Choline as a Cation for the Design of Low-toxic and Biocompatible Ionic Liquids, Surfactants, and Deep Eutectic Solvents

Dissertation

zur Erlangung des Doktorgrades der Naturwissenschaften (Dr. rer. nat.)

der Fakultät für Chemie und Pharmazie

der Universität Regensburg

vorgelegt von

Doris Rengstl

aus Landshut

2013

Official Registration:	10.04.2013
Defense:	30.04.2013
Ph. D. Supervisor:	Prof. Dr. Werner Kunz
Adjudicators:	Prof. Dr. Werner Kunz
	Prof. Dr. Hubert Motschmann
	Prof. Dr. Arno Pfitzner
Chair:	Prof. Dr. Henri Brunner

Für meine geliebten Eltern Antonia und Robert!

Preface

This thesis arises from studies carried out at the Institute of Physical and Theoretical Chemistry (Faculty of Natural Sciences IV) of the University of Regensburg between October 2009 and April 2013 under the supervision of Prof. Dr. W. Kunz. Beside this, some of the presented results of this thesis have been obtained during several stays at the Institute de Chimie Séparative de Marcoule (CEA/CNRS, UM2, ENSCM, France), at the research group of Prof. Dr. H. Cölfen (University of Konstanz, Germany), at HASYLAB/DESY (Hamburg, Germany) and at the Papiertechnische Stiftung (Munich, Germany).

This work would not have been possible without the support and help of many people to whom I would like to express my honest thank.

First of all I would like to express my sincere thank to Prof. Dr. W. Kunz for giving me the opportunity to work independently at his institute and for kindly granting me financial support, for the valuable discussions and at last for the interesting topic.

Additionally, I want to thank Prof. Dr. R. Buchner and PD. Dr. R. Müller (all from the Institute of Physical and Theoretical Chemistry, University of Regensburg) for providing their equipment and also their profound knowledge in concerns of IR, TGA, DSC, density and conductivity. Furthermore, I am grateful to Prof. Dr. R. Buchner for giving me the opportunity to use his nitrogen floated glove box. Without this all the preparations would not have been possible.

Also special thanks to T. Sonnleitner for the introduction in the handling of the high precision conductivity instrument and support concerning the MOPAC calculations. Further thank to Dr. D. Touraud and Prof. Dr. D. Horinek for fruitful discussions (all from the Institute of Physical and Theoretical Chemistry, University of Regensburg).

Furthermore, I am grateful to U. Schießl and M. Avola (both Institute of Anorganic Chemistry, University of Regensburg) for performing DSC measurements and further to Prof. Dr. A. Pfitzner for providing the required equipment.

I would like to express my gratitude to Prof. Dr. G. J. Tiddy (School of Chemical Engineering and Science, University of Manchester) for the long and fruitful discussions concerning

thermotropic phases, the introduction in temperature variable ^{1}H NMR measurements and especially for his special sense of humor. In addition, special thanks to A. Schramm and G. Stühler for performing the temperature dependent ^{1}H NMR measurements and to Prof. Dr. I. Shenderovich for the long discussions concerning the data evaluation (all from the NMR department of the University of Regensburg). Further, thank to the faculty workshops of the University of Regensburg for constructing diverse cells.

I am likewise thankful to Prof. Dr. J. Heilmann (Institute of Pharmaceutical Biology, University of Regensburg) for giving me the chance to perform cytotoxicity tests at his institute. Furthermore, special thanks to his co-workers Dr. B. Kraus and G. Brunner for their continuous support in any practical questions and Dr. B. Kraus for providing her profound knowledge concerning cytotoxicity.

I am grateful to A. Drexler from the Papiertechnische Stiftung at Munich to give me the opportunity to use their spectrophotometer.

I would like to express my gratitude to Dr. O. Diat from the Institute de Chimie Séparative de Marcoule (CEA/CNRS, UM2, ENSCM, France) for his persistent help during the performance of SAXS and WAXS measurements on the liquid crystalline phases and deep eutectic solvents and for his help concerning data evaluation and interpretation. Furthermore, I would like to thank Bruno Corso from the Institute de Chimie Séparative de Marcoule (CEA/CNRS, UM2, ENSCM, France) for SAXS maintenance at the right time.

Further thanks go to Dr. S. de Souza Funari and S. Botta for their excellent experimental and technical support during the beamtime at the HASYLAB/DESY synchrotron radiation facility at Hamburg. In addition, I would like to thank Prof. Dr. G. D. Elliott and M. Van Vorst from the Department of Mechanical Engineering and Engineering Science at the UNC Charlotte (USA) for performing the VP-DSC measurements and their help concerning data evaluation.

I would like to express my gratitude to Prof. Dr. H. Cölfen for giving me the chance to use his conductivity equipment and further to A. Picker and Dr. M. Kellermeier for their technical support during the measurements.

Special gratitude goes to the “Fonds der Chemischen Industrie” for two years of financial support.

I am grateful to A. Picker, Dr. F. Glaab, Dr. U. Nordemann and K. Rengstl for critical reading parts of this manuscript.

Many gratitude to all my colleagues at the institute for the pleasant atmosphere and helpfulness, enjoyable barbecue evenings and the nice hiking tours in the mountains. Special thank goes to J. Eiblmeier for his help during the beamtime at HASYLAB/DESY at Hamburg. Further gratitude to my lab colleague Dr. R. Klein for the nice time and innovative suggestions and also to M. Müller for the great time we had together in the lab.

Infinite thanks to very important persons in my life: my parents, Robert and Antonia, my sister Kristina and my brothers Mathias and Fabian who always encouraged me and gave me strength to reach my aims.

Last but not least, heartfelt thanks to my boyfriend Uwe for his mental support, understanding and encouraging me all the time.

Doris Rengstl

Table of contents

Chapter 1

Introduction

A lot of studies praise choline as a good biocompatible cation of biological origin in ionic liquids, surfactants or deep eutectic solvents.[1-13] In 1960, choline salicylate was found to be a low temperature melting salt, with a melting point of 50°C.[14] Since at this time the interest in choline as cation was low, further investigations on ionic liquids started only some decades later. In the last 20 years the research in ionic liquids rose enormously, at the beginning mostly in order to replace common organic solvents. Further to a low melting temperature, ionic liquids exhibit various other interesting properties like low vapor pressure, high polarity range, high thermal stability and good solvent properties.[1] Firstly, they were considered as a good alternative to conventional organic solvents, but due to versatile properties, their application area grows enormously covering electrochemistry and even biotechnology.[15] Considering the broader field of appliance, the impact of ionic liquids on health, safety and environment moved into the center of research.[15] A lot of commonly used ionic liquids, especially those with imidazolium derivatives, were observed to be toxic in nature.[15] Therefore, research on new biodegradable, biocompatible and low toxic ionic liquids became more and more important in the last two decades. In this context another class of substance, the deep eutectic solvents, has been considered as well.[2, 3, 16] Choline turned out to be a very important cation in the research of non-metal containing deep eutectic solvents (growing interest since 2003).[3] The main research with choline as cation in ionic liquids started in 2007.[1, 7, 11, 17, 18] The factors making choline, chemically known as (2-hydroxyethyl)trimethylammonium, a promising cation are:

- quaternary ammonium ion of biological origin
- essential nutrient for humans[19]
- present in a lot of food (former vitamin B_4)[20]
- essential key functions in the human body, e.g. precursor for acetylcholine or phospholipids[21]
- unsymmetrical, bulky structure

These characteristics classify the choline cation as low toxic and biodegradable. In addition, the bulky and unsymmetrical structure assigns it as a predestined cation for lowering the melting point in ionic liquids or deep eutectic solvents because it hinders regular crystalline packing. This behavior was also found for ionic liquids with tetraalkylammonium ions.[11, 22-26] However, since they act as phase transfer catalyst, they are considered to be toxic.[27-30] Thus, choline is further shown up as an alternative to the tetraalkylammonium cations. Klein *et al.* used choline also as a promising cation for the design of new surfactants.[8, 9, 13, 31] In the same way as it could lower the melting point, it is able to lower the Krafft temperature of surfactants. Choline carboxylate soaps ChC_m with chain length of m = 12, 14, 16 and 18[9, 13,

[31] and choline dodecylsulfate[8] were synthesized. Low cytotoxicity and good biodegradability of these surfactants were confirmed in cytotoxicity tests with the HeLa and SK-MEL-28 cell lines and in standardized biodegradation tests, respectively.[10]

Collins´ concept of "matching water affinities" [33, 34] characterizes choline[32, 33] as "soft" cation, the sulfate headgroup as "soft" anion, and the carboxylate headgroup as "hard" anion. It assumes stronger headgroup-counterion interaction between the sulfate headgroup and choline compared to the carboxylate headgroup. Klein *et al.*[8] confirmed this concept for the choline surfactants and demonstrated that owing to the stronger headgroup-counterion interaction choline dodecylsulfate is less salt sensitive compared to choline dodecanoate. These tests also proved increasing counterion-headgroup interaction of alkylsulfates with growing size of the couterion ($Li^+ < Na^+ < K^+ <$ choline$^+$).[8, 34, 35] Furthermore, an enhanced solubility of these choline surfactants in water was demonstrated without lowering the biocompatibility.[8, 13] This is against the common trend which was observed for alkylsulfate surfactants. Choline should increase the Krafft temperature due to the stronger counterion-headgroup interaction, however, the bulky nature of the choline cation hinders highly ordered crystalline packing of the choline dodecylsulfate.[8] Additionally, the low counterion-headgroup interaction between choline and the carboxylate group and the bulky nature of the choline cation revealed a significant influence on the aqueous phase behavior of these choline carboxylates. In contrast to common alkali soaps, choline soaps form phases with higher curvature between the micellar phase L_1 and the hexagonal phase H_1.[31, 36-40] As already mentioned, choline hinders the packing of these neat choline carboxylate soaps and this results in lower melting temperatures. They show a manifold thermotropic phase behavior and melt below 100°C to a liquid crystalline phase.[9]

These two types of anionic choline surfactants, the choline dodecylsulfate and choline carboxylates ChC_m with m = 12, 14, 16, 18, constitute the starting point of this work.

The first part of this thesis is focused on the synthesis of choline carboxylate ionic liquids. The design of an ionic liquid, which is liquid at room temperature, is divided into two approaches. Firstly, the melting point could be further lowered, beside the use of a bulky unsymmetrical cation, by decreasing the chain length of the carboxylate anion (ChC_m with m = 2, 4, 6, 8, 10) and, secondly, by inserting a double bond into the alkyl chain (choline oleate). Therefore, choline carboxylates ChC_m with chain lengths of m = 2, 4, 6, 8 and 10 and choline oleate were synthesized. At the very beginning of this work, a cooperation was initiated with the group of Cristina Silva Pereira (Instituto de Tecnologia Química e Biológica, Universidade Nova de Lisboa), because they were also interested in these ionic liquids.[18] While her group started with the search for applications of these choline carboxylates, e.g. suberin isolation from cork[41, 42], the present work is focused on the physico-chemical

characterization and the comparison with the long chain choline carboxylates. The cytotoxicity was tested with the human cell lines HeLa and SK-MEL-28 and further tests were prepared to determine the influence of these ionic liquids on biological cell membrane (see Chapter 3). Further, the hydrotrope behavior of choline acetate, choline butanoate and choline hexanoate was investigated (see Chapter 3), and the temperature dependent, lyotropic phase behavior of choline octanoate, choline decanoate and choline oleate in water was established. The influence of the alkyl chain length and the double bond in the alkyl chain on the aqueous phase behavior was determined (see Chapter 4). In addition, the temperature dependent behavior of all neat choline carboxylates was analyzed (see Chapter 5) to reveal the influence of choline as cation, the chain length of the carboxylate anion, and the impact of a double bond in the carboxylate anion on the thermotropic phase behavior.

The second main part of this thesis is focused on the investigation of new promising biocompatible and biodegradable surfactants for a possible application as laundry detergents. It was shown by Klein *et al.*[13] that the solubility of choline soaps is increased compared to alkali soaps. However, their salt sensitivity is high and this rules out the application as detergent.[8] Choline dodecylsulfate (ChS_{12}) was shown as less salt sensitive and possesses a more acidic headgroup compared to the choline carboxylates.[8] Further, their Krafft temperature was decreased compared to sodium dodecylsulfate.[8] A better washability at low temperatures is obtained by increasing the chain length, while the Krafft temperature of the surfactant remains below room temperature. Thus, choline hexadecylsulfate (ChS_{16}) was synthesized as a better washing surfactant. First of all the cytotoxicty was tested with the upwards mentioned cell lines. Further, the temperature dependent binary phase diagrams of choline dodecylsulfate (ChS_{12}) and choline hexadecylsulfate (ChS_{16}) with water were investigated and compared to the sodium analogs and to choline carboxylates (see Chapter 6). In addition, the thermotropic phase behavior was studied and compared to the one of choline carboxylates ChC_m with m = 8, 10 and oleate (see Chapter 7). Last but not least, the washability of choline alkylsulfate surfactants and mixtures of choline alkylsulfates with different chain length or with a common laundry detergent was evaluated with the help of washing, foamability and foam stability tests. Furthermore, the oil solubilization capacity of the pure surfactants was evaluated (see Chapter 8).

As third part of the thesis choline glutarate based deep eutectic solvents were investigated. A strategy to design room temperature liquid deep eutectic solvents composed of choline bicarboxylate and choline chloride (and urea) was evolved. The mixtures were characterized according to their solvent properties with density, viscosity and conductivity measurements.

Since this dissertation deals with a lot of different topics of choline compounds such as synthesis of surfactants, ionic liquids and deep eutectics, and their characterization using a lot of physico-chemical methods, each chapter is written as a self-contained study along the following outline*: Abstract, Introduction, Results and discussion, Conclusion, Experimental and References.* In some cases also an Appendix is available at the end of the dissertation.

1.1 References

1. J. Restolho, J. L. Mata and B. Saramago, *Fluid Phase Equilibr.*, 2012, **322**, 142-147.
2. A. P. Abbott, D. Boothby, G. Capper, D. L. Davies and R. K. Rasheed, *J. Am. Chem. Soc.*, 2004, **126**, 9142-9147.
3. A. P. Abbott, G. Capper, D. L. Davies, R. K. Rasheed and V. Tambyrajah, *Chem. Commun. (Camb.)*, 2003, 70-71.
4. A. P. Abbott, G. Capper, D. L. Davies, H. L. Munro, R. K. Rasheed and V. Tambyrajah, *Chem. Commun. (Camb.)*, 2001, **0**, 2010-2011.
5. J. Pernak, A. Syguda, I. Mirska, A. Pernak, J. Nawrot, A. Pradzynska, S. T. Griffin and R. D. Rogers, *Chemistry*, 2007, **13**, 6817-6827.
6. K. Fujita, D. R. Macfarlane, K. Noguchi and H. Ohno, *Acta Crystallogr. Sect. E Struct. Rep. Online*, 2009, **65**, 709.
7. Y. Fukaya, Y. Iizuka, K. Sekikawa and H. Ohno, *Green Chem.*, 2007, **9**, 1155-1157.
8. R. Klein, M. Kellermeier, D. Touraud, E. Müller and W. Kunz, *J. Colloid Interface Sci.*, 2013**, 392**, 274-80.
9. R. Klein, H. Dutton, O. Diat, G. J. Tiddy and W. Kunz, *J. Phys. Chem. B*, 2011, **115**, 3838-3847.
10. R. Klein, Dissertation, Universität Regensburg, 2011.
11. R. Klein, O. Zech, E. Maurer, M. Kellermeier and W. Kunz, *J. Phys. Chem. B*, 2011, **115**, 8961-8969.
12. R. Klein, M. Kellermeier, M. Drechsler, D. Touraud and W. Kunz, *Colloids and Surfaces A: Physicochem. Eng. Aspects*, 2009, **338**, 129-134.
13. R. Klein, D. Touraud and W. Kunz, *Green Chem.*, 2008, **10**, 433.
14. R. H. Broh-Kahn, *Int. Rec. Med.,* 1960, **173**, 217-33.
15. M. Petkovic, K. R. Seddon, L. P. N. Rebelo and C. Silva Pereira, *Chem. Soc. Rev.*, 2011, **40**, 1383-1403.
16. A. P. Abbott, J. C. Barron, K. S. Ryder and D. Wilson, *Chemistry*, 2007, **13**, 6495-6501.

17. P. Nockemann, B. Thijs, K. Driesen, C. R. Janssen, K. Van Hecke, L. Van Meervelt, S. Kossmann, B. Kirchner and K. Binnemans, *J. Phys. Chem. B*, 2007, **111**, 5254-5263.
18. M. Petkovic, J. L. Ferguson, H. Q. N. Gunaratne, R. Ferreira, M. C. Leitao, K. R. Seddon, L. P. N. Rebelo and C. S. Pereira, *Green Chem.*, 2010, **12**, 643-649.
19. *Food and Nutrition Board, Institute of Medicine, Dietary Reference Intakes for Thiamin, Riboflavin, Niacin, Vitamin B_6, Folate, Vitamin B_{12}, Pantothenic Acid, Biotin, and Choline*, National Academic Press, Washington DC, 1998.
20. S. H. Zeisel and K. A. da Costa, *Nutr. Rev.*, 2009, **67**, 615-623.
21. J. K. Blusztajn and R. J. Wurtman, *Science*, 1983, **221**, 614-620.
22. H. Yu, Y. T. Wu, Y. Y. Jiang, Z. Zhou and Z. B. Zhang, *New J. Chem.*, 2009, **33**, 2385-2390.
23. Z. J. Yu, X. K. Zhang, G. Z. Xu and G. X. Zhao, *J. Phys. Chem.*, 1990, **94**, 3675-3681.
24. R. Zana, J. Schmidt and Y. Talmon, *Langmuir*, 2005, **21**, 11628-11636.
25. R. Zana, M. Benrraou and B. L. Bales, *J. Phys. Chem. B*, 2004, **108**, 18195-18203.
26. R. Zana, *Langmuir*, 2004, **20**, 5666-5668.
27. E. Kutluay, B. Roux and L. Heginbotham, *Biophys. J.*, 2005, **88**, 1018-1029.
28. V. B. Luzhkov and J. Aqvist, *FEBS Lett.*, 2001, **495**, 191-196.
29. M. E. O'Leary, *J. Gen. Physiol.*, 1994, **104**, 523-539.
30. M. E. O'Leary, *J. Gen. Physiol.*, 1994, **104**, 507-522.
31. R. Klein, G. J. T. Tiddy, E. Maurer, D. Touraud, J. Esquena, O. Tache and W. Kunz, *Soft Matter*, 2011, **7**, 6973.
32. K. D. Collins, G. W. Neilson and J. E. Enderby, *Biophys. Chem.*, 2007, **128**, 95-104.
33. K. D. Collins, *Methods*, 2004, **34**, 300-311.
34. J. V. Joshi, V. K. Aswal and P. S. Goyal, *J. Phys. Condens. Matter*, 2007, **19**, 196219/196211-196219/196219.
35. J. V. Joshi, V. K. Aswal, P. Bahadur and P. S. Goyal, *Curr. Sci.*, 2002, **83**, 47-49.
36. V. Luzzati and P. A. Spegt, *Nature*, 1967, **215**, 701-&.
37. P. V. Luzzati, H. Mustacchi, A. Skoulios and F. Husson, *Acta Cryst.*, 1960, **13**, 660-667.
38. V. Luzzati, H. Mustacchi and A. Skoulios, *Discuss. Faraday Soc.*, 1958, **25**, 43-50.
39. G. Lindblom and L. Rilfors, *Biochim. Biophys. Acta, Rev. Biomembr.*, 1989, **988**, 221-256.
40. K. Fontell, *Colloid Polym. Sci.*, 1990, **268**, 264-285.
41. R. Ferreira, H. Garcia, A. F. Sousa, M. Petkovic, P. Lamosa, C. S. R. Freire, A. J. D. Silvestre, L. P. N. Rebelo and C. S. Pereira, *New J. Chem.*, 2012, **36**, 2014-2024.

42. H. Garcia, R. Ferreira, M. Petkovic, J. L. Ferguson, M. C. Leitao, H. Q. N. Gunaratne, K. R. Seddon, L. P. N. Rebelo and C. S. Pereira, *Green Chem.*, 2010, **12**, 367-369.

Chapter 2

Fundamentals

2.1 Hofmeister series and Collins´ concept: Strategy to design ionic liquids or surfactants

Theories on ion effects play an important role in the field of ionic liquids and also in surfactant chemistry. With their help the strength of cation-anion or counterion-headgroup interaction can be explained. The counterion-headgroup interaction influences the phase behavior of surfactants, their Krafft temperature and also the melting point of general ionic substances. The influence of the strength of this counterion-headgroup interaction on the properties of choline ionic liquids or choline surfactants can be shown throughout the whole thesis.

Here, a short summary about the fundamental aspects concerning ion effects is given. In 1880 to 1890 Hofmeister and his coworkers set one of the milestones in the theory of ion effects. They published seven papers with the main title “About the science of the effect of salts”.[1-4] In these papers they show a systematic study on salt effects beyond the impact of different charges. Their conclusions about the salt effects were proofed with several different systems. For example, they established a series of salts according to their ability to precipitate egg-white albumin. These salt series were also studied on the precipitation behavior of sodium oleate, collagen and some more systems.[4] These studies enabled them to arrange salts (not ions) according to their “water withdrawing capability”.[3, 5] One of their main goals was the finding that salts which have a high ability to order water, are very effective in protein precipitation.[3, 4] Many years later and after some refinement, this classification of salts was transferred to isolated ions and appears as what is known today as the “Hofmeister series” (see **Figure 2-1**).[5]

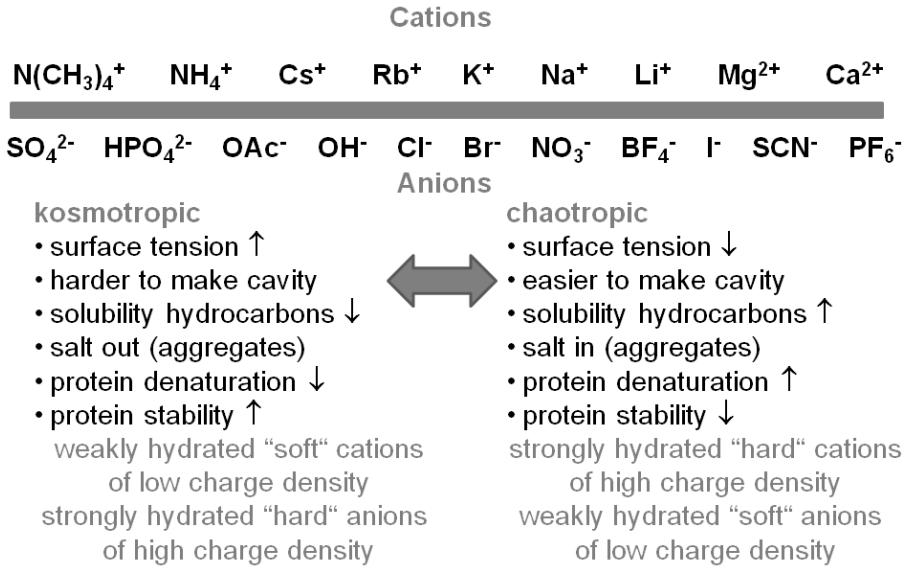

Figure 2-1. The Hofmeister series: Ordering of anions and cations according to their ability to influence the surface tension, the solubility of hydrocarbons, their salting in or salting out effect and protein stabilization. This figure is based on ref [1].

The Hofmeister series are used to explain many phenomena in drug design in pharmaceutical industry, in salting in or salting out processes, in protein stabilization, and in a lot of more pharmacological, physiological and physical processes.[4, 6, 7]

A lot of further studies on ion effects followed. Every year a lot of papers appear in this research area.[1, 3-5] Considering ions in solution, it is necessary not only to study the interaction between the ions, but also to consider the interaction of the ion with surrounding water and also the water structure. For this, it is important to take the charge density into account, which is given by the ratio between the charge and the volume of the ion. In order to consider ion effects on proteins or other macromolecules, even more parameters are necessary. During this work only the consideration of headgroup and counterion in solution was important.

Such a concept which addresses all this points was given by Collin.[3, 6, 7] He orders the ions according to their size to “medium-sized” water. Further, his main ideas are based on the law of “matching water affinities” (see **Figure 2-2**).[7] Thereafter, ion pair formation is dependent on hydration and dehydration processes.[5] Herein, he states that oppositely charged ions, which are in a solution, only form spontaneously inner sphere ion pairs, when their affinity to water is comparable.[7] Collin characterizes two types of ions according to their size to “medium-sized” water (see left-hand panel in **Figure 2-2**). Ions are generally considered as spheres with a point charge. The “hard”, very strongly hydrated ions with a high charge density, called kosmotropes, and the “soft”, very weakly hydrated ions with a low charge density, named chaotropes. The differentiation in the interaction of the ions with each other results from the relative strength of the interaction of the single ion with “medium-sized” water and the interaction of the water molecules in the hydration shell. In the case of the interaction of two oppositely charged, small, “hard” ions, the electrostatic interaction is stronger than their interaction with the “medium-sized” water molecules. Therefore, they can form an inner sphere ion pair and emit the water molecules between each other. Two big (referred to “medium-sized” water) oppositely charged, “soft” ions in water can also form an inner sphere ion pair. Due to their low charge density, their electrostatic interaction is very small and the water molecules are only loosely bound enabling the formation of direct ion pairs without water molecules in between. Concerning the interaction between a “soft” ion and an oppositely charged, “hard” ion, the electrostatic interaction between the ions is not strong enough to destroy the hydration shell of the “hard” ion. Thus, ion pairs formed by a “hard” and a “soft” ion are also separated by water molecules.[1, 6, 7] This concept of “like seeks like” is graphically demonstrated in **Figure 2-2**.

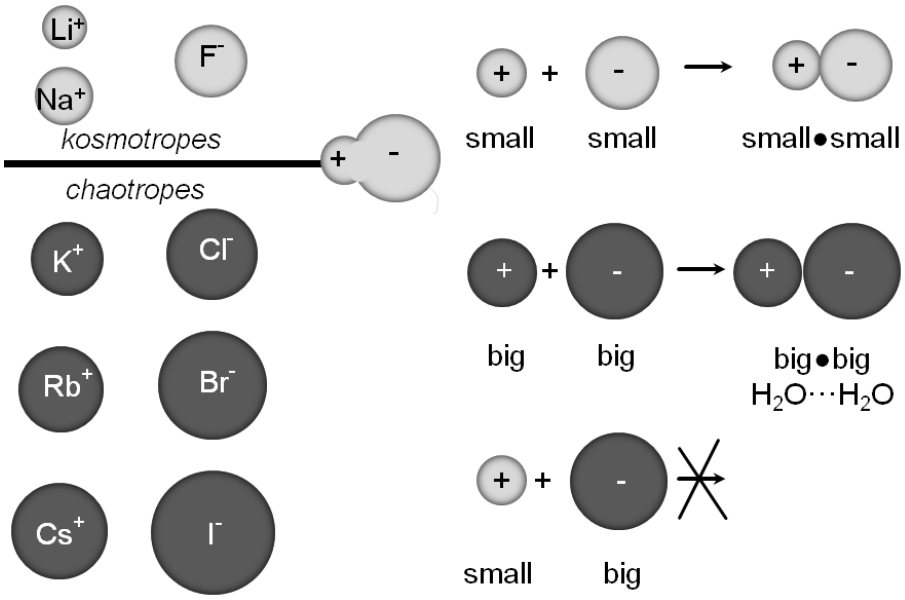

Figure 2-2. Alkali cations and halide anions are divided into kosmotropes (strongly hydrated, "hard" ions, also known as water structure makers) and chaotropes (weakly hydrated, "soft" ions also known as water structure breakers). The ions are drawn accurately to size. The zwitterionic molecule represents the "medium-sized" water.[7] It is shown that the size of the ions is decisive for the ability to form inner sphere ion pairs in aqueous solution. Congeneric ions are able to form inner sphere ion pairs. The combination of mismatching ions brings forth advanced dissociation and the ions like to keep their hydration shell.[1, 7]

This concept of "matching water affinities" can be easily transferred to observations in pharmacy, biology etc. where sulfate, phosphate, carboxylate and ammonium groups are available. The ordering of the isolated ions in the Hofmeister series and their dedicated properties in water can be explained with the Collins´ concept. Taking proteins in solution into account, they possess strongly hydrated carboxylate groups. This group has a high charge density. Therefore, strongly hydrated, "hard" cations interact with the carboxylate group and destabilize the protein (see **Figure 2-1**). Other groups available in proteins are the weakly hydrated amino acid groups. They interact strongly with weakly hydrated anions (reverse Hofmeister series), which destabilize the protein (see **Figure 2-1**).[7] In the last decades, a lot of effects in studies concerning ion specificities in other biological systems[6, 7], in colloid chemistry[3] or due to specific chromatography study[1, 8] were explained by the combination of the Hofmeister series with the Collins´ concept.[6, 7] These studies can also be used to design surfactants with special properties. By knowing the headgroup of the surfactant, the strength of the interaction with the counterion can be explained by the combination of the theory known from Hofmeister series and from Collins´ concept. A lot of studies characterize the carboxylate group as "hard", strongly hydrated headgroup, while the sulfate and sulfonate headgroups are weakly hydrated and "soft". The phosphate headgroup could be set between these two headgroups. The ability to form ion pairs with alkali-metal or ammonium cations was investigated in several studies[3, 9, 10] and is shown in **Figure 2-3.** Additionally, Klein *et al.*[10] proved this concept by investigation of the salt sensitivity of choline

dodecylsulfate and choline dodecanoate. Therefore, the Krafft temperature of dodecylsulfate and dodecanoate with choline, potassium and sodium as cation was measured by adding lithium chloride, sodium chloride, potassium chloride and choline chloride. It was found that the counterion-headgroup interaction increases for the alkylsulfates in this manner: $Li^+ < Na^+ < K^+ <$ choline$^+$, while for the carboxylate surfactants the opposite order was found. Therefore, in aqueous solution choline alkylsulfates are less salt sensitive compared to choline carboxylates.[10]

This result favors the choline dodecylsulfate[10] and choline hexadecylsulfate as promising surfactant in detergency (see Chapter 8). The different counterion-headgroup interactions between the choline carboxylates and choline alkylsulfates has further influence on the structural parameter of the hexagonal and lamellar phases of these surfactants in water (see Chapter 4 and 6).

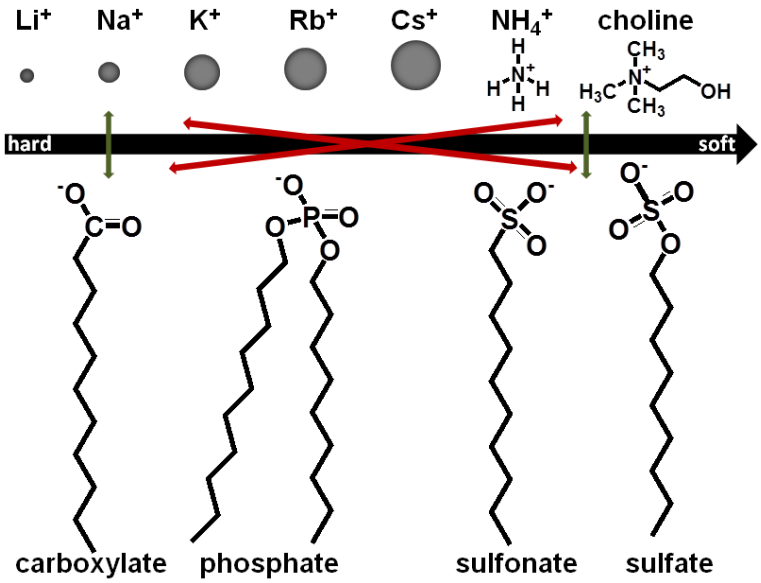

Figure 2-3. The characterization of surfactant headgroups and counterions as “soft” or “hard” ions is shown. Taking into account Collins´ concept of “matching water affinities”, also known as “like seeks like”, the green arrows represent strong headgroup-counterion interaction, while the red arrows represent favored dissociation of the headgroup and counterion in water.[1, 3, 6]

2.2 Surfactants

Surfactants are ubiquitous in our daily life. They are used as laundry detergents (see Chapter 8), in washing and cleaning products as emulsifiers, in pharmaceutical products, in the paper industry and many others. The consumption of surfactants is enormous. Thus, nowadays the focus is set on their easy production from renewable products and also on a high degradation potential and low toxicity of surfactants. The most widely used groups are anionic surfactants.[11]

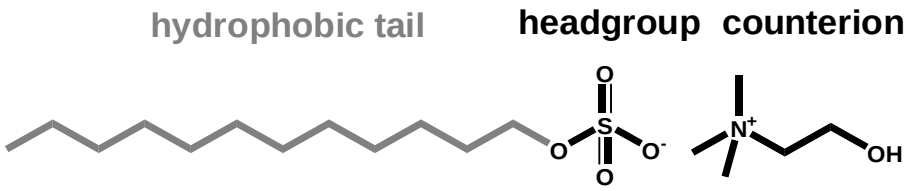

Figure 2-4. Scheme of an anionic surfactant. In this case it is choline dodecylsulfate.

Surfactant class	Structure examples
Anionic	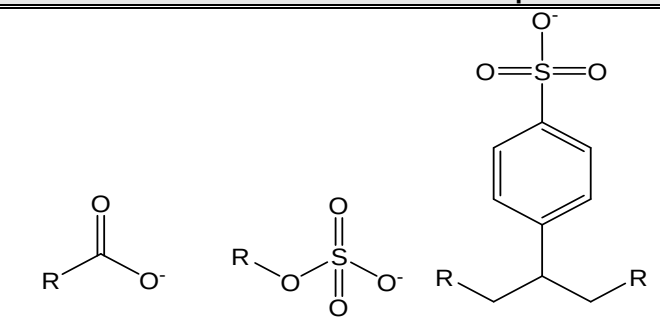 Alkylcarboxylate Alkylsulfate Alkylbenzenesulfonate
Cationic	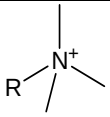 Alkyl quat
Non-ionic	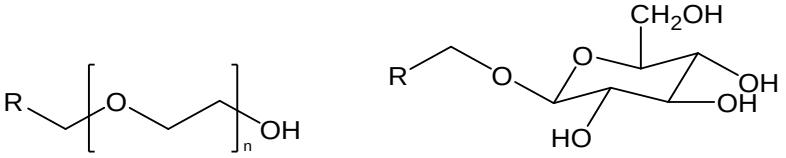 Alkylpolyethylenglycols Alkylglycoside
Zwitterionic	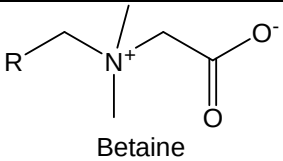 Betaine

Table 2-1. Some representative examples of each surfactant class.

Surfactants are surface active, amphiphilic molecules. They are composed of a hydrophobic tail and the polar headgroup, which is the water-soluble part. The different types of surfactants are classified according to their charge. Negatively or positively charged are

named anionic or cationic, respectively. Zwitterionic ones possess a positive and a negative charge. Completely uncharged surfactants are non-ionic surfactants.[11]

This dissertation is focused on anionic carboxylate (ChC_m with m = 8, 10 and oleate) and alkylsulfate surfactants (ChS_{12} and ChS_{16}) with choline as cation and their physico-chemical characterization. In this section fundamental information about thermotropic phases, Krafft temperature, packing parameter, self-assembly behavior as critical micelle concentration (*cmc*), and lyotropic phases are given.

2.2.1 Adsorption and aggregation behavior

Due to the amphiphilic structure of surfactants the dissolution in solvents, e. g. water, results in a reduction in free energy G. This free energy is further reduced by adsorption of the surfactant at the surface or interface of the solvent and/ or by self-aggregation in the bulk phase.[11-13]

2.2.1.1 Adsorption theory

As mentioned above, one strategy of amphiphilic systems to reduce the free energy is adsorption. Therefore, a surface excess concentration Γ_i can be defined. It is the excess amount of component i in the interface z compared to the bulk phase, with n_i^z as the concentration of component i at the interface z and A is the area of the interface z:

$$\Gamma_i = \frac{n_i^z}{A} \qquad (1)$$

Changes of the free energy dG of a system are given by the following equation with S being the entropy, p the pressure, and V the volume of the system:

$$dG = -SdT + Vdp + \sigma dA + \Sigma \mu_i dn_i \qquad (2)$$

The interfacial tension σ is dependent on the temperature, pressure, and chemical potential μ_i of the components i. At constant temperature and constant pressure the Gibbs equation (see equation (3)) relates the change in the interfacial tension to the shift in the chemical potential μ_i and the surface excess concentration Γ_i:[12, 13]

$$d\sigma = -\Sigma \Gamma_i d\mu_i \qquad (3)$$

For a biphasic system with solvent 1 and uncharged compound 2, the assumption of constant temperature and pressure of the dilute system, a special choice of the dividing surface with $\Gamma_1 = 0$, and $d\mu_2 = RT \cdot d\ln c_2$ (activity coefficient of compound 2 in dilute solution is similar to 1) the Gibbs adsorption isotherm is given as follows:[12, 13]

$$\Gamma_2 = -\frac{1}{RT}\frac{d\sigma}{d\ln c_2} \qquad (4)$$

This equation is valid for uncharged compounds. For charged species the degree of dissociation has to be considered.[13]

2.2.2 Self-assembly behavior of surfactants

Another possibility to reduce the free energy of dissolved surfactants in water is the self aggregation of the surfactant molecules to micelles at low concentrations or to liquid crystalline phases at higher concentration. During aggregation to micelles, the hydrophobic tail of the surfactant is directed towards the interior of the micelles, while the polar headgroup is faced to the polar solvent. Micelle formation can be explained by the “hydrophobic effect”.[13, 14] The “hydrophobic effect” is provoked by two contributions. The first is temperature dependent and explains the influence on the water structure (water is commonly used as solvent). The water molecules around the hydrophobic part of the surfactant possess less degree of freedom. Therefore, fewer conformations are available compared to a water molecule which is not next to a solute. The second contribution is less temperature dependent. It describes the high energy effort to form a cavity in the solvent, mostly water, for the solute. This energy is high because the inter-solvent cohesion forces have to be disturbed and further the solvent molecules are mostly smaller compared to the solute molecules, mainly hydrocarbons. Thus, the “hydrophobic effect” is directly proportional to the area of the hydropobic part of the solute with the solvent.[14]

2.2.2.1 Critical micelle concentration (*cmc*)

The surfactant concentration at which self aggregation appears is called the critical micelle concentration (*cmc*). At the critical micelle concentration two opposite forces arise. One is the energy which is needed to transfer the hydrophobic tails out of water into the interior of the micelles, and the other are the repulsion forces of the headgroups as they converge upon micelle formation. These forces are opposite.[13] As self-assembly is a physico-chemical process and no covalent bonds are formed or broken, the size or shape of aggregates can be easily changed by temperature, concentration, salt content, pH, and pressure.[13] The

concentration dependent aggregation could be well monitored by measuring the concentration dependent change of some physico-chemical properties. As **Figure 2-5** shows, some physico-chemical properties change abruptly at the *cmc*.[11, 15]

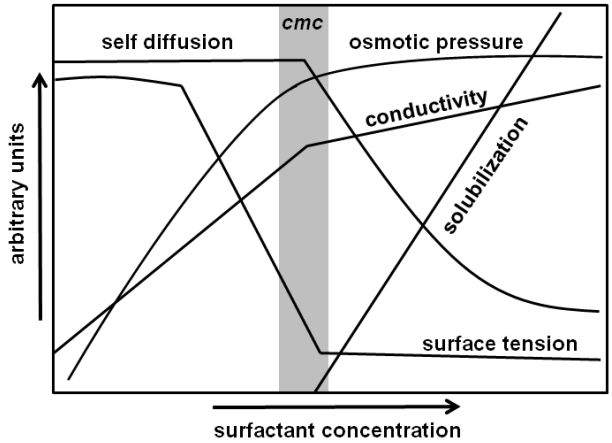

Figure 2-5. Schematic presentation of some concentration dependent physico-chemical properties of surfactants in water.

The *cmc* is strongly dependent on the chemical structure and the charge of the surfactant. Therefore, some general aspects could be given:

- The "hydrophobic effect" results in a decrease of the *cmc* with increasing linear alkyl chain length. This is given in Klevens equation:

$$\log(cmc) = \mathrm{A} - \mathrm{Bm} \qquad (5)$$

- m is the number of carbon atoms in the alkyl chain. A and B are constants. B is dependent on the charge of the headgroup (B = 0.5 for non-ionic; B = 0.3 for monoionic, B = 0.15-0.18 for zwitterionic) and A is constant for a special headgroup.[11] According to this equation (5) the *cmc* of zwitterionic and non-ionic surfactants is reduced by the factor of 10 per addition of two -CH_2- groups to the alkyl chain. For monoionic surfactants the factor is 4.[11, 15]
- Double bonds in the alkyl chain increase the *cmc* compared to their saturated equivalent. [11, 15]
- For linear alkyl chain surfactants the *cmc* decreases with different headgroups in this order: carboxylate (with one C-atom more in the chain) > sulfonate > sulfates.[15]
- An increase in the degree of counterion binding to the headgroup results in a decrease of the *cmc.* This was also found for the choline alkylsulfates. Their *cmc* is smaller than the one of the sodium alkylsulfates (see Chapter 6 and [10]). For soaps the *cmc* should decrease in this row: Choline$^+$ > Cs^+ > K^+ > Na^+ > Li^+. But there was found

no significant difference between the *cmcs´* of the choline soaps, the potassium soaps and the sodium soaps (see Chapter 3 and [16]).[15]

- Cationic surfactants show slightly higher *cmc* values as their corresponding anionic surfactants.[13]

2.2.2.2 Krafft point and solubility

The intersection of the solubility curve and the *cmc* curve is defined as the Krafft point (see **Figure 2-6**). Above this point a rapidly increased surfactant solubilization is found.[13] The Krafft temperature is often measured as the temperature at which the turbidity of a 1 wt% aqueous surfactant solution disappears.[17]

At the Krafft point, the interplay of two opposing thermodynamic forces is observed. One is the free energy of the crystalline state and the other is the free energy of the solubilized state. In general, the free energy of the crystalline state has more influence on the Krafft temperature. Further, a high free energy of the crystalline state indicates high energetically, instable crystals and favors the solubilized state. Thus, the Krafft temperature can be lowered by a hindered crystalline packing or by very well soluble, high dissociated molecules.[17] Branched alkyl chains or functional groups in the alkyl chains, like double bonds, hinder a regular packing (see Chapter 4), cis-double bonds more than trans.[13] Highly dissociated ions decrease the free energy of the solubilized state and lower the Krafft temperature. Therefore, the Krafft temperature of divalent ions is much higher than that of monovalent ions.[13] Considering the counterion-headgroup interaction correlation with the Krafft temperature for alkylcarboxylate and alkylsulfate surfactants, the following is observed: The Krafft temperature increases for alkylsulfates with increasing size of alkali cation (Li^+ < Na^+ < K^+ < Rb^+ < Cs^+)[18, 19], while the one of the alkylcarboxylates decreases[17, 20, 21]. Further, Zana *et al.*[22-24] found that bulky tetraalkylammonium ions lower the Krafft temperature of carboxylate soaps because of the low counterion-headgroup interaction. Klein *et al.* have observed a low Krafft temperature for choline carboxylates ChC_m with m = 12, 14, 16, 18 because choline is a “soft” big counterion which favors a highly dissociated state combined with carboxylates.[16] Additionally, they found, in contrast to the findings for alkysulfates with different sizes of counterions, that choline lowers the Krafft temperature of choline dodecylsulfate.[10] Normally, choline should increase the Krafft temperature due to the strong counterion-headgroup interaction. However, choline hinders the crystallization due to its bulky unsymmetrical nature.[10] This proves the above mentioned observations. The free energy of the crystalline state is more important to lower the Krafft temperature than the free energy of the solubilized state.

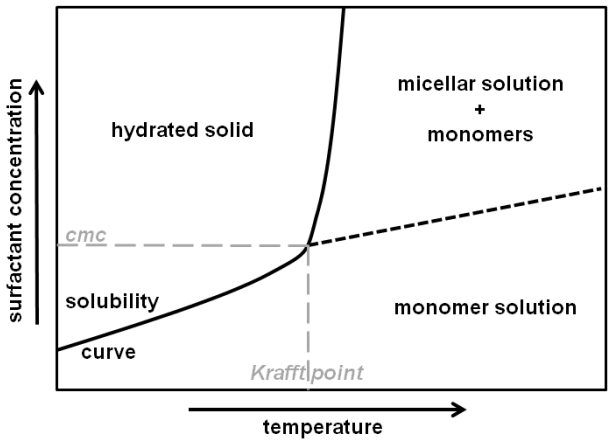

Figure 2-6. Phase diagram of a surfactant in water at the Krafft point region.

2.2.2.3 Correlation of surfactant structure and aggregation behavior with increasing surfactant concentration in water

The shape of micelles often gives information about the lyotropic liquid crystalline phase sequence formed with increasing surfactant concentration. It depends on the geometry of the amphiphilic molecule. The concept of packing constraints links the shape of a surfactant molecule to the shape of the micelles by taking the volume of the hydrocarbon chain ν, the length of the hydrocarbon chain l and the effective area per headgroup a_S into account. The relation between these parameters is described by the packing parameter N_s (see equation (6)). Israelachvilli and coworker gave a thermodynamic description of this concept.[11, 13, 25]

$$N_s = \frac{\nu}{a_S\, l} \qquad (6)$$

The length l and the volume ν of the hydrocarbon chain can be estimated by equation (7) and (8) given by Tanford for saturated, unbranched alkyl chains with n_C C-atoms:[13, 26]

$$l = 1.5 + 1.265\, n_C \qquad (7)$$

$$\nu = 27.4 + 26.9\, n_C \qquad (8)$$

The effective area per headgroup a_S cannot easily be estimated. It strongly depends on the type of headgroup, the size of the counterion and the degree of counterion-headgroup binding (see Chapter 4 and 6). Taking this parameter N_s into account, the following self assembled aggregates at low surfactant concentration could be found (see **Table 2-2**).

Packing parameter N_s	Shape of the aggregates
0.33	Spherical normal micelles with hydrocarbons in the interior of the micelle and the headgroup towards the water
0.5	Elongated cylindrical micelles with undefined length
1	Planar bilayered structures which are conveyed in disc-like micelles or vesicles
>1	Inverted spherical or inverted cylindrical micelles

Table 2-2. Relation between the packing parameter N_s and the shape of the micelles.[13]

Above a certain critical volume fraction of the surfactant in water, a randomly ordered distribution of these aggregates (see **Table 2-2**) is not possible anymore. Ordered structures were formed, if the surfactant is soluble enough. They are called lyotropic liquid crystalline phases. **Figure 2-7** represents the possible liquid crystalline formations of surfactants in water with increasing surfactant concentration.

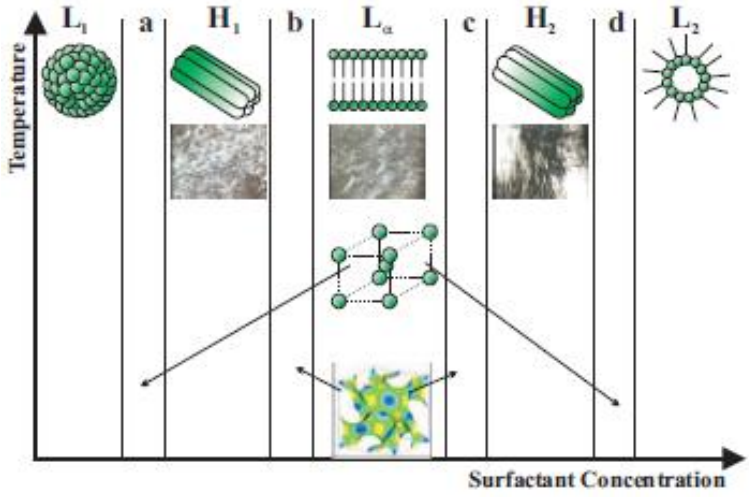

Figure 2-7. Schematic representation of the lyotropic liquid crystalline phases with increasing surfactant concentration is shown as a function of temperature. L_1: normal micelles, H_1: normal hexagonal phase, L_α: lamellar phase, H_2: inverse hexagonal phase, L_2: inverse micelles. a and d are normal and inverse discontinuous cubic phases. Their appearance is dependent on the surfactant structure. b and c are normal or inverse bicontinuous cubic phases. They often can be replaced or complemented by intermediate phases.[27]

Spherical and rod-like micelles are only packed in an ordered structure without a change in the shape until a maximum volume fraction for the packing is reached. This volume fraction is 0.74 for spheres, 0.91 for rods and 1 in case of lamellar bilayers. Above this volume fraction, when the whole available volume is occupied, the curvature of the aggregates is reduced, and they form aggregates with a shape of higher packing limit.[11] The following shapes for micelles result in the following sequences of mesophases with increasing surfactant concentration:

- **Small polar headgroup**: *Disc-like micelles L_1 → lamellar phase L_α*
- ***Medium sized polar headgroup:*** *Rod-like micelles L_1 → normal hexagonal phase H_1 → bicontinuous cubic phase V_1/ intermediate phases → lamellar phase L_α*
- ***Large polar headgroup:*** *Spherical micelles L_1 → discontinuous cubic phase I_1 → normal hexagonal phase H_1 → bicontinuous cubic phase V_1/ intermediate phases → lamellar phase L_α*

It has to be mentioned that reversed phases appear very seldomly. Further, the bicontinuous cubic phase can be replaced by intermediate phases even for long-chain surfactants. It is known that short-chain surfactants, especially EO derivatives with chain length C_n (with $n < 12$) do not form a V_1 phase. They show a direct transition of H_1 to L_α.[11]

The aqueous behavior of choline carboxylates ChC_m with chain length m = 12, 14, 16, 18 is strongly influenced by the huge choline counterion.[28] Due to the bulky structure of choline and the high degree of dissociation of choline carboxylate surfactants, the effective area of the headgroup a_s is increased a lot (see **Figure 2-9**). Therefore, the choline carboxylate soaps prefer mesophases with a high curvature and are able to form spherical micelles, which aggregate at higher surfactant concentration to a discontinuous cubic phase I_1' (see **Figure 2-8**).[28] The following phases can be found for ChC_m with m = 12, 14, 16, 18 with increasing soap concentrations: [28]

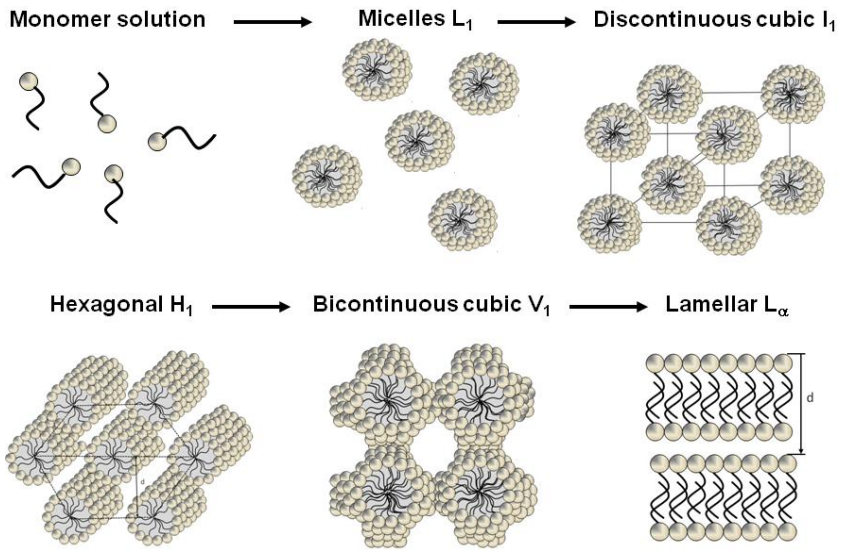

Figure 2-8. Schematic illustration of the sequence of mesophases formed by choline carboxylates ChC_m with m = 12, 14, 16, 18 in water with increasing surfactant concentration.[19, 28]

The other alkali soaps (see **Figure 2-9**) and most of the other mono-anionic surfactants (see **Figure 2-10**) undergo a direct transition from cylindrical micelles to a normal hexagonal phase H_1.[29-33] In Chapter 4, the temperature dependent lyotropic phase behavior of choline

octanoate, choline decanoate and choline oleate is investigated to see the influence of shorter alkyl chains and the insertion of a double bond into the alkyl chain on the lyotropic phase behavior compared to the choline carboxylate soaps ChC_m with m = 12, 14, 16, 18.

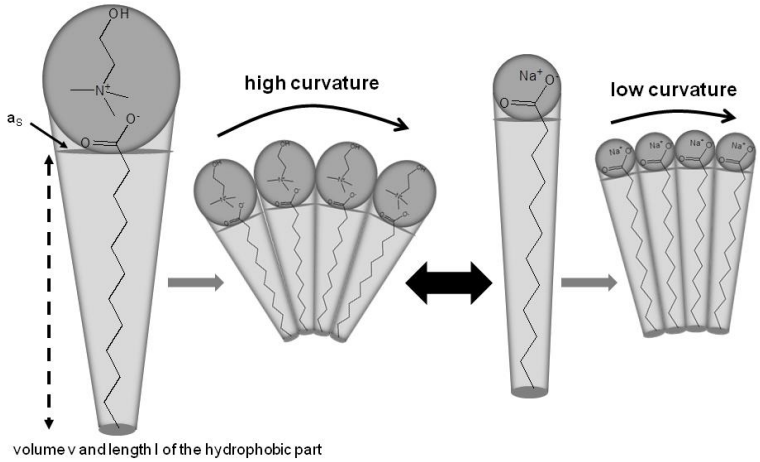

Figure 2-9. Schematic representation of the effect of the different headgroups on the packing behavior of dodecanoate soaps. The choline cation (left) increases compared to the sodium cation (right) the effective area of the headgroup a_S due to the high counterion-headgroup dissociation and its bulky nature. The packing parameter N_s decreases for choline carboxylates compared to sodium carboxylates, since the hydrophobic volume v and the length of the hydrocarbon chain l are the same. Aggregates with higher curvature are formed for choline soaps compared to sodium soaps.[19, 28]

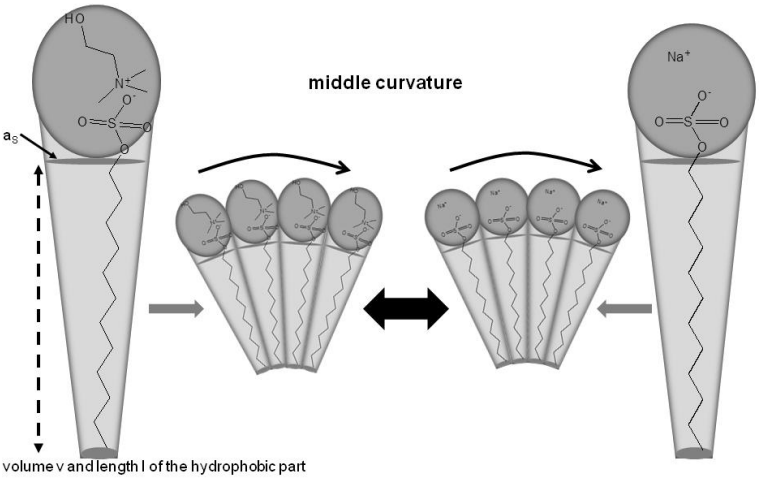

Figure 2-10. The effect of the choline counterion on the alkylsulfate surfactants compared to the sodium cation is low. The effective area of the headgroup a_S is more or less the same for the two cations, because the bigger choline cation shows a higher counterion-headgroup interaction with the sulfate group and due to this it is less dissociated from the sulfate headgroup. Vice versa the interaction of the small sodium cation (right) with the sulfate headgroup is lower and results in a high counterion-headgroup dissociation. Choline does not force an increased packing curvature of the aggregates for alkylsulfate surfactants.

In Chapter 6 the influence of choline on the lyotropic phase behavior of alkylsulfate surfactants compared to the sodium alkylsulfates was investigated. It is observed that choline has no significant influence on the temperature dependent lyotropic phase sequence, as observed for the choline carboxylates. It increases only the solubility of the alkylsulfate surfactant. This can be explained by the opposite effects. Choline is a huge cation, but the

counterion-headgroup interaction with the sulfate is stronger than the interaction of small sodium cation with the sulfate headgroup. Due to this the effective headgroup area of choline dodecylsulfate is more or less the same as the one of sodium dodecylsulfate. They show no increased curvature and a direct transition of cylindrical micelles to the hexagonal phase H_1 with increasing surfactant concentration (see **Figure 2-10** and Chapter 6).[29, 34]

2.2.3 Temperature dependent phase behavior of neat surfactants

Two possibilities exist to transform surfactants into a liquid state. One is the above mentioned dissolution in a solvent. The other is the melting to an isotropic solution. Surfactants have the feature to form with increasing temperature crystalline and liquid crystalline phases before they melt to an isotropic liquid. Alkali soaps (lithium, sodium, potassium, rubidium and cesium) possess various phase polymorphisms forming several phases between the crystalline phase and the isotropic liquid.[12, 35-40] Three main liquid crystalline structures were formed: disc-like structures, ribbon like structures or lamellar, layered structures. In all the liquid crystalline structures the alkyl chains are molten and fluid (see **Figure 2-11**).

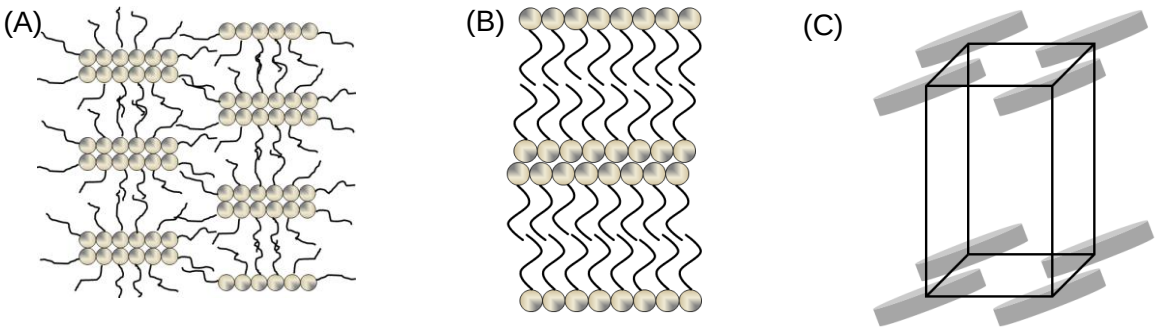

Figure 2-11. Possible arrangements of surfactant molecules in thermotropic liquid crystalline phases. In all structures the alkyl chains are molten and fluid: (A) ribbon-like structure, (B) layered structure (here a non-tilted bilayer is shown, also monolayers or interdigitated layers are possible (tilted or non-tilted)), (C) disc-like structure.[12, 35]

To our knowledge, the thermotropic mesomorphism of the alkylsulfate surfactants is not investigated. On the other hand, the one of the alkali alkanoates like lithium, sodium, potassium, rubidium and cesium alkanoates is established very well.[12, 35-40] Thermotropic mesophases could be formed for carboxylates with chain length m ≥ 4 (dependent on counterion).[41] Sodium alkylcarboxylates with chain lengths of m = 12, 14, 16, 18 form five temperature dependent phases between 100°C and 320°C until they melt to an isotropic liquid. Sodium oleate forms six phases. Normally, they show the following phase sequence with increasing concentration: Curd phase, supercurd phase, subwaxy phase, waxy phase, subneat phase, neat phase and isotropic liquid. In response to the alkyl chain length, some

phases are not formed.[12, 37] In **Figure 2-12** the thermotropic mesomorphism of sodium stearate is shown in the temperature range between 100°C and 320°C.[12]

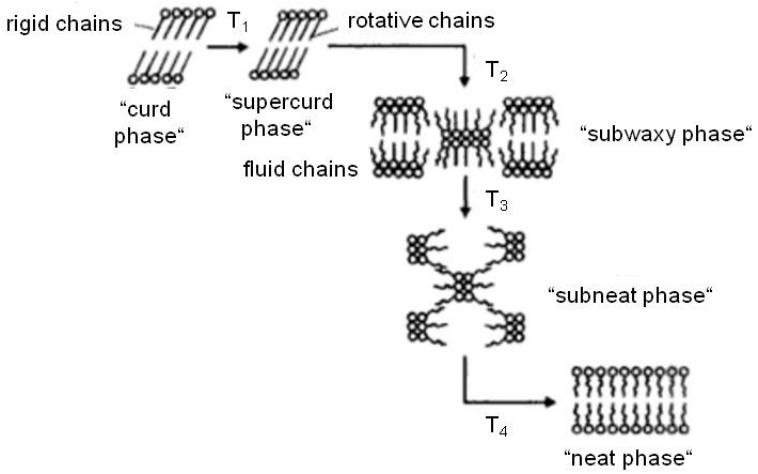

Figure 2-12. Thermotropic mesomorphism of sodium stearate.[12]

The curd and supercurd phase are crystalline phases which possess microfibrous aggregates. In contrast, the subwaxy and waxy phases are more transparent than the curd phase and the chains are fluid. They have a ribbon-like structure and possess no individual fibers or microcrystallines like the curd phase. The subneat phase is a more plastic phase with a grainier texture and is less rigid than the subwaxy phase. The neat phase is similar to the smectic phases which are found in the thermotropic liquid crystalline phases of non-amphiphilic stick-like molecules. It is a two dimensional layered phase.[12, 35]

All alkali metal soaps show in general a similar melting process. It is divided in two major steps which can be explained with increasing temperature. Firstly, the alkyl chains melt before the polar groups get liquid. It is found that the melting point of the alkyl chains increases with increasing alkyl chain length.[31, 35, 39]

Klein *et al.* investigated the melting behavior of choline carboxylate soaps ChC_m with chain lengths of m = 12, 14, 16, 18. Only the temperature range of -20°C to 100°C was investigated, since choline soaps start to decompose at temperatures above 100°C.[42] Three temperature dependent phases were found with increasing temperature: A crystalline and a semi-crystalline interdigitated monolayered phase and a liquid crystalline lamellar bilayered phase.[42] The melting of the alkyl chains is performed before the one of the polar groups, but both melting temperatures increase with growing alkyl chain length. Thus, choline seems to influence the thermotropic mesomorphism because it decreases in general the melting temperature due to its bulky unsymmetrical structure.[42] In Chapter 5, the thermotropic mesomorphism of choline acetate, choline butanoate, choline hexanoate, choline octanoate, choline decanoate and choline oleate was investigated with respect to the influence of the double bond in the alky chain and the alkyl chain length on the temperature dependent

phase behavior of choline carboxylates. The thermotropic mesomorphism of the choline alkylsulfates ChS_{12} and ChS_{16} was established in Chapter 7.

2.2.4 Characterization methods for liquid crystalline phases

2.2.4.1 Small (SAXS) and wide (WAXS) angle X-ray scattering

Scattering methods are useful tools to evaluate the accurate structure of liquid crystalline phases. Only a small sample volume is needed. To evaluate the structure parameters of the liquid crystalline phases, the q-vector dependent reflection pattern of the scattering intensity is used.[11, 43] These spectra are similar to powder diffraction spectra, where Bragg peaks are shown at different ratios. The absolute scattering intensity as a function of the q-vector is not needed, as it is important to investigate the shape and structure of the aggregates for example in microemulsions. The wavelength λ of the incident X-rays should be in the range of the size of the structures which are detected. Synchrotron radiation with a wavelength of 1.5 Å was used to investigate the thermotropic phases shown in Chapter 5 and 7. X-ray radiation was generated with a molybdenum tube with λ = 0.71 Å to establish the lyotropic phases in Chapter 4 and Chapter 6. The wavelength of the X-rays covers in general a range of λ = 0.5-2.3 Å. The scattering vector $\vec{q}$ in liquid crystalline phases is related to the wavelength and the scattering angle θ. It is the modulus between the incident wave vector $\vec{k_i}$ and the scattered wave vector $\vec{k_f}$ (see **Figure 2-13** and equation (9)):[44]

$$q = |\vec{q}| = 2\pi|\vec{k_f} - \vec{k_i}| = \frac{4\pi}{\lambda}\sin\theta \qquad (9)$$

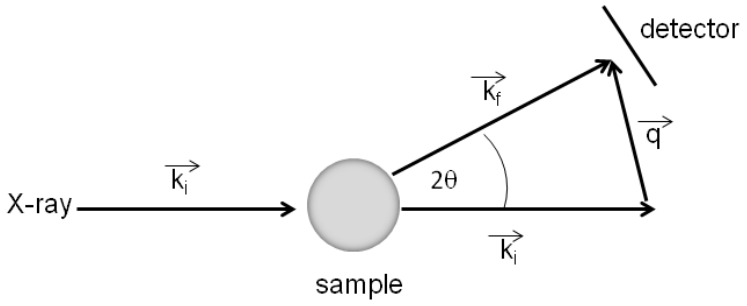

Figure 2-13. Schematic presentation of the correlation between the incident wavevector $\vec{k_i}$ and the scattered wavevector $\vec{k_f}$.

The wave vector is related to the d-spacing in this way: $d = 2\pi/q$. X-rays are scattered by electrons. Thus, inhomogenities in electron distribution in a phase cause X-ray scattering.

The scattering of a single electron is known as Thomson scattering length. The scattering length of a single electron b_0^x is $2.8 \cdot 10^{-15}$ m. Therefore, the scattering length of a molecule i with z electrons is given as $b_i^x = b_0^x \cdot z$.[44, 45]

With the help of X-ray scattering also the crystallinity of a substance could be evaluated. In the small angle X-ray region (q ~ 0.1-0.6 $Å^{-1}$) the packing of the alkyl chains, e.g. lamellar, hexagonal, cubic or layered structure, and the substructure, e. g. orthorhombic, rectangular, triclinic etc., could be evaluated. The wide angle region reflects the crystallinity of the alkyl chains. Crystalline alkyl chains result in defined reflections in the wide angle region (q ~ 0.6-3.0 $Å^{-1}$). Fluid and molten alkyl chains show a broad reflection peak with the maximum assigned around 1.5 $Å^{-1}$ (~ 4.5 Å). This broad peak is characteristic in thermotropic and lyotropic liquid crystalline phases.[12, 31] Beside these downwards explained phases, also nematic phases or gel phases exist, which are not explained in detail.

2.2.4.1.1 Lamellar liquid crystalline phase L_α or layered phases

Layered phases show the same pattern at the small angle region as the normal liquid crystalline lamellar smectic A phase L_α. The Bragg peaks in the small angle region show the ratio of 1 : 2 : 3 : 4 ….[11] The difference is only observed in the wide angle range. As already mentioned, crystalline phases show defined reflections in the wide angle region, while gel phases like the L_β phase reveal a sharp Bragg reflection at 4.2 Å.[11, 31] Liquid crystalline lamellar phases depict a broad peak at 4.5 Å (~ 1.5 $Å^{-1}$). The surfactant molecules could be arranged as shown in the following cases as a normal bilayer/monolayer, and interdigitated monolayer, or a tilted bilayer/monolayer (see **Figure 2-14**).[31] The ordering of the layers is important in the thermotropic mesomorphism of the choline carboxylates ChC_m with m = 8, 10 and oleate (see Chapter 5) and of choline dodecylsulfate and choline hexadecylsulfate (see Chapter 7).

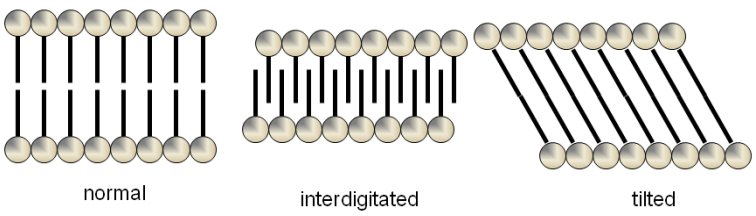

Figure 2-14. Schematic presentation of a normal bilayer, interdigitated monolayer or a tilted bilayer.[31]

The most common lyotropic liquid crystalline phase is the lamellar phase. It is also known as neat phase in the case of the thermotropic liquid crystalline phases of soaps and appears as the high concentrated phase in the majority of binary surfactant water systems. In the lyotropic lamellar phase, surfactant molecules are arranged in bilayers separated by a water layer. The bilayer thickness varies between 1.0-1.9 times of the all-trans alkyl chain length

l_{max}. The bilayer thickness of 1.0 l_{max} reflects a large disorder in the alkyl chains. d describes the repeating spacing which reflects the sum of the water and the bilayer thickness.[11]

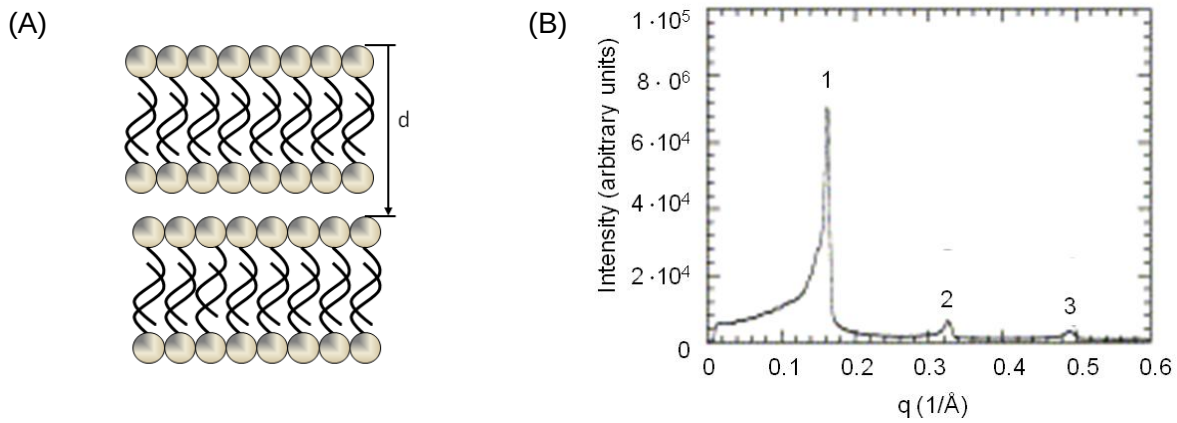

Figure 2-15. (A) Schematic presentation of a lamellar L_α phase with molten alkyl chains. d represents the repeating spacing of the bilayers which include the bilayer thickness and the water layer thickness. (B) SAXS spectrum of a lamellar L_α phase.[11, 46]

2.2.4.1.2 Hexagonal phase (H_1 or H_2)

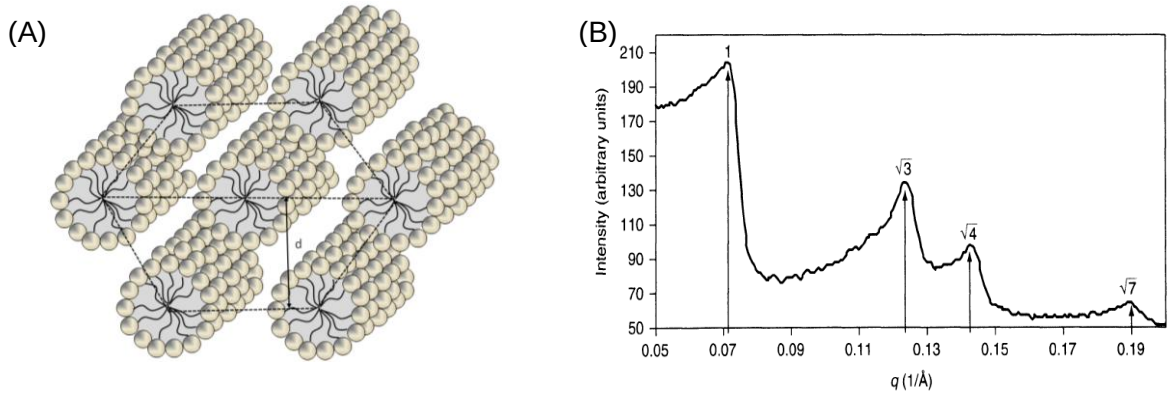

Figure 2-16. (A) Schematic representation of a normal hexagonal phase H_1 and (B) its small angle X-ray spectrum. The d value represents the repeating distance.[11]

The hexagonal phase is, as already explained in section 2.2.2.3, a common mesophase in binary surfactant water systems. Two classes exist. The water continuous normal hexagonal phase H_1 and the alkyl chain length continuous reversed hexagonal phase H_2. Both phases consist of dense packed cylindrical (rod-like) micelles ordered in a hexagonal lattice. They show the same Bragg reflections in the ratio of $1 : \sqrt{3} : \sqrt{4} : \sqrt{7} : \sqrt{12} : \ldots$ and a diffuse reflection of 4.5 Å of the fluid alkyl chains. The phases are more viscous than the lamellar phase. The diameter of the normal cylindrical micelles is 1.3-2.0 times of the all-trans alkyl chain length l_{max}. The intermicellar separation is 8-50 Å.[11]

2.2.4.1.3 Cubic phase (I_1 and I_2 or V_1 and V_2)

The cubic phases are isotropic and very viscous phases. They possess fluid alkyl chains and therefore a broad peak around 4.5 Å. This phase comprises two different aggregate structures, but in a three dimensional network. The discontinuous cubic phase I implies the ordering of normal (I_1) or reversed (I_2) micelles in a cubic lattice, e.g. primitive, face-centered or body-centered. It is placed in the binary water surfactant diagram between the micellar phase and the hexagonal phase. The most often found discontinuous cubic lattices are I*m*3*m*, F*m*3*m* and P*m*3*n*. I*m*3*m* and F*m*3*m* possess only one quasi-spherical structure of micelle which is arranged in a cubic lattice. In the P*m*3*n* phase two different micelle structures are available. The other aggregation consists of bicontinuous cubic structures which build up a three-dimensional network throughout the whole structure. The structure built a surface with saddle points. They have radii of curvature which possess an opposite sign at right angles. This group is labeled with V and often placed between the hexagonal and lamellar phase in the binary phase diagram of water with surfactant.[11] The three main groups are the I*a*3*d* structure which belongs to the gyroid type (G), the primitive cubic bicontinuous phase P*n*3*m*, which belongs to the diamond type D and the Schwarz surface type of bicontinuous cubic phase the I*m*3*m* (P type).[11, 47] In **Table 2-3** the peak ratios of the most common cubic phases are given.[43, 47]

Mesophase	Symmetry	Peak ratio
Discontinuous cubic I	P*m*3*n*	$1:\sqrt{2}:\sqrt{4}:\sqrt{5}:\sqrt{6}:\sqrt{8}$ ...
	I*m*3*m*	$1:\sqrt{2}:\sqrt{4}:\sqrt{6}:\sqrt{8}:\sqrt{10}$ ...
	F*m*3*m*	$1:\sqrt{3}:\sqrt{4}:\sqrt{8}:\sqrt{11}:\sqrt{12}$ ...
	F*d*3*m*	$1:\sqrt{3}:\sqrt{8}:\sqrt{11}:\sqrt{12}:\sqrt{16}$ ...
Bicontinuous cubic V	I*m*3*m*	$1:\sqrt{2}:\sqrt{4}:\sqrt{6}:\sqrt{8}:\sqrt{10}$ ...
	I*a*3*d*	$1:\sqrt{6}:\sqrt{8}:\sqrt{14}:\sqrt{16}:\sqrt{18}$ ...
	P*n*3*m*	$1:\sqrt{2}:\sqrt{3}:\sqrt{4}:\sqrt{6}:\sqrt{8}$ ...

Table 2-3. Symmetry and peak ratio of the most common discontinuous and bicontinuous cubic phases. [43, 47]

2.2.4.2 Temperature variable ^{1}H NMR

As already described in section 2.2.3, the chain flexibility reflects also the crystallinity of the phase as crystalline, semi-crystalline or liquid crystalline. It is a good indicator to characterize the thermotropic mesomorphism of choline carboxylates (Chapter 5) and choline alkylsulfates (Chapter 7). A method to evaluate the chain flexibility is the determination of the spin-spin relaxation time T_{2eff} of the protons in the neat surfactants due to ^{1}H NMR measurements.

^{1}H possesses with spin I = 1/2 two Kern-Zeeman-levels of different energy. Spin states, oriented parallel (m = + 1/2) to the external magnetic field, are lower in energy than the

energy states without an external field. Antiparallel (m = - 1/2) spin states possess a higher energy state referred to the energy level without a magnetic field (see **Figure 2-17**).

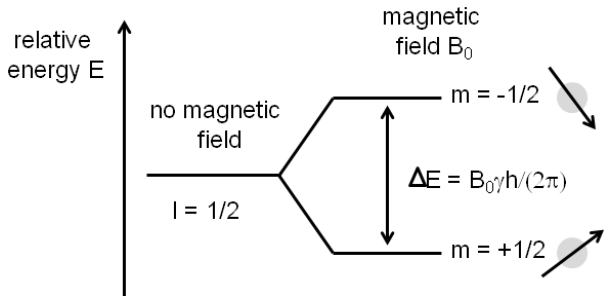

Figure 2-17. Energy profile of nucleus with a spin I of 1/2, as it is the case for ^1H, is shown before and after an external magnetic field B_0 is applied.

The energy difference between the two energy levels ΔE depends on the external magnetic field B_0 and the resonance conditions are given as:

$$h\nu = \Delta E = \gamma \frac{h}{2\pi} B_0 \qquad (10)$$

ν is called the resonance frequency and depends on the external magnetic field B_0.[48] In magnetic resonance experiments relaxation processes appear in the system, which are important to define the flexibility of alkyl chains. The transfer of a nucleus from an energetic higher Kern-Zeeman-level to a lower one is called spin-lattice relaxation. Therefore, energy in form of heat is emitted into the environment. The process depends on the rate constant of $1/T_1$, with T_1 as the longitudinal relaxation time. The other, more important relaxation time is the spin-spin relaxation time, also known as transversal relaxation time T_{2eff}. Hereby, no energy is emitted to another spin system. The relaxation leads only to an entropy increase in the spin system. This time reflects the transversal magnetization and is influenced by the interaction of the nuclear moments of neighbored protons. It is induced by a 90° pulse.[48]
This spin-spin relaxation is also expressed in the line width of a NMR signal. The line width normally depends on the natural line width given by the Heisenbergs´ uncertainty principle. It is further influenced by inhomogenity of the magnetic field, far coupling and also by the spin-spin relaxation processes. Therefore, smaller spin-spin relaxation times T_{2eff} due to a higher crystallinity or lower flexibility in the molecule results in broader line width, and vice versa.[48] Thus, the flexibility of the alkyl chains can be expressed in T_{2eff}.[48] From literature the following values are given for $-CH_2-$ groups in different phases:

- T_{2eff} < 10 µs in crystalline phases[49, 50]
- T_{2eff} = 20-30 µs in gel or semi-crystalline phases[50]

- T_{2eff} = 100-200 µs in lamellar phases[49-52]
- T_{2eff} above 1 ms for "normal liquid"[49]

The T_{2eff} values can be calculated from the half width Δν (= b in Hertz) at half-height (h/2) of a NMR peak (see **Figure 2-18**). The values of T_{2eff} have been used in the characterization of the thermotropic phases (see Chapter 5 and Chapter 7) to monitor the molecular order at different temperatures.[53] In the case of the thermotropic phases of choline carboxylates and alkylsulfates, temperature dependent ^{1}H-NMR spectra were fitted with a combined Lorentzian and Gaussian function. The Lorentzian and Gaussian function are the common found line shapes in NMR spectra. In liquids, mostly homogeneous broadening of the curve shape due to collisional broadening, lifetime broadening or pressure broadening results in a Lorentzian line shape. This means, each molecule is affected in the same way. While in solids where the molecules are rigid with relative fixed orientations inhomogeneous broadening of the line shape appears and is expressed in a Gaussian curvature.[54]

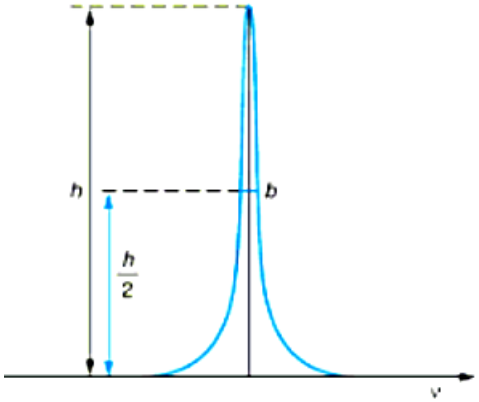

Figure 2-18. Lorentzian line shape of a NMR curve. b (= Δν) represents the half width in Hertz at the half-height, which is used to calculate T_{2eff}.[48] The figure is based on ref. [48].

2.2.4.3 Polarizing optical microscopy

Polarizing optical microscopy is an important method for the characterization of thermotropic and lyotropic mesophases. Each mesophase shows a characteristic texture between the crossed polarizer of the microscope.[12] Mesophases can be classified according to their optical behavior. Cubic phases are optically isotropic, while the hexagonal, lamellar and nematic phases exhibit an optical anisotropy. All materials are characterized by an indicatrix which allows the determination of the prevailing refractive indices.[55, 56] Crystals of high symmetry such as cubic crystals possess a sphere as an optical indicatrix, hence they behave similar to optical isotropic medium. The system is optically fully characterized by a single refractive index.[57, 58]

Crystals of lower symmetry are optically anisotropic. The indicatrix of a hexagonal crystal is an ellipsoid of revolution.[59] The optical properties depend on the propagation direction of the light within the crystal.[55, 57, 58] In a birefringent media the beam is split into two rays with orthogonal polarization. In a polarizing optical microscope the liquid crystal is placed between two crossed polarizers. The birefringent medium acts as a phase retardation plate. Coincides the optical axis with the setting of the crossed polarizers, darkness is observed. In all other cases some light can pass.[55, 56, 58, 60] Therefore, optically anisotropic material is colorful with different textures under the light microscope, while no light passes through in 90° crossed polarizer and analyzer when an optically isotropic material is in between.[55, 58, 60, 61]

In the present work polarizing optical microscopy combined with a hot stage and a temperature control was used to determine the crystallinity of the thermotropic phases of choline octanoate, choline decanoate and choline oleate (see Chapter 5) and choline dodecylsulfate and choline hexadecylsulfate (see Chapter 7). These phases are layered phases and therefore birefringent under the polarizing optical microscope. Due to mechanical agitation of the microscope slides, also the relative viscosity of these phases helps to determine their structure.[11]

Further, in the binary surfactant water system (see Chapter 4 and Chapter 6) the so called penetration scan technique, which was described by Lawrence[62], was used. Therefore, a small amount of surfactant was put between two microscopy slides. A drop of water starts from the outside and penetrates in direction to the middle of the sample. Along the penetration line the different lyotropic phases appear with increasing concentration. This is a simple method to characterize the concentration dependent and also temperature dependent (by equipping the microscope with a hot stage and a temperature control) phase sequence in a binary surfactant water system.

The different lyotropic mesophases can be explained and described owing to their typical textures under the polarizing optical microscope with crossed polarizers. Further, due to mechanical agitation, also the relative viscosity of the different samples can be monitored. Micellar phases are low viscose and isotropic. Cubic phases are also isotropic and very viscous. Hexagonal phases are more viscous than the lamellar phases and both are anisotropic. Lamellar phases often form an oily streaky or focal conic texture.[11, 12] Further, in some cases nematic structures can appear in surfactant systems. They are birefringent under the polarizing optical light microscope. The pattern of nematic phases can be explained as “Schlieren” pattern to distinguish it from the lamellar, hexagonal or cubic phase.[58, 65, 66] An example of a hexagonal phase and a lamellar phase is given in **Figure 2-19**, and a detailed information is found in Chapter 4 and Chapter 6.

(A) 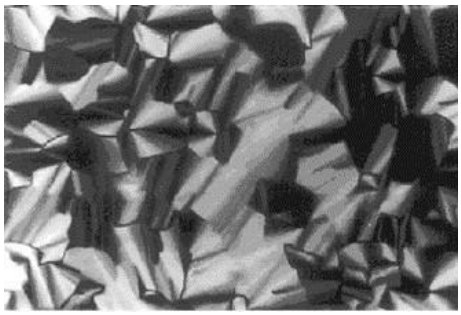 (B) 

Figure 2-19. Polarizing optical microscopy images with crossed polarizers show a possible texture of a hexagonal phase[63] (A) and the oily streaky texture of a lamellar phase[12] (B) (100x magnification).

2.2.5 Application as laundry detergent

Surfactants show a lot of possible applications in cosmetical formulation, in synthesis and a lot of more. In this section the application as washing detergent or more the washing mechanism should be taken into account. The first known washing detergents are the soaps. With increasing knowledge in chemical synthesis even more surfactant classes are found as better detergents compared to soaps. In Chapter 8 the choline alkylsulfates were introduced as a new class of biodegradable surfactants of renewable material, which can make a contribution to more sustainable and eco-balanced washing procedures. In the present section fundamental information about the washing mechanism and the composition of the soil which should be removed during the washing process is given.

Soil on clothes has various origins e.g. from direct contact with the human skin, the atmosphere (e.g. dust particles), food and the working environment. Soil can be classified in three main families: particulate soil, non-fatty soil and fatty soil.[64] The latter is mostly found in lubricating oils of automobiles, food (vegetable and animal oil) and secretions of the human skin (mainly components are free fatty acids, wax, sterol ester, triglyceride, diglyceride, squalene, sterol and paraffin). It is also known that particulate soil adheres on the fabric as oil bond, because it is mostly fixed on the fabric with an oil casing.[65] Thus, the performed washing tests in Chapter 8 are focused on the fatty soil removal.[65]

The soil release from fibers is a complex phenomenon where special care has to be taken regarding different fiber surfaces (cotton fibers are more hydrophilic, polyester fibers more hydrophobic)[66], the chemical finish, the fiber fabric structure, the soil and last but not least the surfactant.[65] Fatty liquid oil removal is the most interesting and important surfactant property in laundry processes. The wettability of the fiber and also the soil within the washing solution are the crucial parameters during the removal process. This process is shortly explained in the following:

Two main models exist which explain the removal of liquid oily soil from flat surfaces. The first one is the so called roll-up mechanism which can be applied for the removal of oily liquid soil from hydrophilic surfaces like cotton as it is schematically shown in **Figure 2-20** (A). The

second mechanism is based on emulsification (see **Figure 2-20** (B)). Emulsification occurs, when low surface energies are observed. This is the case for hydrophobic surfaces like polyesters and many mineral soils or oil-polar soils on flat hydrophobic surfaces. The contact angles are between 0° and 90° so that the whole surface is covered with soil in extreme cases. Consequently, the surfactant solution cannot get into contact with the fiber surface. Due to the lower interfacial tension, agitation can deform the oil film and small emulsion droplets can be formed because of the surfactants stabilization in the aqueous detergent solution. However, also this mechanism is highly influenced by temperature, polar organic alcohols, electrolyte concentrations and surfactant concentrations.[66]

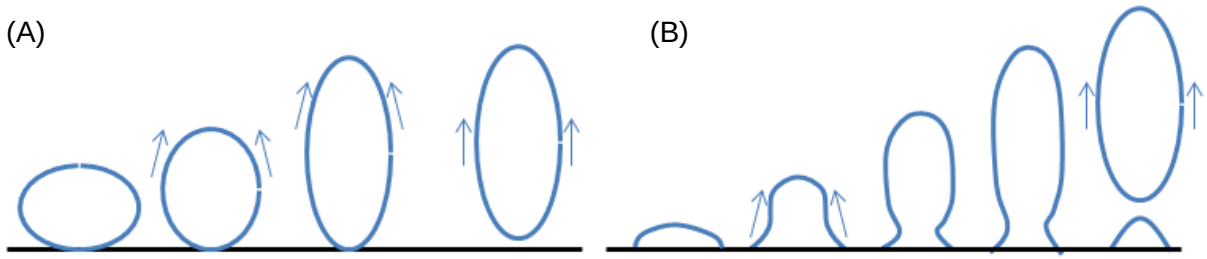

Figure 2-20. Two main mechanisms of oily liquid soil removal from flat surfaces: (A) Roll-up mechanism, mostly found in the removal of soil from hydrophilic surfaces which are partly covered with oily liquid soil. (B) Emulsification is observed during the removal of oily liquid or oil-polar soil from hydrophobic surfaces, which are fully covered with the soil.[66]

To explain the roll-up mechanism (see **Figure 2-21 (II – IV)**) the different values of the interfacial tensions, equal to the free energy per unit of surface, have to be considered. The relation is expressed in Young´s equation (11):

$$\cos\theta = \frac{\gamma_{FW} - \gamma_{FS}}{\gamma_{SW}} \qquad (11)$$

with γ_{FW} as the interfacial surface tension between the fiber and water surface; γ_{FS} the interfacial tension between the fiber surface and the soil surface and γ_{SW} as the interfacial surface tension between the soil and the water phase. For the removal of the liquid oily soil, the contact angle θ has to be 180° so that:

$$-1 = \frac{\gamma_{FW} - \gamma_{FS}}{\gamma_{SW}} \qquad (12)$$

$$\gamma_{FS} = \gamma_{SW} + \gamma_{FW} \qquad (13)$$

In general, hydrophilic surfaces achieve contact angles θ higher than 90°, because the interfacial surface tension between water and the fiber γ_{FW} is smaller than the interfacial

surface tension between the fiber and the liquid soil γ_{FS}. Water wets the fabric and helps to lift up the soil into the washing solution. Moreover, the anionic surfactants adsorb with their headgroups oriented in direction to the detergent solution and lower further the interfacial tension between the fiber and water γ_{FS}. This is essential for the efficiency of this mechanism so that the soil is rolling up and can be detached of the fiber via agitation.[64, 66]

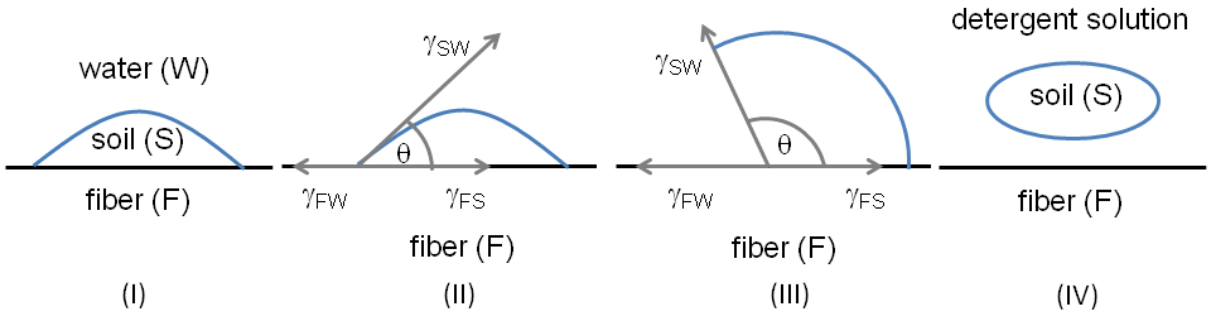

Figure 2-21. Roll-up mechanism for a flat hydrophilic fiber surface. During removal of the soil (II to IV) the contact angle increases thanks to the surfactant and favors the detachment of the soil via agitation (hand or washing machine).[64]

At relatively high surfactant concentrations (above the *cmc*) compared to the oily soil content, direct solubilization of the liquid oily soil into the micelles can also occur.[66] Concerning the surfactant properties, it can be stated that with increasing chain length of the surfactant the wettability behavior is improved. Interestingly, for sodium alkylsulfates it was found that their wetting ability is increased when the sulfate group is chemically attached on a secondary carbon atom. The wetting ability can be further improved by incorporating propylenoxide groups.[67]

As already stated above, the detergency behavior of a surfactant increases with growing linear chain length of the surfactant. Sodium octadecylsulfate shows a better detergency behavior at 60°C compared to shorter chain alkylsulfates, but due to the higher Krafft temperature the washing temperature is increased to 60°C.[67] Therefore, in Chapter 8 it will be shown that with choline as cation for alkylsulfate surfactants the washing process is able at room temperatures also with chain length up to C_{16}.

2.3 Ionic Liquids

Salts like sodium chloride melt at very high temperatures which make them useless as solvent for chemical processes.[68] It was observed that salts with an organic cation melt at lower temperatures. The ones which melt below 100°C are called ionic liquids. The interest in ionic liquids grew enormously in the 21st century. They were also called “designer solvents”, because by varying the cation or anion they change their properties. Further, they possess no measureable vapor pressure and therefore cannot emit volatile organic compounds. Thus, they were introduced as “green solvents”. This has been revised two decades ago because of performed toxicity and biodegradation tests which assigned the commonly used cations as toxic.[69, 70] Nevertheless, the interest in this substance class is very high. Whereas in 1995 almost 20 papers appeared about ionic liquids, in 2001 they were already 300 and this number steadily increases.[71] In this part a short overview of the common ionic liquids and their properties are given. Since the literature about ionic liquids is enormous, here only a small outlook is given.

2.3.1 Types of ionic liquids and general aspects

Ethylammonium nitrate with a melting point of 14°C[72] was the first ionic liquid. Then, in 1951 the organic chloroaluminates were mentioned for the first time, and from 1970 on the interest and research in this class of ionic liquids start with the work of Osteryoung *et al.* and Wilkes *et al..*[69] These ionic liquids were classified by Wasserscheid *et al.* as first generation ionic liquids.[71] They possess anions like hepta- or tetra-chloroaluminate. This type of ionic liquid is very fluid, but disadvantageously also very water instable.[69, 72] In 1990, a lot of combinations of a single cation with a single anion were found to be water and air stable, which stimulated the research field of new “designer solvents”. This second generation ionic liquids are composed of metal-free cation and anion.[69, 73] The interest in industry, synthesis, biology, electrochemistry and a lot of more fields was enormous because these solvents possess a high conductivity, are liquid over a wide range, have low vapor pressure and a low flammability.[74] The following organic cations were commonly used in these ionic liquids: imidazolium, pyridinium, pyrrolidinium, ammonium, and phosphonium.[68, 69] They were combined with a variety of anions (see **Figure 2-22**) including simple halides, fluorinated anions and simple organic anions like acetate or decanoate. The latter were used in this thesis.[69, 73] However, halides are not favored, as they are very hygroscopic. BF_4^- and PF_6^- are very water instable.[69]

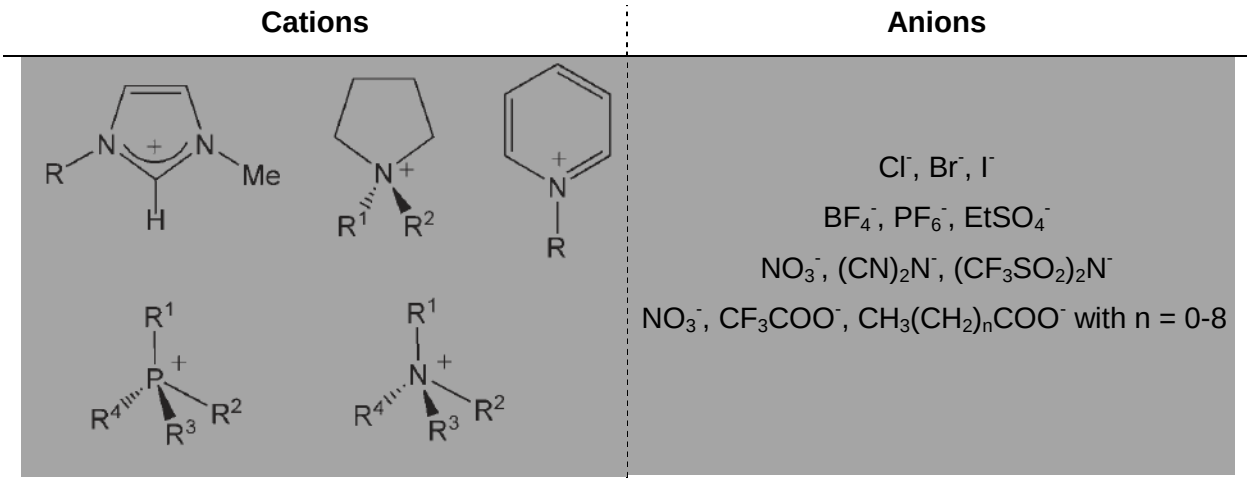

Figure 2-22. Some examples for common used cations and anions in second generation ionic liquids[69]

Since it was found that a lot of the common used ionic liquids are toxic in nature, especially the imidazolium ones, the research in the last two decades was focused on a new generation of ionic liquids containing cations and anions of natural resources, the so called bio-renewable and degradable ionic liquids.[70, 75] Studies on amino acid-based ionic liquids[76, 77] or using choline or choline based ions as cation appeared as well.[42, 78-81]

2.3.2 Physico-chemical properties

As already mentioned, the physico-chemical properties of ionic liquids are very well tunable by selecting task-specific cations or anions. Thus, it is feasible to create ionic liquids for special applications. It is known that the physico-chemical properties can be influenced by impurities like water or stabilizers and a lot of more factors. The purification of ionic liquids with melting points lower or around room temperature is very difficult. Thus, it is necessary to start with pure material. The experiments with choline carboxylates ChC_m with m = 2, 4, 6, 8, 10, oleate, choline succinate, choline glutarate and choline adipate were performed under inertgas atmosphere, because choline carboxylates and bicarboxylates are very hygroscopic. The hygroscopy decreases with increasing chain length. In this section only the melting point, the viscosity, conductivity and toxicity of ionic liquids are considered. The other physico-chemical properties like density, polarity, solubility and vapor pressure were not explained in this part because they are not investigated for the ionic liquids synthesized in the thesis. These ionic liquids are not liquid at room temperature.

2.3.2.1 Melting point

The melting point is the cardinal point in ionic liquid properties`. It is very strongly influenced by impurities and water.[79, 81] As mentioned before, ionic liquids are composed of a cation and an anion. Therefore, the Coulombic attraction is the dominant force in ionic liquids, e.g. the stronger the Coulombic attraction between cation and anion the higher the melting point of the ionic liquid. The term of the Coulombic attraction E_C is given as followed:

$$E_C = \frac{M\, Z^- Z^+}{4\pi\varepsilon_0 r} \qquad (14)$$

with Z^+ and Z^- as the ion charge. M is the Madelung constant, which reflects the packing efficiency, and r is the inter-ion separation.[71] As shown by equation (14), a lower melting point can be addressed by mono-charged anions, cations and big ions. These conditions result in a huge inter-ion separation, a high charge delocalization and a low overall charge density.[71] Taking these aspects into account for the design of ionic liquids, the Coulombic attraction forces can be lowered by increasing the bulkiness and size of the ion and creating an asymmetric charge distribution.[69]

For alkali chloride salts the melting point decreases with increasing cation (from sodium to cesium) from 803°C to 646°C.[82] Comparing these values again with chloride salts combined with an organic cation, for example 1-ethyl-3-methylimidazolium chloride ([EMIM]Cl), the melting point can be lowered to 87°C.[68, 70] In addition, a bulky cation with a low symmetry decreases also the melting point. This could be proved for symmetric 1-methyl-3-methyl-imidazolium chloride compared to unsymmetrical 1-butyl-3-methyl-imidazolium chloride. The melting point is lowered from 125°C to 65°C.[83] Another option to decrease the melting point is to increase the radius of the anion. This could be observed for 1-ethyl-3-methylimidazolium chloride, 1-ethyl-3-methylimidazolium tetrafluoroborate and 1-ethyl-3-methylimidazolium aluminiumtetrachloride. With increasing anion radius ($Cl^- < BF_4^- < AlCl_4^-$) the melting point decreases from 87°C to 15°C to 7°C.[71]

In addition to the Coulombic interaction the van der Waals interaction has to be considered. The melting point increases with increasing alkyl chain length due to the increase of the van der Waals interaction. Thus, the crystalline structure is more favored. 1-Alkyl-3-methylimidazolium tetrafluoroborate and bi(trifyl)imide ionic liquids show the lowest melting point for chain lengths 6 and 8.[71] Especially for choline based ionic liquids also the hydrogen bonds have to be considered for the melting point. Hydroxy groups are able to form hydrogen bonds and increase further the melting point. The insertion of a double bond hinders a regular packing and lowers the melting point.[79]

.

2.3.3 Viscosity and conductivity

Compared to the common molecular solvents, ionic liquids are more viscous. The viscosity ranges mainly from 22 cP to around 40000 cP.[84] For example, the values of water, ethylene glycol or glycerol are 0.890 cP, 16.1 cP and 934 cP, respectively.[71] In general, it can be stated that the viscosity of ionic liquids is dependent on the strength of the van der Waals interactions and also on the tendency of the ionic liquids to form hydrogen bonding.[68] The viscosity of the ionic liquid increases with growing chain length of the alkyl substituent using the same anion. Further, in a series of imidazolium based ionic liquids (with the same cation) the anion affects the viscosity and the following trend could be shown: $[(CF_3SO_2)_2N^-] \leq [BF_4^-] \leq [CF_3CO_2^-] \leq [CF_3SO_3^-] \leq [(C_2H_5SO_2)_2N^-] < [C_3F_7CO_2^-] < [CH_3CO_2^-] \leq [CH_3SO_3^-] < [C_4F_9SO_3^-]$.[71]

Concerning the conductivity, it was found that the conductivity increases for the same anion and different cations in this row: pyridinium ≤ ammonium ≤ sulfonium ≤ imidazolium.[71] The conductivity is also dependent on the anion. In a row of ionic liquids with 1-butyl-3-methylimidazolium the conductivity decreases like: $[DCA^-] > [TA^-] > [TfO^-] > [PF_6^-]$.[85]

Abbott showed that the hole theory, which was first used to explain the ion mobility in high-temperature molten salts, can also be transferred to explain the viscosity and conductivity in ionic liquids.[86] The hole theory states that due to melting of the ionic liquid empty space remains in the liquid. These holes result from thermally induced fluctuations of the local densities. Instead of the ions, the holes are subject of constant flux in ionic liquids. Consequently, ions which are next to holes with a substantial size go into and move. Thereby, the low conductivity and high viscosity of room temperature ionic liquids can be explained because the average hole size is directly related to the temperature and indirect to surface tension γ. Thus, to get sufficiently big holes, generating low viscosity and high conductivity, is difficult at room temperature and can be only achieved with small ions which lower the surface tension.[86, 87] This explains why the optimal fluidity is found for alkyl imidazolium ionic liquids with chain length C_4 or C_6. They are sufficiently small and reduce the surface tension.[86]

A strong temperature dependence of the viscosity η (equation (15)) and specific conductivity κ (equation (16)) could be found for most of the ionic liquids over a wide temperature range. The temperature dependence was described by the empirical Vogel-Fulcher-Tammann (VFT) equation, especially for the ionic liquids which show a glass transition. This VFT equation was fundamentally used to describe the temperature dependent behavior of a glass forming liquid.[88] A and B are fit parameter and $T_{0\eta/\kappa}$ is called the VFT temperature or the ideal glass temperature.[88, 89]

$$\ln(\eta) = \ln(A) + \frac{B}{(T - T_{0\eta})} \qquad (15); \qquad \ln(\kappa) = \ln(A) - \frac{B}{(T - T_{0\kappa})} \qquad (16)$$

The correlation between the temperature dependent molar conductivity Λ and the temperature dependent fluidity (inverse viscosity η^{-1}) can be expressed with the help of the Walden rule (see equation (17)):

$$\Lambda \cdot \eta = k \qquad (17)$$

where k is a temperature dependent constant and Λ the molar conductivity. It is related to the specific conductivity κ with the help of the molar weight M and the density ρ of the ionic liquid ($\Lambda = \kappa$ M/ ρ).[90] The Walden rule was originally introduced for strong electrolytes. It was found that the molar conductivity is inversely proportional to the viscosity of the aqueous solution of a strong electrolyte. The molar conductivity and the inverse viscosity change in the same rate with temperature.[72]

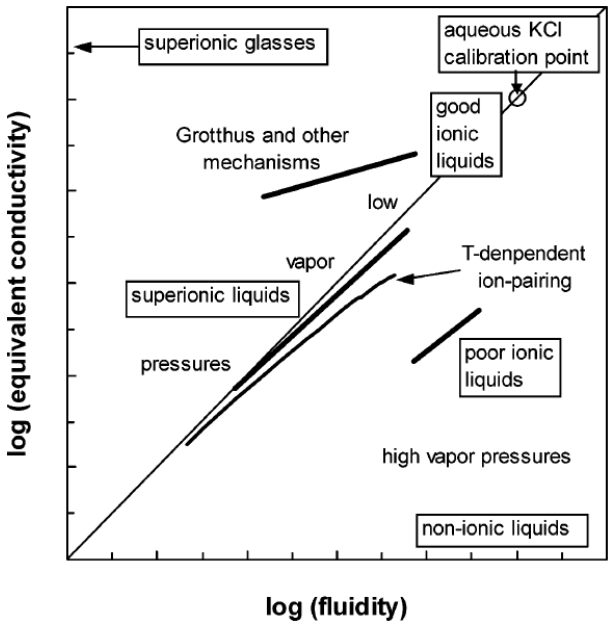

Figure 2-23. Walden plot: Classification of ionic liquids based on the original Walden rule (represented from ref. [91])

Thus, the Walden rule relates the ionic mobility to the fluidity. With the help of the Walden plot (log(Λ) versus log(η^{-1})), the degree of ionicity was tried to visualize. As ideal line, a strong electrolyte was taken. The ideal Walden line represents a liquid where the ions can move independently from each other. The ideal line in the Walden plot can be represented by a 0.01 M potassium chloride solution with a slope of unity (see **Figure 2-23**).[72, 90]

Angell and coworkers[72, 91] and also MacFarlane and coworkers[90] firstly used the Walden plot to characterize ionic liquids in compliance with their degree of ionicity. They characterize ionic liquids according to their vertical deviation to the ideal KCl line as “poor” ionic liquids, “non-ionic” liquids, “good” ionic liquids or “superionic” liquids (see **Figure 2-23**).[91] MacFarlane and coworkers define ionic liquids with a vertical deviation ΔW of unity as “poor” ionic liquids because they exhibit 10% of the ionicity they would express at the ideal line.[90]

2.3.4 Environmental aspects and toxicity

At the starting point of ionic liquid research in 1990, ionic liquids were considered to be the promising “green solvents”. They show a low vapour pressure. Thus, compared to conventional solvents, the inhalational exposure of solvent molecules could be avoided. Therefore, no release of volatile organic compounds (VOCs) was found.[71, 82] Moreover, they were classified as solvents for “clean processes” at which the loss of organic solvent could be avoided and also the consumption of catalyst could be reduced.[68] However, in this consideration the organic solvents, which were needed to synthesize the ionic liquid, were not taken into account. Also their toxicity was not explored in detail. It was always assumed that ionic liquids are not toxic, since they show a low risk for air pollution. However, what remains in the environment and nature? Toxicity studies, also including the ecotoxicity, were performed and it was found that ionic liquids show a certain level of toxicity.[92] These toxicity tests determine the toxicity related to microorganism, cyto-systems, animals and aquatic environments, cells (cytotoxicity), skin irritation and a lot of more.[70, 92] It is not easy to designate the toxicity of ionic liquids because a lot of functional groups are inserted in the anions or cations like alcohols, acids, thiols, alkynes etc..[92, 93]

With the help of toxicity tests, ionic liquids are compared to common organic solvents, e.g. phenol, xylene, dichloromethane and ethanol.[92] Furthermore, many ionic liquids possess longer alkyl chains, especially the cations, making them amenable to act as surfactants. Therefore, the toxicity of ionic liquids is compared to the one of cationic or also anionic surfactants.[94]

They were further characterized due to five ecotoxicological indicators to estimate their risk in environment. The indicators are as followed: Release, spatiotemporal range, bioaccumulation, biological activity and uncertainty.

To summarize the important results obtained from toxicity experiments, it could be mentioned: Imidazolium ionic liquids possess the highest toxicological impact, ammonium ones the lowest. The cytotoxicity of imidazolium and pyridinium ionic liquids is particularly high because their positive site is similar to the binding site of choline and can interact with the anionic binding site of enzymes. Also the toxicity is mostly made up of the cation and is higher for ions with aromatic structures than without aromatic structure.[70] Furthermore, the

toxicity increases with growing hydrophobicity. This is in relation with an increasing alkyl chain length. In addition, the biodegradability of imidazolium, pyridinium, phosphonium and ammonium ionic liquids is very low.[75, 92] However, it can be improved by incorporation of ester, amide, hydroxyl, aldehyde or carboxylic acid groups in the side chains.[70]

At the moment a lot of concepts which relate the structure of an ionic liquid or surfactant to their toxicity exist. The QSAR (quantitative structure-activity relationship) studies made by Roberts *et al.* display that the toxicity rises with increasing hydrophobicity, and no difference in toxicity is found between an ionic liquid and a surfactant.[94, 95]

Additionally, they try to explain with this model that a chemical molecule (ion or uncharged, polarized molecule like alcohol) can interact with an organism due to adsorption on the membrane and penetration into the membrane. They state two different mechanisms to interact with the membrane, namely the polar narcotics and the general narcotics. The polar narcotics operate in a two-dimensional partition. Their hydrophobic chain penetrates the bilayer, while the polar headgroup interact with the phosphatidylcholine head. The general narcotics act in a three dimensional partition. They penetrate the bilayer and are able to move in all directions in the hydrocarbon part of the bilayer.[94, 95] In Chapter 3 the cytotoxicity on the HeLa and SK-MEL-28 cell line is explained to evaluate the skin irritancy of the choline carboxylates ChC_m with m = 2-10, choline oleate and the choline bicarboxylates such as choline succinate, choline glutarate and choline adipate.

2.3.5 Application

The interest in ionic liquids is still very high. The opportunity to create solvents with different properties, not only for the exchange of organic solvents in known processes, but also for the performance of new reactions is given. At the moment, a lot of well known companies produce or use ionic liquids, like Merck KGaA/EMD Chemicals, BASF, DuPont, IoLiTec, Sigma Aldrich (also produces choline acetate).[84] The most popular use of ionic liquids at the moment in industrial application is the $BASIL_{TM}$ (Biphasic Acid Scavenging utilizing Ionic Liquids) process at the BASF AG to synthesize alkoxyphenylphosphines.[84] At the starting point of ionic liquid research, the main aim was the usage in electrochemistry. They are therefore found in lithium batteries, metal plating and solar cells.[84] In synthesis they were feasible as Friedel-Crafts catalysts, e.g. the chloroaluminates[68], or the phosphonium halides serve as reagent in nucleophilic aromatic substitution reactions.[68] Another application can be found in formulation or colloidal chemistry as paint additive, lubricants or dispersing agent.[84]

A further important application field is the biomass processing. The choline carboxylates, for example, were able to extract suberin out of cork.[96, 97] Room temperature ionic liquids like [BMIM][$MeSO_4$] are very efficient in lignocellulosic biomass pretreatment using less harsh conditions compared to the common solvents.[98] A very broad application field is the

dissolution of cellulose. [C_4MIM]Cl is able to dissolve up to 25 wt% cellulose. This is not possible in conventional solvents.[99] Many other ionic liquids are able to dissolve cellulose, but they show disadvantages as a toxic potential or only a low efficiency in cellulose dissolution. Also a COSMO-RS study was done to describe the combinatorial contribution of ionic liquids to their chemical potential to dissolve cellulose.[100] Here only a small outlook of the versatile application fields of ionic liquids was given.

2.4 Deep eutectic solvents

Ionic liquids possess a lot of disadvantages like their high cost of production, the complex synthesis, purification and toxicity in nature. This was the starting point of the deep eutectic solvents. The concept was forced to avoid the disadvantages of the ionic liquids to get a more rational concept of new biocompatible, low cost solvents for industrial application. Solvent properties could not only be tuned by modifying the cation or different anions, but also by different ratios of the two or three components contained in the deep eutectics. Deep eutectics, in general, are composed of two or three cheap, biodegradable, low toxic components which are mixed together to from liquid deep eutectic solvents (see **Figure 2-24**). The purity depends on the purity of the starting products. The components are linked through hydrogen bonds. The melting point of the deep eutectic solvent is lower than the melting points of its starting components. Their solvent properties are very similar to the one of the ionic liquids.[73] Compared to the common ionic liquids, the eutectic mixtures are easy to prepare as a pure mixture. Further they are low cost products and unreactive with water. As the ionic liquids, they are non-volatile and non-flammable. This is an advantage compared to the organic solvents. They are mostly biodegradable and the toxicological properties of the single products are mostly well known.[73, 101] Also the liquid properties of deep eutectics are similar to those of ionic liquids.[101]

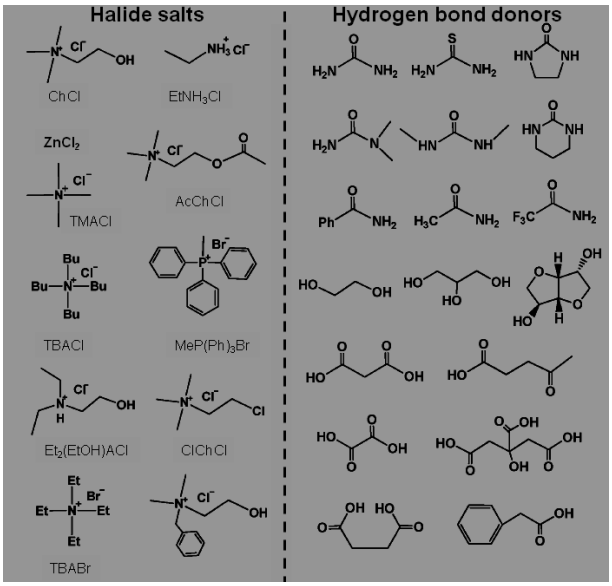

Figure 2-24. Overview of the typical halide salts and hydrogen bond donors used in deep eutectic mixtures (represented from ref. [73]).

Deep eutectics could be formed due to delocalization of charge. The delocalization of charge mostly appears because of hydrogen bonding. This is explained by the following equilibrium.[102]

$$\text{cation} + \text{anion} + \text{complexing agent}$$
$$\updownarrow$$
$$\text{cation} + \text{complex anion} \textbf{ or also } \text{complex cation} + \text{anion}$$

The depression of the melting/freezing point is possible by reason of charge delocalization. The complexing agent mostly forms a complex with the anion to delocalize the charge of the anion. Furthermore, the interaction with the cation is reduced[102] and the greater the ability of the complexing agent to form hydrogen bonding the stronger the decrease of the melting/freezing point, e.g. urea and thiourea form strong hydrogen bonds.[103] Further, as already known for ionic liquids, the lower the symmetry of the cation of the organic salt is, the more diminished is the melting/freezing point (see **Table 2-4**).[103]

R_1	R_2	R_3	R_4	X^-	T_f / °C
CH_3	CH_3	$PhCH_2$	C_2H_4OH	Cl^-	-33
CH_3	CH_3	C_2H_5	C_2H_4OH	Cl^-	-38
CH_3	CH_3	CH_3	$PhCH_2$	Cl^-	26
CH_3	CH_3	CH_3	C_2H_4OAc	Cl^-	-14
CH_3	CH_3	CH_3	C_2H_4Cl	Cl^-	15
CH_3	$PhCH_2$	C_2H_4OH	C_2H_4OH	Cl^-	-6

Table 2-4. Freezing point of mixtures of organic salt $R_1R_2R_3R_4N^+ X^-$ with urea in the molar ratio of 2:1[103]

It seems that the melting/freezing point is dependent on the lattice energy of the deep eutectic, the strength of the interaction of the hydrogen bonding couples with each other, and the change in entropy which arises by formation of the deep eutectic mixture.[73]

2.4.1 Types of deep eutectic solvents

Abbott and coworkers[73, 104] divided the deep eutectics in four main groups:

- Type 1: Metal salt + organic salt : $R_1R_2R_3R_4N^+ X^- \cdot MCl_x$ with M = Zn, Sn, Fe, Al, Ga; (e.g. $ZnCl_2$ + choline chloride[105])
- Type 2: Metal salt hydrate + organic salt: $R_1R_2R_3R_4N^+ X^- \cdot MCl_x \cdot yH_2O$ with M = Cr, Co, Cu, Ni, Fe; (e.g. $CoCl_2 \cdot 6\ H_2O$ + choline chloride[104])
- Type 3: Hydrogen bond donor + organic salt: $R_1R_2R_3R_4N^+ X^- \cdot R_5Z$ with Z = $-CONH_2$, -COOH, -OH; (e.g. choline chloride and urea[103])
- Type 4: Metal chlorides + hydrogen bond donor: $MCl_x \cdot$ hydrogen bond donor like urea, ethylene glycol, acetamide or hexanediol[104]

The mixtures of quaternary ammonium salts with metal salts result in the formation of complex anions e.g. $Al_2Cl_7^-$ or $Zn_2Cl_5^-$. The complex anions cause the decrease of the freezing point and of the lattice energy.[103]
Deep eutectics are very important, especially choline chloride combined with a hydrogen bond donor compound. They show similar physico-chemical properties as observed for imidazolium ionic liquids[106] and thus they should be able to replace them in applications.[73]

2.4.2 Properties of deep eutectic solvents

The density, viscosity and conductivity behavior of deep eutectics is based on the hole theory which is also used to explain the properties of ionic liquids.[73] In this section only the density, conductivity and viscosity behaviors of deep eutectic solvents are explained. The toxicity is generally low because they are fully composed of natural material.

2.4.2.1 Density

The density of most deep eutectics is higher than the density of water. Further, it is found that mostly the density is higher than the density of the hydrogen bond donor substance. This could be explained because of the hole theory. For example, deep eutectics made of $ZnCl_2$ and urea in the ratio of 1:3.5 or $ZnCl_2$ and acetamide in a ratio of 1:4 show the following densities of 1.63 g cm^{-3} and 1.36 g cm^{-3}, respectively. The density of the pure urea is

1.16 g cm^{-3} and of acetamide is 1.32 g cm^{-3}. By including urea to $ZnCl_2$ the hole size decreases and this increases the density.[73, 104]

2.4.2.2 Viscosity and conductivity

Deep eutectic solvents mostly show a very high viscosity. The reason for this high viscosity is in a first range the dense network of hydrogen bonding. Furthermore, the size of the components results mostly in small free volumes and small cavities which results in a low hole mobility. The van der Waal interaction and the electrostatic interaction also play an important role for viscosity. In general, the viscosity can be explained as in the case of ionic liquids by the hole theory. The temperature dependence of the viscosity of most deep eutectic solvents follows the Arrhenius equation (see equation (18)) and decreases with increasing temperature.[73, 107] Therefore, η_0 is a constant and E_η is the activation energy of the viscous flow.[107]

$$\ln(\eta) = \ln(\eta_0) + \frac{E_\eta}{RT} \qquad (18)$$

The viscosity could be lowered by destroying the hydrogen bond network (see Chapter 8) or using smaller molecules to favor the mobility of the ions in the holes.
The conductivity is strongly dependent on the viscosity of the system and increases with increasing temperature following an Arrhenius like behavior as shown in equation (19).[59, 60]

$$\ln(\kappa) = \ln(\kappa_0) - \frac{E_\Lambda}{RT} \qquad (19)$$

where κ_0 is a constant and E_Λ is the activation energy for conductivity.[107] For example, the conductivity could be increased by raising the organic salt content.[73, 102] The relationship between the conductivity and the fluidity (reciprocal viscosity) can be again considered with the help of the Walden rule as explained in section 2.3.3. Deep eutectic solvents can be compared to the ionic liquids due to the Walden plot.[90] Most of the deep eutectic solvents behave as “good” ionic liquids and possess fully dissociated ions.[107]

2.4.3 Application

The application field of deep eutectic solvents should increase in the next years, owing to their versatile properties like sustainability, biodegradability and more task-specificity compared to the ionic liquids.[103] Especially, they should be used to exchange the imidazolium ionic liquids in industrial application.[103, 107] Eutectic mixtures of resorcinol, choline

chloride and urea were used in polycondensation reactions as task-specific solvents to prepare carbons.[108]

Deep eutectics were generally used as solvent with precursor ability to synthesize polymers with controlled chemical composition and morphology.[108] Lidocaine-octanediol based deep eutectics were also used to synthesize elastomers for regenerative medicine. Additionally, they help to load this material with pharmaceutical ingredients, like APIs. Deep eutectics are able to perform an all-in one process, because the deep eutectic could be made of molecules containing the monomers.[108] This can be especially used for the synthesis of carbon material. Therefore, the deep eutectic solvent can be utilized as reaction solvent which contains the precursor material and also a molecule which takes care of the structural organization of the precursor.[108] Further, deep eutectics made up of carboxylic acids and also choline chloride can be used due to their low oral toxicity. They are able to dissolve poorly soluble compounds and can be used as a carrier in pharmacokinetic studies on mice or rats.[73, 109] To sum up, deep eutectic solvents are useful, especially, in drug formulation or synthesis of medicinal compounds, where the application of ionic liquids was limited due to high toxicity. Furthermore, they can be used in many fields in terms of exchanging ionic liquids, like electrochemistry, synthesis etc. However, a huge drawback of deep eutectic solvents in applications is their high viscosity.[73]

2.5 References

1. W. Kunz and R. Neueder, *An Attempt of a General Overview; Chapter 1 in Specific ion effects*, World Scientific, Singapore, 2010.
2. F. Hofmeister, *Arch. Exp. Pathol. Pharmakol.*, 1888, **24**, 247-260.
3. N. Vlachy, B. Jagoda-Cwiklik, R. Vacha, D. Touraud, P. Jungwirth and W. Kunz, *Adv. Colloid Interface Sci.*, 2009, **146**, 42-47.
4. W. Kunz, J. Henle and B. W. Ninham, *Curr. Opin. Colloid Interface Sci.*, 2004, **9**, 19-37.
5. W. Kunz, *Curr. Opin. Colloid Interface Sci.*, 2010, **15**, 34-39.
6. K. D. Collins, G. W. Neilson and J. E. Enderby, *Biophys. Chem.*, 2007, **128**, 95-104.
7. K. D. Collins, *Methods*, 2004, **34**, 300-311.
8. C. R. Harrison, J. A. Sader and C. A. Lucy, *J. Chromatogr. A*, 2006, **1113**, 123-129.
9. I. Lipar, P. Zalar, C. Pohar and V. Vlachy, *J. Phys. Chem. B*, 2007, **111**, 10130-10136.
10. R. Klein, M. Kellermeier, D. Touraud, E. Müller and W. Kunz, *J. Colloid Interface Sci.*, 2013**, 392**, 274-80.

11. K. Holmberg, D. O. Shah and M. J. Schwuger, *Handbook of Applied Surface and Colloid Chemistry*, John Wiley & Sons, LTD, New York, 2002.
12. H. D. Dörfler, *Grenzflächen und kolloid-disperse Systeme: Physik und Chemie*, Springer, Berlin, 2002.
13. D. F. Evans and H. Wennerström, *The colloidal domain: where physics, chemistry, biology, and technology meet*, Wiley-VCH, New York, 1999.
14. B. Kronberg, M. Costas and R. Silveston, *J. Disper. Sci. Technol.*, 1994, **15**, 333-351.
15. M. J. Rosen, L. Fei, Y.-P. Zhu and S. W. Morrall, *J. Surfactants Deterg.*, 1999, **2**, 343-347.
16. R. Klein, D. Touraud and W. Kunz, *Green Chem.*, 2008, **10**, 433.
17. R. G. Laughlin, *The Aqueous Phase Behavior of Surfactants*, Academic Press, San Diego, 1994.
18. M. J. Schwuger, *Kolloid-Z. Z. Polym.*, 1969, **233**, 979-985.
19. R. Klein, Dissertation, Universität Regensburg, 2011.
20. B. L. Bales, M. Benrraou and R. Zana, *J. Phys. Chem. B*, 2002, **106**, 9033-9035.
21. R. Klein, M. Kellermeier, M. Drechsler, D. Touraud and W. Kunz, *Colloids and Surfaces A: Physicochem. Eng. Aspects*, 2009, **338**, 129-134.
22. R. Zana, J. Schmidt and Y. Talmon, *Langmuir*, 2005, **21**, 11628-11636.
23. R. Zana, M. Benrraou and B. L. Bales, *J. Phys. Chem. B*, 2004, **108**, 18195-18203.
24. R. Zana, *Langmuir*, 2004, **20**, 5666-5668.
25. J. N. Israelachvili, D. J. Mitchell and B. W. Ninham, *J. Chem. Soc., Faraday Trans. 2*, 1976, **72**, 1525-1568.
26. C. Tanford, *J. Phys. Chem.*, 1972, **76**, 3020-3024.
27. A. Klaus, Dissertation, Universität Regensburg, 2011.
28. R. Klein, G. J. T. Tiddy, E. Maurer, D. Touraud, J. Esquena, O. Tache and W. Kunz, *Soft Matter*, 2011, **7**, 6973.
29. P. Kékicheff, C. Grabielle-Madelmont and M. Ollivon, *J. Colloid Interface Sci.*, 1989, **131**, 112-132.
30. K. Fontell, *Colloid Polym. Sci.*, 1990, **268**, 264-285.
31. M. D. Small, *The Physical Chemistry of Lipids from Alkanes to Phospholipids*, Plenum Press, New York and London, 1986.
32. S. Hassan, W. Rowe and G. J. T. Tiddy, *in Handbook of Applied Surface and Colloid Chemistry*, Ed. K. Holmberg, John Wiley & Sons Ltd, Chichester, 2002, pp. 465-508.
33. V. Luzzati, A. Tardieu, T. Gulik-Krzywicki, E. Rivas and F. Reiss-Husson, *Nature*, 1968, **220**, 485-488.
34. P. Kekicheff and B. Cabane, *J. Phys. France*, 1987, **48**, 1571-1583.
35. K. Binnemans, *Chem. Rev.*, 2005, **105**, 4148-4204.

36. V. Luzzati and P. A. Spegt, *Nature*, 1967, **215**, 701-&.
37. R. D. Vold, *J. Am. Chem. Soc.*, 1941, **63**, 2915-2924.
38. M. J. Vold, *J. Am. Chem. Soc.*, 1941, **63**, 160-168.
39. M. J. Vold, M. Macomber and R. D. Vold, *J. Am. Chem. Soc.*, 1941, **63**, 168-175.
40. R. D. Vold and M. J. Vold, *J. Am. Chem. Soc.*, 1939, **61**, 808-816.
41. P. Franzosini and M. Sanesi, *Thermodynamic and Transport Properties of Organic Salts*, Pergamon Press, Oxford, 1980.
42. R. Klein, H. Dutton, O. Diat, G. J. Tiddy and W. Kunz, *J. Phys. Chem. B*, 2011, **115**, 3838-3847.
43. K. Holmberg, D. O. Shah and M. J. Schwuger, *Handbook of Applied Surface and Colloid Chemistry*, John Wiley & Sons, LTD, 2002.
44. O. Glatter and O. Kratky, *Small Angle X-ray Scattering*, Academic Press, London, 1982.
45. P. Lindner and T. Zemb, *Neutrons, X-Rays and Light Scattering Methods Applied to Soft Condensed Matter*, Elsevier Science B.V., Amsterdam, 2002.
46. A. Svensson, J. Sjöström, T. Scheel and L. Piculell, *Colloids and Surfaces A: Physicochem. Eng. Aspects*, 2003, **228**, 91-106.
47. G. Lindblom and L. Rilfors, *Biochim. Biophys. Acta, Rev. Biomembr.*, 1989, **988**, 221-256.
48. M. Hesse, H. Meier and B. Zeeh, *Spektroskopische Methoden in der organischen Chemie*, Thieme, Stuttgart, 2011.
49. I. Kamel and A. Charlesby, *J. Polym. Sci. Polym. Phys.*, 1981, **19**, 803-814.
50. C. D. Adam, J. A. Durrant, M. R. Lowry and G. J. T. Tiddy, *J. Chem. Soc. Farad. T. 1*, 1984, **80**, 789-801.
51. R. Y. Dong, M. Wiszniewska, E. Tomchuk and E. Bock, *J. Chem. Phys.*, 1973, **59**, 6266-6268.
52. K. Rendall, G. J. T. Tiddy and M. A. Trevethan, *J. Chem. Soc. Farad. T. 1*, 1983, **79**, 637-&.
53. H. Wennerström, *Chem. Phys. Lett.*, 1973, **18**, 41-44.
54. L. Petrakis, *J. Chem. Educ.*, 1967, **44**, 432.
55. http://www.olympusamerica.com/files/seg_polar_basic_theory.pdf; 01.04.2013.
56. S. A. Nelson, *Uniaxial Minerals, Uniaxial Indicatrix, Optic Sign & Ray Path*,Tulane University, 2010.
57. G. W. Gray, V. Vill, H. W. Spiess, D. Demus and J. W. Goodby, *Physical Properties of Liquid Crystals*, Wiley-VCH Verlag GmbH, Weinheim, 1999.
58. R. E. Newnham, *Properties of materials - anisotropy, symmetry, structure*, Oxford University Press, Oxford, 2005.

59. http://www.uwgb.edu/dutchs/Petrology/Indicatrix.HTM; 03.04.2013.
60. D. B. Murphy, *Fundamentals of Light Microscopy and Electronic Imaging*, John Wiley & Sons, Inc., 2001.
61. http://www.olympusmicro.com/primer/lightandcolor/birefringence.html; 01.04.2013
62. A. S. Lawrence, *Mol. Cryst. Liq. Cryst.*, 1969, **7**, 1-&.
63. V. Ganesh, S. K. Pal, S. Kumar and V. Lakshminarayanan, *Electrochim. Acta*, 2007, **52**, 2987-2997.
64. L. H. T. Tai, *Formulating Detergents and Personal Care Products A Complete Guide to Product Development*, AOCS Press, 2000.
65. G. M. Venkatesh, N. E. Dweltz, G. L. Madan and R. H. Alurkar, *Textile Res. J.*, 1974, **44**, 352-362.
66. C. A. Miller and K. H. Raney, *Colloids and Surfaces A: Physicochem. Eng. Aspects*, 1993, **74**, 169-215.
67. H. W. Stache, *Anionic Surfactants*, Marcel Dekker, Inc., New York, 1996.
68. P. Wasserscheid and W. Keim, *Angew. Chem. Int. Ed. Engl.*, 2000, **39**, 3772-3789.
69. H. Weingärtner, *Angew. Chem. Int. Ed. Engl.*, 2008**, 47**, 654-70.
70. M. Petkovic, K. R. Seddon, L. P. N. Rebelo and C. Silva Pereira, *Chem. Soc. Rev.*, 2011, **40**, 1383-1403.
71. P. Wasserscheid and T. Welton, *Ionic Liquids in Synthesis*, Wiley-VCH Verlag GmbH & Co. KGaA, Weinheim, 2002.
72. W. Xu, E. I. Cooper and C. A. Angell, *J. Phys. Chem. B*, 2003, **107**, 6170-6178.
73. Q. Zhang, K. De Oliveira Vigier, S. Royer and F. Jerome, *Chem. Soc. Rev.*, 2012, **41**, 7108-7146.
74. J. G. Huddleston, A. E. Visser, W. M. Reichert, H. D. Willauer, G. A. Broker and R. D. Rogers, *Green Chem.*, 2001, **3**, 156-164.
75. R. F. Frade and C. A. Afonso, *Hum. Exp. Toxicol.*, 2010, **29**, 1038-1054.
76. S. Kasahara, E. Kamio, T. Ishigami and H. Matsuyama, *Chem. Commun. (Camb)*, 2012, **48**, 6903-6905.
77. H. Ohno and K. Fukumoto, *Acc. Chem. Res.*, 2007, **40**, 1122-1129.
78. J. Restolho, J. L. Mata and B. Saramago, *Fluid Phase Equilibr.*, 2012, **322**, 142-147.
79. Y. Fukaya, Y. Iizuka, K. Sekikawa and H. Ohno, *Green Chem.*, 2007, **9**, 1155-1157.
80. M. Petkovic, J. L. Ferguson, H. Q. N. Gunaratne, R. Ferreira, M. C. Leitao, K. R. Seddon, L. P. N. Rebelo and C. S. Pereira, *Green Chem.*, 2010, **12**, 643-649.
81. N. Muhammad, M. I. Hossain, Z. Man, M. El-Harbawi, M. A. Bustam, Y. A. Noaman, N. B. Mohamed Alitheen, M. K. Ng, G. Hefter and C.-Y. Yin, *J. Chem. Eng. Data*, 2012, **57**, 2191-2196.
82. K. R. Seddon, *J. Chem. Technol. Biot.*, 1997, **68**, 351-356.

83. J. S. Wilkes, J. A. Levisky, R. A. Wilson and C. L. Hussey, *Inorg. Chem.*, 1982, **21**, 1263-1264.
84. N. V. Plechkova and K. R. Seddon, *Chem. Soc. Rev.*, 2008, **37**, 123-150.
85. O. Zech, A. Stoppa, R. Buchner and W. Kunz, *J. Chem. Eng. Data*, 2010, **55**, 1774-1778.
86. A. P. Abbott, *ChemPhysChem*, 2004, **5**, 1242-1246.
87. I. Krossing, J. M. Slattery, C. Daguenet, P. J. Dyson, A. Oleinikova and H. Weingartner, *J. Am. Chem. Soc.*, 2006, **128**, 13427-13434.
88. A. Grandjean, M. Malki, C. Simonnet, D. Manara and B. Penelon, *Phys. Rev. B*, 2007, **75**, 054112.
89. C. A. Angell, *Science*, 1995, **267**, 1924-1935.
90. D. R. MacFarlane, M. Forsyth, E. I. Izgorodina, A. P. Abbott, G. Annat and K. Fraser, *Phys. Chem. Chem. Phys.*, 2009, **11**, 4962-4967.
91. M. Yoshizawa, W. Xu and C. A. Angell, *J. Am. Chem. Soc.*, 2003, **125**, 15411-15419.
92. D. B. Zhao, Y. C. Liao and Z. D. Zhang, *Clean-Soil Air Water*, 2007, **35**, 42-48.
93. S. Stolte, M. Matzke, J. Arning, A. Boschen, W. R. Pitner, U. Welz-Biermann, B. Jastorff and J. Ranke, *Green Chem.*, 2007, **9**, 1170-1179.
94. D. W. Roberts and J. F. Costello, *QSAR Comb. Sci.*, 2003, **22**, 220-225.
95. D. W. Roberts and J. F. Costello, *QSAR Comb. Sci.*, 2003, **22**, 226-233.
96. R. Ferreira, H. Garcia, A. F. Sousa, M. Petkovic, P. Lamosa, C. S. R. Freire, A. J. D. Silvestre, L. P. N. Rebelo and C. S. Pereira, *New J. Chem.*, 2012, **36**, 2014-2024.
97. H. Garcia, R. Ferreira, M. Petkovic, J. L. Ferguson, M. C. Leitao, H. Q. N. Gunaratne, K. R. Seddon, L. P. N. Rebelo and C. S. Pereira, *Green Chem.*, 2010, **12**, 367-369.
98. T. V. Doherty, M. Mora-Pale, S. E. Foley, R. J. Linhardt and J. S. Dordick, *Green Chem.*, 2010, **12**, 1967-1975.
99. R. P. Swatloski, S. K. Spear, J. D. Holbrey and R. D. Rogers, *J. Am. Chem. Soc.*, 2002, **124**, 4974-4975.
100. J. Kahlen, K. Masuch and K. Leonhard, *Green Chem.*, 2010, **12**, 2172-2181.
101. A. P. Abbott, D. Boothby, G. Capper, D. L. Davies and R. K. Rasheed, *J. Am. Chem. Soc.*, 2004, **126**, 9142-9147.
102. A. P. Abbott, R. C. Harris and K. S. Ryder, *J. Phys. Chem. B*, 2007, **111**, 4910-4913.
103. A. P. Abbott, G. Capper, D. L. Davies, R. K. Rasheed and V. Tambyrajah, *Chem. Commun. (Camb.)*, 2003, 70-71.
104. A. P. Abbott, J. C. Barron, K. S. Ryder and D. Wilson, *Chemistry*, 2007, **13**, 6495-6501.
105. A. P. Abbott, G. Capper, D. L. Davies, H. L. Munro, R. K. Rasheed and V. Tambyrajah, *Chem. Commun. (Camb.)*, 2001, **0**, 2010-2011.

106. H. Zhao, G. A. Baker and S. Holmes, *Org. Biomol. Chem.*, 2011, **9**, 1908-1916.

107. A. P. Abbott, D. Boothby, G. Capper, D. L. Davies and R. K. Rasheed, *J. Am. Chem. Soc.*, 2004, **126**, 9142-9147.

108. D. Carriazo, M. C. Serrano, M. C. Gutierrez, M. L. Ferrer and F. del Monte, *Chem. Soc. Rev.*, 2012, **41**, 4996-5014.

109. H. G. Morrison, C. C. Sun and S. Neervannan, *Int. J. Pharm.*, 2009, **378**, 136-139.

Chapter 3

Effect of choline carboxylate ionic liquids on biological membranes

3.1 Abstract

Choline carboxylates, ChC_m, with m = 2-10 and choline oleate are known as biocompatible substances, yet their influence on biological membranes is not well-known, and the effect on human skin has not previously been investigated. The short chain choline carboxylates ChC_m with m = 2, 4, 6 act as hydrotropes, solubilizing hydrophobic compounds in aqueous solution, while the longer chain choline carboxylates ChC_m with m = 8, 10 and oleate are able to form micelles (see **Figure 3-1**).

In the present study the cytotoxicity of choline carboxylates was tested using HeLa and SK-MEL-28 cells. The influence of these substances on liposomes prepared from dipalmitoylphosphatidylcholine (DPPC) was also evaluated to provide insights on membrane interactions. It was observed that the choline carboxylates with a chain length m > 8 influence the bilayer, while the shorter ones had minimal interaction with the liposomes.

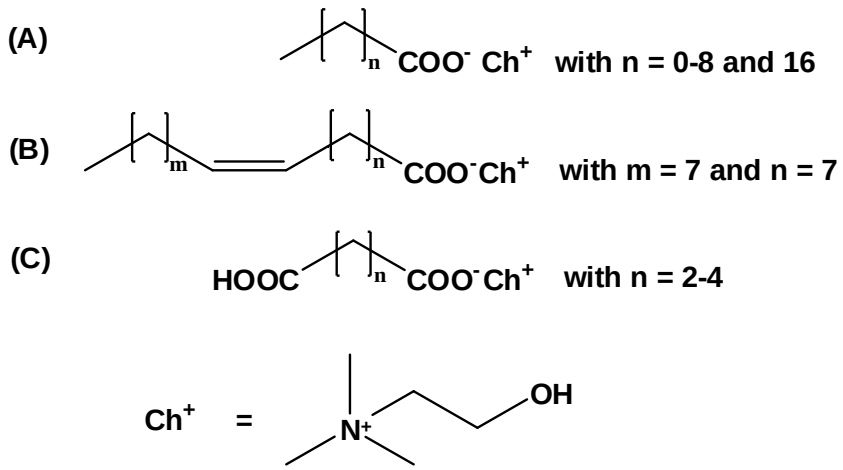

Figure 3-1. Cytotoxicity was measured of choline carboxylates ChC_m with m = 2-10 and 18 (A), of choline oleate (B) and of choline bicarboxylate $ChbiC_m$ with m = 4-6 (C) and also of their respective sodium equivalents.

3.2 Introduction

The investigation of the toxicity of ionic liquids and surfactants is a very important field, since it was found that commonly used cations in ionic liquids like imidazolium or pyridinium are toxic.[1] Further, choline compounds are forbidden in cosmetical products according to the European Cosmetic Directive 76/768/EEC. They are prohibited in cosmetics because they are assigned as quaternary ammonium compounds which are known as phase transfer catalysts and are known to possess intrinsic irritation potential.[2] In order to boost the utilization of choline compounds in future applications, cytotoxicity tests were performed to evaluate the actual skin irritation potential. Previous toxicity experiments considered the charge, the number of ethoxy groups[3] and the hydrophilicity, but in the case of surfactants it

is also very important to consider the critical micelle concentration (*cmc).*[1, 3-5] The cytotoxicity of ionic surfactants is mainly caused by the monomer[3, 6] and the IC_{50} values are found to be below the *cmc*. For nonionic surfactants the IC_{50} values are often above the *cmc*.[3] Many toxicity tests are based on the surfactant or ionic liquid concentration-dependent survival of cells, resulting from the absorption of the substance onto the cell and/or penetration into the cell membrane.[7-9] In a previous study Petkovic *et al*.[10] investigated the toxicity of choline carboxylates ChC_m with m = 2-10 by carrying out tests with filamentous fungi as a model for eukaryotic organisms. Choline carboxylates were found to have a low toxicity to these organisms. Also Muhammad *et al.* found low cytotoxicity levels in the human breast cancer cell line MCF-7 for choline carboxylates ChC_m with m = 2, 3, 4, 6.[11]

The present study is focused on the influence of the choline carboxylates on biological cell membranes like the human skin. Thereby, the question arises, how irritant these choline carboxylates are to biological membrane. Are they penetrating the membrane or do they absorb on it? IC_{50} values, which are the concentration required to cause death in 50% of the cell population, were measured for human cell lines, namely cervix carcinoma cells (HeLa), an alternative to eye irritancy tests on rabbits (Draize test),[12-16] and keratinocytes (SK-MEL-28) which reflect the skin irritancy power. The tests were made on short chain choline carboxylates ChC_m with chain length m = 2-10 and their respective sodium equivalents. To investigate further the influence of the double bond in an alkyl chain on the cytotoxicity, IC_{50} values of choline oleate and choline octadecanoate were measured. Further, the impact of an additional carboxylate group was tested measuring the cytotoxicity of choline bicarboxylates, like choline succinate ($ChbiC_4$), choline glutarate ($ChbiC_5$) and choline adipate ($ChbiC_6$) and their sodium equivalents. The influence of the choline carboxylates ChC_m with m = 2-10 and choline oleate on the cooperativity behavior of liposomes, made out of DPPC and imitating a biological membrane, was investigated at the biological pH of 7.4 to better understand interfacial interactions with membranes.

Furthermore, to be sure that the toxicity results only from the surfactant monomer, and is not influenced by the formation of the micelles, the critical micelle concentration of choline octanoate, choline decanoate and choline oleate was determined with conductivity and surface tension measurements. The hydrotrope behavior of the short chain choline carboxylates like choline acetate, choline butanoate and choline hexanoate was investigated by solubilization of the hydrophobic dye Disperse Red 13 and UV-Vis absorption measurements at 503 nm were performed. This is a common method to characterize a hydrotrope. It is also important to compare the short chain choline carboxylates with common hydrotropes like sodium xylene sulfonate (SXS) to estimate their applicability e.g. for extractions of very hydrophobic, scarcely water soluble pharmaceutical products. Hydrotropes are often used in this field, as they are able to destroy and penetrate the plant

cell wall, which is often a phospholipid bilayer. Hydrotropes solubilize the interior of the cell and upon dilution of water the very hydrophobic pharmaceutical product precipitates and can be separated from the hydrotrope.[17]

The use as extracting solvent for example of organic, water insoluble phytoconstituents [17] plays an important role in pharmacy e.g. in phytochemical extraction for drug and microemulsion formulation.[17, 18] Sodium alkylbenzene sulfonates and sodium butyl monoglycolsulfate (NaBMGS) are used to extract non polar, water insoluble phyto-constituents selectively due to permeabilization of the cell. Also choline hexanoate is able to dissolve suberin out of cork, but the mechanism is not clear. The dissolution process could be able due to breaking up bonds.[19] In addition to the biotechnological aspect, hydrotrope behavior is also an important consideration in determining the influence of this short chain choline carboxylates on dipalmitoylphosphatidylcholine (DPPC) liposomes and in a similar manner on biological membranes like the human skin or plant cells.

3.3 Results and discussion

3.3.1 Hydrotrope behavior

There are two opposite forces which are the decisive factors whether a substance belongs to the group of hydrotropes, which show no or few self aggregation, or to surfactants, which aggregate at the critical micelle concentration (*cmc*) to micelles.[20] These are on the one hand the energy which is needed to transfer the hydrophobic tails of the amphiphil into the interior of the micelle and on the other hand the repulsion force of the headgroups.[21] In this study the hydrophobicity varies with the chain length. It was found that choline carboxylates with chain length $m \geq 8$ behave as surfactants, whereas with $m < 8$ they behave like hydrotropes.[22]

A hydrotrope possesses as well as a surfactant a hydrophilic and a hydrophobic part. Also the form and shape of the amphiphilic molecule play an important role. The hydrophobic part can be cyclic (sodium toluene-, xylene-, benzene sulfonate), branched (sodium 2-ethylhexyl sulfate)[23] or as seen in this study possesses short alkyl chains.[17] Above a certain threshold concentration of hydrotrope in water, often called minimal hydrotrope concentration MHC (≈ 1M) [24], solubilization of a hydrophobic, hardly water soluble compound in the aqueous hydrotrope solution increases exponentially. To evaluate this MHC the departure from linearity of the solubilization curve has to be determined.[25] For many amphiphilic molecules this concentration is hard to determine, because the increase of solubilized hydrophobic molecules, here hydrophobic dye Disperse Red 13, occurs exponentially even at low concentration. The term minimal hydrotrope concentration is thus controversial.[24] The MHC of sodium xylenesulfonate (SXS) is around 0.4 M, sodium p-toluenesulfonate has a value of 0.35 M, and the MHC of sodium butylmonoglycolsulfate (NaBMGS) is 0.8 M. To compare the

solubilizing value of choline carboxylates ChC_m with m = 2, 4, 6 with commonly used hydrotropes the concentration dependent optical densities obtained from UV-Vis measurements, resulting from the dissolved amount of Disperse Red 13 in the aqueous hydrotrope solutions, were determined. The optical density increases exponentially above a certain threshold concentration (see **Figure 3-2** (A)).

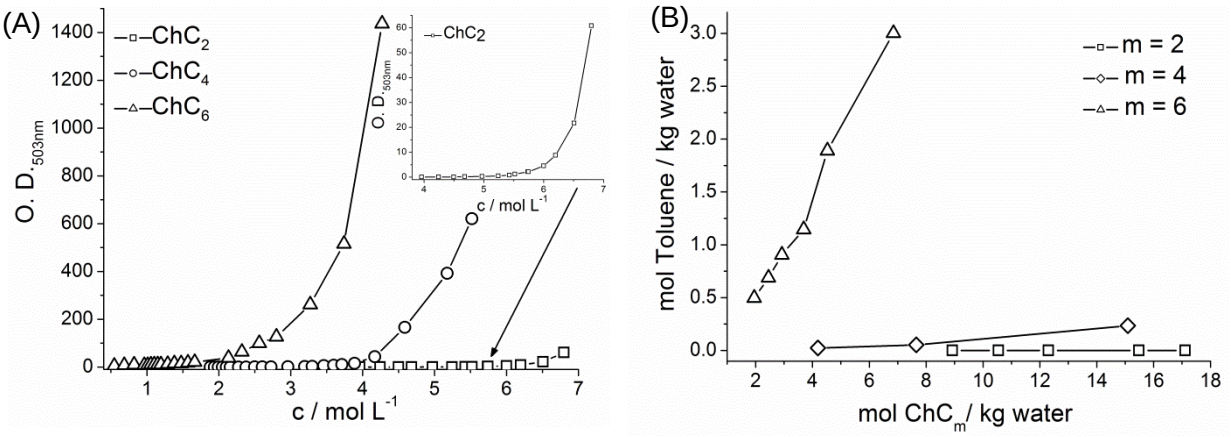

Figure 3-2. (A) Aqueous hydrotrope concentration of ChC_m with m = 2, 4, 6 versus the optical density (O. D. $_{503\ nm}$) value of the dissolved amount of Disperse Red 13 in the hydrotorpe solution taken at the wavelength of 503 nm. (B) Aqueous hydrotrope concentration of ChC_m with m = 2, 4, 6 versus the amount of dissolved toluene in the hydrotrope solution.

This concentration is 1.75 M for choline hexanoate, 3.5 M for choline butanoate and 5.4 M for choline acetate. These values are much higher than the MHCs found for the common hydrotropes, which are described previously. Also comparing the optical densities of Disperse Red 13 solutions at the aqueous hydrotrope concentration of 2.248 M it is observed that Disperse Red 13 is sparingly soluble in the choline carboxylates ChC_m with m = 2, 4, 6 compared to the very efficient hydrotrope SXS (see **Table 3-1**).[24]

Hydrotrope	Optical density $O.D._{503nm}$
CHC_6	54.0
ChC_4	0.2
ChC_2	≤ 0.2
SXS	347.0 [24]

Table 3-1. Optical density O. $D._{503nm}$ values of Disperse Red 13 saturated aqueous hydrotrope solutions at 25°C and a hydrotrope concentration of 2.248 M. The values were measured at 503 nm.

To check the hydrophobicity of these hydrotropes and their ability to extract pharmaceutical compounds out of plants, which contain often aromatic rings e.g. curcumin or piperine[17], toluene was solubilized in aqueous hydrotrope solutions at 25°C. The solubility of toluene in water is 0.008 mol per kg of water.[26] The solubility of toluene in 3.737 mol NaBMGS per kg water is 0.13 mol of toluene per kg water.[27] The solubility of toluene in 3.693 mol choline hexanoate per kg water is 1.14 mol toluene per kg water. Choline butanoate shows at 10.860

mol per kg water a solubility of toluene of 0.13 mol toluene per kg water. In contrast choline acetate decreases the solubility of toluene in water. In general, it could be seen that choline butanoate and choline acetate are not very efficient to increase the solubility of toluene or comparable substances in water. Choline hexanoate is more hydrophobic and shows a better solubilization behavior, but compared to other hydrotropes it is too polar to be efficient.[26, 27] Compared to choline hexanoate and choline butanoate, sodium hexanoate and sodium butanoate are able to self aggregate in aqueous solution.[26, 28] The *cmc* of sodium hexanoate is 1.57 M (20°C) and the one of sodium butanoate is 3.5 M (25°C).[28] The values are in the same concentration range as found for the MHCs´ of the choline ones. Thus, the counterion influences the self aggregation behavior.

3.3.2 Critical micelle concentration (*cmc*)

The *cmc* is further influenced by several factors e.g. by the presence of salts or organic compounds in the solution, the structure of the surfactant, the existence of a second liquid phase, the chain length and temperature. In this study the influence of the temperature (25°C and 40°C), structure (choline stearate vs. choline oleate) and chain length (m = 8, 10) of choline carboxylates on the *cmc* was investigated. It is known that the free energy of micellization, which reflects the chain length of a surfactant, is proportional to the logarithm of the activities in dilute solutions. In dilute solutions the activity can be approximated by the concentration. According to these dependencies the following equation could be found for a surfactant class with variable chain length.[20, 23] The logarithm of the *cmc* shows a linear relation to the surfactant chain length m.

$$\log(cmc) = \mathrm{A} - \mathrm{Bm} \qquad (1)$$

A is a characteristic value at a distinct temperature for the headgroup. B is a constant at the respective temperature. Monoionic headgroups show a value for B of 0.3.[20, 23] Klein *et al.* [22] found for long chain choline carboxylates ChC_m with m = 12, 14, 16 at 25°C the value for A of 1.9 and 0.29 for B. This equation fits also very well with the found *cmc*s for choline octanoate and choline decanoate at 25°C (see **Figure 3-3**). Potassium carboxylates possess the same values for A and B at 25°C.[23]

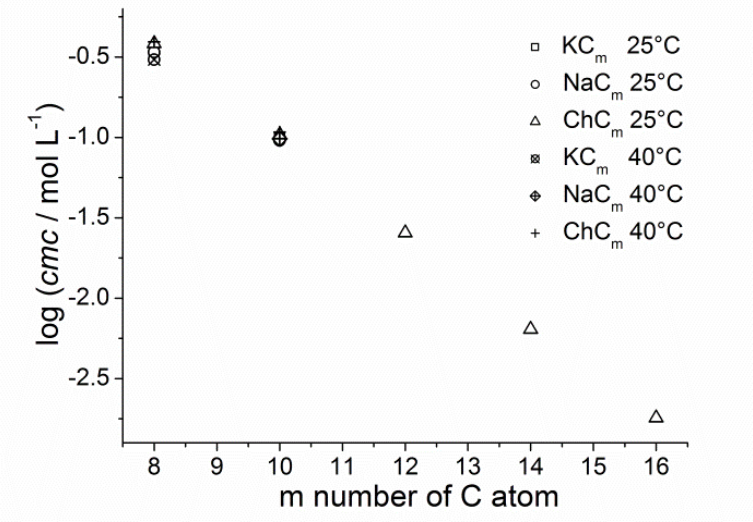

Figure 3-3. Linear dependence of the logarithm of the *cmc* of potassium, sodium, and choline carboxylates of the alkyl chain length m. (25°C: KC_8 [28], KC_{10} [28], NaC_8 [28], NaC_{10} [28], ChC_{12} [22], ChC_{14} [22], ChC_{16} [22]; 40°C: KC_8 [28], NaC_{10} [28])

As seen in **Figure 3-3** the *cmc* of choline carboxylate surfactants does not vary a lot by exchanging the choline cation by sodium or potassium and also by changing the temperature. No significant difference is found between the sodium, potassium and choline octanoates and decanoates in diluted solutions, respectively. Normally, the *cmc* of alkali carboxylates should decrease with increasing size of the alkali counterion[23] and so with decreasing counterion-headgroup binding. Taking into account Collins´ law[29, 30] the counterion-headgroup interaction should increase in this row: $Ch^+ < K^+ < Na^+$, and the *cmc* should decrease: $Ch^+ > K^+ > Na^+$. As seen here (see **Figure 3-3**), the influence of the counterion is negligible in diluted solutions.[23]

From literature it is known that the *cmc* should increase with a double bond in the alkyl chain.[23] This could be also affirmed in the case of choline oleate. The *cmc* of choline octadecanoate could not be measured at 25°C due to the high Krafft temperature of 40°C.[22] The above stated equation (1) predicts a value of 0.45 mM for the *cmc* of choline octadecanoate at 25°C. The *cmc* increases for choline oleate (see **Table 3-2**) which contains a double bond in the alkyl chain compared to choline octadecanoate. Further, an influence of the counterion is seen in the case of choline oleate. Comparing sodium oleate (*cmc* = 2.64 mM[28]) and potassium oleate (*cmc* = 0.80 mM[28]) at 25°C the *cmc* decreases with increasing counterion size and decreasing counterion binding. The value of choline oleate at 25°C is between these concentration values. Therefore, at diluted solutions it is not in line with the alkali cations. At 40°C the *cmc* of choline oleate is more than half of the *cmc* of sodium oleate (*cmc* = 3.00 mM[28]). For choline oleate the micelle ionization degree α at the *cmc* could be calculated (see **Table 3-2**). The value is in the same range as found for the long chain choline carboxylates.[22]

	cmc [a] / mM	*cmc* [b] / mM	α
ChC_8 25°C	383.0	324.9	-
ChC_8 40°C	393.8	360.0	-
ChC_{10} 25°C	103.3	75.0	-
ChC_{10} 40°C	106.8	87.2	-
Choleate 25°C	1.6	1.3	0.30
Choleate 40°C	1.7	1.6	0.24

Table 3-2. Critical micelle concentration *cmc* of choline octanoate, choline decanoate and choline oleate (Choleate) obtained from conductivity[a] and surface tension[b] measurements at 25°C and 40°C. The micelle ionization degree α at the *cmc* could be calculated from the conductivity measurements.

3.3.3 Cytotoxicity

The cytotoxicity was determined performing MTT assays (MTT named as (3-(4,5-dimethylthiazol-2-yl)-2,5-diphenyltetrazolium bromide) on HeLa and keratinocyte cells according to the procedure described by Mosmann *et al.*[31] and modified by Vlachy *et al*.[32] in order to obtain the IC_{50} value of the different choline carboxylates and choline bicarboxylates and to check the usability of the choline carboxylates and choline bicarboxylates in pharmaceutical formulations or other applications. In contrast to these earlier studies[31, 32], Amphotercin B and Penicillin G/ Streptomycinsulfate were not used in the media. The application of choline carboxylates in cosmetical formulation is not possible, because they are forbidden within the European Cosmetic Directive 76/768/EEC (Anex II/ 168) and states that quaternary ammonium compounds are not allowed in cosmetic products. Choline belongs to this group.[2, 33]

In general, cell tests with keratinocytes are a good *in vitro* method to obtain a trustable forecast for the skin irritation potential.[34, 35] To get authentic cytotoxicity results with *in vitro* tests, it is necessary that the substance is completely soluble in the media.[3] As already shown in a lot of studies, choline as cation lowers the Krafft temperature of choline carboxylates.[22, 36, 37] The choline carboxylates ChC_m with m = 8, 10 and oleate show Krafft temperatures lower than 0°C (see Chapter 4 in section 4.3.1).[37] The one of choline nonanoate and the shorter chain ones should be in the same range, because the Krafft temperature decreases with decreasing chain length.[38] The sodium salts show also Krafft temperatures below room temperature.[39-41] Choline octadecanoate possesses a Krafft temperature of $T_{Krafft} \approx 40°C$.[22] However, it could be dissolved directly in the media. In contrast, the corresponding sodium salt was not soluble in the media and could not be tested.[3]

The measured IC_{50} values of the choline carboxylates and choline bicarboxylates, obtained from the SK-MEL-28 cells and the HeLa cells, show a cytotoxicity comparable to the sodium analogs. Therefore, the impact of the cation on the cytotoxicity is very low (see **Figure 3-4**). But no tendency in the cytotoxicity concerning the counterion could be found. Petkovic *et al.*[10] and Klein *et al.*[2] obtained comparable cytotoxicity values of the choline carboxylates and

their respective sodium soaps. On the contrary, they got a slightly higher cytotoxicity for the sodium carboxylates.[2, 10] Therefore, it is obvious that the cytotoxicity is created more by the anion than by choline. It was also observed on tests with alkali salts, that the alkali cation shows no intrinsic toxicity.[42] In contrast to further studies it was shown that the toxicity of carboxylates increases with decreasing size of the cation. This was found for alkali cations as well as for quaternary ammonium ions.[34, 43] The toxicity was explained by the stronger binding of a small cation on the carboxylate headgroup compared to a larger and higher charge diffused cation, like a quaternary ammonium ion. This stronger binding resulted in ion pairs. Such ion pair formation is also the reason for the higher toxicity in pyridinium and imidazolium ionic liquids.[42, 44] However, as already seen for the *cmc*, the difference in counterion binding is negligible in dilute solutions and so the toxicity of these carboxylate soaps is not cation specific. Also a low toxicity of choline is assumed, because it is available in the human body and has a lot of important functions in the choline metabolism.[45] Stolte *et al.*[44] found that quaternary ammonium compounds show in general very low toxicity (EC_{50} < µM) and in biodegradability tests it was observed that choline is biodegradable[46] and can be aerobically decomposed by microorganisms.[47] This affirms what is found in the performed cytotoxicity tests on the choline carboxylates and choline bicarboxylates.

The overall cytotoxicity of these substances is very low. According to the T-SAR concept[8, 9, 42] the cytotoxicity should increase with increasing hydrophobicity and so with increasing chain length. Taking into account imidazolium and pyridinium based ionic liquids with a chain length from C_3 to C_{10} the toxicity of the ionic liquids indeed increases with increasing chain length.[44, 48] To check if also these choline and sodium carboxylates and bicarboxylates follow this trend in cytotoxicity also the odd chain length carboxylates were measured in this study, which are not available in nature from the biosynthesis of fatty acids. It was interesting to see, if the toxicity increases monotonously with increasing chain length or if a non-monotonous behavior is found as for physico-chemical properties (e.g. Krafft point[49]).

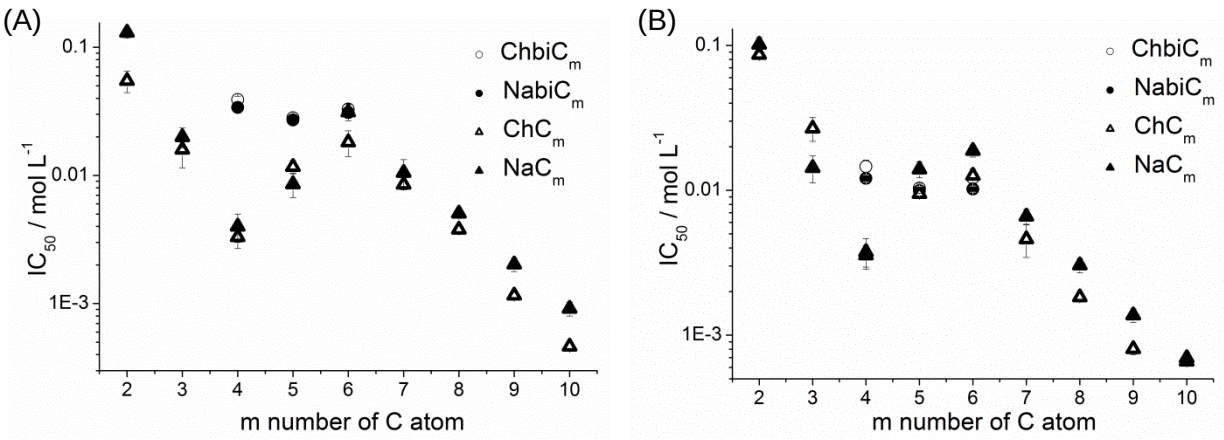

Figure 3-4. IC_{50} values of choline (Δ) and sodium (▲) carboxylates and choline (○) and sodium (●) bicarboxylates obtained with (A) SK-MEL-28 cells and (B) HeLa cells as a function of alkyl chain length *m*.

With both cell lines it was observed that the cytotoxicity increases with increasing alkyl chain length, but not in a linear way. An exception was found for the choline carboxylates ChC_m and also for the sodium carboxylates NaC_m with m = 4-6. In these cases the cytotoxicity decreases with increasing chain length. These results are against the observations seen in the paper of Petkovic *et al.*[10] where the cytotoxicity behaves as explained with the T-SAR concept (Thinking in Structure-Activity Relationship)[42, 44] and increases with increasing chain length. Also the results are not in line with the ones of Muhammad *et al*..[11] There the cytotoxicity of ChC_m with m = 2, 3, 4, 6 decreases with increasing chain length.[11] Muhammad *et al*. tested the cytotoxicity on the human breast cancer cell line MCF-7.[11] This study agrees partly with the results found by Petkovic *et al.*[10] and partly with the one of Muhammad *et al.*[11]. However, the cytotoxicity depends on the considered system and on the cell line that is used for the toxicity test.[1]

The following equations fit well the experimental results and show the partly linear relationship between the different samples.

Hela ChC_m with m = 2-4

$$\log(IC_{50}\ (\text{mol L}^{-1})) = -0.681m + 0.356\ (R^2 = 0.979) \qquad (2)$$

Hela ChC_m with m = 4-6

$$\log(IC_{50}\ (\text{mol L}^{-1})) = 0.264m - 3.435\ (R^2 = 0.916) \qquad (3)$$

Hela ChC_m with m = 6-10

$$\log(IC_{50}\ (\text{mol L}^{-1})) = -0.333m + 0.011\ (R^2 = 0.960) \qquad (4)$$

SK-MEL-28 with m = 2-4

$$\log(IC_{50}\ (\text{mol L}^{-1})) = -0.609m - 0.020\ (R^2 = 0.995) \qquad (5)$$

SK-MEL-28 with m = 4-6

$$\log(IC_{50}\ (\text{mol L}^{-1})) = 0.369m - 3.90\ (R^2 = 0.928) \qquad (6)$$

SK-MEL-28 with m = 6-10

$$\log(IC_{50}\ (\text{mol L}^{-1})) = -0.405m + 0.741\ (R^2 = 0.993) \qquad (7)$$

In literature such breaks in linearity of the cytotoxicity are often found for chain length C_{10} to C_{14}.[2, 6, 50] But to the best of our knowledge it was never found for chain lengths m = 4-6. To check if this discontinuity in cytotoxicity in the line of choline butanoate, choline pentanoate and choline hexanoate could result from the amount of $-CH_2-$ or $-CH_3$ groups in the alkyl chain, the cytotoxicity of choline succinate, choline glutarate and choline adipate was measured with HeLa and SK-MEL-28 cells. Again, a break in cytotoxicity was found for choline glutarate. Thus, it could be that this discontinuity in cytotoxicity is related to the amount of available $-CH_2-$ groups in the alkyl chain.

Roberts *et al.*[8, 9] tried to infer from the octanol water partition coefficients a quantitative structure-activity relationship (QSAR) to explain toxicity. With this model two kinds of mechanisms, which cause the toxicity, could be explained. One mechanism is based on the general narcotics. General narcotics penetrate completely into the bilayer membrane and extend in all directions in the hydrocarbon part of the membrane. The other possibility is the so called polar narcotic. The functional, mostly polar groups of the polar narcotic interact with the phosphatidylcholine headgroups of the membrane and can slightly penetrate into the membrane. Classical anionic surfactants belong to this group of polar narcotics.[8, 9] In general for evaluation of the toxicity it is irrelevant whether a substance is a surfactant or not as long as the IC_{50} value is below the *cmc* of a surfactant.[3, 6, 8]

Taking this model into account to explain the cytotoxicity it seems that the choline carboxylates and sodium carboxylates ChC_m with m = 6, 7, 8, 9, 10 belong to this polar narcotics and interact slightly with the phosphatidyl headgroups while penetrating into the membrane with the alkyl chain. As known from hydrotrope evaluation, choline acetate, choline butanoate and choline hexanoate are very polar substances. Therefore it could be that they only slightly absorb on the membrane, but do not penetrate and the cytotoxicity is more made up by the hydrophilicity of the anion.[42] Taking into account the bicarboxylates, the variation in cytotoxicity could result from the number of $-CH_2-$ groups. In general the bicarboxylates are too polar to affect the cell membrane, as it was assumed for the carboxylates C_m with m = 2, 3, 4, 5, 6. This hypothesis will be discussed in more details in section 3.3.4, where the influence of these substances on DPPC liposomes was investigated.

Furthermore, the cytotoxicity of the choline oleate, sodium oleate and choline octadecanoate was measured to investigate the influence of the double bond in an alkyl chain. Compared to the short chain choline carboxylates (see **Figure 3-4**) the longer chain length carboxylates show a higher cytotoxicity and lower IC_{50} values. Compared to the long chain choline carboxylates (ChC_m with m = 11-16) the IC_{50} value of choline octadecanoate is in the same range for the HeLa and the SK-MEL-28 cells.[2] Also the toxicity of the choline oleate is in the range of choline octadecanoate. A specific influence of the double bond could not be found. The counterion shows also no impact on the cytotoxicity of oleate soaps, as already seen for the other carboxylates (see **Table 3-3**).

Ionic Liquid	HeLa IC_{50} / mmol L^{-1}	SK-MEL-28 IC_{50} / mmol L^{-1}
Choline oleate	0.467 ± 0.034	0.521 ± 0.051
Sodium oleate	0.263 ± 0.027	0.813 ± 0.198
ChC_{18}	0.832 ± 0.143	0.116 ± 0.015

Table 3-3. IC_{50} values of choline oleate, sodium oleate and choline octadecanoate (ChC_{18}) measured with HeLa and SK-MEL-28 cells.

In general the IC_{50} values of sodium oleate measured on different acetate-utilizing methanogens are comparable to the above mentioned results. The values vary temperature dependent between 0.35 mM and 4.30 mM. The tendency of measured cytotoxicity with different systems should be equal, but the exact values depend on the tested organism.[51] From these results oleate soaps can be assigned as polar narcotics.[8, 9]

3.3.4 Lipid bilayer interactions

The following measurements were performed and the data were evaluated within the framework of collaboration by Prof. Dr. G. D. Elliott and M. Van Vorst from the Department of Mechanical Engineering and Engineering Science at the UNC Charlotte (USA).

Choline carboxylate compounds with m = 2-10 and oleate were exposed to DPPC membranes in order to identify trends in lipid bilayer interactions. The melting of the alkyl chains in the liposomes from a gel phase to a liquid crystalline phase takes place at 41.3°C.[52] It could be seen in **Figure 3-5** (A), that as the alkyl chain length m increases, the melting transition temperature of the lipid decreases slightly up to m = 8. Increasing interactions with the acyl chains of the lipid bilayer were suggested. Choline carboxylates with m = 9 and greater displayed more significant interactions with the lipid bilayer because of a greater decrease of the melting transition temperature T_m (see **Figure 3-5** (A)). Choline nonanoate (m = 9) and choline decanoate both significantly decrease the transition temperature and the cooperativity of the transition, as measured by the width of the peak at the midpoint of the transition. The enthalpy of the transition was not significantly altered. In the case of choline nonanoate also significant shouldering was observed (see **Figure 3-5** (B)). This is observed when the inner and outer headgroups are hydrated differentially. For choline decanoate and choline nonanoate at the 10 mM concentration, there is significant interaction of the ionic liquid and the lipid bilayer, consistent with penetration of the compounds into the acyl chain region. Choline oleate significantly disrupts the liposome as the DPPC peak could not be resolved at a choline oleate concentration of 10 mM. Choline oleate probably formed its own micelle under the DSC processing conditions, as we might expect based on what is known about the *cmc*. The determined *cmc* (conductivity: *cmc* = 1.6 mM) is less than the test concentration of 10 mM. In the case of choline oleate the concentration dependence of membrane interactions was investigated. At the IC_{50} concentration there is only a modest depression in the T_m, but as the concentration increased, the T_m and cooperativity decreased considerably, consistent with growing membrane disruption. This would indicate a likely accumulation of choline oleate in the lipid bilayer.

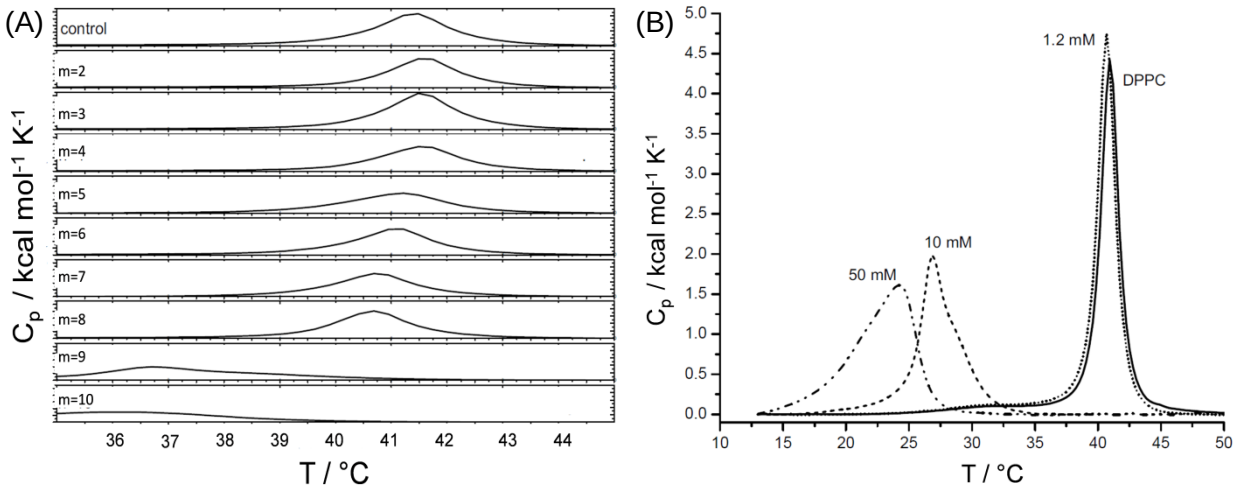

Figure 3-5. (A) DSC curves imaging the melting point of DPPC liposomes with and without (control) the influence of a 10 mM choline carboxylate solution ChC_m with m = 2, 3, 4, 5, 6, 7, 8, 9, 10 at pH 7.40. (B) DSC curves show the influence of choline nonanoate with different concentrations on the melting temperature of the DPPC liposomes from a gel phase to a liquid crystalline phase at pH 7.40: ——— 0 mM ChC_9, ····· 1.2 mM ChC_9, – – – · 10 mM ChC_9, — · · – 50 mM ChC_9.

3.4 Conclusion

Choline carboxylates ChC_m with m = 2, 4, 6 behave like hydrotropes and dissolve Disperse Red 13 exponentially with increasing hydrotrope concentration above a certain threshold concentration. However, compared to the common hydrotropes they are not very efficient at dissolving sparingly water soluble compounds. In contrast to the sodium analogs, choline as a counterion inhibited the self-aggregation of choline hexanoate and choline butanoate. [26, 28] Choline octanoate and choline decanoate behave as their sodium and potassium analogs, exhibiting similar *cmc* values. It was found that the size of the cation and the cation to carboxylate interaction at very diluted aqueous solutions show no influence on the *cmc*. It remains the same. The logarithm of the *cmc* decreases linearly with the chain length. With increasing temperature the *cmc* values increase only slightly. Choline oleate shows an increased *cmc* compared to choline octadecanoate, because of the double bond. But the *cmc* is not in line with the results found for alkali oleate soaps, where the *cmc* decreases with increasing size of the counterion.[28]

The cytotoxicity towards HeLa and SK-MEL-28 cells is not influenced by the cation, but it is very dependent on the anion. A double bond, as seen for choline oleate, has no influence on the toxicity. Cytotoxicity of the choline carboxylates ChC_m and sodium carboxylates NaC_m with m = 2, 3, 4, 5, 6, 7, 8, 9, 10 increased with increasing chain length, but in a non-linear way. The discontinuity in cytotoxicity could result from the amount of $-CH_2-$ groups in the alkyl chain, because this discontinuity was also observed in the row of choline bicarboxylates $ChbiC_m$ with m = 4, 5, 6 for choline glutarate ($ChbiC_5$), which possesses also three $-CH_2-$ groups as choline butanoate (two $-CH_2-$ and one $-CH_3$). Although the lack of a consistent

trend is interesting, most important is that the choline carboxylates ChC_m with m = 2, 3, 4, 5, 6, 7, 8 are very low toxic and do not penetrate or interact only slightly with the bilayer of DPPC liposomes. The longer chain choline carboxylates ChC_m with m = 9 and 10 and choline oleate penetrate into the liposome bilayer. For choline oleate it could already be shown that at concentrations above the IC_{50} value it starts to accumulate in the bilayer. However, according to the cytotoxicity tests with the HeLa and SK-MEL-28 cell line they could be characterized as harmless. In the last tests the liposomes were exposed to choline carboxylate concentrations of 10 mM or higher. The discontinuity of cytotoxicity as found for the cell lines could not be approved, but it could be observed that choline carboxylates starts to interact with biological membranes, when exposed to membranes at concentrations around or higher than the IC_{50} value (see **Figure 3-4** (A)).

3.5 Experimental

3.5.1 Synthesis

The synthesis of choline acetate was done by neutralization of acetic acid (Merck, purity 100%) with 45% methanolic choline hydroxide solution (Sigma Aldrich). The obtained salt was recrystallized twice in diethylether. A white salt was obtained after lyophilization and drying under vacuum atmosphere.

Choline carboxylates (ChC_m) with m = 4, 5, 6, 7, 8, 9, 10, choline oleate and choline bicarboxylates ($ChbiC_m$) with m = 4, 5, 6 were synthesized according to the synthesis route of Petkovic *et al.* but with minor modifications.[10] To the equimolar amount of carboxylic acid, aqueous choline bicarbonate solution was added dropwise. In contrast to the synthesis of Petkovic *et al.*[10] the ionic liquid was lyophilized and then dried for more than two weeks on a high vacuum pump. Heating during this procedure was skipped to avoid decomposition of the choline cation.

The following chemicals were used: Oleic acid (Sigma Aldrich, purity ≥ 99 %), propionic acid (Sigma Aldrich, purity ≥ 99.5 %), butyric acid (Sigma Aldrich, purity ≥ 99 %), valeric acid (Sigma Aldrich, purity ≥ 99 %), hexanoic acid (Sigma Aldrich, purity ≥ 99 %), heptanoic acid (Merck, purity ≥ 99 %), octanoic acid (Sigma Aldrich, purity ≥ 99 %), nonanoic acid (Sigma Aldrich, purity ≥ 97 %), decanoic acid (Alfa Aesar, purity = 99 %), adipic acid (Alfa Aesar, purity ≥ 99 %), glutaric acid (Alfa Aesar, purity ≥ 99 %), succinic acid (Alfa Aesar, purity ≥ 99 %) and 80 wt% aqueous choline bicarbonate solution (Sigma Aldrich, stored at 2°C to avoid decomposition and without stabilizer).

The purity of the choline carboxylates was evaluated with electro-spray mass spectroscopy (ES-MS) and ^{1}H and ^{13}C NMR measurement were performed. Mass spectrometry data were recorded on a ThermoQuest Finnigan TSQ 7000 instrument. The ^{1}H and ^{13}C NMR spectra

were recorded with a Bruker Avance 300 spectrometer at 300 MHz using tetramethylsilane (TMS) as internal standard. Coulometric Karl-Fischer titration was performed on an Abimed MCI analyzer (Model CA-02) to determine the water content.

The sodium salts, which were used for the cytotoxicity tests, were prepared by adding an equimolar amount of 1M sodium hydroxide solution (Merck) to the corresponding carboxylic acid. The sodium salts were lyophilized (> 24 h) and dried under vacuum atmosphere. For the synthesis the above mentioned carboxylic acids were used. Sodium octanoate (Sigma Aldrich, purity ≥ 99 %), sodium decanoate (Sigma Aldrich, purity ≥ 98 %) and sodium oleate (Sigma Aldrich, purity = 99 %) were bought.

Choline acetate: ^{1}H NMR (300 MHz, D_2O, 25°C, TMS): δ = 1.8 (s, 3H; C**H$_3$**), 3.1 (s, 9H; N(C**H$_3$**)$_3$), 3.4 (t, 2H; C**H$_2$**OH), 3.95 (m, 2H; C**H$_2$**N(CH$_3$)$_3$)

^{13}C NMR (300 MHz, D_2O, 25°C, TMS): δ = 23.22 (**C**H$_3$COO$^-$), 53.86 (t, N(**C**H$_3$)$_3^+$), 55.60 (**C**H$_2$OH), 67.38 (N**C**H$_2$), 184.0 (**C**OO$^-$)

ES-MS (H_2O/ MeOH/ MeCN): m/z (%) (+p): 104.0 (100) [M$^+$], 147.9 (6) [M$_1^+$], 207.0 (100) [(2M$^+$ - H)$^+$], 267.1 (11) [(2M$^+$ - M$^-$)$^+$], 430.2 (6), 533.5 (6) [2(2M$^+$ + M$^-$)$^+$], 593.4 (15) [4M$_1^+$], 696.6 (5), 756.7 (5), (p-): 59.1 (2) [M$^-$], 222.0 (100) [(2M$^-$ + M$^+$)$^-$], 385.1 (16)) [(3M$^-$ + 2M$^+$)$^-$], 548.4 (20), 711.5 (6) [12M$^-$], 874.7 (4)

Water content (Karl-Fischer) = 1300 ± 100 ppm

Choline propionate: ^{1}H NMR (300 MHz, D_2O, 25°C, TMS): δ = 0.95 (t, 3H; CH$_2$C**H$_3$**), 2.05 (m, 2H; C**H$_2$**COO$^-$), 3.05 (s, 9H; N(C**H$_3$**)$_3^+$), 3.4 (m, 2H; C**H$_2$**OH), 3.9 (m, 2H; C**H$_2$**N(CH$_3$)$_3^+$)

^{13}C NMR (300 MHz, D_2O, 25°C, TMS): δ = 10.20 (**C**H$_3$CH$_2$), 30.72 (**C**H$_2$COO$^-$), 53.88 (t, N(**C**H$_3$)$_3^+$), 55.61 (**C**H$_2$OH), 67.44 (t, N**C**H$_2$), 184.91 (**C**OO$^-$)

ES-MS (H_2O/ MeOH/ MeCN): m/z (%) (+p): 104.0 (100) [M$^+$], 207.0 (40) [(2M$^+$ - H)$^+$], 281.1 (4) [(2M$^+$ + M$^-$)$^+$], 384.2 (1) [(3M$^+$ - H + M$^-$)$^+$]; (p-): 73.0 (19) [M$^-$], 250.0 (100) [(2M$^-$ + M$^+$)$^-$], 427.2 (12) [(3M$^-$ + 2M$^+$)$^-$], 604.4 (12) [(4M$^-$ + 3M$^+$)$^-$]

Water content (Karl-Fischer) = 3044 ± 100 ppm

Choline butanoate: ^{1}H NMR (300 MHz, D_2O, 25°C, TMS): δ = 0.8 (t, 3H; CH$_2$C**H$_3$**), 1.45 (m, 2H; C**H$_2$**CH$_3$), 2.15 (m, 2H; C**H$_2$**COO$^-$), 3.1 (s, 9H; N(C**H$_3$**)$_3^+$), 3.4 (t, 2H; C**H$_2$**OH), 3.95 (m, 2H; C**H$_2$**N(CH$_3$)$_3^+$)

^{13}C NMR (300 MHz, D_2O, 25°C, TMS): δ = 13.25 (**C**H$_3$CH$_2$), 19.38 (CH$_3$**C**H$_2$), 39.63 (**C**H$_2$COO$^-$), 53.86 (t, N(**C**H$_3$)$_3^+$), 55.60 (**C**H$_2$OH), 67.42 (t, N**C**H$_2$), 184.11 (**C**OO$^-$)

ES-MS (H_2O/ MeOH/ MeCN): m/z (%) (+p): 104.0 (100) [M$^+$], 207.0 (23) [(2M$^+$ - H)$^+$], 295.1 (2) [(2M$^+$ + M$^-$)$^+$], 677.6 (3) [(4M$^+$ + 3M$^-$)$^+$]; (p-): 87.0 (46) [M$^-$], 278.1 (100) [(2M$^-$ + M$^+$)$^-$], 469.3 (10), 660.5 (12) [(4M$^-$ + 3M$^+$)$^-$], 851.7 (2.5), 1042.9 (3)

Water content (Karl-Fischer) = 3303 ± 100 ppm

Choline pentanoate: ^{1}H NMR (300 MHz, D_2O, 25°C, TMS): δ = 0.8 (t, 3H; $CH_2C\mathbf{H_3}$), 1.2 (m, 2H; $C\mathbf{H_2}C\mathbf{H_2}CH_3$), 1.40 (q, 2H; $C\mathbf{H_2}CH_2COO^-$), 2.05 (t, 2H; $C\mathbf{H_2}COO^-$), 3.1 (s, 9H; $N(C\mathbf{H_3})_3^+$), 3.4 (t, 2H; $C\mathbf{H_2}OH$), 3.9 (m, 2H; $C\mathbf{H_2}N(CH_3)_3^+$)
^{13}C NMR (300 MHz, D_2O, 25°C, TMS): δ = 13.23 ($\mathbf{C}H_3CH_2$), 22.06 ($CH_3\mathbf{C}H_2$), 28.16 ($\mathbf{C}H_2CH_2COO^-$), 37.42 ($\mathbf{C}H_2COO^-$), 53.88 (t, $N(\mathbf{C}H_3)_3^+$), 55.60 ($\mathbf{C}H_2OH$), 67.44 (t, $N\mathbf{C}H_2$), 184.13 ($\mathbf{C}OO^-$)
ES-MS (H_2O/ MeOH/ MeCN): m/z (%) (+p): 104.0 (100) [M^+], 207.0 (29) [$(2M^+ - H)^+$], 309.1 (4) [$(2M^+ + M^-)^+$], 514.4 (4) [$(3M^+ + 2M^-)^+$], 719.7 (3) [$(4M^+ + 3M^-)^+$]; (p-): 101.0 (33) [M^-], 306.1 (100) [$(2M^- + M^+)^-$], 511.3 (20) [$(3M^- + 2M^+)^-$], 716.6 (28) [$(4M^- + 3M^+)^-$]
Water content (Karl-Fischer) = 2803 ± 100 ppm

Choline hexanoate: ^{1}H NMR (300 MHz, D_2O, 25°C, TMS): δ = 0.72 (t, 3H; $CH_2C\mathbf{H_3}$), 1.15 (m, 4H; $C\mathbf{H_2}C\mathbf{H_2}CH_3$), 1.40 (q, 2H; $C\mathbf{H_2}CH_2COO^-$), 2.05 (t, 2H; $C\mathbf{H_2}COO^-$), 3.05 (s, 9H; $N(C\mathbf{H_3})_3^+$), 3.4 (t, 2H; $C\mathbf{H_2}OH$), 3.95 (m, 2H; $C\mathbf{H_2}N(CH_3)_3^+$)
^{13}C NMR (300 MHz, D_2O, 25°C, TMS): δ = 13.29 ($\mathbf{C}H_3CH_2$), 21.97 ($CH_3\mathbf{C}H_2$), 25.34 ($CH_3CH_2\mathbf{C}H_2$), 30.95 ($\mathbf{C}H_2CH_2COO^-$), 36.98 ($\mathbf{C}H_2COO^-$), 53.86 (t, $N(\mathbf{C}H_3)_3^+$), 55.60 ($\mathbf{C}H_2OH$), 67.42 (t, $N\mathbf{C}H_2$), 183.45 ($\mathbf{C}OO^-$)
ES-MS (H_2O/ MeOH/ MeCN): m/z (%) (+p): 104.0 (100) [M^+], 207.0 (78) [$(2M^+ - H)^+$], 323.2 (12) [$(2M^+ + M^-)^+$], 542.5 (4) [$(3M^+ + 2M^-)^+$], 761.7 (6) [$(4M^+ + 3M^-)^+$]; (p-): 114.9 (44) [M^-], 334.2 (100) [$(2M^- + M^+)^-$], 553.5 (10) [$(3M^- + 2M^+)^-$], 772.7 (5) [$(4M^- + 3M^+)^-$]
Water content (Karl-Fischer) = 2831 ± 100 ppm

Choline heptanoate: ^{1}H NMR (300 MHz, D_2O, 25°C, TMS): δ = 0.75 (t, 3H; $CH_2C\mathbf{H_3}$), 1.2 (m, 6H; $C\mathbf{H_2}C\mathbf{H_2}C\mathbf{H_2}CH_3$), 1.40 (m, 2H; $C\mathbf{H_2}CH_2COO$-), 2.05 (t, 2H; $C\mathbf{H_2}COO$-), 3.05 (s, 9H; $N(C\mathbf{H_3})_3$), 3.4 (t, 2H; $C\mathbf{H_2}OH$), 3.95 (m, 2H; $C\mathbf{H_2}N(CH_3)_3$)
^{13}C NMR (300 MHz, D_2O, 25°C, TMS): δ = 13.40 ($\mathbf{C}H_3CH_2$), 21.95 ($CH_3\mathbf{C}H_2$), 25.85 ($CH_3CH_2\mathbf{C}H_2$), 28.44 ($\mathbf{C}H_2CH_2CH_2COO^-$), 30.91 ($\mathbf{C}H_2CH_2COO^-$), 37.55 ($\mathbf{C}H_2COO^-$), 53.89 (t, $N(\mathbf{C}H_3)_3^+$), 55.62 ($\mathbf{C}H_2OH$), 67.44 (t, $N\mathbf{C}H_2$), 184.14 ($\mathbf{C}OO^-$)
ES-MS (H_2O/ MeOH/ MeCN): m/z (%) (+p): 104.0 (100) [M^+], 207.0 (23) [$(2M^+ - H)^+$], 337.2 (2) [$(2M^+ + M^-)^+$]; (p-): 128.9 (100) [M^-], 362.1 (54) [$(2M^- + M^+)^-$], 595.5 (3) [$(3M^- + 2M^+)^-$], 828.7 (2) [$(4M^- + 3M^+)^-$]
Water content (Karl-Fischer) = 3120 ± 100 ppm

Choline octanoate: ^{1}H NMR (300 MHz, D_2O, 25°C, TMS): δ = 0.72 (t, 3H; $CH_2C\mathbf{H_3}$), 1.15 (m, 8H; $C\mathbf{H_2}C\mathbf{H_2}CH_3$), 1.40 (m, 2H; $C\mathbf{H_2}CH_2COO^-$), 2.05 (t, 2H; $C\mathbf{H_2}COO^-$), 3.05 (s, 9H; $N(C\mathbf{H_3})_3^+$), 3.4 (t, 2H; $C\mathbf{H_2}OH$), 3.95 (m, 2H; $C\mathbf{H_2}N(CH_3)_3^+$)

^{13}C NMR (300 MHz, D_2O, 25°C, TMS): δ = 13.40 ($\mathbf{C}H_3CH_2$), 22.02 ($CH_3\mathbf{C}H_2$), 25.91 ($CH_3CH_2\mathbf{C}H_2$), 28.27 ($CH_3CH_2CH_2\mathbf{C}H_2$), 28.72 ($CH_3CH_2CH_2CH_2\mathbf{C}H_2$), 31.06 ($\mathbf{C}H_2CH_2COO^-$), 37.61 ($\mathbf{C}H_2COO^-$), 53.86 (t, $N(\mathbf{C}H_3)_3^+$), 55.60 ($\mathbf{C}H_2OH$), 67.41 ($N\mathbf{C}H_2$), 184.30 ($\mathbf{C}OO^-$)

ES-MS (H_2O/ MeOH/ MeCN): m/z (%) (+p): 104.0 (100) [M^+], 207.0 (44) [$(2M^+ - H)^+$], 351.1 (4) [$(2M^+ + M^-)^+$], 598.5 (1) [$(3M^+ + 2M^-)^+$], 845.9 (1) [$(4M^+ + 3M^-)^+$]; (p-): 142.9 (100) [M^-], 390.2 (82) [$(2M^- + M^+)^-$], 637.5 (6) [$(3M^- + 2M^+)^-$], 884.9 (2) [$(4M^- + 3M^+)^-$]

Water content (Karl-Fischer) = 3733 ± 100 ppm

Choline nonanoate: ^{1}H NMR (300 MHz, D_2O, 25°C, TMS): δ = 0.75 (t, 3H; $CH_2C\mathbf{H_3}$), 1.15 (m, 10H; $C\mathbf{H_2}C\mathbf{H_2}CH_3$), 1.45 (m, 2H; $C\mathbf{H_2}CH_2COO^-$), 2.10 (t, 2H; $C\mathbf{H_2}COO^-$), 3.05 (s, 9H; $N(C\mathbf{H_3})_3^+$), 3.4 (t, 2H; $C\mathbf{H_2}OH$), 3.9 (m, 2H; $C\mathbf{H_2}N(CH_3)_3^+$)

^{13}C NMR (300 MHz, D_2O, 25°C, TMS): δ = 13.41 ($\mathbf{C}H_3CH_2$), 22.04 ($CH_3\mathbf{C}H_2$), 25.83 ($CH_3CH_2\mathbf{C}H_2$), 28.54 ($CH_3CH_2CH_2\mathbf{C}H_2$), 28.73 ($CH_3CH_2CH_2CH_2\mathbf{C}H_2$), 31.15 ($\mathbf{C}H_2CH_2COO^-$), 37.44 ($\mathbf{C}H_2COO^-$), 53.85 (t, $N(\mathbf{C}H_3)_3^+$), 55.59 ($\mathbf{C}H_2OH$), 67.42 ($N\mathbf{C}H_2$), 179.30 ($\mathbf{C}OO^-$)

ES-MS (H_2O/ MeOH/ MeCN): m/z (%) (+p): 104.0 (100) [M^+], 207.3 (100) [$(2M^+ - H)^+$], 365.4 (10) [$(2M^+ + M^-)^+$], 626.6 (3) [$(3M^+ + 2M^-)^+$]; (p-): 157.3 (76) [M^-], 315.4 (30) [$(2M^- + H^+)^-$], 418.5 (100) [$(2M^- + M^+)^-$], 679.7 (6) [$(3M^- + 2M^+)^-$]

Water content (Karl-Fischer) = 3532 ± 100 ppm

Choline decanoate: ^{1}H NMR (300 MHz, D_2O, 25°C, TMS): δ = 0.75 (t, 3H; $CH_2C\mathbf{H_3}$), 1.15 (m, 12H; $C\mathbf{H_2}C\mathbf{H_2}CH_3$), 1.40 (m, 2H; $C\mathbf{H_2}CH_2COO^-$), 2.05 (t, 2H; $C\mathbf{H_2}COO^-$), 3.01 (s, 9H; $N(C\mathbf{H_3})_3$), 3.4 (t, 2H; $C\mathbf{H_2}OH$), 3.95 (m, 2H; $C\mathbf{H_2}N(CH_3)_3^+$)

^{13}C NMR (300 MHz, D_2O, 25°C, TMS): δ = 13.45 ($\mathbf{C}H_3CH_2$), 22.09 ($CH_3\mathbf{C}H_2$), 25.96 ($CH_3CH_2\mathbf{C}H_2$), 28.51 ($CH_3CH_2CH_2\mathbf{C}H_2$), 28.61 ($CH_3CH_2CH_2CH_2\mathbf{C}H_2$), 28.71 ($CH_3CH_2CH_2CH_2CH_2\mathbf{C}H_2$), 28.79 ($CH_3CH_2CH_2CH_2CH_2CH_2\mathbf{C}H_2$), 31.21 ($\mathbf{C}H_2CH_2COO^-$), 37.70 ($\mathbf{C}H_2COO^-$), 53.88 (t, $N(\mathbf{C}H_3)_3^+$), 55.62 ($\mathbf{C}H_2OH$), 67.44 ($N\mathbf{C}H_2$), 184.21 ($\mathbf{C}OO^-$)

ES-MS (H_2O/ MeOH/ MeCN): m/z (%) (+p): 104.0 (100) [M^+], 207.0 (57) [$(2M^+ - H)^+$], 379.2 (8) [$(2M^+ + M^-)^+$], 654.6 (2) [$(3M^+ + 2M^-)^+$]; (p-): 170.9 (100) [M^-], 343.2 (3) [$(2M^- + H^+)^-$], 446.3 (53) [$(2M^- + M^+)^-$], 721.7 (4) [$(3M^- + 2M^+)^-$], 997.0 (2) [$(4M^- + 3M^+)^-$]

Water content (Karl-Fischer)= 2252 ± 100 ppm

Choline oleate: NMR (300 MHz, D_2O, 25°C, TMS): δ = 0.75 (t, 3H, C**H**$_3$CH_2),1.19 (m, 20H, CH_2C**H**$_2$),1.40 (m, 2H, C**H**$_2$CH_2COO^-), 1.87 (m, 4H, C**H**$_2$CH=CHC**H**$_2$), 2.06 (m, 2H, C**H**$_2$COO^-), 3.05 (s, 9H; N(C**H**$_3$)$_3^+$), 3.4 (t, 2H; C**H**$_2$OH), 3.95 (m, 2H; C**H**$_2$N$(CH_3)_3^+$), 5.22 (m, 4H; C**H**=C**H**)

^{13}C NMR (300 MHz, D_2O, 25°C, TMS): δ = 13.90 (**C**H_3CH_2), 22.68 (CH_3**C**H_2), 26.40 (CH_3CH_2**C**H_2), 27.25 ($CH_3CH_2CH_2$**C**H_2), 29.46 (CH_2**C**H_2), 29.55 (CH_2**C**H_2), 29.72 ($_2CH_2$**C**H_2), 29.87 (CH_2**C**H_2), 32.01 (**C**$H_2CH_2COO^-$), 37.70 (**C**H_2COO^-), 53.91 (t, N(**C**$H_3)_3^+$), 55.62 (**C**H_2OH), 67.50 (N**C**H_2), 184.00 (**C**OO^-), 129.58 (**C**H=CH), 129.98 (CH=**C**H)

ES-MS (H_2O/ MeOH/ MeCN): m/z (%) (+p): 104.0 (100) [M^+], 207.0 (33) [$(2M^+ - H)^+$], 489.4 (4) [$(2M^+ + M^-)^+$]; (p-): 281.1 (100) [M^-], 563.6 (16) [$(2M^- + H^+)^-$], 666.6 (53) [$(2M^- + M^+)^-$]

Water content (Karl-Fischer) = 3787 ± 100 ppm

Choline succinate: ^{1}H NMR (300 MHz, D_2O, 25°C, TMS): δ = 2.40 (s, 4H; C**H**$_2$C**H**$_2$), 3.10 (s, 9H; N(C**H**$_3$)$_3^+$), 3.40 (t, 2H; C**H**$_2$OH), 3.95 (m, 2H; C**H**$_2$N$(CH_3)_3^+$)

^{13}C NMR (300 MHz, D_2O, 25°C, TMS): δ = 31.31 (**C**H_2COO^-), 53.85 (t, N(**C**$H_3)_3^+$), 55.59 (**C**H_2OH), 67.40 (t, N**C**H_2), 179.70 (**C**OO^-)

ES-MS (H_2O/ MeOH/ MeCN): m/z (%) (+p): 104.0 (100) [M^+], 207.0 (6) [$(2M^+ - H)^+$], 325.1 (24) [$(2M^+ + M^-)^+$]; (p-): 116.9 (100) [M^-], 338.1 (65) [$(2M^- + M^+)^-$]

Water content (Karl-Fischer) = 2221 ± 100 ppm

Choline glutarate: ^{1}H NMR (300 MHz, D_2O, 25°C, TMS): δ = 1.80 (q, 2H; CH_2C**H**$_2$$CH_2$), 2.20 (t, 4H; C**H**$_2$$CH_2$C**H**$_2$), 3.10 (s, 9H; N(C**H**$_3$)$_3^+$), 3.40 (t, 2H; C**H**$_2$OH), 3.92 (m, 2H; C**H**$_2N(CH_3)_3^+$)

^{13}C NMR (300 MHz, D_2O, 25°C, TMS): δ = 21.35 (**C**H_2 CH_2COO^-), 35.12 (**C**H_2COO^-), 53.85 (t, N(**C**$H_3)_3^+$), 55.59 (**C**H_2OH), 67.44 (t, N**C**H_2), 180.67 (**C**OO^-)

ES-MS (H_2O/ MeOH/ MeCN): m/z (%) (+p): 104.0 (100) [M^+], 207.0 (7) [$(2M^+ - H)^+$], 339.2 (8) [$(2M^+ + M^-)^+$], 442.2 (6) [$(3M^+ - H + M^-)^+$]; (p-): 130.8 (100) [M^-], 366.0 (18) [$(2M^- + M^+)^-$]

Water content (Karl-Fischer) = 1521 ± 100 ppm

Choline adipate: ^{1}H NMR (300 MHz, D_2O, 25°C, TMS): δ = 1.45 (m, 4H; CH_2C**H**$_2$$CH_2$), 2.20 (t, 4H; C**H**$_2$$CH_2$C**H**$_2$), 3.09 (s, 9H; N(C**H**$_3$)$_3^+$), 3.40 (t, 2H; C**H**$_2$OH), 3.92 (m, 2H; C**H**$_2N(CH_3)_3^+$)

^{13}C NMR (300 MHz, D_2O, 25°C, TMS): δ = 24.77 (**C**H_2 CH_2COO^-), 35.34 (**C**H_2COO^-), 53.85 (t, N(**C**$H_3)_3^+$), 55.59 (**C**H_2OH), 67.44 (t, N**C**H_2), 180.67 (**C**OO^-)

ES-MS (H_2O/ MeOH/ MeCN): m/z (%) (+p): 104.0 (100) [M^+], 207.0 (10) [$(2M^+ - H)^+$], 353.1 (7) [$(2M^+ + M^-)^+$], 456.3 (10) [$(3M^+ - H + M^-)^+$]; (p-): 144.8 (100) [M^-], 394.1 (28) [$(2M^- + M^+)^-$]

Water content (Karl-Fischer) = 3197 ± 100 ppm

3.5.2 UV-Vis measurements and toluene solubility

To determine the concentration of hydrotrope in water at which the solubilization of hydrophobic dye in the aqueous hydrotrope solution of choline acetate, choline butanoate or choline hexanaote increase, Disperse Red 13 was solubilized as hydrophobic dye. All the solubilization experiments and the UV-Vis measurements were performed in a thermostated room at 25 ± 0.2°C. Different concentrated aqueous hydrotrope solutions were prepared and saturated with Disperse Red 13. These solutions were stirred for 24 h and afterwards filtered to remove the excess of the dye. The amount of the dissolved Disperse Red 13 was determined with UV-Vis measurements on a Varian Cary 3E spectrophotometer. The absorption was measured at the wavelength of 503 nm.[25] The calibration curve with defined amounts of Disperse Red 13 was prepared by dissolving Disperse Red 13 in absolute ethanol (Baker, purity ≥ 99.9 %). Also the solubility of toluene (Sigma Aldrich) in the aqueous hydrotrope solution was performed in the same way. Different concentrated aqueous hydrotrope solutions were prepared and stirred for 24 h. Toluene was put dropwise with a Hamilton syringe into the solution until turbidity appears. The amount of toluene was checked twice, by taking the weight of the vial and by the volume injected with the syringe.[27]

3.5.3 Conductivity

A valuable method to determine the critical micelle concentration *cmc* and also to determine the micelle ionization degree α at the *cmc* is to measure the concentration dependent specific conductivity κ of an aqueous choline carboxylate solution ChC_m with m = 8, 10 and oleate. An autobalance conductivity bridge (Konduktometer 702, Knick), arranged with a Consort SK41T electrode cell was used to measure the specific conductivity. For the calibration 0.01 M, 0.1 M and 1 M potassium chloride solutions were needed to determine the cell constant at 25°C and 40°C.[53] The concentration dependent conductivity was evaluated at 25°C and 40°C. A break in the slope of the plot of concentration versus the specific conductivity κ marks the *cmc* of the respective choline carboxylates (see **Figure 3-6**). The accuracy of the *cmc* values is ± 4 %.

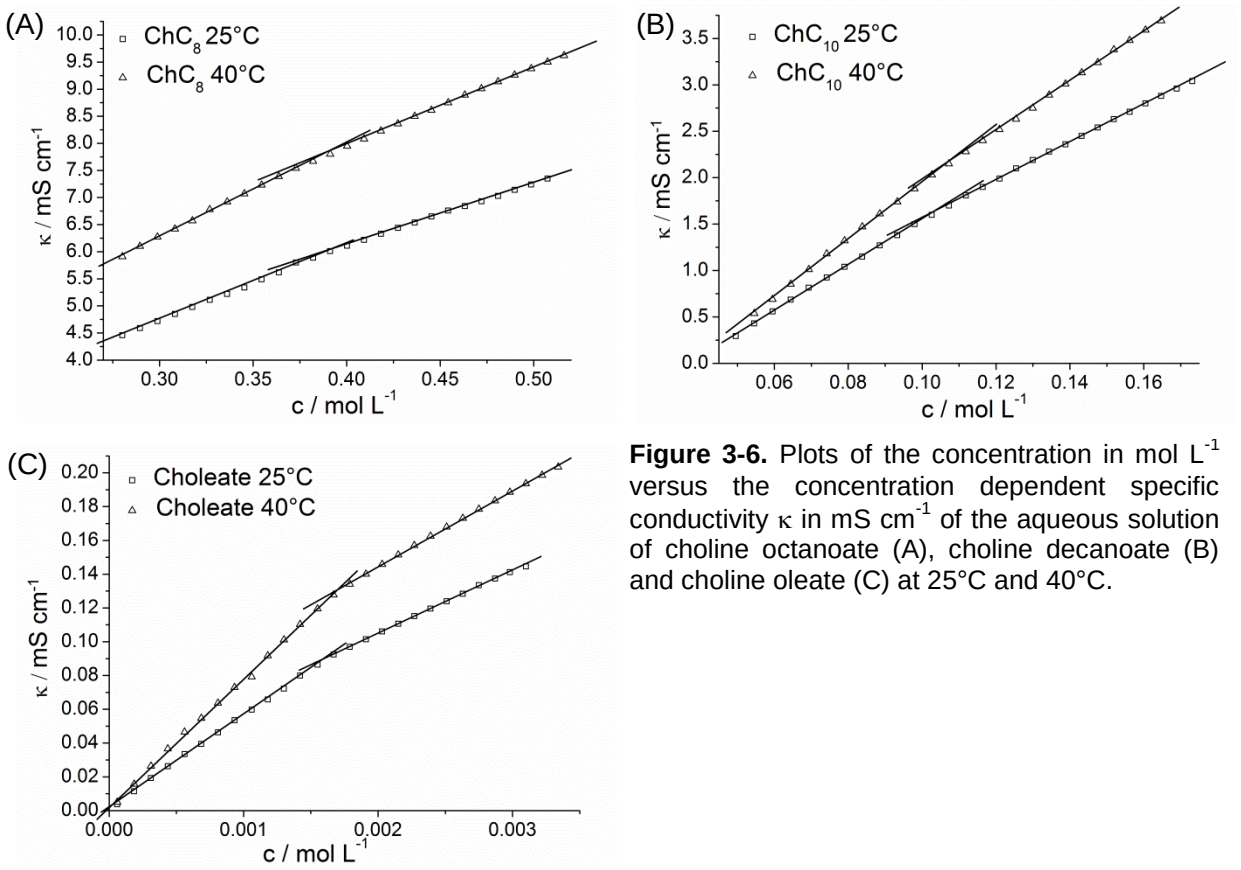

Figure 3-6. Plots of the concentration in mol L^{-1} versus the concentration dependent specific conductivity κ in mS cm^{-1} of the aqueous solution of choline octanoate (A), choline decanoate (B) and choline oleate (C) at 25°C and 40°C.

For the calculation of the micelle ionization degree α at the *cmc* equation (8) presented by Evans *et al.*[54] was used:

$$0 = \left[N^{\frac{2}{3}}(1000 \cdot S_1 - \lambda_{Ch+})\right]\alpha^2 + \lambda_{Ch+}\alpha - 1000 \cdot S_2 \qquad (8)$$

λ_{Ch+} is the counterion conductivity given by Fleming *et al.* as 42.0 S cm^2.[55] N represents the amount of surfactant molecules in the micelle and S_1 the slope before the *cmc* and S_2 the slope above the *cmc*. The micelle ionization degree α could only be calculated for choline oleate. Choline octanoate and choline decanoate are at the limits of this equation (8) and present too small slopes.

	1000·S_1 / S cm^2 mol^{-1}	**1000·S_2 / S cm^2 mol^{-1}**	**α**
Choline oleate 25°C	56.6	37.3	0.30
Choline oleate 40°C	77.1	44.8	0.24

Table 3-4. Slope S_1 and S_2 are obtained from the plot of the concentration versus the specific conductivity κ. The accuracy of the slope is 5 %. The one of the calculated ionization degree α is 7%.

3.5.4 Surface tension

To determine the critical micelle concentration of choline octanoate, choline decanoate and choline oleate at 25°C and 40°C the concentration dependent surface tension σ was measured. The temperature accuracy was 25°C ± 0.1°C and 40°C ± 0.1°C. The measurements were performed with a Krüss tensiometer (model K100 MK2) using a platinum-iridium ring. The data acquisition works automatically and records the surface tension as a function of the concentration. The surface tension was measured during dilution of the soap solution with degassed, bidistilled water. The data correction was done according to the procedure performed by Harkins and Jordan.[56]

3.5.5 Cytotoxicity on HeLa and SK-MEL-28 cells

Tests were performed with the SK-MEL-28 (keratinocytes, CLS 300337) and the HeLa (cervix carcinoma, ATCC CCL17) cell line. In both cases the MTT assay procedure introduced by Mosmann *et al.*[31] was used. It was modified by Vlachy *et al.* [32] The only exception in this study compared to their method was that media was used without Amphotericin B and Penicillin G/ Streptomycinsulfate.[31, 32] During the tests MTT (3-(4,5-dimethylthiazol-2-yl)-2,5-diphenyltetrazolium bromide) a yellow tetrazol is reduced to purple formazan in the living cells.[31] For the stock solutions the substances were directly dissolved in the corresponding media. For each ionic liquid in solution the IC_{50} value (in mol L^{-1}) was determined. The IC_{50} value represents the concentration of tested substance that lowers MTT reduction by 50 % relative to the untreated control. It was calculated for each substance from a concentration-response curve, which was generated on the basis of 8 different concentrations. For a better comparison the IC_{50} values were determined for all substances on the same day (in triplicate). All experiments were repeated three to five times over several weeks, and the average IC_{50} value and its standard deviation (SD) are reported (see **Figure 3-4** and **Table 3-3**). The dose-response curves of the substances are shown in Appendix A.

3.5.6 Calorimetry of model membranes

Large, unilamellar vesicles of DPPC were prepared by extrusion as described by Weaver *et al.*[52], using membranes with a pore size of ≤ 0.2 µm. Lyophilized DPPC powder was hydrated with 20 mM HEPES (4-(2-hydroxyethyl)-1-piperazineethanesulfonic acid) buffer at pH 7.40, which had been pre-warmed to 70°C, and then held at this temperature for 30 minutes, with occasional agitation. Solutions were passed 21 times through 100 nm Nucleopore® track-etched polycarbonate filters (Whatman, Pleasanton, CA) that had been mounted in a mini-

extruder (Avanti Polar Lipids, Alabaster, AL). Liposomes were then refrigerated at 4°C for a minimum of 16 h before use.

A MicroCal VP-DSC microcalorimeter (MicroCal, Northhampton, MA) was used to determine the temperature associated with the transition from the gel to liquid crystalline state of the alkyl chains in the liposomes as described by Weaver *et al.*.[52] An aliquot of the stock lipid vesicle solution was combined with experimental compounds in 20 mM HEPES buffer at pH 7.40 in a 1:1 ratio by volume where dilution resulted in the desired compound experimental concentration in the calorimeter cells. A control (lipid only) thermal scan was acquired for each tested compound. After loading into the calorimeter cells, the samples were allowed to equilibrate 15 minutes at 10°C then scanned from 20°C to 50°C at 60°C per hour with a 16 second filter and passive feedback (gain). Reversibility was determined by rescanning samples after allowing them to cool down to initial temperature. The tests were prepared with choline carboxylates ChC_m with chain length m = 2, 3, 4, 5, 6, 7, 8, 9, 10 and choline oleate.

3.6 References

1. M. Petkovic, K. R. Seddon, L. P. N. Rebelo and C. Silva Pereira, *Chem. Soc. Rev.*, 2011, **40**, 1383-1403.
2. R. Klein, Dissertation, Universität Regensburg, 2011.
3. M. C. Scaife, *Int. J. Cosmet. Sci.*, 1982, **4**, 179-193.
4. M. C. Holmes, *Curr. Opin. Colloid Interface Sci.*, 1998, **3**, 485-492.
5. C. Gloxhuber, *Arch. Toxicol.*, 1974, **32**, 245-270.
6. H. Schott, *J. Pharm. Sci.*, 1973, **62**, 341-343.
7. M. J. Rosen, L. Fei, Y.-P. Zhu and S. W. Morrall, *J. Surfactants Deterg.*, 1999, **2**, 343-347.
8. D. W. Roberts and J. F. Costello, *QSAR Comb. Sci.*, 2003, **22**, 220-225.
9. D. W. Roberts and J. F. Costello, *QSAR Comb. Sci.*, 2003, **22**, 226-233.
10. M. Petkovic, J. L. Ferguson, H. Q. N. Gunaratne, R. Ferreira, M. C. Leitao, K. R. Seddon, L. P. N. Rebelo and C. S. Pereira, *Green Chem.*, 2010, **12**, 643-649.
11. N. Muhammad, M. I. Hossain, Z. Man, M. El-Harbawi, M. A. Bustam, Y. A. Noaman, N. B. Mohamed Alitheen, M. K. Ng, G. Hefter and C.-Y. Yin, *J. Chem. Eng. Data*, 2012, **57**, 2191-2196.
12. H. Eagle, *J. Exp. Med.*, 1955, **102**, 595-600.
13. K. Chiba, I. Makino, J. Ohuchi, Y. Kasai, H. Kakishima, K. Tsukumo, T. Uchiyama, E. Miyai, J. Akiyama, Y. Okamoto, H. Kojima, H. Okumura, Y. Tsurumi, M. Usami, K. Katoh, S. Sugiura, A. Kurishita, M. Sunouchi, A. Miyajima, M. Hayashi and Y. Ohno, *Toxicol. in Vitro*, 1999, **13**, 189-198.

14. W. Yang and D. Acosta, *Toxicol. Lett.*, 1994, **70**, 309-318.
15. M. A. Perkins, R. Osborne, F. R. Rana, A. Ghassemi and M. K. Robinson, *Toxicol. Sci.*, 1999, **48**, 218-229.
16. R. L. Grant, C. Yao, D. Gabaldon and D. Acosta, *Toxicology*, 1992, **76**, 153-176.
17. P. P. Dongre, D. M. Kannur, V. Kosambiya and B. D. Desai, *I.J.P.S.R.*, 2011, **2**, 730-734.
18. G. Horvath-Szabo, Q. Yin and S. E. Friberg, *J. Colloid and Interface Sci.*, 2001, **236**, 52-59.
19. H. Garcia, R. Ferreira, M. Petkovic, J. L. Ferguson, M. C. Leitao, H. Q. N. Gunaratne, K. R. Seddon, L. P. N. Rebelo and C. S. Pereira, *Green Chem.*, 2010, **12**, 367-369.
20. R. G. Laughlin, *The Aqueous Phase Behavior of Surfactants,* Academic Press, San Diego, 1994, pp. 328-330.
21. D. F. Evans and H. Wennerström, *The colloidal domain: where physics, chemistry, biology, and technology meet*, Wiley-VCH, New York, 1999.
22. R. Klein, D. Touraud and W. Kunz, *Green Chem.*, 2008, **10**, 433.
23. M. J. Rosen, *Surfactants and Interfacial Phenomena*, John Wiley & Sons, Inc., New York, 1989.
24. P. Bauduin, A. Renoncourt, A. Kopf, D. Touraud and W. Kunz, *Langmuir*, 2005, **21**, 6769-6775.
25. M. Durand, Y. Zhu, V. Molinier, T. Feron and J. M. Aubry, *J. Surfactants Deterg.*, 2009, **12**, 371-378.
26. P. C. Ho, *J. Chem. Eng. Data*, 1985, **30**, 88-90.
27. S. Kalyanram and V. G. Gaikar, *J. Chem. Eng. Data*, 1994, **39**, 119-121.
28. P. Mukerjee and K. J. Mysels, *Critical Micellar Concentrations of Aqueous Surfactant Systems*, NSRDS-NBS 36, Washington D.C., 1971.
29. K. D. Collins, G. W. Neilson and J. E. Enderby, *Biophys. Chem.*, 2007, **128**, 95-104.
30. K. D. Collins, *Methods*, 2004, **34**, 300-311.
31. T. Mosmann, *J. Immunol. Methods*, 1983, **65**, 55-63.
32. N. Vlachy, D. Touraud, J. Heilmann and W. Kunz, *Colloids Surf., B*, 2009, **70**, 278-280.
33. Clarification of Annex II, Entry 168 of the Cosmetic Directive: *Choline Salts and their Esters e.g. Choline Chloride* (INN), European Commission, SCCS/1237/09, 2009.
34. L. Sanchez, M. Mitjans, M. Infante and M. Vinardell, *Pharm. Res.*, 2004, **21**, 1637-1641.
35. R. Roguet, *Cell Biol. Toxicol.*, 1999, **15**, 63-75.
36. R. Klein, G. J. T. Tiddy, E. Maurer, D. Touraud, J. Esquena, O. Tache and W. Kunz, *Soft Matter*, 2011, **7**, 6973.

37. D. Rengstl, O. Diat, R. Klein and W. Kunz, *Langmuir*, 2013, **29**, 2506-2519.
38. R. G. Laughlin, *The Aqueous Phase Behavior of Surfactants*, Academic Press, San Diego, 1994.
39. E. Blanco, A. Gonzalez-Perez, J. M. Ruso, R. Pedrido, G. Prieto and F. Sarmiento, *J. Colloid and Interface Sci.*, 2005, **288**, 247-260.
40. J. W. McBain, R. D. Vold and M. Frick, *J. Phys. Chem.*, 1940, **44**, 1013-1024.
41. A. González-Pérez, G. Prieto, J. M. Ruso and F. Sarmiento, *Mol. Phys.*, 2003, **101**, 3185-3195.
42. S. Stolte, J. Arning, U. Bottin-Weber, M. Matzke, F. Stock, K. Thiele, M. Uerdingen, U. Welz-Biermann, B. Jastorff and J. Ranke, *Green Chem.*, 2006, **8**, 621-629.
43. M. Maugras, M. R. Infante, C. Gerardin, C. Selve and M. P. Vinardell, *Comp. Biochem. Physio.l C Toxicol. Pharmacol.*, 2001, **128**, 541-545.
44. S. Stolte, M. Matzke, J. Arning, A. Boschen, W. R. Pitner, U. Welz-Biermann, B. Jastorff and J. Ranke, *Green Chem.*, 2007, **9**, 1170-1179.
45. S. H. Zeisel and K. A. da Costa, *Nutr. Rev.*, 2009, **67**, 615-623.
46. R. S. Boethling, E. Sommer and D. DiFiore, *Chem. Rev.*, 2007, **107**, 2207-2227.
47. G. J. Kortstee, *Arch. Microbiol.*, 1970, **71**, 235-244.
48. T. P. Pham, C. W. Cho, J. Min and Y. S. Yun, *J. Biosci. Bioeng.*, 2008, **105**, 425-428.
49. K. Ogino and Y. Ichikawa, *Bull. Chem. Soc. Jpn.*, 1976, **49**, 2683-2686.
50. C. Prottey and T. F. M. Ferguson, *Food Cosmet. Toxicol.*, 1976, **14**, 425-430.
51. C.-S. Hwu and G. Lettinga, *Enzyme Microb. Technol.*, 1997, **21**, 297-301.
52. K. Weaver, M. V. Vorst, R. Vijayaraghavan, D. MacFarlane and G. Elliott, *in review at BBA: Biomembranes*, 2013.
53. D. R. Lide, *CRC - Handbook of Chemistry and Physics*, CR Press, Boca Raton, USA, 2004.
54. H. C. Evans, *J. Chem. Soc.*, 1956, 579-586.
55. R. Fleming, *J. Chem. Soc.* , 1960, 4914-4916.
56. W. D. Harkins and H. F. Jordan, *J. Am. Chem. Soc.*, 1930, **52**, 1751-1772.

Chapter 4

Influence of chain length and double bond on the aqueous behavior of choline carboxylate soaps

4.1 Abstract

In preceding studies Klein *et al.* demonstrated that choline carboxylates ChC_m with alkyl chain lengths of m = 12-18 are highly water soluble (for m = 12, soluble up to 93 wt% soap and 0°C).[1] In addition, choline soaps are featured by an extraordinary lyotropic phase behavior. With decreasing water concentration the following phases were found: micellar phase (L_1), discontinuous cubic phase (I_1' and I_1''), hexagonal phase (H_1), bicontinuous cubic phase (V_1), and lamellar phase (L_α). The present work is focused also on the lyotropic phase behavior of choline soaps, but with shorter alkyl chains or different alkyl chain properties. The aqueous phase behavior of choline soaps with C_8 and C_{10} chain lengths (choline octanoate and choline decanoate) and with a C_{18} chain length with a cis-double bond (choline oleate) was investigated. It was found that choline decanoate follows the lyotropic phase behavior of the longer-chain homologs mentioned above. Choline octanoate in water shows no cubic phases, but an extended, isotropic micellar solution phase. In addition, choline octanoate is at the limit between a surfactant and a hydrotrope, as already seen in Chapter 3. The double bond in choline oleate leads also to a better solubility in water and a decrease of the solubilization temperature. It influences also the packing curvature of the aggregates which results in a loss of discontinuous cubic phases in the binary phase diagram. The different lyotropic mesophases were identified by the penetration scan technique with polarizing optical microscope and visual observations. To clarify the structural behavior small (SAXS) and wide (WAXS) angle X-ray scattering were performed. To further characterize the extended isotropic solution phase in the binary phase diagram of choline octanoate viscosity and conductivity measurements were also carried out.

4.2 Introduction

The aqueous binary phase diagrams of long chain ($\geq C_{12}$) alkali carboxylates and alkali oleate are well known since the pioneering work done by Vold[2,3], McBain[2,4], Luzzati[5], Madelmont and Perron[6], Skoulios, and their coworkers[7]. Basically, they identified the following sequence of mesophases with increasing soap concentration: micellar phase (L_1), hexagonal phase (H_1), bicontinuous cubic phase (V_1), and lamellar phase (L_α). The bicontinuous cubic phase can be replaced or accompanied by intermediated phases.[5,7] Vold pointed out that sodium oleate shows the same phase behavior as the saturated sodium carboxylates.[2,3] These studies[2, 8] also demonstrated that the Krafft temperatures of the alkali carboxylate soaps are higher than room temperature or at least 22°C (sodium oleate[8]; exception 10°C for KC_{12}[9]) and that the solubility of soaps increases with decreasing aliphatic chain length and with changing sodium by potassium. Vold and McBain confirmed the validity

of the Gibbs phase rule for soap systems.[3] They stated a true equilibrium between soap and water so that the phase change is only dependent on temperature, concentration and pressure.[3] Using rheology and ^{1}H NMR diffusometry measurements, Antunes *et al.*[10] found that the micellar growth of sodium oleate is very rapid and shows different micellar shapes with increasing soap concentration (spheres → cylinders → long cylinders) and promotes a phase transition between micellar and a hexagonal phase.

The binary phase diagrams of alkali decanoate (C_{10}) or octanoate (C_8) are similar to those of the before mentioned long chain homologs.[11] Only few literatures are available for these systems. Mostly literature exists on the characterization of the micellar solution. The other phases like hexagonal etc. are only mentioned but not described in detail. The micellar solution of sodium decanoate was explored by De Lisi *et al.*[12] and Vikingstad *et al.*[13], the one of sodium octanoate by Ekwall *et al.*.[14-20] The binary phase diagram of sodium octanoate is slightly different. The micellar solution of sodium octanoate shows three changes in structure seen as a variation in the concentration dependent behavior of some physical chemical parameters like density, viscosity, partial specific volume etc.[14-20] The first change corresponds to the formation of spherical micelles. The second is related to the increase of counterion binding. At the third a transition to an anisometric micellar shape takes place.[14-20] At higher concentration, the phase transition from micellar solution to the hexagonal phase occurs at room temperature, whereas the transition towards the cubic V_1 phase and the lamellar phase L_α appears only at higher temperatures.[21]

In this chapter the focus is set on the interplay between the bulky, non-toxic choline cation and anionic carboxylates with various alkyl chains to show their influence on the lyotropic phase behavior in water compared to long chain choline carboxylates ChC_m with m = 12-18. In detail, the lyotropic phase behavior of choline octanoate (ChC_8), choline decanoate (ChC_{10}) and choline oleate (Choleate) in a temperature range between 0°C and 95°C was investigated. A first rough overview of the different mesophases and their sequence was obtained with the penetration scan method using polarizing optical microscopy. The exact concentrations of the phase changes were evaluated by an optical screening with the help of crossed polarizers. Then, SAXS and WAXS measurements were performed on samples having surfactant concentrations up to 99 wt% to get the structural parameters of the different lyotropic mesophases. The binary phase diagram of choline octanoate in water shows a very broad isotropic micellar solution area, which at temperatures above 70°C remains isotropic up to 100 wt% of surfactant. This part was explored with conductivity, viscosity, dynamic light scattering, SAXS, and WAXS.

4.3 Results and discussion

4.3.1 Krafft temperature T_{Krafft}

One of the most important parameters of surfactants is the Krafft temperature, T_{Krafft}. It describes the solubility of a surfactant. For most applications Krafft temperatures below room temperature are required. A generally accepted practice to approximate this point is to record the temperature at which a 1 wt% surfactant solution becomes transparent. Usually, the Krafft temperature rises with increasing alkyl chain length.[22] It can be lowered by a hindered regular packing of the crystalline lattice, e.g. by introducing a double bond into the alkyl chain or by using a bulky, asymmetric cation like choline. The other possibility is to ensure a high solubility by the appropriate choice of the cation or anion.[23] The Krafft temperature lowering on account of a double bond can be seen by comparing the respective Krafft temperature of sodium stearate (T_{Krafft} = 67°C) and sodium oleate (T_{Krafft} = 22°C).[8] Comparing choline stearate (T_{Krafft} = 40°C)[9] with choline oleate (T_{Krafft} < 0°C, the real value cannot be measured, because it is below the melting temperature of the aqueous surfactant solutions) the difference in the Krafft temperature is even more than 40°C. The low Krafft temperature of choline oleate results from the cis double bond in the alkyl chain and additionally from the bulky and asymmetric structure of the choline cation.

Similarly but less detectable, the Krafft temperature of sodium octanoate is about 0°C[24], the one of sodium decanoate is 2.1°C[25]. The choline analogs have Krafft temperatures below 0°C. It should be mentioned that other quaternary ammonium ions can also lower the Krafft points of carboxylates, but they are much more toxic than the biological choline cation.[9] Furthermore, the low counterion-headgroup interaction in choline carboxylates is another reason for the lower Krafft temperatures compared to the sodium carboxylates.[26, 27, 22]

4.3.2 Penetration scan

The penetration scans were performed as described by Lawrence.[28] This technique is very efficient to evaluate the phase sequence with increasing soap concentration. Different mesophases can be identified by their relative viscosities and their specific textures.[29] The hexagonal phase can be evaluated easily because of the typical pattern[29] and its relatively high viscosity and temperature stability compared to the defective lamellar or nematic phase. The bicontinuous and discontinuous cubic phases can be characterized well by their very high viscosity and their isotropic appearance.[23, 30]

Choline decanoate (see **Figure 4-1** (A)-(D)) behaves like the long chain choline carboxylates.[1] The alternating sequence of isotropic and anisotropic lyotropic liquid crystalline phases can be illustrated very well. It exhibits the following phases with increasing

surfactant concentration: micellar phase L_1, two discontinuous cubic phases $I_1'$and I_1'', hexagonal phase H_1, and a solid phase. The latter one turns at higher temperatures (above the melting point of choline decanoate at around 45.8°C, see Appendix C in section C.3.2) to a liquid crystalline defective lamellar phase dL_α, which could also be named as nematic phase N.[31-33] The formation of the nematic phase could be observed due to the partly visible "Schlieren" texture[32] at temperatures higher than 45.8°C (see **Figure 4-1** (D)).

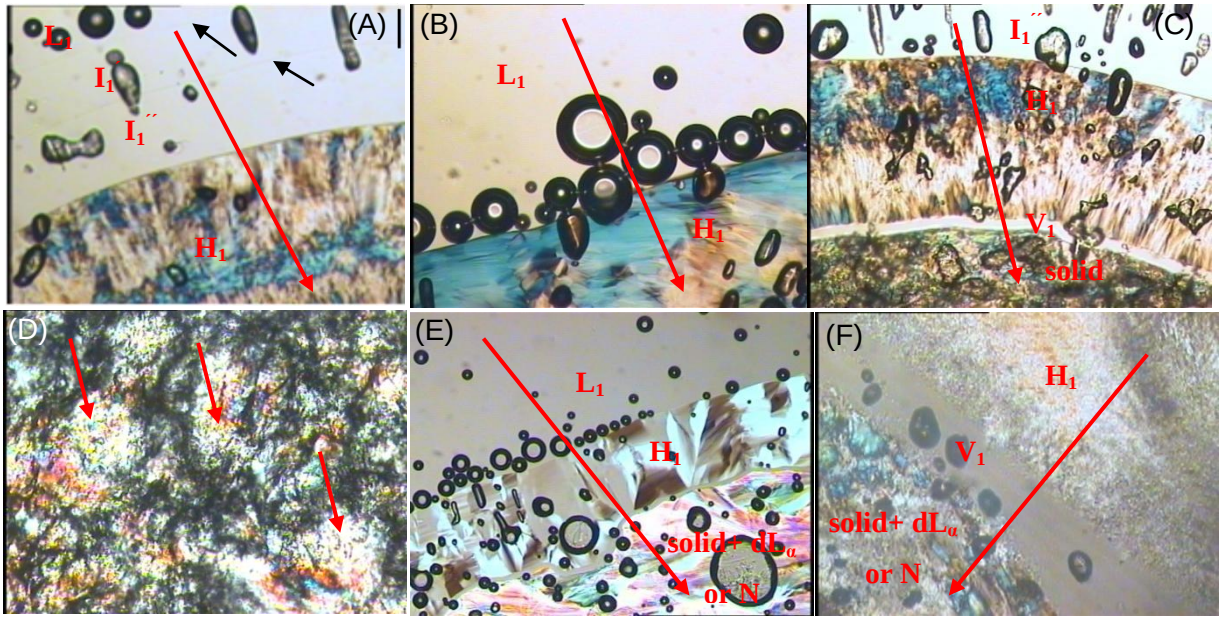

Figure 4-1. Polarizing light microscopy pictures are made with slightly crossed polarizers and 100x magnification. (A)-(C) Penetration scan of ChC_{10}. (A) 30°C, with increasing surfactant concentration: micellar L_1, discontinuous cubic I_1' and I_1'', hexagonal phase H_1; (B): 70°C, with increasing temperature the discontinuous cubic phases I_1' and I_1'' melt; (C): 25°C, almost full sequence of mesophases; with increasing surfactant concentration: discontinuous cubic I_1'', hexagonal H_1, bicontinuous cubic V_1, solid; (D): 70°C, over 45.8°C the solid phase is transferred to a defective lamellar dL_α or nematic N phase; typical "Schlieren" texture of a nematic phase visible at some parts (arrow). (E) Penetration scan of ChC_8 at 25°C: ChC_8 with water shows the phase sequence with increasing surfactant concentration: micellar phase L_1, hexagonal phase H_1, solid (above 30°C defective lamellar dL_α or nematic N). (F) Penetration scan of choline oleate at 25°C: Choline oleate discloses the behavior with increasing concentration: Micellar phase L_1 (missing in the picture), hexagonal phase H_1, bicontinuous cubic phase V_1 and solid + defective lamellar dL_α or nematic N phase. The scale bar in panel (A) is 100 µm. It is the same for all the other images.

In contrast, the long chain choline carboxylates form as highest concentrated phase and above the melting point a lamellar smectic A phase. Another difference, compared to the long chain choline carboxylates[1], appears at the melting of the discontinuous cubic phases at higher temperatures. They melt distinctly obvious at lower temperatures (see **Figure 4-1** (A)). At around 30°C the first discontinuous cubic phase I_1' starts to get liquid and at 70°C (see **Figure 4-1** (B)) all discontinuous cubic phases have turned to the micellar phase L_1. The reason for forming these discontinuous cubic phases in the case of choline carboxylates is the high degree of counterion-headgroup dissociation and the size of the bulky choline cation. The choline cation increases the curvature of these soaps.[1]

The penetration scan of choline octanoate is different from those of the longer-chain ones (see **Figure 4-1** (E)). The discontinuous cubic phases I_1' and $I_1''$and the bicontinuous cubic phase V_1 are absent. This illustrates that choline octanoate is not able to form stable micelles or aggregates, which can be ordered in a discontinuous cubic phase. Another important point is the instability of the lyotropic mesophases with increasing temperature. They all melt above 70°C to a viscous but liquid isotropic phase. The structure and the behavior of this molten phase will be discussed later in section 4.3.4.6.

The cis double bond in the alkyl chain of the choline oleate surfactant inhibits the formation of a discontinuous cubic phase, but not of the bicontinuous cubic phase. Thus, with increasing surfactant concentration the binary phase diagram of choline oleate comprises the following lyotropic phases (see **Figure 4-1** (F)): micellar phase L_1, hexagonal phase H_1, bicontinuous cubic phase V_1 and solid or defective lamellar phase dL_α or nematic phase N (depending on the temperature). Note that in the case of long chain carboxylates like choline hexadecanoate and choline octadecanoate it was found that the solid phase splits at high temperatures into a gel phase L_β and a lamellar phase L_α.[1] Choline oleate does not show a L_β phase.

4.3.3 Binary phase diagrams

The different samples of 1 wt% to 100 wt% soap (ChC_m with m = 8, 10 or choline oleate) water mixtures were heated or cooled in a water bath from 0°C up to 95°C or vice versa. This method was used to evaluate the concentration and temperature dependent phase boundaries. The temperature hysteresis of the heating and cooling phase transitions was found to be smaller than 3°C and can be neglected. In **Figure 4-2** the binary phase diagrams of choline octanoate, choline decanoate and choline oleate with water recorded during heating are shown. The sequence of the different lyotropic phases with increasing choline decanoate concentration is similar to the behavior Klein *et al.* found for the long chain choline carboxylates ChC_m (m = 12-18)[1] with one exception already mentioned: here at highest concentrated phase a defective lamellar dL_α or nematic N phase is found. Comparing the phase diagrams of choline soaps (ChC_m with m = 8, 10, 12[1], 14[1], 16[1], 18[1]) with different alkyl chain lengths, it can be concluded that the phase boundaries are shifted to smaller surfactant concentrations with increasing chain lengths. The only exception is found when comparing the binary diagrams of choline decanoate and choline dodecanaote. The boundary between the hexagonal and the bicontinuous cubic phase in the choline decanoate system is located at similar concentrations.[1]

As stated above choline octanoate with water cannot form any cubic phases. The solubilization temperature is below 0°C up to 98 wt% and then increases up to 35.3°C (see

section C.3.2 in Appendix C). This is the phase transition temperature of pure choline octanoate, which forms above this temperature a liquid crystalline phase.

The double bond in the oleate anion hinders the aggregation to a micellar cubic phase. It only allows the arrangement of the following phases in the binary system of choline oleate: micellar phase L_1, hexagonal phase H_1, bicontinuous cubic phase V_1, and defective lamellar dL_α or nematic N phase. In comparison to the binary phase diagram of choline octadecanoate[1], the solubilization temperature is below 0°C for almost all compositions. This behavior of choline oleate is the consequence of weak counterion binding to the carboxylate headgroup[34] and of the hindered regular crystalline packing. As a further consequence, the phase borders in the binary phase diagram of choline oleate are shifted slightly to smaller soap concentrations compared to the phase diagram of choline octadecanoate.[1]

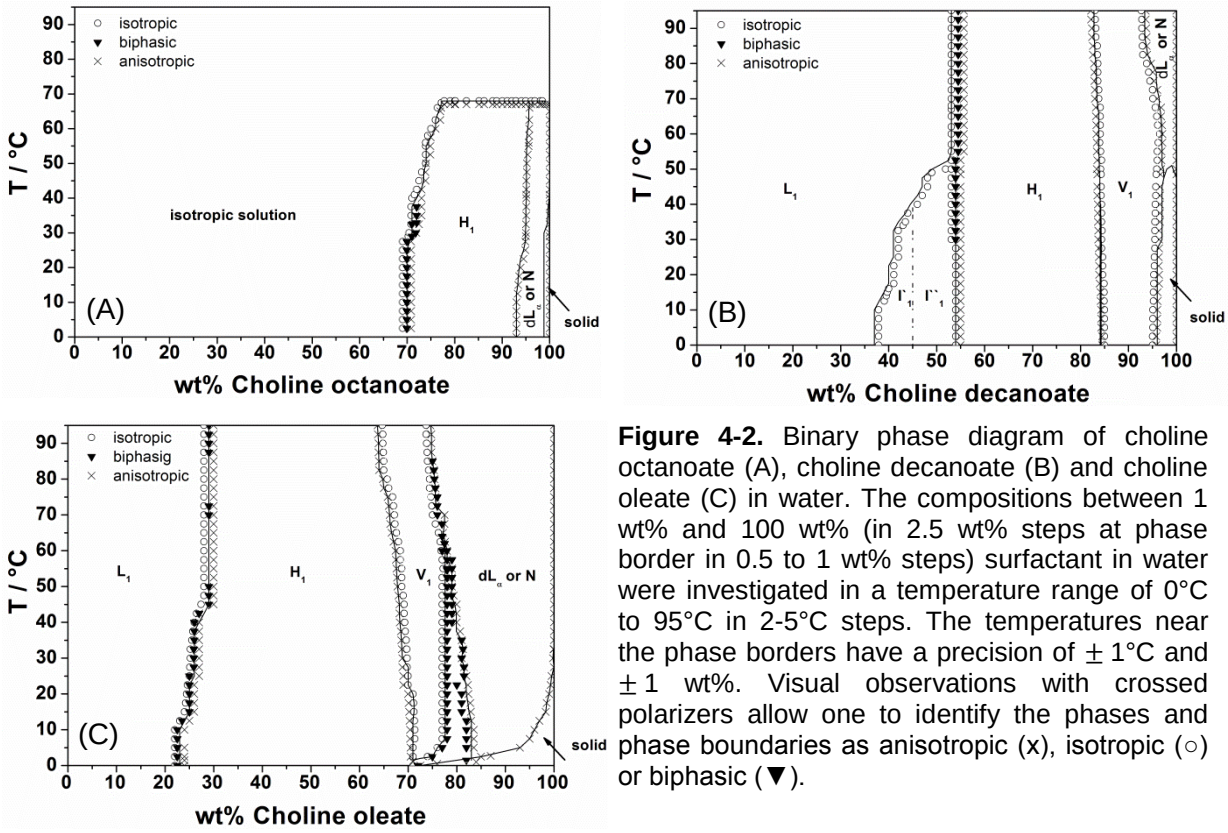

Figure 4-2. Binary phase diagram of choline octanoate (A), choline decanoate (B) and choline oleate (C) in water. The compositions between 1 wt% and 100 wt% (in 2.5 wt% steps at phase border in 0.5 to 1 wt% steps) surfactant in water were investigated in a temperature range of 0°C to 95°C in 2-5°C steps. The temperatures near the phase borders have a precision of $\pm$ 1°C and $\pm$ 1 wt%. Visual observations with crossed polarizers allow one to identify the phases and phase boundaries as anisotropic (x), isotropic (○) or biphasic (▼).

4.3.4 Small (SAXS) and wide (WAXS) angle X-ray scattering data and analysis

In the following part the SAXS and WAXS data and the calculated structural parameter of the three binary phase diagrams are illustrated. The phases were recorded in 1 wt% to 5 wt% steps to show concentration dependent changes in the structure. In addition, this technique was used to verify the phase borders. All SAXS and WAXS data and spectra are shown in Appendix B.

4.3.4.1 Discontinuous cubic phases $I_1´$ and $I_1´´$

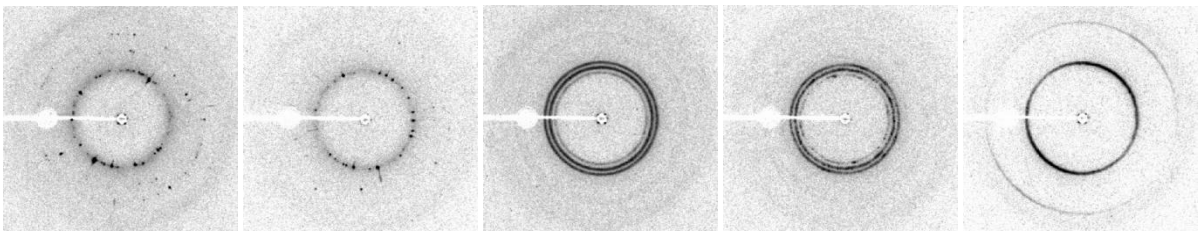

Figure 4-3. Two-dimensional X-ray spectra of different points in the binary choline decanoate with water phase diagram: Pictures from left to right; $I_1´$ 40 wt% ChC_{10}; $I_1´$ 43.8 wt% ChC_{10}; $I_1´´$ 49 wt% ChC_{10}; $I_1´´$ 51.8 wt% ChC_{10}; H_1 60 wt% ChC_{10}.

As already mentioned, the binary phase diagram of choline decanoate contains two discontinuous cubic phases $I_1´$ and $I_1´´$ between the micellar phase L_1 and the hexagonal phase H_1, whereas choline octanoate and choline oleate do not form these micellar cubic phases in water. Normally, these two discontinuous cubic phases do not appear in binary surfactant systems. They are more typical for aqueous systems of monoacylglycerols[35] or membrane lipids like lysophosphatidylcholine[35]. However, dodecyltrimethylammonium chloride shows even two cubic phases between the micellar L_1 and hexagonal H_1 phase.[36] Cubic phases form a three-dimensional lattice (isotropic phase), but they possess no short-range order. This means for example that the hydrocarbon chains are disordered compared to a hexagonal or lamellar liquid crystalline phase and can grow to form big monocrystals. Thus, a proper powder spectrum cannot be expected, instead a dotted X-ray pattern is found.[1,35,36] In **Figure 4-3**, a decrease of the number of dots is observed as well as the formation of continuous rings with increasing choline decanoate concentration, especially when comparing the different two-dimensional X-ray spectra ranging from discontinuous cubic phase $I_1´$ through $I_1´´$ to the hexagonal phase H_1. The second discontinuous cubic phase $I_1´´$ shows more continuous rings and fewer dots in the 2D spectra.

The cubic phase $I_1´´$ could be identified as a P*m*3*n* discontinuous cubic phase. The $I_1´$ phase shows a different pattern compared to $I_1´´$ and is more difficult to characterize. For the characterization models of primitive, body-centered and face-centered cubic phases[35] like

P43*n*[37], $P4_232$[36], F*m*3*c*, F*d*3*m* have been tested, because they often accompany a P*m*3*n* phase.[38]

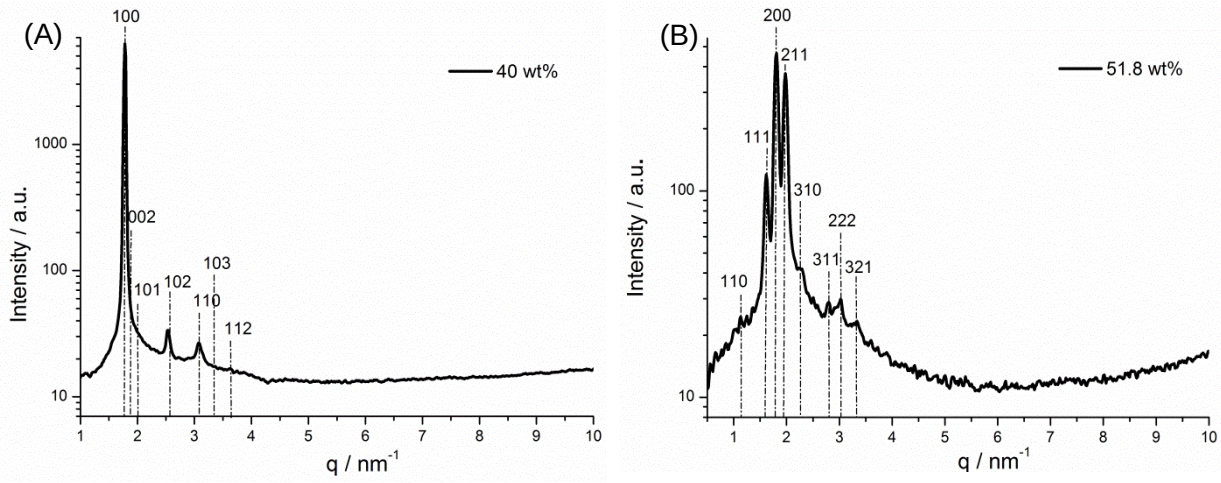

Figure 4-4. Radially averaged SAXS profile of (A) 40 wt% ChC_{10} ($I_1´$) and (B) 51.8 wt% ChC_{10} ($I_1´´$) taken at 25°C. The Miller indices of the reflections that were expected for the $P6_3/mmc$ structure ($I_1´$) or P*m*3*n* structure ($I_1´´$) are indicated with vertical dotted lines.

4.3.4.1.1 Discontinuous cubic phase $I_1´$

This discontinuous cubic phase $I_1´$ is shown in the spectra of samples containing 40 wt% ChC_{10} (see **Figure 4-4** (A)) and 43.8 wt% ChC_{10} (see Appendix B). The phase is very temperature sensitive and melts to a micellar solution above 40°C. This type of discontinuous cubic phase was first discovered in the binary system of nonionic surfactant $C_{12}EO_8$ and water and was investigated by Clerc.[38,39] It has recently been detected in the binary system of long chain choline carboxylates ChC_m with m = 12-18 and water.[1] It could be characterized as a 3D-periodic phase with regular packed direct micelles. All micelles are crystallographically equivalent. The space group shows a hexagonal compact structure of the type $P6_3/mmc$.[38, 39] **Figure 4-4** shows that not all expected reflections for the $P6_3/mmc$ phase could be indexed properly. One reason could be that cubic phases form big crystals and with the used setup this phase could not be measured with a sufficiently high precision. Assuming the $P6_3/mmc$ structure and knowing the volume of the choline decanoate surfactant molecule V_s (see section 4.5.2.8) and the volume fraction of choline decanoate Φ_s the unit cell parameter a of the discontinuous cubic phase $I_1´$ at 25°C is given by the following equation (1):[39,1]

$$a = d\sqrt{\frac{4}{3}(h^2 + k^2 + hk) + \frac{l^2}{R^2}} \qquad (1)$$

The ratio R = c/a for a hexagonal close packing (with unit cell parameter a = b ≠ c) is given in literature as 1.633.[39] For the 40 wt% ChC_{10} and 43.8 wt% ChC_{10} sample an R value of 1.64 was found with the lowest statistical error. This is in the range of a hexagonal packing with quasi-spherical shaped micelles. The volume of the unit cell $V_{unit\ cell}$ and the micelle aggregation number N_{agg}, taking into account two micelles per unit cell, can be calculated. For the calculation the volume of the choline decanoate surfactant molecule V_s and the volume fraction of choline decanoate Φ_s have to be known.[1, 38, 39]

$$V_{\text{unit cell}} = \frac{\sqrt{3}}{2} Ra^3 \qquad (2); \quad N_{agg} = \frac{V_{\text{unit cell}} \frac{\Phi_s}{V_s}}{2} \qquad (3)$$

The obtained values are shown in **Table 4-1**.

wt% ChC_{10}	$V_{unit\ cell}$ / nm³	a / Å	N_{agg}
40	96.9	40.9 ± 0.4	42
43.8	95.8	40.7 ± 0.3	46

Table 4-1. Volume of the unit cell $V_{unit\ cell}$, cell parameter a and aggregation number N_{agg} of the discontinuous cubic phase with $P6_3/mmc$ structure in the aqueous choline decanoate system at 25°C.

4.3.4.1.2 Discontinuous cubic phase I_1''

The second discontinuous cubic phase forms a P*m*3*n* structure. It is a primitive cubic lattice, which is often found between the micellar L_1 and the hexagonal H_1 phase in binary phase diagrams of surfactants. It shows the following X-ray pattern: $\sqrt{2} : \sqrt{4} : \sqrt{5} : \sqrt{6} : \sqrt{8}$.[40, 41] Eriksson *et al.* described the P*m*3*n* structure by a three-dimensional network structure of rod like micelles.[35] Two different types of micelles exist. All in all, the unit cell contains eight micelles. Six of them have a slightly ellipsoidal shape, the other two are more spherical.[39,41]
The present case is described assuming eight spherical micelles. The aggregation number N_{agg} is calculated according to equation (4):[1]

$$N_{agg} = \frac{V_{\text{unit cell}} * \frac{\Phi_S}{V_S}}{8} \qquad (4)$$

taking into account the cell parameter a, the volume fraction of the surfactant Φ_s, the aggregation number N_{agg} and the volume of the unit cell $V_{unit\ cell}$. For different concentrations of choline decanoate the following parameters are obtained for this discontinuous cubic phase I_1'' (see **Table 4-2**):

wt%	45.9	51.8	53.9
a / Å	80.7 ± 0.1	77.8 ± 0.1	76.9 ± 0
Φ_s	0.460	0.519	0.540
N_{agg}	66	66	67
$V_{unit\ cell}$ / nm^3	525.8	471.0	455.1
T / °C	25	25	25

Table 4-2. Cell parameter a, volume fraction of the surfactant Φ_s, aggregation number N_{agg} and volume of the unit cell $V_{unit\ cell}$ are detected of the discontinuous cubic phase of choline decanoate with P*m*3*n* structure.

Table 4-2 shows that the cell parameter a and the volume of the unit cell $V_{unit\ cell}$ slightly decrease with increasing choline decanoate concentration, whereas the aggregation number N_{agg} remains constant. This illustrates a closer packed structure with increasing concentration. Comparing these numbers with the results of Klein *et al.* for the choline carboxylates ChC_m with m = 12-18, they are in good agreement.[1] The cell parameter increases with increasing chain length. The increase is not linear: ChC_{10} a ≈ 78.5 Å; ChC_{12} a ≈ 90 Å; ChC_{14} a ≈ 106 Å; ChC_{16} a ≈ 124.9 Å.[1] Hence, the oblate micelles do not grow linearly. Furthermore, the structures vary from almost spherical oblate micelles to a more flat oblate aggregate with increasing chain length and the aggregation number increases again with increasing chain length.[1] The P*m*3*n* phase formed by choline decanoate, a short chain choline carboxylate, and water is very temperature sensitive. The melting of this phase at higher temperatures is observed only in the binary phase diagram of choline decanoate and not in those of long chain choline carboxylates.[1] The aggregation number in the micelle, as mentioned above, decreases with decreasing alkyl chain length. Thus choline decanoate forms in general smaller micelles. The melting of the cubic phase into micellar phase must be due to the smaller aggregates formed with surfactants with short alkyl chain. With temperature increase the mobility of the micelles gets higher than the interaction between the micelles and results in the melting of the cubic phases (same for I_1').[23]

4.3.4.2 Hexagonal phase H_1

The hexagonal phase appears in all three binary phase diagram systems. Cylindrical micelles with infinite size are packed in a hexagonal planar cell with cell parameter a.[42] In the case of choline decanoate a transition from a P*m*3*n* phase to a hexagonal phase occurs. An epitaxial relationship, where the {211} plane of the discontinuous cubic phase P*m*3*n* is converted to the {100} plane of the hexagonal phase[1,42,43], could be neglected. The long chain choline carboxylates do not show this transition behavior either.[1] The transition behavior of choline octanoate will be discussed in section 4.3.4.6. The one of choline oleate was not investigated further. A transition from a micellar phase, which contains rod like micelles, to a hexagonal phase should take place for choline oleate with water.[23] Only little

information about the binary phase diagrams of sodium or potassium octanoate with water and sodium or potassium decanoate with water could be found in literature. Therefore, the structural parameter of the hexagonal phases cannot be compared. For sodium oleate and potassium oleate following values were found in the literature. The cross sectional area a_s increases with increasing counterion and decreasing couterion headgroup association: sodium oleate (a_s = 55 Å^2 at 100°C and a_s = 52 Å^2 at 65°C)[1,7], potassium oleate (a_s = 58 Å^2 at 100°C and a_s = 52 Å^2 at 20°C).[1,7] Choline oleate does not behave as expected, the cross sectional area is smaller (a_s = 51.9 ± 1.7 Å^2 at 55°C and 28 wt% choline oleate). Comparing the cross sectional area a_s of the alkali stearate with the respective alkali oleate, a small increase is found and in the case of lipophilic radius r_L a decrease.[5, 7] Thus, alkali oleate forms smaller cylindrical micelles, which are not so closely packed.[7] The same is found when comparing choline oleate with choline stearate (ChC_{18}: a_s = 52 Å^2 at 50°C[1]; choline oleate: a_s = 52.8 ± 1.6 Å^2 at 55°C and 31 wt% choline oleate). As it has been already observed, the cross sectional area a_s increases even with temperature and the lipophilic radius r_L decreases. The calculated values for choline oleate were recorded at 25°C and 55°C. So, they cannot be exactly compared with the alkali analogs, which were measured at higher temperature because of the higher Krafft temperatures (31 wt% choline oleate a_s = 50.2 ± 1.5 Å^2 and r_L = 19.3 ± 0.6 Å at 25°C; a_s = 52.8 ± 1.6 Å^2 and r_L = 18.4 ± 0.5 Å at 55°C). By comparing the existing data for different temperatures one can at least state that the tendencies are not similar for the alkali oleate and choline oleate, but the relation between choline stearate and choline oleate is the same as for the alkali homologs.[1, 5, 7] For choline octanoate and choline decanoate the lipophilic radius r_L is 8-10 % smaller than the fully extended length of the alkyl chain. Klein *et al.* found[1] that the effective headgroup area a_s decreases with decreasing alkyl chain length from choline octadecanoate with 52 Å^2 to 46 Å^2 for choline dodecanoate. Here an average value of a_s for choline decanoate of 45 Å^2 and 44.2 Å^2 for choline octanoate was found. These values are in good agreement with the values of the longer chain surfactants.

To summarize, the cross sectional area a_s (see **Figure 4-5** (B)) and the interlayer spacing d (see **Figure 4-5** (C)) decrease with increasing surfactant concentration, while the lipophilic radius r_L (**Figure 4-5** (D)) increases. This can be explained by a stronger and closer packing of the cylindrical micelles in the hexagonal phase with increasing surfactant concentration.

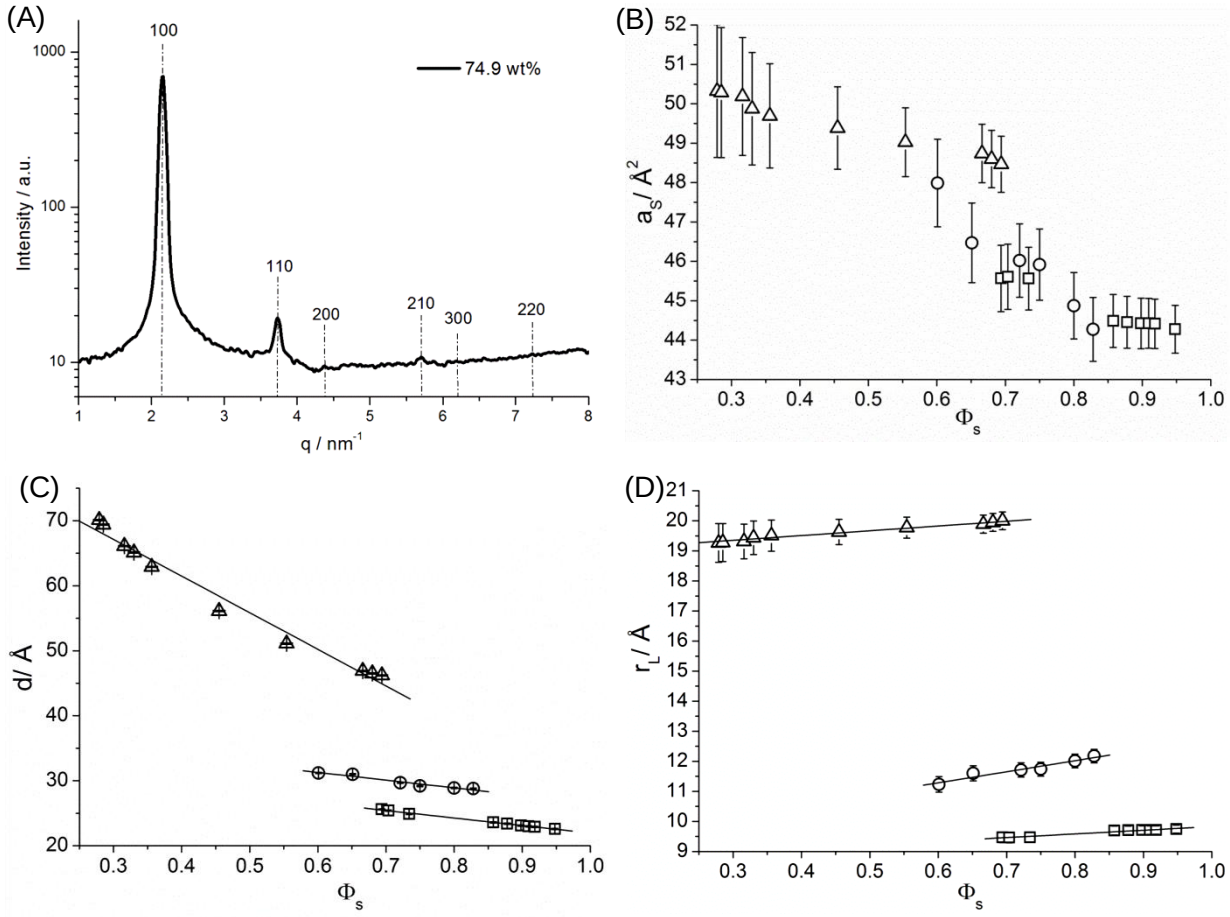

Figure 4-5. (A) Miller indices for the hexagonal phase at 74.9 wt% ChC_{10} at 25°C; (B) cross sectional area at polar-nonpolar interface a_s as a function of volume fraction of surfactant Φ_s for the hexagonal phases; (C) d-interlayer spacing of the Miller index [100] of the hexagonal phase as a function of volume fraction of surfactant Φ_s; (D) radius of the lipophilic part r_L as a function of the volume fraction of surfactant Φ_s of the hexagonal phase; hexagonal phase is formed by choline octanoate (□), choline decanoate (**O**) choline oleate (Δ**)** with water at 25°C. For the calculation of the error bars the following uncertainty was estimated $\Delta q = 0.01$ nm^{-1} and $\Delta\Phi_L = 0.01$.

4.3.4.3 Bicontinuous cubic phase V_1 with I*a*3*d* stucture

The bicontinuous cubic phase identified in the systems of choline decanoate and choline oleate could be clearly assigned to an I*a*3*d* structure. I*a*3*d* is a body centered space group (see **Figure 4-6** (A)). I*a*3*d* is a typical cubic lattice found in several lipid and soap systems between the hexagonal phase H_1 and the lamellar phase L_α.[35] The structure belongs to the gyroid type (G)[23,44] and is described by infinite periodic minimal surfaces.[45,46,44] The bicontinuity is given by two equivalent surfactant media separated by a water film.[47]

In the literature Rancon and Charvolin[43] and later on in a more detailed study Clerc *et al.*[47] spotted an epitaxial relationship for the transition from hexagonal phase H_1 into bicontinuous cubic phase V_1. This epitaxial relation was found between the planes of highest substance density. The {100} plane of the hexagonal phase is transferred into the {211} plane of the cubic phase. The epitaxial relation can be ruled out for the hexagonal to bicontinuous cubic

phase transition in the binary diagram of choline decanoate or choline oleate, because the required condition given by Rancon and Charvolin is not fulfilled. They stated that $2*d_{211}/\sqrt{3}$ of the cubic phase should be equal to the d_{100} spacing of the hexagonal phase.[42, 43, 48]

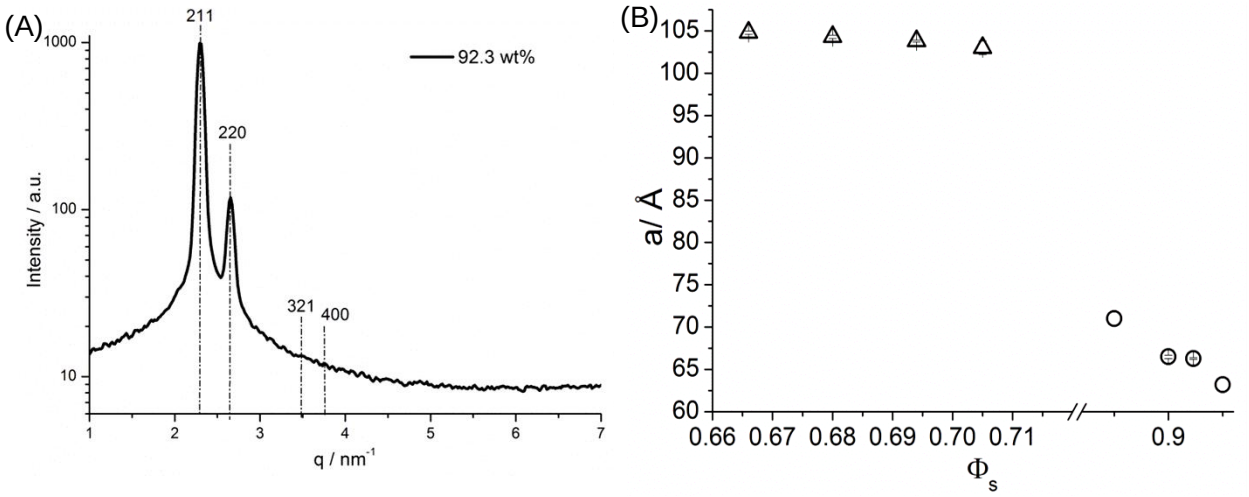

Figure 4-6. (A) Miller indices for the bicontinuous cubic phase V_1 of 92.3 wt% choline decanoate at 25°C; (B) Cell parameter of the bicontinuous cubic phase V_1 of choline decanoate (o) at 25°C and choline oleate (Δ) at 80°C versus the surfactant volume fraction Φ_s. For the calculation of the error bars the following uncertainty was estimated $\Delta q = 0.01$ nm^{-1} and $\Delta\Phi_L = 0.01$.

In this phase the d_{211}-spacings of the highest electron density decrease with increasing surfactant concentration. The unit cell parameter a decreases simultaneously (see **Figure 4-6** (B)). This is caused by a closer packing of the molecules with increasing concentration. In agreement with the concept of infinite periodic minimal surfaces the effective headgroup area is reduced, whereas the alkyl chains are more expanded. However, it should be noted that the calculation of the effective headgroup area a_s and the length of the lipophilic part r_L cannot be done easily taking into account the concept of the infinite periodic minimal surface. This was also seen in other studies.[1] The dimensions of the values of the unit cell parameter a are in accordance with the values found in earlier studies on the long chain choline carboxylates[1] and alkali carboxylates[7,41].

Choline octanoate could not form in water a bicontinuous cubic phase. In the choline octanoate system the intrinsic radius of curvature R_0 should be very high because of the short octanoate chain and the large effective headgroup area. But at higher surfactant concentration the packing parameter favors aggregates with small curvature to lower the unfavorable interaction of water with the hydrophobic chain area at the chain-headgroup interface and to decrease the free energy of packing of the hydrocarbon chains. Therefore, the lowest value for the elastic free energy and a minimal packing energy of the hydrocarbon chains is given by a hexagonal to lamellar phase transition with increasing concentration of choline octanoate.[35,49,50]

4.3.4.4 Interlayer phase

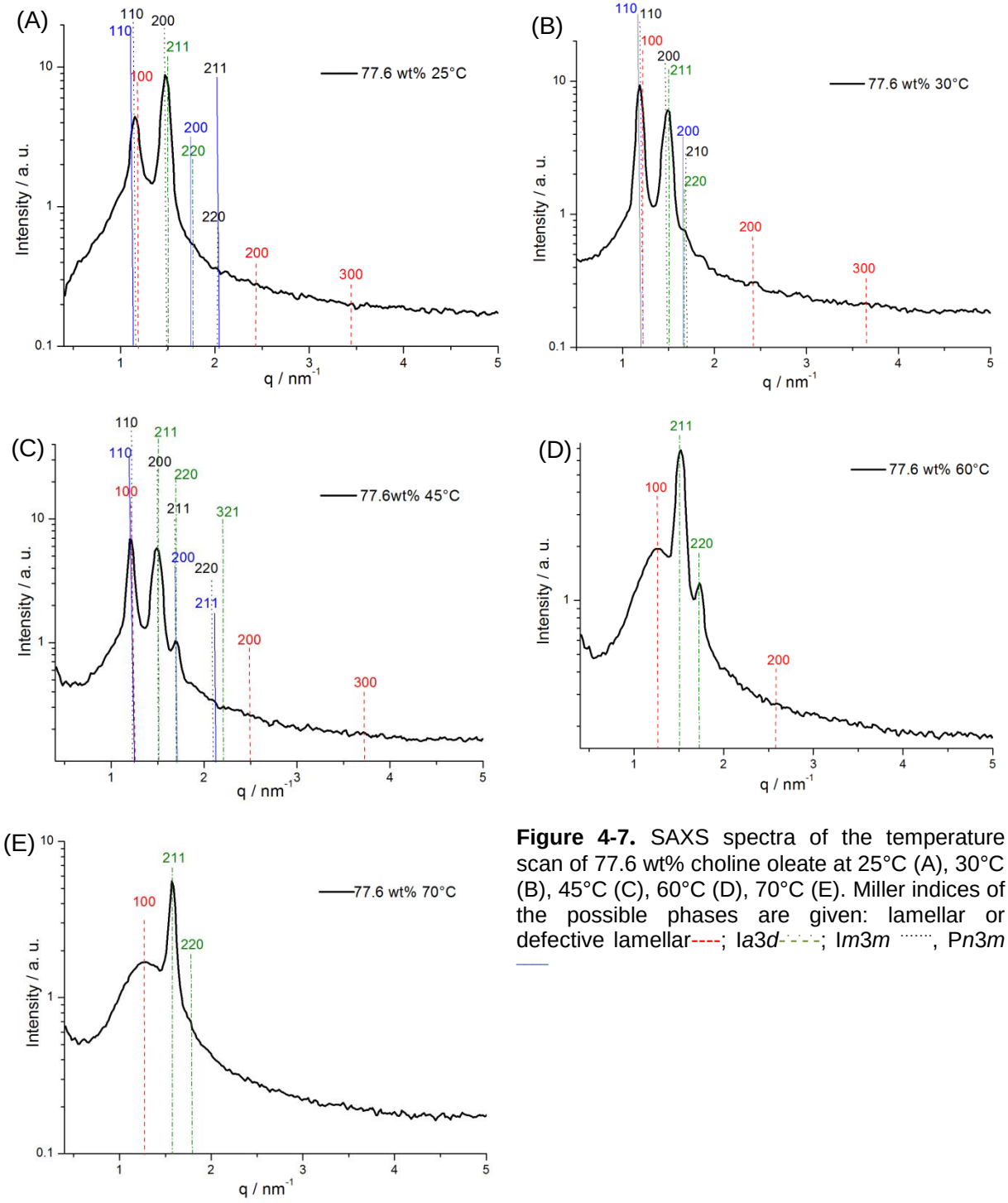

Figure 4-7. SAXS spectra of the temperature scan of 77.6 wt% choline oleate at 25°C (A), 30°C (B), 45°C (C), 60°C (D), 70°C (E). Miller indices of the possible phases are given: lamellar or defective lamellar----; I*a*3*d*-·-·-; I*m*3*m* ·····, P*n*3*m* ——

Choline oleate shows additional phases as compared to choline octanoate and choline decanoate. A two or multi phase system is located between the bicontinuous cubic phase V_1 and the defective lamellar phase dL_α or nematic phase N. It could be that this region even exists for the choline octanoate and choline decanoate system, but the existence region could be too small and not detectable with the used methods. For the system hexaethylene glycol mono-n-dodecylether in water Rancon and Charvolin found an epitaxial phase

transition between the plane of highest electron density of the bicontinuous cubic phase V_1 and the one of the lamellar phase L_α.[43] This phase transition can be ruled out for choline oleate. The condition for this relationship is that d_{211} of the bicontinuous phase and d_{100} of the lamellar phase are equal[43], which is not the case for choline oleate.

Furthermore, this interlayer phase region is featured by a birefringent texture under the polarizing optical microscope. With SAXS this temperature dependent multi or biphasic system could be analyzed in details at 77.6 wt% choline oleate. This concentration was measured at 25°C, 30°C, 45°C, 60°C and 70°C (see **Figure 4-7**). A defective lamellar phase and bicontinuous cubic phases with I*a*3*d* (G, gyroid type), I*m*3*m* (P, primitive type) and P*n*3*m* (D, diamant type) structure could be indexed for the different phases at the above mentioned temperatures. The bicontinuous cubic phases can be described with the model of infinite periodic minimal surfaces (IPMS).[35,51] The transition energy between these three phases is smaller than 0.01 kJ mol^{-1}.[35,51] Thus, it is possible, that they exist simultaneously or could be transferred easily into each other (transition energy for liquid crystalline phases is normally higher than 1 kJ mol^{-1}).[35,51] In general this interlayer phase seems to be a phase of different types of curvatures. This explains also the simultaneous existence of different phases. An equilibrium between choline oleate and water on the one side and the strong base choline hydroxide (pK_a of 13.9)[52] and oleic acid ($pK_a \approx 5$)[53] on the other side could be formed.[54] Therefore, two types of headgroups are available as these are the carboxylic acid group (-COOH) and the carboxylate group ($-COO^-$). On account of the two different headgroups different curvatures could be created and result in the simultaneous existence of different bicontinuous cubic phases. Also the existence of a defective lamellar phase[32, 55] could be explained further to the bicontinuous cubic phases.

4.3.4.5 Defective lamellar phase dL_α or nematic phase N

All three binary phase diagrams comprise as phase with highest concentration of soap a birefringent phase that looks like a defective lamellar dL_α or a nematic N phase (see **Figure 4-8**). Indeed, the light microscopy pictures under crossed polarizers show “Schlieren” textures that could be typical of a nematic phase (see **Figure 4-8** (B)).[32, 33, 55] Moreover, their corresponding reflection patterns in SAXS present only a broad first order reflection without a second or a third Bragg peak. At these concentrations, the second order is not observed due to the first minimum of the bilayers form factor, but it should re-appear when varying the concentration within this small domain of existence. Another explanation is the absence of a long range order along the normal to the layers. Locally this phase forms a lamellar bilayer that can be staked with a short periodicity and characterized by a first order reflection. But defects, formed because of strong local curvature, destroy the long range order of this staking. To differentiate between a defective lamellar phase with holes or long dislocations

and a nematic phase formed by disc-like micelles PFG-NMR should be performed on oriented samples to analyze water diffusion process parallel or perpendicular to the lamellae. These defects could be created due to the simultaneous existence of two types of amphiphiles characterized by either carboxylic acid headgroup or a carboxylate headgroup. Two different headgroups (-COOH, -COO^-) with two different surfaces per polar head can effectively create different curvatures (a detailed description is shown in Chapter 5). The longer chain choline carboxylates do not form this defective lamellar or nematic phase. They create a true lamellar phase as highest concentrated phase.[1] In the following part we can nevertheless compare this structure with the lamellar phases formed normally in this region in the case of sodium soaps and long chain choline carboxylates. Assuming a perfect mixing of two types of soap bilayer thicknesses (if they really exist), the effective headgroup areas and the other parameters can be calculated from the first order peak position and the species concentrations.

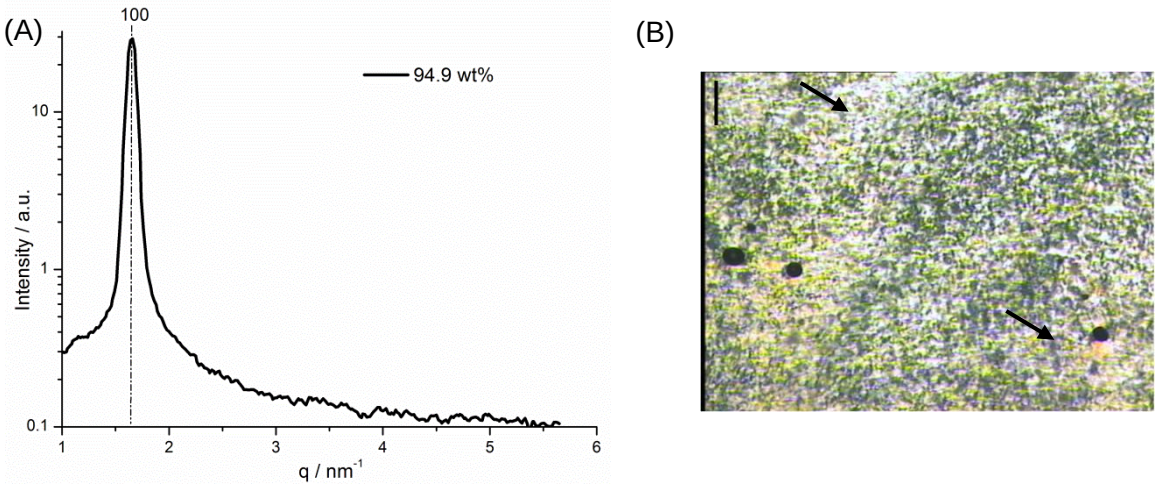

Figure 4-8. (A) SAXS spectrum of a defective lamellar phase dL_α or nematic phase N at 94.9 wt% choline oleate and 25°C. Theoretical peak position is indicated by the vertical line and indexed with the Miller index. A broad first order reflection is seen but the second and third order reflections are missing. (B) Light microscopy image of 94.9 wt% choline oleate shows "Schlieren" typical of a defective lamellar or nematic phase texture (see arrows) (100x magnification).[32] The scale bar is 100 µm.

The parameters and results which were obtained from the SAXS experiments (see **Table 4-3**) are in good agreement with the ones of the long chain choline carboxylates.[1] As expected, the headgroup areas a_s of the choline surfactants are larger than the ones found for the alkali analogs, for example KC_8 at 86°C and 83.2 wt% has a_s = 30.1 Å^2 in comparison to ChC_8 at 25°C and 96.1 wt% having a_s = 36.9 Å^2; KC_{10} at 86°C and 82.8 wt%: a_s = 31.0 Å^2 in comparison to ChC_{10} at 75°C and 96.9 wt%: a_s = 37.6 Å^2.[56] This again supports the idea that large, "soft" counterions show a low interaction with the carboxylate headgroups.[1,34] As can be seen in **Table 4-3**, the d_{100} values decrease with increasing concentration, in the same way the half length of the lipophilic part r_L increases with increasing concentration. The

packing of the bilayer gets closer and the chains are more expanded. This leads to a decrease of the headgroup area a_s with increasing concentration (see **Figure 4-9** (B)). However, a temperature effect is observed. It is observed that with increasing temperature the headgroup area increases and in parallel the half length of the lipophilic part r_L decreases (see Appendix B in section B.1.5).

	wt%	Φ_S	d_{100}/ Å	(r_S-r_L)/ Å	d_W/ Å	d_L/l_{max}
ChC_8 25°C	96.1	0.960	22.7	5.1	0.9	1.1
	96.8	0.967	22.7	5.1	0.7	1.1
	98.0	0.980	22.6	5.2	0.5	1.1
	98.4	0.984	22.5	5.2	0.4	1.1
	98.8	0.988	22.5	5.2	0.3	1.1
ChC_8 40°C	96.8	0.967	22.4	5.1	0.7	1.1
	98.4	0.984	22.3	5.1	0.4	1.1
	99.0	0.990	22.2	5.1	0.2	1.1
ChC_{10} 75°C	96.9	0.969	25.2	5.1	0.8	1.1
	98.1	0.981	25.0	5.1	0.5	1.1
	98.9	0.989	24.9	5.1	0.3	1.1
ChC_{10} 80°C	92.3	0.923	26.8	5.1	2.1	1.1
Choleate 25°C	82.8	0.832	39.3	4.3	6.6	1.0
	91.3	0.915	38.8	4.7	3.3	1.1
	94.9	0.950	38.1	4.8	1.9	1.2
	98.9	0.989	37.0	4.8	0.4	1.2
Choleate 80°C	94.9	0.950	36.5	4.6	1.8	1.1
	98.9	0.989	34.3	4.5	0.4	1.1

Table 4-3. Structural parameters of the locally lamellar parts in the defective lamellar or nematic phase of ChC_m with m = 8, 10 and oleate, as deduced from SAXS measurements: d_{100} values, the thickness of the headgroup counterion layer (r_S-r_L), the thickness of the water layer d_W and (d_L/l_{max}) at different surfactant concentrations and temperatures.

Taking into account the values of the thickness of the headgroup and counterion layer, the (r_S-r_L)-values of **Table 4-3**, and also the ones from the long chain choline carboxylates[1], it is obvious that the thickness of the headgroup and counterion layer is not very dependent on concentration, temperature and alkyl chain length and not on the saturation of the alkyl chain either. The (r_S-r_L)-value is between 4.3 Å and 5.2 Å. An extended choline cation has a length of 8 Å.[1] Therefore, choline must be located perpendicular and not parallel to the alkyl chain length. The ratio of (d_L/l_{max}) indicates that the half length of the bilayer r_L is less or equal to the one of a fully expanded alkyl chain l_{max}. Comparing the half length of the lipophilic bilayer r_L and the headgroup area a_s of choline oleate with the one of choline octadecanoate, a small influence of the double bond can be found. The double bond provokes the opposite effect as in the case of the hexagonal phases. It induces a smaller headgroup area a_s in the defective lamellar phase and also causes more expanded chains compared to the alkyl chains of choline octadecanoate in the lamellar phase.[1]

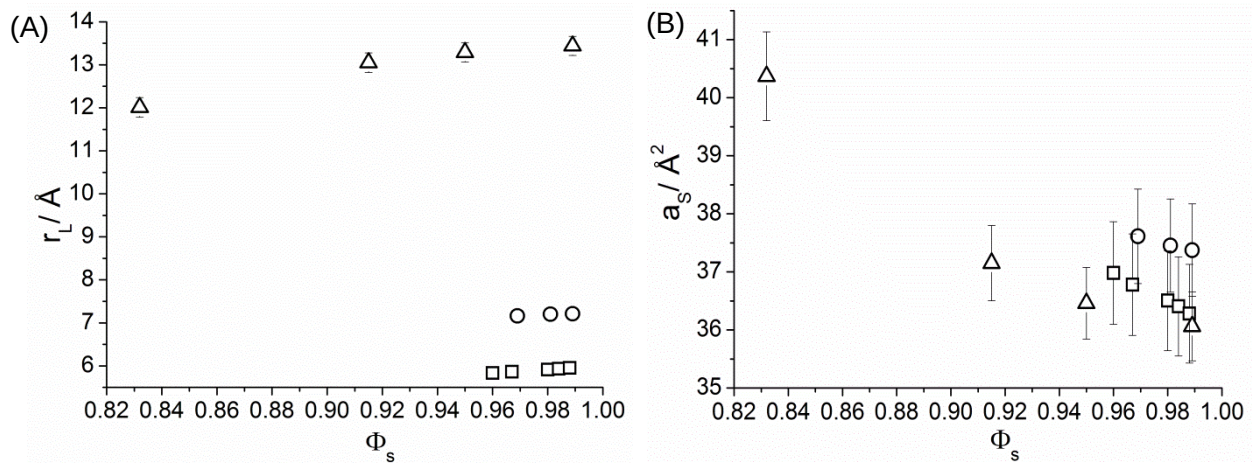

Figure 4-9. (A) Half length of the lipophilic bilayer r_L in the lamellar parts of the defective lamellar or nematic phase of choline octanoate (□), choline decanoate (**O**), and choline oleate (Δ) as a function of the surfactant volume fraction Φ_S; (B) Headgroup area a_s of choline octanoate (□), choline decanoate (**O**), and choline oleate (Δ) in the lamellar parts of the defective lamellar or nematic phase as a function of the surfactant volume fraction Φ_S. For the calculation of the error bars the following uncertainty is estimated: $\Delta q = 0.01$ nm^{-1} and $\Delta\Phi_L = 0.01$.

4.3.4.6 Extended isotropic, micellar phase of choline octanoate in water

The binary phase diagram of choline octanoate shows a huge extended area of an isotropic, liquid solution. This isotropic solution expands up to 70 wt% choline octanoate in the temperature range from 0°C to 95°C and over the entire mixing range at temperatures ranging from 70°C to 95°C (see **Figure 4-2** (A)). To characterize this solution area small (SAXS) and wide (WAXS) angle X-ray scattering, conductivity, and rheological experiments were performed.

According to the WAXS spectra choline octanoate does not form any big aggregates or crystals along the whole concentration range. Also, with polarizing optical microscopy only an isotropic solution was observed for the temperatures and concentrations, in which the isotropic liquid phase exists.

However, the SAXS spectra (see Appendix B in section B.2) measured at 70°C indicate aggregates. To get further inside into the structure, the q-dependence of the first peak maximum of the scattering intensity on the surfactant volume fraction Φ_s was investigated. A decrease of the d-values (in nm) of the first peak maximum of the scattering intensity with increasing choline octanoate concentration is found (see **Figure 4-10** (A)). Taking into account the three dimensional dilution law for spherical aggregates that can be written as follows:[57]

$$\log(d) = \frac{1}{3}\log(K \cdot V_{mic}) - \frac{1}{3}\log(\phi_s) \qquad (5)$$

the different packing types can be accounted for by the constant *K* (for face centered cubic packing $K = \sqrt{2}$).[57] A change in the slope of $-\frac{1}{3}$ corresponds to no change in the form of the aggregates. The line of the logarithm of the d values versus the logarithm of the volume fraction of choline octanoate shows a mean slope of -0.264 (see **Figure 4-10** (A)) with even the possibility of two regimes. Anyway this slope (or these slopes) is (are) bigger than the required slope of $-\frac{1}{3}$ for spherical aggregates in solution along the whole concentration range. Thus it can be concluded that choline octanoate forms in water some spherical aggregates for which the shape and size certainly evolve along the whole concentration range.

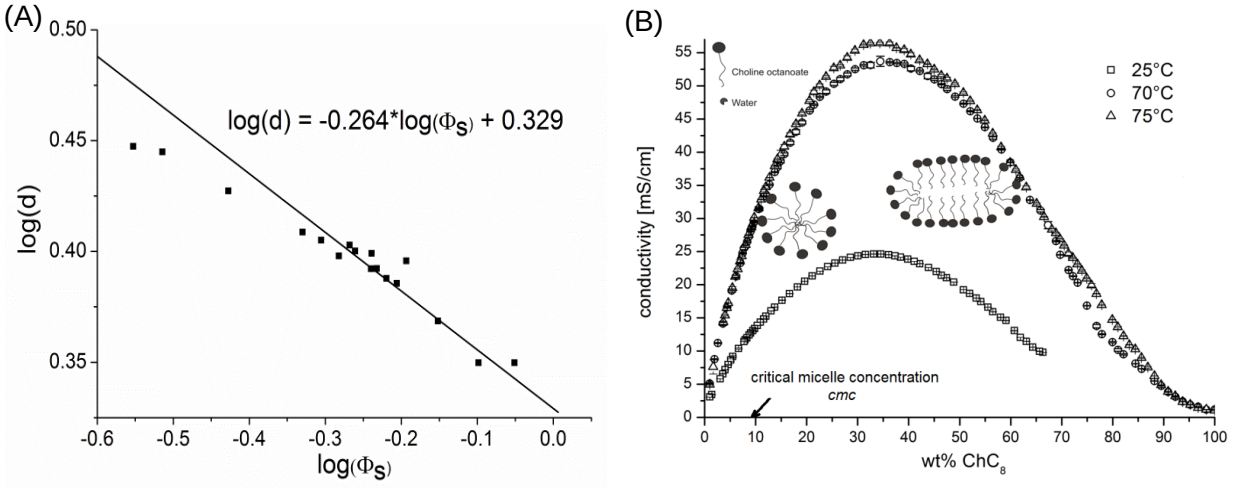

Figure 4-10. (A) Logarithm of the d-spacing log(d) as a function of the logarithm of the volume fraction of choline octanoate log(Φ_S). (B) Specific conductivity as a function of choline octanoate concentration (weight percent) at 25°C (□), 70°C (**O**), and 75°C (Δ): the assumed structures are included in the graph at the respective concentration range. The structure at high choline octanoate concentration (> 96 wt% choline octanoate) could not be determined clearly: two explanations might be possible as explained in the text.

SAXS measurements on different concentrated solutions at 25°C (see previous sections) show a direct change from micellar phase to hexagonal phase without the appearance of a discontinuous cubic phase. This phase transition can only occur via a continuous change of spherical micelles to rodlike, cylindrical micelles before they aggregate to a hexagonal phase.[23]

In conductivity measurements it is observed that the change in structuring is only dependent on the concentration (see **Figure 4-10** (B)) and not on the temperature (see Appendix B in section B.2, and **Figure 4-10** (B)). The conductivity behavior of choline octanoate in water is the same as room temperature imidazolium ionic liquids show in water.[58] On the other hand the shape of the concentration dependent conductivity curve is similar to the one found for the percolation in microemulsions when changing the concentration of the oil phase.[59] Such a percolating behavior in microemulsions is sometimes accompanied by a change in

viscosity[60,61] and in most cases the percolation point is temperature dependent.[61] These two points rule out a percolation behavior in this system.

Another point excludes phase percolation. Measuring the melting point of the hexagonal phase with differential scanning calorimetry with a heating rate of 10 K min^{-1} an average melting enthalpy of around 100 J mol^{-1} is obtained. This value is typical of the melting of a hexagonal phase to cylindrical, wormlike, not connected micelles. The enthalpy to invert the system must be in the kJ mol^{-1} range. However, one more important factor is the packing parameter. If the percolation model is considered at 25°C the aggregation number would change from 0.33 for spherical micelles to 1.2 for reversed cylindrical micelles and at higher concentration to a reversed hexagonal phase. The aggregation number had to decrease again to the aggregation number of 1 which characterizes a lamellar phase. This is against the packing rules.[21, 57]

The conductivity can be explained as follows: At low concentrations, the conductivity increases rapidly because of the high counterion mobility in the diluted aqueous medium. The conductivity of the spherical octanoate aggregates is low. At the highest conductivity value non-spherical, cylindrical, micelles are formed. The counterion mobility is hindered because of the cylindrical aggregates, which favor the aggregation of cations to lower the repulsive forces of the negative headgroups, and the further decrease of the water content (high soap concentration). At higher soap concentration the water layer between the aggregates gets thinner. For the structure in the isotropic solution above 96 wt% two possible options could be explained. One of this could be the appearance of inverted aggregates at very high concentrations (≥ 96 wt%) due to the low water content.[62] The water layer at this concentration above 96 wt% of choline octanoate between the cylindrical aggregates is so thin that choline cations form a shell around the less water molecules. Because of its charge this choline shell is surrounded with carboxylate anions. Thus, more or less reverse structures can be formed in a concentration range above 96 wt% choline octanoate and hide the charge (see **Figure 4-10** (B)). This model is also in agreement with the packing parameter N_s. For spherical micelles the packing parameter has always a value between 0 and 0.33. The packing parameter increases to 0.5 for cylindrical micelles (or normal hexagonal phase N_s = 0.5 and lamellar phase N_s = 1 for 25°C). Concerning the 70°C concentration line or higher the packing parameter changes from 0.5 for cylindrical micelles to higher than 1 for inverted aggregates at very high concentrations (≥ 96 wt%).[23, 63] However, another possible structure at very high concentration could be the existence of a molten salt which forms less ordered microstructure, such as disc like micelles.[62] From literature it is known that pure ionic liquids have a low conductivity.[58] The hexagonal phase melts to cylindrical aggregates in an isotropic solution. The lamellar phase melts to an isotropic solution where the liquid crystalline order is lost. Such a behavior was also found for

typical imidazolium ionic liquids in water. They show the same conductivity curve with decreasing water content.[58] The low conductivity is related to the very viscous system. Also this model is in agreement with the packing parameter. Therefore, the structure of the isotropic solution at very high soap concentration (≥ 96 wt%) could not be solved exactly. The measurements are in agreement with the two explained models.

In rheology experiments the shear stress and the dynamic viscosity were measured under constant shear rate. A Newtonian behavior is found for solutions with concentrations lower than 45 wt% of choline octanoate. At higher concentrations a non-Newtonian behavior is detected. Some of these samples could be described as shear-thickening solutions. The dynamic viscosity does not sensibly change in the measured concentration range from 30 wt% choline octanoate to 95 wt% choline octanoate (from 0.0033 Pas to 0.01 Pas). This minor ongoing increase can be ascribed to the increasing volume fraction of choline octanoate aggregates. The change in aggregate structure must be small and progressive. The continuous increase of viscosity (see **Figure 4-11**) with increasing concentration without a big change in viscosity can be explained by the Einstein equation and modifications of the Einstein equation for more concentrated systems with non-spherical micelles. The equation signifies that the viscosity is determined by the total volume fraction of choline octanoate aggregates and not by the size of the choline octanoate micelles or aggregates.[16,64] This explains the only slight increase in viscosity with increasing concentration. But in general, the solutions are very viscose. The shear-thickening behavior of choline octanoate water solutions with concentrations higher than 45 wt% is in agreement with the supposed mechanism. The viscosity increase occurs with increasing shear rate because of the water layer thinning between the aggregates with increasing shear rate.

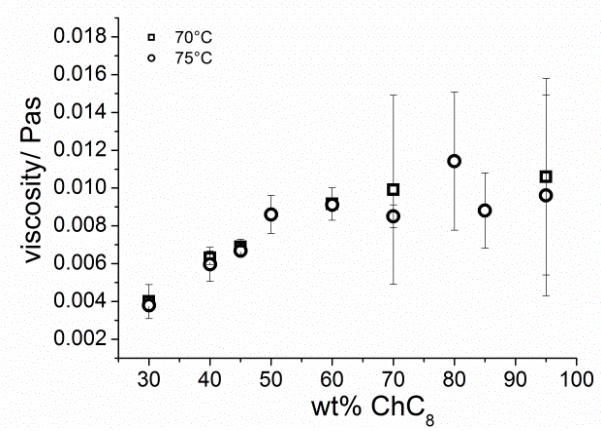

Figure 4-11. Tendencies of zero viscosity of different concentrated choline octanoate water solutions at 70°C (□) and 75°C (**O**).

It is interesting to consider the concentration dependent micellar solution of sodium octanoate, which was described by Ekwall *et al.*.[14-20] In their work they pointed out that at

higher concentrations sodium octanoate forms in water subsequently a hexagonal, bicontinuous cubic and lamellar phase. All of these phases are stable until 100°C. The melting of the hexagonal and lamellar phase in the binary phase diagram of choline octanoate is a result of the shape of the bulky and asymmetric choline cation and the low counterion-headgroup binding.[34] Ekwall established three changes in the concentration dependent behavior of the different physico-chemical parameters the density, partial specific volume, viscosity, vapour pressure, the counterion binding and in the activity of the caprylate ions, measured in various experiments.[14-20] The first change is ascribed to the formation of spherical micelles, the second to a change in water binding onto the micelles, and the third to a structural change of spherical micelles into cylindrical ones. The viscosity did not change very much with concentration. Only a slight increase was observed and a slight change in the slope of the viscosity curve with increasing concentration.[16, 17]

Choline octanoate in water forms spherical micelles (*cmc*) at 9.48 wt% (see Chapter 3). The second change in conductivity results from the change in micellar structure from spherical to cylindrical at around 40 wt% to 45 wt%. This can be demonstrated by conductivity and viscosity measurements. Choline octanoate does not show another breakpoint, as seen in sodium octanoate water solution, which results from different water binding to the carboxylate group of the octanoate molecule as triggered by the counterion. The binding of choline to the headgroup of the octanoate molecule is very low and does not affect the water binding to the octanoate.[34]

Taking into account all the results of these different experiments, the following concentration dependent, but not temperature dependent variations of the choline octanoate aggregates take place. With increasing concentration spherical micelles appear at the *cmc* at 9.48 wt% choline octanoate. These spherical aggregates undergo a transformation to cylindrical rod like micelles at 40 wt% to 45 wt%. The cylindrical micelles start to grow in an epitaxial way, until the interaction of the aggregates and the choline octanoate concentration is too high. Therefore, the aggregates get reversed with a few water molecules inside or it is also possible that molten salts are formed with a less ordered microstructure instead of reversed aggregates. However, it can be mentioned that the cylindrical micelles of choline octanoate are not linked with each other because no increase in the scattering intensity of the different concentration dependent SAXS spectra is seen.

4.3.4.7 Comparison with long chain choline carboxylates and alkali analogs

In the following part the short-chain choline soaps and choline oleate were compared to long chain choline carboxylate ones, ChC_m with m = 12-18, and to the sodium and potassium

analogs. However, the literature on the mesophase characterization concerning decanoate and octanoate soaps, with the exception of the micellar solution, is very limited.

- ChC_m with m = 12-18 form the following phases with increasing surfactant concentration: micellar phase L_1, discontinuous cubic phase I_1' and I_1'', hexagonal phase H_1, bicontinuous cubic phase V_1, and lamellar phase L_α. Beside these, they form intermediate phases between the hexagonal H_1 and bicontinuous cubic phase V_1. These intermediate phases are not found for choline carboxylates ChC_m with m = 8, 10 and oleate. Choline decanoate shows more or less the same lyotropic phase behavior. Choline octanoate forms no cubic phases and choline oleate no discontinuous cubic phases. However, all three choline carboxylates ChC_m with m = 8, 10 and oleate form as highest concentration phase a defective lamellar dL_α or nematic N phase in contrast to the long, saturated chain choline carboxylates.
- Compared to alkali soaps choline carboxylates show better solubility in water (the soap solubility increases from sodium soap to potassium soap and then choline soap[65]) and a lower Krafft temperature.[3,4,7,11,65]
- Neither sodium and potassium octanoate nor sodium and potassium decanoate form discontinuous cubic phases.[11]
- Sodium octanoate and sodium decanoate exhibit a bicontinuous cubic phase V_1 between the hexagonal phase H_1 and the lamellar phase L_α. Sodium decanoate additionally forms an intermediate phase (rod like micelles ordered in a deformed hexagonal lattice) between the hexagonal phase H_1 and the bicontinuous cubic phase V_1.[11]
- Potassium octanoate shows the following phase behavior with increasing surfactant concentration: micellar phase L_1, hexagonal phase H_1, bicontinuous cubic phase V_1 and lamellar phase L_α. Potassium decanoate shows two additional intermediate phases between the hexagonal H_1 and lamellar L_α phase separated by a bicontinuous cubic phase V_1.[11]
- Luzzati *et al.*[7] described the binary phase diagrams of potassium and sodium oleate. They have a higher Krafft boundary compared to choline oleate and show the phase behavior: micellar phase L_1, hexagonal phase H_1, rectangular phase, hexagonal complex phase, lamellar phase L_α. Earlier studies only mentioned two additional intermediate phases between the hexagonal phase H_1 and the lamellar phase L_α, but were not as precise as the studies of Luzzati *et al.*.[3,4,10]
- At higher temperatures choline octanoate forms an extended isotropic, micellar solution over the whole composition range.

4.4 Conclusion

Binary phase diagrams of choline octanoate, choline decanoate and choline oleate with water were determined and analyzed with SAXS and WAXS measurements, polarizing optical microscopy and visual observations. The expanded area of isotropic, micellar solution in the binary choline octanoate system was further studied with conductivity and viscosity measurements. The influence of the different alkyl chains on the phase diagrams is clearly detectable. Choline decanoate behaves similarly to the long chain choline carboxylates ChC_m with m = 12-18 and forms the following lyotropic phases with increasing concentration: micellar phase L_1, discontinuous cubic phase I_1' and I_1'', hexagonal phase H_1, bicontinuous cubic phase V_1, and defective lamellar phase dL_α or nematic phase N. The short chain in choline octanoate induces a large isotropic, micellar solution area in the binary phase diagram and is also responsible for the absence of cubic phases. The double bond in choline oleate hinders the surfactant molecule to create the discontinuous cubic phases, which are present in the binary phase diagram of choline octadecanoate. But all three substances form as highest concentrated phase a defective lamellar or nematic phase instead of a lamellar phase. The interphases, which are partly found in the binary phase diagram of the long chain choline carboxylates ChC_m with m = 12-18 between the hexagonal phase H_1 and the bicontinuous cubic phase V_1, could not be found for the two shorter chain choline soaps. Only choline oleate shows interphases between the bicontinuous cubic phase V_1 and the defective lamellar phase dL_α. It could be that the existence area for the choline octanoate and choline decanoate system is too small. These interphases could result from the simultaneous existence of two headgroups (-COOH and $-COO^-$). In general, the liquid crystal formation starts almost at the same surfactant concentration as in the case of the alkali homologs. Choline oleate and choline octadecanoate form liquid crystals above concentrations of about 22 wt% and 25 wt% of surfactant in water, respectively. The corresponding concentrations of choline octanoate and choline decanoate are in line with the longer chain ones and are shifted to higher values with decreasing alkyl chain length. Compared to the alkali soaps the choline analogs show a more extended hexagonal phase region and only a small defective lamellar or nematic phase region. Choline oleate possesses a lower Krafft temperature than the corresponding alkali soaps. Comparing the binary phase diagrams of the choline carboxylates ChC_m with $m > 8$ to the one of choline octanoate, a transitions from a surfactant to a hydrotrope can be seen in the case of choline octanoate.

All in all, using choline as cation in soaps is a valuable method to decrease their solubilization temperatures and to increase the micellar solution area in the binary phase diagram of short chain carboxylates. For choline oleate, the double bond lowers the Krafft

temperature compared to choline octadecanoate and further widens the range of possible applications of soaps.

4.5 Experimental

4.5.1 Chemicals and sample preparation

Choline octanoate, choline decanoate and choline oleate were synthesized and dried as explained in Chapter 3 in section 3.5.1. Choline octanoate is a slightly yellow powder, choline decanoate is a white powder and choline oleate is a slightly yellow gel. The samples for evaluation of the different lyotropic phases were prepared in the following way: 0.3 g of each sample was chosen, and the surfactant was weighed in the appropriate amount into glass ampoules of 1 cm diameter. The preparation was carried out in a nitrogen glove box to avoid water absorption and to obtain the right weight percents. Then, the exact amount of millipore water was added. The tubes were flame sealed. The closed tubes were centrifuged a few days at 40°C for 6000 rpm and afterwards homogenized at room temperature for several days. The different samples were observed over one and a half year to check if the samples are in thermodynamic equilibrium.

4.5.2 Methods

4.5.2.1 Krafft temperature T_{Krafft}

The Krafft temperatures of the different soaps were measured with a homebuilt apparatus.[66] It is able to monitor the turbidity of a sample by measuring the transmitted light, which is created by a LED with a light-dependent resistor (LDR). The temperature control is given by a computer-controlled thermostat, in which the samples are stored and heated with a constant heating rate of 1°C per hour. To measure the Krafft temperature, solutions of 1 wt% of soap in water were prepared.

4.5.2.2 Visual observation

The first and main characterization of the complete temperature and concentration dependent binary phase diagram was done by visual observations between crossed polarizers. Samples of 0.3 g were prepared from 0 wt% surfactant in water up to 100 wt% surfactant in water in 2.5 wt% steps and near the phase transition border in 0.5 wt% or 1 wt% steps, as explained above. They were temperature equilibrated in a water bath to obtain a temperature accuracy of 0.1 °C. They were recorded in the temperature range from 4°C to

95°C. The samples were controlled every 2-5°C through crossed polarizers. The heating rate was 5°C per hour. This procedure was done with different samples and in time distances of one to two days up to a year. The change in the phase borders was negligible and thermodynamic equilibrium was achieved very fast. Different phases could be identified by their relative viscosity and by polarizer proving their birefringent or isotropic pattern. The cubic phases I_1', I_1'' and V_1 could be identified very fast because of their isotropic appearance and their very high viscosity. The hexagonal phase is more viscous than the defective lamellar and can only appear right after the I_1'' phase. The defective lamellar phase occurs as the phase at highest soap concentration at temperatures around or higher than the Krafft temperature. It is less viscous.

4.5.2.3 Penetration scan

Penetration scans were performed under nitrogen atmosphere and following the same procedure as described by Lawrence.[28] Dry surfactant was added in small amounts between two microscope glass slides. A water drop was deposited on the border of the glass slides and penetrates slowly towards the center of the glass slides. The different mesophases appeared along the penetration way and were characterized by their texture. The phases occured in distinct rings around the center of the surfactant spot. The texture was visualized and monitored on a Leitz Orthoplan polarizing microscope (Wetzlar, Germany) equipped with a JVC digital camera (TK-C130). A Linkham hot stage with a TMS90 temperature controller ($\pm$ 0.5°C) and a CS196 cooling system was mounted. The recorded images had a magnification of 100x. The heating and cooling rate for all samples was around 10 K min^{-1} and the transition temperatures for the heating and cooling cycles were comparable. This method turned out to be very efficient, because the phases and the phase sequence can be rapidly characterized to first approximation with the help of crossed polarizers, and their distinct textures by tapping with a spatula on the glass slides.

4.5.2.4 Small and wide angle X-ray scattering

X-ray scattering measurements were performed at the Institute de Chimie Séparative de Marcoule (CEA/CNRS, UM2, ENSCM, France). The X-ray radiation was generated by a sealed molybdenum tube with a wavelength of λ = 0.71 Å. The tube was mounted on a bench built by XENOCS. A large two-dimensional automatic image plate system (MAR 345, MAR Research, diameter: 345 mm) is used for the scattered beam detection. The pixel resolution of the system was 150 x 150 µm.

The collimation system was a 12:∞ multilayer XENOCS mirror and with two sets of FORVIS scatterless slits the beam area was reduced to 0.8 x 0.8 mm^2. The attainable q-region was

0.2-30 nm^{-1} with an experimental resolution of $\Delta q/q = 0.05$ given by a sample to detector distance of 750 mm and an off-centered detection. The different samples were assembled in 3 mm thick aluminum cells, which were sealed with Kapton foil of 25 µm thickness. The temperature of the samples was controlled by a home-built heater resistance coupled to a Pelletier cooling base. A temperature range from -10°C to 120°C with $\Delta T = \pm 2$°C was achieved. The software FIT2D was used to integrate the two dimensional spectra. The azymuthal integration was performed to obtain the scattering intensity as a function of the scattering vector q (= $(4\pi/\lambda)\cdot\sin\theta$ with θ as the scattering angle and λ as the X-ray wavelength). The acquisition time of the different samples was between 1200 and 3600 seconds. For the spectra analysis only the peak positions were important. Thus, most of the data were shown without subtraction of the empty cell. Therefore, the peak at 4 nm^{-1} results from the Kapton foil.

4.5.2.5 Density

Density measurements were performed to obtain the molar volume and from this the effective molecular volume of the surfactants (see section 4.5.2.8). The density of different surfactant solutions in water of 1 wt% up to 20 wt% mostly in 2.5 wt% steps were measured at 25°C. For the measurements of the densities a vibrating tube densimeter (Anton Paar DMA 5000M) was used. The calibration of the instrument was done with standards.

4.5.2.6 Viscosity

Viscosity measurements were carried out on a Bohlin rheometer (type CVO 120 High Resolution) with a plate/plate geometry (P20mm) under argon atmosphere and at controlled temperature. The calibration was done with a standard oil. The different solutions were measured at 70°C and 75°C at shear rates ranging from 2.96 to 2000 s^{-1}. The viscosity was measured in the concentration range between 30 wt% and 95 wt% choline octanoate.

4.5.2.7 Conductivity

The concentration dependent conductivity was measured with a bar electrode from Metrohm with a cell constant of 0.9 cm^{-1} and a Pt1000 temperature control. This electrode was calibrated by Metrohm for 5°C to 70°C but was tested before even for higher temperatures. The calibration was done with KCl solution. The data were recorded by the program tiamo 2.3 and the 856 conductivity module. The measurements were performed using a homemade measuring cell so that the measurements could be performed under argon atmosphere. They were started at 100 wt% choline octanoate and water was titrated into the

surfactant in 0.5 wt%, 1 wt% or 2 wt% steps with the 905 Titrando from Metrohm. These measurements were done at 70°C and 75°C. The one at 25°C were started at 66 wt% choline octanoate. With these conductivity measurements only the relative evolution of conductivity with decreasing concentration could be recorded. Exact values were measured with an equipment developed by Barthel and co-workers.[67, 68] The calibration of the cell with cell constant 46.13 cm^{-1} was done according to the published procedure.[69] The temperature control was set up with a homemade precision thermostat combined with a cold source (Julabo FP40). The temperature stability of this combined thermostat was < 0.3°C in the temperature range of 25°C to 95°C. The whole concentration range from 0 wt% to 100 wt% could not be measured with this instrument because of problems in cell preparation with higher concentrated samples (see Appendix B in section B.2.2).

4.5.2.8 Calculations

Choline octanoate		Choline decanoate		Choline oleate	
wt%	**ρ in g L^{-1}**	**wt%**	**ρ in g L^{-1}**	**wt%**	**ρ in g L^{-1}**
1.03	997.39	1.00	997.25	1.00	996.61
2.56	997.94	2.50	997.54	2.50	996.16
5.12	998.94	5.00	997.57	5.00	994.74
7.68	999.95	7.50	997.46	7.49	994.60
10.24	1000.91	10.00	997.33	10.00	994.03
12.79	1001.61	12.49	997.11	12.48	993.49
15.33	1001.06	14.99	997.09	-	-
17.88	1002.32	17.49	996.66	-	-
20.42	1002.69	19.93	996.64	-	-

Table 4-4. Measured density values of choline octanoate, choline decanoate and choline oleate in the concentration range of 1 wt% to 20 wt% surfactant at 25°C.

The densities of concentrated aqueous choline carboxylate ChC_m (with m= 8, 10 and choline oleate) solutions (see **Table 4-4**) were measured with a vibrating tube densiometer DMA 5000M of Anton Paar at 25°C (see 4.5.2.5). All the solutions were clear. The molar volume can be derived from the following equation:

$$V_{total} = n_{H_2O} V_{H_2O} + n_s V_s \qquad (6)$$

The total volume of the solution (V_{total}) can be calculated with the known molar masses of the surfactant and water. n_s is the mole of surfactant and V_s the molar volume of surfactant. In **Figure 4-12** the plot of the total volume of solution V_{total} is given as a function of moles of surfactant n_s. The molar volume is constant over the whole concentration range and can be obtained from the slope of the linear regression. With the assumption of 1 mol water the y-axis interception represents the molar volume of water.[1]

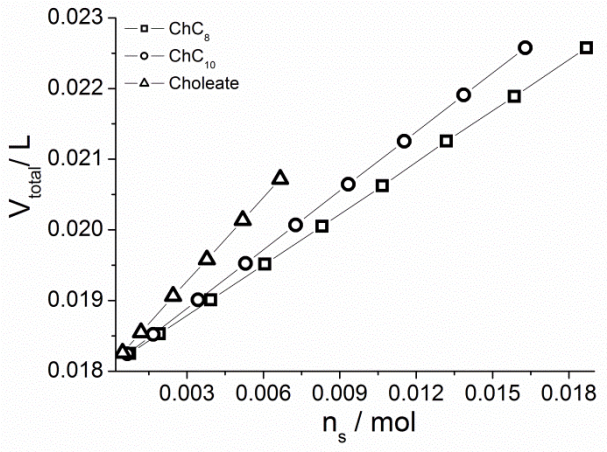

Figure 4-12. Total volume V_{total} as a function of the number of moles n_s of the different choline carboxylates in water (ChC_m with m = 8, 10 and choline oleate).

The average increase of the molar volume from choline octanoate to choline decanoate is given in volume per CH_2-group and is 28.2 Å^3. The difference in molare volume in volume per CH_2-group from choline decanoate to choline dodecanoate (V_s = 0.310 L mol^{-1}) is 27.4 Å^3.[1] These results are roughly in agreement with the results from Tanford, who predicts 26.9 Å for each additional CH_2-group.[70]

	V_S / Å^3	V_L / Å^3	V_{H2O} / L mol^{-1}	l_{max} / Å	ρ_{Surf} / g L^{-1}
ChC_8	403.5	215.7	0.0181	10.4	1017.8
ChC_{10}	459.9	269.5	0.0181	12.9	994.3
Choline oleate	659.3	484.7	0.0181	23.0	971.3

Table 4-5. Volume V_S of one surfactant molecule and the density ρ_{Surf} of the ChC_m with m = 8,10 and choline oleate surfactants at 25°C. The maximum lengths of the alkyl chains and the volume of the lipophilic part V_L were calculated with the equations given by Tanford.[70]

Further, for the calculation of the length of the alkyl chains, a fully extended length of the distinct alkyl chain was assumed and calculated with the equation (7) given by Tanford.[70]

$$l_{max} = 1.5 + 1.265 n_C \qquad (7)$$

with l_{max} as the maximum lengths of alkyl chains in Å and n_C as the number of embedded C-atoms. Also the volume of the alkyl chains V_L can be determined by the expression of Tanford (see equation (8)).[70]

$$V_L = 27.4 + 26.9 n_C \qquad (8)$$

The effective cross-sectional area at the polar-nonpolar interface a_S and the radius or length of the lipophilic part r_L can be calculated from the X-ray data. For these calculations the volume fraction of the surfactant Φ_S and of the lipophilic part Φ_L are required. The volume

fraction Φ_S can be computed by the following equation (9) with *c* as the weight fraction of the surfactant in water.[1]

$$\phi_S = (1 + \frac{\rho_{Surf}(1-c)}{\rho_W c})^{-1} \qquad (9)$$

ρ_w denotes the density of water (ρ_W = 997.1 g L^{-1}). Similarly, the volume fraction of the lipophilic part Φ_L can be calculated taking into account the measured volume of one surfactant molecule V_S and the volume of the lipophilic part V_L.[1]

$$\phi_L = \frac{V_L}{V_S}\,\phi_S \qquad (10)$$

The cross sectional area a_S and the half-thickness of the lipophilic bilayer r_L of the lamellar phases are defined and shown in the equations (11) and (12). The interlayer spacing d is approximated by the position of the first scattering peak (d = 2 π/ q).[5]

$$r_L = \frac{d\phi_L}{2} \qquad (11)$$

$$a_S = \frac{V_L}{r_L} \qquad (12)$$

The hexagonal phase can be characterized by the radius of the lipophilic part r_L and the cross sectional area a_S of the polar-nonpolar interface, see equations (13) and (14):[5]

$$r_L = d\left(\frac{2\phi_L}{\pi\sqrt{3}}\right)^{\frac{1}{2}} \qquad (13)$$

$$a_S = 2\frac{V_L}{r_L} \qquad (14)$$

Exchanging the lipophilic volume fraction with the volume fraction of the surfactant the length of one surfactant molecule r_S can be calculated.[5]

4.6 References

1. R. Klein, G. J. T. Tiddy, E. Maurer, D. Touraud, J. Esquena, O. Tache and W. Kunz, *Soft Matter*, 2011, **7**, 6973.
2. R. D. Vold, R. Reivere and J. W. McBain, *J. Am. Chem. Soc.*, 1941, **63**, 1293-1296.
3. R. D. Vold, *J. Phys. Chem.*, 1939, **43**, 1213-1231.

4. J. W. McBain and W. C. Sierichs, *J. Am. Oil Chem. Soc.*, 1948, **25**, 221-225.
5. P. V. Luzzati, H. Mustacchi, A. Skoulios and F. Husson, *Acta Cryst.*, 1960, **13**, 660-667.
6. C. Madelmont and K. Perron, *Colloid Polym. Sci.*, 1976, **254**, 581-595.
7. P. F. Husson, H. Mustacchi and V. Luzzati, *Acta Cryst.*, 1960, **13**, 668-677.
8. J. W. McBain, R. D. Vold and M. Frick, *J. Phys. Chem.*, 1940, **44**, 1013-1024.
9. R. Klein, D. Touraud and W. Kunz, *Green Chem.*, 2008, **10**, 433.
10. F. E. Antunes, L. Coppola, D. Gaudio, I. Nicotera and C. Oliviero, *Colloids and Surfaces A: Physicochem. Eng. Aspects*, 2007, **297**, 95-104.
11. K. Rendall, G. J. T. Tiddy and M. A. Trevethan, *J. Chem. Soc. Farad. T. 1*, 1983, **79**, 637-&.
12. R. De Lisi, G. Perron, J. Paquette and J. E. Desnoyers, *Can. J. Chem.*, 1981, **59**, 1865-1871.
13. E. Vikingstad, A. Skauge and H. Hoiland, *J. Colloid Interface Sci.*, 1979, **72**, 59-67.
14. P. Ekwall, H. Eikrem and L. Mandell, *Acta Chem. Scand.*, 1963, **17**, 111-122.
15. P. Ekwall, H. Eikrem and P. Stenius, *Acta Chem. Scand.*, 1967, **21**, 1639-1642.
16. P. Ekwall and P. Holmberg, *Acta Chem. Scand.*, 1965, **19**, 455-468.
17. P. Ekwall and P. Holmberg, *Acta Chem. Scand.*, 1965, **19**, 573-583.
18. P. Ekwall, K. E. Lemström, H. Eikrem and P. Holmberg, *Acta Chem. Scand.*, 1967, **21**, 1401-1407.
19. P. Ekwall and P. Stenius, *Acta Chem. Scand.*, 1967, **27**, 1767-1772.
20. P. Stenius and P. Ekwall, *Acta Chem. Scan.*, 1967, **21**, 1643-1646.
21. H. Kelker and R. Hatz, *Handbook of Liquid Crystals*, Verlag Chemie, Weinheim-Deerfield Beach, Basel, 1980.
22. R. G. Laughlin, *The Aqueous Phase Behavior of Surfactants*, Academic Press, San Diego, 1994.
23. K. Holmberg, D. O. Shah and M. J. Schwuger, *Handbook of Applied Surface and Colloid Chemistry*, John Wiley & Sons, LTD, New York, 2002.
24. A. González-Pérez, G. Prieto, J. M. Ruso and F. Sarmiento, *Mol. Phys.*, 2003, **101**, 3185-3195.
25. E. Blanco, A. Gonzalez-Perez, J. M. Ruso, R. Pedrido, G. Prieto and F. Sarmiento, *J. Colloid and Interface Sci.*, 2005, **288**, 247-260.
26. R. Klein, M. Kellermeier, M. Drechsler, D. Touraud and W. Kunz, *Colloids and Surfaces A: Physicochem. Eng. Aspects*, 2009, **338**, 129-134.
27. B. L. Bales, M. Benrraou and R. Zana, *J. Phys. Chem. B*, 2002, **106**, 9033-9035.
28. A. S. Lawrence, *Mol. Cryst. Liq. Cryst.*, 1969, **7**, 1-&.
29. F. B. Rosevear, *J. Am. Oil Chem. Soc.*, 1954, **31**, 628-639.

30. H. D. Dörfler, *Grenzflächen und kolloid-disperse Systeme: Physik und Chemie*, Springer, Berlin, 2002.
31. P. O. Quest, K. Fontell and B. Halle, *Liq. Cryst.*, 1994, **16**, 235-256.
32. O. Dhez, S. Konig, D. Roux, F. Nallet and O. Diat, *Eur. Phys. J. E*, 2000, **3**, 377-388.
33. M. J. Sammon, J. A. Zasadzinski and M. R. Kuzma, *Phys. Rev. Letters*, 1986, **57**, 2834-2837.
34. W. Kunz, *Curr. Opin. Colloid Interface Sci.*, 2010, **15**, 34-39.
35. G. Lindblom and L. Rilfors, *Biochim. Biophys. Acta, Rev. Biomembr.*, 1989, **988**, 221-256.
36. R. R. Balmbra, J. S. Clunie and J. F. Goodman, *Nature*, 1969, **222**, 1159-1160.
37. H. Delacroix, T. Gulik-Krzywicki, P. Mariani and V. Luzzati, *J. Mol. Biol.*, 1993, **229**, 526-539.
38. M. Clerc, *J. Phys. II* 1996, **6**, 961-968.
39. X. Zeng, Y. Liu and M. Imperor-Clerc, *J. Phys. Chem. B*, 2007, **111**, 5174-5179.
40. A. Tardieu, V. Luzzati and F. C. Reman, *J. Mol. Biol.*, 1973, **75**, 711-733.
41. K. Fontell, *Colloid Polym. Sci.*, 1990, **268**, 264-285.
42. P. Mariani, L. Q. Amaral, L. Saturni and H. Delacroix, *J. Phys. II*, 1994, **4**, 1393-1416.
43. Y. Rancon and J. Charvolin, *J. Phys. Chem.*, 1988, **92**, 2646-2651.
44. L. E. Scriven, *Nature*, 1976, **263**, 123-125.
45. V. Luzzati and P. A. Spegt, *Nature*, 1967, **215**, 701-&.
46. V. Luzzati, A. Tardieu, T. Gulik-Krzywicki, E. Rivas and F. Reiss-Husson, *Nature*, 1968, **220**, 485-488.
47. M. Clerc, A. M. Levelut and J. F. Sadoc, *J. Phys. II*, 1991, **1**, 1263-1276.
48. M. Clerc, P. Laggner, A. M. Levelut and G. Rapp, *J. Phys. II France*, 1995, **5**, 901-917.
49. S. M. Gruner, *Proc. Natl. Acad. Sci. U S A*, 1985, **82**, 3665-3669.
50. G. Lindblom, M. Sjölund and L. Rilfors, *Liq. Cryst.*, 1988, **3**, 783-790.
51. S. T. Hyde, S. Andersson, B. Ericsson and K. Larsson, *Z. für Kristallographie*, 1984, **168**, 213-219.
52. H. Iwamoto, R. D. Blakely and L. J. De Felice, *J. Neurosci.*, 2006, **26**, 9851-9859.
53. J. R. Kanicky and D. O. Shah, *J. Colloid Interface Sci.*, 2002, **256**, 201-207.
54. S. E. Friberg, P. Liang, F. E. Lockwood and M. Tadros, *J. Phys. Chem.*, 1984, **88**, 1045-1046.
55. Y. Hendrikx, J. Charvolin and M. Rawiso, *J. Colloid Interface Sci.*, 1984, **100**, 597-600.
56. P. B. Gallot and A. Skoulios, *Kolloid Z. Z. Polym.*, 1965, **28**, 37-43.

57. P. Stepanek, Z. Tuzar, P. Kadlec, F. Nallet and N. P. da Silveira, *Phys. Chem. Chem. Phys.*, 2010, **12**, 2944-2949.
58. A. Stoppa, J. Hunger and R. Buchner, *J. Chem. Eng. Data*, 2009, **54**, 472-479.
59. M. A. van Dijk, G. Casteleijn, J. G. H. Joosten and Y. K. Levine, *J. Phys. Chem.*, 1986, **85**, 626.
60. Z. Saidi, C. Mathew, J. Peyrelasse and C. Boned, *Phys. Rev. A*, 1990, **42**, 872-876.
61. J. Peyrelasse, M. Moha-Ouchane and C. Boned, *Phys. Rev. A*, 1988, **38**, 4155-4161.
62. R. W. Corkery, D. Rousseau, P. Smith, D. A. Pink and C. B. Hanna, *Langmuir*, 2007, **23**, 7241-7246.
63. M. J. Rosen, *Surfactants and Interfacial Phenomena*, John Wiley & Sons, Inc., New York, 1989.
64. V. Vand, *J. Phys. Colloid Chem.*, 1948, **52**, 277-299.
65. J. W. McBain and A. Stewart, *J. Chem. Soc.*, 1933, 924-928.
66. S. Schrödle, R. Buchner and W. Kunz, *Fluid Phase Equilib.*, 2004, **216**, 175-182.
67. J. Barthel, H. Graml, R. Neueder, P. Turq and O. Bernard, *Curr. Topics Solution Chem.*, 1994, 223-239.
68. J. Barthel, R. Wachter and H.-J. Gores, *Mod. Aspects of Eletrochem.*, 1979, **13**, 1-79.
69. J. Barthel, F. Feuerlein, R. Neueder and R. Wachter, *J. Solution Chem.*, 1980, **9**, 209-219.
70. C. Tanford, *J. Phys. Chem.*, 1972, **76**, 3020-3024.

Chapter 5

Influence of chain length and double bond on the thermotropic phase behavior of choline carboxylates

5.1 Abstract

Choline as a cation for carboxylates ChC_m with m = 2, 4, 6, 8, 10 and for oleate increases not only the solubility of carboxylates in water, as seen in the last chapter, it also lowers the melting point due to its bulky and unsymmetrical nature. In general, these carboxylates are ionic liquids, but some of them show also a manifold temperature dependent behavior. In the temperature range between -50°C and 95°C choline acetate (ChC_2), choline butanoate (ChC_4) and choline hexanoate (ChC_6) make only one single phase transition from a crystalline solid to a molten solution. They show the typical melting behavior of a salt. The alkyl chains and the headgroup melt in a one step process. By contrast, the thermotropic behavior of choline octanoate (ChC_8), choline decanoate (ChC_{10}) and choline oleate is more diversified. In the temperature range between -50°C and 95°C these compounds exhibit several different phases and behave more or less like the long chain choline carboxylates ChC_m with m = 12, 14, 16, 18.[1] With increasing temperature the following phases appear: crystalline (Cr), semi-crystalline (CrM), and as the high temperature phase structure a liquid crystalline defective lamellar or nematic structure. An additional phase transition appears in the case of ChC_8. Below 100°C the liquid crystalline phase melts to a liquid solution and marks the transition of a choline carboxylate with only ionic liquid properties to an ionic liquid which can also act as surfactant. The phase behavior of all these neat choline carboxylates was studied with polarizing optical microscopy, differential scanning calorimetry, small (SAXS) and wide (WAXS) angle X-ray scattering and also with NMR spin-spin relaxation. NMR spin-spin relaxation and SAXS reveal that in the cases of choline octanoate, choline decanoate and choline oleate beside the above mentioned temperature dependent phase structure another more fluid like structure is in equilibrium within one single phase along the whole temperature range between -50°C and 95°C. However, this phase behavior could be also explained by assuming that instead of two structures in one phase, two phases (thermodynamically stable or kinetically stabilized) are in equilibrium with each other. Based on the performed measurements, no clear statement could be given.

5.2 Introduction

Compared to the alkali ions, choline is a good counterion to lower the melting point of a salt or to play a special role in deep eutectics. Today a lot of literature exist about choline based ionic liquids like amino acid derivatives[2], choline saccharinate and choline acesulfamate[3], choline hydrogen malate or choline hydrogen tartrate[4] and many more. Choline is not only used as cation because it can lower the Krafft point, the melting temperature and increases the solubility, it is also very important as a novel biocompatible cation which is biodegradable.[5] It is already known as an essential nutrient and has some important

functions in the human body. It plays a significant role in lipid transport, cell membrane signaling (precursor for acetylcholine) and in the methyl group metabolism.[6,7] Biodegradability and biocompatibility of choline ionic liquids open the field for new applications in processes, for example for biodegradation of azo dyes.[8] A well known deep eutectic is choline chloride mixed with urea in the molar ratio 1:2 showing a melting point at 12°C.[9] There also exist deep eutectics with choline chloride or choline acetate and glycerol in different mixing ratios.[10] One application of these mixtures is the solubilization and activation of a lipase to transesterify triglycerides into biodiesel.[10] Further, choline hexanoate is used as an extracting solvent to solubilize suberin (a hydrophobic polymer present in plant cell walls) from cork[11,12] leading to potential new applications in the field of polymers. Since these processes involve rather extended temperature ranges, it is important to know the temperature dependent behavior of the ionic liquid itself. It is well known that soaps have a very complex phase polymorphism that could interfere with any applications. Therefore, this chapter handles the impact of the choline cation on the thermotropic phase behavior of the anhydrous choline carboxylates ChC_m with m = 2, 4, 6, 8, 10 and of choline oleate.

Some earlier studies on choline acetate, choline butanoate and choline hexanoate are present in literature.[13, 14] However, nothing is stated about the thermotropic mesomorphism, only the melting temperature to an isotropic liquid is recorded. The synthesis (exception choline acetate) used in the present study corresponds to the one given by Petkovic *et al.*.[13] Choline bicarbonate and the respective carboxylic acid react to the corresponding choline carboxylates after drying. Muhammad *et al.*[14] also synthesized choline acetate, choline butanoate and choline hexanoate. Their synthesis involved the neutralization of the carboxylic acid with an aqueous solution of choline hydroxide. Their results are completely different to the results presented in this chapter. Muhammad *et al.* obtained at room temperature liquid choline butanoate and choline hexanoate.[14] It is possible that the stabilizer in the used choline hydroxide solution for the synthesis remains in the ionic liquid as impurity.

From former studies on carboxylate soaps combined with mono- or divalent inorganic cations it is known that multiple phases occur between the solid and the isotropic liquid phase, starting with chain length m = 4[1, 15,16-25] and upwards. The phase transitions occur up to 350°C.[1, 16-25] Also in a study about the thermotropic phase behavior of long chain choline carboxylates a manifold temperature dependent phase behavior was found.[1] Choline carboxylates ChC_m with m = 12-18 form in the temperature range between -20°C and 95°C the following phases with increasing temperature: a crystalline interdigitated, monolayered phase, which is transferred above 35°C (the exact temperature depends on the chain length) to a semi-crystalline interdigitated, monolayered phase and at temperatures above 68°C (the exact temperature depends on the chain length) to a liquid crystalline smectic A lamellar phase.[1]

In the present study the influence of shorter chains (m = 2, 4, 6, 8, 10) and a double bond in the alkyl chain (choline oleate) on the thermotropic mesomorphism of choline carboxylates ChC_m is investigated in the temperature range between -50°C and 95°C. The different phases are characterized with polarizing optical microscopy, differential scanning calorimetry, NMR spin-spin relaxation and small (SAXS) and wide (WAXS) angle X-ray scattering. Furthermore, the thermal stabilities were estimated with thermogravimetric measurements.

5.3 Results and discussion

5.3.1 Thermogravimetric analysis

Choline carboxylates ChC_m with m = 2, 4, 6, 8, 10 and choline oleate degrade all in a one step process (curves see Appendix C). The decomposition temperatures of these choline carboxylates (see **Table 5-1**) increase slightly with growing alkyl chain length, but not in a linear way as observed for the long chain choline carboxylates.[1] ChC_2 shows a slightly higher decomposition temperature compared to the other investigated carboxylates. The short chain choline carboxylates seem to be slightly more stable than the saturated long chain choline carboxylates. These results are against the common tendency that decomposition temperatures increase with increasing chain length.[1] The differences of the decomposition temperatures compared to those reported by Petkovic *et al.* vary from 2°C for ChC_2 to 47°C for ChC_{10} and can result from the different heating rate of 5 K min^{-1} compared to 10 K min^{-1}, used in the present study.[13] In the study of Muhammad *et al.*[14] about ChC_m with m = 2, 4, 6 the decomposition temperatures are measured with the same heating rate of 10 K min^{-1}.[14] These authors used another method of synthesis, but their decomposition temperatures T_{dec} are in the same range. In the study of Muhammad *et al.*[14] the decomposition temperatures are not determined by the onset of mass loss, as it was processed here, instead, the value of the highest peak intensity of the derivative weight loss curve was taken.[14] Note that in the other studies[13, 14] the value of choline oleate was not reported. For alkali carboxylates the thermal stability is very different. Sodium carboxylates with chain lengths m = 2, 4, 6, 8 and 10 are stable to temperatures above 350°C[16, 19, 26] as is potassium oleate.[27, 28] Sodium oleate shows a thermal stability up to more than 260°C.[17, 29, 30]

Ionic liquid	T_{dec} / °C	Ionic liquid	T_{dec} / °C
ChC_2	207	**ChC_8**	208
ChC_4	202	**ChC_{10}**	215
ChC_6	204	**Choline oleate**	207

Table 5-1. Decomposition temperatures T_{dec} of ChC_m with m = 2, 4, 6, 8, 10 and choline oleate are shown. They were measured with a heating rate of 10 K min^{-1}.

5.3.2 Polarizing optical microscopy

Visual observations showed that choline carboxylates decompose by heating for a longer time over 100°C. This decomposition was accompanied by a brown coloration. Thus, the investigated temperature range for the measurements was limited to the range from -50°C to 95°C. Another interesting observation was made by heating an anhydrous neat sample of the choline carboxylates in a sealed glass tube. Choline carboxylates ChC_m with chain length m = 2, 4, 6, 8 melt to an isotropic liquid under 95°C, while ChC_{10} and choline oleate remain solid-like.

Polarizing optical microscopy is used to identify the different mesophases due to their typical characteristic textures. Two types of substances are found. One has an one step melting process to an isotropic liquid or vice versa. The other type of substance does not liquefy below 100°C to an isotropic melt, but forms several temperature dependent phases in the recorded temperature range. ChC_8 shows a combination between the two types.

ChC_m with m = 2, 4, 6 undergo only a transition from a crystalline solid to an isotropic melt. With polarizing microscopy the crystalline phases could be visualized very well at low temperatures (see Appendix C in section C.2). During the microscopy experiments it was observed that in general the melting process occurred over a larger temperature range (around 10°C) compared to the crystallization process (around 2°C). The temperature scans for anhydrous ChC_m with m = 8, 10 and oleate imaged with polarizing optical microscopy using crossed polarizers were recorded four times in the temperature range between -50°C and 95°C. The first cycle is not very meaningful. The first three heating and cooling cycles were measured with 10 K min^{-1} heating rate (see Appendix C in section C.2), the fourth with a heating rate of 1 K min^{-1} (see **Figure 5-1**, **Figure 5-2**, and **Figure 5-3**). With this method details in the time-dependence of the phase transitions could be detected.

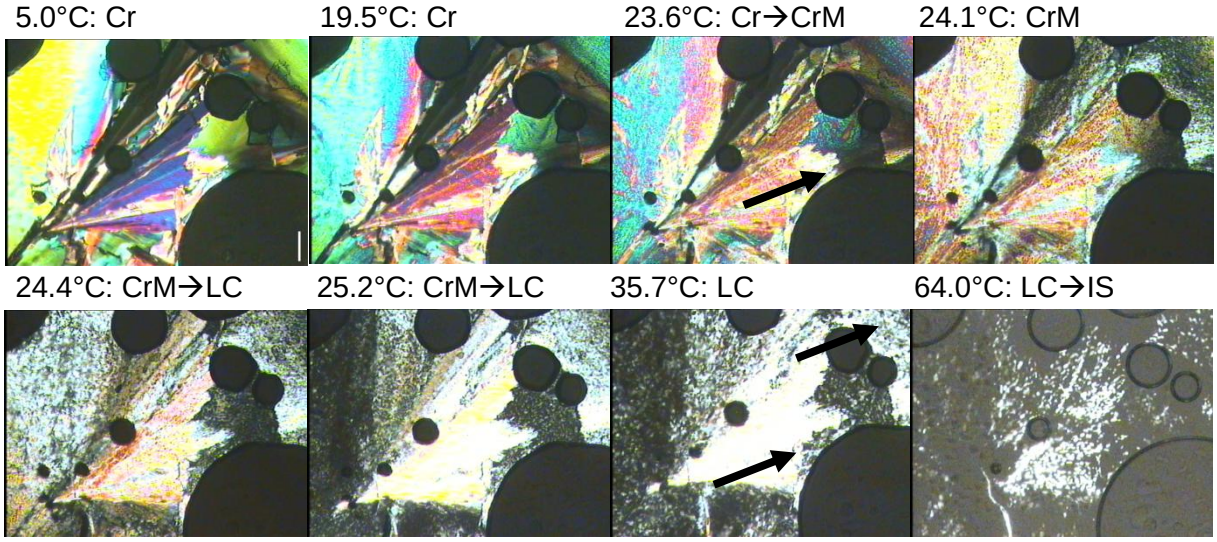

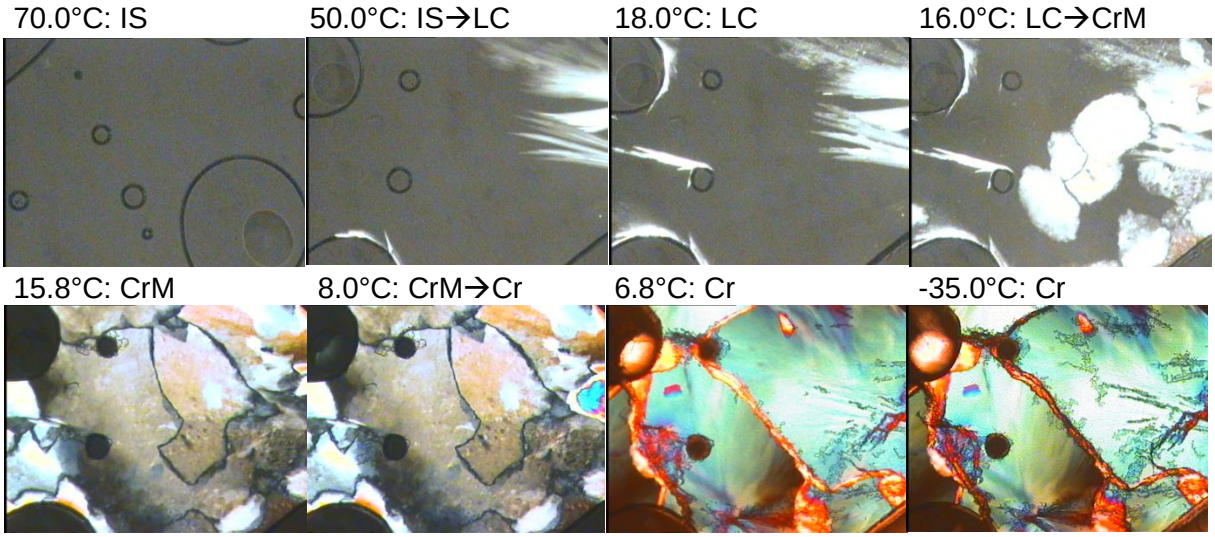

Figure 5-1. Polarizing optical microscopy (with crossed polarizers and 100x magnification) images of the thermotropic phases of anhydrous choline octanoate during the fourth heating and cooling cycle with a heating rate of 1 K min^{-1}. The temperature range between -50°C and 95°C was imaged. The micrographs were taken from the same sample spot during the cycle. Both, the heating cycle and the cooling cycle, show four different phases. With increasing temperature the following phases are formed: crystalline (Cr), semi-crystalline (CrM), liquid crystalline defective lamellar or nematic phase (LC), and isotropic, very viscous melt (IS). The arrows mark the "Schlieren" texture in the liquid crystalline phase, typical of a nematic phase, and also changes in the structure which characterize the respective phase. The scale bar (see image 5°C) is 100 µm. It is the same for all images.

Independently of the heating rate in all four heating and cooling cycles the following phases appear for neat, anhydrous ChC_m with m = 8, 10 and oleate starting at low temperatures: crystalline phase (Cr), semi-crystalline phase (CrM) and a liquid crystalline phase (LC). The latter could be characterized as a defective lamellar phase or a nematic phase. ChC_8 shows an additional phase at higher temperature, the isotropic melt (IS). The transition temperatures depend only slightly on the heating rate (ΔT = 1-3°C, exception for ChC_8 at the last transition at cooling cycle ΔT = 10) and the melting of the semi-crystalline phase to a liquid crystalline phase and the crystallization during the cooling cycle is not time dependent. This is in accordance with the results found by Klein *et al.*[1] and Gallot *et al.*[25]. They also found that the high temperature liquid crystalline phase is the most stable phase for carboxylates combined with a big counterion.[1, 25, 31] A time dependent phase transition was found for each substance for the last transition at the cooling cycle. This transition step is related to the change from a semi-crystalline phase to a crystalline phase, e.g. with 1 K min^{-1} the transition temperature was 10°C higher in the case of ChC_8 than the transition temperature found with the heating rate of 10 K min^{-1}. This time dependence in phase transition could be explained by assuming that the low temperature transition is the crystallization of the alkyl chains and the faster the cooling rate the more hindered is the crystallization of the chains. The electrostatic interactions between the polar groups and the bulky cation hinder the crystallization of the alkyl chains. The influence of this force on the crystallization behavior increases with decreasing chain length. Therefore, this phase

transition is very time dependent and is more influenced by the choline cation with decreasing chain length.

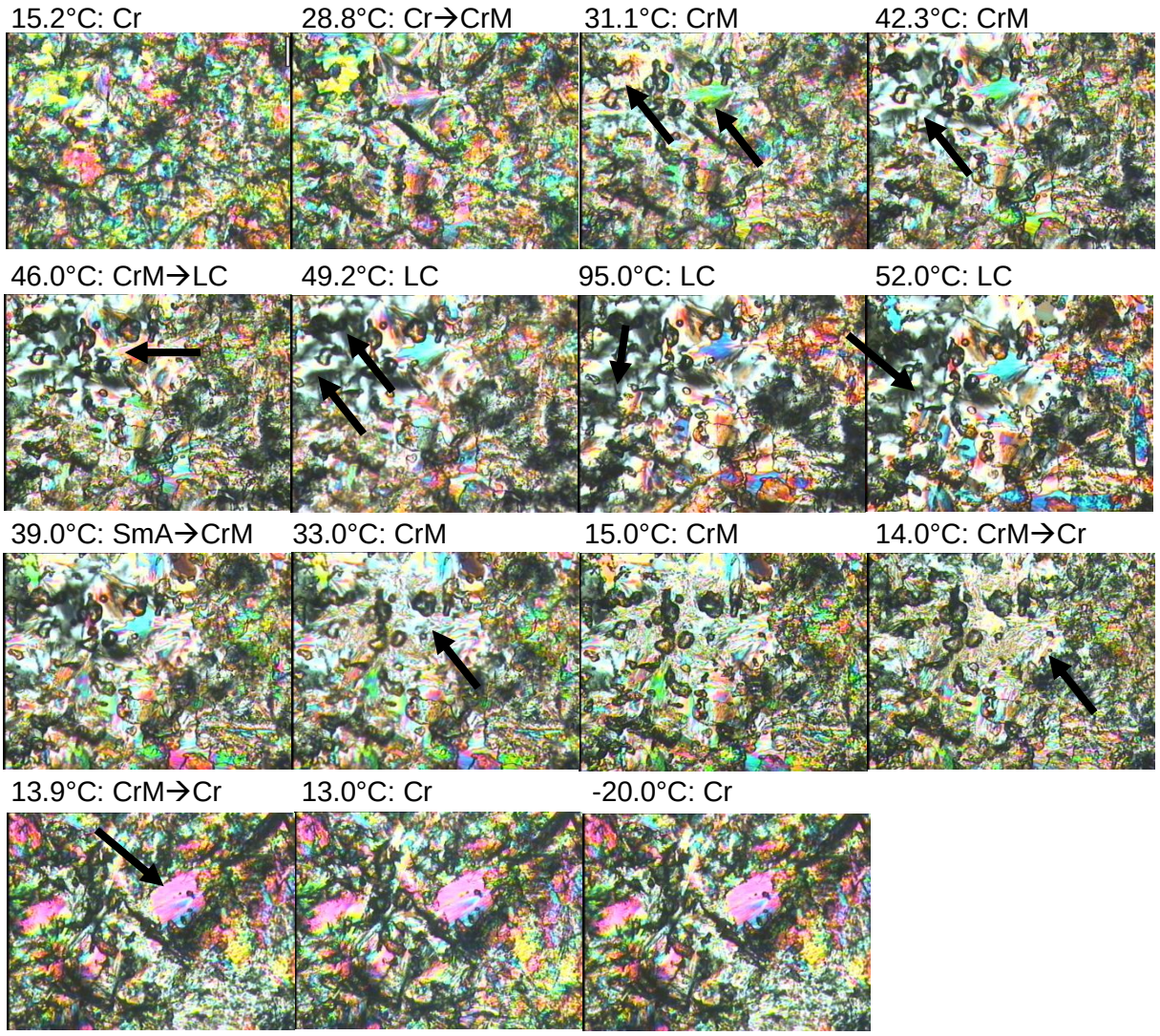

Figure 5-2. Optical polarizing microscopy images (with crossed polarizers and 100x magnification) of the temperature dependent phases of anhydrous choline decanoate are shown during the fourth heating and cooling cycle with the heating rate of 1 K min^{-1}. The temperature range between -50°C and 95°C was imaged. The micrographs were taken from the same sample spot during the cycle.In the heating cycle and the cooling cycle occur three different phases. With increasing temperature the following phases are formed: crystalline (Cr), semi-crystalline (CrM), and defective lamellar or nematic liquid crystalline phase (LC). Choline decanoate does not melt into an isotropic melt below 100°C due to the longer chain compared to choline octanoate. The arrows mark the change in structure and the "Schlieren" texture of the liquid crystalline phase (LC). The "Schlieren" texture is typical for a nematic phase. The scale bar (see image recorded at 15.2°C) is 100 µm. It is the same for all images.

Consider the different polarizing light microscopy images of the fourth temperature cycles between -50°C and 95°C: as already mentioned the low temperature phase is a crystalline phase. With increasing temperature the crystals disappear progressively, but not abruptly. The phase transition is accompanied by an increase in volume. This can be seen very well in the light microscopy images of ChC_m with m = 8, 10 recorded with the heating rate of 1 K min^{-1} see **Figure 5-1**, **Figure 5-2**. In **Figure 5-3** considering the images of -50°C and

-18°C the change in the structure seems to be smaller in the case of choline oleate compared to the other two soaps. This will be explained in detail later on.

Also, an increase in volume is visible in the phase transition from the semi-crystalline phase to the liquid crystalline phase. None of the three substances show any homogeneous liquid crystalline phase. Some parts have a focal conic texture as seen in a lamellar phase, and even a typical “Schlieren” pattern for a nematic liquid crystalline phase could be found.

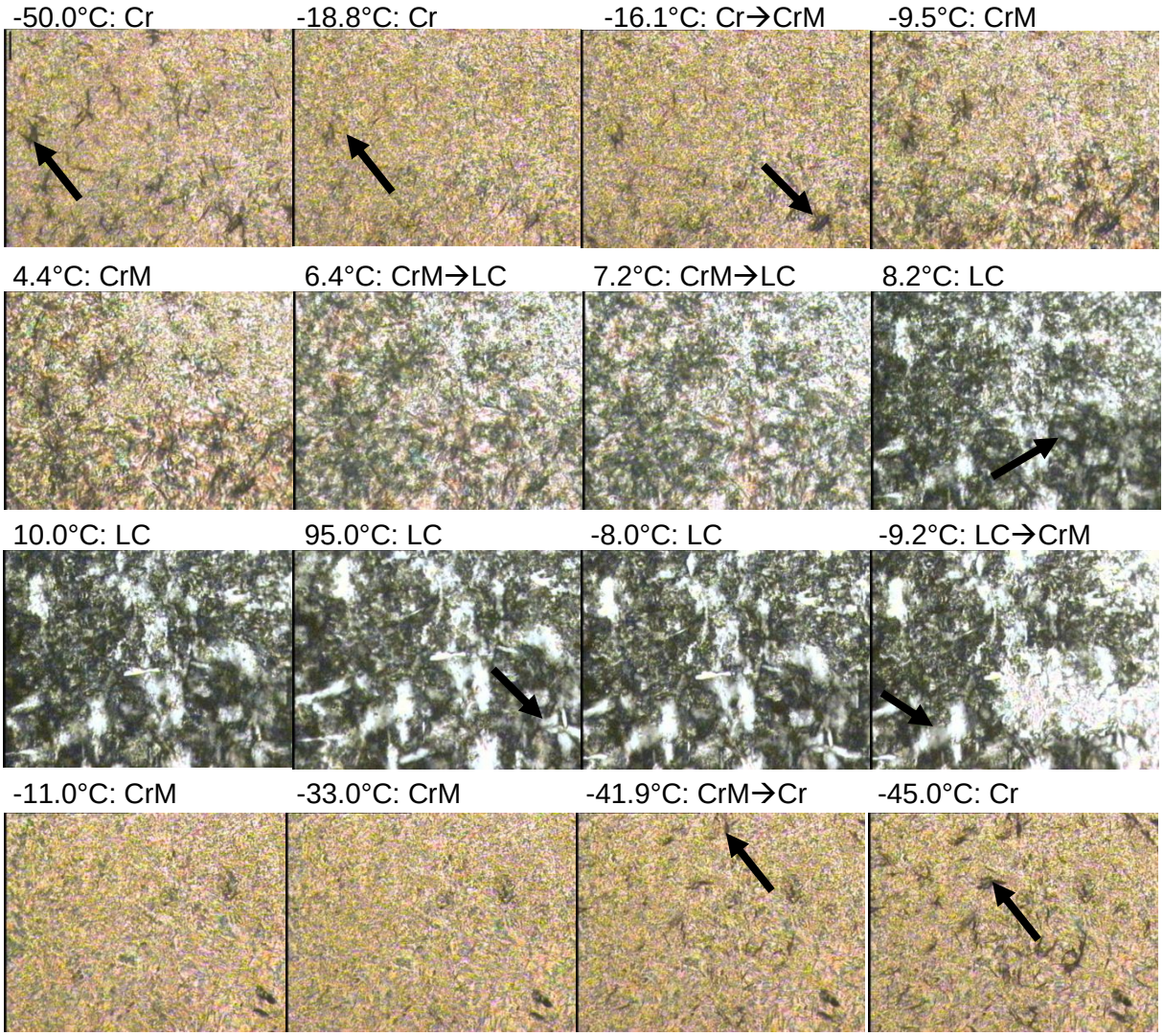

Figure 5-3. Optical polarizing microscopy images (with crossed polarizers and 100x magnification) of the thermotropic phases of anhydrous choline oleate during the fourth heating and cooling cycle with the heating rate of 1 K min^{-1} are shown. The micrographs were taken from the same sample spot during the cycle. The arrows mark changes in the structure. Details as for **Figure 5-2**. The scale bar (see image recorded at -50.0°C) is 100 µm. It is the same for all images.

Due to these experiments it could be observed that the first melting and the last crystallization are the melting and crystallization of the chains. The second reversible transition must involve the polar regions.[32] The volume change in case of choline oleate seems to be higher in this step and lower in the first step compared to the other substances. This could be explained by the influence of the double bond. It is easier to explain this

process on the heating cycle. In the first melting step it seems that the alkyl chains of choline oleate could only be molten slightly due to the existence of the double bond (the degree of crystallinity is lower in the crystalline phase of choline oleate compared to the one of choline octadecanoate[1] because of the double bond). The increase of the volume in the second transition is much higher because of the simultaneous melting of the polar groups and the partly molten alkyl chains.

5.3.3 Differential scanning calorimetry (DSC)

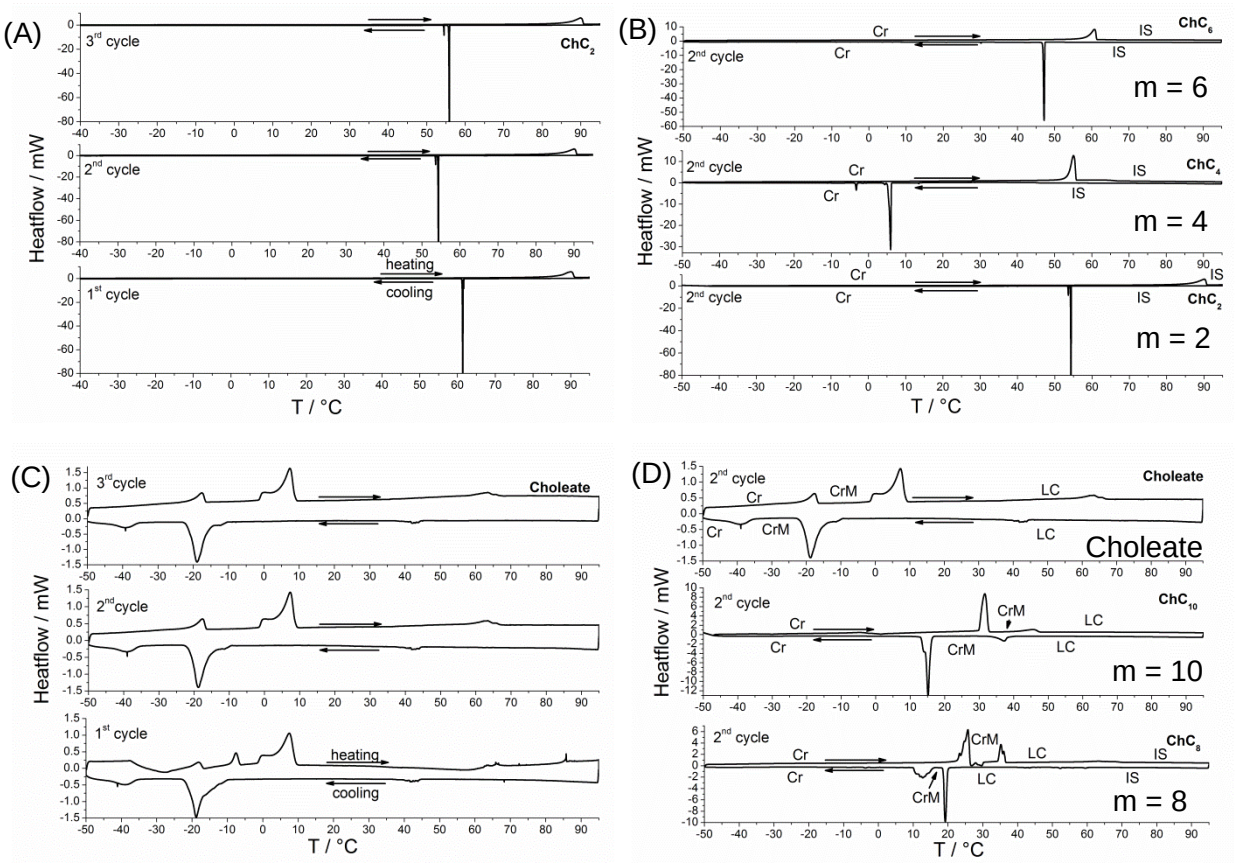

Figure 5-4. (A) DSC curves of anhydrous neat choline acetate measured during three heating and cooling cycles in the temperature range between -50°C and 95°C with a heating rate of 1 K min^{-1}. (B) DSC curves of the second heating and cooling cycle of choline acetate, choline butanoate and choline hexanoate with a heating rate of 1 K min^{-1}. A transition from a crystalline phase (Cr) to an isotropic melt (IS) is observed. (C) DSC curves of anhydrous neat choline oleate. Three heating and cooling cycles were measured in the temperature range from -50°C to 95°C with a heating rate of 1 K min^{-1}. (D) DSC curves of the second heating and cooling cycle of neat choline octanoate, choline decanoate and choline oleate measured in the same manner. With increasing temperature the following phases appear: crystalline phase (Cr), semi-crystalline phase (CrM), liquid crystalline phase (LC). In the case of choline octanoate and choline oleate a further transition was found at higher temperatures. For choline octanoate it should be the transition of the LC phase to an isotropic melt (IS). The one of choline oleate should be related to a phase change in the liquid crystalline phase (LC). The phase structures were assigned taking into account the results from section 5.3.2.

DSC curves were recorded between -50°C and 95°C (three cycles). The first cycle sometimes shows different melting and crystallization temperatures and enthalpies compared to the second and third cycle due to the formation of polymorphic metastable phases.[1, 18, 19] Three cycles are preferred, because the accordance of the second and the third cycle shows the reproducibility of the phase transitions, the temperature stability of the sample and also proves a non-leaking sample holder.

From literature it is known that the number of phase transitions is dependent on the alkyl chain length but more on the nature and the coordination ability of the cation.[15, 32] With DSC experiments the same phase changes were found as observed with the microscope (see **Figure 5-4** and Appendix C in section C.2 and C.3). An additional phase transition occurs for choline oleate at around 62.9°C at heating and 42.3°C at cooling. This phase transition was not observed under the microscope (see **Figure 5-3**). Therefore it could result from the double bond. The heating rate in the DSC experiments was 1 K min^{-1}. The heating and cooling cycle recorded with polarizing light microscopy with heating rate 1 K min^{-1} (**Figure 5-1**, **Figure 5-2**, **Figure 5-3**) show good agreement with the phase transition temperatures obtained from the DSC curves.

Taking into account the different DSC curves (see **Figure 5-4**) always a temperature hysteresis could be found due to the slow nucleation during the cooling cycle. High values of temperature hystereses are more related to the melting and crystallization temperature of crystalline phases, small ones to the melting or crystallization of liquid crystalline phases.[1, 33, 34] In the following discussion only the second and the third DSC curves for the different neat choline carboxylates ChC_m with m = 2, 4, 6, 8, 10 and oleate are considered. The melting and crystallization temperatures of ChC_m with m = 2, 4, 6 show a high reproducibility (see section C.3.2 in Appendix C). The variation of the respective temperatures at the second and the third cycle vary between 0.0°C and 0.7°C. The melting and crystallization temperatures differ from the transition temperatures found with polarizing light microscopy measurements (ΔT = 4-10°C). These discrepancies could result from the different heating and cooling rates used for the different methods (optical polarizing microscopy: 10 K min^{-1}; DSC: 1 K min^{-1}) or from the different amount of used sample. The heating cycle shows one sharp reproducible first-order transition. During the cooling cycle ChC_6 shows a first order transition and ChC_m with m = 2, 4 a defined sharp transition temperature with several sharp peaks. Thus, both substances exhibit several unstable metaphases before they crystallize in a stable phase. The temperature hystereses (ΔT = 13-49°C) are in accordance with the melting of a crystalline phase. Normally, sodium or potassium carboxylates (without m = 2) show the melting of the alkyl chains as a first phase transition and the melting of the polar groups as the second or further transitions.[15, 32] In the case of these short chain choline carboxylates the influence of the chain length on the melting behavior is very low. The alkyl chains

combined with choline as cation are too short to show strong van der Waals interactions with each other. This interaction is disrupted by the strong cohesive forces of the polar groups. The interactions of the polar headgroup and choline dominate and also the size of the choline cation shows an influence. Therefore, only one phase transition could be seen. This phase change should be mostly controlled by the melting of the polar groups (see **Figure 5-4** (A) and (B)). Compared to the sodium or potassium butanoate and sodium or potassium hexanoate the amount of possible mesophases is limited due to the bulky choline cation. As already mentioned, sodium acetate shows only a melting temperature, while sodium butanoate show two and sodium hexanoate three transition temperatures.[16]

The melting and crystallization temperatures of the choline carboxylates ChC_m with m = 2, 4, 6 and 8 (ChC_8 highest temperature transition) illustrate an increase with alkyl chain length with the exception of choline acetate (see **Figure 5-5** (A)). A decrease of the temperature hysteresis is seen with increasing alkyl chain length. Therefore, the alkyl chain seems to act as a template and helps to start the crystallization of the neat substance at the cooling cycle. Sodium carboxylates NaC_m with m = 2, 4, 6, 8 show the same tendency of the melting temperatures as found for choline carboxylates ChC_m with m = 2, 4, 6, 8.[15, 16]

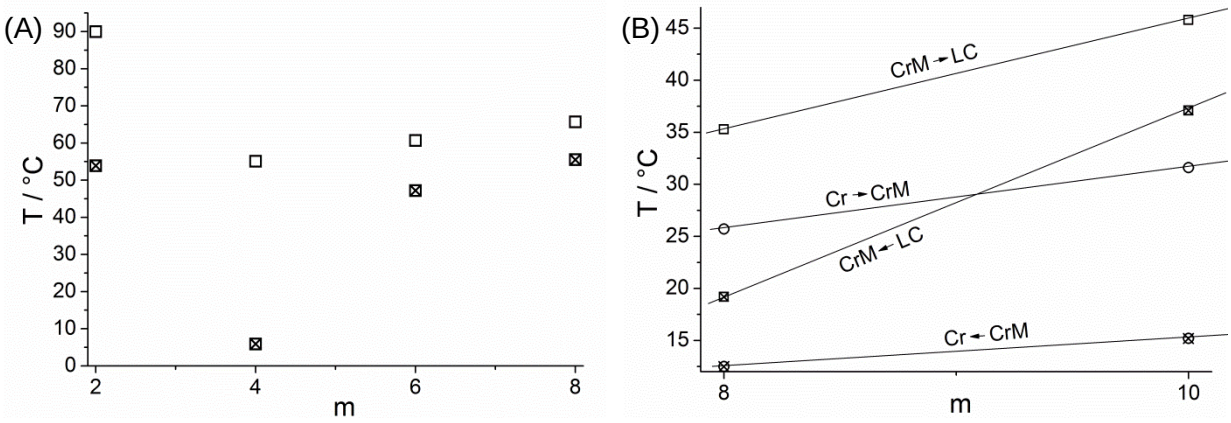

Figure 5-5.(A) Melting □ and crystallization ☒ temperatures of choline carboxylates ChC_m with m = 2, 4, 6, 8 (ChC_8 melts to an isotropic liquid (IS)). (B) Low temperature transition at heating ○ and cooling ⊗ cycle and high temperature transition at heating □ and cooling ☒ cycle of choline carboxylates ChC_m with m = 8, 10. The straight lines connect the corresponding transition temperatures of m = 8, 10. All temperatures are taken from the second DSC curve of the respective choline carboxylates ChC_m with m = 2, 4, 6, 8, 10.

Considering the second and third DSC curve of ChC_8 (see Appendix C in section C.3), ChC_{10} (see Appendix C in section C.3) and choline oleate (see **Figure 5-4** (C)) the transition temperatures are well reproducible and differ only slightly between the different cycles (≈ 1°C).

In general, comparing the DSC curves with the one of the longer chain choline carboxylates ChC_m with m = 12, 14, 16, 18[1], they seem to agree completely with the one recorded for choline decanoate. Therefore, it could be assumed that similar phases are present. The first

temperature hysteresis, characterizing the transition from a crystalline phase to a semi-crystalline phase or vice versa, is around 16.4°C in the case of ChC_{10}. The second is approximately 8.7°C and shows the melting of a semi crystalline phase to a liquid crystalline one at the heating cycle or vice versa at the cooling cycle.[1, 18, 25, 31] The values of the temperature hysteresis of the long chain choline carboxylates ChC_m with m = 12, 14, 16, 18 are in the same range.[1] The ones of ChC_8 differ slightly. The temperature hystereses of ChC_8 for the first two phase transitions are almost equal (see **Figure 5-5** (B)). The first temperature hysteresis has a value around 13.2°C and the second around 16.1°C. This means the ordering effect of the short chains is influenced by the ionic interaction of the polar groups and the bulkiness of the choline cation. The whole melting and crystallization process is strongly dominated by the bulky choline cation. With decreasing chain length the bulky unsymmetrical choline cation influences more and more the stability and the formation ability of the phases. This could also be observed on the last transition at the cooling cycle of ChC_m with m = 8, 10. The multipeak in the DSC curve results from unstable mesophases (see **Figure 5-4** (D)). This was also seen in the case of lithium carboxylates.[35] As it is observed here for the choline carboxylates the influence of the cation on formation of stable mesophases starts with ChC_{10}, but gets more pronounced in the case of ChC_8. A broad multipeak is observed in the cooling curve of ChC_8 around 12.5°C. Also lithium carboxylates have this change in linearity of enthalpy and entropy from chain length eleven to twelve.[35]

Choline oleate forms more or less the same temperature dependent phases as the long chain choline carboxylates.[1] However, the phase transitions occur at lower temperatures compared to choline octadecanoate[1] owing to the less dense chain packing because of the cis-double bond. The temperature hysteresis for the low temperature transition is ΔT = 21.7°C and for the high temperature transition, occurring for the transition of the semi-crystalline to liquid crystalline phase and vice versa, a value of ΔT = 26°C is obtained. Thus, the cis-double bond hinders the crystallization to another phase compared to the saturated carboxylates and result in these high values for the temperature hystereses. The third and highest temperature transition (T_{heat} = 62.9°C, T_{cool} = 42.3°C) could not be found for the long chain choline carboxylates due to the limited investigated temperature range until 95°C, or this phase does not exist for the saturated long chain carboxylates and result from the double bond. However, a phase transition due to different conformations at the double bond, like trans-cis-trans conformation to skew-cis-skew or vice versa or other cases, is not possible, as these different types of conformation were even found in the different temperature dependent phases of oleic acid[36] and triolein[36, 37]. Such a phase transition needs a transition enthalpy higher than 0.7 kJ mol^{-1}, which was found here (see **Table 5-3**).

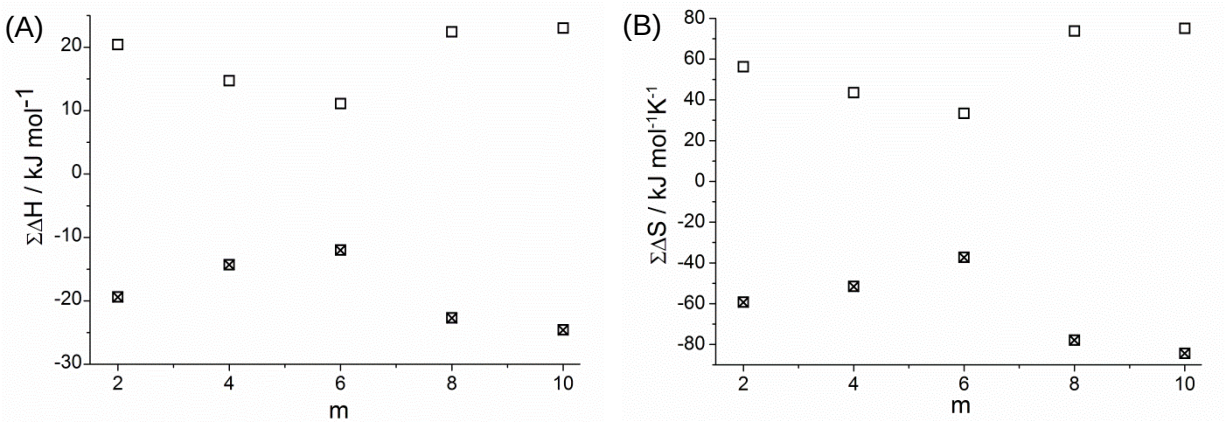

Figure 5-6. (A) Total enthalpy of the second heating □ and cooling ☒ cycle of choline carboxylates ChC_m with m = 2, 4, 6, 8, 10. All substances melt to an isotropic melt (exception choline decanoate). Choline decanoate does not melt under 95°C to an isotropic solution, so the melting enthalpy is missing and this could be the reason for the lower enthalpy increase or decrease. (B) The same behavior was observed for the total entropy of the second heating □ and cooling ☒ cycle obtained from DSC.

The total enthalpy of the phase changes of the choline carboxylates between -50°C and 95°C decreases during the heating cycle linearly with -2.3 kJ mol^{-1} per $-CH_2-$ group for ChC_m with m = 2, 4, 6 and increases with 1.9 kJ mol^{-1} per $-CH_2-$ with decreasing temperature (see **Figure 5-6** (A)). For ChC_m with m = 6, 8, 10 the sum of the enthalpy and sum of the entropy of the phase transitions increases during the heating cycle and decreases during the cooling cycle. However, the enthalpy change does not show a linear behavior. The transition enthalpy of ChC_{10} on the heating cycle is probably too small, because the melting to an isotropic melt occurs at temperatures higher than 95°C. The same is found on the cooling cycle. For the respective alkanols and carboxylic acids, the transition enthalpy increases with increasing alkyl chain length.[31] The sum of the transition enthalpies of the sodium carboxylates NaC_m with m = 2, 4, 6, 8, 10 show the same tendencies as found for the choline carboxylates.[15] Therefore, it can be concluded that the transition enthalpies for carboxylate soaps with shorter alkyl chains are always influenced by the counterion.

	ChC_2		**ChC_4**		**ChC_6**	
	$\sum\Delta H$ / kJ mol^{-1}	**$\sum\Delta S$ / J $mol^{-1}K^{-1}$**	**$\sum\Delta H$ / kJ mol^{-1}**	**$\sum\Delta S$ / J $mol^{-1}K^{-1}$**	**$\sum\Delta H$ / kJ mol^{-1}**	**$\sum\Delta S$ / J $mol^{-1}K^{-1}$**
1. heating	19.8	54.5	15.3	43.5	11.1	33.4
1. cooling	-18.8	-56.2	-14.8	-51.6	-12.0	-37.7
2. heating	20.4	56.2	14.7	43.5	11.1	33.3
2. cooling	-19.4	-59.3	-14.3	-51.6	-12.0	-37.3
3. heating	20.4	56.1	14.8	43.8	11.3	33.9
3. cooling	-18.6	-56.8	-14.2	-51.6	-11.8	-36.7

Table 5-2. Sum of all enthalpies or entropies of the phase transitions of choline acetate, choline butanoate and choline hexanoate at the heating or cooling cycle in the temperature range between -50°C and 95°C. Of each sample three cycles were recorded with DSC.

	ChC_8			ChC_{10}		Choline oleate		
	ΔH_1 / kJ mol^{-1}	ΔH_2 / kJ mol^{-1}	ΔH_3 / kJ mol^{-1}	ΔH_1 / kJ mol^{-1}	ΔH_2 / kJ mol^{-1}	ΔH_1 / kJ mol^{-1}	ΔH_2 / kJ mol^{-1}	ΔH_3 / kJ mol^{-1}
1. heating	14.3	7.1	1.3	20.0	3.1	2.7	14.1	0.7
1. cooling	-9.8	-11.5	-1.2	-21.4	-3.2	-3.1	-14.6	-0.6
2. heating	14.4	6.7	1.4	19.8	3.2	2.8	14.0	0.6
2. cooling	-9.6	-11.6	-1.5	-21.3	-3.2	-2.9	-14.6	-0.7
3. heating	14.1	6.7	1.1	20.1	3.3	2.7	14.2	0.7
3. cooling	-9.6	-11.7	-1.1	-21.4	-3.2	-3.0	-14.2	-0.7

Table 5-3. Different transition enthalpies of the different phase transitions along the heating or cooling cycle of choline octanoate, choline decanoate and choline oleate. The numbers 1, 2 and 3 label the different phase transitions in the temperature range between -50°C and 95°C with increasing temperature.

As already observed above, choline octanoate, choline decanoate and choline oleate show more or less the same phase behavior as the saturated long chain choline carboxylates ChC_m with m = 12, 14, 16. 18.[1] The enthalpy for the phase change from crystalline to semi-crystalline increases from ChC_m with m = 8, 10 (see **Table 5-3**). This is in agreement with the melting of the alkyl chains, due to an increase of the van der Waals interaction with increasing chain length. The enthalpy to form the liquid crystalline phase decreases with increasing chain length. Therefore, the influence of the counterion is higher in the case of choline octanoate than for choline decanoate. For the long chain choline carboxylates the opposite behavior was observed.[1] Therefore, the melting behavior of the long chain choline carboxylates[1] with chain length m = 12, 14, 16, 18 is more influenced by the chain length, while for short chain carboxylates ChC_m with m = 2, 4, 6, 8, 10 the melting is more controlled by the counterion choline.

In the case of choline oleate the transition temperatures were shifted to lower temperatures and the sum of the enthalpy ($\sum\Delta H_{heat}$ = 17.3 kJ mol^{-1}; $\sum\Delta H_{cool}$ = -18.3 kJ mol^{-1}) and entropy ($\sum\Delta S_{heat}$ = 62.5 J mol^{-1}K^{-1}; $\sum\Delta S_{cool}$ = -72.3 J mol^{-1}K^{-1}) at the heating cycle and at the cooling cycle is much smaller compared to the saturated choline stearate ($\sum\Delta H_{heat}$ = 36.0 kJ mol^{-1} and $\sum\Delta S_{heat}$ = 105.7 J mol^{-1}K^{-1}; $\sum\Delta H_{cool}$ = -34.0 kJ mol^{-1} and $\sum\Delta S_{cool}$ = -102.8 J mol^{-1}K^{-1})[1]. The same behavior was found for sodium stearate ($\sum\Delta H$ = 57.9 kJ mol^{-1}) compared to sodium oleate ($\sum\Delta H$ = 35.6 kJ mol^{-1}).[17] This aspect could be explained due to the presence of the cis-double bond in the alkyl chain of oleate. A tight packing as in the case of the saturated alkyl chains is not possible for oleate soaps. In general, less energy is needed to melt the chains or for phase transitions because of the not so dense general packing. Also the increase of the entropy during a heating cycle or the decrease of the enthalpy for cooling cycle due to phase changes is not so high compared to the stearate chain.[17] However, it seems that choline oleate forms the same phases as found for the saturated choline carboxylates. One exception is the third phase transition which shows a low enthalpy value (see **Table 5-3**). The other is found in the way of chain melting, comparing the energy needed for phase

transitions. Comparing the above mentioned sums of the enthalpies of choline oleate and choline stearate with the respective sodium ones, the enthalpy values of the sodium equivalents are much higher. Here the influence of the unsymmetrical bulky choline cation gets obvious. It hinders a general tight packing in the neat soap. The low temperature transition is dominated by the melting of the paraffinic chains so that they are partially molten and disordered. In the temperature range from -50°C to 95°C this enthalpy takes 64% of total enthalpy in the case of choline octanoate, 86 % of total enthalpy in the case of choline decanoate and 53-76 % of total enthalpy for the long chain choline carboxylates.[1] For choline oleate it is around 16% of the total enthalpy, because of the double bond the alkyl chains are not so dense packed in the crystalline phase compared to the saturated alkyl chains. However, in the semi-crystalline phase the alkyl chains are still hindered due to the existence of the double bond. Most of the enthalpy, almost 80 % of the total, is needed for the second phase transition. Choline oleate shows the following behavior. In the crystalline phase, formed at low temperatures, the chains are crystalline, but not so dense packed as the saturated ones. With further heating they become slightly molten, but are more inflexible as the saturated ones in this phase because of the cis-double bond. At the second phase transition a simultaneously melting of the polar groups and also of the oleate chains is observed. Choline oleate exhibits another phase transition at higher temperatures, but the obtained phase is still liquid crystalline.

5.3.4 Temperature dependent SAXS and WAXS

X-ray scattering is a method to characterize the long range structure of liquid crystals like lamellar, cubic phases etc. using small angle X-ray scattering, but also to obtain details about the flexibility of the alkyl chains from wide angle X-ray scattering. The transition temperatures of the different thermotropic phases received with this method are more or less in good agreement with the transition temperatures obtained from DSC measurements. Any differences could result again from different amounts of used substances. Comparing the temperature dependent spectra of ChC_8 (see Appendix C in section C.4), ChC_{10} (see **Figure 5-8**) and choline oleate (see Appendix C in section C.4), several sharp reflections at low temperatures and wide-angle q range appear in the spectra for all samples. They result from the crystalline nature of the low temperature phase and are typical for crystalline paraffinic chains. With increasing temperature the reflections disappear continuously. At higher temperatures they are molten and result in a broad reflection around 1.5 A^{-1}. This broad reflection is characteristic for molten alkyl chains. The small angle q region illustrates reflections which characterize long range packing. They characterize the temperature dependent phases already seen for long chain choline carboxylates[1] with an exception in the high temperature liquid crystalline phase. Instead of a smectic A phase choline octanoate,

choline decanoate and choline oleate form a defective lamellar or nematic phase structure. Further, the SAXS spectra indicate the presence of a second structure in the neat surfactant phase because some additional peaks which do not belong to the main structure of the phase appear. As mentioned in section 5.1, another explanation is possible. Instead of two structures in one phase, two thermodynamically stable phases could be in equilibrium with each other. Kinetically stablized metastable phases could not be approved, because after one year no change in the phase behavior could be found, but kinetic stabilization of such phases can of course not be ruled out completely. However, taking into account the result of the light microscopy section 5.3.2, macroscopically only one phase is observed and no clear statement could be given, which phase behavior is obvious for “neat” choline carboxylates. Therefore, in the next sections the existence of two structures in one phase is favored, keeping in mind that also two phases could be in equilibrium with each other.

Keeping this in mind, the main structure of the phase can be characterized as follows:

Low temperature structure: At low temperatures ChC_m with m = 8, 10 and oleate show a crystalline phase structure. The detailed crystalline packing like triclinic, monoclinic, etc. could not be evaluated. A lamellar bilayer phase could be ruled out by reason of missing reflections. Instead, there is formed a hydrocarbon monolayer sandwiched between the ionic layers. In the small angle region two to three reflections could be found assigning an interdigitated monolayered phase structure. More reflections could not be seen due to the limited q-range. The highest d-values, characterizing this phase, are 21.0 Å at 20°C for ChC_8, 24.6 Å at 20°C for ChC_{10} and 35.6 Å at -30°C for choline oleate. These values could result from an almost fully extended alkyl chain (like decanoate: 12.9 Å)[42] and two choline cations (about 14 Å). This is in good agreement with the long chain choline carboxylates ChC_m with m = 12, 14, 16, 18.[1] The values of choline oleate and choline octadecanoate (35.9 Å at 20°C) are not so different. However, the temperature range of the existence of the phase is lowered to very low temperatures in the case of choline oleate.

Middle temperature structure: The main phase structure is characterized by a semi-crystalline, interdigitated monolayer. It might be thought to be a rotator or gel ($L_{ß}$) phase, but the reflection at 4.2 Å[31, 39], which is typical of such a phase, is missing. The high angle range in the X-ray spectra shows several reflections. Thus, the chains in this phase structure are in motion, but with some restriction due to limited chain flexibility. To rule out other phase structurings the polymorphism of triolein, which possesses three temperature dependent phases, was taken into account especially for choline oleate.[37] Also the different temperature dependent mesophases of oleic acid were considered.[36] However, the reflections do not agree with the one observed in the semi-crystalline phase structure of choline oleate. Due to the existence of the interdigitated layer the lesser flexible oleate chains compared to the saturated alkyl chains in the semi-crystalline phase structure could be explained. With WAXS

measurements it was seen that the first phase transition shows the melting of the chains. The chains are not very flexible in the semi-crystalline structure of the neat choline oleate phase, because they are hindered due to the arrangement of the cis-double bond and forced in a special position (see **Figure 5-7**). Saturated alkyl chains are more flexible in the semi-crystalline phase, but still somewhat crystalline.

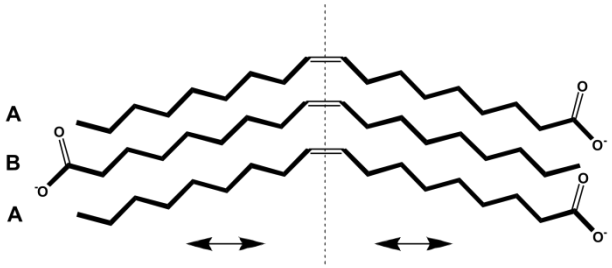

Figure 5-7. Interdigitated monolayer of oleate molecules is shown. Molecules A and B are similar to each other if the layer is symmetric. In a tilted interdigitated monolayer two types of molecules are found (A and B). The cis-double bond increases the crystallinity of the oleate chains in the semi-crystalline structure of the phase compared to the saturated long chain carboxylates.

High temperature phase structure: The main structure of the phase at higher temperatures is a bilayered structure. It could be a defective lamellar structure or a nematic phase structure as will be discussed later. This structuring possesses no long range order. The first order reflection is very broad. The second order reflection could not be observed in the case of ChC_m with m = 8, 10 due to the limited q-range and in the case of choline oleate it has a low intensity. This could indicate that locally a lamellar bilayer appears. Taking into account the long range order it results in a nematic structure or a defective lamellar structure. These defects which link the locally lamellar parts could result from the formation of another curvature. In the lamellar part the curvature is infinite. Different headgroups (here $-COO^-$ and -COOH) could create different curvatures so that these defects are formed in a lamellar structure. This structure shows the X-ray pattern of a bilayer but with broader first order reflection which indicate that the long range order is missing.[40, 41] The bilayer thickness found for ChC_8 is 18.6 Å, 21.2 Å for ChC_{10} and 30.7 Å for choline oleate. Klein *et al.* established an equation (1) which characterize the chain length m dependent bilayer thickness d for the neat long chain choline carboxylates ChC_m with m = 12, 14, 16, 18:[1]

$$\frac{d}{(Å)} = (11 \pm 1) + (1.21 \pm 0.08)m \qquad (1)$$

This equation agrees with the value for the length of a liquid CH_2-group given by Tanford (one liquid CH_2-group is 1.26 Å long).[42] The bilayer thicknesses of ChC_8, ChC_{10} and choline oleate mentioned above are in accordance with the lower limit of the calculated bilayer thickness taking into account the respective m values. Therefore, in the case of choline octanoate and choline decanoate the influence of the cation can be seen. The influence is also obvious comparing the cross sectional area of the different choline carboxylates ChC_m with m = 8, 10, 12, 14, 16, 18.[1]

The cross sectional area increases slightly in the case of ChC_8 and ChC_{10} (see **Table 5-4**) compared to the long chain choline carboxylates ChC_m with m = 12, 14, 16, 18 (a_s = 39.8-41.3 Å^2)[1]. Choline oleate shows a higher cross sectional area (see **Table 5-4**) and a smaller bilayer thickness d of 30.7 Å compared to choline octadecanoate (a_s = 41.3 Å^2 and d = 32.9 Å).[1] The bend in the oleate alkyl chain forced by the cis-conformation of the double bond causes a decrease in the bilayer thickness, but the polar-nonpolar interface area increases due to the bulkier alkyl chain. Furthermore, sodium carboxylates have a cross sectional area of the interface between the polar and nonpolar layer of ~ 40 Å^2. Therefore, also the bulky choline counterion influence the packing and increases the cross sectional area, not only by its bigger size also because of the lower counterion-headgroup binding with the carboxylate group compared to the sodium cation.[43, 44] It has to be mentioned that the values for sodium carboxylates are measured at temperatures higher than 100°C and normally the cross sectional area increases slightly with temperature.[1, 31, 32, 45]

	a_s / Å^2	d-d_L / Å	d_L / Å	T / °C
ChC_8	43.5	8.6	10.0	70
ChC_{10}	43.6	8.7	12.4	90
Choleate	43.0	8.1	22.6	90

Table 5-4. Cross sectional area a_s at the polar-nonpolar interface of the lamellar parts of the defective lamellar or nematic liquid crystalline phase, thickness of the polar layer d-d_L and thickness of the lipophilic bilayer d_L at 90°C. Choline octanoate forms this phase until 70°C, above 70°C it is molten.

Choline octanoate shows another phase at higher temperatures. This is an isotropic melt. Over 70°C a broad reflection at 0.3 Å^{-1} characterizes a molten phase. The structure of this phase could not be evaluated in detail as seen in section 4.3.4.6 in Chapter 4. Due to the DSC measurements choline oleate should possess another phase transition at the heating cycle around 62.9°C and at the cooling cycle at 42.3°C. With SAXS measurements no additional phase transition of the superior packing at this temperature range was observed. The layer distance remains the same. Thus, the phase transition does not result from a change in the packing. It could result from a change in the second structure of the phase, but it could not be evaluated in detail.

As stated above, choline carboxylates do not form a single-structured phase. There is always a main structure, which is described above. The smaller part of the phase forms a more flexible structure. The additional reflections found in the SAXS spectra could result from the structure formed by the smaller part of phase. For example the double peak in the SAXS spectra of choline oleate at 0.3°C (see Appendix C in section C.4.2) or ChC_{10} at the second heating cycle at 80.0°C (see **Figure 5-8** (C)) illustrates the existence of a second structure in the phase of “neat” surfactant. Also from some 2D-spectra the existence of this structure could be assumed. Therefore, the composition in the “neat” surfactant phase is not uniform and the architecture of the second structure of the phase could not be identified. Also it could

not be evaluated if really two structures exist in one phase or if two phases (thermodynamically stable or kinetically stabilized) are in equilibrium with each other.

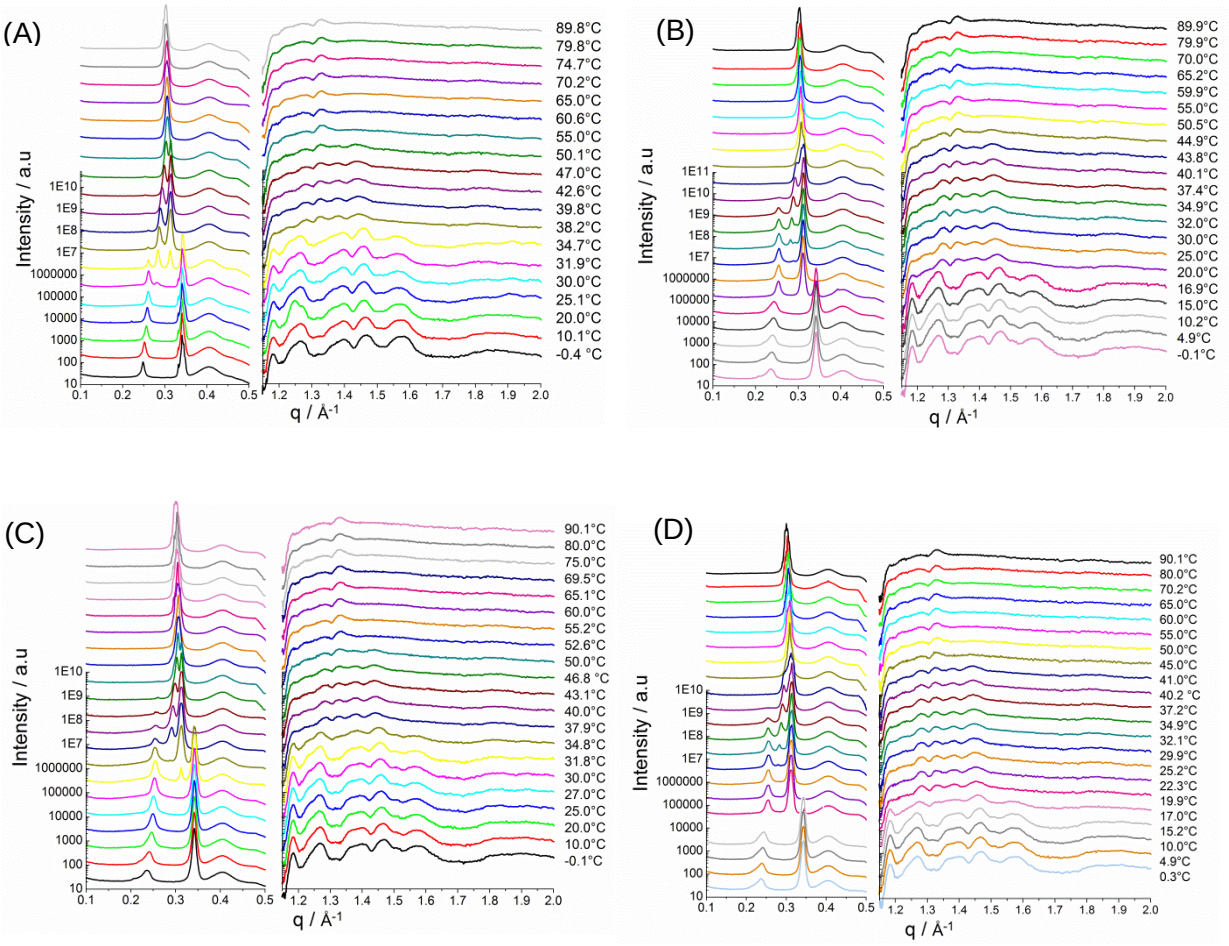

Figure 5-8. Temperature dependent X-ray spectra of choline decanoate. The heating rate is 1 K min^{-1}. Two cyles were recorded: (A) First heating of sample (freshly molten), (B) first cooling of freshly molten sample, (C) second heating of reheated sample, (D) second cooling of reheated sample. At low temperatures a lot of peaks were present in the wide angle region. They result from the crystalline paraffinic chains. With increasing temperatures the peaks disappear. At higher temperatures a broad peak around 1.5 $Å^{-1}$ arises, resulting from the molten alkyl chains.

However, the existence of two headgroups: the carboxylate headgroup and the carboxylic acid headgroup could be assumed. From literature it is known that triethanolammonium oleate, a hygroscopic substance, can form liquid crystalline phases at room temperature because of the transition to the uncharged triethanolamine and the oleic acid which form the solvent of the liquid crystalline phase.[46] The cation choline is comparable to triethanolammonium and, as already mentioned, the neat choline carboxylates are very hygroscopic. Therefore, the following equilibrium could exist in the neat choline carboxylate soap (see **Figure 5-9**).

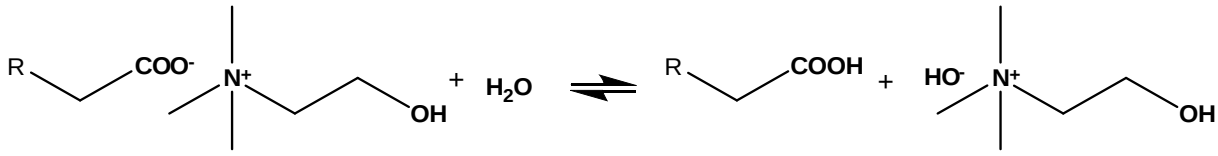

Figure 5-9. The equation shows the equilibrium between choline soap and water and choline hydroxide and the respective carboxylic acid.

The different pK_a values are: oleic acid $pK_a \approx 5$; octanoic acid $pK_a = 4.89$, the one of choline decanoate should be slightly higher[47, 48]; choline hydroxide $pK_a = 13.9$[49]. Therefore, the equilibrium between the carboxylic acid and the carboxylate is definitely possible. It could explain the existence of a second structuring and of a defective lamellar or nematic high temperature structure in the phase. This equilibrium (see **Figure 5-9**) explains the existence of two different headgroups ($-COO^-$ and -COOH) and because of this the possibility to create different curvatures. Defects in the lamellar phase could be created due to the different curvatures and could destroy the long range order of the smectic A phase and therefore result in a defective lamellar or nematic phase structure and further cause the existence of a second structure.[40] However, it will be shown in Chapter 7 that this is only a hypothesis for the appearance of the second structure and the defective lamellar or nematic structure at high temperature in neat choline carboxylates. The existence of the carboxylic acid could not be proved with other performed measurements, as infrared spectroscopy (IR), but it could not be excluded.

5.3.5 Temperature variable ^{1}H NMR

Proton (^{1}H) NMR studies were undertaken as another independent method for phase characterization. The main anisotropic interaction of protons in a solid is the homonuclear dipolar coupling between neighboring nuclear dipoles. This interaction results in a broadening of NMR lines. Anisotropic motion in non-crystalline regions reduces this effect and isotropic reorientation in the liquid state averages it out. Thus, the residual homonuclear ^{1}H dipole-dipole coupling differs in crystalline, semi-crystalline and liquid crystalline phases of choline soaps (see **Figure 5-10**) and provides a possibility to monitor qualitatively the temperature dependence of the rotational and translational molecular motions. These molecular motions are related to the flexibility of the alkyl chains in the different phases. This dependence can be expressed in terms of the spin-spin relaxation time T_{2eff}. The characteristic values of T_{2eff} for $-CH_2-$ groups in different phases are: < 10 µs in crystalline surfactants[50, 51]; 20-30 µs in gel or semi-crystalline phases[51]; 100-200 µs in lamellar phases[50-53]. In a "normal" liquid T_{2eff} is above 1 ms.[50] The spin-spin relaxation time can be obtained

directly from the free induction decay, FID, but this procedure is favorable for one phase systems only.[1]

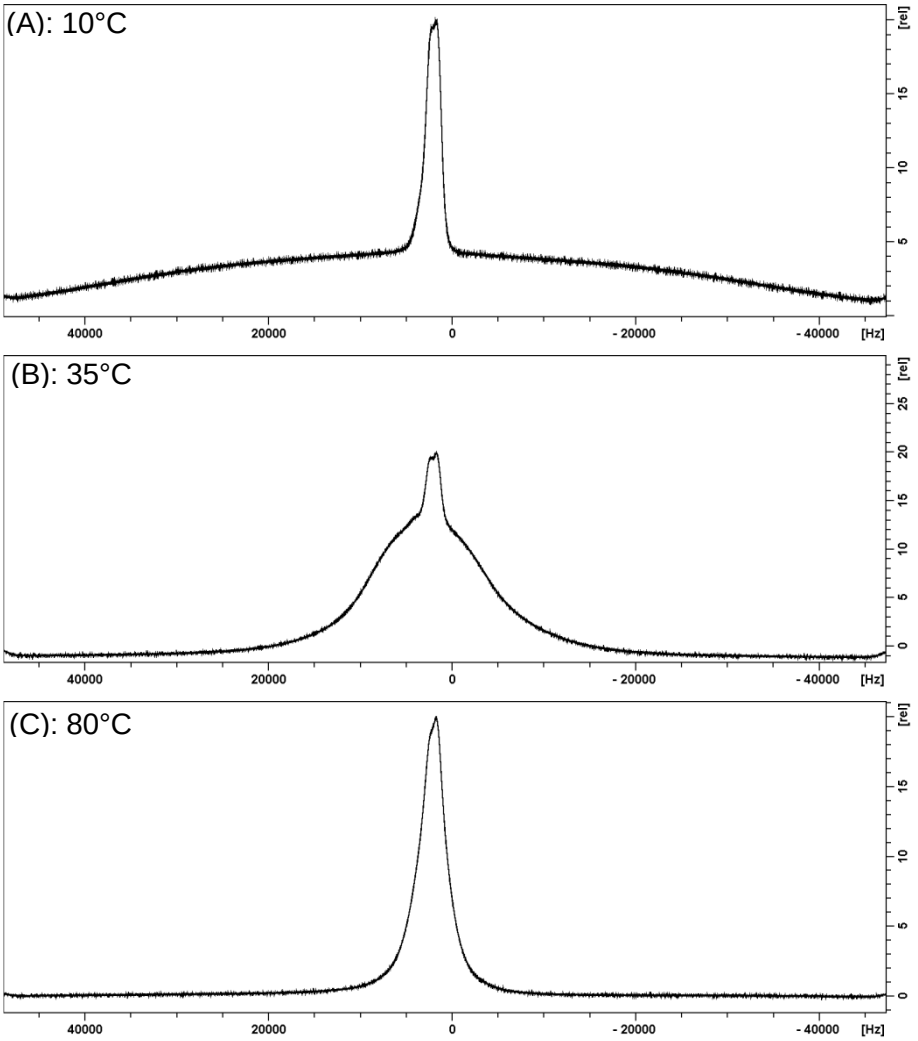

Figure 5-10. Temperature variable ^{1}H NMR spectra of neat choline decanoate demonstrate the presence of the phase heterogeneity in the sample. Besides (A) a 30 kHz broad peak at 10°C associated with the crystalline structure, (B) a 15 kHz broad peak at 35°C assigned to the semi-crystalline structure and (C) a 2 kHz broad peak at 80°C attributed to the liquid crystalline structure, the spectra exhibit further partially overlapped sharp peaks resulted from a second flexible, liquid-like structure in the phase of neat choline decanoate.

Here the spin-spin relaxation time T_{2eff} was calculated from the half width (in Hertz) at half-height of an NMR peak, whose line-shape has been fitted with a Gaussian-Lorentzian equation. The values of T_{2eff} have been used to monitor the molecular order at different temperatures (see **Figure 5-11**).[54] The attribution of the spectral pattern depicted on **Figure 5-10** to a superposition of a broad and sharp line arise from decanoate (H_{19}) and choline (H_{14}), respectively, can be rejected for the reason of the very different integral intensities of these lines. Instead, it has been assumed that the spectra are dominated by superimposed broad peaks resulting from the protons of the -CH_2-, -CH_3 and hydroxyl groups of choline and the respective carboxylate anion arrested in the main structure of the phase and that the

sharp peak of small integral intensity should be attributed to the second, minor phase structure. For each structure the ratio of the choline cation to carboxylate anion has been fixed to 1:1 molar that is the intensity of the respective NMR peak related to the number of protons of the cation and anion. The analysis of experimental spectra demonstrates that the ratio between the main and minor structures in the phase of neat anhydrous ChC_{10} and choline oleate does not depend on temperature. About 91.3 % of the molecules of ChC_{10} and 86.1 % of the molecules of choline oleate form the main phase structure. In the case of ChC_8 the amount of the minor structure of the phase increases strongly with temperature (4 % of overall intensity at 5°C and 100 % of overall intensity at 70°C and higher). In all cases the minor structuring should be attributed to a flexible, liquid-like phase structure.

The heating/cooling rates throughout were 1 K min^{-1}. ChC_{10} and choline oleate show similar relaxation times for the same structure of the main part of the phases as explained before. Only the semi-crystalline structure of choline oleate with relaxation times around 13 µs is, as already mentioned, more ordered. The relaxation time values for the liquid crystalline phase structure of ChC_8 are slightly smaller than expected for a defective lamellar phase structuring (see **Figure 5-11**) that indicates a restricted molecular mobility in this system. For the complete data set concerning the relaxation times and the amount of the main structure of the phase see in section C.5 in Appendix C.

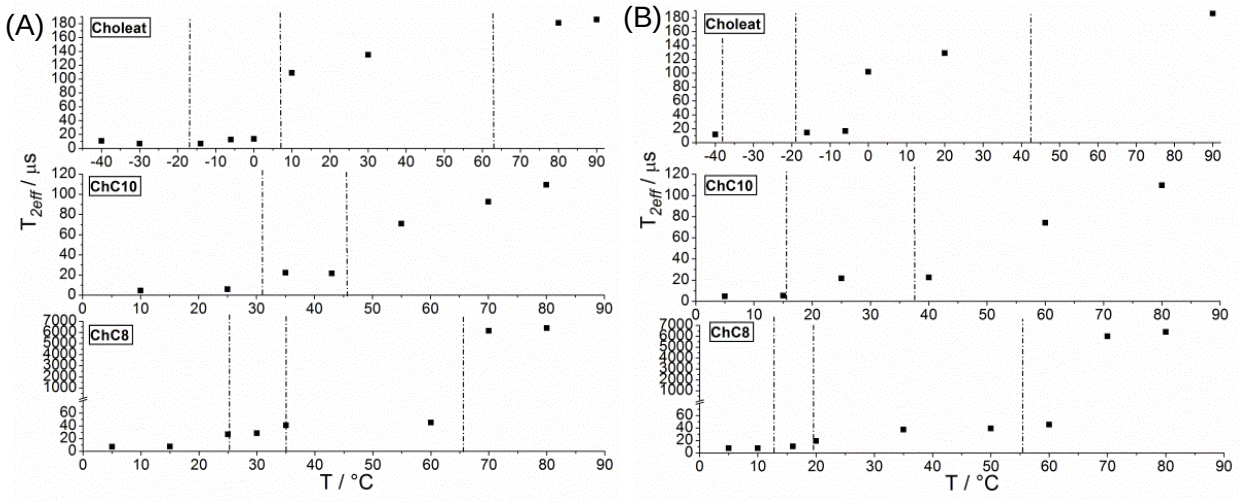

Figure 5-11. Temperature dependent spin-spin relaxation time T_{2eff} of the structure of the main part of the phase of anhydrous choline octanoate, choline decanoate and choline oleate. (A) The heating cycle of a reheated sample and (B) the cooling cycle are shown. The vertical lines mark the transition temperatures as obtained with DSC measurements.

As already mentioned, the structure formed by a minor part of the molecules in the phase is a flexible, liquid-like one exhibiting quasi-isotropic molecular motion. It can be formed due to the presence of both the carboxylic acid and the choline carboxylate.

However, also with this method it was not possible either to check if only one phase with two structures is formed for neat choline carboxylates (as explained above) or if two thermodynamically stable/kinetically stabilized phases/metastable phases, a more solid-like phase and a liquid-like phase, are in equilibrium with each other.

5.3.6 Comparison with alkali carboxylates

Here a short overview of the thermotropic phase behavior of carboxylates with varying inorganic cation is given. Normally, the alkali alkanoates show an increase in the transition temperature to the isotropic melt with increasing cation size.[16, 17, 23-25] The lithium cation is an exception.[23] However, also choline does not follow this trend.[1] All alkali alkanoates from sodium to cesium have been investigated by Skouklios, Vold and a lot of more.[17, 32] They found that the melting process of the alkali carboxylates in general is characterized by two steps: First the melting of the alkyl chains and then the one of the polar groups. The last melting temperature decreases with increasing alkyl chain length, because the balance between the polar and nonpolar region is stronger for short chain alkanoates and the polar interaction hinders the chain melting.[32] The nature of the cation has a stronger influence on the appearance of mesophases in short chain alkali alkanoates than in the long chain alkanoates.[32]

Most of the anhydrous long chain sodium alkanoates with chain length from laurate to stearate pass different thermotropic phases with increasing temperature. Typically, five temperature dependent phases are formed until they melt to an isotropic liquid. These phases appear in the temperature range from 100°C to 320°C. Sodium oleate forms six temperature dependent phases and a direct transition to isotropic phase without the formation of a lamellar phase was observed.[17] The phase transitions of the temperature dependent phases of sodium oleate are also shifted to lower temperatures (first phase transition 40°C; last phase transition 237°C). The total heat of fusion of sodium oleate is smaller than the one of sodium stearate. In the case of sodium stearate a closer packing of the chains is possible (sodium stearate ΔH_f = 57.9 kJ mol^{-1} > sodium oleate ΔH_f = 35.6 kJ mol^{-1}).[17] Studies suggested that the heat of transition and the transition temperature should increase linearly with the alkyl chain length. But in the case of sodium alkanoates this linearity could not be proved in experiments. Therefore the changes in the balance between the polar and non-polar groups are more important than the simple effect of the chain length.[17, 32] Concerning the short chain sodium alkanoates: sodium acetate shows only a transition from a crystalline phase to a liquid melt. Three phases could be evalutated in the case of sodium butanoate and four for sodium hexanoate. The last phase is the transition to the isotropic melt. For sodium octanoate four phases are observed, for sodium decanoate five phases are formed, which end in the isotropic melt.[15] The problem concerning these

short chain sodium alkanoates is the accurate characterization of the different phases. It occurs to be more complicated compared to the one of the long chain carboxylates.[15, 16] However, it is known that the sodium alkanoates with chain length 6 to 10 do not form a subneat phase (disc like structure)[55] compared to the long chain ones.[32]

With increasing temperature lithium alkanoates from laureate to eicosanoate show the following phases: lamellar II, lamellar I, plastic crystal (ribbon like structure), melt. The lithium heptanoate, octanoate, nonanoate and decanaote form the same phases with the exception of the plastic ribbon like crystal. The short chain lithium carboxylates (m = 3-11) show again higher energies of fusion because of the hindered fusion due to the huge interaction of the polar groups.[35]

5.4 Conclusion

In this study the different mesophases of the choline carboxylates ChC_m with m = 2, 4, 6, 8, 10 and oleate, taking into account the influence of the chain length, the variation of the chain properties, and also the impact of the choline cation, were investigated. These choline carboxylates were compared to the longer chain ones (m = 12, 14, 16, 18).[1] Only the temperature range from -50°C to 95°C was investigated. Higher temperatures were avoided to prevent the thermal decomposition of the choline cation. Compared to the alkali cation, the influence of choline on the thermotropic phase behavior of the carboxylates is significant. In general, the transition temperatures are shifted to much lower temperatures. The influence of the choline cation increases with decreasing chain length. Especially, this is observed focusing on choline acetate, choline butanoate and choline hexanoate. They only form one stable crystal phase and melt directly to an isotropic liquid. In contrast, the alkali alkanoates with the same chain lengths could create more mesophases due to the smaller cation. The longer chain choline carboxylates like the choline octanoate and the choline decanoate are able to form mesophases, but as seen with light microscopy, DSC, WAXS, and SAXS measurements the stability of the mesophases decreases from choline decanoate to choline octanoate. During the cooling cycle the last transition to the crystalline phase is very temperature dependent and shows the influence of the cation on the crystallization of the alkyl chains. Choline as a cation increases the hygroscopic behavior of carboxylates, especially with decreasing chain length. This could have a significant influence on the thermotropic behavior of neat choline carboxylates. Water could not be removed completely (3000-4000 ppm usually remained). Therefore, it is possible that the equilibrium between the choline carboxylate and water and the choline hydroxide and carboxylic acid is formed. As a consequence, two different structures are found in one phase for (nearly) neat choline octanoate, choline decanoate and choline oleate in the temperature range between -50°C

and 95°C. A small part of the phase shows a structure with a very flexible, liquid-like behavior, but the structure of the main part of the phase is similar to the one of the longer chain choline carboxylates ChC_m with m = 12, 14, 16, 18.[1] The compositions of the two parts of the phase are not known exactly. Due to the different headgroups (-COO^- and -COOH) different curvatures can occur in a phase. However, the existence of the carboxylic acid could not be proved with infrared spectroscopy (IR) measurements, because the specific antisymmetric stretching of the carboxylic acid (-COH; $\nu \approx 1700$ cm^{-1}) is overlapping with the -COH stretching of choline cation. The structure of the main part of the phase is temperature dependent: at low temperatures a crystalline, interdigitated monolayer structure is formed, at middle temperatures a semi-crystalline, interdigitated monolayer phase structure appears. The existence of the $L_ß$ phase could be ruled out by X-ray measurements. At high temperatures a liquid crystalline defective lamellar or nematic phase structure was observed. The longer chain choline carboxylates (m = 12-18) form at highest temperature phase a smectic A lamellar phase.[1] In the defective lamellar or nematic phase structure, found in this study, locally a lamellar bilayer is formed, but owing to the different headgroups, defects appear within the bilayers having a different curvature, which reduces the long range order of a smectic A lamellar phase. Choline octanoate shows another phase transition to an isotropic melt. For choline oleate also another phase is found at higher temperatures. It was only observed by DSC measurements and has a transition enthalpy of 0.6-0.7 kJ mol^{-1}. This phase transition does not change the bilayer thickness of the defective lamellar phase structure. It could result from structural changes in the second, minor structure of the phase. Furthermore, the double bond lowers the transition temperatures compared to the choline stearate.

However, as already mentioned in the discussion it could not be clearly checked whether a phase with two structures is observed for the choline carboxylates along the whole temperature range or if equilibrium between two thermodynamically stable/kinetically stabilized phases/metastable phases exists. Macroscopically one phase is found. Another point is, it could not be evaluated if and which components are available in the phase beside the choline carboxylates.

As mentioned in the introduction, choline butanoate and choline hexanoate were found by the group of Muhammad *et al.*[14] as liquid at room temperature. This result could not be confirmed. It could be that the different synthesis methods and the used starting products and the stabilizers inside lead to the apparent lower melting temperature.

To sum up, it could be observed that the influence of the bulky choline cation on the thermotropic phase behavior is very strong and increases with decreasing chain length. Furthermore, choline octanoate, choline decanoate and choline oleate form two different structures in the neat surfactant phase or another possible explanation of the results is that

two phases which are in equilibrium with each other are formed along the whole investigated temperature range. The melting temperatures of all considered choline carboxylates are lower than 100°C and so the choline carboxylates ChC_m with m = 2, 4, 6, 8, 10 and oleate can be classified as ionic liquids.

5.5 Experimental

5.5.1 Chemicals and sample preparation

The choline carboxylates ChC_m with m = 2, 4, 6, 8, 10 and choline oleate were prepared as described in Chapter 3 in section 3.5.1. The purity of the choline carboxylates was evaluated with electro-spray mass spectroscopy (ES-MS) and ^{1}H and ^{13}C NMR measurement were performed. Mass spectrometry data were recorded on a ThermoQuest Finnigan TSQ 7000 instrument. The ^{1}H and ^{13}C NMR-spectra were recorded with a Bruker Avance 300 spectrometer at 300 MHz using tetramethylsilane (TMS) as internal standard. Coulometric Karl-Fischer titration was performed on an Abimed MCI analyzer (Model CA-02) to determine the water content. The average water content was found between 1300 ppm and 3600 ppm (see section 3.5.1 in Chapter 3). Furthermore, to prevent the sample of water contamination the choline carboxylates were stored and the samples were prepared in a glove box floated with nitrogen. All experiments were carried out under nitrogen atmosphere or in vacuum.

5.5.2 Methods

5.5.2.1 Differential scanning calorimetry (DSC)

The different phase transition temperatures, the melting (T_m) and the crystallization temperature (T_c) were determined on a Perkin-Elmer DSC 7. The sample preparation has been done in a nitrogen floated glove box. Around 5-15 mg of the sample was placed in aluminum pans. The different choline carboxylates ChC_m with m = 2, 4, 6, 8, 10 and oleate were scanned in the temperature range between -50°C and 95°C. The temperature range was limited to 95°C to avoid thermal degradation. These samples were all investigated with a heat rate of 1 K min^{-1}. From each sample three cycles were measured. As reference an empty aluminum pan was used. Enthalpy and temperature calibration was performed by measuring high purity indium as a standard. The temperature of the peak maximum/minimum is taken as the transition temperature. To calculate the transition enthalpies the integrated whole peak area, the sample mass, the heating and cooling rate and the molar mass of the substance were taken into account.

5.5.2.2 Thermogravimetric analysis

Decomposition temperatures (T_{dec}) and the thermal stabilities were quantified in aluminum pans under a constant nitrogen flow using a thermogravimetric analyzer from Perkin-Elmer (TGA 7). The heating rate was 10 K min^{-1}. T_{dec} was obtained by taking the onset of the mass loss. It was evaluated by the intersection of the baseline before decomposition and the tangent to the mass loss versus the temperature.

5.5.2.3 Polarizing optical microscopy

The light microscopy images were measured on a Leitz Orthoplan microscope (Wetzlar, Germany) fitted with a JVC digital camera (TK-C130) and a Linkham hot stage equipped with a TMS90 temperature controller (± 0.5°C) and a CS196 cooling system. The measurements were performed in a nitrogen glove box to avoid the contamination with water from the air. A spatula tip of substance was put between two microscope slides. At least three heating and cooling cycles were recorded with a heating and cooling rate of about 10 K min^{-1} (ChC_m with m = 2, 4, 6, 8, 10 and oleate) and one with 1 K min^{-1} (ChC_m with m = 8, 10 and oleate).

5.5.2.4 Small and wide angle X-ray scattering

Small and wide angle X-ray scattering experiments were performed with the DORIS III equipment at DESY in Hamburg. The A2 beamline runs experiments at fixed energy of 8 keV. The operating wavelength was 0.15 nm. The samples were measured during two heating and cooling cycles. The heating rate was 1 K min^{-1}. Due to the very hygroscopic nature of the choline carboxylates two types of self-constructed sample cell were built so that the preparation of the cell and the measurement could be completely done in nitrogen or vacuum atmosphere. For ChC_m with m = 2, 4, 6, 8, 10 the cell was made of stainless steel plates with a 7 mm diameter hole. The thickness of the sample was 2.8 mm. The Jumo Imago 500 was used as a temperature control. The holes were covered from both sides with Kapton foil. The cell of choline oleate was made of copper and a cooling system and a temperature controller, using a PT 100 element, were included. The samples were measured in vacuum to avoid contamination with water. The scattered beam was detected with one linear positron sensitive gasfilled detector for the WAXS region and a MarCCD detector for the SAXS region. The MarCCD detector has a resolution of 1024 x 1024 px and a pixel size of 158 x 158. The sample to detector distance was given as 789.07 mm.

The two dimensional spectra were integrated using the IDL software in order to obtain the scattered intensity as a function of the scattering vector q. The scattering vector q is written as $q = (4\pi/\lambda)\cdot\sin\theta$ with θ being the scattering angle and d can be written as $d = 2\pi/q$. X-ray

measurements were performed in the q-region from 0.1 $Å^{-1}$ to 0.5 $Å^{-1}$ and 1.15 $Å^{-1}$ to 2.0 $Å^{-1}$. The SAXS and WAXS spectra were recorded simultaneously. By reason of necessary special arrangement of the SAXS and WAXS detectors, the range from 0.5 $Å^{-1}$ to 1.15 $Å^{-1}$ could not be recorded. The peak at 0.4 $Å^{-1}$ results from the Kapton foil of the cell.

5.5.2.5 Temperature variable ^{1}H NMR

NMR measurements were carried out on a Bruker Avance 400 MHz instrument. The neat powder was prepared in a 20.3 cm long NMR tube 507-HP from NORELL with an outer diameter of 5 mm in nitrogen atmosphere. The heating and cooling rates during the measurements were 1 K min^{-1}. The measurements of the temperature cycle were started at low temperatures. The cycles of heating and cooling were done twice, to check the reproducibility. The 1D spectra were fitted with 1D WINNMR using the Deconvolution2 fitting, taking into account the Gaussian-Lorentzian equation, to get the half width at half-height of the NMR peak ($\Delta\nu$ in Hz) and to calculate T_{2eff} ($T_{2eff} = (\pi \cdot \Delta\nu)^{-1}$); see Appendix C section C.5)[1, 51, 56, 53].

The measurements for choline oleate were recorded from -40°C to 90°C. From DSC it is known that the lowest temperature phase transition occurs down to -50°C. Thus, it could be that the spectra of -40°C for choline oleate shows a phase which is not in full equilibrium.

5.6 References

1. R. Klein, H. Dutton, O. Diat, G. J. Tiddy and W. Kunz, *J. Phys. Chem. B*, 2011, **115**, 3838-3847.
2. P. Moriel, E. J. Garcia-Suarez, M. Martinez, A. B. Garcia, M. A. Montes-Moran, V. Calvino-Casilda and M. A. Banares, *Tetrahedron Lett.*, 2010, **51**, 4877-4881.
3. P. Nockemann, B. Thijs, K. Driesen, C. R. Janssen, K. Van Hecke, L. Van Meervelt, S. Kossmann, B. Kirchner and K. Binnemans, *J. Phys. Chem. B*, 2007, **111**, 5254-5263.
4. Y. Fukaya, Y. Iizuka, K. Sekikawa and H. Ohno, *Green Chem.*, 2007, **9**, 1155-1157.
5. G. J. Kortstee, *Arch. Microbiol.*, 1970, **71**, 235-244.
6. S. H. Zeisel and K. A. da Costa, *Nutr. Rev.*, 2009, **67**, 615-623.
7. J. T. Penry and M. M. Manore, *Int. J. Sport Nutr. Exerc. Metabol.*, 2008, **18**, 191-203.
8. S. Sekar, M. Surianarayanan, V. Ranganathan, D. R. MacFarlane and A. B. Mandal, *Environ. Sci. Technol.*, 2012, **46**, 4902-4908.
9. A. P. Abbott, G. Capper, D. L. Davies, R. K. Rasheed and V. Tambyrajah, *Chem. Commun. (Camb.)*, 2003, 70-71.
10. H. Zhao, G. A. Baker and S. Holmes, *Org. Biomol. Chem.*, 2011, **9**, 1908-1916.

11. R. Ferreira, H. Garcia, A. F. Sousa, M. Petkovic, P. Lamosa, C. S. R. Freire, A. J. D. Silvestre, L. P. N. Rebelo and C. S. Pereira, *New J. Chem.*, 2012, **36**, 2014-2024.
12. H. Garcia, R. Ferreira, M. Petkovic, J. L. Ferguson, M. C. Leitao, H. Q. N. Gunaratne, K. R. Seddon, L. P. N. Rebelo and C. S. Pereira, *Green Chem.*, 2010, **12**, 367-369.
13. M. Petkovic, J. L. Ferguson, H. Q. N. Gunaratne, R. Ferreira, M. C. Leitao, K. R. Seddon, L. P. N. Rebelo and C. S. Pereira, *Green Chem.*, 2010, **12**, 643-649.
14. N. Muhammad, M. I. Hossain, Z. Man, M. El-Harbawi, M. A. Bustam, Y. A. Noaman, N. B. Mohamed Alitheen, M. K. Ng, G. Hefter and C.-Y. Yin, *J. Chem. Eng. Data*, 2012, **57**, 2191-2196.
15. P. Franzosini and M. Sanesi, *Thermodynamic and Transport Properties of Organic Salts*, Pergamon Press, Oxford, 1980.
16. M. J. Vold, M. Macomber and R. D. Vold, *J. Am. Chem. Soc.*, 1941, **63**, 168-175.
17. R. D. Vold, *J. Am. Chem. Soc.*, 1941, **63**, 2915-2924.
18. A. M. Amorim Da Costa, H. D. Burrows, C. F. G. C. Geraldes, J. J. C. Teixeira-Dias, C. G. Bazuin, D. Guillon, A. Skoulios, E. Blackmore, G. J. T. Tiddy and D. L. Turner, *Liq. Cryst.*, 1986, **1**, 215-226.
19. P. Pacor and H. L. Spier, *J. Am. Chem. Soc.*, 1968, **45**, 338-&.
20. L. Jongen, K. Binnemans, D. Hinz and G. Meyer, *Liq. Cryst.*, 2001, **28**, 819-825.
21. L. Jongen, K. Binnemans, D. Hinz and G. Meyer, *Liq. Cryst.*, 2001, **28**, 1727-1733.
22. L. Jongen, K. Binnemans, D. Hinz and G. Meyer, *Mater. Sci. Eng. C*, 2001, **18**, 199-204.
23. B. Gallot and A. Skoulios, *Kolloid Z. Z. Polym.*, 1966, **209**, 164-169.
24. B. Gallot and A. Skoulios, *Mol. Cryst.*, 1966, **1**, 263-292.
25. B. Gallot and A. Skoulios, *Kolloid Z. Z. Polym.*, 1966, **213**, 143-150.
26. C. Madelmont and K. Perron, *Colloid Polym. Sci.*, 1976, **254**, 581-595.
27. J. W. McBain and W. J. Elford, *J. Chem. Soc.*, 1926, 421-438.
28. J. W. McBain and W. C. Sierichs, *J. Am. Oil Chem. Soc.*, 1948, **25**, 221-225.
29. R. D. Vold, *J. Phys. Chem.*, 1939, **43**, 1213-1231.
30. J. W. McBain and W. W. Lee, *Oil & Soap*, 1943, **20**, 17-25.
31. M. D. Small, *The Physical Chemistry of Lipids from Alkanes to Phospholipids*, Plenum Press, New York and London, 1986.
32. K. Binnemans, *Chem. Rev.*, 2005, **105**, 4148-4204.
33. F. Mathevet, P. Masson, J. F. Nicoud and A. Skoulios, *J. Am. Chem. Soc.*, 2005, **127**, 9053-9061.
34. C. G. Bazuin, D. Guillon, A. Skoulios, A. M. A. Dacosta, H. D. Burrows, C. F. G. C. Geraldes and J. J. C. Teixeiradias, *Liq. Cryst.*, 1988, **3**, 1655-1670.
35. P. Ferloni and E. F. Westrum, *Pure and Appl. Chem.*, 1992, **64**, 73-78.

36. F. Kaneko, K. Yamazaki, K. Kitagawa, T. Kikyo, M. Kobayashi, Y. Kitagawa, Y. Matsuura, K. Sato and M. Suzuki, *J. Phys. Chem. B*, 1997, **101**, 1803-1809.
37. C. Akita, T. Kawaguchi and F. Kaneko, *J. Phys. Chem. B*, 2006, **110**, 4346-4353.
38. R. Klein, G. J. T. Tiddy, E. Maurer, D. Touraud, J. Esquena, O. Tache and W. Kunz, *Soft Matter*, 2011, **7**, 6973.
39. D. M. Small, *J. Lipid Res.*, 1984, **25**, 1490-1500.
40. O. Dhez, S. Konig, D. Roux, F. Nallet and O. Diat, *Eur. Phys. J. E*, 2000, **3**, 377-388.
41. P. O. Quest, K. Fontell and B. Halle, *Liq. Cryst.*, 1994, **16**, 235-256.
42. C. Tanford, *J. Phys. Chem.*, 1972, **76**, 3020-3024.
43. K. D. Collins, *Methods*, 2004, **34**, 300-311.
44. K. D. Collins, G. W. Neilson and J. E. Enderby, *Biophys. Chem.*, 2007, **128**, 95-104.
45. A. E. Skoulios and V. Luzzati, *Acta Crystallogr.*, 1961, **14**, 278-286.
46. S. E. Friberg, P. Liang, F. E. Lockwood and M. Tadros, *J. Phys. Chem.*, 1984, **88**, 1045-1046.
47. J. R. Kanicky and D. O. Shah, *Langmuir*, 2003, **19**, 2034-2038.
48. S. Salentinig, L. Sagalowicz and O. Glatter, *Langmuir*, 2010, **26**, 11670-11679.
49. H. Iwamoto, R. D. Blakely and L. J. De Felice, *J. Neurosci.*, 2006, **26**, 9851-9859.
50. I. Kamel and A. Charlesby, *J. Polym. Sci. Polym. Phys.*, 1981, **19**, 803-814.
51. C. D. Adam, J. A. Durrant, M. R. Lowry and G. J. T. Tiddy, *J. Chem. Soc. Farad. T. 1*, 1984, **80**, 789-801.
52. R. Y. Dong, M. Wiszniewska, E. Tomchuk and E. Bock, *J. Chem. Phys.*, 1973, **59**, 6266-6268.
53. K. Rendall, G. J. T. Tiddy and M. A. Trevethan, *J. Chem. Soc. Farad. T. 1*, 1983, **79**, 637-&.
54. H. Wennerström, *Chem. Phys. Lett.*, 1973, **18**, 41-44.
55. H. D. Dörfler, *Grenzflächen und kolloid-disperse Systeme: Physik und Chemie*, Springer, Berlin, 2002.
56. E. S. Blackmore and G. J. T. Tiddy, *Liq. Cryst.*, 1990, **8**, 131 - 151.

Chapter 6

Aqueous behavior of choline alkylsulfates ChS_m with m = 12, 16

6.1 Abstract

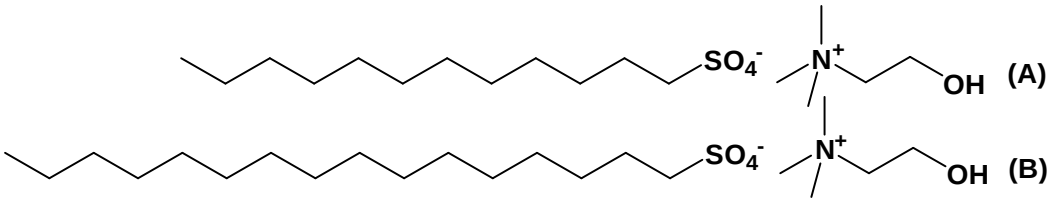

Figure 6-1. Molecular structure of choline dodecylsulfate (A) and choline hexadecylsulfate (B)

Sodium soaps belong to one of the oldest known surfactants. They are biocompatible and are composed of natural products, the fatty acids. But a lot of problems were found in applications with sodium soaps concerning their usability in formulation or washing application. They are very sensitive to salts and possess high Krafft temperatures. Choline as cation for carboxylate soaps lowers the Krafft temperature, but the salt sensitivity and the high pH of the carboxylate soaps remain.[1, 2] The sodium alkylsulfates are used due to their low pH and their low salt sensitivity. But the long chain ones show a high Krafft point. Choline alkylsulfates were thought to be a good alternative without the above mentioned problems. They are less salt sensitive and show neutral pH in applications. In the present study it was tested if longer chain choline alkylsulfates could be used due to a lower Krafft temperature in formulation compared to their sodium homologs. The Krafft temperature of choline hexadecylsulfate (ChS_{16}) was investigated and compared to the one of choline dodecylsufate (ChS_{12}) and its sodium analog. Furthermore, the *cmc* and the aqueous phase behavior of these two choline alkylsulfates ChS_m with m = 12, 16 were investigated with small and wide angle X-ray scattering measurements, polarizing optical light microscopy, conductivity, surface tension measurements, and visual observations. Finally, the cytotoxicity was tested with HeLa and SK-MEL-28 cells.

6.2 Introduction

Sodium dodecylsulfate (NaS_{12}) is a very common low cost surfactant. It belongs to the class of alkylsulfate surfactants. Compared to normal soaps, this class of surfactant does not show high pH in application due to the more acidic sulfate headgroup. In general, alkylsulfates are biodegradable, low toxic and are synthesized from renewable raw material.[3-5] Sodium dodecylsulfate is used in several formulations, such as shampoo, shower gel or washing powder.[3, 4] However, the longer homologs are not very common in application, because of their low solubility at room temperature. For example sodium hexadecylsulfate has a high Krafft temperature of 46°C.[6] It is desirable to lower the Krafft temperatures of long chain alkylsulfates to get a broader field of application. For choline carboxylate soaps it could be

shown that choline lowers the Krafft temperature of these fatty acid soaps.[2, 7, 8] Taking into account Collins´ concept of "matching water affinities"[9, 10] choline belongs to the "soft" cations and binds stronger to the "soft" sulfate headgroup than the "hard" counterion sodium. This headgroup-counterion interaction should influence the Krafft temperature. This influence could also be observed for alkali cations. The Krafft temperature increases for alkylsulfates with increasing size of alkali cation ($Li^+ < Na^+ < K^+ < Rb^+ < Cs^+$)[11, 12], while the one of the alkylcarboxylates decreases with increasing size of alkali cation.[13-15] However, Klein *et al.*[12] found that the Krafft temperature of choline dodecylsulfate is around 0°C and decreases compared to the one of sodium dodecylsulfate. Therefore, the importance of the bulky, unsymmetrical structure of the choline cation on the Krafft temperature is higher than the headgroup-counterion interaction.[12] Most of the tetraalkylammonium counterions combined with alkylsulfates (solubility of alkylsulfates increase: $K^+ < Na^+ < NR_4^+$)[2, 15-19] and alkylcarboxylates[15-19] show a similar effect as found for choline. In this study, further to the counterion dependence, also the chain length dependent tendency of the Krafft temperatures of choline alkylsulfates ChS_m with m = 12, 16 was investigated.

Concerning the application of surfactants in formulation or other fields, the binary phase behavior with water and the characterization of the lyotropic phase behavior is very important. Sodium dodecylsulfate and sodium hexadecylsulfate possess a rich concentration and temperature dependent phase behavior in water. The one of sodium hexadecylsulfate was investigated by Usol´tseva *et al.*.[16] The Krafft boundary, the concentration and temperature dependent crystal solubility boundary of surfactants below the Krafft eutectic,[13] is above 56°C. With increasing concentration the following phase sequence was found: micellar phase, hexagonal phase, deformed hexagonal phase, rectangular phase and lamellar phase.[16] The Krafft boundary is about 20°C higher than the one which was found for sodium dodecylsulfate.[16] The binary phase diagram of sodium dodecylsulfate was reviewed several times. In 1959, Luzzati *et al.*[17, 18] found that sodium dodecylsulfate forms a hexagonal phase with increasing surfactant concentration, then a complex hexagonal phase and at higher temperatures and concentrations a lamellar phase. These phases were characterized with SAXS experiments. In 1983, Yano *et al.*[19] extended a study on the transition of the micellar sodium dodecylsulfate solution to the hexagonal phase at low surfactant concentration. They found that spherical micelles transform to cylindrical ones, which at higher concentrations are ordered in a hexagonal lattice. In 1996, Itri *et al.*[20] made a study investigating the micellar solution to hexagonal phase transition and proposing a model for the hexagonal phase. They stated micellar growth during the phase transition and gave a model of finite micelles which are hexagonally arranged in the hexagonal phase. This model could explain the existence of several hexagonally packed structures or also the formation of a nematic phase. In 1987, Kekicheff *et al.*[21-23] published another study which presents

another phase sequence with increasing sodium dodecylsulfate concentration in water. They found four intermediate phases between the hexagonal phase and the lamellar phase. These interphases are with increasing surfactant concentration: a two-dimensional monoclinic phase, a rhombohedral phase, a cubic phase and a tetragonal phase. The phases were investigated with SANS and SAXS measurements and by calorimetry. In 1992, Lopez *et al.*[24] found a nematic phase between the hexagonal and complex hexagonal phase. As a conclusion, it seems to be difficult to evaluate the right phase sequence. In literature the widely accepted phase sequence is the one given by Kekicheff *et al.*.[21-23]

In this study the binary phase diagrams of choline dodecylsulfate and choline hexadecylsulfate with water were characterized with small (SAXS) and wide angle (WAXS) X-ray scattering measurements, polarizing optical light microscopy, penetration scan technique and visual observations. Further, the critical micelle concentration (*cmc*) was determined with concentration dependent surface tension and conductivity measurements. Also the Krafft temperature of choline hexadecylsulfate was determined. Klein *et al.*[1] have already shown a rough binary phase diagram of choline dodecylsulfate established with visual observation. In this study a refined picture was given.

6.3 Results and discussion

6.3.1 Critical micelle concentration (*cmc*)

In this study the *cmc* of choline hexadecylsulfate at 25°C and 40°C was investigated. The *cmc* of this long chain alkylsulfate at 40°C is interesting for further use in washing powder applications. The known *cmc* of choline dodecylsulfate at 25°C[1] was measured again as a standard for choline hexadecylsulfate. The *cmc* of choline hexadecylsulfate was determined by two methods: the concentration dependent measurement of the conductivity[a], and the concentration dependent evaluation of the surface tension[b] (see **Table 6-1**). The *cmc* values obtained from the different methods are comparable, but not identical, which is an expected result.[25, 26] What is known from literature and by comparing the *cmc* values of choline dodecylsulfate with the one of sodium dodecylsulfate:[1] the *cmc*s of dodecylsulfates decrease with increasing size of the counterion ($Li^+ > Na^+ > K^+ > Cs^+ > N(CH_3)_4^+ > N(CH_3)_3(CH_2)_2OH^+ > N(C_2H_5)_4^+$).[1, 4] Similar results are obtained for the *cmc* values of choline hexadecylsulfate (ChS_{16}) and sodium hexadecylsulfate (NaS_{16}). Tetraethylammonium hexadecylsulfate ($TEAS_{16}$) is an exception (see **Table 6-1**).[4]

The *cmc* of choline hexadecylsulfate increases with increasing temperature. The surface tension at the *cmc* of choline hexadecylsulfate at 25°C is 40.84 $\pm$ 0.03 mN m^{-1} and at 40°C it is 40.56 $\pm$ 0.01 mN m^{-1}. The one of choline dodecylsulfate at 25°C is 41.55 $\pm$ 0.09 mN m^{-1}. Thus, the longer chain choline alkylsulfates are as expected slightly more surface active than

the shorter chain ones. As already known, the logarithm of the *cmc* is linearly dependent on the surfactant chain length[27] and decreases with increasing number of carbon atoms m (see equation (1)):

$$\log(cmc) = \mathrm{A} - \mathrm{Bm} \qquad (1)$$

Taking into account the *cmc* values, evaluated from the surface tension measurements at 25°C, the following relation between *cmc* (in mol L^{-1}) and chain length, expressed with m, was found (see equation (2)):

$$\log(cmc) = 0.94 - 0.28\mathrm{m} \qquad (2)$$

For the sodium analogs the B value is 0.3 and the A value is 1.513.[4, 28] Therefore, the A and B values of the choline alkylsulfates are in rough agreement with the sodium ones at 25°C. The area per molecule A_s of choline hexadecylsulfate is almost constant at different temperatures. Also the area does not significantly change with the alkyl chain length (see **Table 6-1**). However, comparing the one of choline dodecylsulfate (A_s = 62.6 ± 0.2 Å^2) with the one of NaS_{12} (A_s = 60 ± 0.2 Å^2)[29] it is obvious that the area per molecule is slightly influenced by the size of the counterion (Ch^+ > Na^+). This behavior is also reflected in the surface excess concentration.[29] On the other hand, it is similar for choline dodecylsulfate and choline hexadecylsulfate.

	cmc [a] **/ mM**	***cmc*** [b] **/ mM**	**α**	**A_s / Å^2**	**Γ / mol m^{-2}**
ChS_{16} 25°C	0.37 ± 0.03	0.32 ± 0.01	0.25 ± 0.03	61.2 ± 0.6	$2.71 \cdot 10^{-6}$
ChS_{16} 40°C	0.44 ± 0.01	0.40 ± 0.03	0.24 ± 0.00	62.3 ± 0.1	$2.66 \cdot 10^{-6}$
NaS_{16} 25°C	0.45[4]	-	0.20[30]	-	-
NaS_{16} 40°C	0.58[4, 26]	-	-	-	-
$TEAS_{16}$ 25°C	1.2[4] (method not specified)		-	-	-
ChS_{12} 25°C	5.99 ± 0.06[1]	4.09 ± 0.03	0.30[31]	62.6 ± 0.2	$2.65 \cdot 10^{-6}$

Table 6-1. Physico-chemical properties of choline hexadecylsulfate at 25°C and 40°C in comparison to choline dodecylsulfate, sodium (NaS_{16}) and tetraethylammonium ($TEAS_{16}$) hexadecylsulfate: critical micelle concentration (*cmc*) obtained from conductivity[a] and surface tension[b] measurements, micelle ionization degree α at the *cmc* (determined from conductivity data), area per molecule A_s and surface excess concentration Γ, derived from concentration dependent surface tension measurements.

From the micelle ionization degree α at the *cmc* it can be inferred that association of choline on the micelle increases with increasing alkyl chain length and also with increasing temperature (see **Table 6-1**). Compared to the sodium alkylsulfates NaS_m with chain length m = 12, 14, 16, 18 the micelle ionization degree α at the *cmc* shows a similar behavior with increasing chain length from α = 0.25 (NaS_{12}) to α = 0.20 (NaS_{16}). For sodium octadecysulfate a much lower counterion association of 0.32 was observed.[30] Therefore, the interaction of sodium with the sulfate headgroup at the *cmc* of the respective surfactants is

slightly stronger than that of choline, but both increase from alkyl chain length C_{12} to C_{16} in a similar manner. This is contrary to Collins´ concept of "matching water affinities".[9, 10] An interesting point is also the comparison of the choline alkylsulfates with the choline carboxylates ChC_m with m = 12, 14, 16. The α value decreases considerably with increasing chain length in the case of the choline carboxylates ChC_m with m = 12, 14, 16 (ChC_{12} α = 0.33; ChC_{14} α = 0.28; ChC_{16} α = 0.18).[12] The decrease in α is much stronger than for the choline alkylsulfates (ChS_{12} to ChS_{16}). A change is seen in the interaction of the choline with the headgroup. Comparing the α values of ChS_{12} and ChC_{12} the interaction of the sulfate with the choline cation is much higher than the interaction of the carboxlate group with choline. This is in line with Collins` concept that the interaction of "soft" cation with "soft" anion is stronger (ChS_{12}) than the one of "soft" cation with "hard" anion (ChC_{12}).[9, 10, 12] However, in the case of the longer chain surfactants as ChS_{16} and ChC_{16} the interaction of choline is much higher with the carboxylate headgroup than with the sulfate headgroup. Therefore, choline hexadecanoate should be less salt sensitive than choline hexadecylsulfate in dilute systems. Thus, the micelle ionization degree α does not follow Collins` law of "matching water affinities"[9, 10] comparing the tendencies of α for the different choline carboxylate[2], choline alkysulfate (see **Figure 6-1**) and sodium alkylsulfate surfactants[30].

6.3.2 Krafft temperature T_{Krafft}

Choline is a bulky unsymmetrical cation. It can lower the Krafft temperature T_{Krafft} of surfactants because it hampers the regular packing of the surfactant molecule in the crystalline lattice.[2] The measured Krafft temperature T_{Krafft} (temperature at which the turbidity of a 1 wt% surfactant solution disappears[13]) of choline hexadecylsulfate was 16°C. It is 30°C lower than the corresponding one for sodium hexadecylsulfate (T_{Krafft} = 46°C).[6, 32] The one of potassium hexadecylsulfate should be higher than 41°C.[11] However, literature about the Krafft temperature of hexadecylsulfate surfactants is very rare. The one of choline dodecylsulfate was already determined by Klein *et al.* and choline dodecylsulfate was found to be soluble down to 0°C.[1] For both choline alkylsulfate surfactants ChS_m with m = 12, 16 it can be stated: the influence of the bulky, unsymmetrical nature of the choline cation on the Krafft temperature is larger, whereas the interaction of choline with the sulfate headgroup is only slightly stronger than the interaction of the sulfate headgroup with sodium. The important point is that choline hexadecylsulfate shows a Krafft temperature lower than 25°C and can be used for further applications at room temperature compared to the respective sodium surfactant. The application of sodium hexadecylsulfate is restricted because of the high Krafft temperature.

6.3.3 Cytotoxicity on HeLa and SK-MEL-28 cells

The cytotoxicity value is important for applications. It was measured *in vitro* with two human cell lines: the keratinocytes (SK-MEL-28) and the cervix carcinoma cells (HeLa). The keratinocytes mimic the skin irritancy power, while the HeLa cells are an alternative to the eye irritancy tests, namely the Draize test, on rabbits.[33-36] Such tests were already performed by Klein *et al.*[1] using the HeLa and SK-MEL-28 cell line according to the procedure described by Mosmann *et al.*[37] and modified by Vlachy *et al*.[38]. However, they have used an antibiotic in the medium. They compared the cytotoxicity of sodium dodecylsulfate with the one of choline dodecylsulfate. No influence of the counterion on the cytotoxicity was found. The cytotoxicity is mainly influenced by the hydrophobicity of the anion.[39, 40] In this study the comparison with the cytotoxicity of sodium hexadecylsulfate was not possible because it precipitates in the cell media and could not be dissolved completely. Therefore, only the alkyl chain length dependent IC_{50} values were investigated for the choline alkylsulfates ChS_m with m = 12, 16 (see **Figure 6-2**). For both cell lines a decrease in the IC_{50} values and an increase in cytotoxicity is observed with increasing chain length corresponding to a lower cytotoxicity and eye irritancy of ChS_{12} compared to ChS_{16}. This behavior was expected and is in line with the chain length dependence of IC_{50} values of the choline carboxylates ChC_m with m = 12, 14, 16.[12]

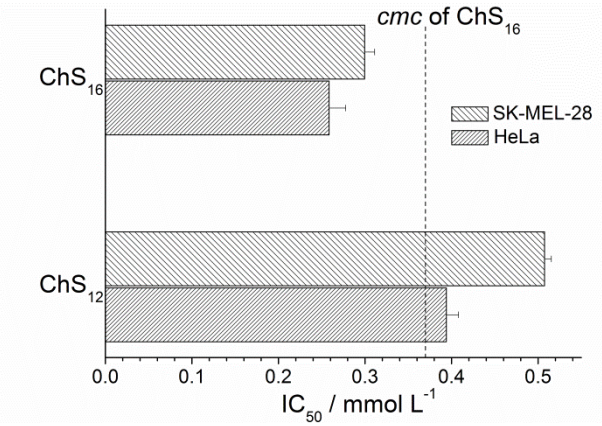

Figure 6-2. Comparison of the IC_{50} values of choline hexadecylsulfate and choline dodecylsulfate evaluated with the help of MTT (3-(4,5-dimethylthiazol-2-yl)-2,5-diphenyltetrazolium bromide) assays on two human cell lines (SK-MEL-28 and HeLa cell line). The vertical line marks the *cmc* value of ChS_{16} at 25°C. The one of ChS_{12} is 5.99 ± 0.06 mmol L^{-1}.[1]

To sum up, it is already known that alkylsulfates show a low oral toxicity (metabolized through ω and β oxidation). Furthermore, no carcinogenic, mutagenic and teratogenic properties and also a very low skin irritation potential were found in other studies.[4] Therefore, they are widely used in common surfactant formulations, like tooth paste, shampoo, washing powder, and a lot of other formulations.[4] Taking into account the chain length dependent

cytotoxicity of alkylsulfate surfactants, it increase with increasing chain length and the highest toxicity at room temperature was found for the dodecylsulfate anion.[32] As already mentioned in Chapter 3, only surfactant monomers show impact on the cytotoxicity, not the micelles, and also the cytotoxicity is strongly dependent on the solubility and the Krafft temperature of the surfactant.[32] Therefore, sodium dodecylsulfate, an alkylsulfate surfactant with a Krafft point lower than room temperature,[32] is used at very high concentrations (much higher than the IC_{50} value) for cell lysis to release proteins.[41] With choline as cation the cytotoxicity of choline hexadecylsulfate could be measured and is higher than the one of choline dodecylsulfate because the Krafft temperature of ChS_{16} is lower than room temperature and also the *cmc* (see **Table 6-1**) is higher than the IC_{50} value of ChS_{16} (see **Figure 6-2**).

6.3.4 Binary phase diagrams of ChS_{12} and ChS_{16} with water

The temperature and concentration dependent aqueous phase behavior of choline dodecylsulfate and choline hexadecylsulfate was investigated to observe the influence of the choline cation compared to the sodium one and the impact of the chain length on the lyotropic phase behavior. A rough lyotropic phase diagram of choline dodecylsulfate (only visual observation) was already investigated by Klein *et al.*.[1]

6.3.4.1 Penetration scan

To gain a first overview of the concentration and temperature dependent phases formed by aqueous choline dodecylsulfate and choline hexadecylsulfate, penetration scans were performed and light microscopy images using crossed polarizers were recorded at different temperatures. The penetration scans were prepared according to the procedure described by Lawrence.[42] Due to this technique information about the mesophases can be obtained with the help of their specific texture and relative viscosity. The liquid crystalline phases are ordered in definite rings around the center of the sample and the surfactant concentration increases to the sample´s midpoint.[43]

Choline dodecylsulfate and choline hexadecylsulfate reveal the same sequence of mesophases with increasing concentration (see **Figure 6-3** and **Figure 6-4**): micellar solution L_1, hexagonal phase H_1, bicontinuous cubic phase V_1, hydrated crystal and at higher temperatures defective lamellar dL_α or nematic N phase. The cubic phase is an isotropic phase with a relative high viscosity. It appears for choline dodecylsulfate in water at 10°C. In the case of choline hexadecylsulfate in water it is formed above 55°C. For each substance this phase extends with increasing temperature.

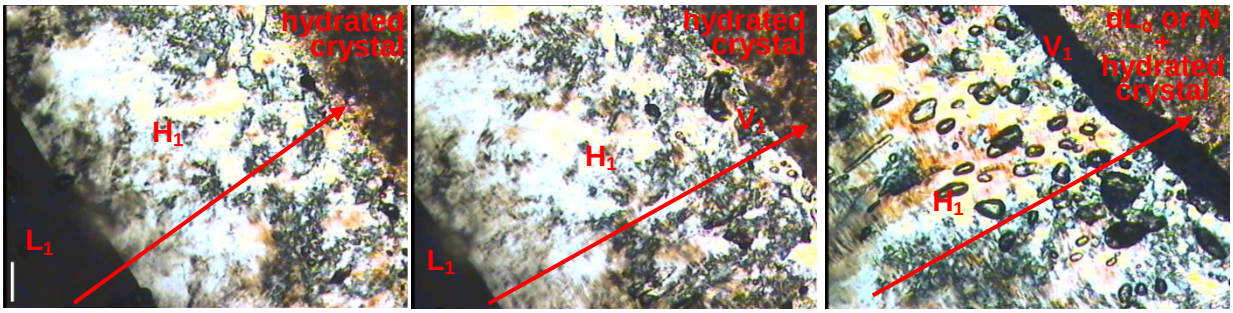

(A) (B) (C)

Figure 6-3. Light microscopy images recorded through crossed polarizers with a magnification of 100x. (A) With increasing concentration choline dodecylsulfate shows the following phases in water at 0°C: micellar solution L_1, hexagonal phase H_1, hydrated crystal. (B) at 20°C: a bicontinuous cubic phase appears between the hexagonal phase H_1 and the hydrated crystal. (C) at 55°C: with increasing temperature the cubic phase V_1 increases and also a defective lamellar dL_α or nematic N phase appears between the cubic V_1 phase and the hydrated crystal. The scale bar (see image (A)) is 100 µm. It is the same for all images (A)-(C).

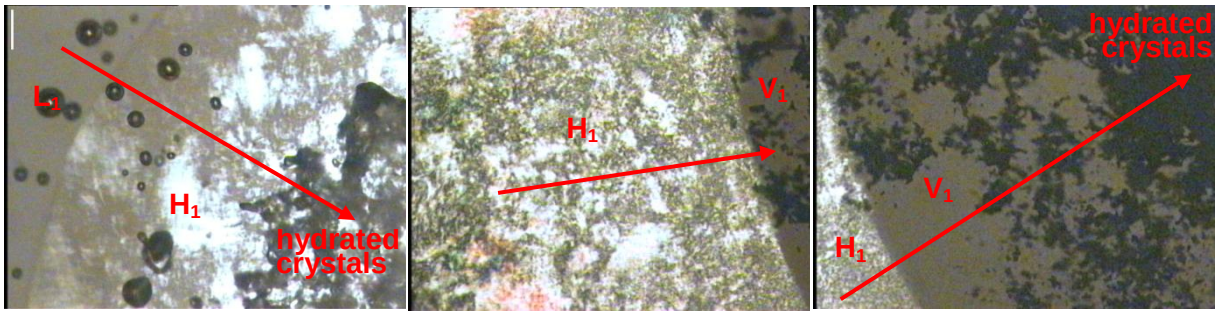

(A) (B) (C)

Figure 6-4. Penetration scan of choline hexadecylsulfate at (A) 28°C, (B) and (C) at 80°C. The light microscopy images are recorded with crossed polarizers and a magnification of 100x. (A): With increasing concentration of choline hexadecylsulfate a micellar phase L_1, homogeneous hexagonal phase H_1 and a hydrated crystal are formed. Further the crystal solubility boundary moves to higher concentration. In figure (B) and (C) a bicontinuous cubic phase V_1 appears between the hexagonal phase H_1 and the hydrated crystal. The scale bar (see image (A)) is 100 µm. It is the same for all images (A)-(C).

The hexagonal phase of the two substances show a homogeneous texture. They do not form such interphases, like deformed hexagonal phases or rectangular phases, as found for the sodium analogs.[16, 20, 23, 44]

6.3.4.2 Visual observations

Visual observations were used to evaluate the concentration and temperature dependent phase borders of the above mentioned lyotropic phases. The binary phase diagrams of choline dodecylsulfate and choline hexadecylsulfate were observed through crossed polarizer in the concentration range between 1 wt% and 100 wt% surfactant in 2.5 wt% steps (at phase borders in 0.5-1 wt% steps). The different samples were heated or cooled in a water bath in the temperature range from 0°C up to 98°C. To evaluate the crystal solubility boundary, which is the concentration and temperature dependent line between crystalline and molten alkyl chains also including the Krafft boundary,[13] DSC measurements were

performed. Therefore, the transition temperature T_C, characterizing the melting of the hydrated crystals to a liquid crystalline phase, was measured with DSC for some concentrations. The temperature difference of the phase transitions found for the heating or cooling cycle are smaller than 4°C and are considered to be sufficiently small so that the binary phase diagrams of choline dodecylsulfate and choline hexadecylsulfate with water were established from the heating cycle (see **Figure 6-5**). Choline dodecylsulfate shows the same phase sequence with increasing concentration as choline hexadecylsulfate. At 25°C the following phases are found for choline dodecylsulfate with increasing surfactant concentration: micellar phase L_1, hexagonal phase H_1 (above 39 wt%), bicontinuous cubic phase V_1 (above 85 wt%), and above 92 wt% a hydrated crystal is formed which transforms to a defective lamellar dL_α or nematic N phase for temperatures higher than 77°C. With extending the alkyl chain length from C_{12} to C_{16}, the phase borders are shifted to lower concentrations and the area of the hexagonal phase increases. Further the T_C-line of choline hexadecylsulfate in water increases along the whole concentration range and is much higher than the one found for choline dodecylsulfate in water (see **Figure 6-5**). In the case of choline hexadecylsulfate in water it starts at very low concentrations (1 wt% ChS_{16}) at 16°C and increases almost linearly to 45°C at 88 wt% ChS_{16}. Above 88 wt% ChS_{16} and 45°C it rises strongly to 100 wt% ChS_{16} at 98°C (see **Figure 6-5** (B)). Whereas for choline dodecylsulfate in water small T_C values were found at much higher concentration (87 wt% ChS_{12}) and a pronounced increase is found for concentrations higher than 87wt% of choline dodecylsulfate (see **Figure 6-5** (A)). Sodium dodecylsulfate shows a richer lyotropic phase behavior.[18, 21-23, 45] Instead of the cubic phase sodium hexadecylsulfate possesses a deformed hexagonal and rectangular phase.[16] The Krafft boundary of sodium hexadecylsulfate is 20°C higher than the one of sodium dodecylsulfate.[16] Compared to the choline equivalents the sodium alkylsulfates show higher crystal solubility boundaries.[16, 44] Further, for choline alkylsulfates (ChS_{12} and ChS_{16}) a smaller micellar solution area in the binary phase diagram is observed and the border of the micellar phase to hexagonal phase is shifted to lower concentrations compared to the sodium alkylsulfates.[16, 44] In the case of the sodium equivalent surfactants it was also found that the concentration of the hexagonal phase was shifted to lower concentrations of sodium alkylsulfate with increasing chain length.[16]

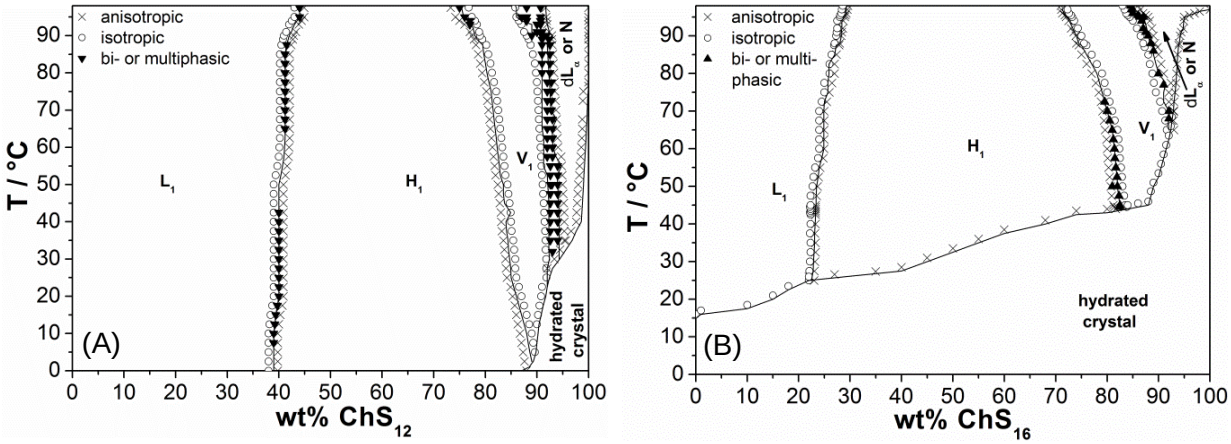

Figure 6-5. Binary phase diagram of choline dodecylsulfate (A) and choline hexadecylsulfate (B) with water recorded in the temperature range between 0°C and 98°C (in 2-5°C steps) during the heating cycle. The different concentrations of 1 wt% to 100 wt% ChS_m with m = 12, 16 (in 2.5 wt% steps and at the phase borders in 0.5-1 wt% steps) were observed during the heating cycle through crossed polarizers. Anisotropic (x), isotropic (○), and biphasic or multiphasic (▼) phases could be evaluated. The accuracy of the phase borders is ± 1°C and ± 1 wt%.

6.3.4.1 Small (SAXS) and wide (WAXS) angle X-ray scattering data and analysis

The following sections present the SAXS analysis of the different liquid crystalline phases to confirm the phase mapping, introduced in the preceding sections, and to give a further structural understanding. The spectra were recorded in 0.5 wt% to 10 wt% steps to obtain information about the structure and the structural parameters. All SAXS and WAXS spectra and data are presented in Appendix D in section D.2.

6.3.4.1.1 Hexagonal phase H_1

Over a wide concentration range choline dodecylsulfate and choline hexadecylsulfate in water show the X-ray pattern of a hexagonal phase $1 : \sqrt{3} : \sqrt{4} : \sqrt{7}$.[23] The lyotropic phase region of the hexagonal phase is concentration, temperature and chain length dependent (ChS_{12}: 38-89 wt%; ChS_{16}: 22-82 wt% at 40°C). A complex hexagonal phase shows the same X-ray pattern as a normal hexagonal phase. To distinguish the differences, polarizing optical light microcopy of the diverse concentrations in the above mentioned concentration range was performed[17] and only a normal hexagonal phase was observed. This could also be approved comparing the structural parameters. The d-spacing of a complex hexagonal phase should be twice the one of a normal hexagonal phase.[17, 18] Even tetragonal phases etc. could be excluded. Therefore, the phase sequence in this region is not so manifold as the one observed for the sodium equivalents.[16, 21-23] In **Figure 6-6** (C) it is shown that the d-spacing of the Miller index [100] of the hexagonal phase decreases linearly with increasing surfactant volume fraction independently of the chain length. This could be explained by a

more dense packing of the micellar cylinders in the hexagonal phase with increasing concentration. Furthermore, slight temperature dependence is found (see **Figure 6-6** (C)). With increasing temperature the d-spacing decreases.

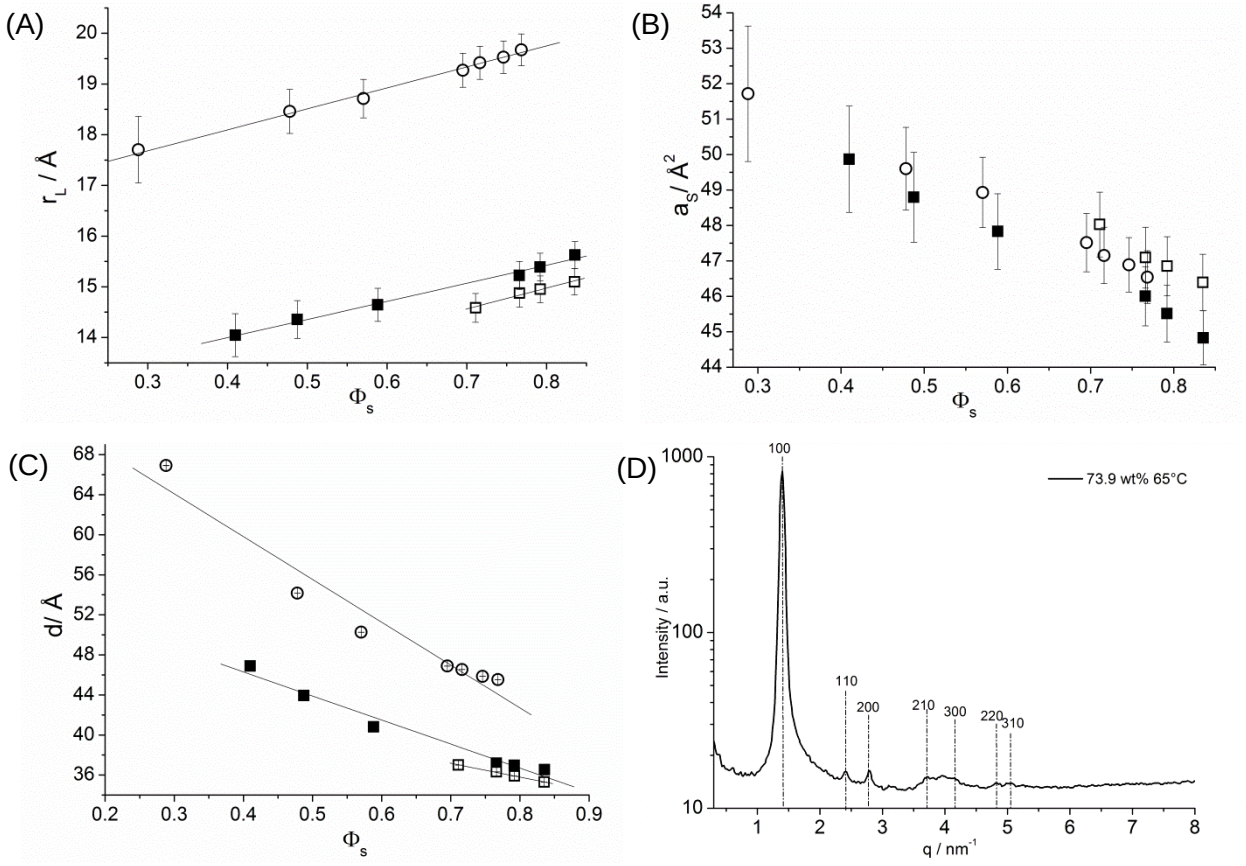

Figure 6-6. The radius of the lipophilic part r_L (A), the cross-sectional area at the polar-nonpolar interface a_s (B) and the interlayer spacing d of the Miller index [100] (C) are shown as a function of volume fraction of the surfactant Φ_s for the hexagonal phase of ChS_{12} (at 25°C (■) and at 50°C(□)) and ChS_{16} (at 50°C (○)). For the calculation of the error bars the following uncertainties were estimated Δq = 0.01 nm^{-1} and $\Delta\Phi_L$ = 0.01. (D) SAXS spectra of 73.9 wt% ChS_{16} at 65°C. The vertical lines represent the Miller indices. The broad peak around 4 nm^{-1} belongs to the Kapton foil.

Accordingly, the lipophilic radius r_L of the hexagonal phases increases linearly with rising concentration. The determined slopes of $\Delta r_L/\Delta\Phi_S$ vary within the experimental error between 4.09 and 4.14 at 50°C and describe a linear growth of the cylindrical radius r_L with increasing concentration Φ_S independently of chain length. The calculated slopes are similar to the slopes found for cylindrical growth in the hexagonal phase of choline carboxylates ChC_m with m = 8-18 and oleate.[8, 43] Therefore, the cylindrical growth of choline surfactants is only dependent on the concentration and not on the headgroup or temperature. r_L is around 8-9 % shorter than the length of the fully extended alkyl chain. This is in good accordance with literature.[46] The lipophilic radius r_L increases within the experimental error at a given volume fraction by 1.185 Å for each additional -CH_2- group in the alkyl chain. This agrees roughly with the value of 1.265 Å that Tanford *et al.*[47] gave for the addition of one -CH_2- group in an

alkyl chain. Also the effective cross-sectional area at the polar-nonpolar interface a_s decreases with increasing surfactant concentration. The value is almost chain length independent. The tendencies found for the d-spacing, the lipophilic length r_L and the cross-sectional area at the polar-nonpolar interface a_s are comparable with the tendencies found for the sodium equivalents.[16-18, 23]

However, comparing the values of a_s found for sodium and choline dodecylsulfate at the same concentration: NaS_{12} (a_s = 50 Å^2)[17] > ChS_{12} (a_s = 48 Å^2); they do not correlate with the difference in size of the cations (Na^+ < Ch^+). Rather, they reflect the stronger counterion-headgroup binding of choline with sulfate compared to sodium.

6.3.4.1.2 Bicontinuous cubic phase V_1 with I*a*3*d* structure

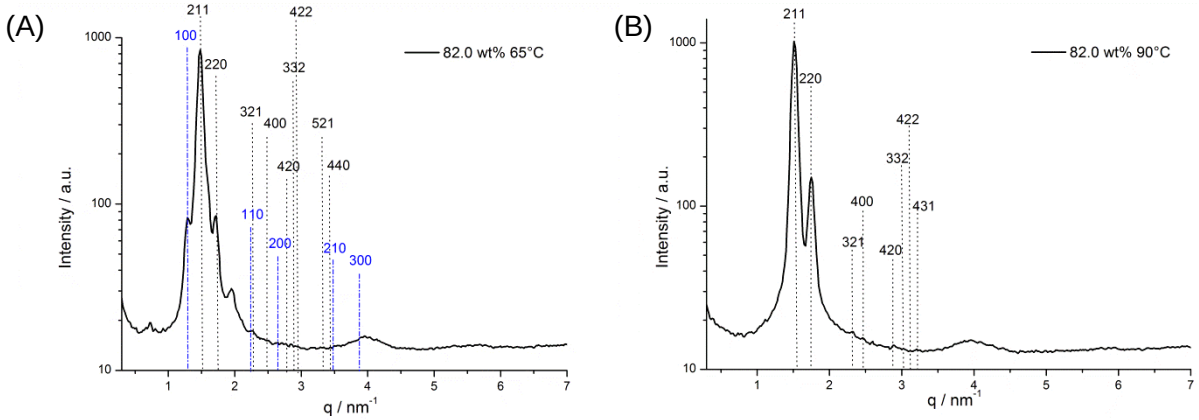

Figure 6-7. (A) SAXS spectrum of the biphasic region between the hexagonal phase and the bicontinuous cubic phase V_1 with I*a*3*d* structure of 82.0 wt% ChS_{16} and 65°C. The black dotted lines (…..) denote the Miller indices assigning the I*a*3*d* structure. The blue lines (_ _ _ _) assign the Miller indices of the hexagonal phase. (B) SAXS spectrum of the bicontinuous cubic phase V_1 with I*a*3*d* structure at 82 wt% ChS_{16} and 90°C. The black dotted lines (…..) indicate the Miller indices assigning the bicontinuous cubic phase with I*a*3*d* structure.

The phase region at concentrations above the hexagonal phase is characterized as a bicontinuous cubic phase V_1 with I*a*3*d* structure. This structure is one of the three bicontinuous cubic structures, which possess a mean curvature of zero and can be described with the model of the infinite periodic minimal surfaces (IPMS).[48-51] It is a three dimensional structure. Further the I*a*3*d* space group can be assigned to the gyroid (G) type surface.[49, 51] It belongs to the body centered space groups and shows the following X-ray pattern for the d-spacings: $\sqrt{3}:\sqrt{4}:\sqrt{7}:\sqrt{8}:\sqrt{10}:\sqrt{11}$ (see **Figure 6-7** (B)).[49] At the phase border to the hexagonal phase a biphasic region is found in the binary phase diagram of choline hexadecylsulfate with water. In this region the coexistence of the hexagonal phase and the bicontinuous cubic phase with I*a*3*d* structure could be assigned. The coexistence region of the two phases could also result from a non-equilibrium between the two phases at the

phase border. The d-spacings of these phases correlates with the d-spacings of the ones found for the one phase regions of the hexagonal phase and the bicontinuous cubic phase with I*a*3*d* structure (see **Figure 6-7** (A) and Appendix D). Therefore, the existence of interphases as found for the sodium equivalents could be neglected.[16-18, 23, 44, 45] Also the interphase $I4_132$, found in this concentration region as an interphase in the binary phase diagram of choline carboxylates with m = 12-18 with water, could not be detected.[43] Mostly an epitaxial transition was found from a hexagonal phase to a bicontinuous cubic phase with I*a*3*d* structure. This transformation is alined between the planes of highest electron density. The $\{100\}$ plane of the hexagonal phase is transformed to the $\{211\}$ plane of the bicontinuous cubic phase.[52] No epitaxial relation could be assigned, because the required condition that $2*d_{211}/\sqrt{3}$ of the cubic phase should be equal to the d_{100} spacing of the hexagonal phase is not fulfilled (see **Figure 6-7** (A)).[52-54]

Concerning the bicontinuous cubic phase with I*a*3*d* structure, the d-spacing of the Miller index (211) decreases with increasing surfactant concentration and rising temperature and it increases with extending the chain length from C_{12} to C_{16}. Also the unit cell parameter a could be calculated. It is dependent on the temperature, the volume fraction of the surfactant Φ_s and the chain length of the choline alkylsulfate surfactant ChS_m with m = 12, 16. It decreases linearly with the increasing volume fraction of the surfactant Φ_s and increasing temperature. The unit cell parameter rises also linearly with the chain length around 4 Å per additional $-CH_2-$ group (see **Figure 6-8**). The unit cell parameter of choline alkylsulfates ChS_m with m = 12 (a ≈ 75 Å) and m = 16 (a ≈ 95 Å)[43] is bigger than the one of ChC_m with m = 12, 16 because of the additional $-CH_2-$ group and the bigger sulfate headgroup. Within the scope of the IPMS it is difficult to calculate the other parameters like the length of the lipophilic part r_L and the area per surfactant headgroup a_s.

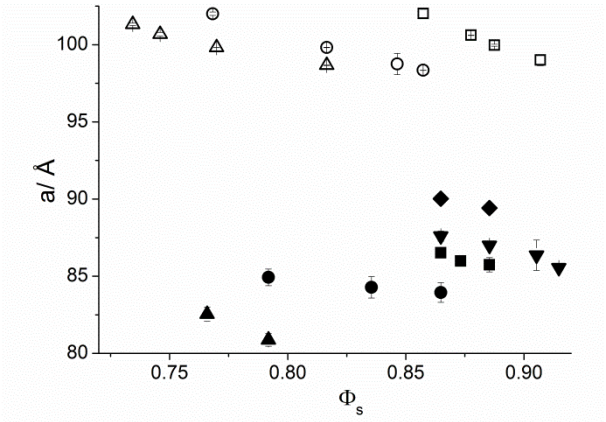

Figure 6-8. Unit cell parameter a shown at different temperatures as a function of the volume fraction Φ_s of the surfactant ChS_{12} and ChS_{16} in water: (♦) ChS_{12} at 25°C, (▼) ChS_{12} at 50°C, (■) ChS_{12} at 65°C, (□) ChS_{16} at 65°C, (●) ChS_{12} at 90°C, (○) ChS_{16} at 90°C, (▲) ChS_{12} at 95°C and (Δ) ChS_{16} at 95°C. For the calculation of the error bars the following uncertainties were estimated $\Delta q = 0.01$ nm^{-1} and $\Delta\Phi_L = 0.01$.

The cubic phase found in the binary phase diagram of sodium dodecylsulfate was characterized as an I*m*3*m* phase and not as an I*a*3*d* phase.[23] Sodium hexadecylsulfate shows no cubic phase in the binary phase diagram with water.[16]

6.3.4.1.3 Multi-phasic region: Additional bicontinuous cubic phase with I*m*3*m* structure

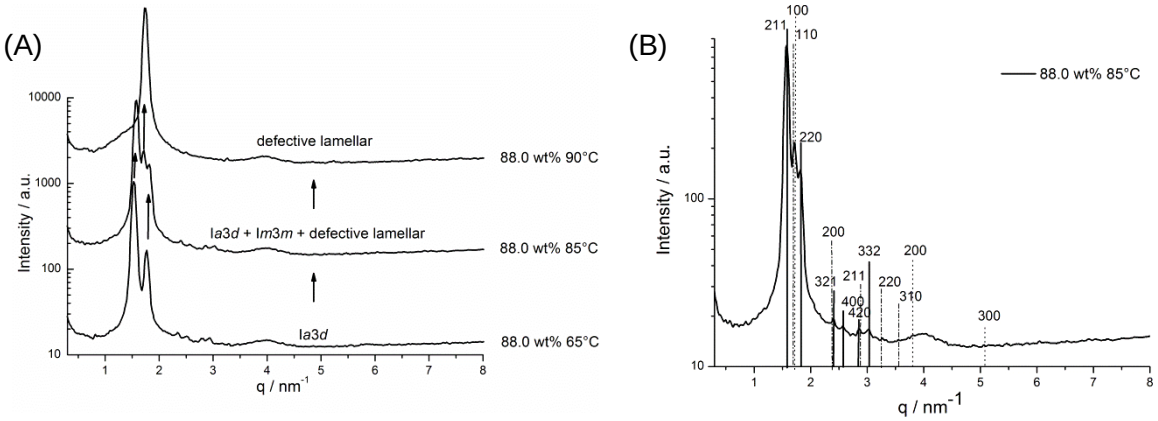

Figure 6-9. (A) Temperature induced phase transition for 88.0 wt% ChS_{16} in water. With increasing temperature the following phases appear: one phase region: bicontinuous cubic phase V_1 with I*a*3*d* structure; three phase region with bicontinuous cubic phase with I*a*3*d* structure, another bicontinuous cubic phase with I*m*3*m* structure and defective lamellar or nematic phase; one phase region: defective lamellar or nematic phase. (B) SAXS-spectrum of 88.0 wt% ChS_{16} at 85°C. Miller indices are assigned for the phases with structure I*m*3*m* (_._._._), I*a*3*d* (_____), and defective lamellar or nematic (…….) which appear in the multi-phasic region between the bicontinuous cubic phase with I*a*3*d* structure and the defective lamellar or nematic phase.

Rançon *et al.*[52, 53] suggested an epitaxial transformation of the bicontinuous cubic phase with I*a*3*d* structure into a lamellar phase. They explained this transformation with the help of the binary system of the nonionic surfactant hexaethylene glycol mono-n-dodecylether in water. The plane of highest electron density of the bicontinuous cubic phase with I*a*3*d* structure is converted to the plane of the highest electron density of the lamellar phase and their d-spacings are equal.[52, 53] In **Figure 6-9** (B) it is obvious that this transition could not occur, because the d-spacings are not equal to each other (d_{211} (I*a*3*d*) ≠ d_{100} (L_α))[52] and some additional reflections characterize the appearance of a third phase. With increasing concentration and temperature the transition to the defective lamellar or nematic phase occurs via a three phasic system. This region arises only in a concentration range of 2 wt% and is very temperature dependent both in the choline dodecylsulfate and in the choline hexadecylsulfate water system (see Appendix D in section D.2.4). As seen in **Figure 6-9** (A) the region could be monitored with SAXS during a temperature scan. The heating rate was around 1 K min^{-1}. It is not only a phase transition between the bicontinuous cubic phase with I*a*3*d* structure and the defective lamellar phase. Some reflections could also be assigned to a

bicontinuous cubic phase with I*m*3*m* structure. This phase structure appears also in the binary phase diagram of sodium dodecylsulfate in water.[23] Tetragonal, orthorhombic, rhombohedral or other cubic phases could not be found.[23] The I*a*3*d* phase structure and the I*m*3*m* phase structure belong both to the bicontinuous cubic phases which are explained to possess infinite periodic minimal surfaces (IPMS) with a mean curvature of zero.[48-51] In general two identical interwoven structures of amphiphilic molecules are separated by a small water layer. In the I*m*3*m* structure two identical structures are made up by rods which are connected six by six with 90° angle in between. In the case of I*a*3*d* three by three rods are connected within a 120° angle.[55] These two identical interwoven structures are separated by a water film with zero mean curvature. The structure is three dimensional. Normally, changes between the three bicontinuous cubic phases (gyroid type (I*a*3*d*), diamond type (P*n*3*m*) and Schwarz surface (I*m*3*m*)) which possess IPMS structure appear without change in the curvature. Hyde *et al.*[56] explained that the phase transition from the I*a*3*d* phase structure to the diamond type (D) of bicontinuous cubic phase is related to a transition energy lower than 0.01 kJ mol^{-1}.[48] In general the I*a*3*d* structure is more stable than the I*m*3*m* structure[55], as seen in this phase diagram. The coexistence and the existence of these structures can be explained with the concept of bilayer frustration, as introduced by Charvolin et al..[55] Therefore, changes in the concentration of surfactant or the temperature could easily induce the occurrence or coexistence of another IPMS structure.[55] This explanation is also in accordance with the results obtained with penetration scan technique, because it is difficult to distinguish the two cubic phases in a penetration scan.

6.3.4.1.4 Defective lamellar phase dL_α or nematic phase N

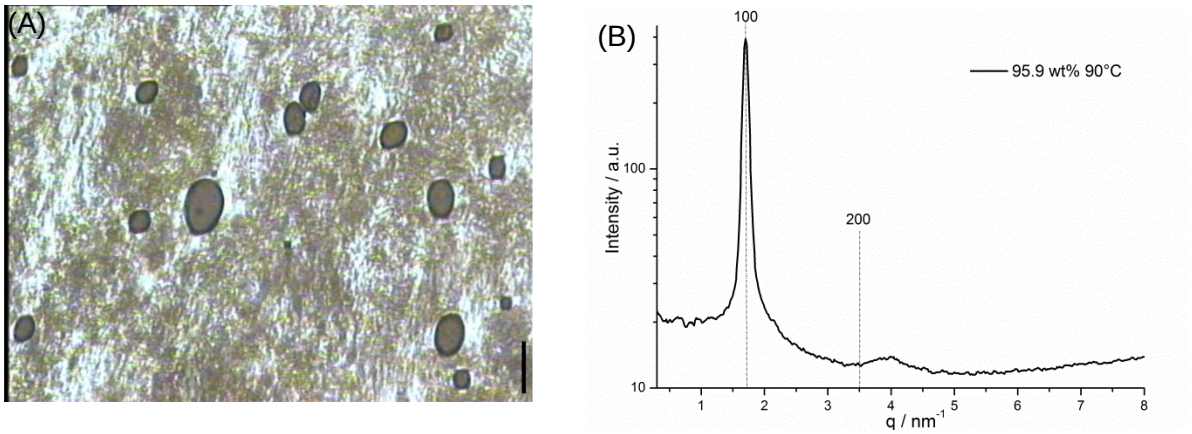

Figure 6-10. (A) Polarizing optical light microscopy image recorded with crossed polarizers of the defective lamellar or nematic phase of 95.9 wt% choline dodecylsulfate at 90°C. It shows “Schlieren” typical of a defective lamellar or nematic phase texture (100x magnification). The scale bar in image (A) is 100 µm. (B) Miller indices illustrate the peak position for the defective lamellar phase or nematic phase of 95.9 wt% choline dodecylsulfate at 90°C. Only a broad first order reflection is seen, but the second and third order reflections are missing. The line at Miller index [200] indicate the position of the second reflection. The broad reflection at 4 nm^{-1} results from the Kapton foil.

At highest surfactant concentration choline dodecylsulfate and choline hexadecylsulfate in water form a defective lamellar or nematic phase. This phase is also a very important phase in soap formulation. The phase region in the binary phase diagram of ChS_{12} and ChS_{16} in water is much smaller as observed for the binary phase diagram of the sodium equivalents.[16-18, 21, 22] However, as already observed in the case of choline carboxylates ChC_m with m = 8, 10 and oleate[8] also these SAXS spectra of the choline alkylsulfates ChS_m with m = 12, 16 in water show only a first Bragg reflection, but no second or third order reflection. The reflection peaks are slightly broader than expected for a lamellar smectic A or C phase. As already explained[8] in Chapter 4 in section 4.3.4.5 the second peak could be the minimum of the first Bragg reflection, but then it should re-appear by changing the concentration. Another explanation could be that defects are formed in the lamellar bilayer.[57-59] Such defects could also be created for example in a temperature induced transition from a lamellar phase to a nematic phase.[57] In case of the choline alkylsulfates it could be due to the existence of two different headgroups as it was explained for the highest concentration phase of choline carboxylates ChC_m with m = 8, 10 or oleate in water (see Chapter 4 in section 4.3.4.5).[8] However, the pK_a of the alkylsulfate is lower than 2.[60, 61] Thus, the assumed equilibrium between the choline alkysulfate and water with choline hydroxide and alkylsulfuric acid is shifted totally to the side of the choline alkylsulfate and water. Another possibility which considers the existence of a second headgroup could be the hydrolysis of alkylsulfate anion. Bethell *et al.*[60] have proposed an autocatalysed hydrolysis of sodium dodecylsulfate above 80°C to dodecanol and the hydrogensulfate anion (this mechanism will be explained in more details in Chapter 7 in section 7.3.5). Most of our SAXS spectra measured of the defective lamellar phase at different surfactant concentration were performed at 90°C. Therefore, if hydrolysis also appears in choline alkylsulfate water solution, it should process at 90°C. Though, the dodecanol or hexadecanol could not be confirmed with IR measurements, because the specific peak of the dodecanol or hexadecanol alcohol group overlap[62] with the one of the hydroxyl group of choline and the alkylsulfate stretching (see section 7.5.2.6 in Chapter 7).[63] Consequently, the existence of the fatty alcohol could not be excluded or proved completely. Further, with the help of ^{1}H and ^{13}C NMR and ES-MS measurements impurities could be neglected. The defects, available in the lamellar phase, could either be created because of the possible second headgroup, the alcohol group further to the sulfate headgroup, and force the formation of different curvatures. Or a further explanation would be that due to the bulky, unsymmetrical nature of the choline cation different curvatures could be formed and create the defects in the defective lamellar or nematic phase.

As observed from the SAXS spectra, defects are available in the lamellar bilayer and destroy the long range order. Only locally lamellar bilayered regions could be found. Also light microscopy pictures, recorded at the respective concentration range, show no typical focal

conic texture of a lamellar smectic A phase. The texture is a “Schlieren” texture which was found for a defective lamellar or nematic phase (see **Figure 6-10** (A)).[57, 64, 65]

However, to differentiate between a defective lamellar phase and a nematic phase formed by disc-like micelles PFG-NMR should be performed on oriented samples to analyze water diffusion processes parallel or perpendicular to the lamellae.

From 70 wt% to 82 wt% sodium dodecylsulfate forms a lamellar smectic A phase. The values for the half length of the lypophilic radius r_L vary from 11 Å to 12.5 Å. They increase slightly with concentration, while the cross-sectional area at the polar-nonpolar interface a_s decreases with increasing concentration (70 wt% to 82 wt%) from 41 $Å^2$ to 35 $Å^2$. Furthermore, the d-spacing of the Miller index [100] decreases with increasing concentration.[17, 18, 66] For sodium hexadecylsulfate no information on structural parameter was found in literature. For the lamellar phases of sodium carboxylate soaps[17, 18, 66] and of choline carboxylate soaps[8, 43] it was found that the polar-nonpolar interface a_s is independent of the chain length and also slightly dependent on the temperature. The choline soaps show a slightly bigger interface area compared to the sodium soaps because of the bigger choline cation. The comparison of the polar-nonpolar interface area a_s of sodium dodecylsulfate (70 wt% to 82 wt% from 41 $Å^2$ to 35 $Å^2$)[17] and choline dodecylsulfate (at 90°C: 92.9 wt% ChS_{12} a_s = 35.6 $Å^2$; 97.0 wt% ChS_{12} a_s = 34.8 $Å^2$) is not possible, because the measured surfactant concentrations are not the same. Normally, the value of the area of the polar-nonpolar interface does not vary with different chain length at the same concentration. Here the choline hexadecylsulfate shows a slightly higher value. Also in the case of choline hexadecylsulfate the half length of the lipophoilic bilayer r_L is 50 % of the extended alkyl chain length l_{max}, while for choline dodecylsulfate it is around 60 % of an extended alkyl chain length. All in all, it indicates a high disorder of the paraffinic chains in both cases. However, the slightly bigger area of the polar-nonpolar interface a_s and smaller half length of the lipophilic bilayer r_L in the defective lamellar or nematic phase of choline hexadecylsulfate suggest that the molecular axis is more tilted in the locally formed bilayers in the case of choline hexadecylsulfate compared to choline dodecylsulfate. This is typical of a smectic C phase.[67, 68] Smectic C phases also show a “Schlieren” pattern in light microscopy and the same X-ray pattern such as a smectic A phase.[69]

To sum up: Defects were created in the lamellar phase because of the formation of different curvatures. They could result from the presence of two different headgroups, or, what is more probable, because of the bulky, unsymmetrical nature of the choline cation. The long range order of the lamellar phase is interrupted and locally lamellar phases are found with the molecular axis perpendicular to the bilayer axis (see smectic A), like in the case of choline dodecylsulfate. For choline hexadecylsulfate the locally lamellar parts are observed with the molecular axis not perpendicular to the bilayer axis (see smectic C phase).[69]

However, the overall structure can be assigned as defective lamellar phase or nematic phase.

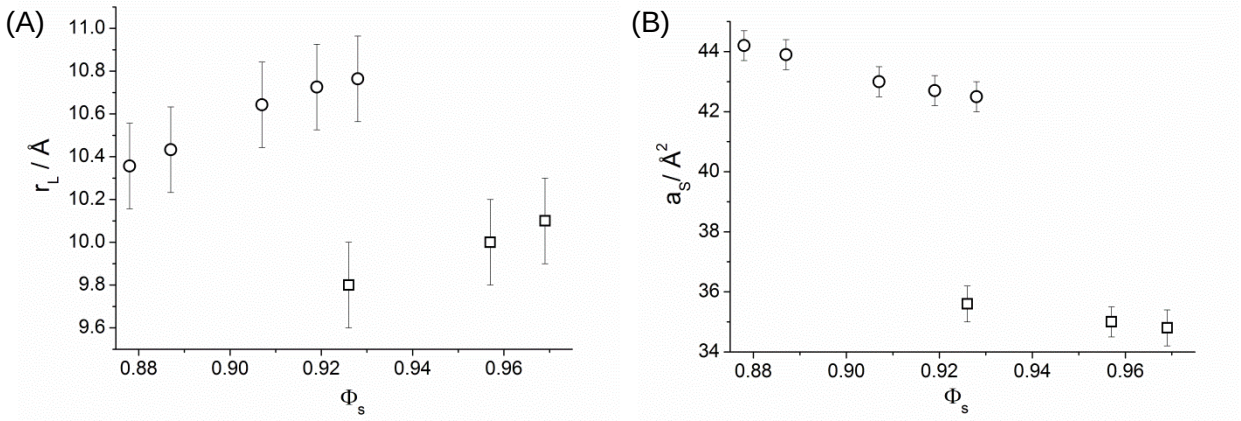

Figure 6-11. (A) Half length of the lipophilic bilayer r_L as a function of the volume fraction of the surfactant Φ_S. (B) Cross-sectional area at the polar-nonpolar interface a_s as a function of the volume fraction of the surfactant Φ_S. The values are obtained from the binary phase diagram region of the defective lamellar phase of ChS_{12} (□) and ChS_{16} (○) at 90°C. For the calculation of the error bars the following uncertainties were estimated $\Delta q = 0.01$ nm^{-1} and $\Delta\Phi_L = 0.01$.

	wt%	Φ_S	T / °C	d_{100} / Å	d_L / l_{max}	(r_s-r_L) / Å	d_w / Å
ChS_{12}	95.9	0.957	50	35.7	1.2	6.9	1.5
	92.9	0.926	90	35.7	1.2	6.7	2.6
	95.9	0.957	90	35.1	1.2	6.8	1.5
	97.0	0.969	90	34.9	1.2	6.8	1.1
	89.0	0.885	95	34.5	1.1	6.2	4.0
ChS_{16}	92.9	0.928	80	35.3	1.0	5.5	2.6
	88.0	0.878	90	35.7	1.0	5.3	4.4
	88.9	0.887	90	35.6	1.0	5.3	4.0
	90.9	0.907	90	35.5	1.0	5.5	3.3
	92.1	0.919	90	35.3	1.0	5.5	2.9
	92.9	0.928	90	35.1	1.0	5.5	2.5

Table 6-2. Structural parameters of the locally bilayered parts of the defective lamellar or nematic phase calculated from the SAXS data of different concentrated samples of choline dodecylsulfate and choline hexadecylsulfate with water. The d_{100}-values are shown as well as the ratio of the lipophilic bilayer d_L and the all-trans length of the alkyl chain l_{max}, the thickness of the polar region (r_s-r_L) and the thickness of the water layer between the bilayers d_w.

In **Table 6-2** it is shown that the thickness of the water layer d_w in the locally bilayered parts of the defective lamellar or nematic phase decreases linearly with increasing concentration independently of the chain length. Also the thickness of the polar region (r_s-r_L) is in general bigger than the one for ChC_{16} (4.7 Å)[43] because of the bigger sulfate group. However, it is smaller than the length of a choline cation (~ 8 Å) so that the choline cation is arranged with its long axis perpendicular to the bilayer axis. The polar-nonpolar interface a_s of the choline carboxylates[43] is more or less in the same range as the one of the sulfates. The same was found for the hexagonal phase: the stronger headgroup-counterion binding reduces the effective charge of the sulfate group compared to the one of the carboxylate group and

adjusts the bigger size of the sulfate headgroup compared to the carboxylate headgroup. A similar area of the interface region results.[43]

6.4 Conclusion

The binary phase diagrams of choline dodecysulfate and choline hexadecylsulfate with water were investigated to observe the influence of the chain length on the solubility behavior and on the lyotropic phase sequence.

It was found that choline is able, contrary to the increasing counterion-headgroup binding, to decrease the Krafft temperatures of choline dodecylsulfate[1] and especially of choline hexadecylsulfate below room temperature. Further, the *cmc*s of these choline alkylsulfates ChS_m with m = 12, 16 were found to be slightly lower than the one of the sodium alkylsulfates due to the stronger counterion-headgroup binding of choline with sulfate compared to sodium. However, in contrast to the choline carboxylates, choline as cation is not able to increase the curvature of alkylsulfates in such a manner that they can form discontinuous cubic phases[43] at surfactant concentrations below the hexagonal phase. As already seen in an earlier study[12] the toxicity of sodium and choline dodecylsulfate is comparable. Furthermore, the cytotoxicity of choline hexadecylsulfate is slightly higher than the one of choline dodecylsulfate.

The aqueous phase behavior of choline alkylsulfates is similar to the one of choline carboxylates ChC_m with m = 10-18 and oleate[8, 43] (see Chapter 4), but not to the one of the sodium equivalents. The phase behavior of the sodium equivalents is more manifold.[16-18, 21-23, 66]

With increasing concentration the following phases appear for choline alkylsulfates: micellar phase L_1, hexagonal phase H_1, bicontinuous cubic phase V_1 (I*a*3*d*), three phasic system (I*m*3*m*, I*a*3*d* and defective lamellar) and defective lamellar or nematic phase. The choline carboxylates ChC_m with m = 10-18[8, 43] form the same phases with two exceptions. Two discontinuous cubic phases were found between the micellar solution and the hexagonal phase. Further an additional phase with I4_132 [43] structure was found (exception ChC_{10}) between the hexagonal phase and the bicontinuous cubic phase V_1 with I*a*3*d* structure, instead of the additional phase with I*m*3*m* structure which was observed between the bicontinuous cubic phase with I*a*3*d* structure and the defective lamellar phase in the binary phase system of the choline alkylsulfates.

The absence of the discontinuous cubic phases can be explained by assuming that the sulfate headgroup is slightly bigger than the carboxylate one so that choline could not increase enough the curvature for the choline alkylsulfates in water. Another point is the stronger counterion-headgroup interaction of the sulfate headgroup with choline compared to

the carboxylate headgroup and thus, a low degree of dissociation can be assumed for choline alkylsulfates. As a consequence discontinuous cubic phases, mesophases with high curvature, could not be formed. Further it could be approved that in diluted solutions choline alkylsulfates ChS_m with m = 12, 16 form spherical micelles with increasing concentration which are transferred to cylindrical micelles, before they are ordered in a hexagonal phase. This spherical micelle to cylindrical micelle formation was also found for sodium dodecylsulfate.[19] In the case of choline alkylsulfates as well as for the choline carboxylates, the defective lamellar or nematic phase region is smaller than the one found for the sodium equivalents[8, 16-18, 21-23, 43, 66]. On the other side the hexagonal phase region increases in the binary phase diagram of choline alkylsulfates in water compared to sodium alkylsulfates. [8, 16-18, 21-23, 43, 66]. For the hexagonal phase as well as for the defective lamellar phase it was found that the area of the polar-nonpolar interface a_s is more or less the same for the choline alkylsulfates ChS_m with m = 12, 16 as well as for ChC_m with m = 12 and 16.[43] The effective charge of the sulfate anion is reduced due to the stronger interaction of choline with the sulfate headgroup compared to the carboxylate headgroup. Therefore, the repulsion of the sulfate headgroups in the polar region of the aggregates is lowered which results in a similar polar-nonpolar interface area in the hexagonal and defective lamellar phase for the two types of choline surfactants in water.

All in all, it could be shown that the choline alkylsulfates, especially the longer chain ones, are a good alternative to the common sodium alkylsulfates in application. They are less salt sensitive, show an acidic pH value in water and further have Krafft temperatures below room temperature.

6.5 Experimental

6.5.1 Synthesis and sample preparation

Choline dodecylsulfate and choline hexadecylsulfate were synthesized according to the procedure established by Klein *et al.*[1, 5] for choline dodecylsulfate. An ion exchanger I of Merck (strong acid ion exchange) was first flushed with 1 M HCl solution (Merck) and then successively with millipore water to obtain a pH of 7. Afterwards the ion exchanger was loaded with choline cations using the salt choline chloride (purity ≥ 98 %, Sigma Aldrich). A 1 M salt solution was prepared to load the resin until the resulted effluent has a pH of 8-9 (the amount of used choline chloride corresponds to 4 times the maximum cation exchange capacity). To ensure complete ion exchange, a 0.1 M choline hydroxide solution (Taminco) was used until the effluent had a pH of 10. To remove the excess of base, the column was flushed with millipore water (pH ≈ 7). Afterwards, a 0.1 M aqueous sodium dodecylsulfate solution (salt: purity ≥ 99.9 %, Merck) passed the column at room temperature. The amount

of used surfactant was lower than 1/3 of the minimum resin capacity. The Krafft temperature of sodium hexadecylsulfate is 46°C.[6] Thus, the concentration of the aqueous sodium hexadecylsulfate solution was lowered to 0.02 M and the solution and the column containing the resin were tempered at 60°C during the ion exchange. The water was removed with freeze drying. The white powder was further dried for 1 week at 10^{-2} mbar in a desiccator.
To verify the purity ^{1}H NMR, ^{13}C NMR and ES-MS were performed. The mass spectrometry was carried out with a ThermoQuest Finnigan TSQ 7000 instrument. The NMR spectra were recorded on a Bruker Avance 300 spectrometer at 300 MHz with tetramethylsilane (TMS) as internal standard.

Choline dodecylsulfate: ^{1}H NMR (300 MHz, $CDCl_3$, 25°C, TMS): δ = 0.85 (t, 3H; $CH_2C\mathbf{H_3}$), 1.25 (m, 18H; $C\mathbf{H_2}C\mathbf{H_2}CH_3$), 1.65 (q, 2H; $C\mathbf{H_2}CH_2SO_4^-$), 3.3 (s, 9H; $N(C\mathbf{H_3})_3$), 3.65 (t, 2H; $C\mathbf{H_2}OH$), 4.0 (t, 2H; $C\mathbf{H_2}N(CH_3)_3$), 4.1 (t, 2H; $C\mathbf{H_2}SO_4^-$)
^{13}C NMR (300 MHz, $CDCl_3$, 25°C, TMS): δ = 14.16 ($\mathbf{C}H_3CH_2$), 22.72 ($CH_3\mathbf{C}H_2$), 25.86 ($CH_3CH_2\mathbf{C}H_2$), 29.39-29.67 ($\mathbf{C}H_2CH_2$), 31.94 ($\mathbf{C}H_2CH_2SO_4^-$), 54.56 ($N(\mathbf{C}H_3)$), 56.50 ($\mathbf{C}H_2OH$), 67.80 ($S\mathbf{C}H_2$), 68.09 ($N\mathbf{C}H_2$),
ES-MS (H_2O/ MeOH/ MeCN): m/z (%) (+p): 104.0 (100) [M^+], 147.9 (19), 473.2 (37) [$(2M^+ + M^-)^+$], 517.3 (4) [$(M^+ + M_1^+ + M^-)^+$]; (p-): 264.9 (100) [M^-], 634.3 (16) [$(2M^- + M^+)^-$], 678.4 (1)

Choline hexadecylsulfate: ^{1}H NMR (300 MHz, $CDCl_3$, 25°C, TMS): δ = 0.85 (t, 3H; $CH_2C\mathbf{H_3}$), 1.25 (m, 26H; $C\mathbf{H_2}C\mathbf{H_2}CH_3$), 1.65 (q, 2H; $C\mathbf{H_2}CH_2SO_4^-$), 3.3 (s, 9H; $N(C\mathbf{H_3})_3$), 3.65 (t, 2H; $C\mathbf{H_2}OH$), 4.0 (t, 2H; $C\mathbf{H_2}N(CH_3)_3$), 4.1 (m, 2H; $C\mathbf{H_2}SO_4^-$)
^{13}C NMR (300 MHz, $CDCl_3$, 25°C, TMS): δ = 14.16 ($\mathbf{C}H_3CH_2$), 22.72 ($CH_3\mathbf{C}H_2$), 25.87 ($CH_3CH_2\mathbf{C}H_2$), 29.40-29.73 ($\mathbf{C}H_2CH_2$), 31.95 ($\mathbf{C}H_2CH_2SO_4^-$), 54.55 ($N(\mathbf{C}H_3)$), 56.56 ($\mathbf{C}H_2OH$), 67.70 ($S\mathbf{C}H_2$), 68.08 ($N\mathbf{C}H_2$),
ES-MS (H_2O/ MeOH/ MeCN): m/z (%) (+p): 103.8 (100) [M^+], 147.7 (3), 529.4 (19) [$(2M^+ + M^-)^+$], 954.9 (0.5) [$(3M^+ + 2M^-)^+$]; (p-): 321.1 (100) [M^-], 746.7 (8) [$(2M^- + M^+)^-$]

6.5.2 Methods

6.5.2.1 Surface tension

The critical micelle concentration of choline hexadecylsulfate ChS_{16} was obtained at 25°C and 40°C by concentration dependent surface tension σ measurements. The one of ChS_{12} was also quantified at 25°C to compare this value with existing data[1] and to have a standard for ChS_{16}. The temperature accuracy was 25°C ± 0.1°C and 40°C ± 0.1°C. The measurements were carried out on a Krüss tensiometer (model K100 MK2) using a platinum-iridium ring. The data acquisition was done automatically and recorded the surface tension

as a function of the concentration. The surface tension was measured during dilution of the surfactant solution with degassed, milipore water. The data correction was accomplished according to the procedure performed by Harkins and Jordan.[70] Plotting the surface tension σ with the log of the concentration, as done in earlier studies on ChS_{12}[1, 31], only the *cmc* could be evaluated. The plot of the ln(c) versus the surface tension σ allows us to calculate the excess concentration of surface molecules per unit area by using the Gibbs adsorption equation (3): [29]

$$-\mathrm{d}\sigma = \mathrm{RT}\left[\Gamma_{S_m^-}\,\mathrm{d}\left(\ln c_{S_m^-}\right) + \Gamma_{Ch^+}\,\mathrm{d}(\ln c_{Ch^+})\right] \qquad (3)$$

at the surface electroneutrality is required so that $\Gamma_{S_m^-} = \Gamma_{Ch^+} = \Gamma$ and also $c_{S_m^-} = c_{Ch^+} = c$, if no other electrolyte is in the solution (S_m^- lables the sulfate anion with chain length m = 12 or 16). Therefore, the slope of the curve at lower concentrations than the *cmc* can be used to calculate the excess surface concentration of surface molecules per unit area Γ. Taking into account the before mentioned conditions the following equation (4) can be used:[29]

$$\Gamma = -\frac{1}{2\mathrm{RT}}\,\frac{\mathrm{d}\sigma}{\mathrm{d}(\ln c)} \qquad (4)$$

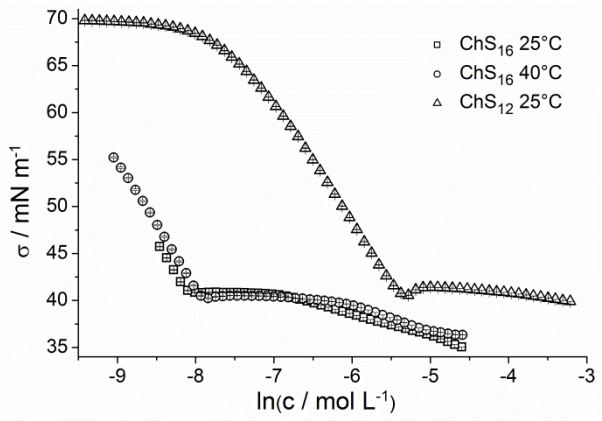

Figure 6-12. The surface tension σ is shown as a function of the natural logarithm ln(c) of the concentration of choline dodecylsulfate at 25°C (Δ) or choline hexadecylsulfate at 25°C (□) and 40°C (○) with water. The breakpoint in the concentration dependent surface tension marks the *cmc*.

6.5.2.2 Conductivity

Another method to evaluate the critical micelle concentration of choline hexadecylsulfate ChS_{16} was to measure the specific conductivity κ of an aqueous choline hexadecylsulfate solution during subsequent increase of the soap concentration in the solution. The measurement was performed according to the procedure explained in Chapter 3 in section 3.5.3. The accuracy of the *cmc* values is ± 5%.

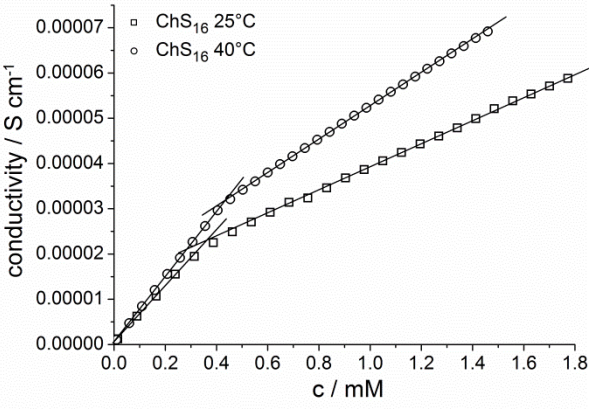

Figure 6-13. Plot of the concentration in mM versus the concentration dependent specific conductivity κ values in S cm^{-1} of the aqueous solution of choline hexadecylsulfate at 25°C (□) and 40°C (○).

The micelle ionization degree α at the *cmc* was calculated taking into account the equation deduced by Evan[30], as described in Chapter 3 in section 3.5.3. In **Table 6-3** the slope S_1 before the *cmc* and the slope S_2 above the *cmc* in the plot of the concentration versus the specific conductivity κ and the micelle ionization degree α at the *cmc* is given.

	1000·S_1 / Scm^2 mol^{-1}	**1000·S_2 / Scm^2 mol^{-1}**	**α**
ChS_{16} 25°C	57.08 ± 8.20	24.65 ± 1.92	0.25 ± 0.03
ChS_{16} 40°C	73.27 ± 0.01	36.75 ± 0.01	0.24 ± 0.01

Table 6-3. Slopes S_1 and S_2 obtained from the plot of the concentration versus conductivity of choline hexadecylsulfate in water at 25°C and 40°C, and the calculated values of the micelle ionization degree α at the *cmc* and the respective temperature are listed.

6.5.2.3 Krafft temperature T_{Krafft}

Krafft temperatures were inferred from temperature dependent turbidity measurements, which were done with a homebuilt apparatus.[71] A solution of 1 wt% of choline hexadecylsulfate in water was prepared. The temperature dependent turbidity of this sample was measured. The sample was irradiated with a LED of a light dependent resistor (LDR). The transmitted light was measured as a function of the temperature and reflects the turbidity of the sample. The sample was stored in a computer-controlled thermostat. The heating rate was 1°C per hour.

6.5.2.4 Density

To obtain the molar volume of the choline alkylsulfate surfactants ChS_m with m = 12, 16 the density of diluted aqueous surfactant solutions was measured. The concentration range of the surfactant solutions was 1 wt% to 20 wt%, mostly in 2.5 wt% steps. The choline dodecylsulfate solutions were measured at 25°C, the one of choline hexadecylsulfate at 25°C and 40°C. A vibrating tube densiometer (Anton Paar DMA 5000M) was used for the density measurements. The instrument was calibrated with standards. The obtained data were listed in **Table 6-4**.

ChS_{12} at 25°C		ChS_{16} at 25°C		ChS_{16} at 40°C	
wt%	**ρ in g L^{-1}**	**wt%**	**ρ in g L^{-1}**	**wt%**	**ρ in g L^{-1}**
0.99	997.5	1.00	997.5	1.00	992.4
2.48	998.2	2.50	997.6	2.50	990.4
4.99	999.6	4.99	998.4	4.99	993.1
7.51	1000.0	7.37	999.1	7.37	993.1
15.19	1003.8	11.08	999.9	11.08	994.0
20.04	1006.4	12.43	1000.5	12.43	993.9
-	-	15.01	1000.9	15.01	994.4
-	-	17.46	1001.3	17.46	994.8
-	-	19.15	1001.5	19.15	993.3

Table 6-4. Densities of the aqueous solutions of ChS_m with m = 12, 16 measured at 25°C and 40°C.

The molar volumes can be obtained due to the fitting procedure explained in Chapter 4 in section 4.5.2.8. The calculated data were shown in **Table 6-5**.

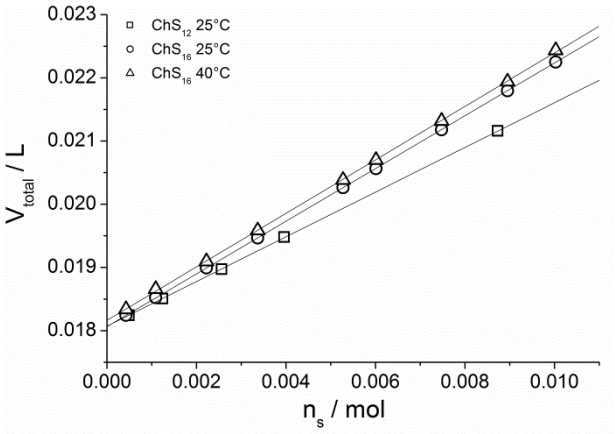

Figure 6-14. Total volume V_{total} as a function of the number of moles n_s of the different aqueous choline alkylsulfate solutions (ChS_m with m = 12 at 25°C (□); m = 16 at 25°C (○) and 40°C (Δ)).

	V_s / L mol^{-1}	V_{H2O} / L mol^{-1}
ChS_{12} 25°C	0.354	0.0181
ChS_{16} 25°C	0.417	0.0181
ChS_{16} 40°C	0.423	0.0182

Table 6-5. Molar volume V_s of the surfactant ChS_m with m = 12, 16 obtained from the fitting of the density data of the aqueous surfactant solutions according to the procedure explained in Chapter 4 in section 4.5.2.8.

Taking into account the molar volume of 0.352 L mol^{-1} Klein *et al.*[1] found for choline dodecylsulfate, it is in good agreement with the molar volume obtained here. Concerning the molar volumes at 25°C for choline dodecylsulfate and choline hexadecylsulfate (see **Table 6-5**), the molar volume increases of 0.0158 L mol^{-1} (26.2 Å^3) per each additional -CH_2- group. This is in good agreement with the value Tanford *et al.* predicted (26.9 Å^3).[47]

6.5.3 Cytotoxicity on HeLa and SK-MEL-28 cells

Cytotoxicity tests were performed with the SK-MEL-28 (keratinocytes, CLS 300337) and the HeLa (cervix carcinoma, ATCC CCL17) cell line. In both cases the MTT (3-(4,5-dimethylthiazol-2-yl)-2,5-diphenyltetrazolium bromide) assay procedure introduced by Mosmann[72] and modified by Vlachy *et al.* was performed.[38] The only exception was that media were used without Amphotercin B and Penicillin G/Streptomycinsulfate. The experiments were carried out according to the procedure described in Chapter 3 in section 3.5.5. The respective dose-response curves are shown in Appendix D in section D.1.

6.5.3.1 Visual observations

To assign the lyotropic phases, different concentrations of water with choline alkylsulfate ChS_m with m = 12, 16 were prepared. 0.3 g of each sample was weighed in glass ampoules with 1 cm diameter. The tubes were flame sealed. The concentration range of the different samples was 1 wt% to 100 wt% of choline alkylsulfate ChS_m with m = 12, 16 in water. The concentration steps were 2.5 wt% and near the phase transition border the concentration steps were scaled down to 1 wt% or 0.5 wt%. The flame sealed tubes were centrifuged a few days at 40°C for 6000 rpm and afterwards homogenized at room temperature for several days. This procedure was repeated over one year to be sure of thermodynamic equilibrium and reproducibility of the different phases.

To obtain the temperature and concentration dependent phase diagrams visual observations were made. The differently concentrated samples were tempered in a water bath. The temperature accuracy was 0.1 °C. The temperature range between 0°C and 98°C was recorded. The heating rate was 10°C per hour and the samples were checked every 2-5°C through crossed polarizers. Due to this method isotropic and birefringent phases could be

evaluated and also the relative viscosity of the different samples could be checked. Lamellar phases could be evaluated because they appear normally at higher soap concentration and are less viscous compared to the hexagonal phase. The bicontinuous cubic phase is an isotropic phase with a high relative viscosity. The hexagonal phase should appear at concentrations lower than the one of the bicontinuous cubic phase and the hexagonal phase is more viscous than the lamellar phase.

6.5.3.2 Penetration scan

The penetration scans were prepared on microscope slides and performed in nitrogen atmosphere. They were recorded following the procedure described in Chapter 4 in section 4.5.2.3.

6.5.3.3 Small and wide angle X-ray scattering

X-ray measurements and data analysis were performed as described in Chapter 4 in section 4.5.2.4. The acquisition time of the different samples was 900 seconds. Mainly the peak position was important for the phase characterization. Consequently, the spectra could be used without background subtraction. The peak at 4 nm^{-1} resulted from the Kapton foil.

6.5.3.4 Equation and parameter

The maximum length of the alkyl chain in Å was calculated with MOPAC[73] calculation and with the equation of Tanford[47] (see equation (5)) for a fully extended alkyl chain with n_c embedded C-atoms in the alkyl chain. The same values were obtained.

$$l_{max} = 1.5 + 1.265 n_C \qquad (5)$$

Further, the volume of the alkyl chain V_L was also determined by the expression of Tanford:[47]

$$V_L = 27.4 + 26.9 n_C \qquad (6)$$

The values of the molar volumes of the surfactants V_S were estimated with density measurements (see section 6.5.2.4 and **Table 6-5**). The density ρ_{surf} was obtained by measuring the densities of surfactant water solutions with increasing surfactant concentration. These densities were extrapolated up to 100 wt% of surfactant.

	V_S / Å^3	V_L / Å^3	l_{max} / Å	ρ_{Surf} / g L^{-1}
ChS_{12}	587.8	350.2	16.7	1044.0
ChS_{16}	692.4	457.8	21.7	1020.7

Table 6-6. The volume of the lipophilic part of the surfactant V_L and the maximum length of the alkyl chain l_{max} were calculated with the equations presented by Tanford[47] and MOPAC[73]. The density of ChS_m with m = 12, 16 and the volume of one surfactant molecule V_S are given at 25°C.

The X-ray data are used to calculate the radius or length of the lipophilic part r_L and also the effective cross-sectional area at the polar-nonpolar interface a_S of the hexagonal phase and the lamellar parts of the defective lamellar or nematic phase. The calculation of these data includes the volume fraction of the lipophilic part Φ_L and the one of the surfactant Φ_S. For the assessment of the volume fraction of the surfactant Φ_S and the one of the lipophilic part Φ_L the density of the surfactant ρ_{Surf}, the volume of the lipophilic part V_L, and the volume of a surfactant molecule V_S are required and shown in **Table 6-6**. The equations to calculate the above mentioned parameters are given in Chapter 4 in section 4.5.2.8.

6.6 References

1. R. Klein, M. Kellermeier, D. Touraud, E. Müller and W. Kunz, *J. Colloid Interface Sci.*, 2013**, 392**, 274-80.
2. R. Klein, D. Touraud and W. Kunz, *Green Chem.*, 2008, **10**, 433.
3. A. Schmalstieg and G. W. Wasov, *Ed. K. Holmberg, John Wiley & Sons Ltd.*, 2002, 271-293.
4. H. W. Stache, *Anionic Surfactants*, Marcel Dekker, Inc., New York, 1996.
5. W. Kunz, M. Kellermeier, R. Klein, E. Maurer, D. Touraud, *Biologically Acceptable Choline Compounds and their Use as Tensides*, EP 2010-152626 (University of Regensburg, Germany), 2010.
6. I. Piirma and S. R. Chen, *J. Colloid Interface Sci.*, 1980, **74**, 90-102.
7. R. Klein, M. Kellermeier, T. Pöpper, G. J. Schneider and W. Kunz, *Structural Characterization of Aqueous Solutions of Choline Carboxylate Surfactants*. In Hasylab Annual Report 2006, Hasylab: Hamburg, 2006; pp 1215-1216.
8. D. Rengstl, O. Diat, R. Klein and W. Kunz, *Langmuir*, 2013, **29**, 2506-2519.
9. K. D. Collins, *Methods*, 2004, **34**, 300-311.
10. K. D. Collins, G. W. Neilson and J. E. Enderby, *Biophys. Chem.*, 2007, **128**, 95-104.
11. M. J. Schwuger, *Kolloid-Z. Z. Polym.*, 1969, **233**, 979-985.
12. R. Klein, Dissertation, Universität Regensburg, 2011.
13. R. G. Laughlin, *The Aqueous Phase Behavior of Surfactants*, Academic Press, San Diego, 1994.
14. B. L. Bales, M. Benrraou and R. Zana, *J. Phys. Chem. B*, 2002, **106**, 9033-9035.

15. R. Klein, M. Kellermeier, M. Drechsler, D. Touraud and W. Kunz, *Colloids and Surfaces A: Physicochem. Eng. Aspects*, 2009, **338**, 129-134.
16. N. V. Usol´tseva, N. M. Kormilitsyn and L. N. Zhukova, *Koloidnyi Zhurnal*, 1989, **51**, 601-603.
17. P. F. Husson, H. Mustacchi and V. Luzzati, *Acta Cryst.*, 1960, **13**, 668-677.
18. P. V. Luzzati, H. Mustacchi, A. Skoulios and F. Husson, *Acta Cryst.*, 1960, **13**, 660-667.
19. S. Yano, K. Tadano and K. Aoki, *Mol. Cryst. Liq. Cryst.*, 1983, **92**, 99-104.
20. R. Itri, L. Q. Amaral and P. Mariani, *Phys. Rev. E Stat. Phys. Plasmas Fluids Relat. Interdiscip. Topics*, 1996, **54**, 5211-5216.
21. P. Kékicheff, *J. Colloid Interface Sci.*, 1989, **131**, 133-152.
22. P. Kekicheff and B. Cabane, *Acta Crystallogr. B*, 1988, **44**, 395-406.
23. P. Kekicheff and B. Cabane, *J. Phys. France*, 1987, **48**, 1571-1583.
24. R. Lopez, L. A. Fucugauchi and J. H. Fendler, *Mikrochim. Acta*, 1992, **106**, 11-20.
25. B. Lindman, in *Handbook of Applied Surface and Colloid Chemistry*, Ed. K. Holberg, D. O. Shah and M. J. Schwuger, John Wiley & Sons, LTD, New York, 2002, Vol. 1, Chapter 19.
26. P. Mukerjee and K. J. Mysels, *Critical Micelle Concentrations of Aqueous Surfactant Systems*, U.S. Government Printing Office, Washington, D.C., 1971.
27. M. J. Rosen, *Surfactants and Interfacial Phenomena*, John Wiley & Sons, Inc., New York, 1989.
28. K. Holmberg, D. O. Shah and M. J. Schwuger, *Handbook of Applied Surface and Colloid Chemistry*, John Wiley & Sons, LTD, New York, 2002.
29. R. J. E. Stokes, D. Fennell, *Fundamentals of Interfacial Engineering*, Wiley-VCH Inc., 1996.
30. H. C. Evans, *J. Chem. Soc.*, 1956, 579-586.
31. R. Klein, Dissertation, Universität Regensburg, 2011; Counterion condensation of choline dodecylsulfate recalculated with right value for molar volume V_m 0.354 L mol^{-1}.
32. H. Schott, *J. Pharm. Sci.*, 1973, **62**, 341-343.
33. H. Eagle, *J. Exp. Med.*, 1955, **102**, 595-600.
34. K. Chiba, I. Makino, J. Ohuchi, Y. Kasai, H. Kakishima, K. Tsukumo, T. Uchiyama, E. Miyai, J. Akiyama, Y. Okamoto, H. Kojima, H. Okumura, Y. Tsurumi, M. Usami, K. Katoh, S. Sugiura, A. Kurishita, M. Sunouchi, A. Miyajima, M. Hayashi and Y. Ohno, *Toxicol. in Vitro*, 1999, **13**, 189-198.
35. W. Yang and D. Acosta, *Toxicol. Lett.*, 1994, **70**, 309-318.

36. M. A. Perkins, R. Osborne, F. R. Rana, A. Ghassemi and M. K. Robinson, *Toxicol. Sci.*, 1999, **48**, 218-229.
37. T. Mosmann, *J. Immunol. Methods*, 1983, **65**, 55-63.
38. N. Vlachy, D. Touraud, J. Heilmann and W. Kunz, *Colloids Surf., B*, 2009, **70**, 278-280.
39. S. Stolte, M. Matzke, J. Arning, A. Boschen, W. R. Pitner, U. Welz-Biermann, B. Jastorff and J. Ranke, *Green Chem.*, 2007, **9**, 1170-1179.
40. S. Stolte, J. Arning, U. Bottin-Weber, M. Matzke, F. Stock, K. Thiele, M. Uerdingen, U. Welz-Biermann, B. Jastorff and J. Ranke, *Green Chem.*, 2006, **8**, 621-629.
41. C. Prottey and T. F. M. Ferguson, *Food Cosmet. Toxicol.*, 1976, **14**, 425-430.
42. A. S. Lawrence, *Mol. Cryst. Liq. Cryst.*, 1969, **7**, 1-&.
43. R. Klein, G. J. T. Tiddy, E. Maurer, D. Touraud, J. Esquena, O. Tache and W. Kunz, *Soft Matter*, 2011, **7**, 6973.
44. P. Kékicheff, C. Grabielle-Madelmont and M. Ollivon, *J. Colloid Interface Sci.*, 1989, **131**, 112-132.
45. P. Kékicheff, C. Grabielle-Madelmont and M. Ollivon, *J. Colloid Interface Sci.*, 1989, **131**, 112-132.
46. S. Hassan, W. Rowe and G. J. T. Tiddy, *in Handbook of Applied Surface and Colloid Chemistry*, Ed. K. Holmberg, John Wiley & Sons Ltd, Chichester, 2002, pp. 465-508.
47. C. Tanford, *J. Phys. Chem.*, 1972, **76**, 3020-3024.
48. S. T. Hyde, S. Andersson, B. Ericsson and K. Larsson, *Z. für Kristallographie*, 1984, **168**, 213-219.
49. G. Lindblom and L. Rilfors, *Biochim. Biophys. Acta, Rev. Biomembr.*, 1989, **988**, 221-256.
50. S. Andersson, S. T. Hyde, K. Larsson and S. Lidin, *Chem. Rev.*, 1988, **88**, 221-242.
51. K. Larsson and F. Tiberg, *Curr. Opin. Colloid Interface Sci.*, 2005, **9**, 365-369.
52. Y. Rancon and J. Charvolin, *J. Phys. Chem.*, 1988, **92**, 2646-2651.
53. Y. Rancon and J. Charvolin, *J. Phys. Chem.*, 1988, **92**, 6339-6344.
54. P. Mariani, L. Q. Amaral, L. Saturni and H. Delacroix, *J. Phys. II*, 1994, **4**, 1393-1416.
55. J. Charvolin and J. F. Sadoc, *J. Physique*, 1987, **48**, 1559-1569.
56. S. T. Hyde, *Curr. Opin. Solid St. M.*, 1996, **1**, 653-662.
57. O. Dhez, S. Konig, D. Roux, F. Nallet and O. Diat, *Eur. Phys. J. E*, 2000, **3**, 377-388.
58. Y. Hendrikx, J. Charvolin and M. Rawiso, *J. Colloid Interface Sci.*, 1984, **100**, 597-600.
59. M. J. Sammon, J. A. Zasadzinski and M. R. Kuzma, *Phys. Rev. Letters*, 1986, **57**, 2834-2837.

60. D. Bethell, R. E. Fessey, E. Namwindwa and D. W. Roberts, *J. Chem. Soc., Perkin Trans. 2*, 2001, **0**, 1489-1495.
61. A. F. Hollemann, E. Wiberg and N. Wiberg, *Lehrbuch der Anorganischen Chemie*, Walter de Gruyter, Berlin, 2007.
62. M. Hesse, H. Meier and B. Zeeh, *Spektroskopische Methoden in der organischen Chemie*, Thieme, Stuttgart, 2011.
63. J. J. Leitch, J. Collins, A. K. Friedrich, U. Stimming, J. R. Dutcher and J. Lipkowski, *Langmuir*, 2012, **28**, 2455-2464.
64. D. Constantin, P. Davidson and C. Chaneac, *Langmuir*, 2010, **26**, 4586-4589.
65. H. D. Dörfler, *Grenzflächen und kolloid-disperse Systeme: Physik und Chemie*, Springer, Berlin, 2002.
66. H. Delacroix, T. Gulik-Krzywicki, P. Mariani and V. Luzzati, *J. Mol. Biol.*, 1993, **229**, 526-539.
67. W. L. McMillan, *Phys. Rev. A*, 1973, **8**, 1921-1929.
68. S. Kalaivani, T. Narasimhaswamy, B. B. Das, N. P. Lobo and K. V. Ramanathan, *J. Phys. Chem. B*, 2011, **115**, 11554-11565.
69. M. D. Small, *Handbook of Lipid Research 4: The Physical Chemistry of Lipids*, Plenum Press, New York, 1986.
70. W. D. Harkins and H. F. Jordan, *J. Am. Chem. Soc.*, 1930, **52**, 1751-1772.
71. S. Schrödle, R. Buchner and W. Kunz, *Fluid Phase Equilib.*, 2004, **216**, 175-182.
72. T. Mosmann, *J. Immunol. Methods*, 1983, **65**, 55-63.
73. J. J. P. Stewart, *MOPAC 2009, Stewart Computational Chemistry*, Colorado Springs, CO, USA.

Chapter 7

Thermotropic phase behavior of choline alkylsulfates ChS_m with m = 12, 16

7.1 Abstract

This chapter deals with the thermotropic phase behavior of choline alkylsulfates ChS_m with m = 12, 16. In Chapter 5 a very interesting thermotropic phase behavior of choline carboxylates ChC_m with m = 8, 10 and choline oleate was observed. These choline carboxylates form simultaneously two different structures in one phase along the whole temperature range between -50°C and 95°C. The main structure of the phase is temperature dependent and could be evaluated by small angle (SAXS) and wide angle (WAXS) X-ray scattering measurements. The following main structures were observed with increasing temperature in the temperature range between -50°C and 95°C: interdigitated crystalline monolayer, interdigitated semi-crystalline monolayer and liquid crystalline defective lamellar structure. The second structure shows a more liquid-like behavior. However, the structure and temperature dependence could not be evaluated in detail. As already explained in chapter 5, no clear statement could be given if really two structures exist in one phase or if two phases (thermodynamically stable or kinetically stabilized) exist simultaneously and are in equilibrium with each other. Beside this the choline alkylsulfates ChS_m with m = 12, 16 behave similarly. They also form two structures in one phase or two phases which are in equilibrium with each other in the neat choline alkylsulfate in the temperature range between 0°C and 98°C. To explain the observed results two structures in one phase are assumed, but also the other case of two phases which are in equilibrium with each other is possible.
Here the structuring of the main part of the phase is more manifold compared to the choline carboxylate ones. With increasing temperature they form the following phases: first crystalline interdigitated monolayer (Cr1), second crystalline interdigitated monolayer (Cr2), first semi-crystalline bilayered structure (CrM1), second semi-crystalline bilayered structure (CrM2) and a defective lamellar or nematic liquid crystalline structure (LC). The structure of the smaller part of the phase is more liquid-like, but again the temperature dependence and the exact structure could not be clarified in detail. To characterize the phases SAXS, WAXS, temperature variable ^1H NMR, differential scanning calorimetry and polarizing optical microscopy measurements were carried out. Further, pH, IR and liquid NMR measurements were performed, to check if the alkylsulfate anion hydrolysed to a notable extent.

7.2 Introduction

Thermotropic phases are temperature dependent phases which sometimes are formed by solvent free surfactants.[1, 2] The stability of the structure in thermotropic phases depends on various interactions, amongst them ionic ones between the headgroups and counterions, van der Waals interactions between the hydrophobic alkyl chains, and in some cases also hydrogen bonding plays an important role.[2] As described in Chapter 5, the thermotropic

phase behavior of the classical soaps is very well characterized.[3-14] However, as far as we know, the one of the alkali alkylsulfates is not investigated yet.[1] For these surfactants the aqueous behavior is more interesting with regard to formulation issues (skin-friendly personal-care products)[15] and also for industrial applications.[16, 17] Several studies concern the temperature dependent behavior of sodium dodecylsulfate mixtures with water (40 wt% sodium dodecylsulfate in water: temperature scan between -20°C to 44°C)[18] and the phase transitions of the system sodium dodecylsulfate, hexanoic acid and water in the temperature range between -12°C and 80°C with different concentrations.[19] Even the thermotropic phase behavior of cationic gemini surfactants combined with equally charged mixtures of sodium dodecylsulfate was investigated in the temperature range between 20°C and 200°C.[2]

In a former study on the thermotropic phase behavior of choline carboxylates ChC_m with m = 8, 10 and oleate (see Chapter 5) two structures in the neat phase of choline carboxylates ChC_m with m = 8, 10 and oleate in the temperature range between -50°C and 95°C were found. Further, it is also possible that instead of the two structures in one phase, two phases are in equilibrium with each other and thermodynamically stable or kinetically stabilized. A clear statement could not be given.

In the present chapter the question was considered if this behavior is common for neat choline surfactants with different headgroups. For this purpose the thermotropic phase behavior of the neat choline alkylsulfates ChS_m with m = 12, 16 was investigated. Temperature variable ^{1}H NMR measurements were performed to obtain the spin-spin relaxation time T_{2eff}. Further, differential scanning calorimetry measurements (DSC), small (SAXS) and wide (WAXS) angle X-ray scattering measurements were conducted. pH, liquid ^{1}H NMR and IR measurements were further carried out to obtain information about the presence of dodecanol, or hexadecanol, or hydrogensulfate due to hydrolysis.

7.3 Results and discussion

7.3.1 Thermogravimetric analysis

Klein *et al.*[20] already compared the thermal decomposition behavior of choline dodecylsulfate with the one of sodium dodecylsulfate. They found a two step thermal decomposition for the former and a one step for the latter. They assigned the first decomposition temperature to the disintegration of the alkylsulfate part and the second decomposition to the decomposition of the choline cation. The comparison of the C_{12} chain length surfactants with C_{16} ones supports this hypothesis (see **Figure 7-1** and **Table 7-1**). However, it should be added that the second decomposition of the choline alkylsulfates ChS_m with m = 12, 16 describes not only the decomposition of the choline cation, but also the further thermal degradation of the alkyl chain. The first decomposition temperature of the choline alkylsulfates is similar to the one of

the sodium equivalents, as it reflects the partial decomposition of the alkyl chain and increases with chain length. However, even the second decomposition does not occur at the same temperature for ChS_{12} and ChS_{16}. Thus, it could not only be assigned to the thermal degradation of the choline cation, but it could also be observed that the choline alkylsulfate degrades up to 500°C until 95 % mass loss. The sodium equivalents are more stable, as they degrade only up to 74 % mass loss in the same temperature range. Therefore, the second decomposition temperature of the choline alkylsulfates shows a further thermal degradation of the alkyl chain combined with the one of the choline cation.

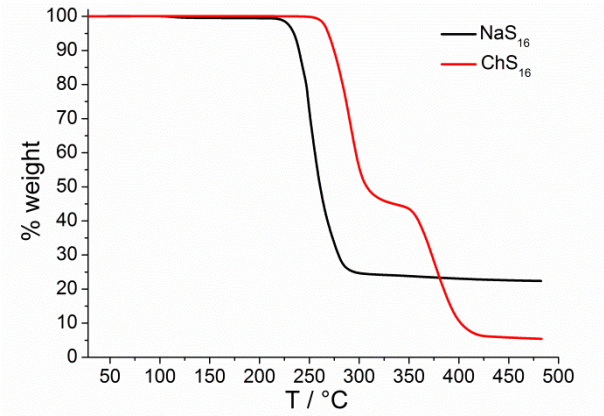

Figure 7-1. TGA curves of ChS_{16} and NaS_{16} measured in the temperature range between 30°C and 500°C.

Comparing the thermal stabilities of the choline carboxylates and of choline alkylsulfates it can be concluded that the sulfates are much more stable than the carboxylates with the same chain length (T_{dec} ≈ 190-202°C)[21].

Compound	T_{1dec} / °C	T_{2dec} / °C
ChS_{12}	252[20]	330[20]
NaS_{12}	221[20]	-
ChS_{16}	270	356
NaS_{16}	239	-

Table 7-1. Decomposition temperatures T_{dec} of choline alkylsulfates ChS_m with m = 12, 16 compared to sodium dodecylsulfate (NaS_{12}) and sodium hexadecylsulfate (NaS_{16}). They were measured from room temperature up to 500°C with a heating rate of 10 K min^{-1} and with constant nitrogen flow.

However, from pre-experiments in sealed glass tubes it was observed that choline alkylsulfate surfactants ChS_m with m = 12, 16 decompose, as the choline carboxylate soaps (see Chapter 5 in section 5.3.2) by heating for a longer time above 100°C. A brown coloration was detected. Thus, the investigated temperature range was limited from 0°C to 98°C for further characterization experiments.

7.3.2 Polarizing optical microscopy

For the purpose of distinguishing between crystalline, semi-crystalline and liquid crystalline phases and also to characterize the mesophases, polarizing optical microscopy was used.
For each sample three heating and cooling cycles were recorded. The first cycle was performed to obtain a flat film between the glass slides. The second cycle was measured with a heating rate of 10 K min^{-1} (see Appendix E in section E.1) the third with a rate of 1 K min^{-1} (see **Figure 7-2** and **Figure 7-3**). No significant differences are found between the transition temperatures obtained with the different heating rates. The phase transitions are reversible. With increasing temperature the following phases could be identified: first crystalline phase (Cr1), second crystalline phase (Cr2), first semi-crystalline phase (CrM1) and second semi-crystalline phase (CrM2). These phase transitions are very fast and within a range of 3°C. The change between the crystalline phases is not so obvious. In semi-crystalline phase transitions a change in the volume is visible and the birefringence increases (see **Figure 7-2** and **Figure 7-3**). The last transition to the liquid crystalline phase is very slow and occurs in a temperature range of 9°C. For the liquid crystalline phase a heterogeneous phase texture is observed. Parts with “Schlieren” texture and sometimes areas with focal conic texture appear.

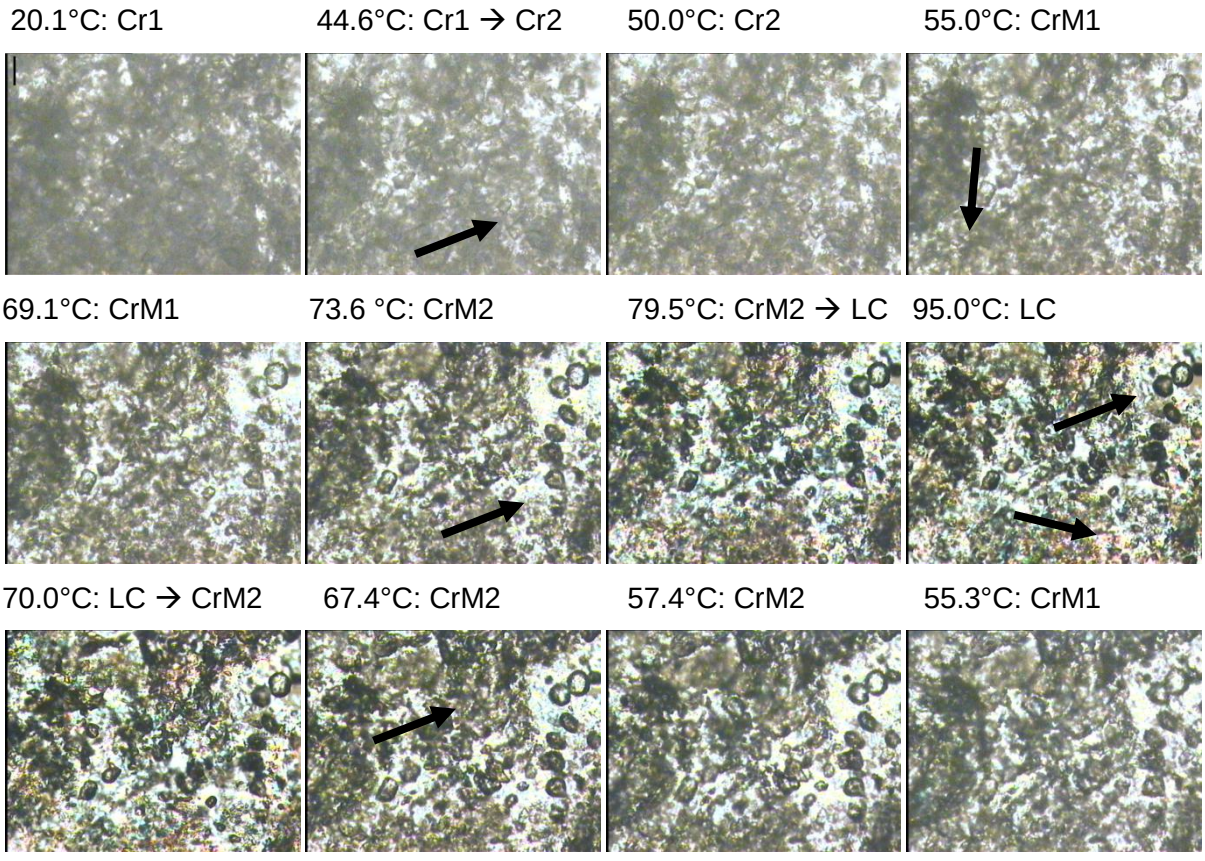

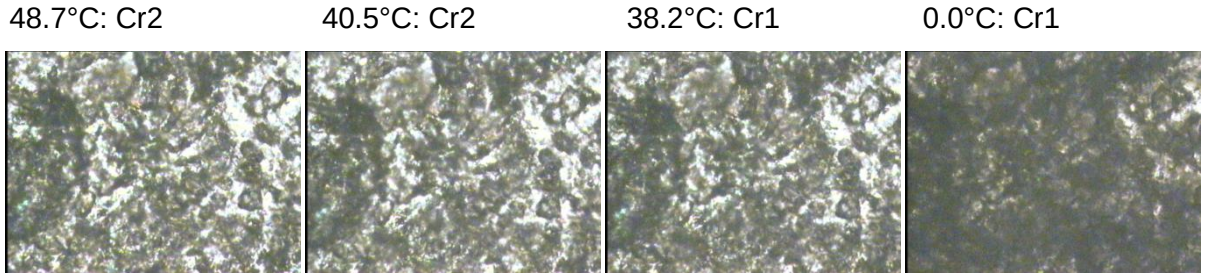

Figure 7-2. Polarizing optical micrographs of neat choline dodecylsulfate. The images were taken from the same sample spot during the third heating and cooling cycle with a heat rate of 1 K min^{-1} in the temperature range between 0°C and 95°C. With increasing temperature the following phases appear: first crystalline phase (Cr1), second crystalline phase (Cr2), first semi-crystalline phase (CrM1), second semi-crystalline phase (CrM2). The transition to the liquid crystalline phase (LC) is very slow. The Cr1 and Cr2 phase show a high crystallinity. The change to the CrM1 and then to the CrM2 occurs with a decrease in viscosity and increase in birefringence. In the liquid crystalline phase the viscosity is very low and partly "Schlieren" texture is visible (arrows). The phase is not very homogeneous. The arrows also mark changes in the structure. The scale bar (see image recorded at 20.1°C) is 100 µm. It is the same for the other images.

Therefore, a similar liquid crystalline phase as found for the high temperature phase of the neat choline carboxylate soaps with m = 8, 10 and oleate can be formed (see Chapter 5). From the investigation of the classical soap behavior[22,21] it is known that with increasing temperature the alkyl chains start to melt continuously before the headgroup counterion layer melts. The same was observed for choline soaps (see Chapter 5 and [21]). During the phase transition from crystalline to semi-crystalline the alkyl chains start to melt, while in the liquid crystalline phase they are completely molten. Due to the longer alkyl chains the influence of the choline cation on the melting behavior is not so pronounced as it is revealed for the thermotropic phases of the short chain choline carboxylates ChC_m with m = 2, 4, 6, 8, and 10 (see Chapter 5).

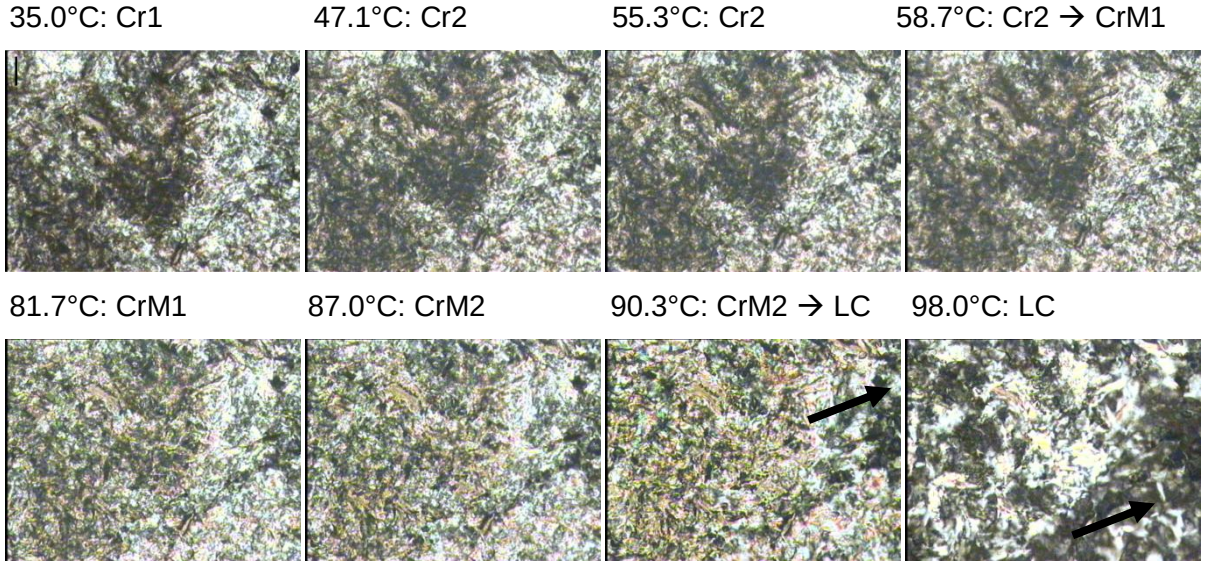

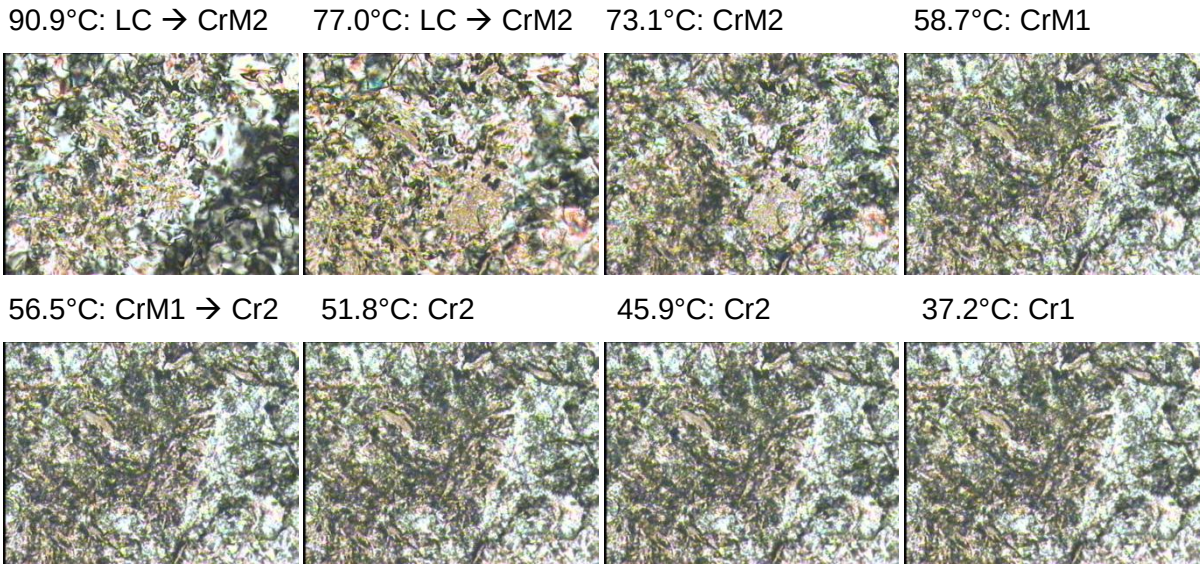

Figure 7-3. Polarizing optical micrographs of thermotropic phases of choline hexadecylsulfate recorded in a temperature scan from 0°C to 98°C and vice versa. The micrographs were taken from the same sample spot during the third cycle. The heating rate was 1 K min^{-1}. With increasing temperature the following phases appear: first crystalline phase (Cr1), second crystalline phase (Cr2), first semi-crystalline phase (CrM1), second semi-crystalline phase (CrM2). The transition to the liquid crystalline phase (LC) is very slow. The Cr1 and Cr2 phase show a high crystallinity. They change to the CrM1 and then to the CrM2 which is connected with an increase in birefringence and a decrease in viscosity. In the liquid crystalline phase the viscosity is very low and partly "Schlieren" texture is apparent (arrows). The scale bar (see image recorded at 35.0°C) is 100 µm. It is the same for the other images.

7.3.3 Differential scanning calorimetry (DSC)

DSC measurements are a further independent method to evaluate the transition temperatures. In addition, enthalpies and entropies of the phase transitions of the different thermotropic phases could be determined. The measurements were performed in the temperature range between 0°C and 95°C. For each substance three cycles were conducted. The first cycle of choline dodecylsulfate (see **Figure 7-4** (A)) shows different phase transitions compared to the second and the third one because of the formation of polymorphic metastable phases. This phenomenon is already known from the investigation of the temperature dependent phase behavior of choline carboxylates (see Chapter 5 and [21]) and other surfactants.[1, 11] The second and the third cycle prove the reproducibility of the phase transitions. In the following only the second heating and cooling cycle, which is similar to the third one, is considered.

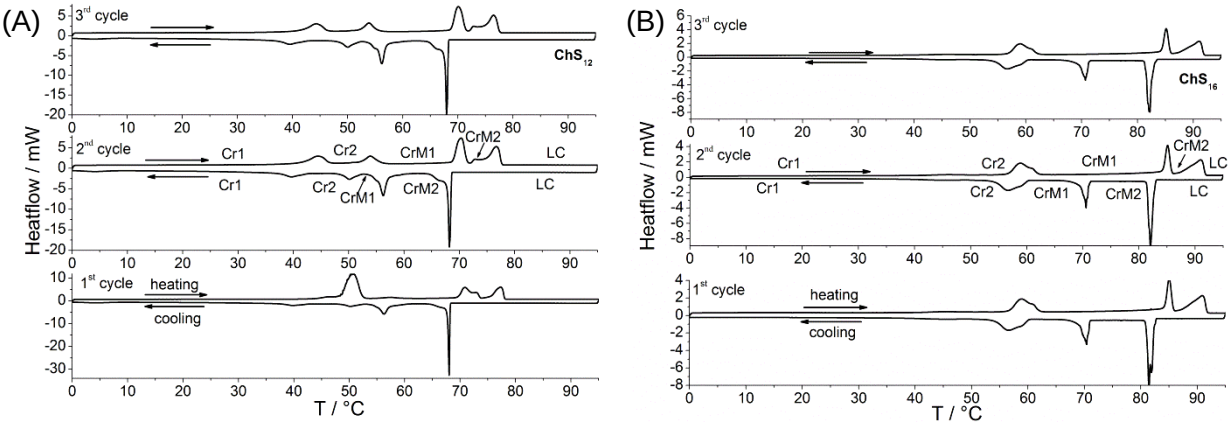

Figure 7-4. DSC curves of anhydrous choline dodecylsulfate (A) and choline hexadecylsulfate (B) measured in the temperature range between 0°C and 95°C. Both, the heating and the cooling cycle, show four phase transitions. The lowest temperature transition of choline hexadecylsulfate is not so pronounced. According to the microscopy measurements the following phases could be attributed to the transitions. With increasing temperature the following phases are formed: first crystalline phase (Cr1), second crystalline phase (Cr2), first semi-crystalline phase (CrM1), second semi-crystalline phase (CrM2) and liquid crystalline phase (LC).

The transition temperatures derived from DSC measurements (see Appendix E in section E.2) are similar to the ones obtained from the light microscopy measurements. The four transition temperatures of the different thermotropic phase transitions of choline dodecylsulfate are lower during both, the heating and the cooling cycle, compared to the ones of choline hexadecylsulfate (see **Figure 7-4**). This can be explained with the shorter alkyl chain length of choline dodecylsufate which results in less van der Waals interactions compared to C_{16} chain. Phase transitions on the cooling cycle show temperature hystereses which result from the slow nucleation. Via these hysteresis values the melting process could be slightly evaluated.[21, 23] The values of the temperature hystereses of the phase transition between the first (Cr1) to the second crystalline phase (Cr2) and the transition from the second crystalline phase (Cr2) to the first semi-crystalline phase (CrM1) are for ChS_m with m = 12 and 16 between 2.5°C and 4.9°C. The hysteresis value of the transition of the first (CrM1) to the second semi-crystalline phase (CrM2) is around 14.5°C for both substances, while the one of the transition of the second semi-crystalline (CrM2) to the liquid crystalline phase (LC) is around 9°C. These values reveal (see **Figure 7-5**) a slow chain melting and rigid alkyl chains in the two crystalline phases. Moreover, the first semi-crystalline phase seems to have only slightly disordered alkyl chains, while they start to melt and be more flexible in the second semi-crystalline phase. This is indicated by the huge value of the temperature hysteresis ($\Delta T \approx 14.5°C$).[4] The liquid crystalline phase should possess completely molten alkyl chains as assigned by the last hysteresis.

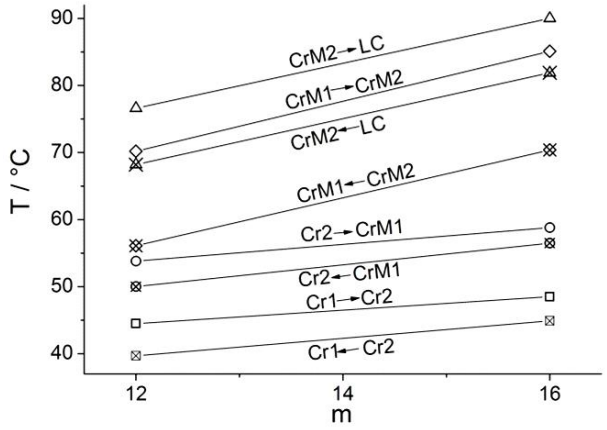

Figure 7-5. Transition temperatures of the different temperature dependent phases of the second heating (bare symbols) and cooling (crossed symbols) cycle of ChS_m with m = 12 and 16 obtained from DSC measurements. The following phases are formed with increasing temperature: first crystalline phase (Cr1), second crystalline phase (Cr2), first semi-crystalline phase (CrM1), second semi-crystalline phase (CrM2), liquid crystalline phase (LC). The straight lines connect the corresponding transition temperatures of m = 12 and 16 (not fitted).

The same behavior could be observed comparing the single enthalpy and entropy values of the respective phase transitions (see **Table 7-2**). The sum of the enthalpies of the phase transitions of choline dodecylsulfate ($\sum\Delta H_{heat}$ = 38.1 kJ mol^{-1}) and choline hexadecylsulfate ($\sum\Delta H_{heat}$ = 53.8 kJ mol^{-1}) (see Appendix E in section E.2) with increasing temperature in the range between 0°C and 95°C is similar to the enthalpy values of dodecane (36.8 kJ mol^{-1})[24] or hexadecane (53.3 kJ mol^{-1})[24] fusion. This explains that the systematic melting of the surfactant is more dependent on the alkyl chain length and therefore on the van der Waals interactions between the alkyl chains, rather than on the interactions between the polar groups.

Taking **Figure 7-6** into account, the sum of the enthalpies/entropies obtained for the transitions of the phases Cr1 to Cr2 and Cr2 to CrM1 represent the transition enthalpy/entropy for the transition of the crystalline phase Cr to the semi-crystalline phase CrM, while the sum of the enthalpy/entropy of the transitions of CrM1 to CrM2 and CrM2 to LC gives the enthalpy/entropy for the phase transition of the semi-crystalline phase CrM to the liquid crystalline phase LC (vice versa for the cooling cycle). The following discussion is based on the heating cycle. The same behavior is found for the cooling cycle. The phase transition enthalpy/entropy of the crystalline phase Cr towards the semi-crystalline phase CrM is strongly dependent on the chain length and increases with growing paraffinic chain length by 3.1 kJ mol^{-1} or 9.4 J $mol^{-1}K^{-1}$ per $-CH_2-$ group. The other transition from the semi-crystalline phase CrM to the liquid crystalline phase LC is only slightly influenced by the chain length. The enthalpy/entropy increases with growing chain length by 0.8 kJ mol^{-1}/1.5 J $mol^{-1}K^{-1}$ per $-CH_2-$ group. These increases of the transition enthalpies and entropies with the alkyl chain length can be related to the increasing van der Waals interactions in the same direction.

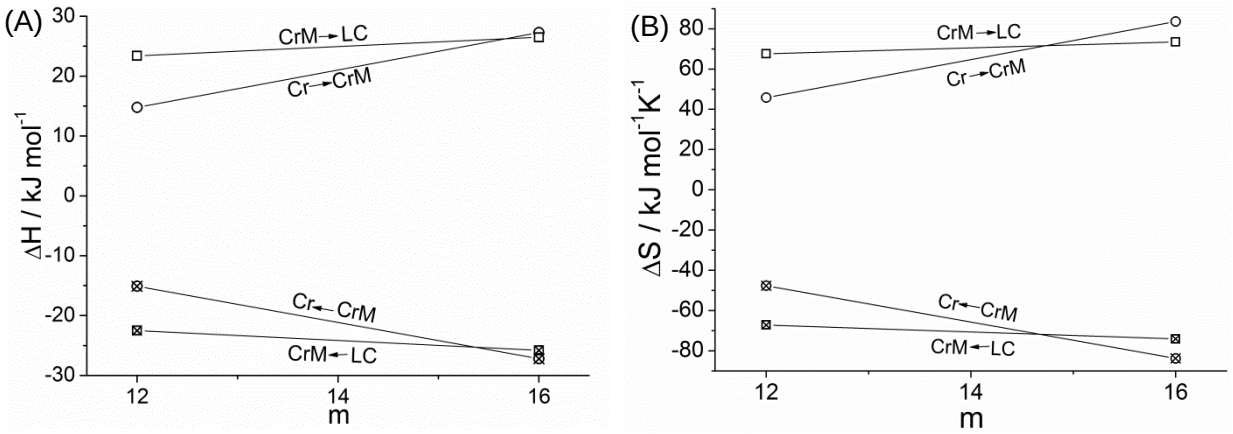

Figure 7-6. Transition enthalpies (A) and transition entropies (B) of the respective phase transition of the thermotropic phases of choline alkysulfates ChS_m with m = 12 and 16 are shown as a function of the chain length m. The values are obtained from DSC measurements between the temperature range of 0°C and 95°C of reheated samples. As the transition enthalpy and transition entropy of the crystalline phase Cr to the semi-crystalline phase CrM, the sum of the single transition enthalpies/entropies of the Cr1 to Cr2 and Cr2 to CrM1 was taken (○ heat; ⊗ cool). For the ones of the phase transition of the semi-crystalline phase CrM to the liquid crystalline phase LC the sum of the transition enthalpies/entropies of the phase transition CrM1 to CrM2 and CrM2 to LC was taken (☐ heat; ☒ cool). The straight lines connect the corresponding transition enthalpies/entropies of m = 12 and 16 (not fitted).

Comparing the single transition enthalpies and entropies of the respective choline alkylsulfates (see **Table 7-2**) the following could be observed. The chains are very rigid in the two crystalline phases and only slightly disordered in the first semi-crystalline phase. This could be assumed because the first two transitions have an overall transition enthalpy/entropy of 38.7 % (ChS_{12}) or 50.8 % (ChS_{16}) of the overall transition enthalpy/entropy. The transition of the first semi-crystalline phase to the second semi-crystalline phase requires 34.6 % (ChS_{12}) or 29.6 % (ChS_{16}) of the overall transition enthalpy/entropy and indicates partly molten alkyl chains in the second semi-crystalline phase. The enthalpy/entropy value of the transition of the second semi-crystalline phase to the liquid crystalline phase is the same for the both alkyl chain lengths and is 26.7 % (≈ 10.2 kJ mol^{-1}; ChS_{12}) or 19.6 % (≈ 10.6 kJ mol^{-1}; ChS_{16}) of the overall transition enthalpy. This indicates that the paraffinic chains are fully disordered in the liquid crystalline phase. The last transition is more related to the melting of the polar groups and not so dependent on the alkyl chain length. As already found for other thermotropic phase transitions of longer chain surfactants[3, 21], also here the total enthalpy and entropy variation is smaller in the cooling cycle than in the heating cycle. However, a more detailed discussion of the structure is given in the X-ray scattering section 7.3.4 and NMR section 7.3.5.

	ChS_{12}				ChS_{16}			
	ΔS_1 / J mol^{-1} K^{-1}	ΔS_2 / J mol^{-1} K^{-1}	ΔS_3 / J mol^{-1} K^{-1}	ΔS_4 / J mol^{-1} K^{-1}	ΔS_1 / J mol^{-1} K^{-1}	ΔS_2 / J mol^{-1} K^{-1}	ΔS_3 / J mol^{-1} K^{-1}	ΔS_4 / J mol^{-1} K^{-1}
1. heat	75.8		38.1	27.8	33.5	52.7	42.6	29.8
1. cool	-24.6	-21.2	-38.4	-31.4	-33.7	-48.8	-43.3	-31.2
2. heat	23.9	21.9	38.5	29.1	30.8	52.5	44.5	29.1
2. cool	-26.0	-21.7	-39.1	-28.1	-35.6	-48.2	-43.2	-30.9
3. heat	24.2	21.0	38.2	29.4	33.5	53.9	42.4	29.5
3. cool	-25.2	-20.9	-37.9	-30.3	-31.5	-51.5	-44.1	-30.5
	ChS_{12}				ChS_{16}			
	ΔH_1 / kJ mol^{-1}	ΔH_2 / kJ mol^{-1}	ΔH_3 / kJ mol^{-1}	ΔH_4 / kJ mol^{-1}	ΔH_1 / kJ mol^{-1}	ΔH_2 / kJ mol^{-1}	ΔH_3 / kJ mol^{-1}	ΔH_4 / kJ mol^{-1}
1. heat	25.1		13.1	9.7	10.8	17.5	15.1	10.9
1. cool	-7.7	-6.9	-12.6	-10.7	-10.7	-16.1	-14.9	-11.1
2. heat	7.6	7.2	13.2	10.2	9.9	17.4	15.9	10.6
2. cool	-8.1	-7.0	-12.9	-9.6	-11.3	-15.9	-14.8	-11.0
3. heat	7.7	6.9	13.1	10.3	10.8	17.9	15.2	10.8
3. cool	-7.9	-6.8	-12.5	-10.3	-10.0	-17.0	-15.2	-10.8

Table 7-2. Single entropies and enthalpies of the different phase transitions of ChS_m with m = 12, 16 of the three heating and cooling cycles recorded by DSC measurements in the temperature range between 0°C and 95°C. The numbers 1, 2, 3, and 4 are assigned to the transitions with increasing temperature.

7.3.4 Temperature dependent SAXS und WAXS

As it was already shown in Chapter 5 in section 5.3.4 X-ray scattering is a very efficient method to evaluate structural details of different thermotropic phases. Here, lower q region characterizes the long range order and the packing of the chains, while the higher q region specifies the flexibility and fluidity of the alkyl chains.

Unfortunately, reliable spectra of the two heating and cooling cycles of neat choline dodecylsulfate were not recordable. The measured spectra give raise to the assumption that neat choline dodecylsulfate was decomposed. This fact was further confirmed by NMR. Due to a lack of beamtime at DESY in Hamburg the measurements could not be reproduced so that only the results of choline hexadecylsulfate are shown. However, by taking into account the results of the other performed characterization methods (see section 7.3.2, 7.3.3 and 7.3.5), it could be assumed that the structure of the thermotropic phases of choline dodecylsulfate should be similar to the one of choline hexadecylsulfate.

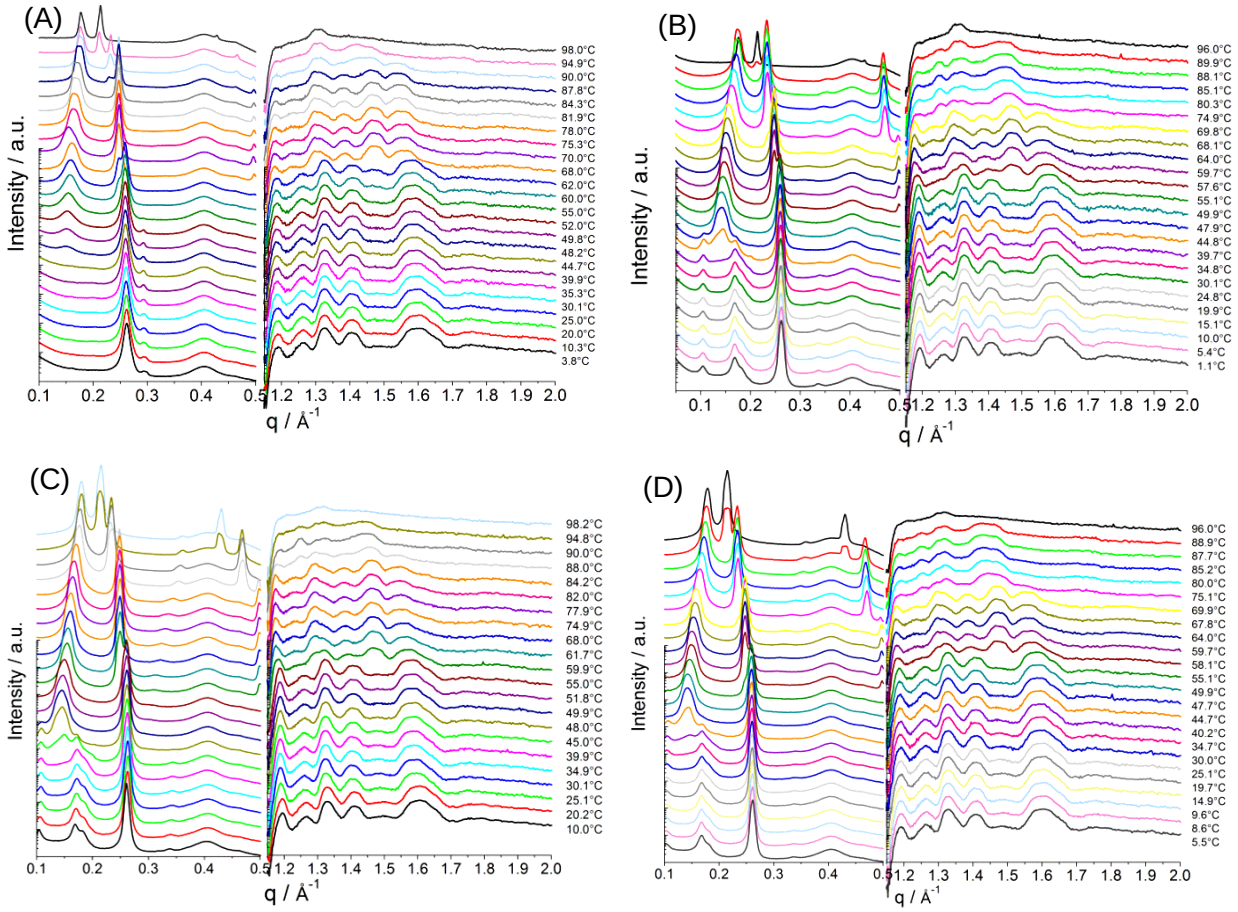

Figure 7-7. SAXS und WAXS spectra of the first heating (A), first cooling (B), second heating (C) and second cooling (D) cycle of neat choline hexadecylsulfate. The measurements were performed in a temperature range between 0°C and 98°C and with a heating rate of 1 K min^{-1}. The peak around 0.4 $Å^{-1}$ results from the Kapton foil. At 98°C a broad peak arises around 1.5 $Å^{-1}$ and indicates the molten alkyl chains.

As already found for the thermotropic phases of choline carboxylates in Chapter 5 choline hexadecylsulfate shows as well a continuous melting of the chains with increasing temperature (see **Figure 7-7**). The sharp reflections at the higher q-range disappear with increasing temperature and the disorder of the alkyl chains and the fluidity of the paraffinic chains increase. At maximum temperature a broad peak at around 1.5 A^{-1} indicates the fully molten alkyl chains (see **Figure 7-7** (C) at 98.2°C). For the cooling cycle the same behavior was found the other way round.

The small q region indicates again the simultaneous existence of two structures in one phase for the different thermotropic phases of neat choline hexadecylsulfate as it was already observed for the choline carboxylates (see Chapter 5). This can be assumed as additional peaks, which could not be assigned to the main structure, were observed in this low q region. However, also here it could even be possible that instead of the two structures in one phase the simultaneous existence of two phases in equilibrium occurs. The phases may be thermodynamically stable or kinetically stabilized. But as mentioned in the case of choline

carboxylates, the phase behavior is explained as two structures in one phase, but also the other case should be taken into account.

Therefore, the main structure of the thermotropic phases of choline hexadecylsulfate can be assigned with increasing temperature as follows:

First crystalline structure Cr1: An interdigitated monolayered structure with tilted alkyl chains can be assigned due to the existence of two small angle reflections. The highest d-value is 36.8 Å at 20.2°C (see **Figure 7-7** (C)). This corresponds to the length of a fully extended hexadecyl chain (≈ 21.7 Å)[25] and 14 Å for two choline cations.[21] The length of two sulfate groups is around 7-8 Å (MOPAC calculation[26]). In addition, a lot of defined reflections are found in the high q range which characterize the crystallinity of the alkyl chains. The rigid bilayered structure (curd phases), as found for the low temperature thermotropic phase of classical soaps[24, 27], could not be confirmed because the identified d-values are too small. The phase sequence with increasing temperature is more similar to the one found for low temperature structures of thermotropic phases of choline carboxylates (see Chapter 5 in section 5.3.4 and [21]). Details on crystalline packing of the structure (e.g. orthorhombic, monoclinic, triclinic, etc.) could not be obtained yet.

Second crystalline structure Cr2: Another interdigitated monolayered phase with less tilted alkyl chains as before is observed. Two reflections indicate the phase structure. The highest d-value increases slightly with increasing temperature (42.9 Å at 51.8°C, see **Figure 7-7** (C)). Again the detailed structure could not be revealed. The alkyl chains are still crystalline. This is indicated by the defined reflections in the wide angle q-range.

First semi-crystalline structure CrM1: The structure is a bilayer with slightly molten alkyl chains. The change in the flexibility of the alkyl chains can be seen by the decreased and shifted defined reflections in the wide angle region. The assigned reflections at 4.2 Å (≈ 1.5 $Å^{-1}$) and 4.0 Å (≈ 1.6 $Å^{-1}$)[27] are typical for a $L_{\beta'}$ gel phase. However, the existence of further reflections at the wide angle range excludes the presence of a gel phase. The bilayered structure could be assigned by two reflections. The highest d-value is around 38.8 Å at 74.9°C (see **Figure 7-7** (C)). Taking into account the approximation of the molar volume of choline hexadecylsulfate (see Chapter 6, **Table 6-6**.) and the equation (11) and (12) (see Chapter 4) the thickness of the lipophilic bilayer d_L and the cross-sectional area a_s can be calculated. The lipophilic bilayer thickness d_L is around 25.7 Å. Here, the half length of the lipophilic bilayer is 59.1 % of a fully extended hexadecyl chain length (≈ 21.7 Å)[25]. The thickness of the polar layer (sulfate headgroup plus choline) is 13.2 Å. This value is moderate considering the sulfate headgroup (≈ 3.5-4 Å (MOPAC calculation[26])) and the length of a fully extended choline cation (≈ 7-9 Å[21]). The cross-sectional area a_s is around 35.6 $Å^2$.

Second semi-crystalline structure CrM2: Again a semi-crystalline bilayered structure is found. The chains are more molten and show a higher degree of flexibility. Because of this the

lipophilic bilayer distance d_L decreases to 23.7 Å at 88°C. This value results in a half length of the lipophilic bilayer of around 54.4 % compared to the fully extended hexadecyl chain length (≈ 21.7 Å)[25]. Additionally, the value of the highest d-spacing and the length of the polar layer decrease at 88°C to 35.7 Å and 12.0 Å, respectively, compared to CrM1 (see **Figure 7-7** (C)). The cross-sectional area a_s, however, increases with temperature to 38.7 Å^2.

Liquid crystalline structure LC: A defective lamellar or nematic structure is formed. The highest d-spacing decreases slightly to 35 Å at 98°C (**Figure 7-7** (C)). Now, the alkyl chains are completely molten and fluid. The lipophilic length of the bilayer d_L is reduced to 23.1 Å. Thus, the half length of the lipophilic bilayer is around 53.2 % of the fully extended hexadecyl chain length (≈ 21.7 Å)[25]. The cross-sectional area a_s is amplified to 39.6 Å^2 at 98°C. It is slightly smaller compared to the cross-sectional area a_s found for the liquid crystalline high temperature phase of choline carboxylates ChC_m with m = 12-18 at 90°C (the a_s values vary in a non-linear way for ChC_m with m = 12-18 between 39.8 Å^2 to 41.3 Å^2).[21] The value of a_s for the high temperature phase of choline hexadecylsulfate should be higher due to the sulfate headgroup being slightly bigger than the carboxylate headgroup. Moreover, the cross sectional area increases with temperature. The smaller cross-sectional area measured for the defective lamellar or nematic structure of choline hexadecylsulfate could result from the stronger interaction between the “soft” sulfate anion and the “soft” choline cation compared to the interaction between the “hard” anion carboxylate and the “soft” cation choline. Collins’ law of “matching water affinities” [28, 29] could also be transferred to a liquid crystalline system.[30] Thus, the stronger interaction between the sulfate headgroup and the choline counterion diminishes the effective charge at the sulfate anion and therefore reduces the headgroup repulsion in the polar part of the lamellar bilayer. Another reason for the discrepancies could be the error which was made during the approximation of the molar volume.

Furthermore, no smectic A phase which was assigned as the high temperature phase for neat choline hexadecanoate[21] was identified for choline hexadecylsulfate at high temperatures. A broad reflection was found at the first d-spacing which corresponds to a defective lamellar or nematic phase of neat choline hexadecylsulfate. This could be the consequence of the creation of defects[31], which destroy the long range order. This phase was also found in Chapter 6 as the highest concentrated liquid crystalline phase in the binary phase diagram of ChS_{12} and ChS_{16} with water. The reason for creating such defects will be explained in the next section 7.3.5. A second peak in the small angle region (≈ 29.2 Å, **Figure 7-7** (C) at 98°C) could result from the second phase structure or demonstrate that the phase transition is not in equilibrium and needs thus higher temperatures or more time to reach equilibrium state.

All in all, it is obvious that two structures appear in one phase of neat choline alkylsulfate along the whole temperature range. The second structure is characterized by additional

peaks in the small angle region, but the detailed structure could not be evaluated. Furthermore, another possibility instead of two structures in one phase is the simultaneous existence of two different phases, which are thermodynamically stable or kinetically stabilized. However, the method used here does not allow to render a conclusive judgement.

7.3.5 Temperature variable ^{1}H NMR

^{1}H NMR was used to provide a further independent method characterizing the thermotropic phases and their phase transitions. As already explained in Chapter 5 in section 5.3.5 the homonuclear dipolar coupling between the neighboring nuclear dipoles is the main anisotropic interaction of protons in a solid phase. This anisotropic interaction creates broad NMR lines. This broadening of the lines is reduced by increasing chain flexibility by the anisotropic motion in non-crystalline regions and isotropic reorientation in the liquid state. Thus, the phase change can be qualitatively visualized by the broadening of the NMR lines (see **Figure 7-8**). The chain flexibility can be expressed with the help of the spin-spin relaxation time T_{2eff}. Therefore, characteristic values for the -CH_2- groups can be found in literature for the different phases: T_{2eff} < 10 µs[32, 33] for crystalline phases; gel or semi-crystalline phase T_{2eff} ≈ 20-30 µs[33]; lamellar phases T_{2eff} ≈ 100 µs[32-35], but this value can vary a lot. It can be up to 200 µs or slightly smaller than 100 µs. A "normal" liquid shows values > 1 ms[32].

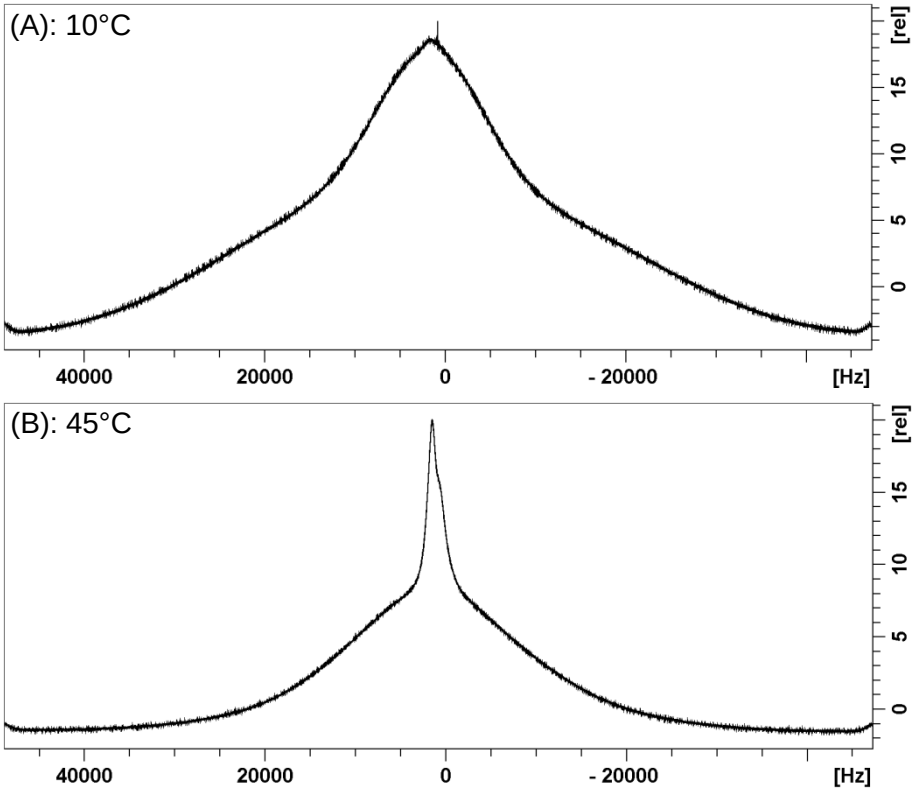

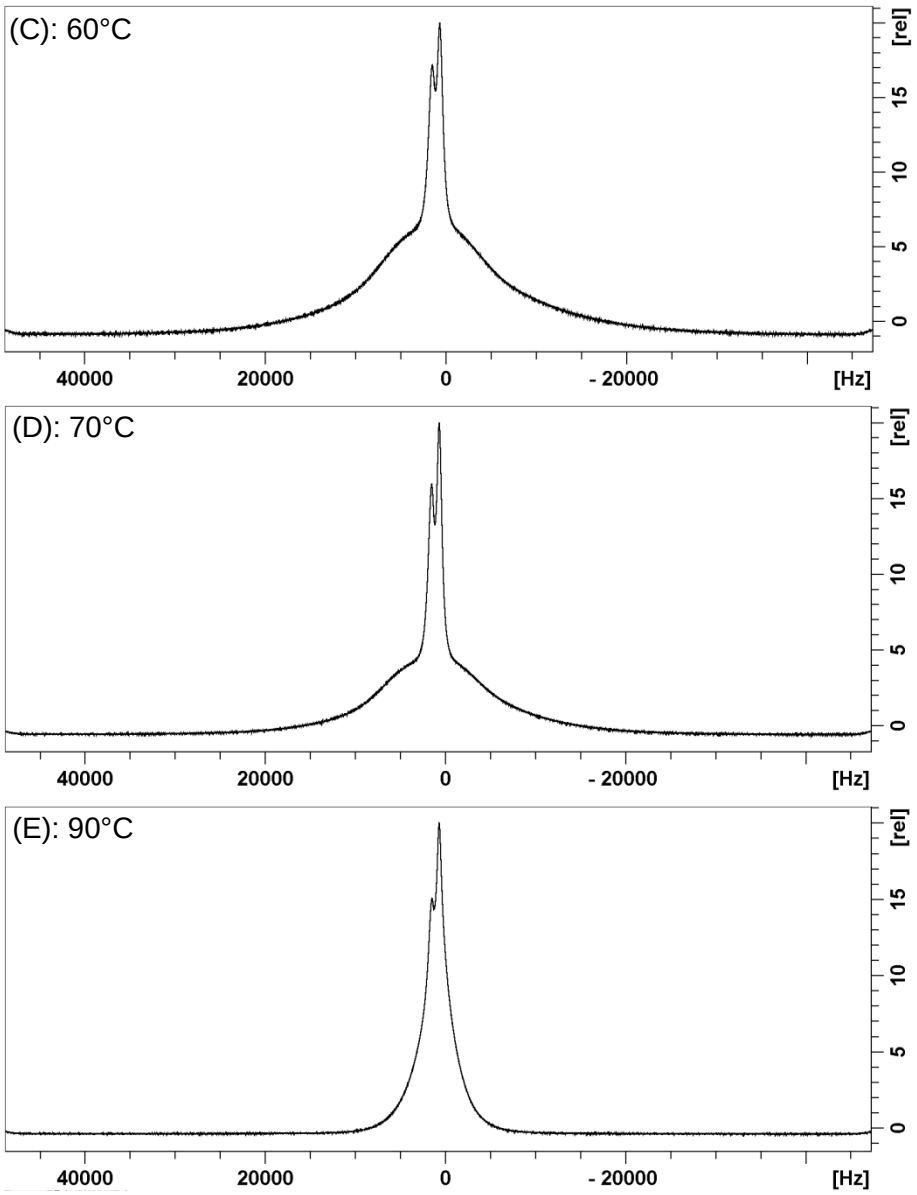

Figure 7-8. Temperature dependent ^{1}H NMR spectra of the neat choline dodecylsulfate are shown. The phase heterogeneity is visualized. Each spectrum contains a broader peak which varies with the crystallinity of the main structure and several sharp peaks which result from the non-averaged dipole-dipole couplings between the protons of choline dodecylsulfate in the more liquid-like structure. The spectra are measured at the following temperatures and the broader peak results from the following main structures: (A) 10°C: first crystalline phase Cr1, (B) 45°C: second crystalline phase Cr2, (C) 60°C: first semi-crystalline phase CrM1, (D) 70°C: second semi-crystalline phase CrM2, (E) 90°C: liquid crystalline phase LC.

The T_{2eff} times are calculated from the half width (in Hertz) at the half-height of the different NMR peaks. Hereby the temperature dependent spectra were fitted using a Gaussian-Lorentzian equation. The Lorentzian equation describes the theoretical shape of the NMR peak, while the Gaussian equation takes field inhomogeneities into account.[36] The values of T_{2eff} have been used to get an idea of the chain flexibility and molecular order at the different temperatures (see **Figure 7-9**).[37] With this method two different structuring could be monitored in one phase. Here, each spectrum of the respective temperature contains a broad NMR peak, which belongs to the main structuring of the phase. A more fluid, liquid-like

structure could be identified due to several sharp NMR peaks belonging to the single protons of the choline alkylsulfates ChS_m with m = 12, 16 in the liquid-like structure (see **Figure 7-8**). During the fitting procedure the ratio between the choline cation and the alkylsulfate anion was fixed to 1:1 molar so that the overall intensity of the NMR peak belongs to the number of protons of the choline cation and the alkylsulfate anion. Taking the overall intensity into account, the amount of main and minor structure in the single phase could be determined (see Appendix E in section E.3). The amount of the minor phase is temperature independent and more or less similar for the two choline alkylsulfates ChS_m with m = 12 and 16. In the case of ChS_{12} this value is determined to 13.6 ± 3.5 % of the overall intensity for the minor phase and 18.1 ± 4.5 % for ChS_{16}.

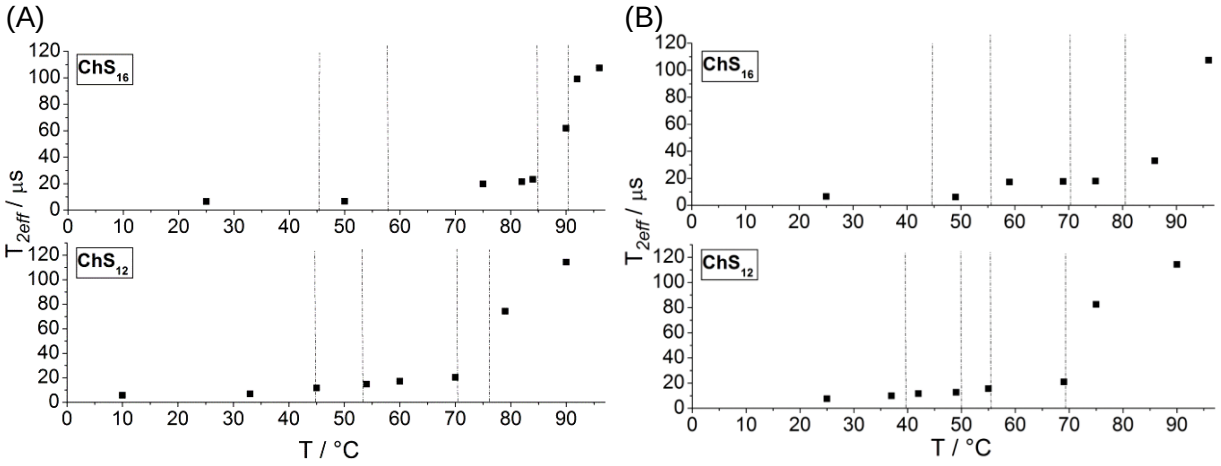

Figure 7-9. Temperature dependent spin-spin relaxation times T_{2eff} of the main structure of anhydrous choline dodecylsulfate and choline hexadecylsulfate are shown. The vertical lines mark the transition temperatures evaluated with DSC for different thermotropic phases of reheated choline dodecylsulfate and choline hexadecylsulfate at the heating (A) and cooling cycle (B).

Comparing the molecular motion in the main structuring, which is expressed by the spin-spin relaxation time T_{2eff}, the two choline alkylsulfates behave very similarly. It is obvious that the chain flexibility is rather restricted in the two crystalline phases Cr1 and Cr2. The spin-spin relaxation time T_{2eff} for Cr1 and Cr2 is lower than 10 µs and 12.6 µs, respectively. The flexibility of the alkyl chains in the two semi-crystalline phases CrM1 and CrM2 increases slightly. The spin-spin relaxation time T_{2eff} covers the range from 16.7 µs to 25.2 µs. These values also point out a very restricted flexibility of the alkyl chains. In the liquid crystalline structure the flexibility increases a lot and the chains are molten. The spin-spin relaxation time T_{2eff} varies between 82 µs and 114.3 µs. Further, the transition temperatures of the main structure are slightly different compared to DSC measurements, but this refers to the different amount of used substance for each method (NMR: 2-3 g, DSC smaller than 30 mg). The existence of a second, more liquid-like structure could also be approved with this method. As explained above not only the existence of two structures in one phase but also

the simultaneous existence of two phases which are in equilibrium with each other (thermodynamically stable or kinetically stabilized) is a possible explanation for the measured data. However, with the performed measurements it could not be clarified exactly which of these two phase behaviors appears in neat choline alkylsulfates along the investigated temperature range. Therefore, the experimental data are explained as two structures in one phase, but also the other case could be an explanation for the phase behavior of neat choline alkylsulfates.

In the case of the thermotropic phases of choline carboxylates (see Chapter 5) the second structuring in the neat choline carboxylate phase and the defects in the high temperature defective lamellar or nematic phase structure could be explained either by the unsymmetrical, very bulky choline cation or by the appearance of a second headgroup. In general, choline surfactants are hygroscopic and contain a few thousand ppm of water. The equilibrium between choline carboxylate and water with choline hydroxide and carboxylic acid could be assumed because the pK_a of the carboxylic acids is around 4.5.[38, 39] Thus, two different headgroups (-COOH and $-COO^-$) are available and different curvatures could be formed. They create defects in the lamellar liquid crystalline structure, the main structure at high temperatures, as well as a second structure in the neat surfactant phase, existing along the whole investigated temperature range.

This equilibrium could be excluded for the thermotropic phases of the choline alkylsulfates ChS_m with m = 12, 16. Neat choline alkylsulfates contain 1500 ppm to 2500 ppm water (measured with coulometric Karl-Fischer titration) due to the hygroscopic nature of choline. However, the hygroscopic behavior is not so pronounced as for the carboxylate soaps. The pK_a of the alkylsulfate is lower than 2.[30, 40] To our knowledge the exact values are not listed in literature. This value is too small so that the upwards mentioned equilibrium (here explained for the choline alkylsulfates) between the choline alkylsulfate and water with the alkylsulfuric acid and choline hydroxide will be shifted completely to the side of water and choline alkylsulfate. Another possibility explaining the existence of two different headgroups to create different curvatures could be the hydrolysis of the alkylsulfate anion (see **Figure 7-10**) so that these two headgroups, the hydroxyl group of the fatty alcohol (-OH) and the sulfate group ($-SO_4^-$), are present in the phase.

Literature exists on the hydrolysis behavior of sodium dodecylsulfate in water. The hydrolysis rate increases with increasing temperature.[40] With the help of computer simulations Bethell *et al.*[40] calculated the rate coefficients for the different hydrolysis steps (see **Figure 7-10**). The hydrolysis mechanism is an autocatalytic mechanism (see **Figure 7-10**).[40, 41]

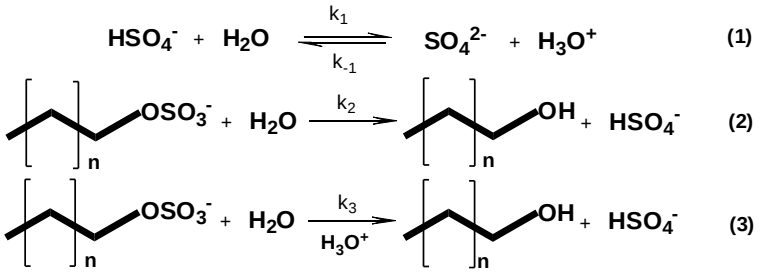

Figure 7-10. Hydrolysis of neutral sodium dodecylsulfate water solution is shown. k_1, k_{-1}, k_2 and k_3 are the rate coefficients. For neutral aqueous solutions of sodium dodecylsufate $k_1 = 1.66 \cdot 10^8$ mol $kg^{-1}s^{-1}$ and $k_{-1} = 1 \cdot 10^{10}$ mol $kg^{-1}s^{-1}$. The computer simulations and experiments take the temperature range of 80°C to 100°C and the concentration range of 1 wt% to 70 wt% into account. k_2 and k_3 are temperature and concentration dependent, but in general $k_2 < k_3$.[40]

The study investigated the concentration range of almost 0 wt% up to 70 wt% sodium dodecylsulfate in water in the temperature range between 80°C and 100°C. Here, no linearity of the hydrolysis rate as a function of concentration could be observed.[40] Moreover, the hydrolysis rate can be influenced by the counterion even if no law could be identified in this case.[40] Another study reveals more detailed information about the temperature dependent hydrolysis. It is known that sodium dodecylsulfate shows a decomposition of 5 % in water by heating for 30 hours at 70°C and a dehydration of 50 to 60 % by heating for one hour at 125°C.[42]

Such a hydrolysis would explain the simultaneous existence of the fatty alcohol and the alkylsulfate anion of the fatty alcohol in the phase, but it has to be taken into account that these studies were performed only at concentrations up to 70 wt% surfactant. Furthermore, in the neat choline alkylsulfates ^{1}H NMR measurements suggest two structures at temperatures below 80°C and before heating the sample for the first time. In such a case this hydrolysis must even occur at temperatures below 80°C.[40]

It was not possible to verify the existence of the hydrogensulfate anion with time dependent pH measurements of 4.6 wt% aqueous solution of heated and unheated neat choline alkylsulfates ChS_m with m = 12, 16 (see section 7.5.8). The existence of the fatty alcohol could neither be approved nor excluded with IR measurements because the specific peak of the dodecanol or hexadecanol alcohol group overlap[43] with the one of the hydroxyl group of choline and the alkylsulfate streching[44] (see section 7.5.7 and **Figure 7-11**). Further, the purity of the neat choline alkylsulfate was proved with ^{1}H and ^{13}C NMR and mass spectrometry. Therefore, impurities could be excluded as explanation. Another possibility for the appearance of two structures as well as in the thermotropic phases of choline carboxylates ChC_m with m = 8, 10 and oleate (see Chapter 5) as well as in the thermotropic phases of choline alkylsulfate ChS_m with m = 12, 16 and also for the defects in the lamellar liquid crystalline phase, could be the nature of the choline cation. The choline cation is a very bulky, unsymmetrical cation. It seems that it is able to create different structures with different curvatures in one phase due to its unsymmetric and bulky appearance. In comparison,

different curvatures are also possible in lyotropic phases like lyotropic micellar cubic phases[45, 46] e.g. the P*m*3*n* structure. Micelles of different shape are packed in a micellar cubic phase. [46-49] Also gel phases can possess different curvatures, as seen in hexadecyldimethylethylammonium bromide with water.[27, 46] To sum up, some possible explanations for the appearance of the second more liquid-like structure and the defects in the defective lamellar or nematic liquid crystalline structure are given, but could not be approved with the performed methods and have to be further investigated. Furthermore, it could not be evaluated, if really two structures in one phase exist or if two phases are in equilibrium with each other (thermodynamically stable or kinetically stabilized). Both case scenarios are possible.

7.4 Conclusion

Neat choline alkylsulfates ChS_m with m = 12, 16 show a rich thermotropic phase behavior in the temperature range between 0°C and 98°C. The different phases were characterized with polarizing optical microscopy, differential scanning calorimetry, small and wide angle X-ray scattering and ^{1}H NMR. The melting behavior of the choline alkylsulfates ChS_m with m = 12, 16 was found to be similar to the one of the choline carboxylates ChC_m with m = 8, 10 and oleate (see Chapter 5). First the alkyl chains start to melt and afterwards the polar groups. However, in the case of the choline alkylsulfates the melting process is more influenced by the length of the alkyl chain than by the counterion. Also two different structures are found in one phase along the whole temperature range. The second structure could also be characterized as a more liquid-like structure, but the detailed structure could not be evaluated. The structuring of the main part of the phase is analyzed in detail and is more manifold than the one of the choline carboxylates. Choline hexadecylsulfate shows the following main structures with increasing temperature: first a crystalline interdigitated monolayer with tilted alkyl chains is formed (Cr1). Then a second crystalline interdigitated monolayer appears with less tilted alkyl chains (Cr2). After that the monolayer is transformed to a semi-crystalline bilayered structure (CrM1). In the second semi-crystalline bilayered structure the alkyl chains are more fluid and they melt completely in the liquid crystalline defective lamellar or nematic structure at higher temperatures. The structure of choline dodecylsulfate could not be assigned with SAXS and WAXS measurements, but a similar structure could be assumed comparing the results obtained from the other performed methods. The phase behavior of neat choline alkylsuflates was explained by taking into account two structures in one phase, but it should be kept in mind that another possible explanation for the found results in the measurements is the simultaneous existence of two different phases which are in equilibrium with each other and thermodynamically stable or

kinetically stabilized. For a clear statement further measurements should be performed. What is obvious from light microscopy measurements is that macroscopically only one phase was found and also it could not be determined in pH or IR measurements which components are available in neat choline alkylsulfates.

The cross-sectional area a_s of choline hexadecylsulfate in the defective lamellar bilayered structure is 39.6 $Å^2$ at 98°C. The ones of choline carboxylates ChC_m with m = 12-18 at 90°C are in the range of a_s 39.8 $Å^2$ to 41.3 $Å^2$.[21] Normally, this behavior should be the other way round because the sulfate headgroup is slightly bigger compared to the carboxylate headgroup. Collins' law of "matching water affinities" [28, 29] states that the interaction of choline with the sulfate anion in aqueous solution is stronger than with the carboxylate anion. This theory is applied to liquid crystalline state.[30] Therefore, the effective charge at the sulfate headgroup could be lowered because of the stronger choline-sulfate interaction compared to the interaction of choline with the carboxylate group. The headgroup repulsion at the sulfate anion in the polar layer of the bilayer is reduced and this could explain the smaller a_s value compared to the one of the choline carboxylate soaps.

Furthermore, the melting enthalpy increases from chain length C_{12} to C_{16}. The first three phase transitions are more related to the melting of the alkyl chains, while the last phase transition is more related to the melting of the polar groups.

The defects in the high temperature defective lamellar or nematic liquid crystalline structure and the existence of the second structure (or second phase) in neat choline alkylsulfates in the temperature range between 0°C and 98°C could be explained in the case of the choline alkylsulfates by the bulky, unsymmetrical nature of choline. The existence of the alcohol, as a second headgroup formed due to hydrolysis, could not be excluded completely and is another possible explanation. Due to the alcohol group and the sulfate headgroup different curvatures could be formed and could create defects. However, to get an exact explanation further measurements have to be performed.

Comparing the thermotropic phase behavior with the one of choline carboxylates[21] (see Chapter 5) it is found that all substances are molten to liquid crystalline phases below 100°C and can be assigned as an ionic liquid.

7.5 Experimental

7.5.1 Chemicals and sample preparation

The choline alkylsulfates ChS_m with m = 12, 16 were synthesized via ion exchange as reported in Chapter 6 in section 6.5.1. The purity was confirmed with mass spectrometry, ^1H and ^{13}C NMR measurements. Mass spectrometrical data were recorded on a ThermoQuest Finnigan TSQ 7000 instrument. The ^1H and ^{13}C NMR spectra were measured on a Bruker

Avance 300 spectrometer at 300 MHz using tetramethylsilane (TMS) as internal standard. The water content of the products was determined by coulometric Karl-Fischer titration, using an Abimed MCI analyzer (Model CA-02). The data are shown in Chapter 6 in section 6.5.1.

7.5.2 Methods

7.5.2.1 Thermogravimetric analysis

The decomposition temperatures (T_{dec}) of choline hexadecylsulfate ChS_{16} and sodium hexadecylsulfate NaS_{16} were measured and determined according to the procedure explained in Chapter 5 in section 5.5.2.2. The temperature range between 30°C and 500°C was recorded.

7.5.2.2 Differential scanning calorimetry (DSC)

DSC was used to determine the different phase transition temperatures, the melting (T_m) and the crystallization temperature (T_c) and to calculate the transition enthalpies and entropies of the different phase transitions of choline dodecylsulfate and choline hexadecylsulfate. The measurements and the calculations were done as described in Chapter 5 in section 5.5.2.1. The investigated temperature range was between 0°C and 95°C.

7.5.2.3 Polarizing optical microscopy

Light microscopy images were recorded with a Leitz Orthoplan microscope (Wetzlar, Germany) equipped with a JVC digital camera (TK-C130) and a Linkham hot stage with a TMS90 temperature controller (± 0.5°C) and a CS196 cooling system. Images were taken in the temperature range from 0°C to 98°C in a nitrogen glove box to avoid cross contamination with water from air. A small amount of substance was put between two microscope slides. Three heating and cooling cycles were recorded of each sample. The first two ones were performed with a heating rate of 10 K min^{-1}, the third with heating rate of 1 K min^{-1}.

7.5.2.4 Small and wide angle X-ray scattering

The X-ray scattering experiments in the small and wide angle q-range were performed with the DORIS III equipment at DESY in Hamburg as described in Chapter 5 in section 5.5.2.4. The samples were prepared in the nitrogen glove box in cells made of stainless steel plates with a 7 mm diameter hole. The thickness of the sample was 2.8 mm. To cover the holes from both sides Kapton foil was used. The temperature range from 0-98°C was recorded with a heating rate of 1 K min^{-1}.

7.5.2.5 Temperature variable ^{1}H NMR

NMR measurements were carried out on a Bruker Avance 400 instrument and were conducted and the samples were prepared as explained in Chapter 5 in section 5.5.2.5.

7.5.2.6 IR measurements

The IR spectra were done with an FT/IR 610 instrument from Jasco using the software Spectra Management Software. The IR spectra were recorded in the wavelength region from 450-3700 cm^{-1}. From each spectrum 60 scans were performed. They were measured with diffuse reflectance. The samples were mixed with potassium bromide and the spectrum of potassium bromide was subtracted as background. A spectrum was recorded of choline chloride (Sigma Aldrich, purity ≥ 98%), 1-dodecanol (Sigma Aldrich, purity ≥ 98%), neat choline dodecylsulfate and neat choline hexadecylsulfate. To prove thermal decomposition a sample of choline dodecylsulfate and choline hexadecylsulfate heated for 30 minutes to 95°C was also investigated. As seen in **Figure 7-11** the significant peaks, which characterize dodecanol and also hexadecanol were overlapped by peaks resulting from the sulfate stretching vibrations ($\nu(SO_4^-)$ = 958 cm^{-1}, 980 cm^{-1}, 1064 cm^{-1}, 1210 cm^{-1}, 1250 cm^{-1}).[44] The broad peak of the -OH stretching ((ν(OH) = 3200-3550 cm^{-1})[43] of the alcohol overlaps with peak of the -OH stretching of choline and also with the water peak which is present in the spectra of all substances (except dodecanol) due to the hygroscopic behavior of choline.

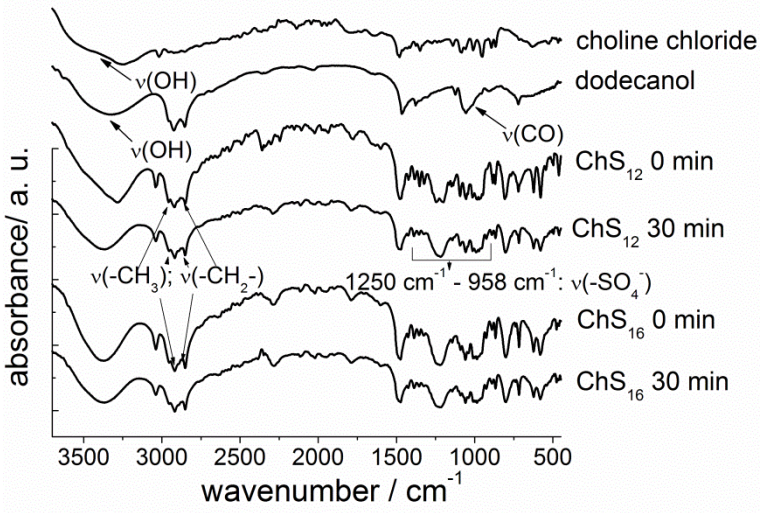

Figure 7-11. IR spectra of choline chloride, dodecanol, choline dodecylsulfate (ChS_{12} 0 min), choline dodecylsulfate heated for 30 minutes to 95°C (ChS_{12} 30 min), choline hexadecylsulfate (ChS_{16} 0 min) and choline hexadecylsulfate heated for 30 minutes to 95°C (ChS_{16} 30 min).

7.5.2.7 pH measurements

Neat choline dodecylsufate and neat choline hexadecylsulfate were heated for 30 minutes to 95°C to prove temperature induced hydrolysis. Aqueous solutions with 4.6 wt% of choline alkylsulfate ChS_m (m = 12, 16) were prepared with the heated samples and the unheated samples. The pH of the unheated solutions was measured after 0 min, 1 h and 72 h later at 25°C to evaluate if hydrolysis in aqueous solution at room temperature occurs. The same was done with aqueous solutions of the heated sample. The obtained pH was the same for all solutions (6.2 for the 4.6 wt% choline dodecylsulfate solutions and 6.8 for the 4.6 wt% choline hexadecylsuflate solutions in water). The pH was measured by using a glass microelectrode (Mettler-Toledo, InLab Micro) immersed in the solutions. The electrode was connected to a Schott CG-843 laboratory pH meter and values were read out automatically.

7.6 References

1. G. Tiddy, *Phys. Rep.*, 1980, **57**, 1-46.
2. Y. Wang and E. F. Marques, *J. Phys. Chem. B*, 2006, **110**, 1151-1157.
3. A. M. Amorim Da Costa, H. D. Burrows, C. F. G. C. Geraldes, J. J. C. Teixeira-Dias, C. G. Bazuin, D. Guillon, A. Skoulios, E. Blackmore, G. J. T. Tiddy and D. L. Turner, *Liq. Cryst.*, 1986, **1**, 215-226.
4. C. G. Bazuin, D. Guillon, A. Skoulios, A. M. A. Dacosta, H. D. Burrows, C. F. G. C. Geraldes and J. J. C. Teixeiradias, *Liq. Cryst.*, 1988, **3**, 1655-1670.
5. P. Ferloni and E. F. Westrum, *Pure and Appl. Chem.*, 1992, **64**, 73-78.
6. B. Gallot and A. Skoulios, *Kolloid Z. Z. Polym.*, 1966, **209**, 164-169.
7. B. Gallot and A. Skoulios, *Mol. Cryst.*, 1966, **1**, 263-292.
8. B. Gallot and A. Skoulios, *Kolloid Z. Z. Polym.*, 1966, **213**, 143-150.
9. P. B. Gallot and A. Skoulios, *Kolloid Z. Z. Polym.*, 1965, **28**, 37-43.
10. L. Jongen, K. Binnemans, D. Hinz and G. Meyer, *Liq. Cryst.*, 2001, **28**, 819-825.
11. L. Jongen, K. Binnemans, D. Hinz and G. Meyer, *Liq. Cryst.*, 2001, **28**, 1727-1733.
12. L. Jongen, K. Binnemans, D. Hinz and G. Meyer, *Mater. Sci. Eng. C*, 2001, **18**, 199-204.
13. P. Pacor and H. L. Spier, *J. Am. Chem. Soc.*, 1968, **45**, 338-&.
14. M. L. Phillips, T. M. Barbara, S. Plesko and J. Jonas, *J. Chem. Phys.*, 1986, **84**, 5143.
15. H. W. Stache, *Anionic Surfactants*, Marcel Dekker, Inc., New York, 1996.
16. R. G. Laughlin, *The Aqueous Behavior of Surfactants*, Academic Press, San Diego, 1994.

17. J. W. McBain and W. W. Lee, *Oil & Soap*, 1943, **20**, 17-25.
18. T. Kawai, J. Umemura and T. Takenaka, *Bull. Inst. Chem. Res.,*, 1983, **61**, 314-323.
19. M. P. McDonald and W. E. Peel, *J. Chem. Soc., Faraday Trans. 1*, 1976, **72**, 2274-2283.
20. R. Klein, M. Kellermeier, D. Touraud, E. Müller and W. Kunz, *J. Colloid Interface Sci.*, 2013**, 392**, 274-80.
21. R. Klein, H. Dutton, O. Diat, G. J. Tiddy and W. Kunz, *J. Phys. Chem. B*, 2011, **115**, 3838-3847.
22. K. Binnemans, *Chem. Rev.*, 2005, **105**, 4148-4204.
23. F. Mathevet, P. Masson, J. F. Nicoud and A. Skoulios, *J. Am. Chem. Soc.*, 2005, **127**, 9053-9061.
24. M. D. Small, *The Physical Chemistry of Lipids from Alkanes to Phospholipids*, Plenum Press, New York and London, 1986.
25. C. Tanford, *J. Phys. Chem.*, 1972, **76**, 3020-3024.
26. J. J. P. Stewart, *MOPAC 2009, Stewart Computational Chemistry*, Colorado Springs, CO, USA.
27. H. D. Dörfler, *Grenzflächen und kolloid-disperse Systeme: Physik und Chemie*, Springer, Berlin, 2002.
28. K. D. Collins, G. W. Neilson and J. E. Enderby, *Biophys. Chem.*, 2007, **128**, 95-104.
29. K. D. Collins, *Methods*, 2004, **34**, 300-311.
30. A. F. Hollemann, E. Wiberg and N. Wiberg, *Lehrbuch der Anorganischen Chemie*, Walter de Gruyter, Berlin, 2007.
31. O. Dhez, S. Konig, D. Roux, F. Nallet and O. Diat, *Eur. Phys. J. E*, 2000, **3**, 377-388.
32. I. Kamel and A. Charlesby, *J. Polym. Sci. Polym. Phys.*, 1981, **19**, 803-814.
33. C. D. Adam, J. A. Durrant, M. R. Lowry and G. J. T. Tiddy, *J. Chem. Soc. Farad. T. 1*, 1984, **80**, 789-801.
34. R. Y. Dong, M. Wiszniewska, E. Tomchuk and E. Bock, *J. Chem. Phys.*, 1973, **59**, 6266-6268.
35. K. Rendall, G. J. T. Tiddy and M. A. Trevethan, *J. Chem. Soc. Farad. T. 1*, 1983, **79**, 637-&.
36. B. L. Al'tshuler and V. N. Prigodin, *Sov. Phys. JETP*, 1989, **68**, 198-209.
37. H. Wennerström, *Chem. Phys. Lett.*, 1973, **18**, 41-44.
38. S. Salentinig, L. Sagalowicz and O. Glatter, *Langmuir*, 2010, **26**, 11670-11679.
39. J. R. Kanicky and D. O. Shah, *Langmuir*, 2003, **19**, 2034-2038.
40. D. Bethell, R. E. Fessey, E. Namwindwa and D. W. Roberts, *J. Chem. Soc., Perkin Trans. 2*, 2001, **0**, 1489-1495.
41. K. Lunkenheimer, F. Theil and K. H. Lerche, *Langmuir*, 1992, **8**, 403-408.

42. S. Yano, K. Tadano and K. Aoki, *Mol. Cryst. Liq. Cryst.*, 1983, **92**, 99-104.
43. M. Hesse, H. Meier and B. Zeeh, *Spektroskopische Methoden in der organischen Chemie*, Thieme, Stuttgart, 2011.
44. J. J. Leitch, J. Collins, A. K. Friedrich, U. Stimming, J. R. Dutcher and J. Lipkowski, *Langmuir*, 2012, **28**, 2455-2464.
45. R. R. Balmbra, J. S. Clunie and J. F. Goodman, *Nature*, 1969, **222**, 1159-1160.
46. K. Fontell, *Colloid Polym. Sci.*, 1990, **268**, 264-285.
47. A. Tardieu, V. Luzzati and F. C. Reman, *J. Mol. Biol.*, 1973, **75**, 711-733.
48. X. Zeng, Y. Liu and M. Imperor-Clerc, *J. Phys. Chem. B*, 2007, **111**, 5174-5179.
49. H. Delacroix, T. Gulik-Krzywicki, P. Mariani and V. Luzzati, *J. Mol. Biol.*, 1993, **229**, 526-539.

Chapter 8

Choline alkylsulfates as a biological alternative to common washing powder surfactants

8.1 Abstract

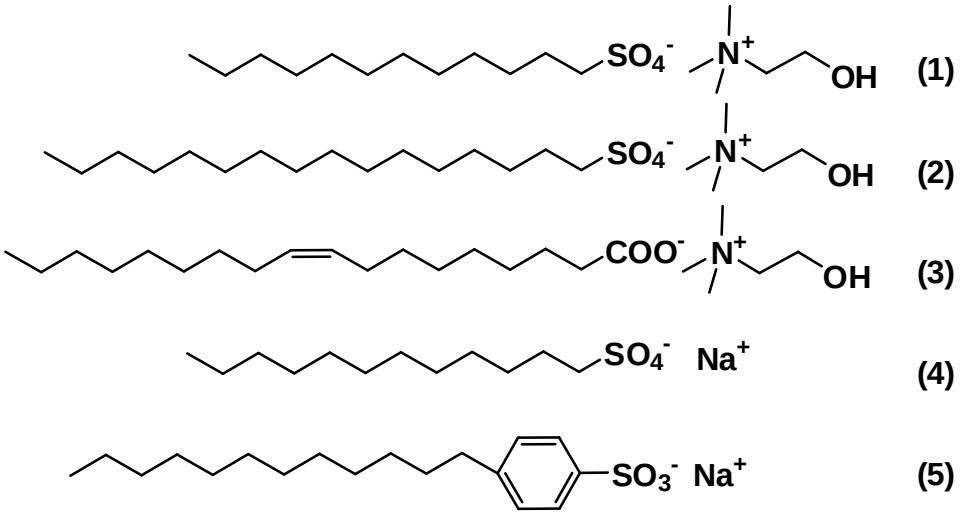

Figure 8-1. The most common surfactants in washing detergency formulation like sodium dodecylsulfate (4) and sodium dodecylbenzenesulfonate (5) were compared with choline dodecylsulfate (1), choline hexadecyl sulfate (2), and choline oleate (3).

In 1998 in Europe the annual consumption of laundry detergents as powder was 3.100.000 tons, the one of liquid laundry detergents was 560.000 tons. These amounts increase each year.[1] Therefore, the research in new biocompatible, more efficient, economically friendly surfactants always continues. Surfactants used in detergency should possess the ability of increasing the wettability of the washing solution on hydrophobic fibers. Further, they should be able to solubilize the soil in the washing solution and prevent the clothes of redeposition of the soil. Their foam should reduce the mechanical stress caused by the washing machine during the washing process. In this chapter it is shown that the mixture of long chain choline alkylsulfates (ChS_{16}) with a common washing surfactant, like sodium dodecylbenzenesulfonate, or with shorter chain choline alkylsulfates, like choline dodecylsulfate (ChS_{12}), show a better washing behavior as it is obtained with the single surfactant solution. This synergism is the more pronounced the more the mixed surfactants differ in their chemical nature. The choline alkylsulfates show several advantages compared to the commonly used surfactants. Their Krafft temperatures T_{Krafft} are lower than 25°C up to chain length C_{16} so that the applied washing temperature can be lowered as well. Moreover, they show low salt sensibility and low toxicity. In addition, it is possible to synthesize the alkylsulfates from the fatty alcohol, which can be obtained from natural oils, like coconut oil or palm oil. But – most important – European resources can also be used to synthesize ChS_{16}. Thus, they can be regarded as a new promising class of anionic surfactants. Their positive properties are manifold and comprise advantages like low production costs. With a future large-scale production of choline hydroxide the prices can go down to those of today´s low

cost surfactants. Lastly, they consist of renewable materials and enable efficient laundry cleaning already at room temperature so that they can make a contribution to more sustainable and eco-balanced washing procedures.

8.2 Introduction

Common laundry detergents consist at least of the following eight substances: surfactant, builder, bleaching agent, enzymes, fillers, fabric softening clay, dye-transfer inhibiting ingredient, and at least, and only in washing powders, an optical brightener. Here, surfactants and builders are the most important ones with the former contributing of 15-40 % to the total detergent formulation.[2, 3]

A lot of studies and reviews exist in the field of surfactants used in detergency.[2-4] Anionic surfactants are the oldest known surfactant group. The first anionic surfactants are the soaps (carboxylates), but in the last 75 years the market of synthetic surfactants started to grow with the increasing knowledge in chemical synthesis. In 1932 the first linear alkylsulfate was introduced in detergency formulation. It was made from animal and vegetable fat by esterification to the fatty alcohol which was subsequently transferred to an alkylsulfate via sulfonation. During the second world war, however, these fats got rare and in 1946 the alkylbenzenesulfonates (ABS) were invented, which were produced from petroleum derivatives. However, these ABS were not biodegradable so that linear alkylbenzenesulfonates (LAS) replaced the ABS in the following. These LAS precipitated in hard water upon calcium complexation. Due to this inconvenience LAS was mixed with highly soluble methyl-subsituted alkylsulfates. A lot of other anionic surfactants like methylestersulfonates or alkylglycerylethersulfonates were used in detergency formulation. But here, mostly the high Krafft temperatures hindered the use of longer chain surfactants to obtain a better washing behavior or the manufacturing costs were too high.[2-4] Beside these anionic surfactants some cationic (e.g. quaternary ammonium), zwitterionic (e.g. alkylbetaine or amidobetaine) and especially non-ionic surfactants (e.g. alkylpolyglycosides (APG)) are also used for laundry formulations.[2, 4]

Washing processes can differ a lot in different areas of the world. In the United States it is common to wash in short cycle times, with warm water, and low surfactant concentration. In Japan similar conditions are preferred with the difference that washing is carried out in cold water. In Europe longer cycle times, high surfactant concentration, and higher temperatures are used.[3, 4] By using choline as counterion higher surfactant concentrations can be dissolved at lower temperature and favor thus the decrease of the washing temperature. Therefore, in the last years not only the biodegradability and ecotoxicity was put into the

focus of research, but also the cost efficiency and energy consumption play an important role.

In general, the most used group of surfactant is the anionic one because they are easy to produce with low manufacturing costs and they are very efficient.[2] The here investigated choline alkylsulfates ChS_{12} and ChS_{16} are such anionic surfactants with an impact in high performance.

In this study the detergency behavior of the pure choline alkylsulfates like choline dodecylsulfate (ChS_{12}) and choline hexadecylsulfate (ChS_{16}) was compared to the one of common utilized surfactants like sodium dodecylsulfate (NaS_{12}) and sodium dodecylbenzenesulfonate (NaDB). Further mixtures (1:1 molar) of choline hexadecylsulfate with choline dodecylsulfate or sodium dodecylbenzenesulfonate were investigated. First the solubilizing behavior of the single surfactants was tested by comparing the microemulsion area of a pseudo ternary system composed of surfactant, 1-pentanol, decane or tricaprylin, and water. Additionally, washing tests were performed with aqueous solutions containing all the surfactants and surfactant mixtures mentioned above as well as a further surfactant, namely choline oleate (see **Figure 8-1**). In addition to the washing tests the foam stability and foamability of the different aqueous surfactant/surfactant mixture solutions were tested. Tests were made to clarify if the foam stability and foamability correlate with the detergency behavior of the surfactants or surfactant mixture solutions.

To reduce the influence of further factors the aqueous surfactant/surfactant mixture solutions were used without the addition of builder or other additives in all the tests. Millipore water was utilized to compare the pure washing ability without taking additional effects of hard water etc. into account.[4] To test the influence of the temperature on the washing behavior the solubility tests were performed at 25°C and 40°C.

8.3 Results and discussion

8.3.1 Solubilization capacity of anionic surfactants

Alkylsulfate surfactants have become one of the most important surfactant classes with the beginning of petrochemistry and the progress in chemical engineering. They could be produced in large amount and are at the moment the most used surfactants in all industrial sectors.[5] However, one crucial point about sodium alkylsulfates like the C_{16} ones is their Krafft temperature of 46°C[6] which requires higher washing temperatures than 40°C.

In this section pure surfactants like sodium dodecylsulfate, sodium dodecylbenzenesulfonate, choline dodecylsulfate and choline hexadecylsulfate were investigated regarding their oil solubilization capacity. Thus, the temperature dependence of the microemulsion area formed by the different surfactants was investigated. A cosurfactant was added into the formulation

as tests without cosurfactant showed only very tiny areas of solubilized decane which made proper comparisons of temperature dependent phase diagrams impossible. Therefore, pentanol was used as cosurfactant, which was already applied in a former study by Friberg *et al.*[7] to prove the temperature dependent behavior of cleaning detergents. Millipore water was taken as polar phase. Decane as a typical hydrocarbon was taken as oil phase. Further, in the case of choline surfactants it was exchanged by tricaprylin, a triglyceride, which appears more often in oily soils.[4] The area of the microemulsion (grey highlighted in **Figure 8-2** (A)-(L)) characterizes the solubilizing power of the surfactant. Here, the following observations can be made:

- For all pseudo ternary phase diagrams a temperature effect was observed. The solubilization of decane or tricaprylin increases with increasing temperature for almost all surfactants. An exception is stated for sodium dodecylbenzenesulfonate. Here, the liquid crystalline phase expands with increasing temperature and lowers thus the solubilization capacity of sodium dodecylbenzenesulfonate for decane.
- Choline hexadecylsulfate (see **Figure 8-2** (I)-(L)) has the best potential to solubilize oily soil. It shows the largest microemulsion area for both temperatures. Further liquid crystalline phases were formed neither at 25°C nor at 40°C nor by using decane or tricaprylin as oil phase.
- Sodium dodecylsulfate (see **Figure 8-2** (A) and (B)) shows the worst solubilizing power for decane of all surfactants used here. Furthermore, a high potential to create liquid crystals by solubilizing oily soil was observed.
- Comparing choline dodecylsulfate (see **Figure 8-2** (E) and (F)) and sodium dodecylbenzenesulfonate (see **Figure 8-2** (C) and (D)) by solubilizing decane and taking the different molar masses ($M(NaDB) < M(ChS_{12})$) into account, sodium dodecylbenzenesulfonate and choline dodecylsulfate reveal more or less a similar solubilization behavior.
- Considering the different oil phases in the pseudo ternary phase diagrams of the choline alkylsulfates (see **Figure 8-2** (G), (H), (K), and (L)): the microemulsion area decreases due to the more branched and bulky tricaprylin molecule compared to decane. Here, the solubilization capacity of choline dodecylsulfate compared to choline hexadecylsulfate for tricaprylin is slightly smaller (see $M(ChS_{12}) < M(ChS_{16})$).

To sum up, it is obvious that choline as cation hinders the formation of liquid crystalline phases (compare NaS_{12} with ChS_{12}; **Figure 8-2** (A), (B) and (E), (F)). Due to the lowering of the Krafft temperature of longer chain alkylsulfates with choline as cation, they can be used at 25°C in detergency formulation. As it is seen here, they show a better solubilization

behavior compared to the ones with shorter chains. For a more precise evaluation, the phase diagrams could be prepared again instead of weight percent in mole fraction.

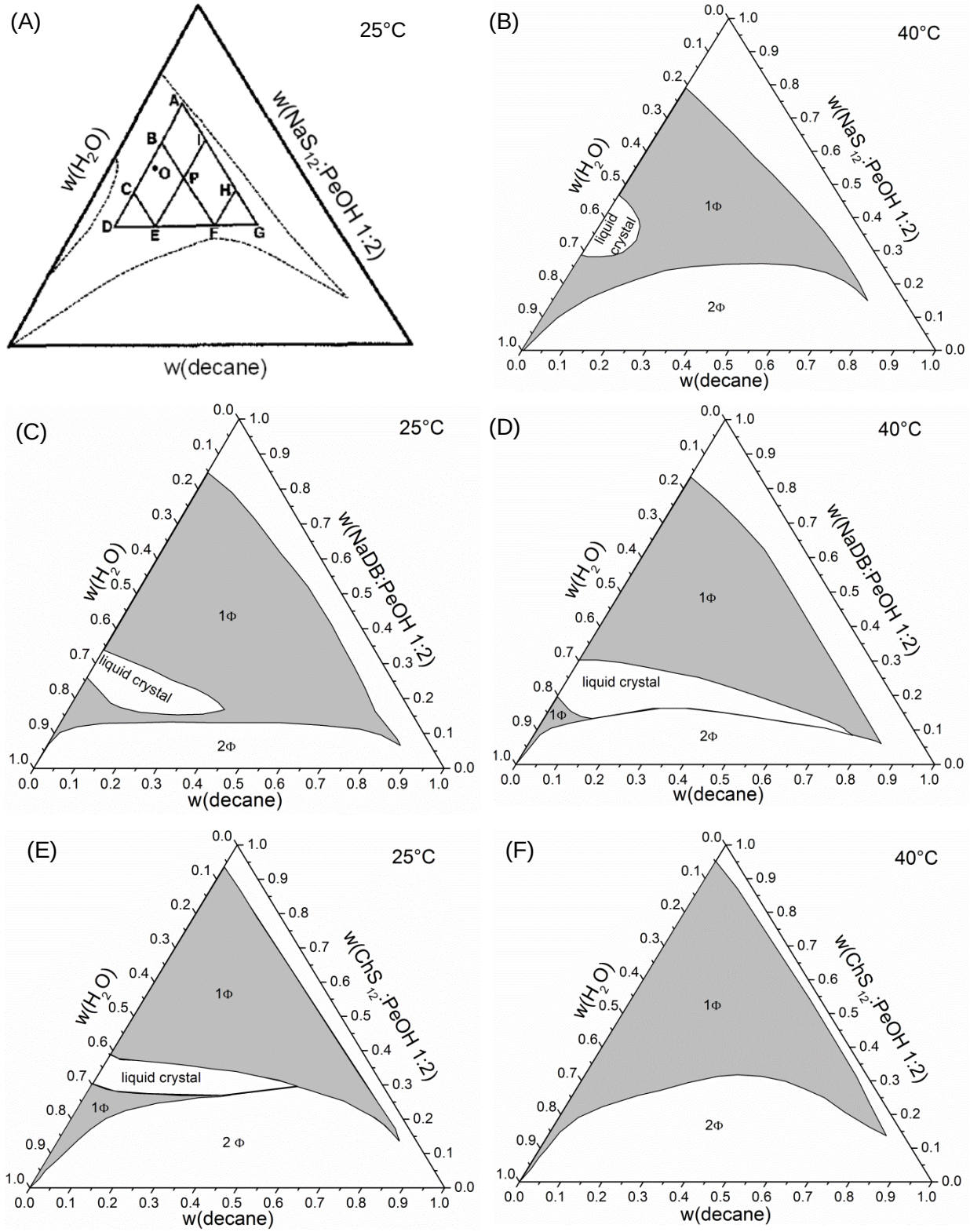

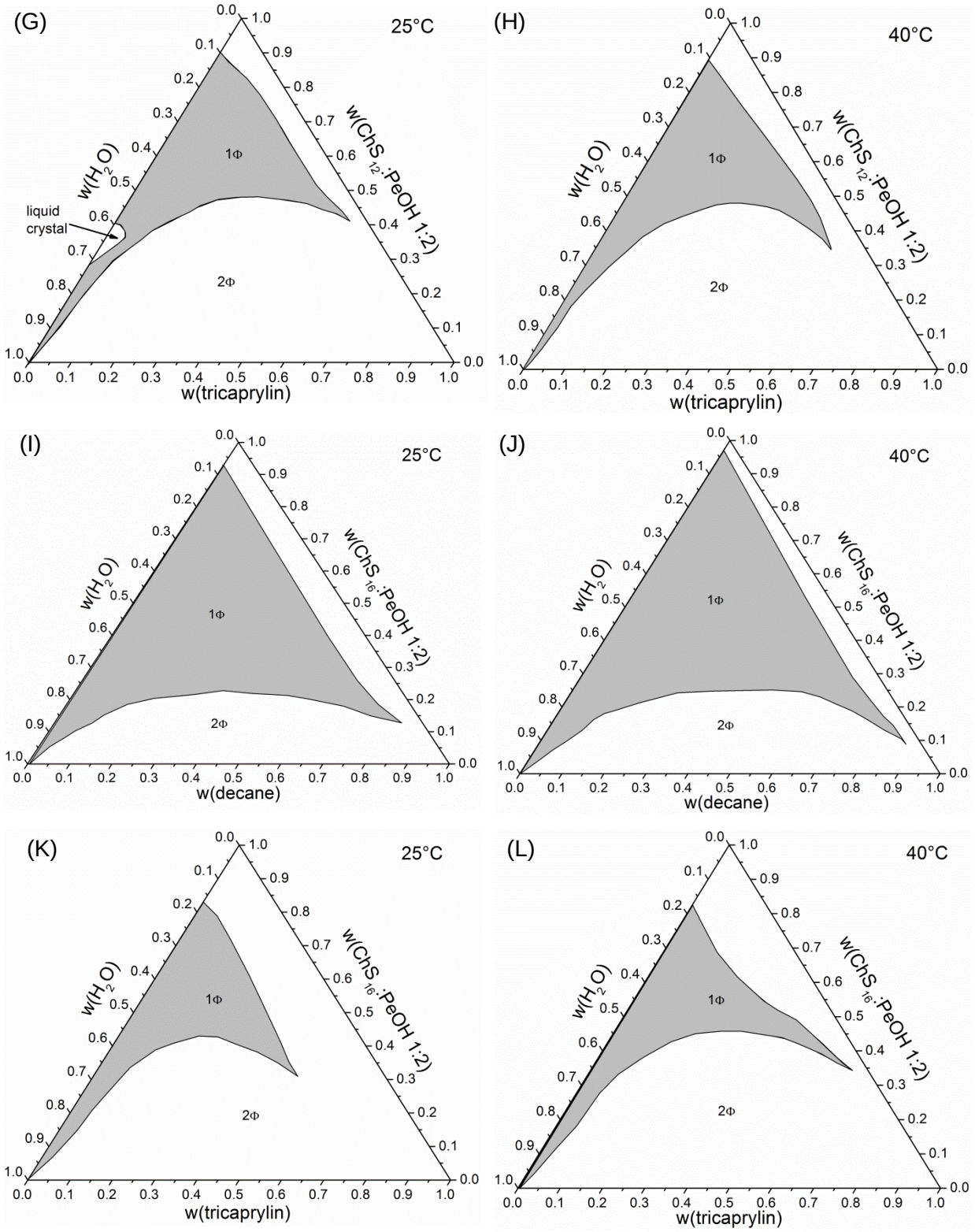

Figure 8-2. Pseudo ternary phase diagrams (see (A)-(L)) were prepared. They consist of water, 1-pentanol as cosurfactant, and the oil phase and the surfactant vary: NaS_{12} and decane at 25°C ((A) prepared by Ceglie *et al.*[8]) and 40°C (B); NaDB and decane at 25°C (C) and 40°C (D); ChS_{12} and decane at 25°C (E) and 40°C (F); ChS_{12} and tricaprylin at 25°C (G) and 40°C (H); ChS_{16} and decane at 25°C (I) and 40°C (J); and ChS_{16} and tricaprylin at 25°C (K) and 40°C (L). As surfactants sodium dodecylsulfate NaS_{12}, sodium dodecylbenzenesulfonate NaDB, choline dodecylsulfate ChS_{12} and choline hexadecylsulfate ChS_{16} were used. The weight ratio between surfactant and cosurfactant was kept constant at 1:2. As oil phase decane or tricaprylin were taken.

8.3.2 Washing tests on cotton fiber

The soil release from fibers is a complex phenomenon where special care has to be taken regarding the following points: the different fiber surfaces (cotton fibers are more hydrophilic, polyester fibers more hydrophobic) [9], the chemical finish, the fiber fabric structure, the type of soil and last but not least the detergency surfactant.[10] The wettability of the fiber, the soil removal of the fiber, and also the stabilization of soil in the washing solution to prevent them from redeposition on the fiber are the crucial parameters during the washing process. The performed washing tests are focused on the fatty soil removal. To this end, a soil containing the most common grease and oil found in food and human skin secret was prepared. As explained in Chapter 2 in section 2.2.5 two main washing mechanisms exist for the removal of liquid oily soil, as they are the “roll-up mechanism” and the “emulsification”. The prepared washing tests should be more dominated by the “roll-up mechanism”. During the series of experiments the surface of the fiber was comparable by using exclusively standardized hydrophilic cotton fibers (Wool Galoon Fabric style: n-500 from testex). The variable in the washing procedure is the type of surfactant/surfactant mixture which was used. The following surfactants and surfactant mixtures in water, respectively, are utilized: sodium dodecylsulfate (NaS_{12}), sodium dodecylbenzenesulfonate (NaDB), choline dodecylsulfate (ChS_{12}), choline hexadecylsulfate (ChS_{16}), choline oleate, and 1:1 molar mixtures of choline hexadecylsulfate with choline dodecylsulfate (ChS_{16} : ChS_{12}) and choline hexadecylsulfate with sodium dodecylbenzenesulfonate (ChS_{16} : NaDB). For each system the following concentrations were tested: 9.5 mM, 14.8 mM, 0.5 wt%, 0.7 wt% and 1 wt%. The washing tests were investigated using the two molar concentrations to compare the washing efficiency regarding the single surfactant molecule. Comparing the results of the washing tests performed with the last three concentrations the washing ability according to the used amount of surfactant was evaluated (all data see Appendix F).

As explained in section 8.5.4, the color of the dyed cotton fiber, which was soaked with dyed fatty soil, was measured before and after the washing process with a spectrophotometer. With this approach the color could be determined with the help of the L*, a*, b* color system and the color difference ΔE*ab could be calculated. This color difference can be directly related to the washing ability of the surfactant or surfactant mixture solution under the assumption that the reduction in dye intensity is directly proportional to the decrease of color and thus to the amount of oily soil.

Figure 8-3 shows the difference in color measured of cotton fibers which were originally soaked with dyed oily soil and washed with the above mentioned pure surfactant or surfactant mixture solutions with concentrations of 9.5 mM and 14.8 mM. The two concentrations are above the *cmc* values of the surfactants. Both surfactant mixtures show the best washing ability independently of the concentration. The difference in the washing

ability of the surfactant mixture solution composed completely of choline alkylsulfate surfactants is insignificantly smaller compared to the one of choline hexadecylsulfate with common surfactant sodium dodecylbenzenesulfonate. For the pure surfactant solutions rising washing ability is observed with increasing surfactant concentrations. Choline oleate shows the longest chain length but the least efficient washing behavior. Carboxylates show a lower washing ability compared to the sulfate or sulfonate surfactants. Further, sodium dodecylbenzenesulfonate reveals a better washing behavior than sodium dodecylsulfate and the choline alkylsulfates at concentrations of 9.5 mM. However, with ascending concentration the washing behavior of ChS_{12} and ChS_{16} increases and at 14.9 mM the choline alkylsulfates show the best washing ability compared to the other pure surfactant solutions. Moreover, it should be mentioned that ChS_{12} shows a better washing ability than NaS_{12} for both concentrations. Choline as cation has a small influence on the washing ability. Maybe it operates as cosurfactant due to its alcohol group.

Further comparison of the washing ability results of the 0.5 wt%, 0.7 wt% and 1 wt% concentrated surfactant or surfactant mixture washing solutions is made in Appendix F. The cost efficiency, which is reflected in the amount of surfactant needed for an efficient washing result, could be evaluated. For the different concentrations (in wt%) the mixtures show again a much better washing behavior. The pure surfactant mixtures of NaS_{12}, ChS_{12} and NaDB behave more or less similar, while the one of ChS_{16} is slightly lower. Again, choline oleate is a very bad detergent.

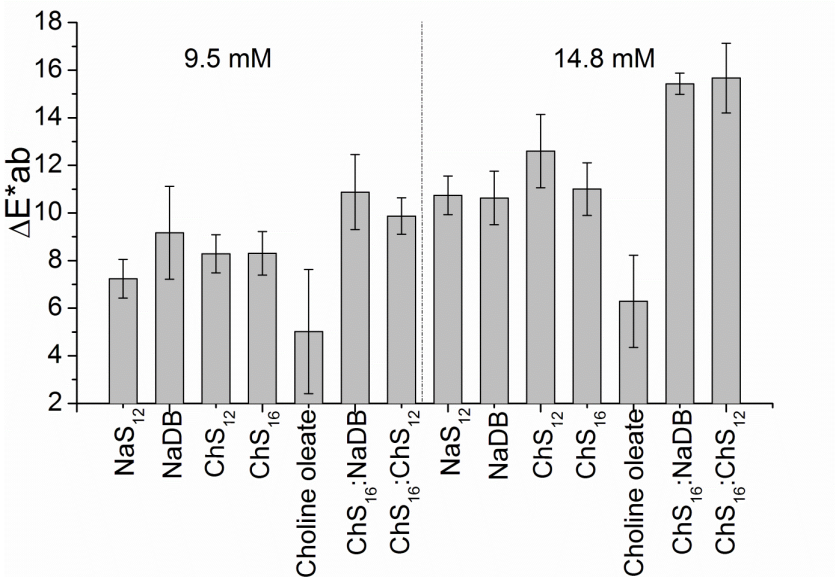

Figure 8-3. Presentation of differences in the color intensity ΔE*ab of sudan black B on the cotton fiber before and after washing of the cotton fiber in presence of various surfactant water solutions. The following surfactants and surfactant mixtures are used in concentrations of 9.5 mM (left) and 14.8 mM (right): NaS_{12}, NaDB, ChS_{12}, ChS_{16}, choline oleate, mixture of 1:1 molar of ChS_{16} : NaDB and ChS_{16} : ChS_{12}. In Appendix F the molar concentrations (9.5 mM and 14.8 mM) are shown recalculated as concentration in wt% for the respective surfactants/surfactant mixtures.

In general, it could be shown that surfactant mixtures show a much better detergency than the corresponding pure surfactants. Long chain surfactants show a better wettability behavior, while the short chain surfactants stabilize the micelles to remove the soil and increase the solubilization behavior. Choline improves slightly the washing ability of the surfactant. In this section, the washing behavior was tested without taking the effects of water hardness or temperature into account. These parameters will be addressed in subsequent studies, where the same tests are performed at room temperature and with hard water.

8.3.3 Foam stability and foamability

Foam slightly reduces the mechanical forces on clothes, which are produced by the washing machine during the washing process. However, too much foam compromises the wettability of the surfactant.[11] Thus, surfactants with a high detergency and the ability to produce semi-stable foams should be the best washing detergents. The surfactant solutions and surfactant mixture solutions, which were used for the washing tests, were tested for their foaming behavior and foam stability.

Foam is a dispersion of gas bubbles in a liquid. It is prepared in the washing process due to agitation. At the beginning sphere foam appears, a temporary dilute dispersion. Here, the gas bubbles are separated by thick liquid films. With increasing time, the foam ages and the film walls drain. At the end, the gas bubbles change to polyhedral gas cells, which possess junction points of interconnecting channels between the polyhedral gas. They are known as plateau borders, where the film walls meet at an angle of 120°C (see **Figure 8-4**).[12] It is known for aqueous surfactant mixtures that the foam drainage kinetics, the lensing of the liquid layer, is reduced by increasing the surface viscosity. In this case the cohesion force in the surface film is increased.[12]

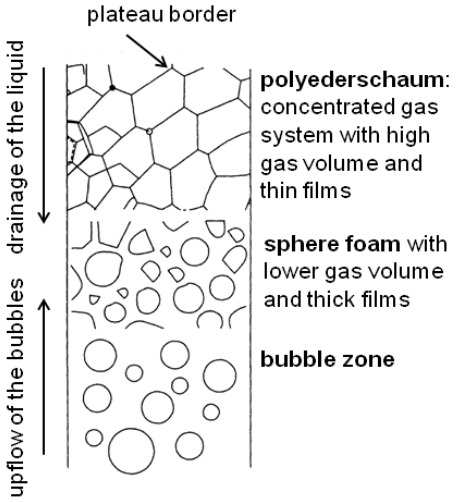

Figure 8-4. Different areas appear in a column during formation and drainage of a foam.[12]

In this section, the foamability and foam stability of different surfactant/surfactant mixture solutions were measured by a dynamic foam analyzer DFA100 from Krüss. The obtained results were not compared with literature. The comparability of foam stabilities is very difficult because the foaming behavior depends, for instance, on the utilized foam forming instrument, on the surfactant concentration, the impurities of the surfactant, and the temperature.[5] Since it is known from literature that hard water increases the foam volume and its stability compared to soft water[5], all experiments are carried out with millipore water.

The foamability of the different surfactants or surfactant mixtures is more or less similar as shown in **Figure 8-5** (A). Only sodium dodecylbenzenesulfonate shows a slightly reduced foamability. Furthermore, the foamability is not influenced by the cation (see **Figure 8-5** (A): ChS_{12} vs. NaS_{12}). Comparing the foam half-life times of the different solutions (see **Figure 8-5** (B)), it becomes obvious that the aqueous surfactant mixtures and the choline oleate solution perform very stable foams. The fact that mixtures produce more stable foams is already known from literature.[12] The stable foam formed by choline oleate results from the long alkyl chain. As observed in section 8.3.2, the good foamability and foam stability of choline oleate foams reduce the wettability and detergency power of the surfactant, while in the case of the surfactant mixtures, the different lengths of the alkyl chains stabilize the foam and further increase the wettability of the washing solution on the fiber and also the solubilization of the soil in the washing solution.

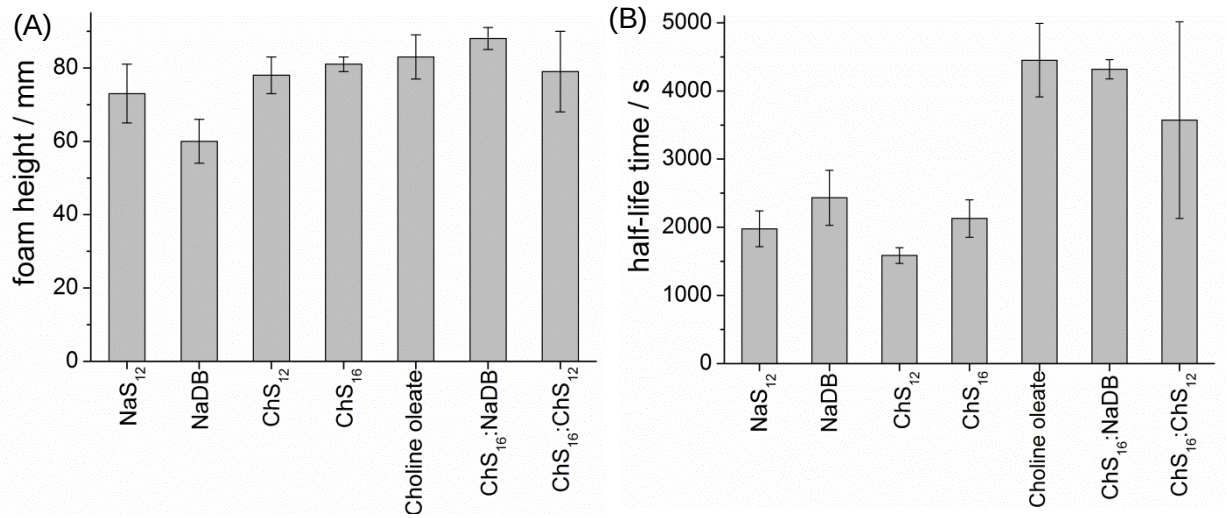

Figure 8-5. (A) Foam heights of the different surfactant/surfactant mixture solutions which are measured directly after the foaming process. (B) Half-life times (in seconds) of the different surfactant/surfactant mixture solutions which reflect the foam stability. The concentration of the surfactant or surfactant mixture solutions is 9.5 mM.

8.4 Conclusion

In this chapter it could be shown that choline alkylsulfates are a promising new class of laundry detergents. In pseudo ternary phase diagrams the extension of the microemulsion area was compared. The diagrams were prepared with decane or tricaprylin as oil phase, millipore water as polar phase, pentanol as cosurfactant, and sodium dodecylsulfate, sodium dodecylbenzenesulfonate, choline dodecylsulfate or choline hexadecylsulfate as surfactant. The microemulsion area reflects the oil solubilization capacity of the surfactant. Choline hexadecylsulfate reveals the best solubilization capacity due to the longer alkyl chain. Sodium dodecylbenzenesulfonate and choline dodecylsulfate have the same efficiency to solubilize decane, while sodium dodecylsulfate is not very efficient. Choline, however, reveals a slight impact on the solubilizing power of the surfactant and reduces the formation of liquid crystalline phases compared to the sodium cation. Maybe it acts as cosurfactant due to its hydroxyl group. Further, in washing tests choline oleate is found to be a less efficient washing detergent. In the case of washing solutions with a single alkylsulfate, the choline cation again increases slightly the washing ability compared to sodium. In general, it was found that mixtures of choline hexadecylsulfate with sodium dodecylbenzenesulfonate or choline dodecylsulfate obtain the best washing behavior as a result of combining longer and shorter alkyl chains. Furthermore, these mixtures possess a high foamability and foam stability. Therefore, they can protect clothes from mechanical forces produced by the washing machine and further obtain their good washing ability and wettability of the fiber during the washing process.

It can be summarized that mixtures of choline alkylsulfates are a very efficient laundry detergent. They can be used up to chain length C_{16} at room temperature, which reduces the

energy consumption during the washing process. They are further biodegradable and less salt sensitive, and can be produced from fatty alcohol obtained from natural oil.
However, all these experiments are performed in millipore water without taking the water hardness into account. Future studies will be performed with hard water and the washing tests should be also carried out at room temperature in order to determine the influence of the temperature on the washing behavior.

8.5 Experimental

8.5.1 Synthesis of surfactants

Choline dodecylsulfate and choline hexadecylsulfate were synthesized with an ion exchange following the method described in Chapter 6 in section 6.5.1. Choline oleate was prepared according to the procedure explained in Chapter 3 in section 3.5.1. Sodium dodecylsulfate (purity ≥ 99.9 %) was bought from Merck. Sodium dodecylbenzenesulfonate was synthesized from dodecylbenzenesulfonic acid (purity ≥ 96 % (contains unsulphonated compound < 2.5 wt% and free sulfuric acid < 2 wt%), Sigma Aldrich), because the technical product shows only a purity of 80 %. The dodecylbenzenesulfonic acid contains only para-substituted benzene cycles, but with different branching. For the synthesis an equimolar amount of 1M sodium hydroxide solution was added to the dodecylbenzenesulfonic acid. After lyophilisation a white yellow powder was obtained. The surfactant was recrystallized in petrol ether. To evaluate the purity ^{1}H NMR was conducted.

Sodium dodecylbenzenesulfonate: ^{1}H NMR (300 MHz, D_2O, 25°C, TMS): δ = 0.5 - 1.5 (broad peak results from the protons of the different substituted chain), 2.9 (s, -C**H**(C_6H_4)-), 7.0 (d, 2H; -CH(C_6**H_2** H_2)-), 7.6 (d, 2H; -CH(C_6**H_2**H_2)-)

8.5.2 Surface tension

To characterize the sodium dodecylbenzenesulfonate, surface tension was measured as a function of the concentration at 25°C according to the procedure described in Chapter 6 in section 6.5.2.1. Also the *cmc* value was obtained as explained in Chapter 6 in section 6.5.2.1. The measured *cmc* value was 1.6 mM (see **Figure 8-6**). Comparing this *cmc* value with the *cmc* values known at 25°C for the neat sodium dodecylbenzenesulfonate surfactants Na-n-DB substituted at different C_n atoms (C1-C6) (Na-1-DB Krafft temperature higher than 25°C, Na-2-DB: 1.04 mM, Na-3-DB: 1.38 mM, Na-4-DB: 1.65 mM, Na-5-DB: 1.94 mM, Na-6-DB: 2.53 mM[13]), this value is in good agreement.

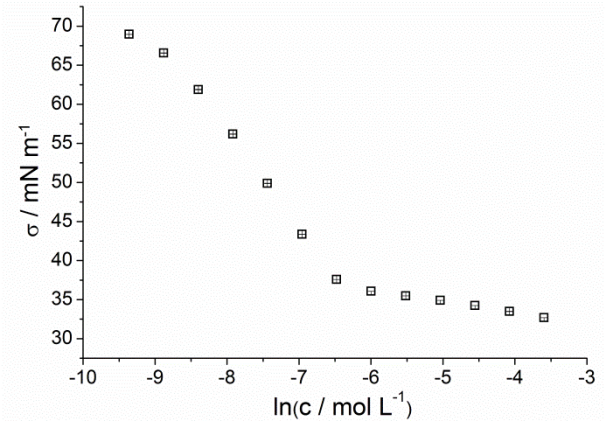

Figure 8-6. Surface tension of aqueous sodium dodecylbenzenesulfonate solution as a function of the natural logarithm of its concentration.

8.5.3 Preparation of pseudo ternary phase diagrams

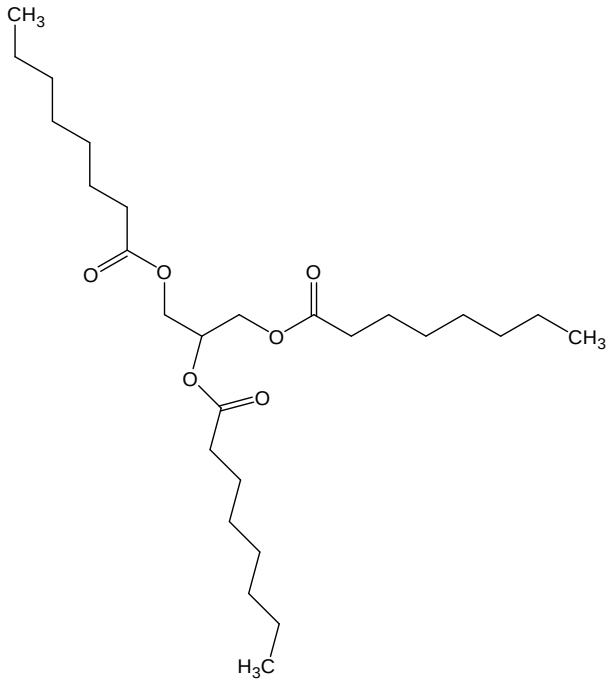

Figure 8-7. Molecular structure of tricaprylin.

The pseudo ternary phase diagrams were conducted following the procedure of Ceglie *et al.*[14] and Friberg *et al.*[7]. A constant weight ratio of 1:2 between the surfactant and cosurfactant was used. The pseudo ternary phase diagrams were prepared in 1 wt% steps on the pure water surfactant/cosurfactant line by adding oil and in 1 wt% steps on the pure oil surfactant/cosurfactant line by adding water. The pseudo ternary phase diagrams were only performed with the pure surfactants choline dodecylsulfate, choline hexadecylsulfate, sodium dodecylsulfate and sodium dodecylbenzenesulfonate at 25°C and 40°C. As cosurfactant 1-pentanol (purity ≥ 99 %, Sigma Aldrich) was used in all cases. The polar phase was

millipore water and the oil phase was n-decane (purity ≥ 99 %, Alfa Aesar). Additional ternary phase diagrams with choline dodecylsulfate and choline hexadecylsulfate were conducted with tricaprylin (purity ≥ 90 %, Fluka) to evaluate the influence of a triglyceride as oil phase.

8.5.4 Washing tests

For the washing tests a standardized hydrophilic cotton fiber (named Wool Galoon Fabric (style: N-500) purchased from testex) was utilized with a length of 2 cm and width of 5 cm. It has a hydrophilic surface and was uniformly soaked with a mixture of soil colored with the black dye sudan black B. Sudan black B (Sigma Aldrich) is a lysochromic, fat soluble dye and belongs to the class of azo dyes (see **Figure 8-8**). It shows an absorption maximum at 598 nm and is often used in microscopy experiments as staining agent for triglycerides or lipids.[15, 16]

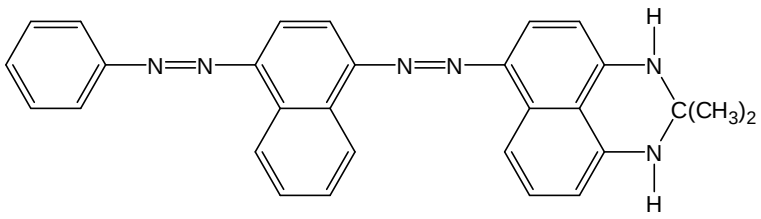

Figure 8-8. Molecular structure of sudan black B.

The cotton fiber was soaked with the dyed oily soil mixture in the ratio of 0.225 g dyed oily soil to 1 g of cotton fiber. This mixture is not enough to saturate the cotton fiber with the oil/grease/dye mixture. Therefore, the removal of oily soil is proportional to the removal of dye and can be evaluated by measuring the difference in color intensity of the dyed cotton fiber before and after the washing process.

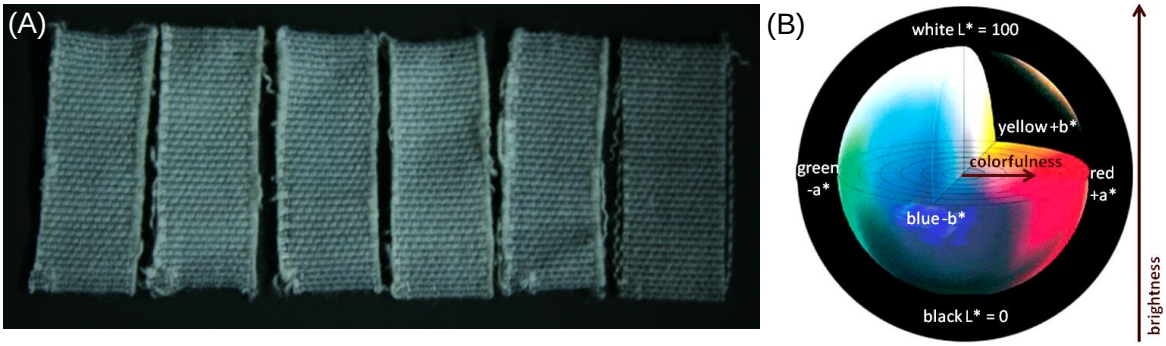

Figure 8-9. (A) Dyed cotton fibers which were soaked with oily soil. Following the picture series from left to right: The first five cotton fibers were washed with 9.5 mM surfactant solution: NaDB, ChS_{12}, ChS_{16}, NaS_{12}, choline oleate. The difference in color could be hardly evaluated by eye. The fiber on the right sight is only soaked with oily dyed soil, but not washed. (B) L*, a*, b* color system. The L* value corresponds to the brightness a* and b* to the colorfulness. The colorfulness increases with increasing absolute values of a* and b*.[17] Scheme is taken from ref.[17].

After the drying process of the oily soil on the cotton fiber, the following washing steps were performed at 40°C: the dyed cotton (see **Figure 8-9** (A)) was placed in a 250 ml Erlenmeyer flask and 10 ml of the corresponding washing solution was added. The closed Erlenmeyer flask was shaken in simultaneously ways for 30 seconds. Afterwards, the washing solution was removed. The cotton fiber was washed again with 50 ml of millipore water. The closed Erlenmeyer flask was shaken again for 15 seconds. The washing water was removed and the last washing step with millipore water was repeated. Then the cotton fiber was dried.

As washing solution the following aqueous surfactant or surfactant mixture solutions were used: sodium dodecylsulfate, sodium dodecylbenzenesulfonate, choline dodecylsulfate, choline hexadecylsulfate, choline oleate, and the 1:1 molar mixtures of choline dodecylsulfate and choline hexadecylsulfate, and further choline hexadecylsulfate and sodium dodecylbenzenesulfonate.

The following concentrations of surfactant/surfactant mixture in millipore water were utilized: 9.5 mM, 14.8 mM, 0.5 wt%, 0.7 wt% and 1 wt%. All concentrations are above the different *cmc* values and also all surfactants possess Krafft temperatures below 25°C.

Furthermore, the composition of the dyed oily soil is similar to secretion of the human skin and grease found in food.[10] It contains:

29 wt% triolein (purity = 65 %, Sigma Aldrich), 28.5 wt% oleic acid (purity 94.5 %, Sigma Aldrich), 18.5 wt% ethyl oleate (contains 74.5 % oleic acid, Sigma Aldrich), 14 wt% squalene (purity = 99 %, Fluka), 7 wt% cholesterol (purity = 95 %, Sigma Aldrich), 3 wt% cholesteryl palmitate (purity = 97 %, Sigma Aldrich). 0.5 wt% of the overall sebum is made out of the dye sudan black B (Sigma Aldrich).

As already mentioned above, the removed oily soil during the washing process correlates with the removed amount of dye and is proportional to the decreased color intensity and brightness of the dyed cotton fiber. This color difference can be calculated due to the measured L*, a*, b* values (see **Figure 8-9** (B)) of the color of the dye before and after the washing step. For this purpose, the color and brightness of the dyed cotton was measured after the dying process and after the washing process at five defined points on the dyed cotton fiber with the spectrophotometer Elrepho SE 071 from Lorentzen & Wettre. As utilized software L&W Elrepho Colour Brightness was taken. In addition, the standardized light D65 was used as light source. In this context normed D65 light is similar to the natural light with a more realistic UV light part.

The color difference ΔE*ab [17, 18] can be calculated according to the following equation (1):

$$\Delta E^{*}ab = \sqrt{\Delta L^{*2} + \Delta a^{*2} + \Delta b^{*2}} \qquad (1)$$

The L value corresponds to the brightness, a* and b* to the colorfulness. The colorfulness increases with increasing absolute values of a* and b*.[17] The higher the value of ΔE*ab the bigger is the difference in color and the better is the washing ability of the surfactant or the surfactant mixture. The difference in brightness can be evaluated with the value of ΔL* ($\Delta L^* = L^*_{before} - L^*_{after}$).[17, 18]

The whole washing procedure and the evaluation of the color difference was performed twice to prove the reproducibility. All washing tests were performed at 40°C, but it will be a future project to conduct all experiments also at 25°C to check the washing behavior at room temperature. The ΔL* and ΔE*ab values of the aqueous solutions of pure surfactant and surfactant mixture with concentrations of 9.5 mM, 14.8 mM, 0.5 wt%, 0.7 wt% and 1 wt% are shown in Appendix F.

8.5.5 Foam stability and foamability

The surfactant solutions and surfactant mixture solutions used for the washing tests were tested regarding their foaming behavior and foam stability. The concentration of 9.5 mM was used for the foam stability test. 14.8 mM surfactant solutions are too stable and show a too high foamability. At the measured concentration the *cmc* of each surfactant was reached. Each solution was individually measured for five times. The foam stability and foamability were determined with the foaming instrument DFA 100 from Krüss (see **Figure 8-10** (A)). The surfactant solution was added in a glass column (4 cm in diameter and 25 cm height) and foamed by blowing air for 10 seconds through a porous frit with a gas flow rate of 0.3 L min^{-1}. The foams produced in this way show a good reproducibility in most cases. The foam stability was evaluated by measuring the half-life time of the foam. This time was reached when the foam height decreased to 50 % of the original height (see **Figure 8-10** (B)).

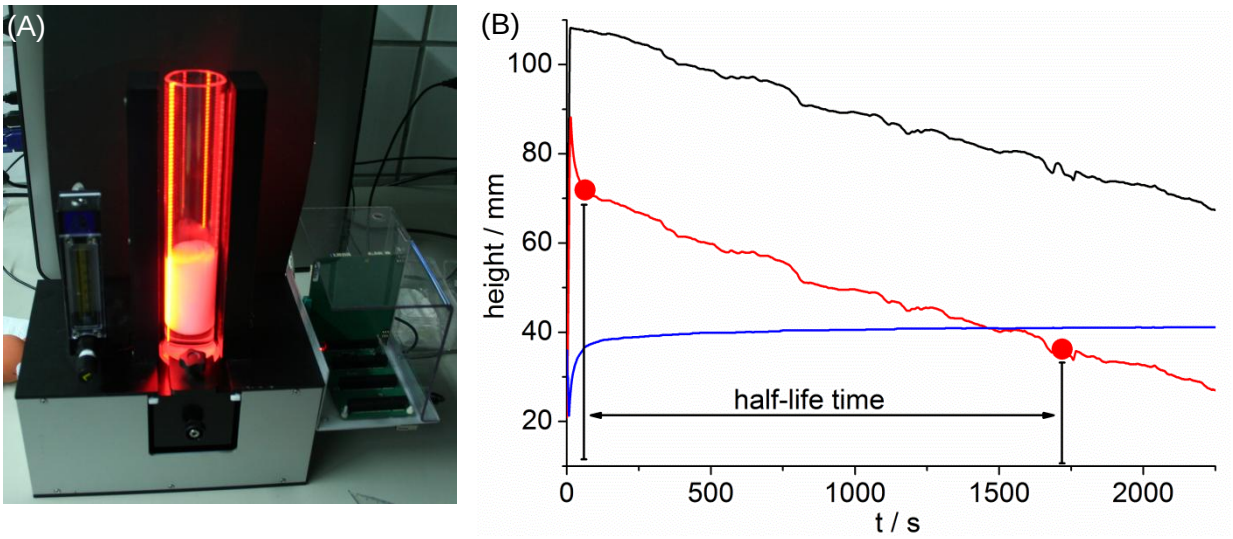

Figure 8-10. (A) DFA 100 from Krüss. (B) Drawing to illustrate the determination of the half-life time. The half-life time is a parameter to characterize the foam stability. The black line marks the total height, the red line the height of the foam and the blue line the liquid height.

This instrument (see **Figure 8-10** (A)) detects the height of the surfactant solution, the foam height and the overall height over the whole measurement time. This is visualized with a red light emitting electrode which sends light from one side of the column to the other side where photo diodes detects the signal. The foams of aqueous choline oleate, choline dodecylsulfate mixed in 1:1 molar with choline hexadecylsulfate and choline hexadecylsulfate mixed 1:1 molar with sodium dodecylbenzenesulfonate were measured manually. The foams were too stable, therefore the upper part of the foam was already drained. Thus, the foam got too transparent and could not reduce the red light from the led.

8.6 References

1. D. Bajpai and V. K. Tyagi, *J. Oleo Sci.*, 2007, **56**, 327-340.
2. Y. Yangxin, Z. Jin and A. E. Bayly, *Chin. J. Chem. Eng.*, 2008, **16**, 517-527.
3. J. J. Scheibel, *J. Surfactants Deterg.*, 2004, **7**, 319-328.
4. L. H. T. Tai, *Formulating Detergents and Personal Care Products A Complete Guide to Product Development*, AOCS Press, 2000.
5. H. W. Stache, *Anionic Surfactants*, Marcel Dekker, Inc., New York, 1996.
6. I. Piirma and S. R. Chen, *J. Colloid Interface Sci.*, 1980, **74**, 90-102.
7. S. E. Friberg and J. H. Fang, *J. Am. Oil Chem. Soc.*, 1984, **61**, 801-804.
8. A. Ceglie, K. P. Das and B. Lindman, *J. Colloid and Interface Sci.*, 1987, **115**, 115-120.
9. C. A. Miller and K. H. Raney, *Colloids and Surfaces A: Physicochem. Eng. Aspects*, 1993, **74**, 169-215.

10. G. M. Venkatesh, N. E. Dweltz, G. L. Madan and R. H. Alurkar, *Textile Res. J.*, 1974, **44**, 352-362.
11. M. Liphard and A. Giza, *Tenside Surf. Det.*, 1997, **34**, 410-416.
12. R. J. Pugh, *Foams and Foaming. Chapter 2 in Handbook of Applied Surface and Colloid Chemistry*, John Wiley & Sons, LTD, New York, 2002.
13. J. G. Ma, B. J. Boyd and C. J. Drummond, *Langmuir*, 2006, **22**, 8646-8654.
14. A. Ceglie, K. P. Das and B. Lindman, *J. Colloid and Interface Sci.*, 1986, **115**, 115-120.
15. E. Gurr, *Synthetic dyes in biology, medicine and chemistry*, Academic Press, London, England, 1971.
16. R. W. Sabnis, *Handbook of Biological Dyes and Stains: Synthesis and Industrial Applications*, John Wiley & Sons, Jersey, 2010.
17. N. Pauler, *Optische Eigenschaften von Papier*, AB Lorentzen & Wettre, Schweden, 2012.
18. N. Pauler, *Paper Optics - optical and colour science in the pulp and paper industry*, AB Lorenzten & Wettre, Schweden, 2012.

Chapter 9

Deep eutectic solvents based on choline glutarate

9.1 Abstract

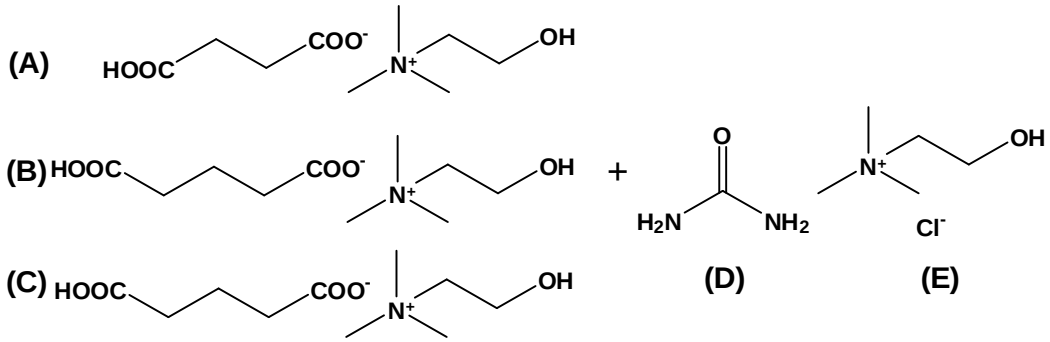

Figure 9-1. Molecular structure of (A) choline succinate ($ChbiC_4$), (B) choline glutarate ($ChbiC_5$) and (C) choline adipate ($ChbiC_6$). Further choline glutarate was mixed with urea (D) and choline chloride (E) to form deep eutectic mixtures.

In this chapter a strategy is established for the design of low toxic, room temperature liquid deep eutectic solvents which are entirely composed of natural materials. From literature it is well known that, in general, deep eutectic solvents based on choline chloride and bicarboxylic acids are not liquid at room temperature, with one exception: a 1:1 molar mixture of malonic acid and choline chloride.[1] Therefore, the starting point of this study was to decrease the melting point of the bicarboxylic acid by using succinic, glutaric and adipic acid. Firstly, the formation of choline bicarboxylate ionic liquids was realized by exchanging one proton with the bulky unsymmetrical choline as cation (see **Figure 9-1** (A)-(C)). However, resulting ionic liquids were still solid at room temperature. In a further step deep eutectic mixtures with choline chloride and choline bicarboxylate ionic liquids, as hydrogen bond donor, were prepared. The only binary mixtures found to be sufficiently liquid at room temperature were choline glutarate/choline chloride mixtures at compositions containing 95-98 wt% of choline glutarate. In a following set of experiments urea was employed as another hydrogen bond donor. All obtained mixtures (with and without urea) were characterized by density, conductivity and viscosity measurements suggesting that all mixtures represent liquids with fully dissociated ions, which can move independently in the mixture (Walden plot). Therefore, they are considered as “good” ionic liquids and thus for example can be used to exchange toxic ionic liquids in application processes. Further, a small outlook containing application possibilities is given. It is demonstrated that choline dodecylsulfate is readily soluble in these mixtures, forming aggregates in the deep eutectic solvent at temperatures exceeding 55°C.

9.2 Introduction and strategy

Interesting deep eutectic solvents are obtained by mixing two or three cheap, biodegradable and low toxic solids (sometimes also a liquid and a solid)[2] to form a new liquid phase with a melting point lower than the melting points of the single components. This liquid phase is generated by self-association of the substances through hydrogen bonds.[2] The main advantages of deep eutectic mixtures can be found in the easy tuning of their physico-chemical properties by simply changing either the components involved or the applied mixing ratio. They are promising new liquids to replace toxic ionic liquids or common organic solvents in applications, e.g. in pharmaceutical formulation[3], dissolution or treatment of biomass[4-6], etc..[2, 7] The first deep eutectic mixture without metal salt mentioned in literature was a mixture of choline chloride and urea in a molar ratio of 1:2.[7] The freezing point of this mixture was determined to be 12°C, therefore being substantially lower than the melting points of both pure substances (urea: 133°C, choline chloride: 302°C). From these experiments it was deduced that hydrogen bonds, being formed between urea and the chloride anion, are mainly responsible for the observed decrease of the freezing point.[7] In addition, mixtures of thiourea with oxalate anions show the same behavior.[8] Conductivity and viscosity data of choline chloride with urea reveal that the choline chloride is completely dissociated and the ions move independently. Due to these advantageous properties the use of such mixtures opens the possibility to replace e.g. toxic imidazolium ionic liquids by more sustainable compounds.[7] Another interesting work focuses on the production of deep eutectic mixtures with high viscosities from bicarboxylic acids and choline chloride. As for all deep eutectics, the fluidity was found to be linked to the size of the mobile species as well as to the size of the holes allowing the mobility.[9] Further analysis unveiled that one chloride ion is complexed by two carboxylic acids, resulting in the delocalization of charge and thus in a depression of the freezing point.[9] However, an important point is that, apart from equimolar mixtures of choline chloride and malonic acid, most deep eutectic solvents containing choline chloride and bicarboxylic acids are solid at room temperature.[9]

As a consequence, a novel strategy was applied to make a step forward towards novel, room temperature liquid deep eutectic mixtures composed of natural products:

In a first attempt exchange of one proton of the bicarboxylic acids used (succinic, glutaric and adipic acid) by one bulky choline cation was performed to lower the melting point of the mixtures, as this already turned out to be a successful strategy to lower the melting point of choline carboxylates[10] (see Chapter 5) and choline alkylsulfates (see Chapter 7). Within these experiments performed in this work, ionic liquids were successfully generated, but their melting points were still above room temperature. Therefore, a further portion of choline chloride was added to the obtained choline bicarboxylate ionic liquids in order to destroy the

hydrogen bond network of the second, still protonated acid group. In a third step, the influence of urea, representing a strong hydrogen bond donor, on the density, viscosity and conductivity behavior of these mixtures was investigated.

In this chapter deep eutectic mixtures containing choline glutarate, choline chloride and sometimes urea were investigated. The components of the deep eutectic mixture are low toxic and from biological origin. Choline is biocompatible and known as former vitamin B_4. It has some important key functions in the human body, e.g. as a precursor for phospholipids and acetylcholine.[11] Further, glutaric acid is contained in natural food products and fruits. It has also a high bacteriostatic activity and is metabolized very rapidly in the human body.[12] In addition, the cytotoxicity of the pure choline bicarboxylate was found to be low according to low skin irritancy in cytotoxicity tests (see Chapter 3). Urea is highly water soluble and not toxic to human body. It is produced in the body in mammalian metabolism and even salvaged due to the metabolic activity of the colonic microflora and thus further used in the body. On the other side it can be easily excreted in the urine.[13]

The investigated deep eutectic mixtures, prepared and discussed in this chapter, have the following compositions:

- **DEEP1**: 96.00 wt% $ChbiC_5$, 4.00 wt% ChCl
- **DEEP1Urea**: 92.80 wt% $ChbiC_5$, 3.87 wt% ChCl, 3.33 wt% urea
- **DEEP2**: 98.00 wt% $ChbiC_5$, 2.00 wt% ChCl
- **DEEP2Urea**: 96.34 wt% $ChbiC_5$, 1.97 wt% ChCl, 1.69 wt% urea

Further, choline bicarboxylate ionic liquids, namely choline succinate ($ChbiC_4$), choline glutarate ($ChbiC_5$), and choline adipate ($ChbiC_6$), and the above mentioned deep eutectic mixtures were characterized by thermogravimetric and differential scanning calorimetric measurements. In addition, temperature dependent viscosities, conductivities and densities of all prepared deep eutectic mixtures were examined in a temperature range between 25-85°C for comparison with typical ionic liquids according to the Walden plot. Beyond this, three different choline containing surfactants (choline dodecylsulfate, hexadecylsulfate and oleate) were solubilized in the deep eutectic solvents in order to examine these mixtures on potential structuring effects by means of small and wide angle X-ray scattering experiments.

9.3 Results and discussion

9.3.1 Decomposition and melting/crystallization temperatures of choline bicarboxylate ionic liquids and deep eutectic mixtures

The thermal decomposition of pure choline bicarboxylates $ChbiC_m$ with m = 4, 5, 6 (see **Table 9-1** and **Figure 9-9**) is a one step decomposition. Increasing decomposition temperatures were observed with increasing chain lengths, however not showing any linear correlation. Observed decomposition temperatures (T_{dec}) of the deep eutectic mixtures are altogether above those of the pure ionic liquids. While thermal decomposition of the deep eutectics not containing urea proceeds in a singular step, a two-step mechanism is observed for deep eutectics prepared with urea. In the latter case, decomposition of urea in the system takes place in the temperature range between around 160°C to 250°C according to literature[14, 15], while choline glutarate and choline chloride start to decompose at the temperature given in **Table 9-1**.

Compound	T_{dec}/ °C		$ChbiC_4$		$ChbiC_5$	$ChbiC_6$
$ChbiC_4$	242.9		T_1/ °C	T_2/ °C	T_1/ °C	T_1/ °C
$ChbiC_5$	243.3	1. heat	-	61.9	39.3	86.0
$ChbiC_6$	245.2	1. cool	-	-	-	13.35
DEEP1	268.7	2. heat	21.9	61.0	-	84.9
DEEP1Urea	282.4	2. cool	-	-	-	10.1
DEEP2	273.0	3. heat	24.0	60.6	-	84.8
DEEP2Urea	280.3	3. cool	-	-	-	9.2

Table 9-1. Decomposition temperatures (T_{dec}) of choline succinate, choline glutarate, choline adipate and examined deep eutectic mixtures together with melting and crystallization temperatures (T_1 and T_2) are shown. The numbers 1, 2 mark the transition temperatures with increasing temperature at the heating cycle (and the respective values at the cooling cycle) of the three pure ionic liquids $ChbiC_m$ with m = 4, 5, 6 obtained for all three cycles measured with DSC in the temperature range from -80°C to 95°C.

Melting points of succinic, glutaric and adipic acid are published to be 185°C, 97.5°C and 153.5°C, respectively.[16] Obviously, the choline cation is capable to lower the melting temperatures of the choline bicarboxylates $ChbiC_m$ with m = 4, 5, 6 (see **Table 9-1**), as already pointed out in Chapter 5 (for choline carboxylates)[10] and Chapter 7 (for choline alkylsulfates)[17], respectively. The reason for this effect is doubtless the bulky and unsymmetrical structure of the choline cation that hinders the arrangement of a regular packing and thus lowers the melting temperatures of the choline bicarboxylates $ChbiC_m$ with m = 4, 5, 6. Due to the exchange of one proton of the bicarboxylic acid with a choline cation, the hydrogen bond network formed in the pure acid becomes partly destroyed, leading to a reduction of intermolecular stabilities. Comparison of melting and crystallization temperatures

found for the choline carboxylates ChC_4 (T_m = 55.1°C; T_c = 5.9°C; see Appendic C in section C.3.2), ChC_5 (T_m = 31°C; T_c = not known[18]) and ChC_6 (T_m = 60.7°C; T_c = 47.2°C; see Appendic C in section C.3.2) in literature with data received in the present study, reveals the tendency that carboxylates possessing an odd number of C-atoms exhibit lower melting points than carboxylates with even numbers of C-atoms. However, no tendency was observed when comparing the melting temperatures of choline carboxylates and bicarboxylates having the same chain length. It also seems that, compared to choline carboxylates ChC_m with m = 4, 5, 6, crystallization of bicarboxylates is more hindered due to the additional acid group. Therefore, crystallization of choline adipate (see **Figure 9-2** (C)) occurs at lower temperatures, while choline succinate (see **Figure 9-2** (A)) was found to crystallize during the heating cycle. This means that crystallization starts at around -80°C but with very low rates, consequently continuing during the heating cycle. In contrast, choline glutarate (see **Figure 9-2** (B)) could not be recrystallized in the temperature range until -80°C, still remaining liquid in the second and third heating cycle recorded during DSC measurements at heating rates of 1 K min^{-1}, thus showing that recrystallization takes place at temperatures below -80°C.

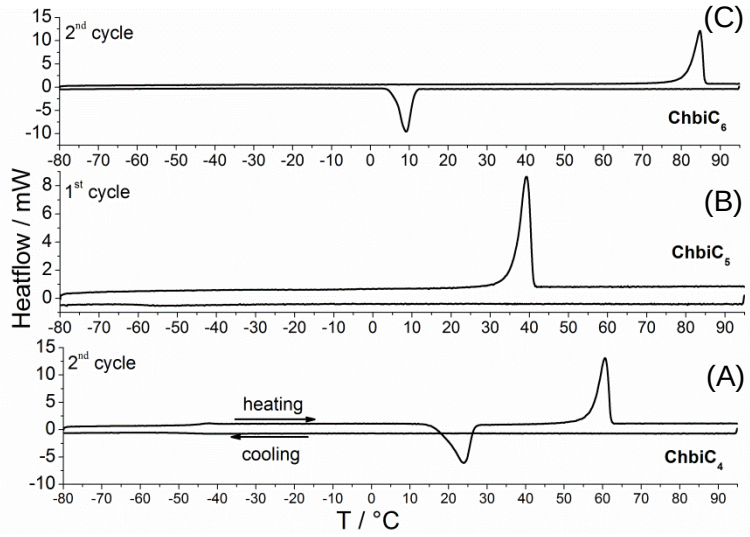

Figure 9-2. DSC curves of (A) choline succinate (second cycle), (B) choline glutarate (first cycle), (C) choline adipate (second cycle). Measurements were performed in the temperature range from -80°C to 95°C at a heating and cooling rate of 1 K min^{-1}.

It is known that hydrogen bonds between the organic salt and the hydrogen bond donor cause charge delocalization and depression of the melting point in the deep eutectics of bicarboxylic acid combined with choline chloride (two carboxylic acid groups complex one chloride ion)[9] and choline chloride with urea[7]. We take profit of this phenomenon in this work for the synthesis of deep eutectics. As hydrogen bond donor, choline glutarate forms a complex with present chloride ions (DEEP1 and DEEP2). Charge is delocalized and results in a decrease of the melting point of the mixture compared to the pure substances. In the

frame of this work, also the influence of urea, representing another type of hydrogen bond donor, was tested while keeping constant the choline chloride/choline glutarate molar ratio (see DEEP1Urea and DEEP2Urea) (see **Figure 9-3**). Only deep eutectic mixtures with choline glutarate were investigated because from pretests it was observed that the mixtures of choline glutarate/choline chloride with 95 wt% to 98 wt% of choline glutarate are liquid at room temperature and possess the lowest freezing points compared to other compositions. Concerning mixtures of choline succinate and choline adipate with choline chloride, no stable room temperature liquid deep eutectic mixtures were observed.

DSC measurements performed for the determination of glass and freezing temperatures at a heating rate of 1 K min^{-1} and a temperature range of -80°C to 25°C were not successful, therefore requiring the execution of manual and non-automatized investigations. As the melting points of choline chloride and urea are 302°C and 133°C,[7] respectively, depression of the melting point of the deep eutectics is very high. When a heating rate of 1°C per 30 minutes was applied, all three mixtures were stable until 4°C. Unfortunately, stability measurements at lower temperatures were not possible under chosen experimental conditions. At temperatures of -18°C DEEP1 remains liquid for a period of 3 days, afterwards tending to crystallize. Similar results were obtained for the DEEP2 system, where crystallization commences after storage at -18°C for 7-8 days. In contrast to these systems, all other mixtures provide higher liquid phase stabilization. After eight weeks, crystallization was found to occur. From all recorded data it can be concluded that addition of urea successfully delays the crystallization processes in the examined deep eutectic solvents at -18°C.

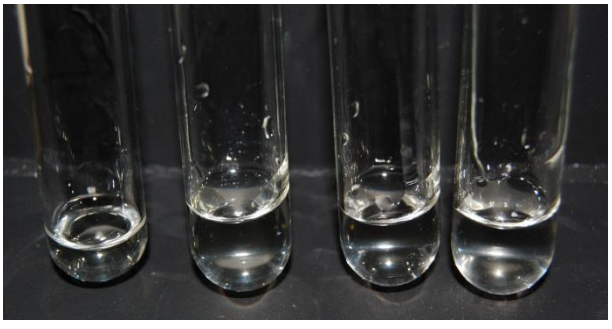

Figure 9-3. Deep eutectic mixtures at 20°C. Left to right: DEEP1, DEEP1Urea, DEEP2, DEEP2Urea

9.3.2 Density

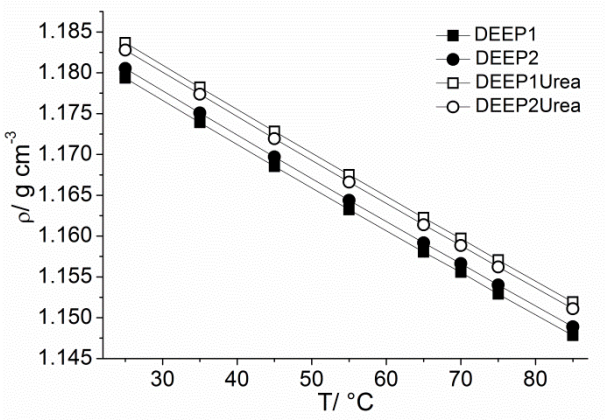

Figure 9-4. Temperature dependent density values of the four deep eutectic mixtures ((■) DEEP1, (•) DEEP2, (□) DEEP1Urea, (○) DEEP2Urea) in the temperature range from 25°C to 85°C.

As expected, all examined deep eutectics possess densities higher than water.[2] In general, one should assume that densities of the deep eutectic mixtures tend to increase with increasing fractions of choline chloride. However this assumption could not be confirmed for the urea-free deep eutectics, because the difference in the amounts of choline chloride used in the deep eutectic mixtures of DEEP1 and DEEP2 is too small.[2] While the molar ratio between choline glutarate and choline chloride remains the same in both DEEP1/DEEP1Urea and DEEP2/DEEP2Urea systems, only urea was added in a molar ratio of 1:2 for choline chloride/urea.[7] Taking into account the hole theory, which is used to explain the conductivity behavior and packing in deep eutectics,[2, 9] the average hole radius decreases by introducing urea to the mixtures, therefore leading to a density increase (see **Figure 9-4**).[2]

9.3.3 Conductivity

Specific conductivities, measured for the four deep eutectic mixtures in the temperature range from 25°C to 85°C, were found to vary between 0.01370 and 0.70226 mS cm^{-1}, thus being in accordance to the conductivity values typically found for ionic liquids.[19] However, compared to imidazolium ionic liquids the conductivities of the presently studied systems are lower to some extent.[20, 21] Higher conductivities were also reported from deep eutectic mixtures composed of a bicarboxylic acid and choline chloride in different ratios[9] as well as from 1:2 molar mixture of urea and choline chloride.[2] However, obtained values agree well with results described for the choline oligoether carboxylate ionic liquid (Ch-TOTO).[22]

Specific conductivities of DEEP1, DEEP1Urea, DEEP2, and DEEP2Urea were found to be temperature dependent. As seen in **Figure 9-5**, a linear correlation exists between the natural logarithm of the specific conductivity κ and the reciprocal temperature. Consequently,

the Arrhenius equation (1)[9, 23, 24] can be used as a fitting equation, but also the Vogel-Fulcher-Tammann equation (2)[22, 25] is suitable (see **Figure 9-5** (B)) for the evaluation of the temperature dependent changes in conductivities:

$$\ln(\kappa) = \ln(\kappa_0) - \frac{E_\Lambda}{RT} \quad (1); \qquad \ln(\kappa) = \ln(\kappa_0) - \frac{E_{\Lambda VFT}}{R\,(T - T_{0\kappa})} \quad (2)$$

For the Arrhenius model a temperature independent activation energy of conductivity E_Λ is assumed, while the Vogel-Fulcher-Tammann model proposes a temperature dependent activation energy $E_{\Lambda VFT}$.[25] $T_{0\kappa}$ thereby represents an ideal glass temperature.[22, 25] However, both models are of empirical nature and can be used as fitting model for the purpose of this study. The Arrhenius model is thereby preferred because the introduction of a further variable in the fitting process ($T_{0\kappa}$) seems to be not favorable. Nevertheless, both models were applied to allow comparison of the data with the choline oligoether ionic liquid reported previously.[22]

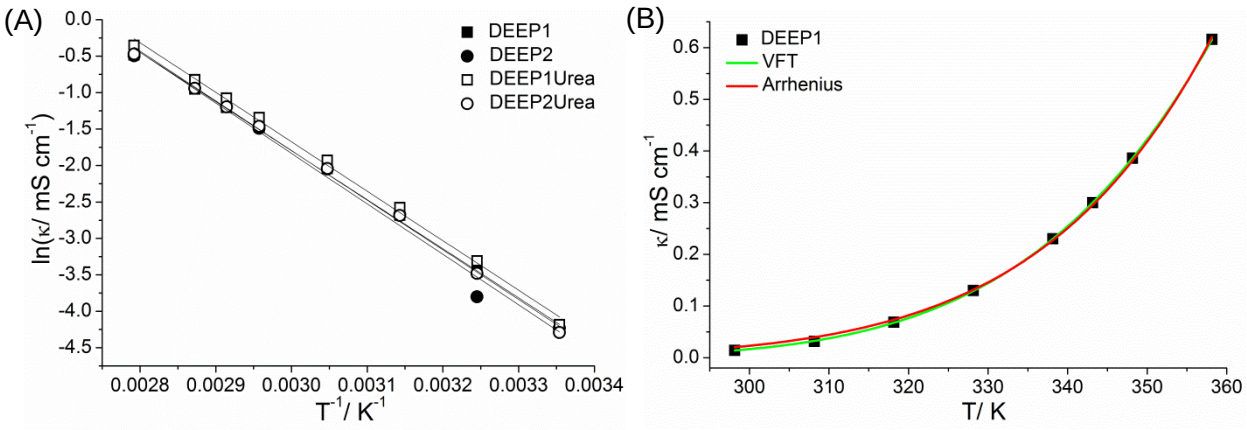

Figure 9-5. (A) Plot of the natural logarithm of the specific conductivity κ of the deep eutectics ((■) DEEP1, (•) DEEP2, (□) DEEP1Urea, (○) DEEP2Urea) versus the reciprocal temperature (Arrhenius fit R^2 = 0.989 to 0.998). (B) Comparison of the fitting of the temperature dependent conductivity values of DEEP1 (■) fitted with the Arrhenius equation (R^2 = 0.999; red line) and the Vogel-Fulcher-Tammann equation (R^2 = 0.999; green line).

Values obtained from the two fittings for the activation energies are shown in **Table 9-2**. The activation energy of conductivity does not depend on the amount of choline chloride or urea used in the deep eutectic mixtures, and measured conductivities of all compositions were basically the same. Activation energies are comparable with the one observed for the deep eutectic mixture of succinic acid and choline chloride (E_Λ = 54.3 ± 4.1 kJ mol^{-1}).[9] The one of malonic acid (E_Λ = 29.0 ± 1.2 kJ mol^{-1}) and oxalic acid (E_Λ = 34.6 ± 1.5 kJ mol^{-1}) with choline chloride are lower according to the smaller size of the molecules and increasing charge per

molecule.[9] Also the choline oligoether ionic liquid Ch-TOTO shows a much smaller activation energy $E_{\Lambda VFT}$ = 0.090 ± 0.001 eV as found here.[22]

	Arrhenius model		Vogel-Fulcher-Tammann model		
	$\ln(\kappa_0$ / mS cm^{-1})	E_Λ / kJ mol^{-1}	κ_0 / 10^3 mS cm^{-1}	$E_{\Lambda VFT}$ / kJ mol^{-1} (eV)	$T_{0\kappa}$ / K
DEEP1	18.4 ± 0.4	56.0 ± 1.1	5 ± 1	15.4 ± 0.8 (0.16 ± 0.01)	154 ± 5
DEEP1Urea	18.7 ± 0.4	56.5 ± 1.2	4 ± 1	14.1 ± 0.7 (0.15 ± 0.01)	157 ± 13
DEEP2	18.2 ± 1.0	55.6 ± 2.8	3 ± 3	15 ± 2 (0.15 ± 0.02)	162 ± 4
DEEP2Urea	18.6 ± 0.4	56.6 ± 1.2	5 ± 1	15.0 ± 0.7 (0.16 ± 0.01)	157 ± 5

Table 9-2. Determination of activation energies of conductivitiy according to the Arrhenius (E_Λ) and Vogel-Fulcher Tammann model ($E_{\Lambda VFT}$), respectively.

9.3.4 Viscosity

Temperature dependent viscosities, obtained for the deep eutectic solvent mixtures from dynamic viscosity measurements, are influenced by the amount of choline chloride as well as by the amount of urea in the mixture. Viscosities of the deep eutectic solvents were found to significantly increase with increasing quantities of hydrogen bonds present in the mixtures.[2] As a consequence, viscosity decreases with increasing amounts of choline chloride in the hydrogen bond donor choline glutarate (see **Figure 9-6**: the amount of choline chloride increases from DEEP2 to DEEP1). In addition, a re-increase in viscosity is observed when urea, representing another hydrogen bond donor, is added to the system (see **Figure 9-6**: the amount of urea increases from DEEP1 to DEEP1Urea and from DEEP2 to DEEP2Urea). In general, viscosity changes are quite small between the different mixtures due to the small changes in the ratios between the different components in the deep eutectic mixtures.

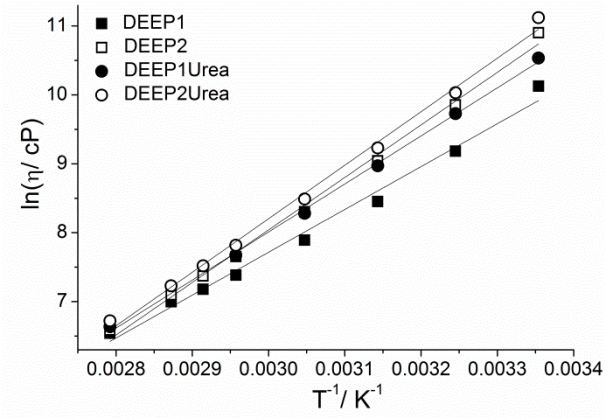

Figure 9-6. Plot of the natural logarithm of the viscosity η of the four deep eutectic mixtures ((■) DEEP1, (□) DEEP2, (•) DEEP1Urea, (○) DEEP2Urea) versus the reciprocal temperature (Arrhenius fit R^2 = 0.989 to 0.998).

Viscosities obtained in the temperature range between 25°C and 85°C are in accordance with values typically found for highly viscous ionic liquids[19], but are higher than those found for choline oligoether carboxylate Ch-TOTO[22] and for the above mentioned bicarboxylic acid/choline chloride mixtures[9].

The activation energy of the viscous flow E_η was calculated according to the Arrhenius law (see equation (3)):[9, 23]

$$\ln(\eta) = \ln(\eta_0) + \frac{E_\eta}{RT} \qquad (3)$$

Considering the obtained values, listed in **Table 9-3**, it can be concluded that the equimolar mixture of succinic acid and choline chloride requires a higher energy for viscous flow (E_η = 74.1 ± 0.8 kJ mol^{-1}).[9] This discrepancy can be explained by the presence of a stronger hydrogen bond network in the bicarboxylic acid-containing system compared to DEEP1, DEEP1Urea, DEEP2 and DEEP2Urea.

Energy values of the eutectic mixtures of choline chloride and oxalic or malonic acid are smaller, possibly due to the smaller molecules.[9]

	Arrhenius model	
	ln(η_0 / cP)	**E_η / kJ mol^{-1}**
DEEP1	-10.9 ± 0.8	51.7 ± 2.2
DEEP1Urea	-14.8 ± 0.6	63.4 ± 1.7
DEEP2	-12.9 ± 0.4	58.0 ± 1.1
DEEP2Urea	-15.1 ± 0.6	64.5 ± 1.7

Table 9-3. Determined activation energies for the viscous flow E_η obtained from temperature dependent viscosity data of the deep eutectic solvents fitted with the Arrhenius model.

9.3.5 Walden plot

An interplay between the molar conductivity, also represented by the ion mobility, and the fluidity, reciprocal viscosity, can be observed in the Walden plot (see **Figure 9-7**). The Walden plot is a useful tool to compare ionic liquids with deep eutectics and to determine the ion association in deep eutectic mixtures.[9] The Walden plot was used by Angell and coworkers to characterize ionic liquids according to their degree of ionicity.[26-28] They used this plot to categorize ionic liquids as “good” or “poor” ionic liquids, “superionic” liquids and so on.[27] The theory is based on Walden´s observation[27, 29] that the equivalent conductivity of a strong electrolyte in an aqueous solution is inversely proportional to the viscosity. The equivalent conductivity and inverse viscosity are influenced by temperature in the same way.[27, 29] According to Angell *et al.* it is possible to give a statement about the cation and anion association by the use of the Walden rule.[26, 27] The black line in **Figure 9-7** has a slope

of 1 and marks the region of fully dissociated salts like a dilute solution of 0.01 M KCl.[26, 27] This means that ions in solution are able to move independently of their ambient ions. Angell *et al.* introduced the ΔW value, the vertical deviation to this ideal line, to characterize ionic liquids according to this value. In this context, "good" ionic liquids are fully dissociated and show a ΔW < 1. Ionic liquids with ΔW = 1 exhibit only 10 % of the ionic conductivity as would have been expected at the ideal line of 0.01 M KCl.[28]

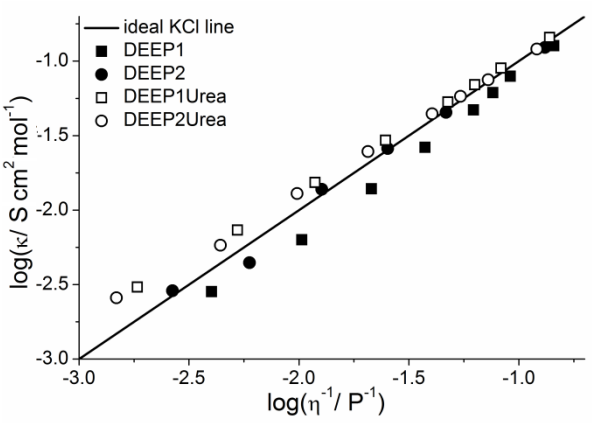

Figure 9-7. Walden plot, comparing the deep eutectic mixtures ((■) DEEP1, (•) DEEP2, (□) DEEP1Urea, (○) DEEP2Urea) at different temperatures (25°C to 85°C) with the ideal line for 0.01 M KCl (black line).

Points depicted in **Figure 9-7** represent the temperature dependent molar conductivities and fluidities of DEEP1, DEEP2, DEEP1Urea and DEEP2Urea, visibly being very close to the ideal line of the Walden plot. All points show a vertical deviation which is smaller than 0.25 (see **Table 9-4**). Consequently, choline chloride and choline glutarate are fully dissociated in the deep eutectic mixtures and behave like "good" ionic liquids, and no ion pairs should exist in the examined deep eutectic solvents.

T / °C	25	35	45	55	65	70	75	80
DEEP1	0.16	0.22	0.20	0.16	0.13	0.11	0.07	0.07
DEEP1Urea	-0.17	-0.09	-0.06	-0.02	0.00	-0.01	-0.02	-0.03
DEEP2	-0.03	0.12	-0.04	-0.01	0.01	-	-	0.03
DEEP2Urea	-0.24	-0.12	-0.12	-0.08	-0.04	-0.03	-0.01	0.00

Table 9-4. Vertical deviation ΔW of the deep eutectic mixtures from the ideal KCl line is shown in the Walden plot at different temperatures (see **Figure 9-7**). The table presents the ΔW values for the different temperatures.

9.3.6 Outlook – dissolution of choline surfactants in deep eutectic solvents

During our search of useful applications for these deep eutectic solvents, several questions arise. Is structuring possible in these deep eutectic solvents? Can they be used to dissolve biomass, e.g. cellulose? Is it possible to use them in formulation? A lot of further experiments could be made, but only a few preliminary tests were performed. Dissolution of cellulose was found to be impossible, as it seems that the hydroxyl groups of choline are linked to cellulose due to hydrogen bonds, thus stabilizing the cellulose system.[30] As a consequence, destruction of intermolecular hydrogen bonds in cellulose by carboxylate anions is blocked.

A promising formulation could be the dissolution of choline surfactants in the deep eutectic solvents. Therefore, 2 wt% of choline dodecylsulfate, hexadecylsulfate or oleate were dissolved in the four examined deep eutectic solvents. At room temperature, surfactant crystals remain solid in the observed systems, but upon heating to 50°C, the mixtures of 2 wt% choline dodecylsulfate in the deep eutectic solvents became transparent and no birefringence was observed during microscopical analysis with crossed polarizers. In contrast, no complete dissolution of the surfactant was observed at temperatures up to 90°C for mixtures containing 2 wt% surfactant either choline oleate or choline hexadecylsulfate. Only the system of DEEP1Urea with surfactant was analysed with X-ray scattering experiments. No temperature dependent behavior of the SAXS and WAXS spectra was found and also no self-structuring of the pure deep eutectic solvent was observed (see **Figure 9-8** (A)). This observation is in good agreement with the assumption that deep eutectic solvents are non-volatile and show very small isothermal compressibilities. This can be assumed taking into account the absolute intensity at q = 0 and bearing into mind that the absolute intensity I(q = 0) is directly proportional to the temperature T and the isothermal compressibility χ_T ($I(q = 0) \sim T \cdot \chi_T$).[31] When 2 wt% of choline dodecylsulfate were added to the DEEP1Urea system, parts of the surfactant still remained undissolved up to temperatures of 45°C. Defined reflections are found in the WAXS region and prove the existence of a crystalline substance. In the SAXS region, a defined peak at 3.07 nm^{-1} was observed, belonging to the alkyl chain length of the surfactant being at 16.86 Å, according to Tanford.[32] This d-spacing is referred to this chain length.

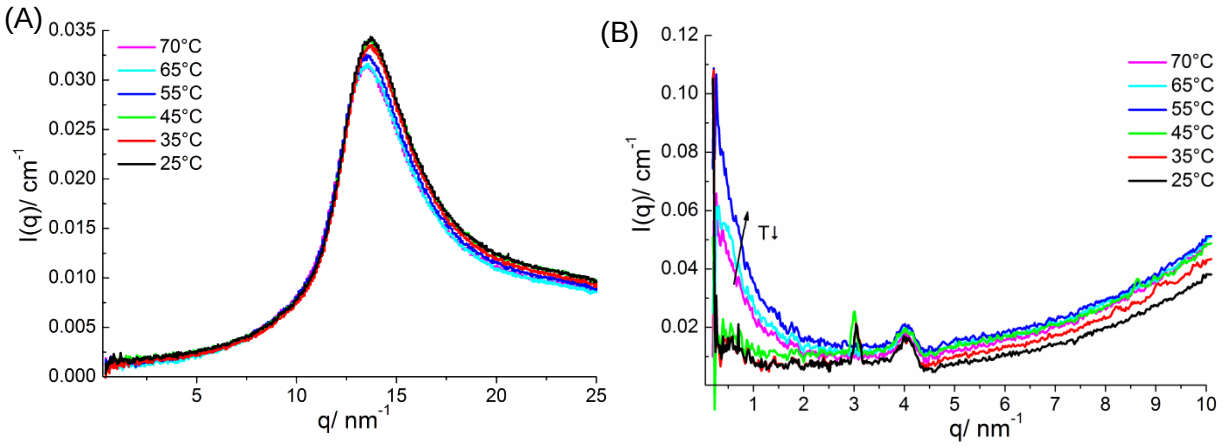

Figure 9-8. (A) SAXS and WAXS spectra of DEEP1Urea at 25°C, 35°C, 45°C, 55°C, 65°C and 70°C (B) SAXS spectra of 2 wt% choline dodeclysulfate in DEEP1Urea at the same temperatures. The reflection at 4 nm^{-1} results from Kapton foil and bad background subtraction caused by the alignment of the instrument.

In the SAXS spectra of 2 wt% choline hexadecylsulfate or choline oleate in DEEP1Urea defined reflections of 2.51 nm^{-1} or 1.51 nm^{-1} were also found, resulting from the alkyl chains of the surfactants. From **Figure 9-8** (B) it can be deduced that aggregates appear in the system of 2 wt% choline dodecylsulfate in DEEP1Urea at 55°C, 65°C and 70°C. Obviously, only choline dodecylsulfate is capable to form aggregates in DEEP1Urea. To evaluate the size and shape of the aggregates, higher scattering intensities and even lower q values are necessary. Therefore, the use of synchrotron radiation is essential for the analysis of this system. In summary, it was nevertheless demonstrated that formation of aggregates is possible in these deep eutectic solvents.

9.4 Conclusion

A successful two-step strategy to form room temperature liquid, deep eutectic solvents containing low toxic bicarboxylic acids was presented within this chapter: In a first step, hydrogen bond networks, usually existing in systems of pure bicarboxylic acids, get destroyed simply by quantitatively exchanging protons of one carboxylic group by choline cations, resulting in significantly lowered melting points. The remaining second protonated carboxylic group is still capable to form hydrogen bonds, thus leading to a delocalization of the charge in the examined deep eutectic solvents. In a second step, the choline bicarboxylate ionic liquid was mixed with choline chloride to destroy the hydrogen bond network in the choline bicarboxylate.

This two step strategy towards “green” deep eutectic solvents was found to work especially well when using glutaric acid (using 95-98 wt% choline glutarate in the mixture of choline glutarate with choline chloride), resulting in a highly viscous (but liquid) deep eutectic solvent at room temperature. With succinic acid and adipic acid no reasonable mixtures were

observed. They are not completely liquid at room temperature. Eutectic compositions of other studied systems containing either pure adipic, oxalic or succinic acid mixed with choline chloride were solid at room temperature and their freezing points were determined to be T_f = 85°C, 34°C and 71°C, respectively.[9] The only observed system representing a deep eutectic mixture being liquid at room temperature is a composition of malonic acid and choline chloride having a freezing point at 10°C.[9] Preliminary tests have shown that mixtures of choline succinate and choline chloride exhibit a melting point higher than 25°C but lower than 65°C, therefore being lower than observed for mixtures of succinic acid and choline chloride.

The disadvantages of the deep eutectic solvents synthesized within the frame of this work are their observed high viscosities and low conductivities. In the future, it is worth to further examine mixtures of either choline oxalate or choline malonate and choline chloride for their physico-chemical properties, as it might be expected that these systems could represent improved room temperature deep eutectic mixtures with lower viscosities due to the smaller molecules. This would represent a potentially suitable strategy to decrease the melting point of carboxylic acid group-containing deep eutectic solvents for room temperature applications. At the moment, beside the here characterized system, only levulinic acid combined with choline chloride in the ratio 2:1 and the above mentioned mixture of malonic acid with choline chloride are known to be deep eutectic solvents containing a carboxylic acid group and being liquid at room temperature.[2, 33]

Another potential strategy towards lower viscosities in such mixtures might be the finding of dependence between the amount of used choline chloride and observed viscosities, as higher amounts of choline chloride in the system, as shown in this work, are capable to destroy hydrogen bonds between the acid groups to a higher degree.

In addition, it was demonstrated within this study that the addition of a second hydrogen bond donor (urea) also has a strong influence on the viscosity of choline glutarate/choline chloride deep eutectic solvents, where increasing viscosities were observed with increasing amounts of the second hydrogen bond donor urea. Nonetheless, fully dissociated anions and cations were observed in the examined deep eutectic solvents, as inferred from Walden plots (depicted in **Figure 9-7**). It was further demonstrated that choline dodecylsulfate is capable to form aggregates in DEEP1Urea.

In view of possible applications for the examined deep eutectic solvents, observed high viscosities of these mixtures strongly limit their potential suitability for electrochemical applications. On the other hand, one might indeed think of their potential use in formulations for pharmaceutical issues, as the examined systems are advantageous in terms of their easy preparation (even the ionic liquid shows an easy and cheap synthesis route), their non-toxicity and their biological origin, which further allows an easy decomposition by the human body. In addition, these systems are non-reactive with water. One possible application even

due to their low oral toxicity could be the use as carriers in pharmacokinetic studies on mice or rats to increase the admittance of scarcely soluble substances in water. This application was already approved as possible for choline chloride urea mixtures and mixtures of malonic acid with choline chloride.[3]

9.5 Experimental

9.5.1 Synthesis of choline bicarboxylate ionic liquids and deep eutectic solvents

Details for the synthesis and the characterization, with regard to the purity, of choline bicarboxylates, like choline succinate ($ChbiC_4$), choline glutarate ($ChbiC_5$) and choline adipate ($ChbiC_6$), are already explained in Chapter 3 in section 3.5.1.

At room temperature all three ionic liquids are white solids. Choline succinate was already synthesized by Fukaya *et al.*, therein described to be of viscous nature but not being solid.[34] However, the described synthesis route of Fukaya *et al.* differs from the one used in the present work. Thus, explaining the difference in the observed state of aggregation possibly by an enhanced and more efficient drying process used in the frame of this work. Deep eutectics were prepared in a glove box under dry nitrogen flow atmosphere to avoid contamination with traces of water stemming from air humidity.

Deep eutectics were prepared with a molar ratio of 1:2 for choline chloride (purity ≥ 98 %, Sigma Aldrich) and urea (molecular biology grade, Serva), respectively, as it was stated by Abbott *et al.*[7] to be the best composition. Four deep eutectic solvents with different compositions were prepared (the exact compositions are given in section 9.2): DEEP1, DEEP1Urea, DEEP2, DEEP2Urea.

The mixtures of the pure substances were stirred for 24 hours at 60°C until a viscous clear liquid was obtained. Subsequently, all mixtures were post-dried for one week in high vacuum, after which coulometric Karl-Fisher titration was performed for the determination of the water contents (typical values listed below).

$ChbiC_4$: 2221±100 ppm; $ChbiC_5$: 1521 ± 100 ppm; $ChbiC_6$: 3197±100 ppm; DEEP1: 71 ± 100 ppm; DEEP1Urea: 930 ± 80 ppm; DEEP2: 519 ± 100 ppm; DEEP2Urea: 714 ± 100 ppm

9.5.2 Methods

9.5.2.1 Thermogravimetric analysis

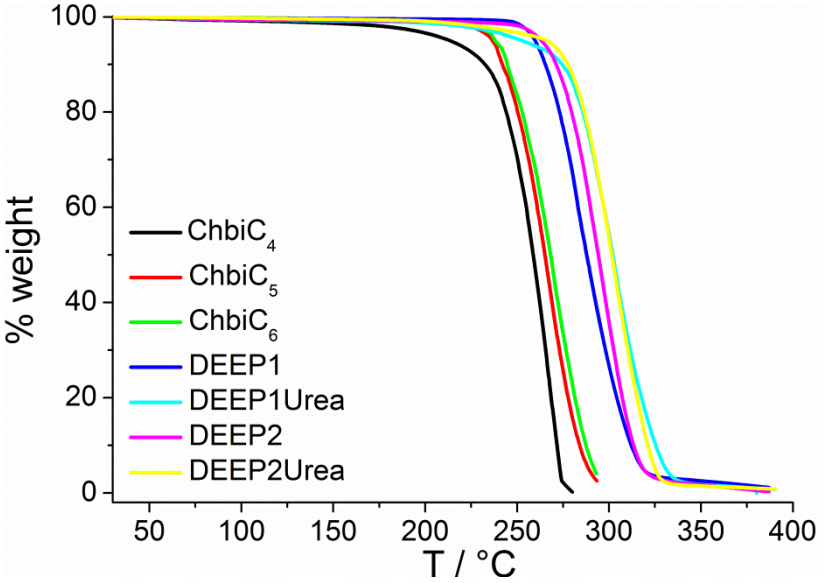

Figure 9-9. Graph of % weight versus temperature for the determination of decomposition temperatures T_{dec}.

Decomposition temperatures (T_{dec}) were measured by means of a thermogravimetric analyzer (TGA7, Perkin-Elmer) in a temperature range of 30 to 300°C or 30 to 400°C for $ChbiC_m$ with m= 4, 5, 6 and deep eutectics, respectively. All measurements were performed under constant nitrogen flow. Decomposition temperatures were determined from the onset of mass loss derived from the intersection of the baseline before thermal decomposition with the tangent during mass loss. The % weight as a function of the temperature is shown for each substance in **Figure 9-9**.

9.5.2.2 Differential scanning calorimetry (DSC)

Melting points, glass transition temperatures T_g as well as freezing points T_f of the ionic liquids $ChbiC_m$ with m = 4, 5, 6 (see **Figure 9-2** and **Figure 9-10**) and deep eutectic mixtures were analyzed by means of differential scanning calorimetry on a DSC30 (Mettler) in a three-cycle mode, using a heating rate of 1 K min^{-1}.

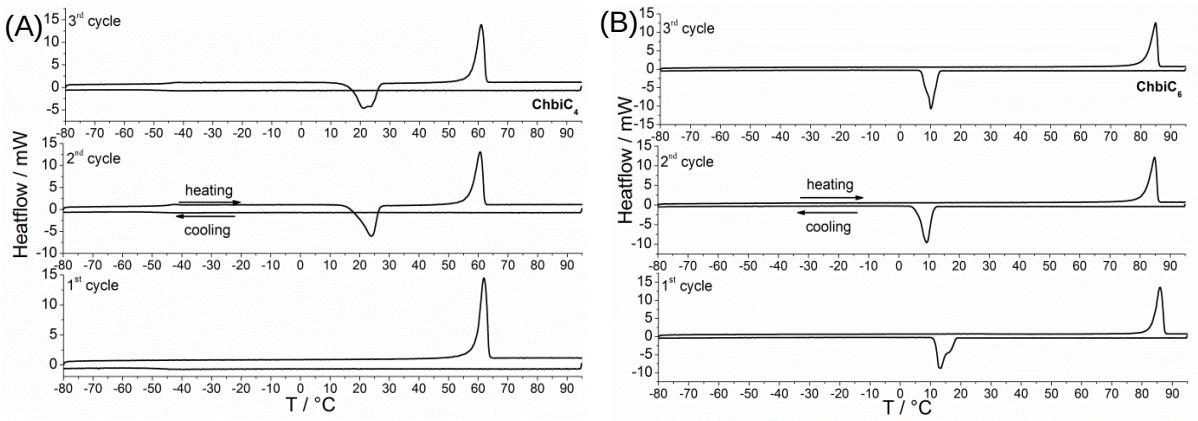

Figure 9-10. DSC curves of choline succinate (A) and choline adipate (B) are shown. Three cycles were recorded in the temperature range between -80°C and 95°C.

Samples were prepared in a glove box under nitrogen atmosphere and sealed in aluminum pans. Measurements were performed in nitrogen atmosphere by continuously flushing the instrument with nitrogen to avoid contamination with water. Examined temperature ranges were -80 to 95°C and -80°C to 25°C for ionic liquids or deep eutectic mixtures, respectively. In case of the deep eutectics, no glass temperatures or freezing points were determinable within the examined temperature range. Therefore, attempts were made to manually evaluate the crystallization points of the deep eutectics by continuously cooling down the four different deep eutectic mixtures from 25°C to 4°C at a heating rate of 1 K per 30 minutes before subsequent storage at -18°C for several days.

Comparison of the different values for the melting/crystallization enthalpy and entropy of all ionic liquids reveals no remarkable discrepancy and almost no influence of the chain length was observed (see **Table 9-5**).

	$ChbiC_4$				**$ChbiC_5$**		**$ChbiC_6$**	
	ΔH_1 / kJ mol^{-1}	**ΔS_1 / J mol^{-1} K^{-1}**	**ΔH_2 / kJ mol^{-1}**	**ΔS_2 / J mol^{-1} K^{-1}**	**ΔH_1 / kJ mol^{-1}**	**ΔS_1 / J mol^{-1} K^{-1}**	**ΔH_1 / kJ mol^{-1}**	**ΔS_1 / J mol^{-1} K^{-1}**
1. heat			25.2	75.1	24.0	76.7	36.5	102.0
1. cool			-	-	-	-	-30.9	-109.3
2. heat	-22.0	-74.5	23.3	69.7	-	-	35.6	99.1
2. cool	-	-	-	-	-	-	-30.2	-105.4
3. heat	-21.7	-73.1	23.2	69.5	-	-	36.5	99.1
3. cool	-	-	-21.7	-73.1	-	-	-29.9	-106.3

Table 9-5. Melting and crystallization enthalpies and entropies of choline succinate ($ChbiC_4$), choline glutarate ($ChbiC_5$) and choline adipate ($ChbiC_6$) obtained from DSC measurements in the temperature range from -80°C to 95°C. The numbers 1, 2 mark the transitions with increasing temperature (heating cycle) and the respective values at the cooling cycle.

9.5.2.3 Density

Densities (ρ) of DEEP1, DEEP1Urea, DEEP2, DEEP2Urea were determined at 25°C; 35°C, 45°C, 55°C, 65°C, 70°C, 75°C and 85°C by using a vibrating tube densimeter (DMA 5000M, Anton Paar) after calibration with standards. Received densities were used for the calculation of molar concentrations and molar volumes (V_m), necessary for the determination of the equivalent conductivity Λ_m. The uncertainty was calculated to $\pm$ 0.0001 g cm^{-3}.

T/°C	DEEP1		DEEP1Urea		DEEP2		DEEP2Urea	
	ρ	V_m	ρ	V_m	ρ	V_m	ρ	V_m
25	1.1794	195	1.1837	177	1.1805	197	1.1828	188
35	1.1739	196	1.1782	178	1.1751	198	1.1774	189
45	1.1685	197	1.1728	179	1.1697	199	1.1719	190
55	1.1633	198	1.1675	180	1.1644	200	1.1666	190
65	1.1580	199	1.1623	181	1.1592	201	1.1614	191
70	1.1556	199	1.1597	181	1.1566	202	1.1588	192
75	1.1529	199	1.1571	181	1.1540	202	1.1562	192
85	1.1478	200	1.1519	182	1.1489	203	1.1511	193

Table 9-6. Densities ρ (g cm^{-3}) and molar volumes V_m (cm^3 mol^{-1}) of deep eutectics, measured at temperatures between 25°C and 85°C.

9.5.2.4 Conductivity

T/°C	DEEP1		DEEP1Urea		DEEP2		DEEP2Urea	
	κ	Λ_m	κ	Λ_m	κ	Λ_m	κ	Λ_m
25	0.01412	0.00275	0.01522	0.00270	0.01456	0.00287	0.01370	0.00257
35	0.03136	0.00614	0.03653	0.00651	0.02234	0.00443	0.03080	0.00581
45	0.06855	0.01349	0.07595	0.01359	0.06917	0.01378	0.06814	0.01292
55	0.12965	0.02563	0.14533	0.02612	0.12915	0.02585	0.12985	0.02472
65	0.22992	0.04565	0.26090	0.04710	0.22544	0.04533	0.23169	0.04432
70	0.29971	0.05963	0.34098	0.06170	-	-	0.30276	0.05803
75	0.38600	0.07698	0.43846	0.07952	-	-	0.39003	0.07493
85	0.61598	0.12339	0.70226	0.12793	0.60926	0.12359	0.62434	0.12048

Table 9-7. Specific conductivities κ (mS cm^{-1}) and equivalent conductivities (S cm^2 mol^{-1}) of the different deep eutectics at different temperatures.

Temperature dependent specific conductivities κ (data see **Table 9-7**) were measured at different temperatures (25°C, 35°C, 45°C, 55°C, 65°C, 70°C, 75°C, 85°C), using a custom-designed apparatus, composed of a precision thermostat, a sine generator, a symmetrical Wheatstone bridge with Wagner earth and a resistance decade.[35-37] Temperature control was achieved by a combination of a homebuilt precision thermostat and a commercial thermostat (Julabo FP40), yielding a temperature stability of ± 0.01 K. Samples were stored under nitrogen atmosphere in a capillary cell, each of them containing a three-electrode setup. The cell constant α was 34 cm^{-1}. The electrical resistance was recorded at frequencies ranging from 100-10000 Hz. To eliminate disturbing effects caused by electrode polarization, the

resistance R was extrapolated to $R_\infty = \lim_{\nu\to\infty} R(\nu)$.[36] Specific conductivities were calculated according to $\kappa = \alpha/R_\infty$. The temperature dependence of the cell constant was determined to be negligible [38] and the uncertainty was estimated to be $< 1\%$.

9.5.2.5 Viscosity

T/°C	DEEP1	DEEP1Urea	DEEP2	DEEP2Urea
	η	η	η	η
25	24.980	54.280	37.610	67.540
35	9.720	19.040	16.780	22.750
45	4.687	8.458	7.881	10.200
55	2.671	4.043	3.951	4.860
65	1.610	2.104	2.145	2.480
70	1.312	1.587	1.638	1.841
75	1.094	1.206	1.251	1.380
85	0.693	0.724	0.761	0.829

Table 9-8. Temperature dependent viscosity data of the different deep eutectics given in Pas.

Temperature dependent viscosities η were measured on a Bohlin rheometer (CVO 120 High Resolution) with a plate/plate geometry (P20mm) (data see **Table 9-8**). The instrument was equipped with a temperature control unit, allowing the investigation at different temperatures (25°C, 35°C, 45°C, 55°C, 65°C, 70°C, 75°C, 85°C). Shear rates were varied between 0.00375 s^{-1} and 262 s^{-1}. Results show that all deep eutectic mixtures are Newtonian fluids, having a constant shear stress to shear rate behavior at all examined temperatures. In addition, all experiments were performed under argon atmosphere. The uncertainty of about 1 % was taken into account and the instrument was calibrated with calibration oil recommended by Bohlin instruments.

9.5.2.6 Small and wide angle X-ray scattering

X-ray measurements were performed at the Institute de Chimie Séparative de Marcoule (CEA/CNRS, UM2, ENSCM, France) on an instrument introduced in Chapter 4 in section 4.5.2.4. The different samples were assembled in 3 mm thick aluminum cells, which were sealed with Kapton foil of 25 µm thickness. The measurement were conducted at temperatures ranging between 25°C to 70°C with $\Delta T = \pm 2$°C. Two-dimensional spectra were integrated with the FIT2D software. Azymuthal integration was performed to obtain the scattering intensity as a function of the scattering vector q ($= (4\pi/\lambda)\cdot\sin\theta$; with θ the scattering angle and λ the X-ray wavelength). Acquisition time of the different samples was 3600 seconds. The empty cell was measured. Further the solvent DEEP1Urea and 2 wt% of surfactant in DEEP1Urea were investigated. As surfactant choline dodecylsulfate, choline hexadecylsulfate and choline oleate were taken. To obtain the absolute intensity of the

spectra of DEEP1Urea the empty cell was subtracted from the spectra of DEEP1Urea. To get the absolute intensity of the solutions containing the surfactant the empty cell and the concentration related intensity of the pure solvent DEEP1Urea was subtracted from the spectrum of 2 wt% surfactant in DEEP1Urea.

9.6 References

1. A. P. Abbott, D. Boothby, G. Capper, D. L. Davies and R. K. Rasheed, *J. Am. Chem. Soc.*, 2004, **126**, 9142-9147.
2. Q. Zhang, K. De Oliveira Vigier, S. Royer and F. Jerome, *Chem. Soc. Rev.*, 2012, **41**, 7108-7146.
3. H. G. Morrison, C. C. Sun and S. Neervannan, *Int. J. Pharm.*, 2009, **378**, 136-139.
4. H. Garcia, R. Ferreira, M. Petkovic, J. L. Ferguson, M. C. Leitao, H. Q. N. Gunaratne, K. R. Seddon, L. P. N. Rebelo and C. S. Pereira, *Green Chem.*, 2010, **12**, 367-369.
5. T. V. Doherty, M. Mora-Pale, S. E. Foley, R. J. Linhardt and J. S. Dordick, *Green Chem.*, 2010, **12**, 1967-1975.
6. R. P. Swatloski, S. K. Spear, J. D. Holbrey and R. D. Rogers, *J. Am. Chem. Soc.*, 2002, **124**, 4974-4975.
7. A. P. Abbott, G. Capper, D. L. Davies, R. K. Rasheed and V. Tambyrajah, *Chem. Commun. (Camb.)*, 2003, 70-71.
8. S. Saito, M. Lee and W.-Y. Wen, *J. Am. Chem. Soc.*, 1966, **88**, 5107-5112.
9. A. P. Abbott, D. Boothby, G. Capper, D. L. Davies and R. K. Rasheed, *J. Am. Chem. Soc.*, 2004, **126**, 9142-9147.
10. R. Klein, H. Dutton, O. Diat, G. J. Tiddy and W. Kunz, *J. Phys. Chem. B*, 2011, **115**, 3838-3847.
11. J. K. Blusztajn, *Science*, 1998, **281**, 794-795.
12. H. L. Merten and G. L. Bachman, *J. Food Sci.*, 1976, **41**, 463-464.
13. A. Jackson, *Arch. Dis. Child.*, 1994, **70**, 3-4.
14. A. M. Wynne, *J. Chem. Educ.*, 1987, **64**, 180.
15. P. A. Schaber, J. Colson, S. Higgins, D. Thielen, B. Anspach and J. Brauer, *Thermochim. Acta*, 2004, **424**, 131-142.
16. M. D. Small, *The Physical Chemistry of Lipids from Alkanes to Phospholipids*, Plenum Press, New York and London, 1986.
17. R. Klein, M. Kellermeier, D. Touraud, E. Müller and W. Kunz, *J. Colloid Interface Sci.*, 2013**, 392**, 274-80.
18. M. Petkovic, J. L. Ferguson, H. Q. N. Gunaratne, R. Ferreira, M. C. Leitao, K. R. Seddon, L. P. N. Rebelo and C. S. Pereira, *Green Chem.*, 2010, **12**, 643-649.

19. O. Zech, M. Kellermeier, S. Thomaier, E. Maurer, R. Klein, C. Schreiner and W. Kunz, *Chemistry*, 2009, **15**, 1341-1345.
20. O. Zech, A. Stoppa, R. Buchner and W. Kunz, *J. Chem. Eng. Data*, 2010, **55**, 1774-1778.
21. P. Wasserscheid and W. Keim, *Angew. Chem. Int. Ed. Engl.*, 2000, **39**, 3772-3789.
22. R. Klein, O. Zech, E. Maurer, M. Kellermeier and W. Kunz, *J. Phys. Chem. B*, 2011, **115**, 8961-8969.
23. J. O. M. Bockris and A. K. N. Reddy, *Modern Electrochemistry*, Plenum Press, New York, 1970.
24. A. P. Abbott, J. C. Barron, K. S. Ryder and D. Wilson, *Chemistry*, 2007, **13**, 6495-6501.
25. A. Grandjean, M. Malki, C. Simonnet, D. Manara and B. Penelon, *Phys. Rev. B*, 2007, **75**, 054112.
26. M. Yoshizawa, W. Xu and C. A. Angell, *J. Am. Chem. Soc.*, 2003, **125**, 15411-15419.
27. W. Xu, E. I. Cooper and C. A. Angell, *J. Phys. Chem. B*, 2003, **107**, 6170-6178.
28. D. R. MacFarlane, M. Forsyth, E. I. Izgorodina, A. P. Abbott, G. Annat and K. Fraser, *Phys. Chem. Chem. Phys.*, 2009, **11**, 4962-4967.
29. P. Walden, *Z. Phys. Chem., Stoechiom. Verwandtschaftsl.*, 1906, **55**, 207-249.
30. A. P. Abbott, T. J. Bell, S. Handa and B. Stoddart, *Green Chem.*, 2006, **8**, 784-786.
31. D. Orthaber, A. Bergmann and O. Glatter, *J. Appl. Crystallogr.*, 2000, **33**, 218-225.
32. C. Tanford, *J. Phys. Chem.*, 1972, **76**, 3020-3024.
33. Z. Maugeri and P. D. de Maria, *RSC Adv.*, 2012, **2**, 421-425.
34. Y. Fukaya, Y. Iizuka, K. Sekikawa and H. Ohno, *Green Chem.*, 2007, **9**, 1155-1157.
35. J. Barthel, H. Graml, R. Neueder, P. Turq and O. Bernard, *Curr. Topics Solution Chem.*, 1994, 223-239.
36. J. Barthel, F. Feuerlein, R. Neueder and R. Wachter, *J. Solution Chem.*, 1980, **9**, 209-219.
37. J. Barthel, R. Wachter and H.-J. Gores, *Mod. Aspects of Eletrochem.*, 1979, **13**, 1-79.
38. R. A. Robinson and R. H. Stokes, *Electrolyte Solutions*, Butterworth, London, 1959.

Chapter 10

Summary

This work was divided into three main parts:

1. The synthesis of choline carboxylates ChC_m with chain lengths of m = 2, 4, 6, 8, 10 and choline oleate was investigated. Subsequently, the effects of the choline cation, the alkyl chain length of the carboxylate anion, and the introduction of a double bond in the alkyl chain of the anion on the aqueous phase behavior of these carboxylates and on the thermotropic mesomorphism of the neat substances were analyzed. Further, the cytotoxicity of the choline carboxylates was determined on HeLa and SK-MEL-28 cells.

2. The synthesis of choline dodecylsulfate (ChS_{12}) and choline hexadeylsulfate (ChS_{16}) was made and the cytotoxicity, the temperature dependent aqueous phase behavior, and the temperature dependent phase behavior of the neat substance were investigated. In addition, their application as efficient, biocompatible laundry detergents was approved with washing, foam stability and foamability tests and by investigation of the oil solubilization capacity of the surfactant.

3. A strategy was proposed to design low toxic, room temperature liquid deep eutectic solvents, composed of choline bicarboxylate and choline chloride (and urea). The density, viscosity and conductivity properties of these deep eutectic solvents were investigated.

1. Choline carboxylates ChC_m with m = 2-10 and choline oleate

Short chain choline carboxylates (ChC_m with m = 2-10) and choline oleate were synthesized in order to characterize the influence of the chain length on the aqueous and thermotropic phase behavior. However, it should be mentioned that neither the short chain choline carboxylates nor choline oleate was found to be a room temperature liquid ionic liquid. In cytotoxicity tests on HeLa and SK-MEL-28 cells a slight increase of the cytotoxicty of the choline carboxylate was observed with growing chain length, but in a non linear way. However, all investigated choline carboxylates are approved as harmless (in general high IC_{50} values). The double bond in choline oleate and the choline cation show no influence on the cytotoxicity. Short chain choline carboxylates, including chain length m = 8, do only interact with the DPPC (dipalmitoylphophatidylcholine) liposomes (mimicking human cell membrane), while choline nonanoate, decanoate and oleate penetrate the membranes. In summary, choline carboxylates start to interact with biological membranes more or less at

concentrations around or higher than the IC_{50} value observed in cytotoxicty tests (see Chapter 3).

Investigating the aqueous behavior and the thermotropic behavior, a change from a pure ionic liquid (chain length m < 8; acting in aqueous solution as hydrotrope) to an ionic liquid with surfactant properties (chain length m ≥ 8) was observed. Choline acetate, choline butanoate and choline hexanoate are found to be very inefficient and polar hydrotropes compared to common ones such as sodium xylene sulfonate. In addition, choline hinders the self aggregation for chain lengths m = 4, 6, while sodium analogs are able to aggregate. The *cmc* values of choline octanoate, choline decanoate and choline oleate are in line with earlier results for choline carboxylates with m = 12-18 (log(*cmc*) = 1.9 – 0.29 m; m as the number of C-atoms in the alkyl chain).[1] Similarly, *cmc* values of sodium, potassium and choline carboxylates show no influence of cation size on the *cmc* (see Chapter 3).

Enhanced water solubility and low Krafft temperatures below 0°C are found for choline carboxylate surfactants ChC_m with m = 8, 10 and oleate. Firstly, the Krafft temperature of choline oleate is lowered compared to choline octadecanoate (T_{Krafft} = 40°C)[1] due to a hindered packing resulting from the cis-double bond. Additionally, the Krafft temperatures of choline carboxylates are lowered by two contributory factors due to the choline cation. The crystalline packing of the surfactant is effectively hindered by the bulky, unsymmetrical nature of the choline cation. Further, increased solubility in water is a result of a high degree of dissociation of the choline salts (see Chapter 4).

These two aspects influence also the packing behavior of choline carboxylates in water, resulting in a large headgroup area a_s of the choline carboxylate surfactant molecule. Therefore, mesophases with high curvature, like a discontinuous cubic phase I_1' and I_1'', are formed between the micellar and the hexagonal phase region. The influence of the different alkyl chain lengths and the double bond in the alkyl chain on the aqueous phase behavior was explained according to packing constrains. Choline decanoate behaves similarly to the long chain choline carboxylates ChC_m with m = 12-18[2] and forms the following lyotropic phases with increasing concentrations: micellar phase L_1, discontinuous cubic phase I_1' and I_1'', hexagonal phase H_1, bicontinuous cubic phase V_1, and defective lamellar phase dL_α or nematic phase N. The discontinuous cubic phases of choline decanoate are instable compared to m = 12-18 and melt to a micellar phase (from 30°C to 70°C). In addition, the short chain in choline octanoate induces a large isotropic, micellar solution area in the binary phase diagram and is also responsible for the absence of cubic phases (discontinuous cubic I_1' and I_1'' as well as bicontinous cubic V_1). Furthermore, I_1' and I_1'', which are present in the binary phase diagram of choline octadecanoate[2], are absent in the binary phase diagram of choline oleate due to the double bond. As highest concentrated phase, a defective lamellar

or nematic phase instead of a lamellar smectic A phase (found for ChC_m with m = 12-18)[2] is formed by all three substances in water. The defects could result from the simultaneous existence of two headgroups (-COOH and $–COO^-$). Compared to the alkali soaps, the choline analogs show a more extended hexagonal phase region and only a small defective lamellar or nematic phase region.

Furthermore, the extended, micellar isotropic solution area of choline octanoate expands up to 70 wt% over the whole temperature range from 0°C up to 95°C and above 70°C over the whole concentration range. The short chain in the octanoate anion forms temperature instable lyotropic phases which melt above 70°C. The following aggregates are formed along the concentration range between 1 wt% and 100 wt%. Above the *cmc* (9.48 wt% ChC_8) spherical micelles are formed, transforming to cylindrical rod like micelles at 40 wt% to 45 wt%. With increasing concentrations the cylindrical micelles grow epitaxially until the interaction between the micelles is too high so that molten salts with a less ordered microstructure or reversed aggregates at concentrations above 96 wt% are formed. Both structure suggestions are possible according to the packing rules (see Chapter 4).

The thermotropic phase behavior of the choline carboxylates ChC_m with m = 2, 4, 6, 8, 10 and oleate was investigated in the temperature range from -50°C to 95°C considering the influence of the chain length, the variation of the chain properties, and also the impact of the choline cation. A significant influence of the choline cation on the thermotropic mesomorphism was observed compared to the sodium cation. In general, the transition temperatures are clearly shifted to lower temperatures. The impact of the choline cation increases with decreasing chain length. This behavior is observed especially for choline acetate, choline butanoate and choline hexanoate (contrary to sodium analogs). They only form one stable crystal phase and melt directly to an isotropic liquid. The longer chain choline carboxylates, like the choline octanoate and the choline decanoate, are able to form mesophases, but the stability of the mesophases decreases from choline decanoate to choline octanoate due to the shortening of the alkyl chain length and the influence of the choline cation on the crystallization behavior. Choline octanoate, choline decanoate and choline oleate show a comparable thermotropic mesophase behavior. With the help of ^1H NMR and SAXS measurements two structures are evaluated in one neat surfactant phase along the whole temperature range between -50°C to 95°C. However, with these methods it could not be given a clear statement if really two structures in one phase are formed or if two phases are created along the whole temperature range which are in equilibrium with each other and thermodynamically stable or kinetically stabilized. From light microscopy only one macroscopical phase was observed. Also it could not be evaluated which compounds are available in the neat choline carboxylates. In the thesis the phase behavior was explained as

two structures in one phase of neat choline carboxylates, but also the other case could be a possible explanation.

The following main structuring could be assigned with increasing temperature: a crystalline structure with an interdigitated monolayer is created at low temperatures, a semi-crystalline interdigitated monolayer structure is formed at middle temperatures (existence of the $L_ß$ phase could be ruled out) and a liquid crystalline stucture is observed at high temperatures. It is characterized as a defective lamellar phase or a nematic phase. A lamellar bilayer is formed locally, but defects appear within the bilayers, which reduce the long range order of a smectic A lamellar phase (phase found for m = 12-18)[3]. Choline octanoate displays another phase transition to an isotropic melt. The second structure of the phase was not assigned in detail. The appearance of the defects in the lamellar structure of the main structure at high temperatures and the second structure, which exists along the whole temperature range, can result from the bulky, unsymmetrical nature of the choline cation or from the existence of a second headgroup ($-COO^-$ and –COOH) as explained in Chapter 5. It should also be concluded that the double bond in the case of choline oleate shifts all transition temperatures to lower temperatures compared to choline octadecanoate due to the hindering of the crystallization of the surfactant.

Concerning application studies, our cooperating group of Cristina Silva Pereira (Instituto de Tecnologia Química e Biológica, Universidade Nova de Lisboa) in Portugal observed that choline carboxylates, especially choline hexanoate, were very efficient in dissolution of suberin domains from cork biopolymers.[4] A further possible application could be in pharmaceutical formulations.

2. Choline alkylsulfates ChS_m with m = 12, 16

The Krafft temperature of choline hexadecylsulfate is found to be 16°C. Therefore, it is obvious that the stronger counterion-headgroup interaction, as proposed in Collins´ law of “matching water affinities”, has only slight influence on the Krafft temperature. The crystallization is more hindered by the unsymmetrical bulky structure of the choline cation. The Krafft temperature of choline dodecylsulfate was already investigated by Klein *et al.*[5] and found to be 0°C or lower. Thus, the Krafft temperature increases with chain length. Further, the *cmc*s of these choline alkylsulfates ChS_m with m = 12 (evaluated by Klein et al.[5]) and 16 are found to be slightly lower than the one of the sodium alkylsulfates. Choline as cation lowers the crystal solubility boundary in the binary water choline alkylsulfate system from 0 wt% to at least 90 wt% surfactant around 20°C compared to the sodium analogs. In

addition, no discontinuous cubic phases could be found between the micellar and the hexagonal phase, due to the stronger counterion-headgroup interaction of choline with the sulfate headgroup compared to carboxylate. In contrast to the choline carboxylates, the headgroup area could not be increased enough to create aggregates with higher curvature. With increasing surfactant concentration, the following phases appear for choline alkylsulfates: micellar phase L_1, hexagonal phase H_1, bicontinuous cubic phase V_1 (I*a*3*d*), three phasic system (I*m*3*m*, I*a*3*d* and defective lamellar) and defective lamellar or nematic phase. The phase behavior of the sodium equivalents is richer.[6-12]

As already observed for choline carboxylates, the hexagonal phase region increases and the defective lamellar or nematic phase region decreases compared to the sodium alkylsulfates [2, 6-13]. For the hexagonal phase as well as for the defective lamellar or nematic phase, it was found that the area of the polar-nonpolar interface a_s of choline alkylsulfates ChS_m with m = 12, 16 is comparable with the one of the respective phases in the binary system of choline carboxylates ChC_m with m = 12 and 16.[2] Taking Collins´ law of "matching water affinities" into account, the effective charge of the sulfate anion in the polar region of the aggregate is reduced due to the stronger interaction of choline with the sulfate headgroup compared to the carboxylate headgroup, which results in a lower sulfate headgroup repulsion. In addition, the cytotoxicity of choline alkylsulfates increases slightly with growing chain length (m = 12 to m = 16; see Chapter 6).

The thermotropic phase behavior of choline dodecylsulfate and choline hexadecylsulfate was not comparable with the one of the sodium analogs due to missing literature data. A very manifold thermotropic phase behavior in the temperature range between 0°C and 98°C was observed. Three similarities are assigned compared to the thermotropic mesomorphism of choline carboxylates: Firstly, the alkyl chains start to melt and afterwards the polar groups. Here, the melting process is more influenced by the length of the alkyl chains than by the counterion. Again, two different structures are found in one phase along the whole temperature range. The second structure presumably is characterized as a more liquid-like structure, but the detailed structure could not be evaluated. And last but not least they all melt at temperatures below 100°C to a liquid crystalline phase and are assigned as ionic liquids.

As already explained for the thermotropic phases of choline carboxylates, it could not be evaluated with the performed measurements if really only one phase of neat choline alkylsulfate exist with two structures in it or if two thermodynamically stable phases or kinetically stabilized metastable phases which are in equilibrium exist along the whole temperature range for neat choline alkylsulfates. The phase behavior of neat choline

alkylsulfate is explained in this thesis as the existence of two structures in one phase, but also the other case of two phases which are in equilibrium is a possible explanation.
The detailed structure of the main part of the phase is characterized with increasing temperature as follows: first crystalline interdigitated monolayer with tilted alkyl chains (Cr1), second crystalline interdigitated monolayer with less tilted alkyl chains (Cr2), first semi-crystalline bilayered structure with partly molten alkyl chains (CrM1), second semi-crystalline bilayered structure with more fluid alkyl chains (CrM2), but with some restrictions in flexibility, and liquid crystalline defective lamellar or nematic structure at higher temperatures with completely molten chains. The first three phase transitions are more related to the melting of the alkyl chains, while the last phase transition is referred to the melting of the polar groups. Furthermore, the melting enthalpy increases from chain length C_{12} to C_{16}.
Again, defects in the high temperature defective lamellar or nematic liquid crystalline structure and the appearance of a second more liquid like structure (or a second phase) in neat choline alkylsulfates between 0°C and 98°C are assigned. As it was already observed in the thermotropic mesomorphism of the choline carboxylates, the bulky, unsymmetrical nature of the choline cation is an obvious explanation for these structures. Further, the existence of a second headgroup, the fatty alcohol group, due to hydrolysis of alkylsulfate anion is possible. Concerning two headgroups, different curvatures can be formed and defects can be created (see Chapter 7).

Last but not least, choline alkylsulfates could be approved as a new promising class of laundry detergents. Choline alkylsulfates are suitable for application in detergency due to their low salt sensitivity, easy synthesis from natural compounds and high solubility at room temperature up to chain length m = 16. In washing tests, foam stability and foamability measurements, mixtures of choline hexadecylsulfate with choline dodecylsulfate or a common washing detergent as sodium dodecylbenzenesulfonate turned out to be very efficient washing detergents compared to the pure surfactants and also to common laundry detergents (sodium dodecylsulfate and sodium dodecylbenzenesulfonate). The mixtures featured high foamability and foam stability without lowering the washing ability. Also choline slightly improves the stabilization of the soil in the water solution, and presumably can act as cosurfactant. However, all these experiments were performed with millipore water to see the different washing behavior resulting from the surfactant properties. They should be tested also under normal washing conditions to determine the influence of the water hardness, and further, the washing tests should be conducted at room temperature (here 40°C). Additional tests should be also carried out with mixtures of longer choline alkylsulfate surfactants.

3. Deep eutectic solvents

A successful two-step strategy to create room temperature liquid, deep eutectic solvents containing low toxic bicarboxylic acids is presented. Firstly, hydrogen bond networks, which exist in systems of pure bicarboxylic acids, are simply destroyed by quantitatively exchanging protons of one carboxylic group by choline cations. This results in significantly lowered melting points. The remaining second protonated carboxylic acid group is still capable to form hydrogen bonds. These hydrogen bonds are destroyed in a second step by adding choline chloride (increasing amounts decrease viscosity of deep eutectic solvent) to the choline bicarboxylate ionic liquid.

This two step strategy towards obtaining low toxic, room temperature liquid deep eutectic solvents is found to work especially well when using glutaric acid (using 95-98 wt% choline glutarate in the mixture choline glutarate/choline chloride). Highly viscous and liquid deep eutectic solvents at room temperature were created. Succinic acid and adipic acid did not show satisfactory results. The mixtures were not completely liquid at room temperature.

In addition, it was demonstrated that the addition of a second hydrogen bond donor (urea) increases the viscosity of choline glutarate/choline chloride deep eutectic solvents. As deduced from a Walden plot, fully dissociated anions and cations could be postulated and the deep eutectic solvents can be ranked as “good” ionic liquids according to the classification introduced by Angell et al..[14, 15] For a lower viscosity, it would be desirable to prepare deep eutectic solvents with oxalic or malonic acid according to this strategy. It was further demonstrated that choline dodecylsulfate is capable to form aggregates in this deep eutectic mixtures. Therefore, an application in surfactant formulation is possible. A further application could be in pharmaceutical formulations, as it is already approved for other deep eutectic solvents.[16]

As it could be shown in this work, choline is a desirable counterion of biological origin which can be used to created low toxic, biodegradable surfactants, ionic liquids and deep eutectic mixtures. All studies used choline as bulky, unsymmetrical cation of biological origin to lower the melting/Krafft temperatures of these substances and to widen their field of application. This strategy is a useful concept transferable to the design of further new promising, biocompatible substances.

10.1 References

1. R. Klein, D. Touraud and W. Kunz, *Green Chem.*, 2008, **10**, 433.
2. R. Klein, G. J. T. Tiddy, E. Maurer, D. Touraud, J. Esquena, O. Tache and W. Kunz, *Soft Matter*, 2011, **7**, 6973.
3. R. Klein, H. Dutton, O. Diat, G. J. Tiddy and W. Kunz, *J. Phys. Chem. B*, 2011, **115**, 3838-3847.
4. H. Garcia, R. Ferreira, M. Petkovic, J. L. Ferguson, M. C. Leitao, H. Q. N. Gunaratne, K. R. Seddon, L. P. N. Rebelo and C. S. Pereira, *Green Chem.*, 2010, **12**, 367-369.
5. R. Klein, M. Kellermeier, D. Touraud, E. Müller and W. Kunz, *J. Colloid Interface Sci.*, 2013**, 392**, 274-80.
6. P. Kékicheff, *J. Colloid Interface Sci.*, 1989, **131**, 133-152.
7. P. Kekicheff and B. Cabane, *Acta Crystallogr. B*, 1988, **44**, 395-406.
8. P. Kékicheff and B. Cabane, *J. Phys. France*, 1987, **48**, 1571-1583.
9. H. Delacroix, T. Gulik-Krzywicki, P. Mariani and V. Luzzati, *J. Mol. Biol.*, 1993, **229**, 526-539.
10. P. V. Luzzati, H. Mustacchi, A. Skoulios and F. Husson, *Acta Cryst.*, 1960, **13**, 660-667.
11. P. F. Husson, H. Mustacchi and V. Luzzati, *Acta Cryst.*, 1960, **13**, 668-677.
12. N. V. Usol´tseva, N. M. Kormilitsyn and L. N. Zhukova, *Koloidnyi Zhurnal*, 1989, **51**, 601-603.
13. D. Rengstl, O. Diat, R. Klein and W. Kunz, *Langmuir*, 2013, **29**, 2506-2519.
14. M. Yoshizawa, W. Xu and C. A. Angell, *J. Am. Chem. Soc.*, 2003, **125**, 15411-15419.
15. W. Xu, E. I. Cooper and C. A. Angell, *J. Phys. Chem. B*, 2003, **107**, 6170-6178.
16. H. G. Morrison, C. C. Sun and S. Neervannan, *Int. J. Pharm.*, 2009, **378**, 136-139.

Appendix A Effect of choline carboxylate ionic liquids on biological membranes

A.1 HeLa dose-response curves

Each of these curves represents one of the three to five dose-response curves established over several months for each substance with the HeLa cell line.

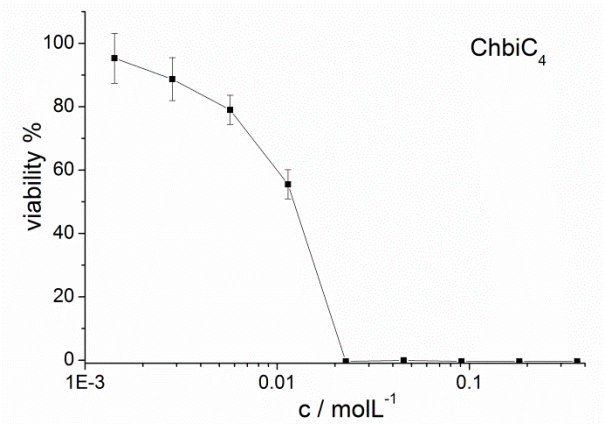

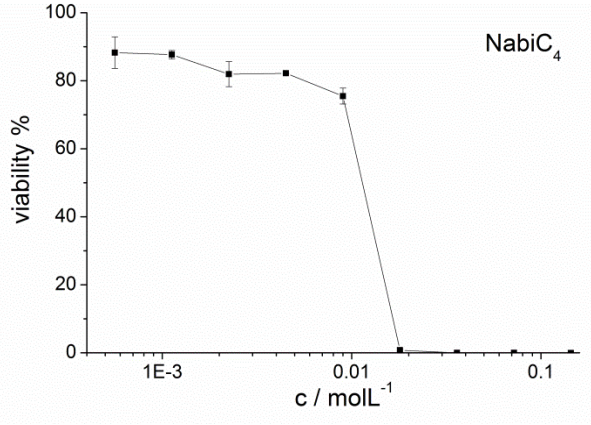

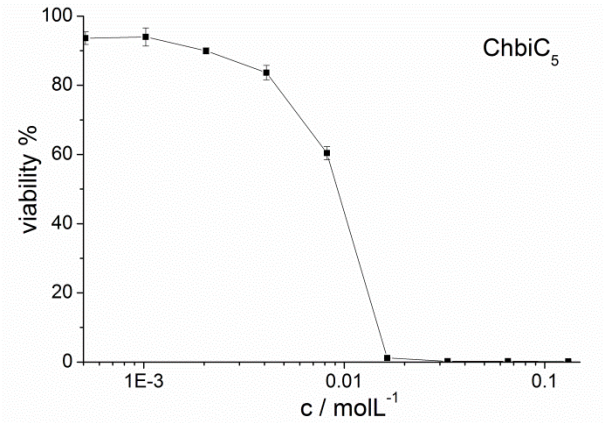

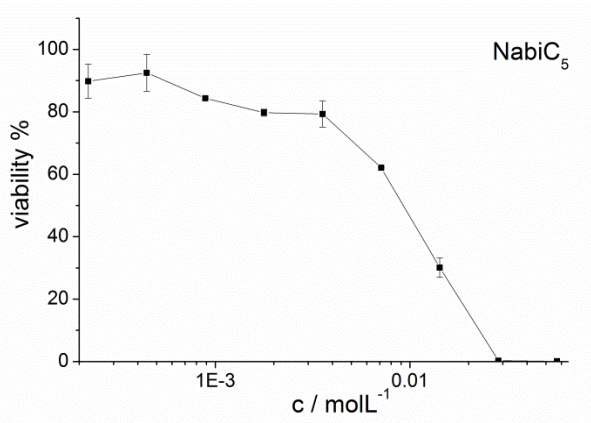

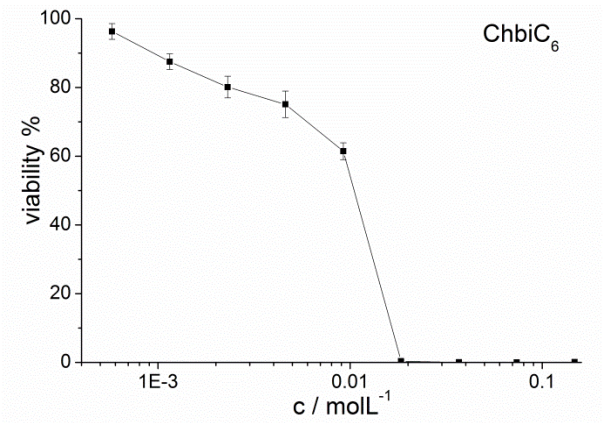
ChbiC6
viability %
c / molL-1
1E-3
0.01
0.1

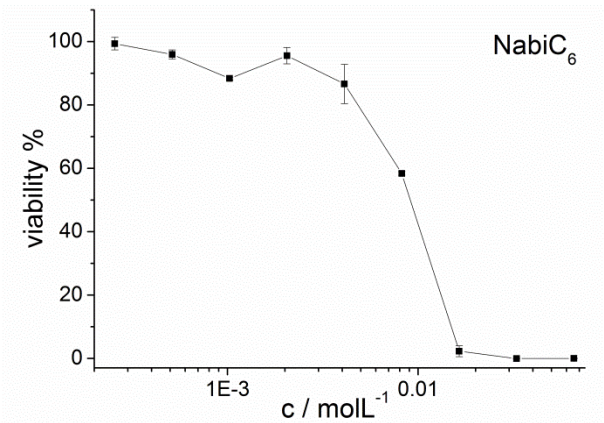
NabiC6
viability %
c / molL-1
1E-3
0.01

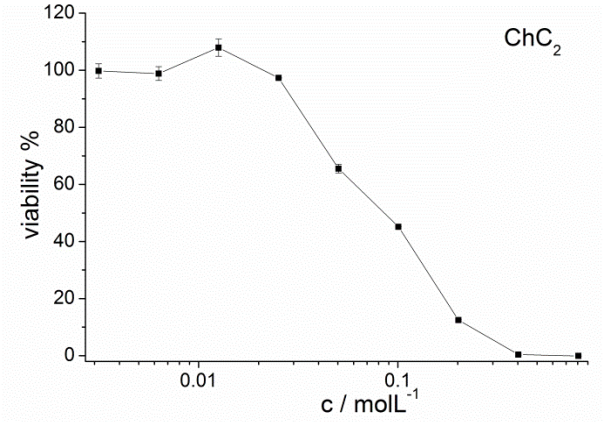
ChC2
viability %
c / molL-1
0.01
0.1

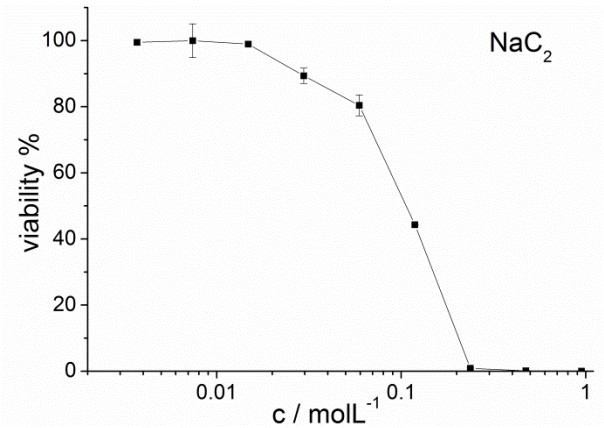
NaC2
viability %
c / molL-1
0.01
0.1
1

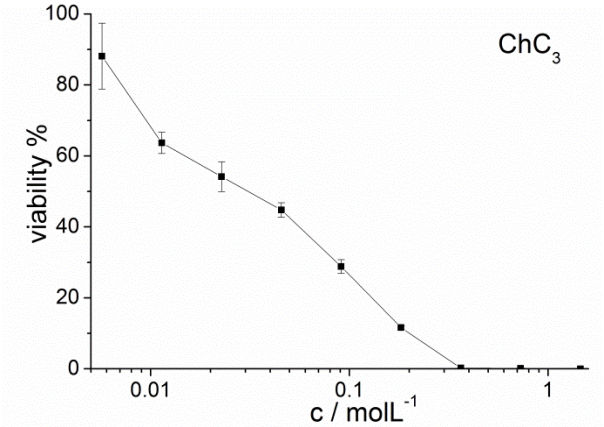
ChC3
viability %
c / molL-1
0.01
0.1
1

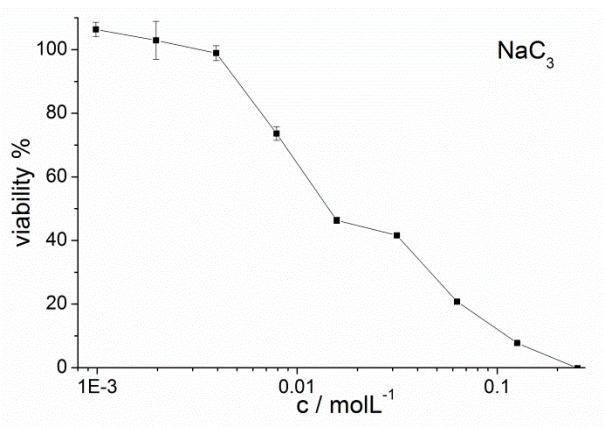
NaC3
viability %
c / molL-1
1E-3
0.01
0.1

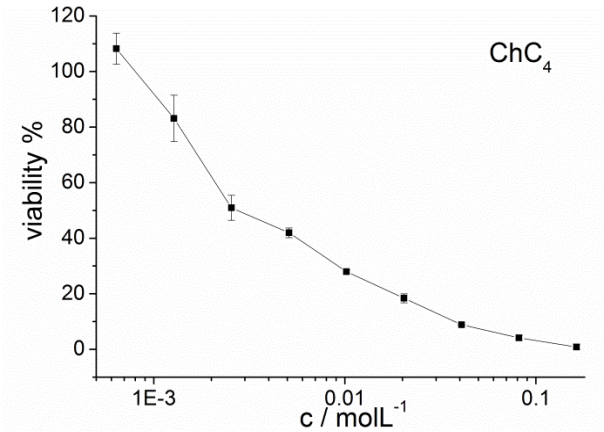
ChC4
viability %
c / molL-1
1E-3
0.01
0.1

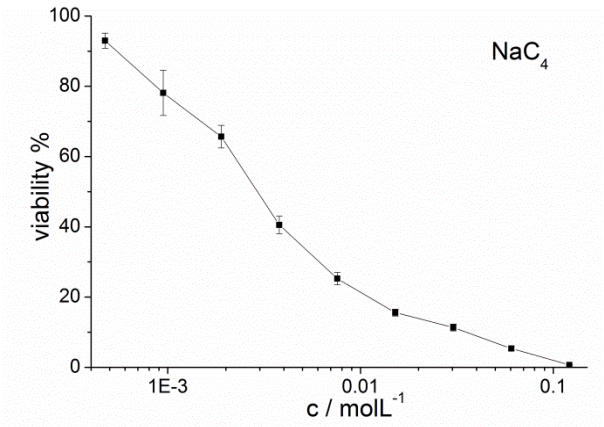
NaC4
viability %
c / molL-1
1E-3
0.01
0.1

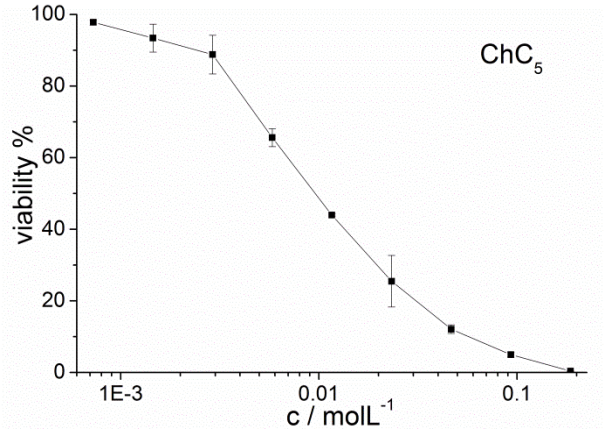
ChC5
viability %
c / molL-1
1E-3
0.01
0.1

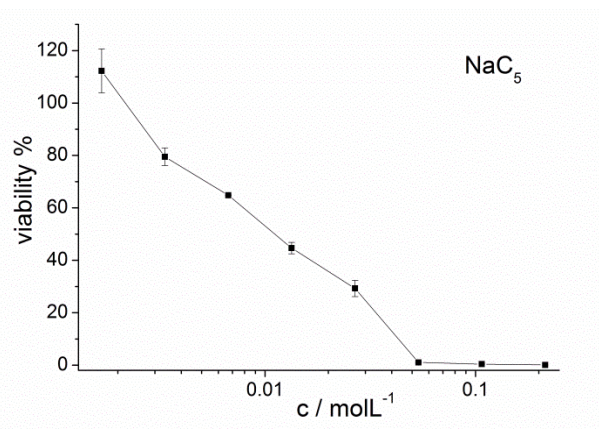
NaC5
viability %
c / molL-1
0.01
0.1

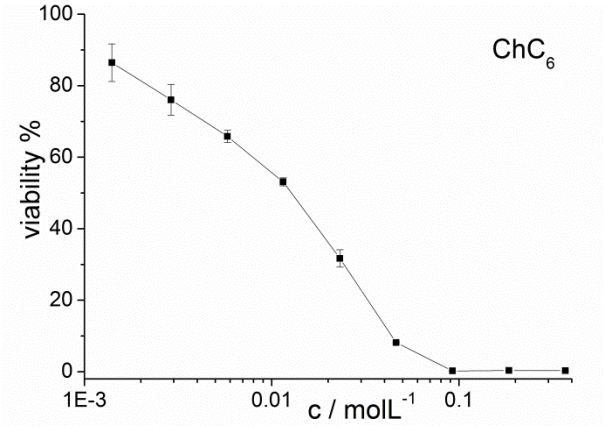
ChC6
viability %
c / molL-1
1E-3
0.01
0.1

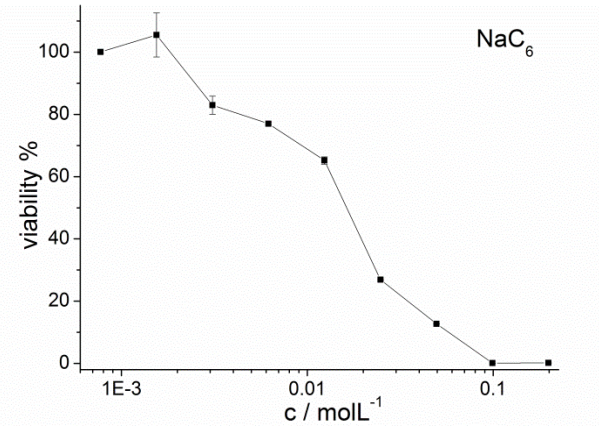
NaC6
viability %
c / molL-1
1E-3
0.01
0.1

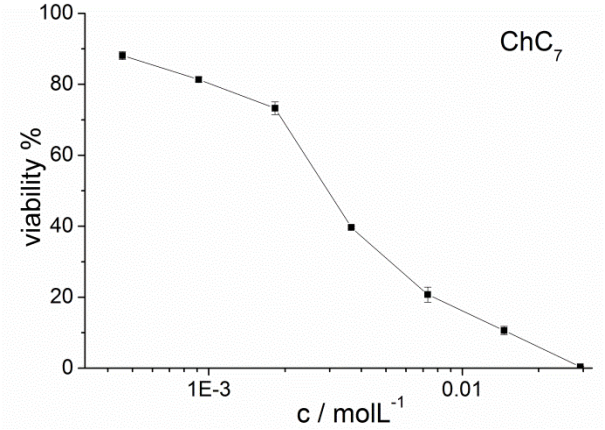
ChC7
viability %
c / molL-1
1E-3
0.01

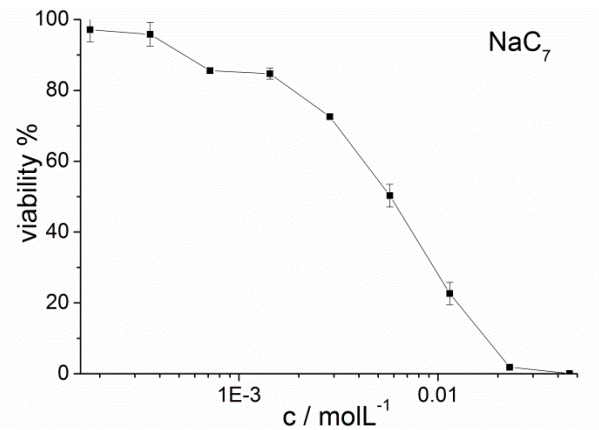
NaC7
viability %
c / molL-1
1E-3
0.01

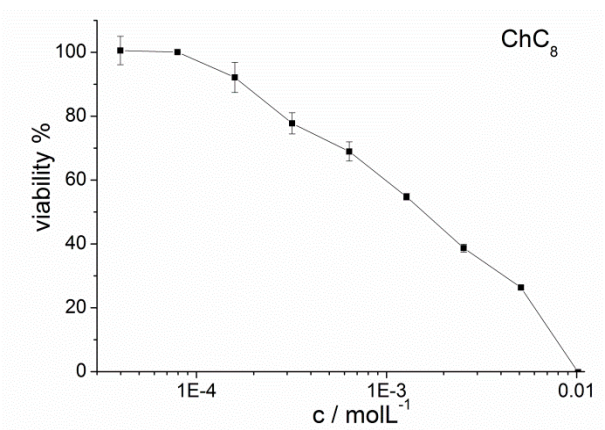
ChC8
viability %
c / molL-1
1E-4
1E-3
0.01

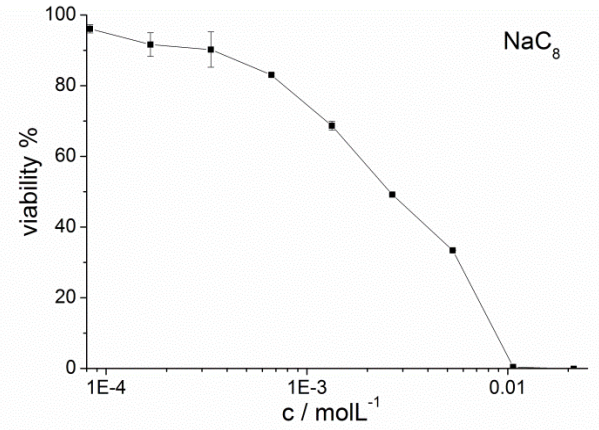
NaC8
viability %
c / molL-1
1E-4
1E-3
0.01

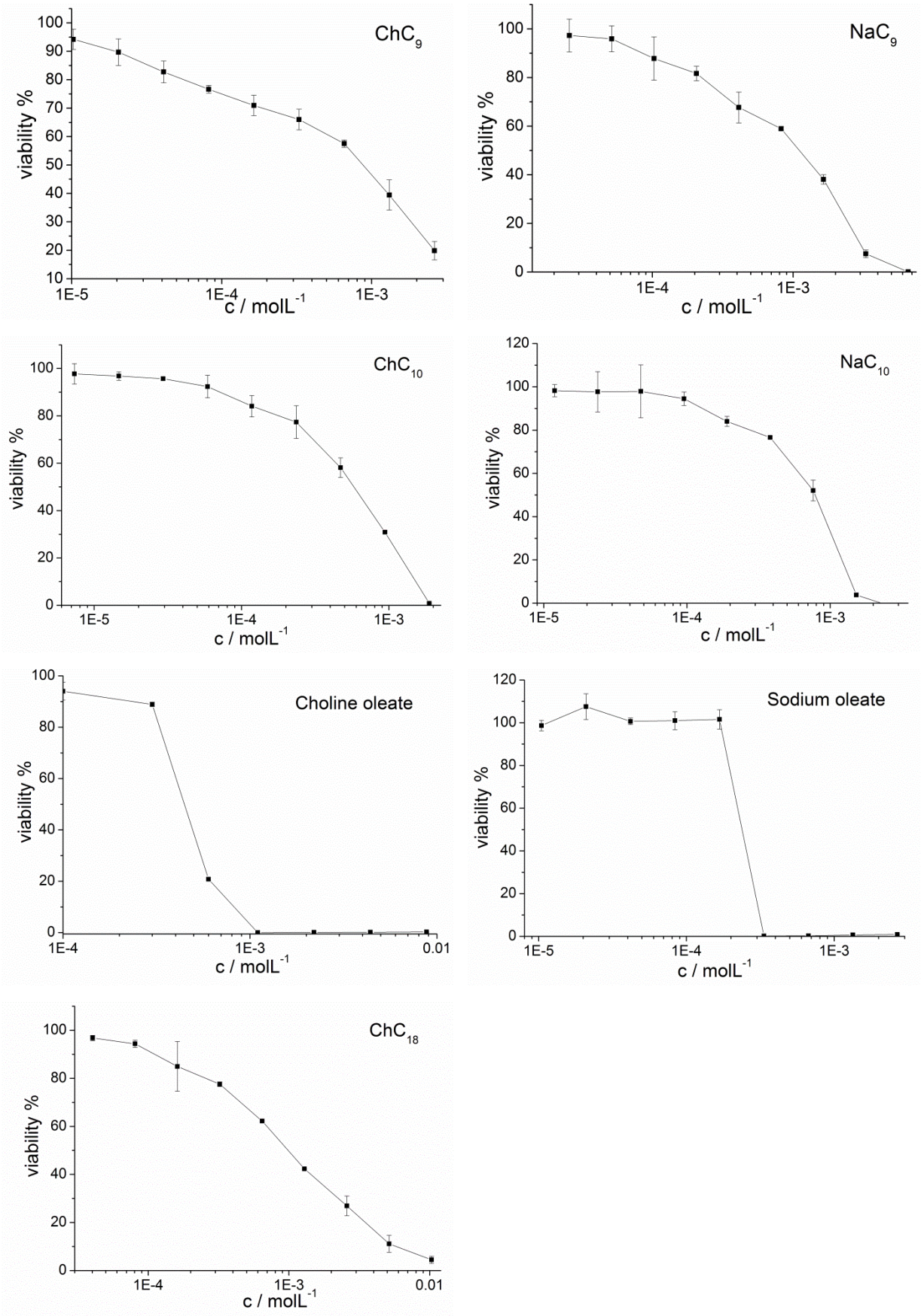

Figure A1-1. The diagrams show the dose-response curves of the different choline carboxylates ChC_m with m = 2-10, 18 and oleate and choline bicarboxylates $ChbiC_m$ with m = 4, 5, 6 and the ones of their respective sodium salts obtained with HeLa cells.

A.2 SK-MEL-28 dose-response curves

Each of these curves represents one of the three to five dose-response curves established over several months for each substance with the SK-MEL-28 cell line.

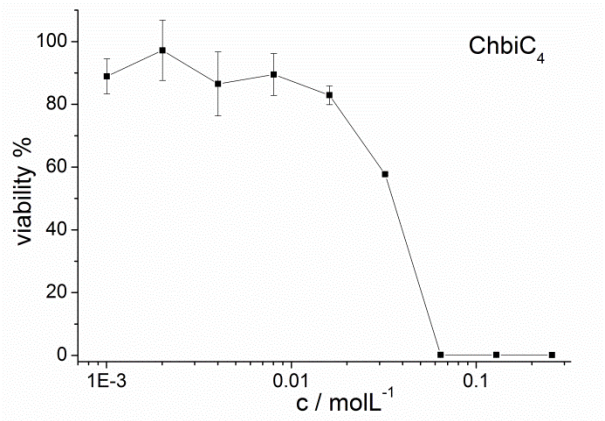

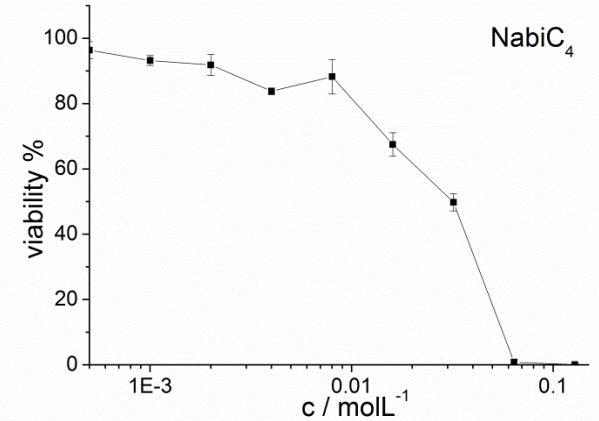

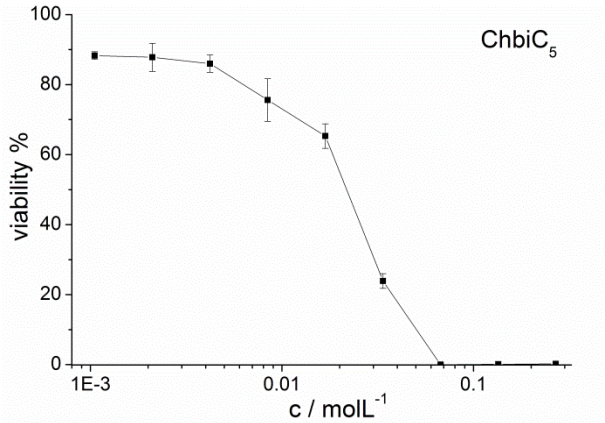

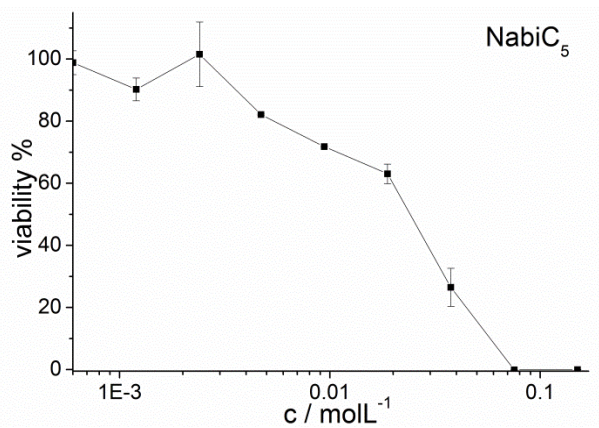

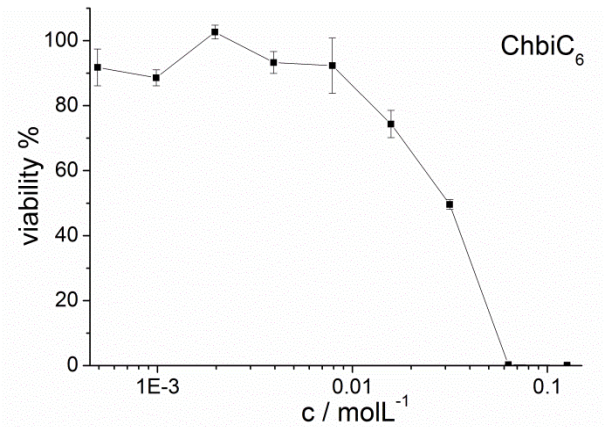

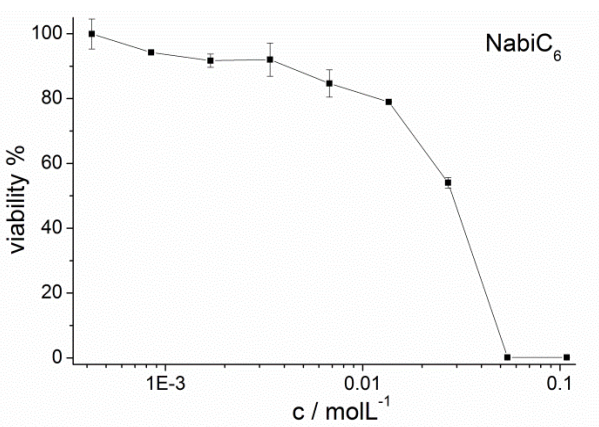

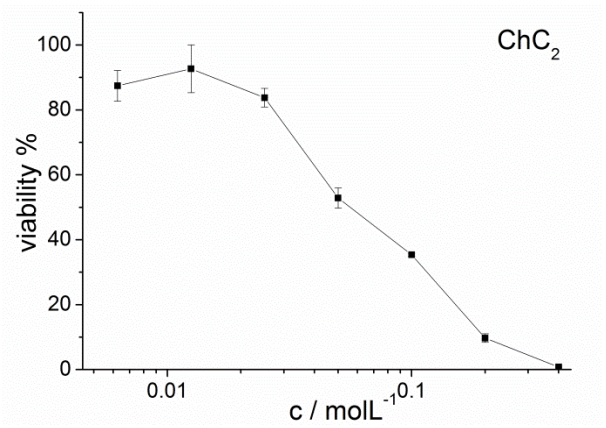
ChC2
viability %
c / molL-1

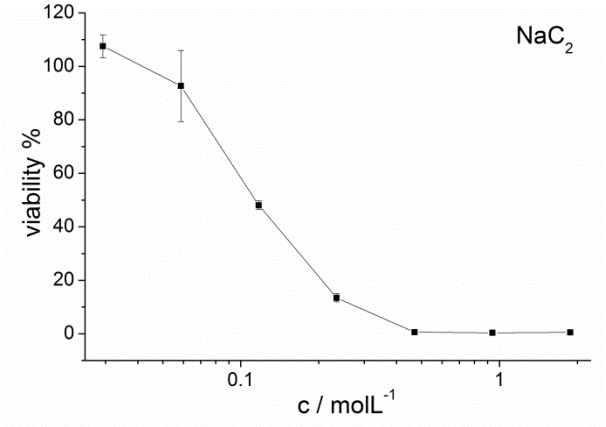
NaC2
viability %
c / molL-1

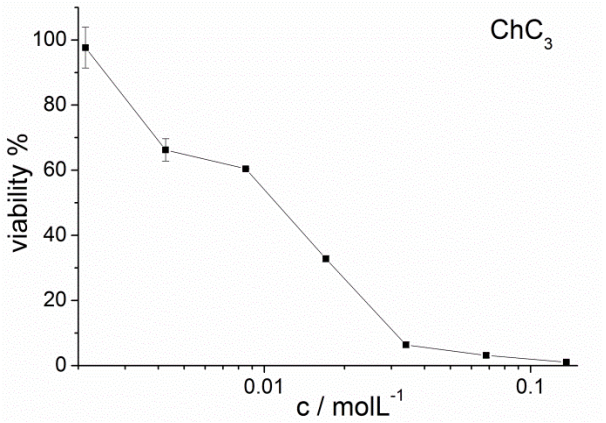
ChC3
viability %
c / molL-1

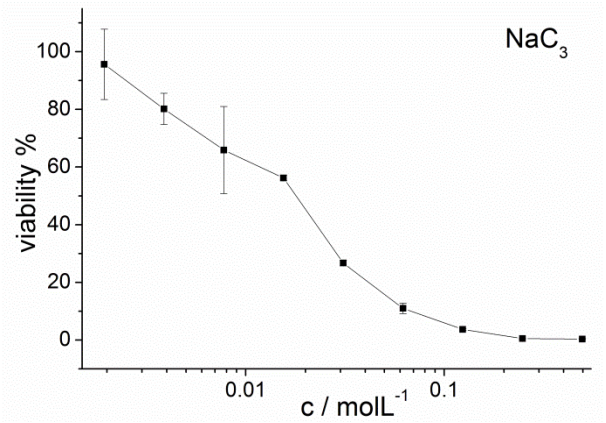
NaC3
viability %
c / molL-1

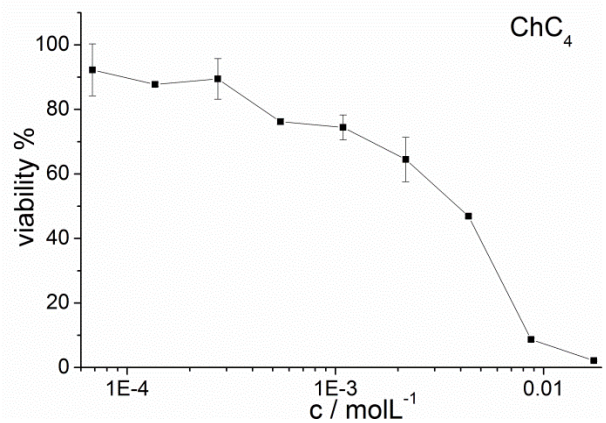
ChC4
viability %
c / molL-1

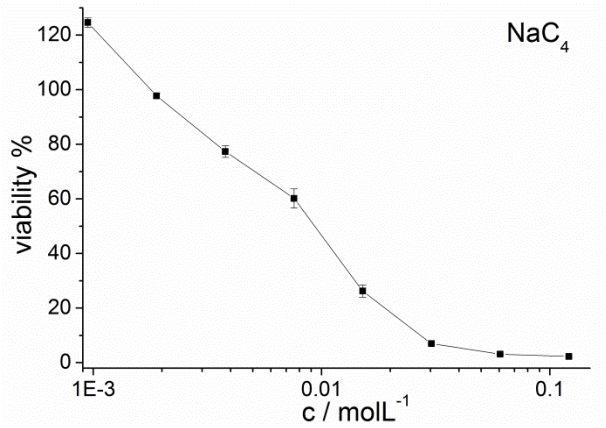
NaC4
viability %
c / molL-1

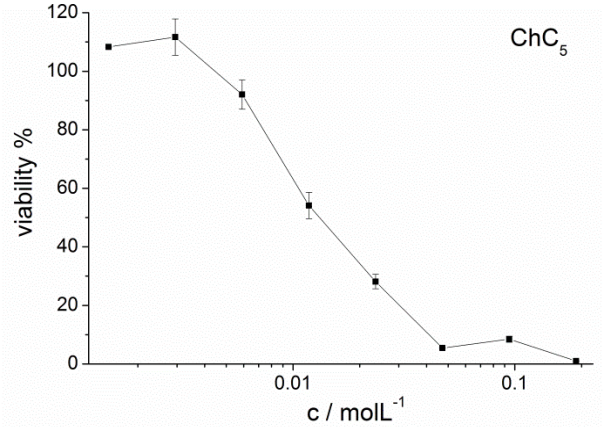
ChC5
viability %
c / molL-1

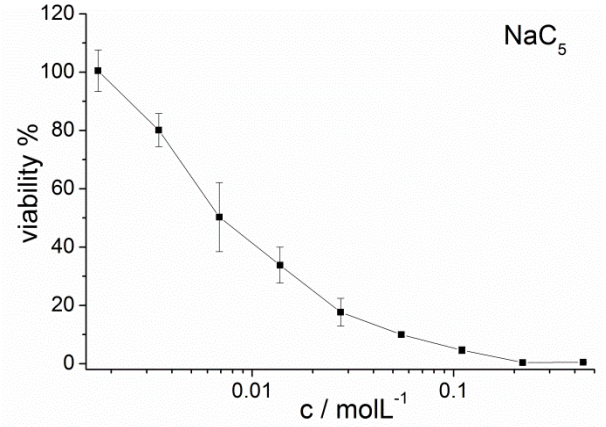
NaC5
viability %
c / molL-1

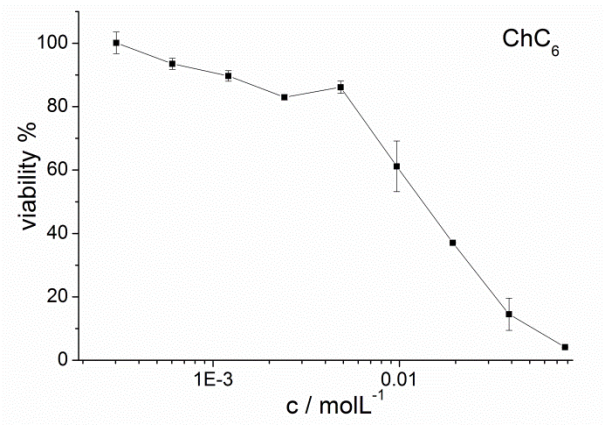
ChC6
viability %
c / molL-1
1E-3
0.01

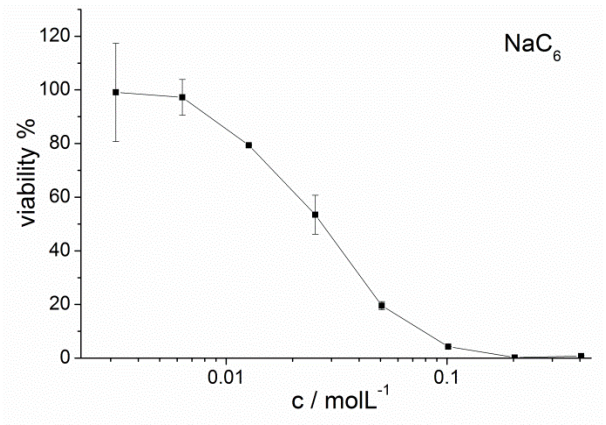
NaC6
viability %
c / molL-1
0.01
0.1

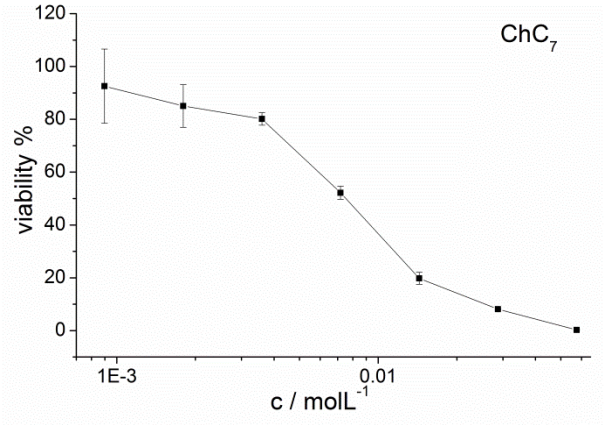
ChC7
viability %
c / molL-1
1E-3
0.01

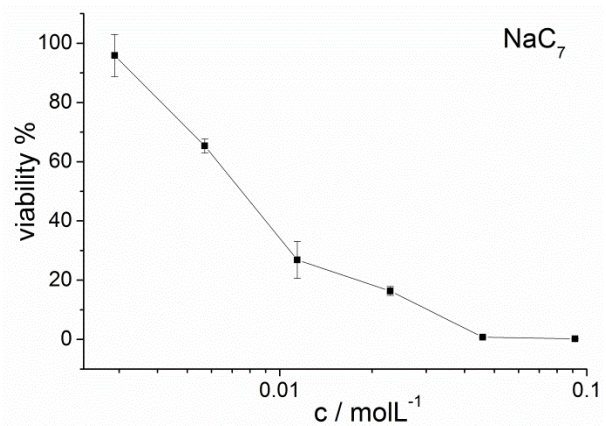
NaC7
viability %
c / molL-1
0.01
0.1

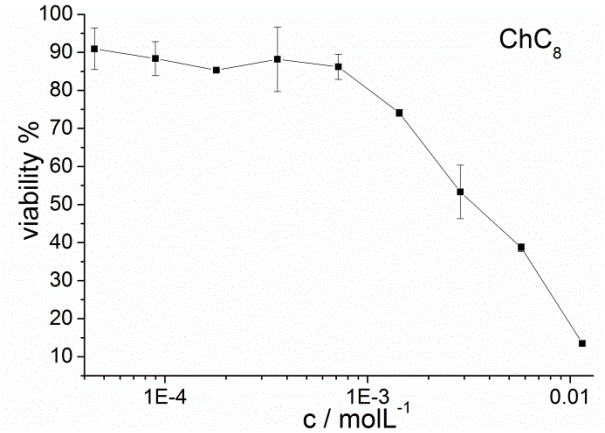
ChC8
viability %
c / molL-1
1E-4
1E-3
0.01

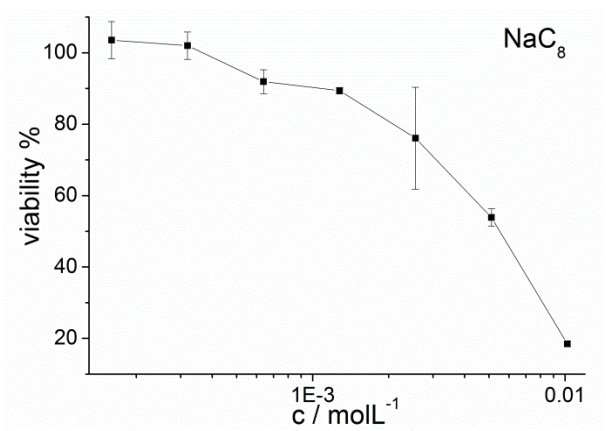
NaC8
viability %
c / molL-1
1E-3
0.01

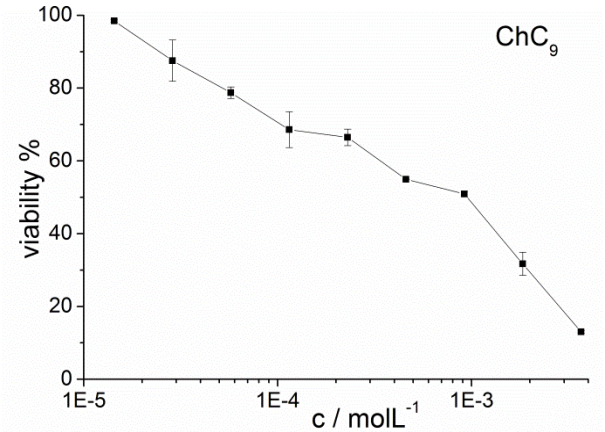
ChC9
viability %
c / molL-1
1E-5
1E-4
1E-3

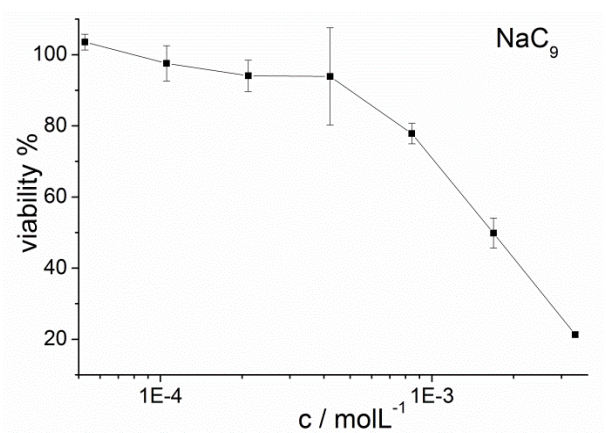
NaC9
viability %
c / molL-1
1E-4
1E-3

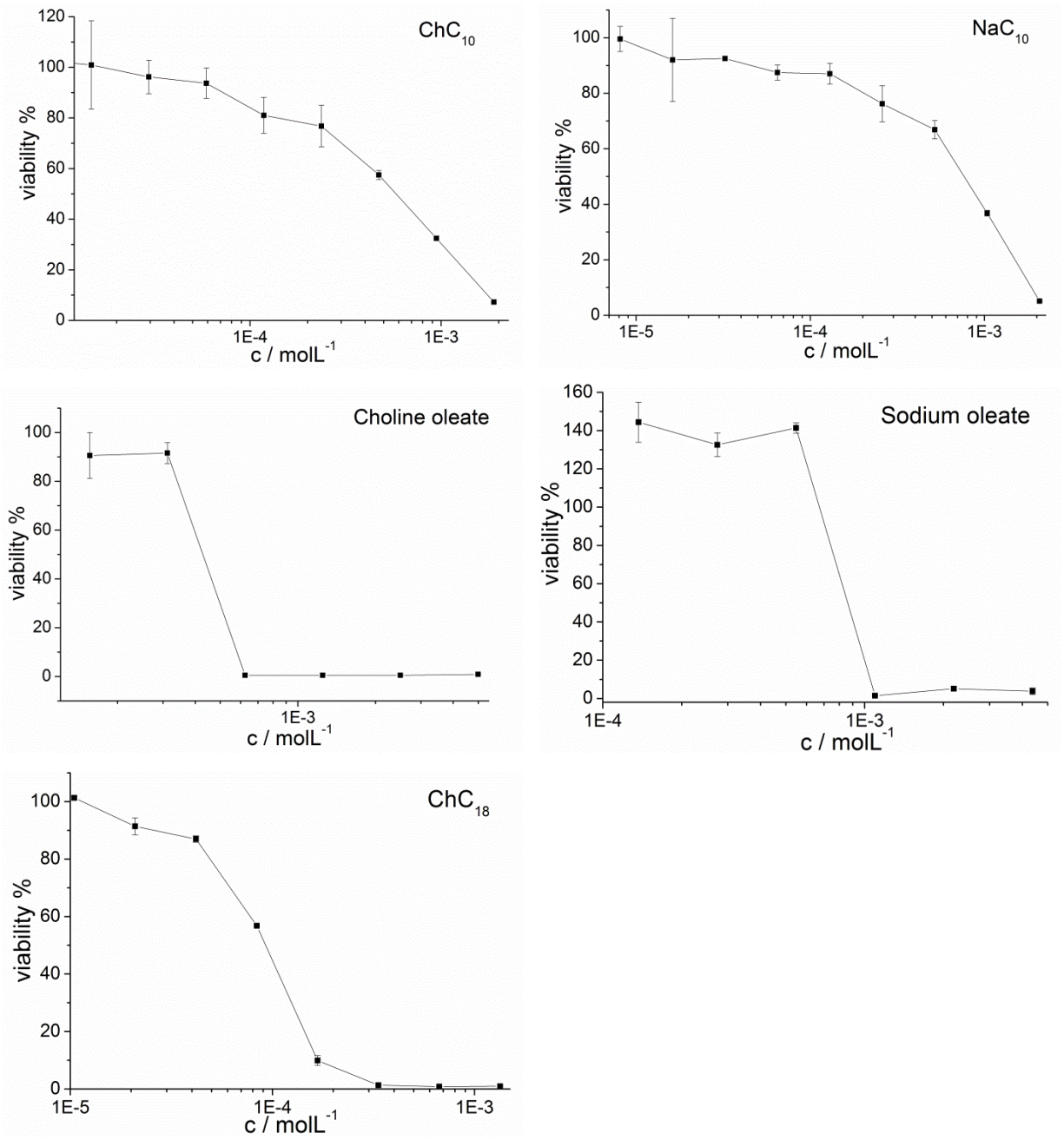

Figure A2-1. The diagrams show the dose-response curves of the different choline carboxylates ChC_m with m = 2-10, 18 and oleate and the different choline bicarboxylates $ChbiC_m$ with m = 4, 5, 6 and the ones of their respective sodium salts obtained with SK-MEL-28 cells.

Appendix B Influence of chain length and double bond on the aqueous behavior of choline carboxylate soaps

B.1 Small (SAXS) and wide (WAXS) angle X-ray scattering

B.1.1 Discontinuous cubic phase I_1' with structure type $P6_3/mmc$

This discontinuous cubic phase I_1' was only observed in the binary phase diagram of choline decanoate.

	Discontinuous cubic I_1' - ChC_{10}	
wt%	40	43.8
d_{100} / Å	35.5	35.4
d_{002} / Å	-	-
d_{101} / Å	-	-
d_{102} / Å	24.7	24.4
d_{110} / Å	20.4	20.4
d_{103} / Å	18.8	18.8
d_{112} / Å	17.3	17.2

Table B1-1. X-ray diffraction data of the discontinuous cubic phase I_1' measured for different choline decanoate concentrations at 25°C. The experimental d-values are given with the corresponding Miller indices.

B.1.2 Discontinuous cubic phase I_1'' with structure type P*m*3*n*

The P*m*3*n* discontinuous cubic phase shows the following X-ray pattern: $\sqrt{2}:\sqrt{4}:\sqrt{5}:\sqrt{6}:\sqrt{8}$. It is only observed in the binary phase diagram of choline decanoate. **Table B1-2.** contains the X-ray diffraction data and the corresponding Miller indices and **Figure B1-1.** the respective X-ray spectra of the discontinuous cubic phase I_1'', which is measured for different concentrations of choline decanoate samples.

	Discontinuous cubic $I_1^{''}$ - ChC_{10}		
wt%	45.9	51.8	53.9
d_{110} / Å	57.1	55.0	54.4
d_{200} / Å	40.3	38.9	38.5
d_{210} / Å	36.0	34.8	34.4
d_{211} / Å	32.9	31.7	31.4
d_{220} / Å	28.5	27.5	27.2
d_{310} / Å	25.5	-	24.3
d_{222} / Å	23.4	22.4	22.2
d_{320} / Å	22.4	21.6	21.3
d_{321} / Å	21.6	20.8	20.6
d_{400} / Å	-	19.5	-
A / Å	80.7 ± 0.1	77.8 ± 0.1	76.9 ± 0
Φs	0.460	0.519	0.540
N_{agg}	66	66	67
T / °C	25	25	25

Table B1-2. X-ray diffraction data of the discontinuous cubic phase $I_1^{''}$ obtained for different choline decanoate concentrations at 25°C. The experimental d-values are given with the corresponding Miller indices.

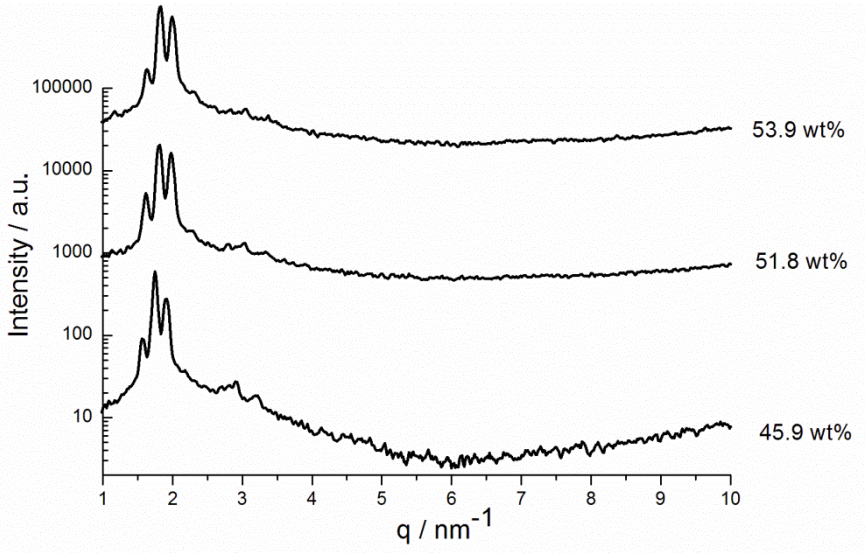

Figure B1-1. SAXS spectra of the discontinuous cubic phase $I_1^{''}$ obtained for differently concentrated samples of choline decanoate at 25°C.

B.1.3 Hexagonal phase H_1

B.1.3.1 SAXS data and calculated parameter

	Hexagonal – H_1										
	wt%	**d_{100} / Å**	**d_{110} / Å**	**d_{200} / Å**	**d_{210} / Å**	**d_{300} / Å**	**d_{220} / Å**	**d_{310} / Å**	**a / Å**	**Φs**	**$Φ_L$**
ChC_8 at 25°C	69.8	25.6	14.8	-	9.8	8.7	7.5	-	29.8 ± 0.3	0.694	0.371
	70.8	25.4	14.4	12.5	9.4	8.3	7.2	6.9	28.9 ± 0.2	0.704	0.376
	73.8	24.9	14.2	12.3	9.3	-	-	-	28.6 ± 0.1	0.734	0.392
	86.0	23.6	13.6	11.8	8.9	7.8	-	-	27.2 ± 0.1	0.858	0.458
	88.0	23.4	13.5	11.6	8.8	7.8	-	-	26.9 ± 0	0.878	0.469
	90.0	23.1	13.3	11.5	8.7	7.7	-	-	26.7 ± 0	0.898	0.480
	91.1	23.0	13.2	11.4	-	7.6	-	-	26.4 ± 0.1	0.909	0.486
	92.0	22.9	13.2	11.4	-	7.6	-	-	26.4 ±0	0.918	0.491
	94.9	22.6	13.0	11.2	-	8.5	-	-	26.0 ± 0.1	0.948	0.507
ChC_{10} at 25°C	60.0	31.2	18.0	15.6	11.8	10.4	-	-	36.1 ± 0	0.601	0.352
	65.0	31.0	17.9	15.5	11.8	-	8.9	-	35.8 ± 0.1	0.651	0.381
	72.0	29.7	17.2	14.9	11.2	9.9	8.6	-	34.3 ± 0.1	0.721	0.422
	74.9	29.2	16.9	14.4	11.0	-	-	-	33.6 ± 0.2	0.750	0.439
	80.0	28.9	16.7	14.6	10.9	9.7	-	-	33.5 ± 0.1	0.800	0.469
	82.8	28.8	16.5	14.3	-	-	-	-	33.1 ± 0.1	0.828	0.485
ChC_{10} at 85°C	65.0	28.7	16.6	14.4	-	-	-	-	33.2 ± 0	0.651	0.381
	80.0	28.1	16.2	14.1	10.8	9.4	-	-	32.6 ± 0.2	0.800	0.469
Ch-oleate at 25°C	27.4	70.1	40.3	34.9	26.4	23.3	20.2	19.4	69.9 ± 0.1	0.279	0.205
	28.0	69.4	39.9	34.5	26.1	22.8	19.8	19	68.9 ± 0.3	0.285	0.210
	31.0	66.1	38.2	33.1	25.2	22.0	-	-	66.3 ± 0.3	0.316	0.232
	32.4	65.1	38.3	33.1	24.8	21.7	19.3	18.2	65.8 ± 0.6	0.330	0.242
	35.0	62.9	36.3	31.4	-	-	18.2	17.5	62.9 ± 0	0.356	0.262
	44.9	56.1	31.9	27.6	20.8	18.4	15.9	-	55.3	0.455	0.335

									± 0.4		
	54.8	51.1	28.6	24.7	18.7	16.5	14.3	13.7	49.7 ± 0.4	0.554	0.408
	66.0	46.9	27.1	23.4	17.7	15.6	13.5	13.0	46.9 ± 0	0.666	0.490
	67.4	46.5	26.5	22.9	17.3	15.3	13.3	12.7	46.0 ± 0.2	0.680	0.500
	68.8	46.2	26.7	23.1	17.5	15.4	13.3	12.8	46.2 ± 0	0.694	0.510
Ch-oleate at 55°C	28.0	67.2	38.8	33.6	25.4	22.4	-	-	67.2 ± 0.1	0.285	0.210
	31.0	62.8	36.3	31.4	24.0	20.9	18.2	17.5	63.0 ± 0.2	0.316	0.232

Table B1-3. X-ray diffraction data of the hexagonal phases of ChC_8, ChC_{10} and choline oleate (Choleate) at different temperatures. The table comprises the Miller indices, unit cell parameter a, volume fraction of surfactant Φ_s and volume fraction of the lipophilic part Φ_L of the hexagonal phase.

B.1.3.2 SAXS spectra

B.1.3.2.1 Choline octanoate at 25°C

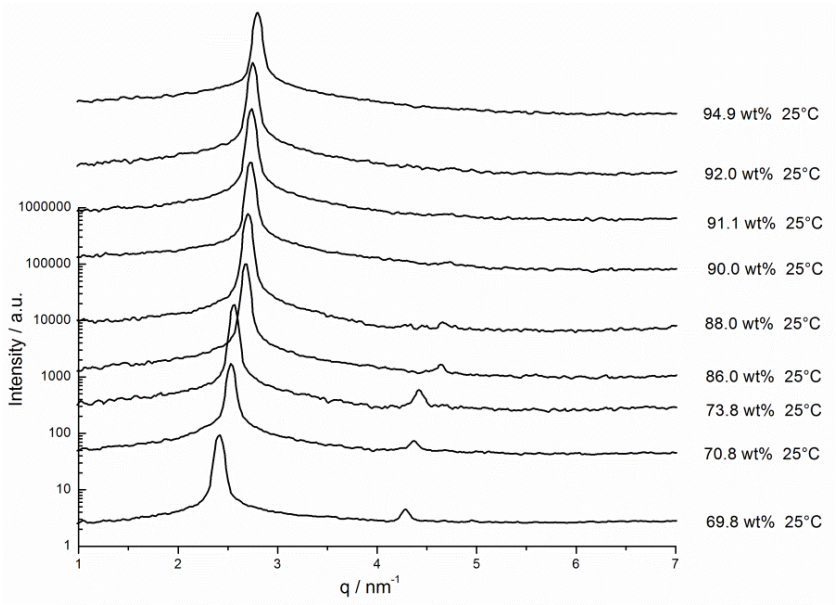

B.1.3.2.2 Choline decanoate at 25°C and 85°C

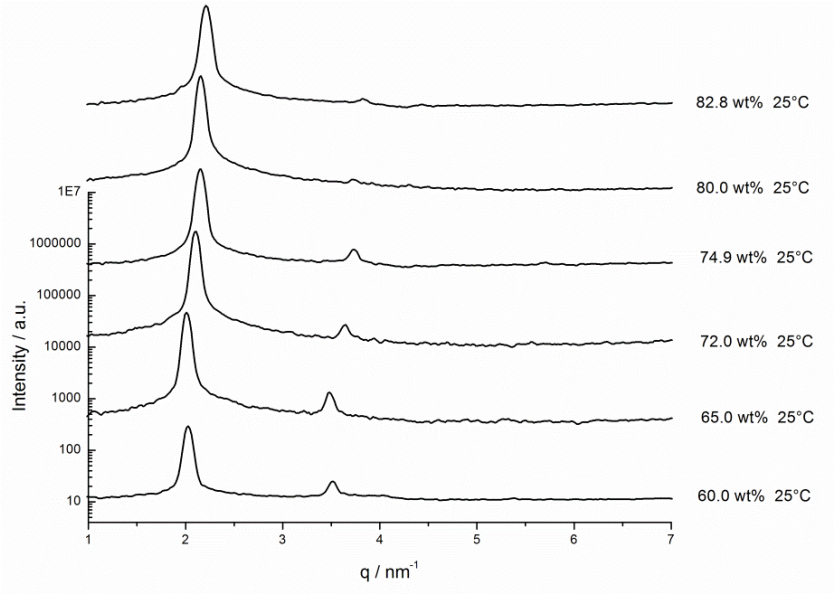

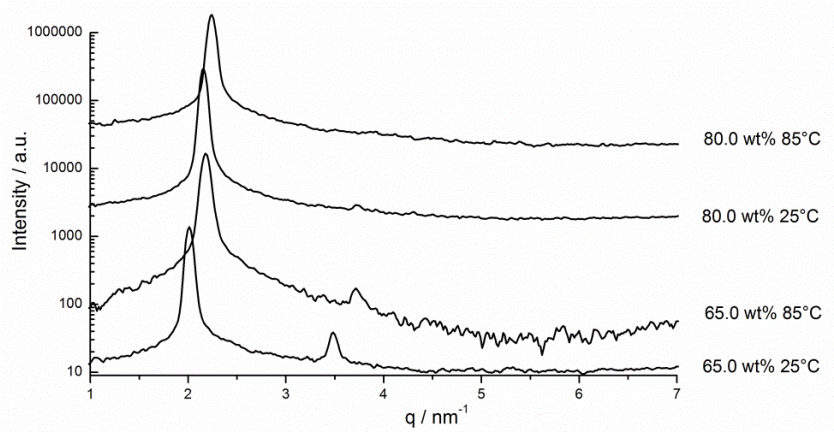

B.1.3.2.3 Choline oleate at 25°C and 55°C

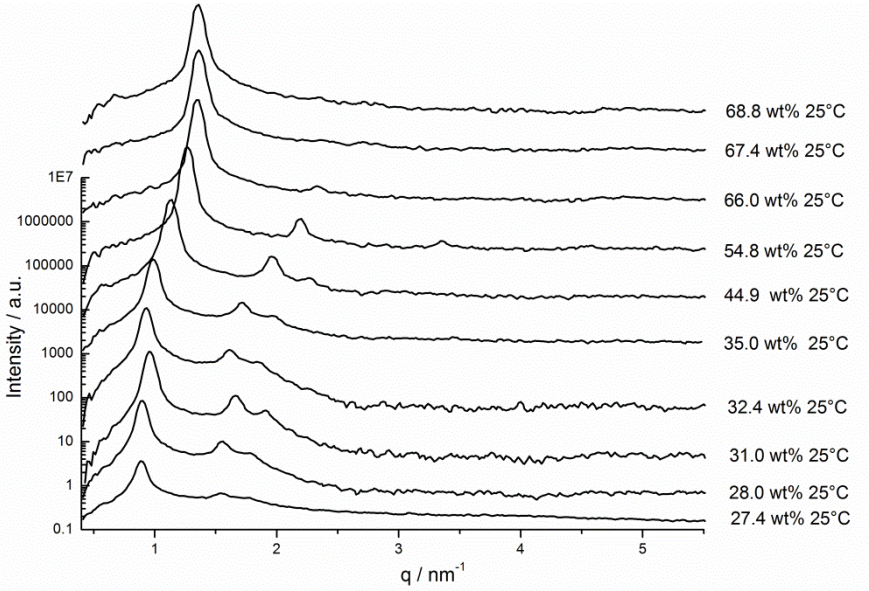

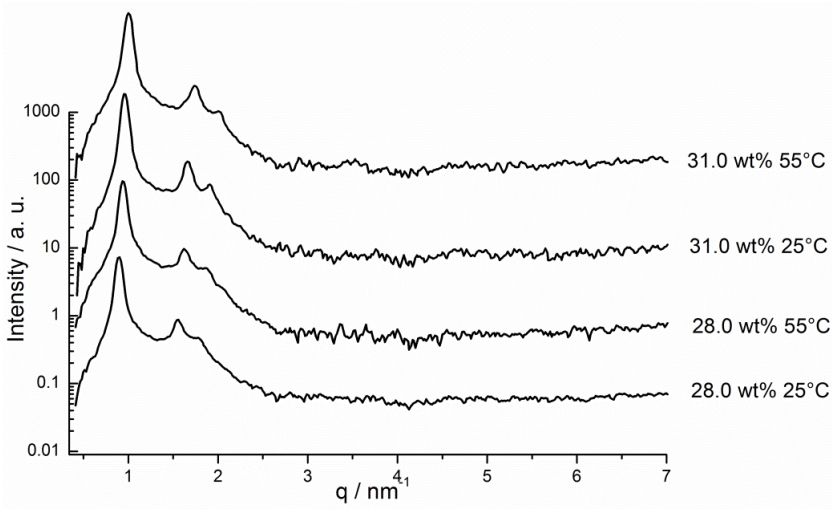

In the case of choline oleate the existence of a hexagonal complex, a rectangular or hexagonal deformed phase was ruled out. The Miller indices of these phase types do not fit with the experimental data.[1, 2]

B.1.4 Bicontinuous cubic phase V_1 with I*a*3*d* structure

B.1.4.1 SAXS data and calculated parameter

	Bicontinuous cubic V_1 with I*a*3*d* structure								
	wt%	**d_{211} / Å**	**d_{220} / Å**	**d_{321} / Å**	**d_{400} / Å**	**d_{420} / Å**	**d_{332} / Å**	**a / Å**	**Φs**
ChC_{10} at 25°C	85.0	29.0	25.1	-	-	15.9	15.1	71.0 ± 0	0.850
	90.0	27.2	23.5	17.7	-	-	-	66.5 ± 0.2	0.900
	92.3	27.0	23.5	17.7	16.6	-	-	66.3 ± 0.1	0.923
	95.0	25.8	22.3	16.9	15.8	-	-	63.2 ± 0	0.950
Ch-oleate at 25 °C	70.0	42.7	37.2	28.0	26.2	23.4	22.3	104.8 ± 0.2	0.705
	72.4	44.6	38.8	-	-	-	-	109.4 ± 0.4	0.729
Ch-oleate at 80 °C	66.0	42.7	37.0	28.0	-	23.4	22.4	104.8 ± 0.2	0.666
	67.4	42.5	37.0	27.8	-	23.4	22.2	104.3 ± 0.2	0.680
	68.8	42.4	36.7	27.7	26.0	23.3	22.1	103.8 ± 0.1	0.694
	70.0	42.1	36.4	27.5	25.8	23.3	21.7	103.0 ± 0.8	0.705

Table B1-4. X-ray diffraction data of the bicontinuous cubic phase with I*a*3*d* structure of ChC_{10} and Choleate at different temperatures are presented. The Miller indices, unit cell parameter a and volume fraction of surfactant Φ_s of the bicontinuous cubic phase V_1 are comprised in the table.

B.1.4.2 SAXS spectra

B.1.4.2.1 Choline decanoate at 25°C

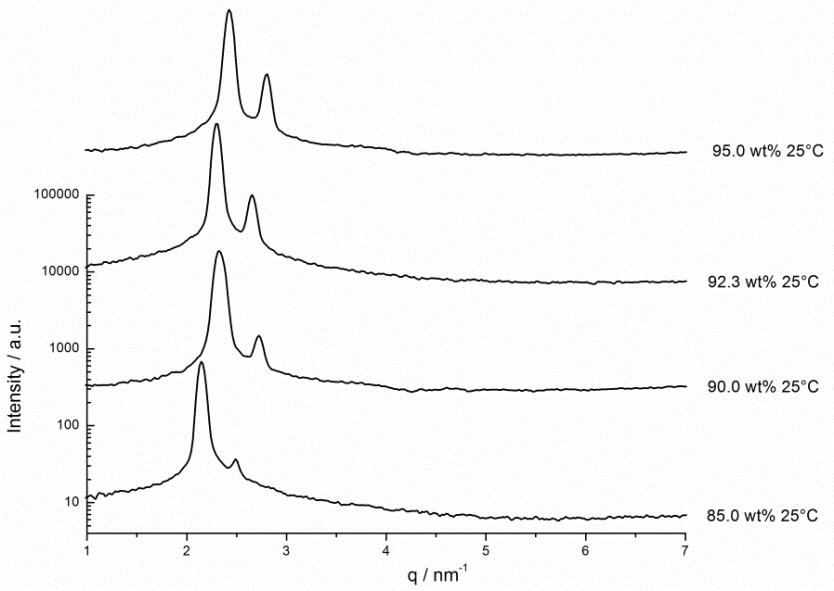

B.1.4.2.2 Choline oleate at 25°C and 80°C

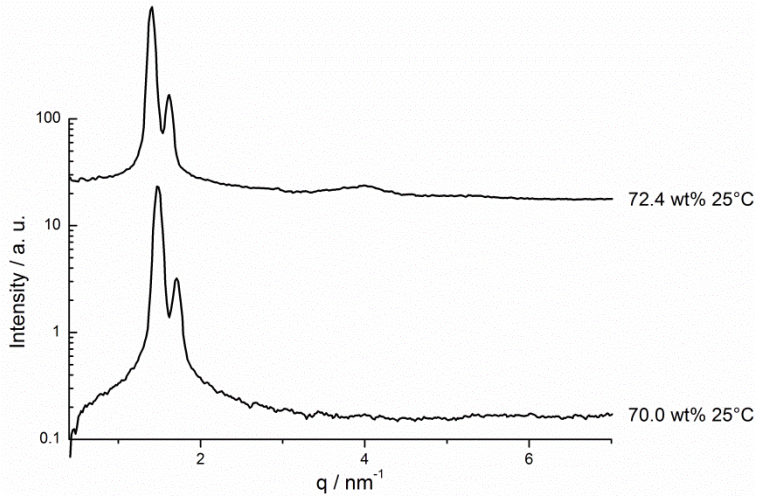

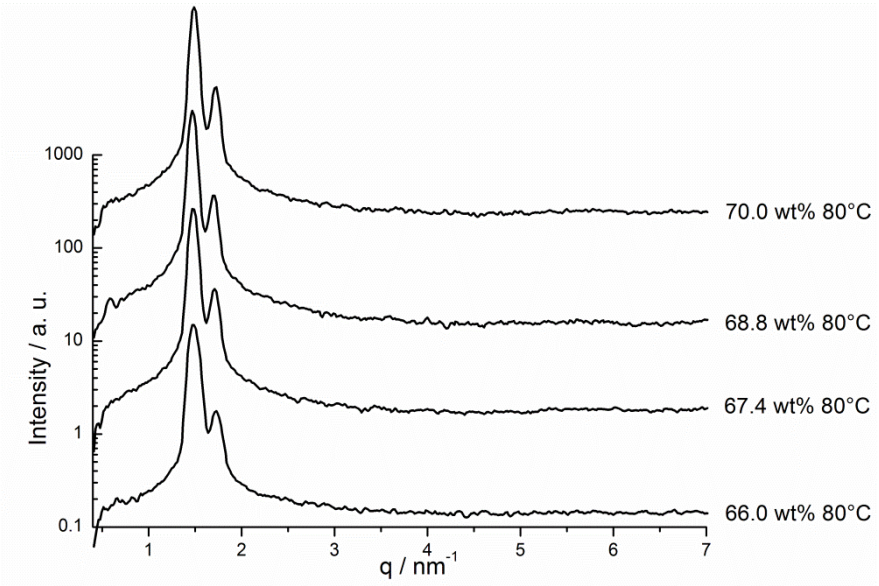

B.1.5 Defective lamellar phase dL_α or nematic phase N

B.1.5.1 SAXS data and calculated parameter

	Lamellar phase dL_α or nematic phase N								
	wt%	**d_{100} / Å**	**d_{200} / Å**	**d_{300} / Å**	**d_{400} / Å**	**r_L / Å**	**Φs**	**$Φ_L$**	**T / °C**
ChC_8	96.1	22.7	11.5	-	-	5.83	0.960	0.513	25
	96.8	22.7	11.5	-	-	5.86	0.967	0.517	25
	98.0	22.6	11.5	-	-	5.91	0.980	0.524	25
	98.4	22.5	11.4	7.6	-	5.93	0.984	0.526	25
	98.8	22.5	11.4	-	-	5.95	0.988	0.528	25
	96.8	22.4	-	-	-	5.80	0.967	0.517	40
	98.4	22.3	11.3	-	-	5.86	0.984	0.526	40
	99.0	22.2	10.7	-	-	5.87	0.990	0.529	40
ChC_{10}	96.9	25.2	-	-	-	7.16	0.969	0.568	75
	98.1	25.0	-	-	-	7.20	0.981	0.575	75
	98.9	24.9	-	-	-	7.21	0.989	0.580	75
	92.3	26.8	13.7	-	-	7.25	0.923	0.541	80
Ch-oleate	82.8	39.3	19.6	13.2	9.8	12.01	0.832	0.611	25
	91.3	38.8	19.4	13.0	9.7	13.05	0.915	0.673	25
	94.9	38.1	19.3	12.9	-	13.29	0.950	0.699	25
	98.9	37.0	17.5	11.6	-	13.44	0.989	0.727	25
	94.9	36.5	18.3	12.2	-	12.76	0.950	0.699	80
	98.9	34.3	17.2	-	-	12.49	0.989	0.727	80

Table B1-5. X-ray diffraction data of defective lamellar phase dL_α or nematic phase N of ChC_8, ChC_{10} and Choleate at different temperatures are presented. The Miller indices, half length of the lipophilic part r_L, volume fraction of surfactant $Φ_s$ and volume fraction of the lipophilic part $Φ_L$ of the defective lamellar dL_α or nematic N phase are given in the table.

B.1.5.2 SAXS and WAXS spectra

SAXS spectra of the defective lamellar phase dL_α or nematic phase N of the binary phase diagrams of choline octanoate, choline decanoate and choline oleate with water are illustrated. A broad first reflection peak for a birefringent phase is characteristically of a short range order within a non isotropic phase such as a defective lamellar or a nematic phase. Long range order is missing. Higher order reflections were not observed.

B.1.5.2.1 Choline octanoate at 25°C or 40°C

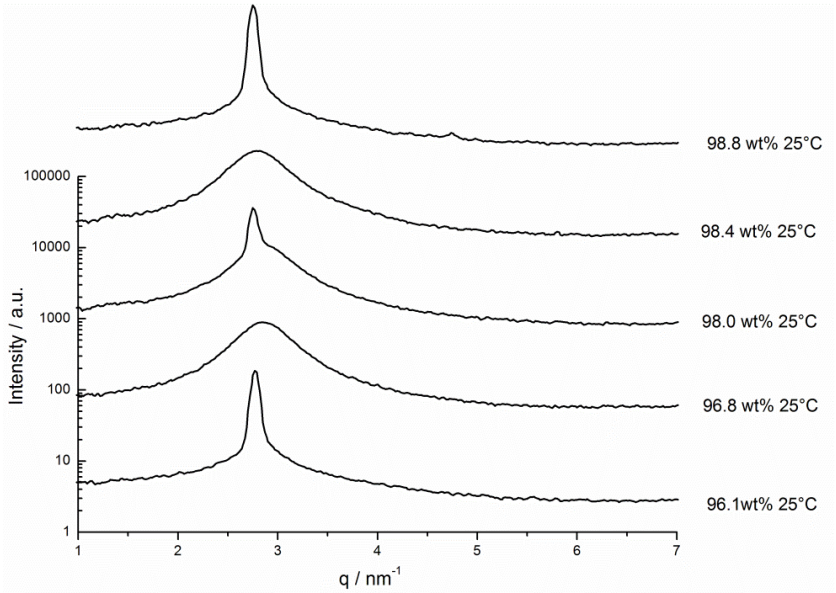

.

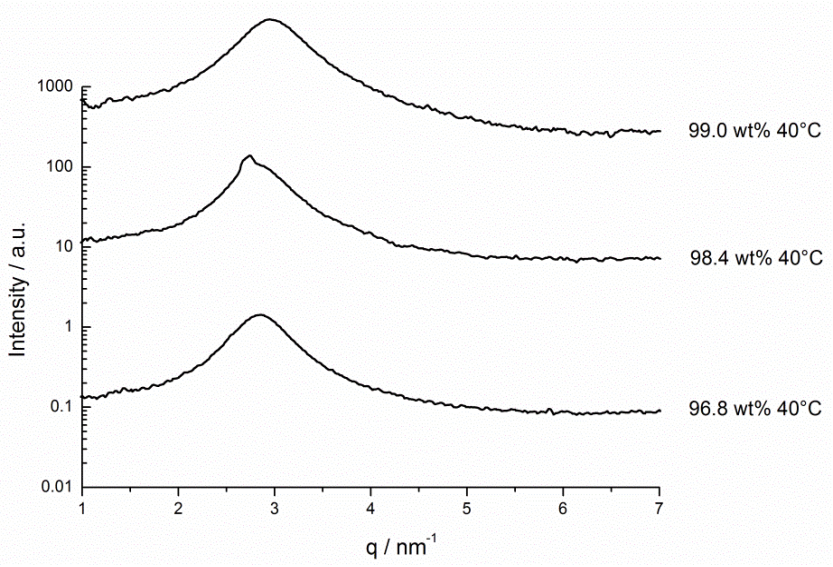

B.1.5.2.2 Choline decanoate at 25°C and 75°C

SAXS and WAXS spectra of differently concentrated choline decanoate samples at 25°C illustrate phases below the crystal solubility boundary.

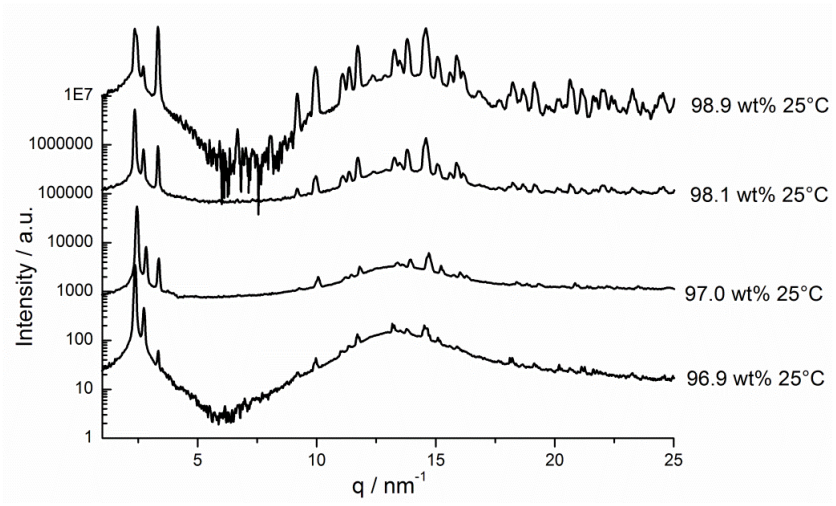

SAXS spectra of differently concentrated choline decanoate samples at 75°C show the defective lamellar phase dL_{α} or nematic phase N above the crystal solubility boundary.

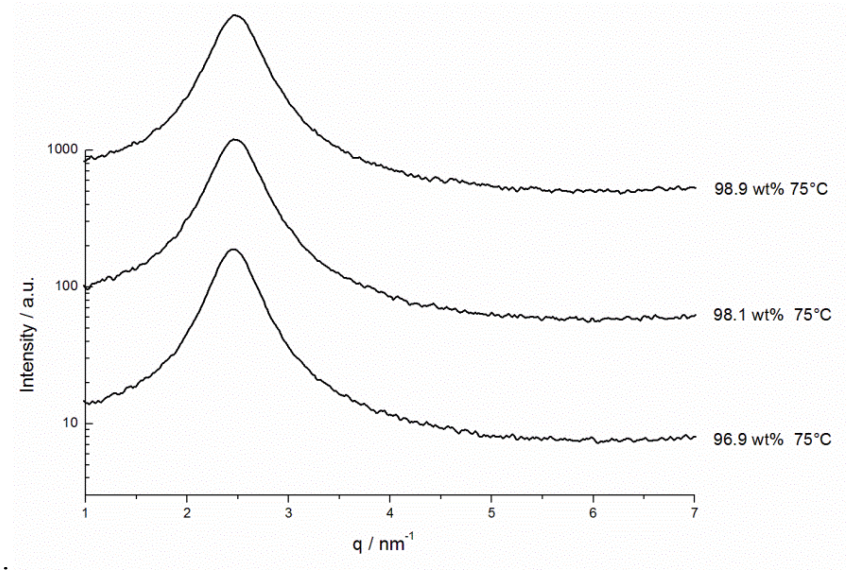

B.1.5.2.3 Choline oleate at 25°C and 80°C

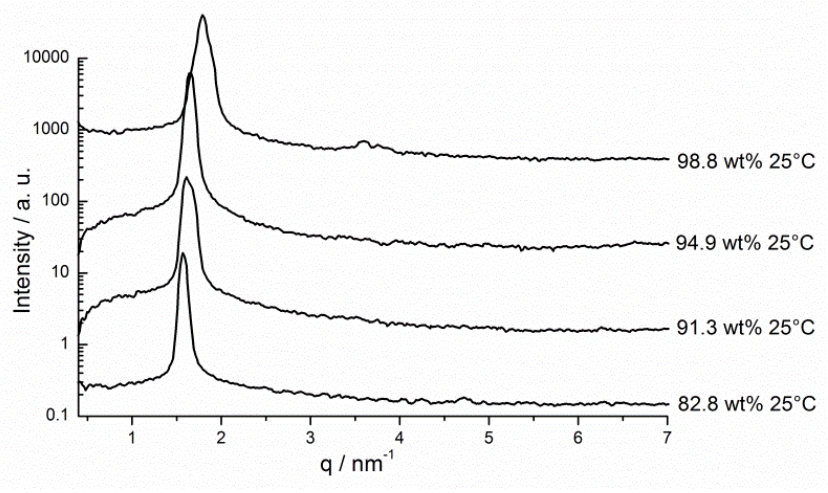

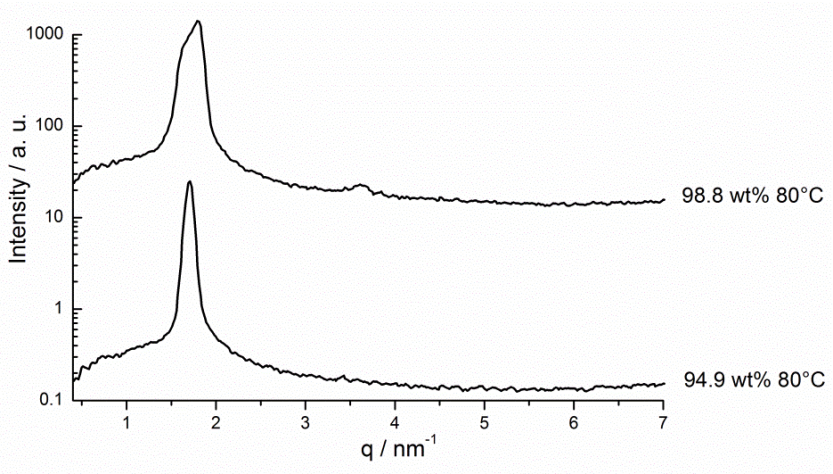

B.2 Extended isotropic, micellar phase of choline octanoate in water

B.2.1 SAXS and WAXS spectra of choline octanoate water mixtures at 70°C

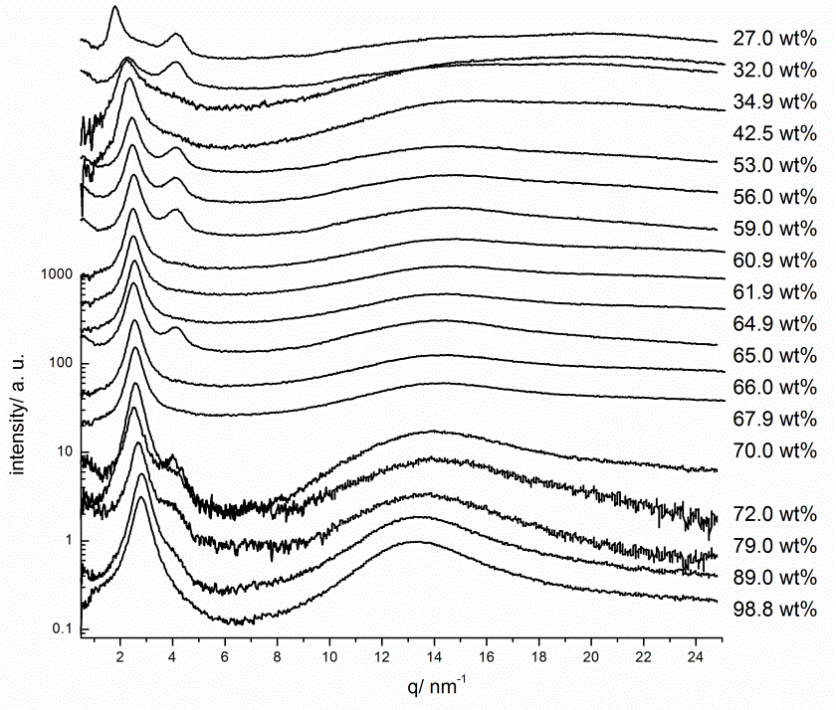

Figure B2-1. SAXS and WAXS spectra of different concentrated choline octanoate water solutions at 70°C. Some spectra show a peak at 4 nm^{-1} resulting from the Kapton foil.

B.2.2 High precision conductivity

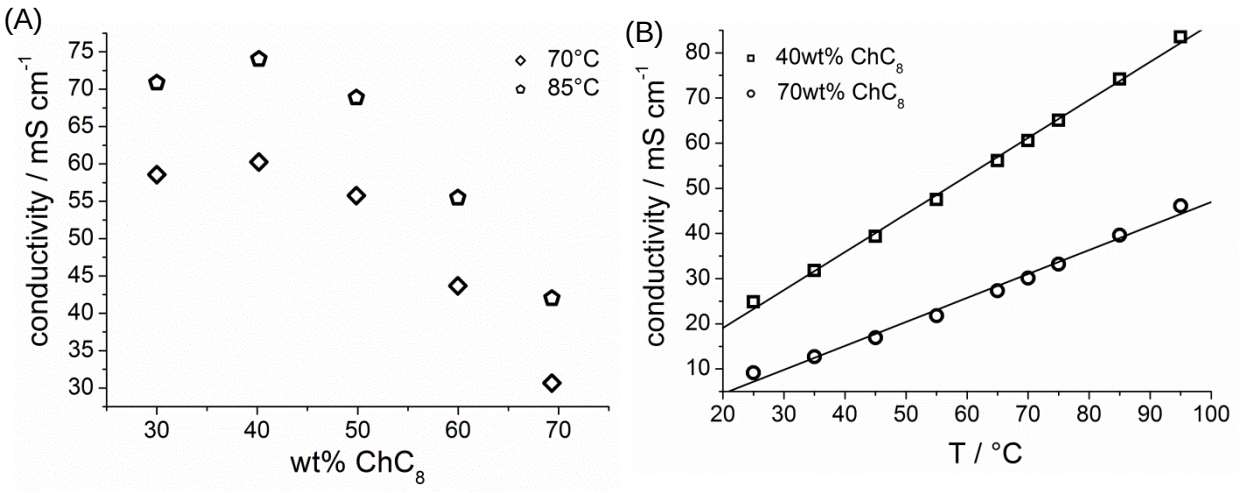

Figure B2-2. (A) Specific conductivity as a function of choline octanoate concentration measured at 70°C and 85°C with a high precision conductivity instrument. (B) Conductivity measured as a function of temperature of 40 wt% and 70 wt% choline octanoate water solutions

From this conductivity data (see **Figure B2-2**. (A) and (B)) and the conductivity measurements shown in the Chapter 4 in section 4.3.4.6 it could be evaluated: The change of the aggregate structure is only dependent on temperature and not on concentration. The shown conductivity values in Chapter 4 in section 4.3.4.6 are not the exact values. These are slightly higher and were determined with a more precise apparatus for some selected compositions (see **Figure B2-2 (A)**). They could not be measured at higher concentrations on the homebuilt precise conductivity instrument due to preparation problems with the high precision cell. Therefore, the whole curve was evaluated with bar electrode from Metrohm with a cell constant of 0.9 cm^{-1} and a Pt1000 temperature control which does not show such exact conductivity values. Further, in **Figure B2-2**. (B) it was approved that the conductivity increases more or less linearly with temperature for the different concentrations.

B.3 References

1. P. F. Husson, H. Mustacchi and V. Luzzati, *Acta Cryst.*, 1960, **13**, 668-677.
2. P. V. Luzzati, H. Mustacchi, A. Skoulios and F. Husson, *Acta Cryst.*, 1960, **13**, 660-667.

Appendix C Influence of chain length and double bond on the thermotropic phase behavior of choline carboxylates

C.1 Thermogravimetric analysis

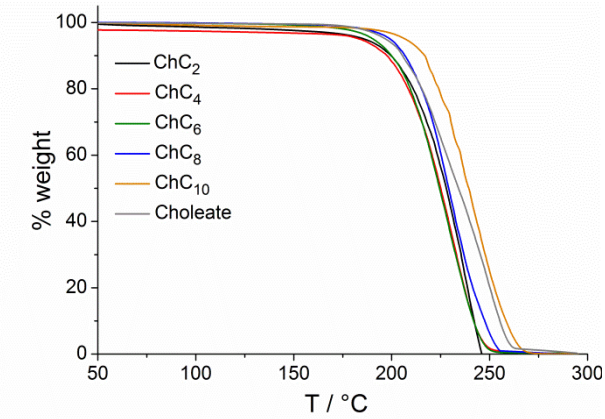

Figure C1-1. Thermogravimetry curves of the different neat choline carboxylates ChC_m with m = 2, 4, 6, 8, 10 and choline oleate to determine the decomposition temperatures and the thermal stability

C.2 Polarizing optical microscopy

The temperature range between -50°C and 95°C was recorded for each sample. Here the second heating and cooling cycle recorded with the heating rate of 10 K min^{-1} is shown. The magnification of the samples is 100x. Sample position and the light intensity is kept constant during the measurement.

C.2.1 Choline acetate

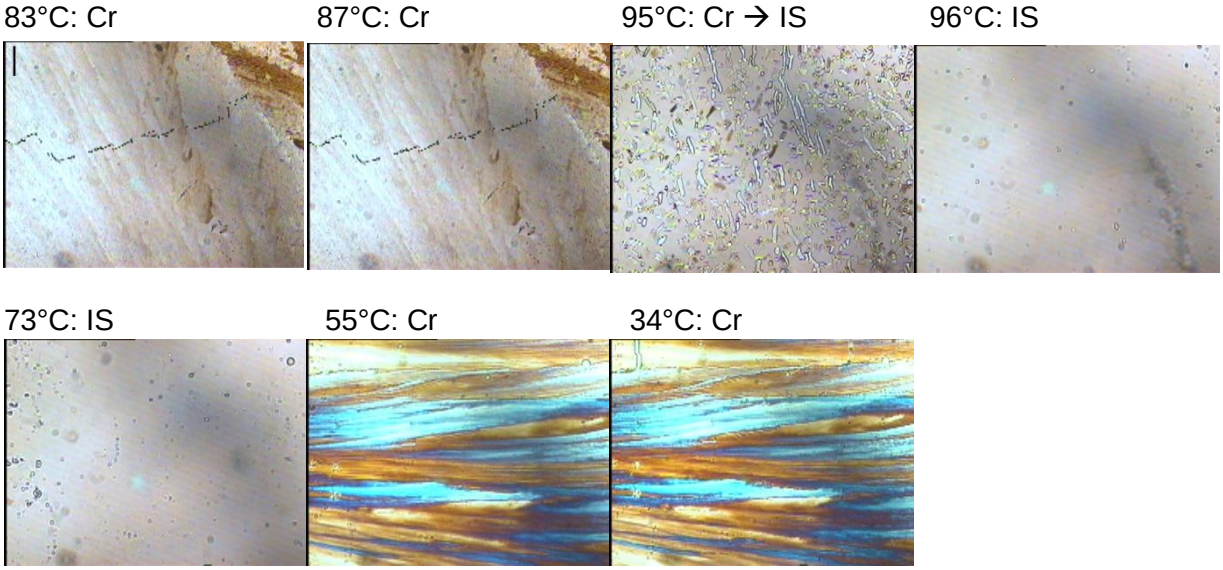

Figure C2-1. Polarizing optical microscope images show the second heating and cooling cycle of anhydrous choline acetate. The heating rate was 10 K min^{-1}. They were recorded with half-crossed polarizer. Choline acetate is an ionic liquid which shows only one phase transition between -50°C and 95°C from a solid (Cr) to an isotropic solution (IS). The melting temperature is 96°C and the crystallization temperature is 56°C. The melting of the solid occurs in a temperature range of 10°C, the crystallization only of 2°C. The temperatures are in good accordance with the temperatures obtained with DSC, but with a heating rate of 1 K min^{-1}. The scale bar (see image recorded at 83°C) is 100 µm. It is the same for the other images.

C.2.2 Choline butanoate

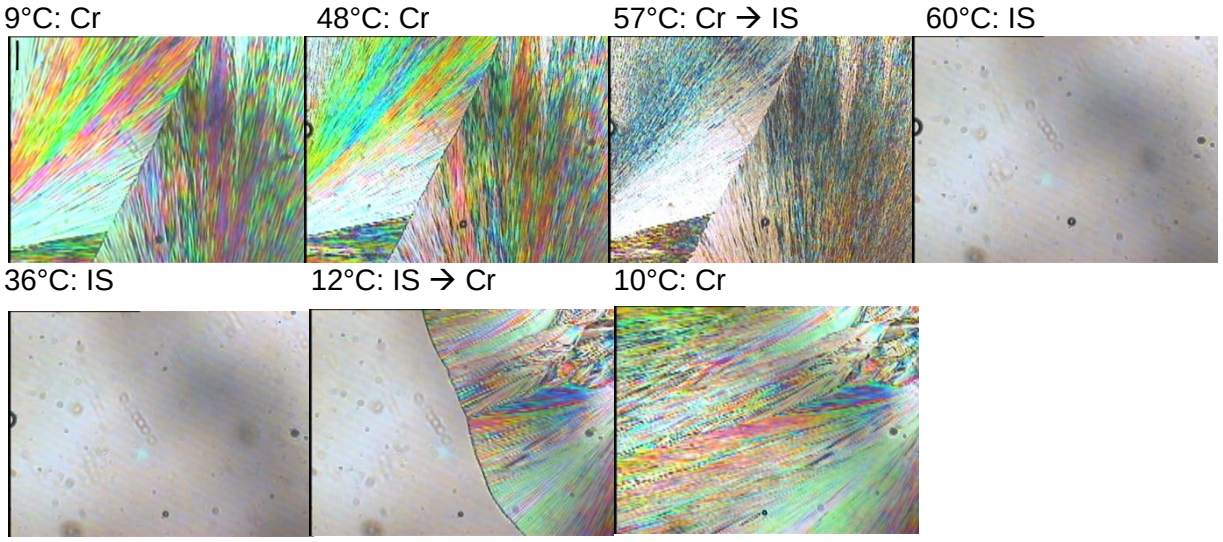

Figure C2-2. Polarizing optical microscope images show the second heating and cooling cycle of anhydrous choline butanoate. The heating rate was 10 K min^{-1}. They were recorded with half crossed polarizer. Choline butanoate is an ionic liquid which shows only a phase transition between -50°C and 95°C. The melting temperature is 58°C and the crystallization temperature is 11°C. The melting of the solid (Cr) to an isotropic solution (IS) occurs in a temperature range of 10°C, the crystallization only of 2°C. The transition temperatures are in good accordance with the obtained temperatures from DSC measurements with heating rate of 1 K min^{-1}. Slight difference is found at the crystallization temperature. The scale bar (see image recorded at 9°C) is 100 µm. It is the same for the other images.

C.2.3 Choline hexanoate

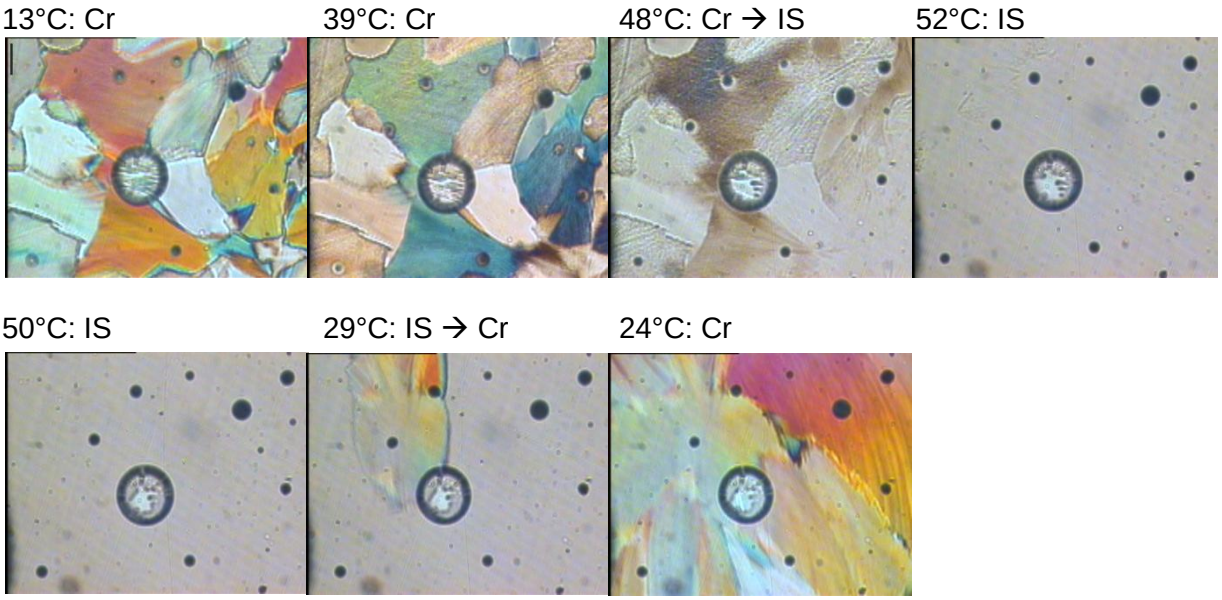

Figure C2-3. Polarizing optical microscope images show the second heating and cooling cycle of anhydrous choline hexanoate. The heating rate was 10 K min^{-1}. They were recorded with half crossed polarizer. Choline hexanoate is an ionic liquid which shows only a phase transition between -50°C and 95°C. The melting temperature is 52°C and the crystallization temperature is 29°C. The melting of the solid (Cr) to an isotropic solution (IS) occurs in a temperature range of 10°C the crystallization only in 3°C. The transition temperatures are slightly different compared to the one obtained from DSC with a heating rate of 1 K min^{-1}. The scale bar (see image recorded at 13°C) is 100 µm. It is the same for the other images.

C.2.4 Choline octanoate

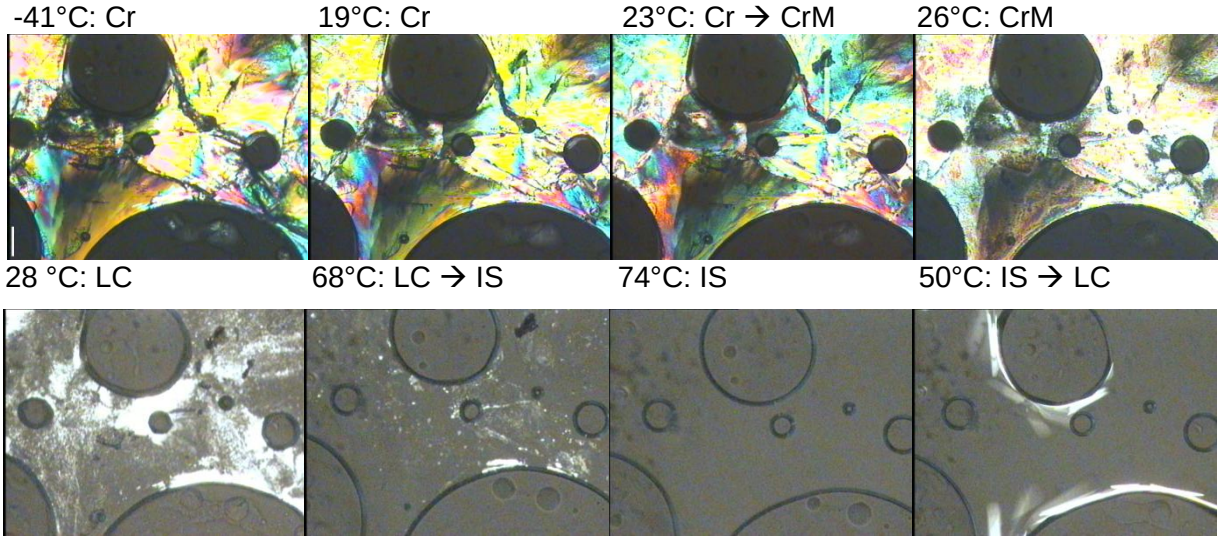

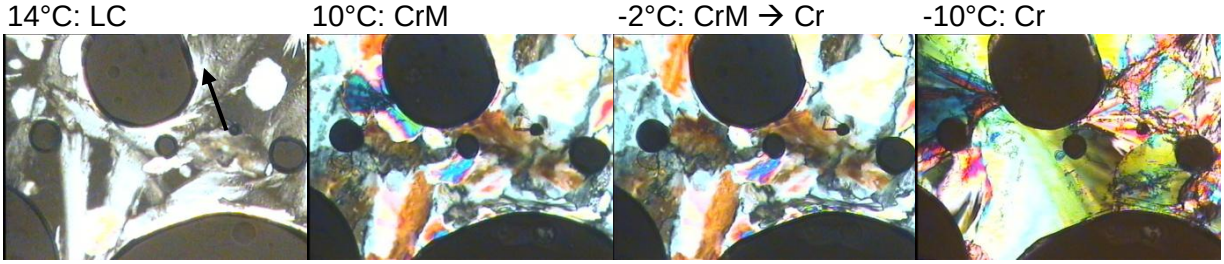

Figure C2-4. Polarizing optical microscope images show the second heating and cooling cycle of anhydrous choline octanoate. The heating rate was 10 K min^{-1}. During each cycle four different phases occur: the crystalline phase Cr at low temperatures, the birefringent semi-crystalline phase CrM, the defective lamellar or nematic liquid crystalline phase LC and as high temperature phase the isotropic viscous melt. The arrow marks the “Schlieren” texture, which is typical of a nematic phase. The scale bar (see image recorded at -41°C) is 100 µm. It is the same for the other images.

C.2.5 Choline decanoate

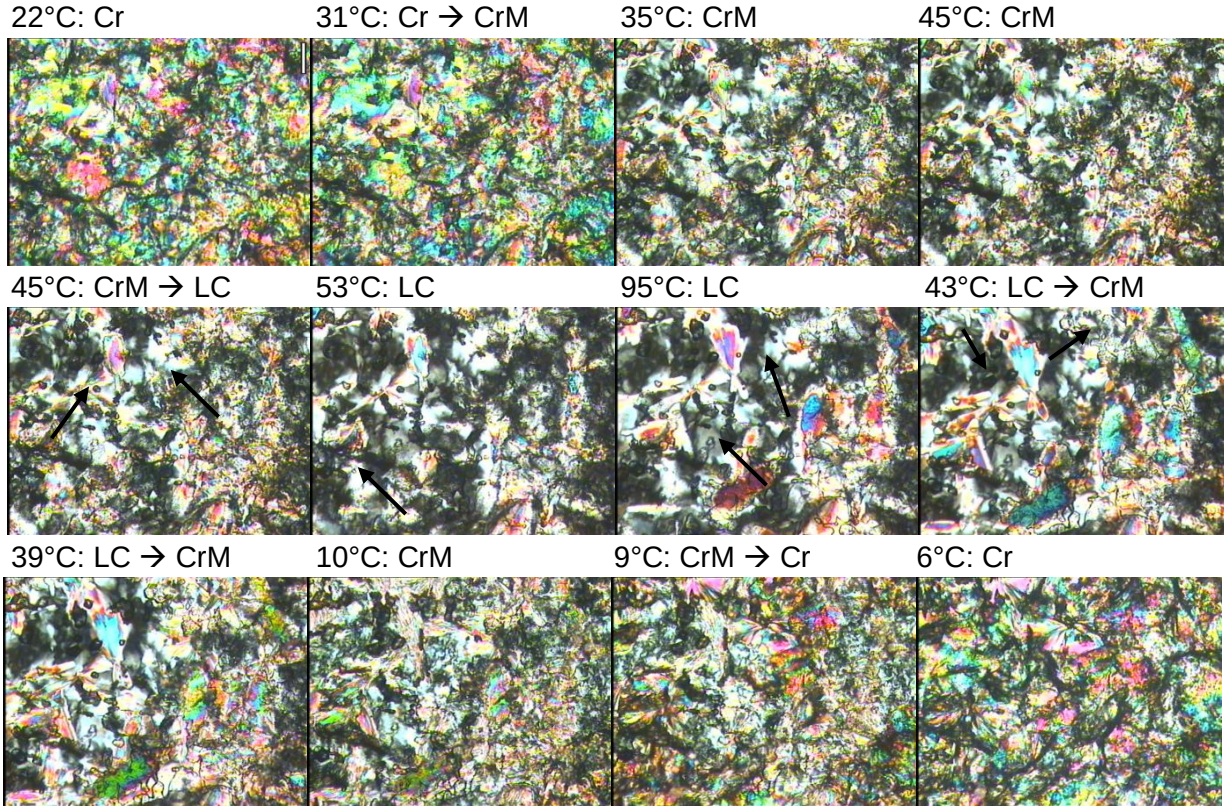

Figure C2-5. Polarizing optical microscope images show the second heating and cooling cycle of anhydrous choline decanoate. The heating rate was 10 K min^{-1}. During each cycle three different phases occurs: the crystalline phase Cr at low temperatures, the birefringent semi-crystalline phase CrM, the defective lamellar or nematic liquid crystalline phase LC. The arrows mark the “Schlieren” texture. The scale bar (see image recorded at 22°C) is 100 µm. It is the same for the other images.

C.2.6 Choline oleate

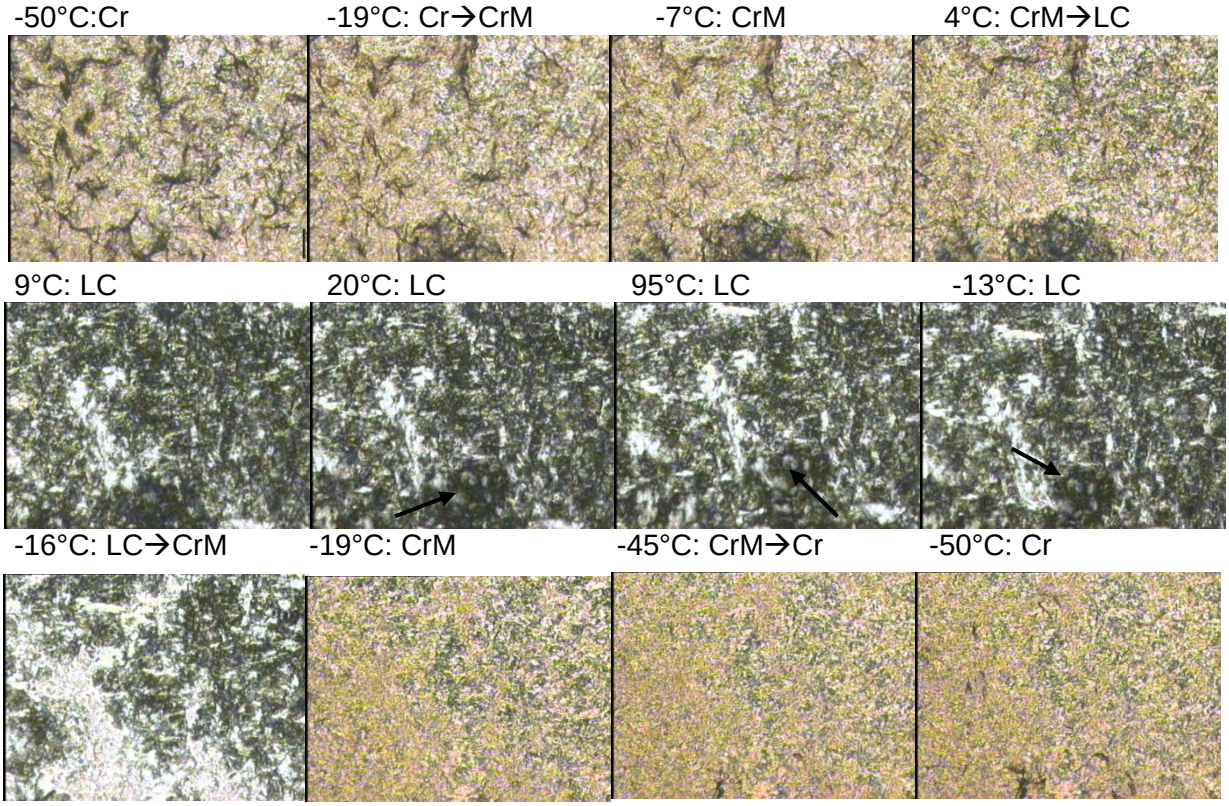

Figure C2-6. Polarizing optical microscope images show the second heating and cooling cycle of anhydrous choline oleate soap. The heating rate was 10 K min^{-1}. During each cycle three different phases occurs. The crystalline phase Cr at low temperatures, the birefringent semi-crystalline phase CrM at middle temperature range, the defective lamellar or nematic liquid crystalline phase LC at higher temperatures. The arrows mark the “Schlieren” texture. The scale bar (see image recorded at -50°C) is 100 µm. It is the same for the other images.

C.3 Differential scanning calorimetry (DSC)

C.3.1 DSC curves

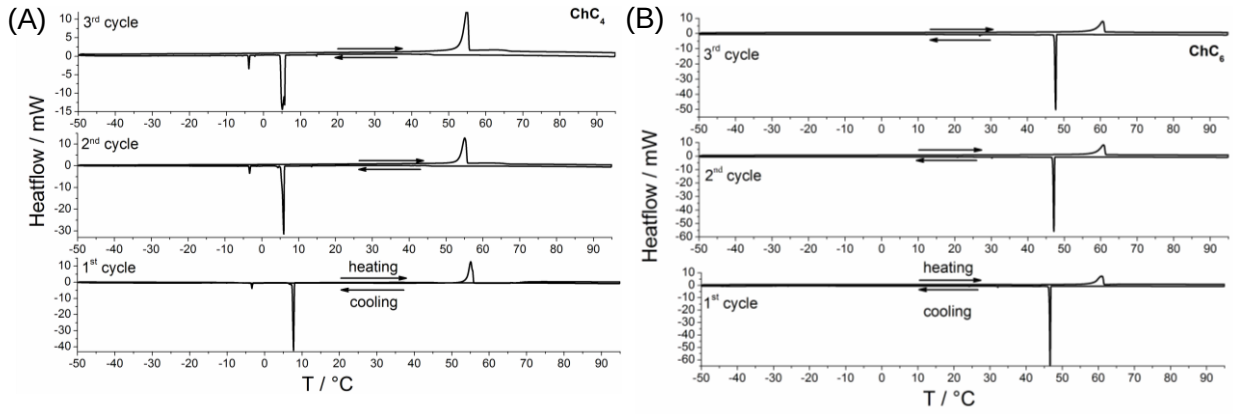

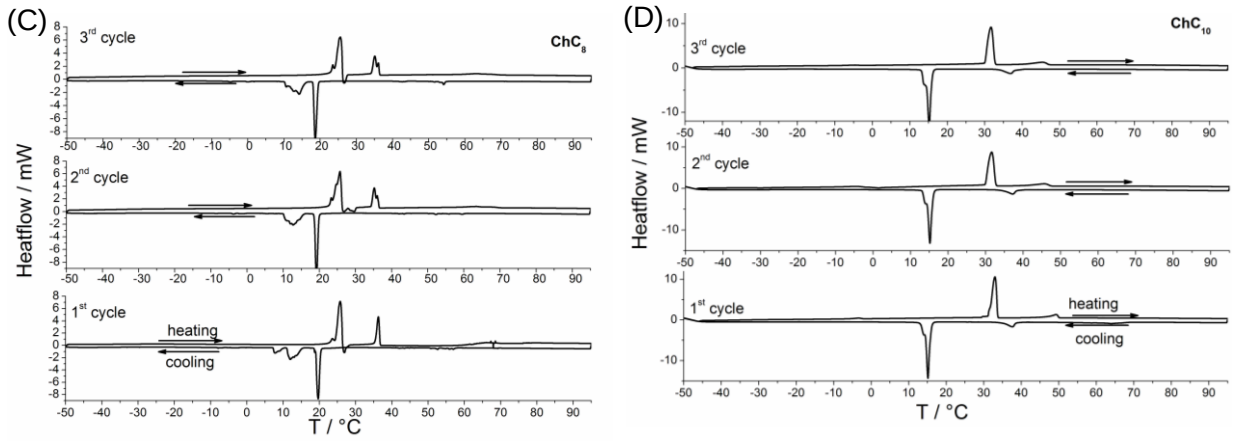

Figure C3-1. DSC curves of choline butanoate (A), choline hexanoate (B), choline octanoate (C) and choline decanoate (D). For all samples three curves were recorded with a heating rate of 1 K min^{-1} between -50 °C and 95 °C.

C.3.2 Transition temperature

The transition temperatures were obtained from the three DSC curves recorded for each sample with a heat rate of 1 K min^{-1}. The temperature of the peak maximum/minimum (heat/cool) is taken as the transition temperature. The numbers 1, 2 and 3 mark the transitions with increasing temperature (heating cycle) and the respective values at the cooling cycle.

	ChC_2	**ChC_4**	**ChC_6**
	T_1 / °C	**T_1 / °C**	**T_1 / °C**
1. heating	89.9	55.0	60.9
1. cooling	61.3	7.6	46.6
2. heating	90.0	55.1	60.7
2. cooling	53.9	5.9	47.2
3. heating	90.2	54.8	60.8
3. cooling	54.2	5.3	47.9

Table C3-1. Melting and crystallization temperatures of the three heating and cooling cycles of choline acetate, choline butanoate and choline hexanoate obtained from DSC measurements.

	ChC_8			**ChC_{10}**		**Choline oleate**		
	T_1 / °C	**T_2 / °C**	**T_3 / °C**	**T_1 / °C**	**T_2 / °C**	**T_1 / °C**	**T_2 / °C**	**T_3 / °C**
1. heating	25.7	36.2	66.4	32.9	49.3	-18.2	7.1	64.9
1. cooling	12.1	19.6	56.3	15.3	37.5	-39.5	-19.1	41.9
2. heating	25.7	35.3	65.7	31.6	45.8	-17.6	7.2	62.9
2. cooling	12.5	19.2	55.5	15.2	37.1	-39.3	-19.2	42.3
3. heating	25.6	35.2	65.1	31.6	45.5	-17.9	7.2	62.8
3. cooling	12.9	18.8	54.5	15.0	36.8	-39.4	-18.8	42.2

Table C3-2. Transition temperatures of the different phase changes of choline octanoate, choline decanoate and choline oleate. Of each substance three cycles were recorded with DSC.

C.3.3 Transition enthalpy

	ChC_8		ChC_{10}		Choline oleate	
	$\sum\Delta H$ / kJ mol^{-1}	$\sum\Delta S$ / J mol^{-1}K^{-1}	$\sum\Delta H$ / kJ mol^{-1}	$\sum\Delta S$ / J mol^{-1}K^{-1}	$\sum\Delta H$ / kJ mol^{-1}	$\sum\Delta S$ / J mol^{-1}K^{-1}
1. heating	22.7	74.5	23.1	75.0	17.4	62.7
1. cooling	-22.5	-77.2	-24.6	-84.6	-18.3	-72.7
2. heating	22.4	73.7	23.0	75.0	17.3	62.5
2. cooling	-22.7	-77.9	-24.6	-84.4	-18.3	-72.3
3. heating	22.0	72.4	23.3	76.1	17.6	63.2
3. cooling	-22.4	-76.9	-24.6	-84.7	-17.8	-70.5

Table C3-3. Sum of the transition enthalpies in the temperature range between -50°C and 95°C obtained from the three DSC cycles of choline octanoate, choline decanoate and choline oleate.

C.3.4 Transition entropy

	ChC_8			ChC_{10}		Choline oleate		
	ΔS_1 / J mol^{-1} K^{-1}	ΔS_2 / J mol^{-1} K^{-1}	ΔS_3 / J mol^{-1} K^{-1}	ΔS_1 / J mol^{-1} K^{-1}	ΔS_2 / J mol^{-1} K^{-1}	ΔS_1 / J mol^{-1} K^{-1}	ΔS_2 / J mol^{-1} K^{-1}	ΔS_3 / J mol^{-1} K^{-1}
1. heating	47.8	22.8	3.8	65.5	9.5	10.5	50.3	1.9
1. cooling	-34.3	-39.2	-3.6	-74.3	-10.4	-13.3	-57.5	-1.8
2. heating	48.0	21.6	4.1	64.9	10.1	11.1	49.8	1.7
2. cooling	-33.7	-39.7	-4.4	-74.0	-10.4	-12.4	-57.7	-2.2
3. heating	47.2	21.9	3.3	65.9	10.2	10.6	50.5	2.1
3. cooling	-33.5	-40.0	-3.5	-74.4	-10.3	-12.8	-55.6	-2.1

Table C3-4. Transition entropies of the different phase transitions of choline octanoate, choline decanoate and choline oleate were obtained from DSC measurements in the temperature range between -50°C and 95°C. Each cycle was recorded three times. The numbers 1, 2 and 3 label the different phase transitions with increasing temperature (heating cycle) and the respective ones at the cooling cycle.

C.4 Small (SAXS) and wide (WAXS) angle X-ray scattering

C.4.1 SAXS and WAXS spectra of choline octanoate

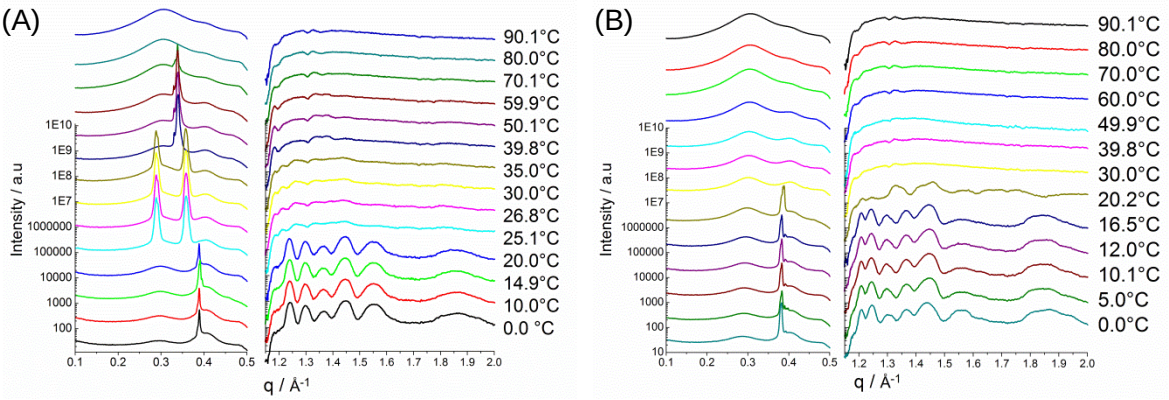

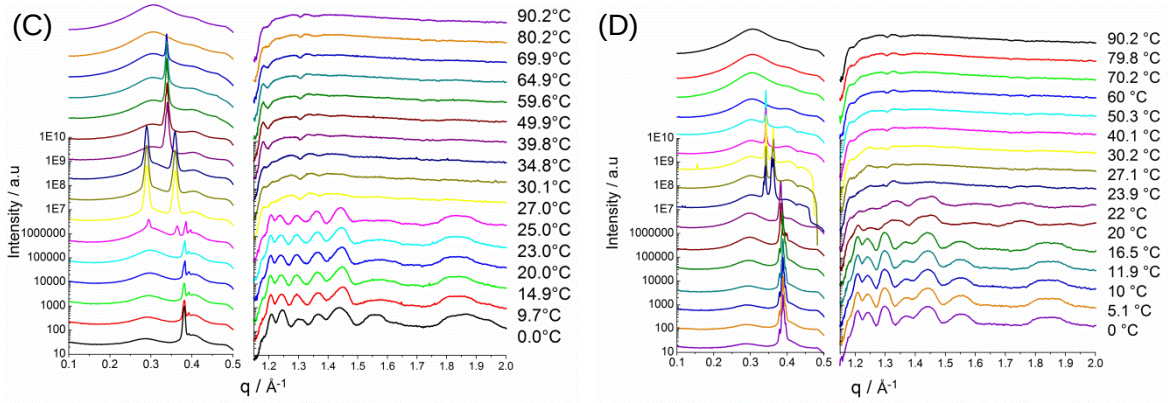

Figure C4-1. SAXS and WAXS spectra of the first heating (A) and cooling (B) cycle (freshly molten sample) and the second (reheated) heating (C) and cooling (D) cycle of choline octanoate. The heating rate was 1 K min^{-1}.

C.4.2 SAXS and WAXS spectra of choline oleate

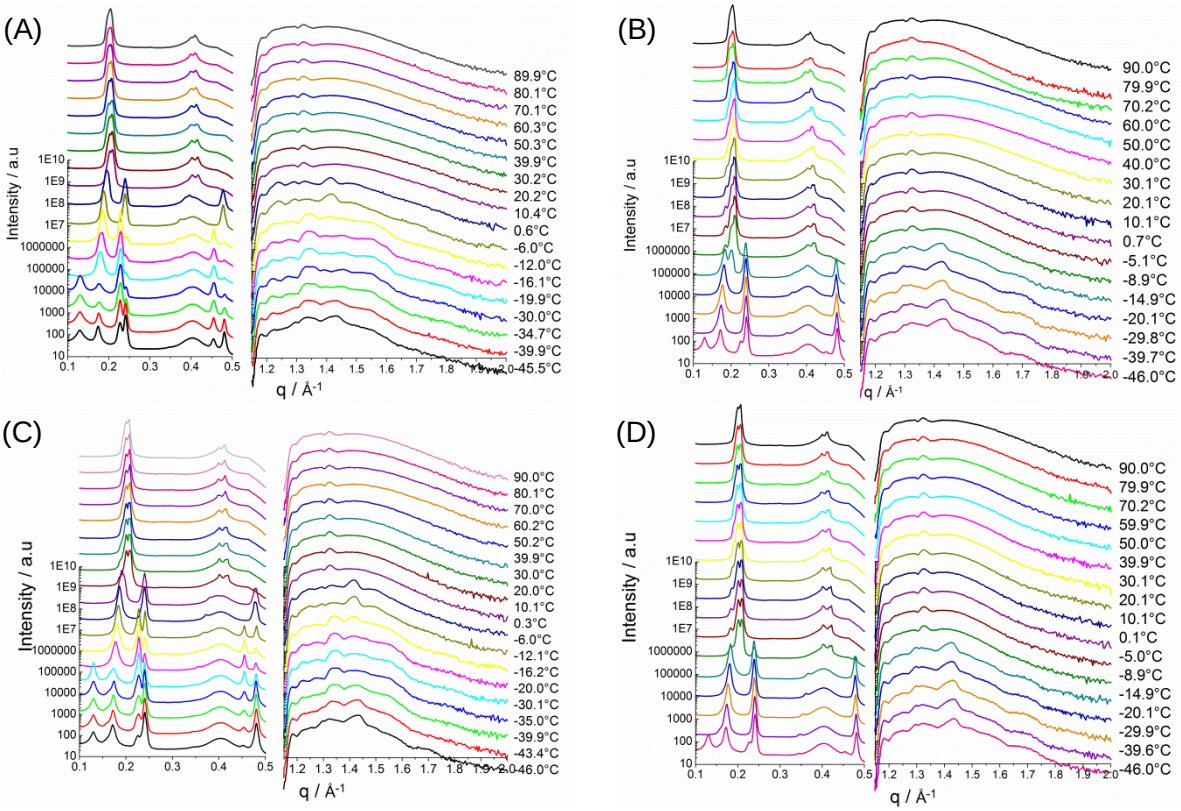

Figure C4-2. SAXS and WAXS curves of the first heating (A) and cooling (B) cycle (freshly molten sample) and the second (reheated) heating (C) and cooling (D) cycle of choline oleate. The heating rate was 1 K min^{-1}.

C.4.3 Temperature dependent d-spacings

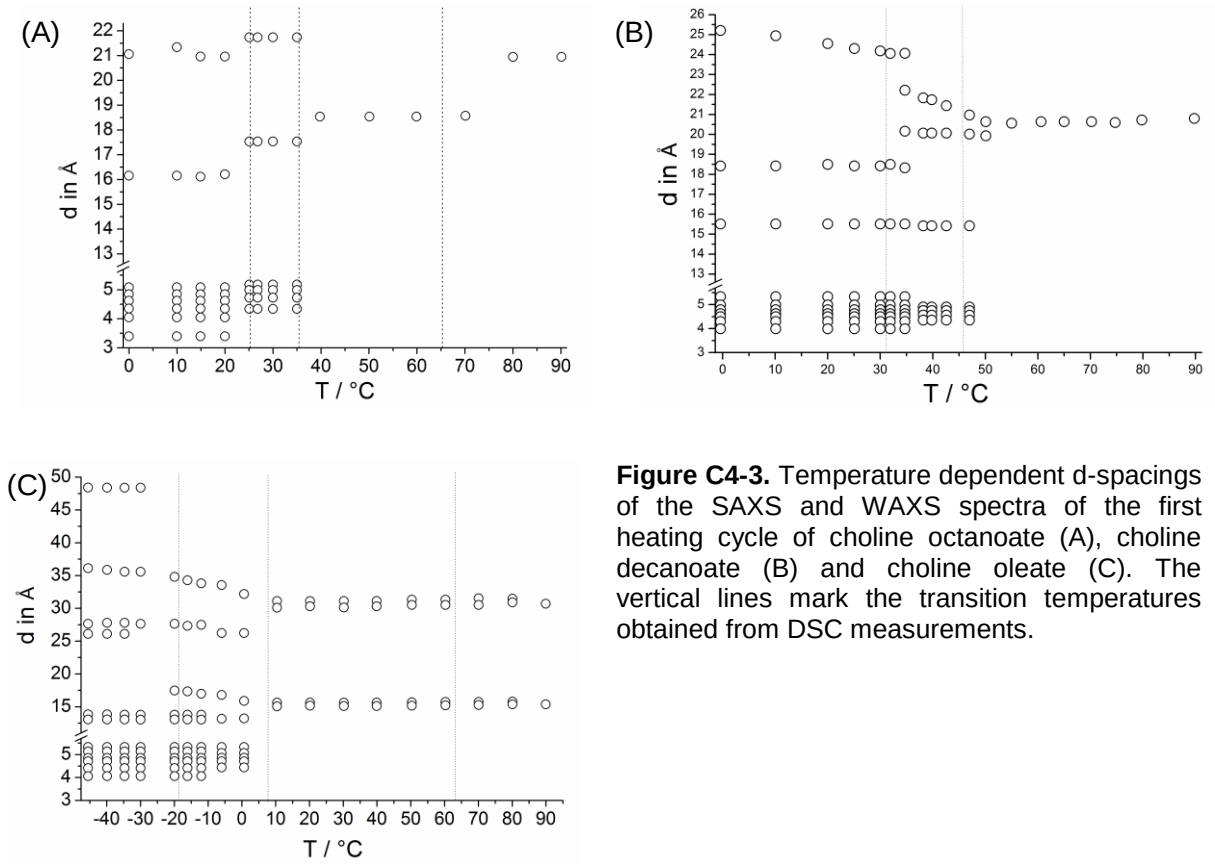

Figure C4-3. Temperature dependent d-spacings of the SAXS and WAXS spectra of the first heating cycle of choline octanoate (A), choline decanoate (B) and choline oleate (C). The vertical lines mark the transition temperatures obtained from DSC measurements.

C.5 NMR proton spin-spin relaxation times T_{2eff}

First heating cycle	Choline octanoate		Choline decanoate		Choline oleate	
T / °C	*T_{2eff} / µs of main structure*	*percent of main structure*	*T_{2eff} / µs of main structure*	*percent of main structure*	*T_{2eff} / µs main structure*	*percent of main structure*
-40	-	-	-	-	9.5	97.0
-30	-	-	-	-	6.4	90.0
-14	-	-	-	-	6.4	80.1
-6	-	-	-	-	12.2	82.4
0	-	-	-	-	12.8	82.3
5	3.9	96.9	4.5	90.7	-	-
10	-	-	-	-	110.1	85.7
15	4.1	95.9	-	-	-	-
25	26.1	87.5	6.8	88.5	-	-
30	27.0	88.6	-	-	141.4	81.1
35	30.4	81.9	19.2	96.0	-	-
43	-	-	23.2	92.1	-	-
45	44.1	80.8	-	-	-	-
55	-	-	53.1	96.1	-	-
60	49.2	53.5	-	-	-	-
70	-	-	83	94.6	-	-
80	>5600	0.0	109	92.3	170.7	80.1
90	-	-	-	-	189.0	79.0
70	-	-	-	-	-	-
60	48.0	45.6	68.8	88.2	-	-
50	40.0	77.3	-	-	-	-
40	-	-	22.9	94.1	-	-
35	30.0	83.9	-	-	-	-
25	-	-	21.5	97.3	-	-
20	5.3	94.1	-	-	116.6	79.3
16	4.7	95.5	-	-	-	-
15	-	-	4.9	89.1	-	-
10	4.4	97.1	-	-	-	-
5	3.8	97.5	4.2	92.2	-	-
-5	-	-	3.8	93.5	-	-
-6	-	-	-	-	12.6	81.1
-16	-	-	-	-	12.6	89.8
-40	-	-	-	-	11.2	94.6
Second heating cycle						
T / °C	*T_{2eff} / µs of main structure*	*percent of main structure*	*T_{2eff} / µs of main structure*	*percent of main structure*	*T_{2eff} / µs main structure*	*percent of main structure*
-40	-	-	-	-	10.6	96.5
-30	-	-	-	-	6.7	84.7
-14	-	-	-	-	6.6	80.0
-6	-	-	-	-	12.6	80.4
0	-	-	-	-	13.5	79.2
5	7.1	95.1	-	-	-	-

10	-	-	4.5	91.1	109.0	90.2
15	7.5	93.8	-	-	-	-
25	26.5	85.4	5.9	84.1	-	-
30	28.6	86.8	-	-	135.0	87.4
35	40.9	83.9	22.2	95.2	-	-
43	-	-	21.6	92.9	-	-
45	-	-	-	-	-	-
55	-	-	70.8	85.1	-	-
60	45.2	58.1	-	-	-	-
70	>5600	0.0	92.7	87.7	-	-
80	>5600	0.0	109.5	88.4	181.0	87.6
90	-	-	-	-	186.0	87.3
70	>5600	0.0	-	-	-	-
60	45.4	54.2	74.2	84.7	-	-
50	39.4	71.7	-	-	-	-
40	-	-	22.5	93.5	-	-
35	37.3	80.0	-	-	-	-
25	-	-	21.5	93.4	-	-
20	19.1	76.8	-	-	129.0	90.4
16	10.4	89.7	-	-	-	-
15	-	-	5.2	88.9	-	-
10	7.6	94.4	-	-	-	-
5	7.5	96.8	4.7	91.4	-	-
0	-	-	-	-	102.0	90.9
-5	-	-	4.4	92.2	-	-
-6	-	-	-	-	16.7	86.2
-16	-	-	-	-	14.3	87.5
-40	-	-	-	-	11.7	95.1

Table C5-1. Temperature dependent spin-spin relaxation time T_{2eff} of choline octanoate, choline decanoate and choline oleate obtained from ^{1}H NMR measurements

Appendix D Aqueous behavior of choline alkylsulfates ChS_m with m = 12, 16

D.1 Cytotoxicity

D.1.1 HeLa dose-response curves

The curves were established over several weeks with the HeLa cells and represent one of the four dose-response curves of choline dodecylsulfate and choline hexadecylsulfate.

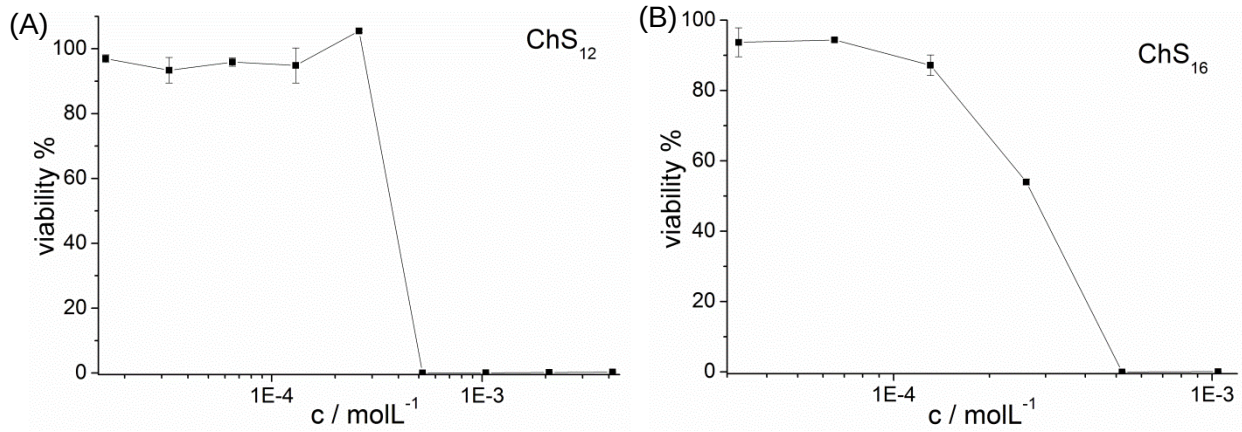

Figure D1-1. Dose-response curve of choline dodecylsulfate (A) and choline hexadecylsulfate (B) established with HeLa cells.

D.1.2 SK-MEL-28 dose-response curves

The curves were established with the SK-MEL-28 cells over several weeks and represent one of the four dose-response curves of choline dodecylsulfate and choline hexadecylsulfate.

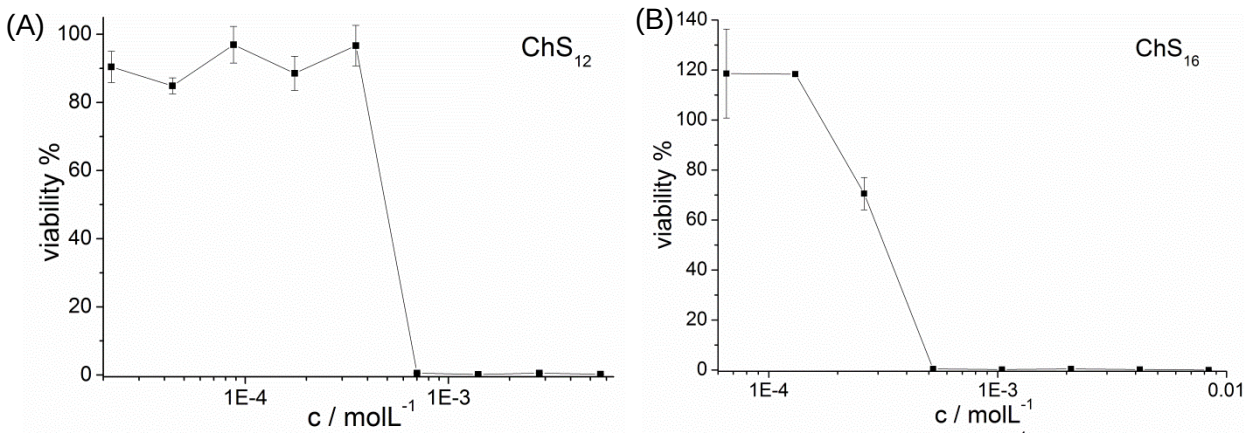

Figure D1-2. Dose-response curve of choline dodecylsulfate (A) and choline hexadecylsulfate (B) generated with SK-MEL 28 cells.

D.2 Small (SAXS) and wide (WAXS) angle X-ray scattering

D.2.1 Hexagonal phase H_1

D.2.1.1 SAXS data and calculated parameter

Hexagonal – H_1											
ChS_{12}											
wt%	**T / °C**	**d_{100} / Å**	**d_{110} / Å**	**d_{200} / Å**	**d_{210} / Å**	**d_{300} / Å**	**d_{220} / Å**	**d_{310} / Å**	**a / Å**	**Φs**	**$Φ_L$**
42.1	25	46.9	27.1	23.4	17.7	-	-	-	54.2	0.410	0.244
49.9	25	43.9	25.4	22.0	16.6	14.6	12.7	-	50.7	0.487	0.290
59.9	25	40.8	23.6	20.4	15.4	-	11.8	-	47.1	0.588	0.350
77.4	25	37.2	21.5	18.6	14.1	12.4	10.7	10.3	42.9	0.766	0.456
79.9	25	37.0	21.3	18.5	14.0	12.3	10.7	10.3	42.7	0.792	0.472
84.2	25	36.5	21.5	18.3	-	-	-	-	42.5	0.835	0.498
72.0	50	37.0	21.3	18.5	14.0	12.3	10.7	10.3	42.7	0.711	0.424
77.4	50	36.3	21.0	18.2	-	-	-	-	41.9	0.766	0.456
79.9	50	35.9	20.7	18.0	13.6	-	-	10.0	41.5	0.792	0.472
84.2	50	35.3	20.4	17.6	13.3	11.8	10.2	9.8	40.8	0.835	0.498
77.4	90	34.7	20.0	17.4	13.1	11.5	10.0	34.7	40.0	0.766	0.456
72.0	95	34.9	20.2	17.5	13.2	11.6	10.1	34.9	40.3	0.711	0.424
ChS_{16}											
29.3	50	66.9	38.6	33.5	25.3	21.8	19.4	18.6	77.1	0.288	0.190
48.4	50	54.2	31.3	27.1	20.5	18.2	15.6	15.2	62.7	0.478	0.316
57.6	50	50.3	28.3	25.1	19.0	16.8	14.5	14.0	57.6	0.570	0.377
70.0	50	46.9	27.1	23.4	17.7	-	13.5	13.0	54.1	0.695	0.460
72.1	50	46.5	27.1	23.4	17.7	15.8	13.5	13.0	54.2	0.716	0.474
75.0	50	45.9	26.5	22.9	17.3	-	13.3	12.7	53.0	0.746	0.493
77.2	50	45.5	26.3	22.8	17.2	15.2	13.1	12.6	52.6	0.768	0.508
73.9	65	44.9	25.9	22.4	17.0	15.0	13.0	12.4	51.8	0.734	0.486
73.9	90	43.6	25.2	21.8	16.5	-	12.6	12.1	50.4	0.734	0.486
70.0	95	43.9	25.4	22.0	16.6	14.6	12.7	12.2	50.8	0.695	0.460

Table D2-1. X-ray diffraction data for the hexagonal phases of choline dodecylsulfate and choline hexadecylsulfate with water including the experimental d-values with the corresponding Miller indices, unit cell parameter a (Δa = 0.0 - 0.9) and volume fraction of the surfactant $Φ_S$ and of the lipophilic part $Φ_L$.

D.2.1.2 SAXS spectra of the hexagonal phase of ChS_{12} with water

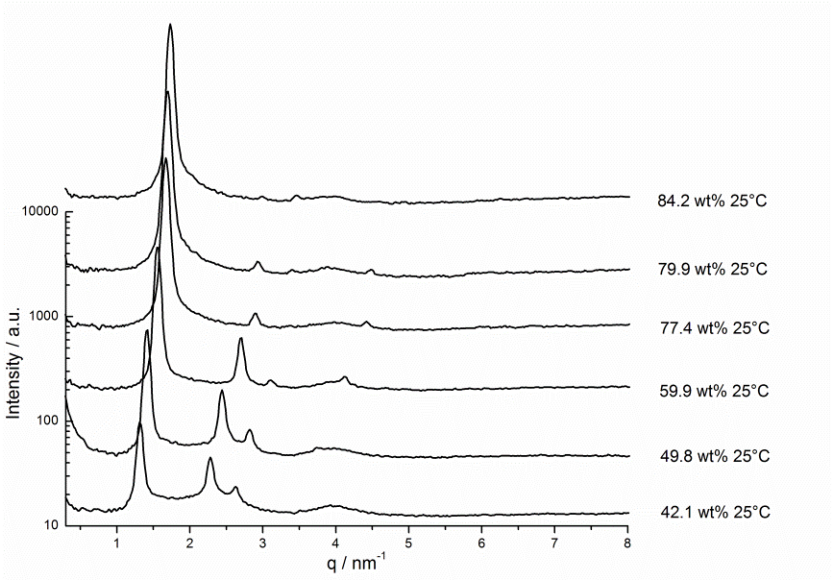

Figure D2-1. SAXS spectra of the hexagonal phase of choline dodecylsulfate with water at 25°C

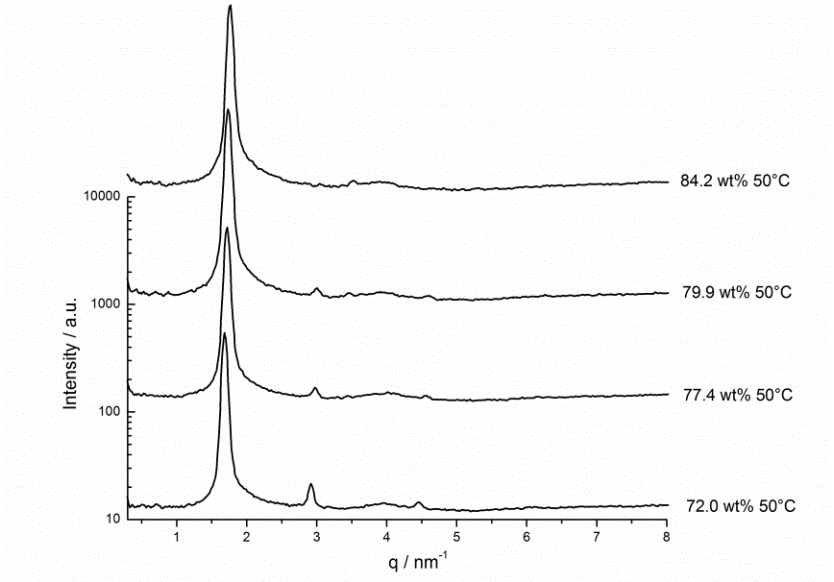

Figure D2-2. SAXS spectra of the hexagonal phase of choline dodecylsulfate with water at 50°C

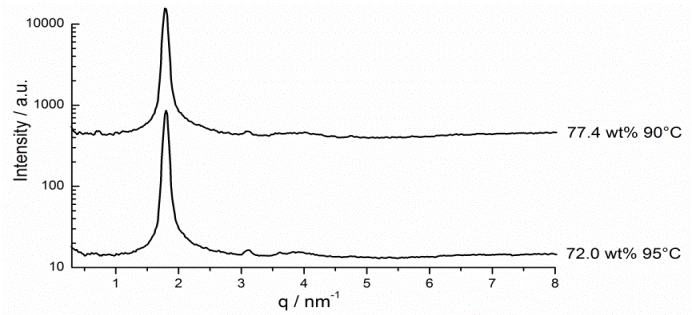

Figure D2-3. SAXS spectra of the hexagonal phase of choline dodecylsulfate with water at 90°C and 95°C

D.2.1.3 SAXS spectra of the hexagonal phase of ChS_{16} with water

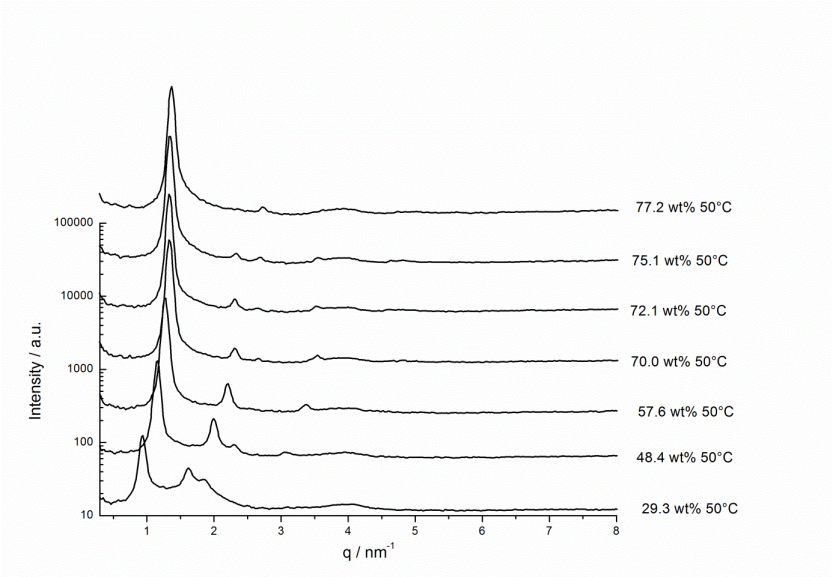

Figure D2-4. SAXS spectra of the hexagonal phase of choline hexadecylsulfate with water at 50°C.

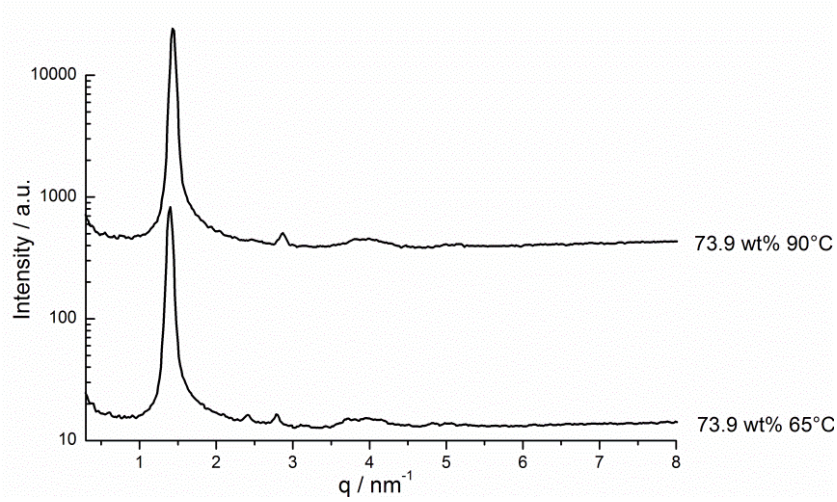

Figure D2-5. SAXS spectra of the hexagonal phase of choline hexadecylsulfate with water at 65°C and 95°C

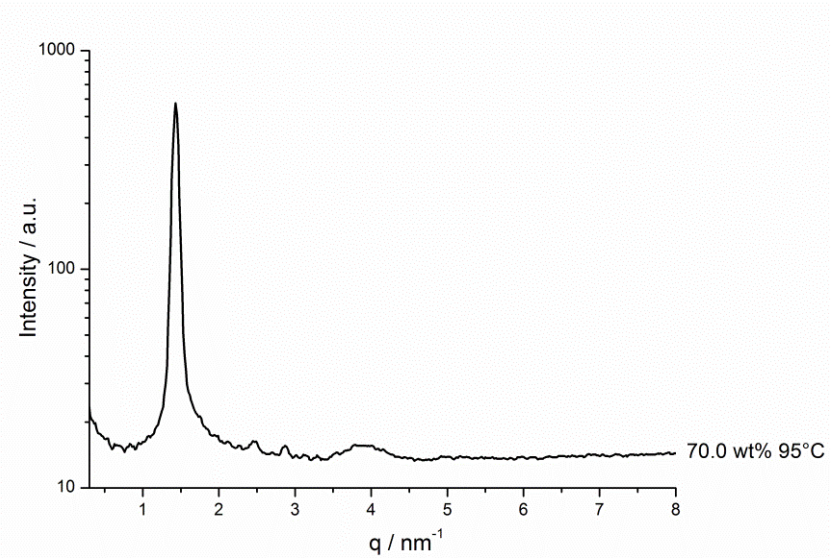

Figure D2-6. SAXS spectrum of the hexagonal phase of choline hexadecylsulfate with water at 95°C

D.2.2 Biphasic region: Hexagonal phase H_1 and bicontinuous cubic phase with I*a*3*d* structure

D.2.2.1 SAXS data of the biphasic region

Biphasic system: Hexagonal phase H_1 and I*a*3*d*									
ChS_{16}									
wt%	**T /°C**	**d_{100} / Å**	**d_{110} / Å**	**d_{200} / Å**	**d_{210} / Å**	**d_{300} / Å**	**a / Å**	**Φs**	**$Φ_L$**
82.0	50	49.1	29.0	24.5	18.6	16.4	56.9	0.817	0.540
82.0	65	48.7	28.1	24.4	18.4	16.2	56.2	0.817	0.540
84.9	65	48.0	27.7	24.6	18.5	-	56.1	0.846	0.560
wt%	**T/°C**	**d_{211} / Å**	**d_{220} / Å**	**d_{321} / Å**	**d_{400} / Å**	**d_{420} / Å**	**a / Å**	**Φs**	**$Φ_L$**
82.0	50	43.3	37.5	28.4	26.5	23.8	106.2	0.817	0.540
82.0	65	42.5	36.8	27.8	26.0	42.5	104	0.817	0.540
84.9	65	41.6	36.0	27.2	25.5	41.6	101	0.846	0.560

Table D2-2. X-ray diffraction data for the biphasic region with a hexagonal and bicontinuous cubic phase with I*a*3*d* structure: The experimental d-values and the corresponding Miller indices, unit cell parameter a (Δa = 0.0 - 0.8) and volume fraction of the surfactant Φ_S and of the lipophilic part Φ_L of the hexagonal and bicontinuous cubic phase with I*a*3*d* structure at different concentrations of choline hexadecylsulfate with water are given.

D.2.2.2 SAXS spectra

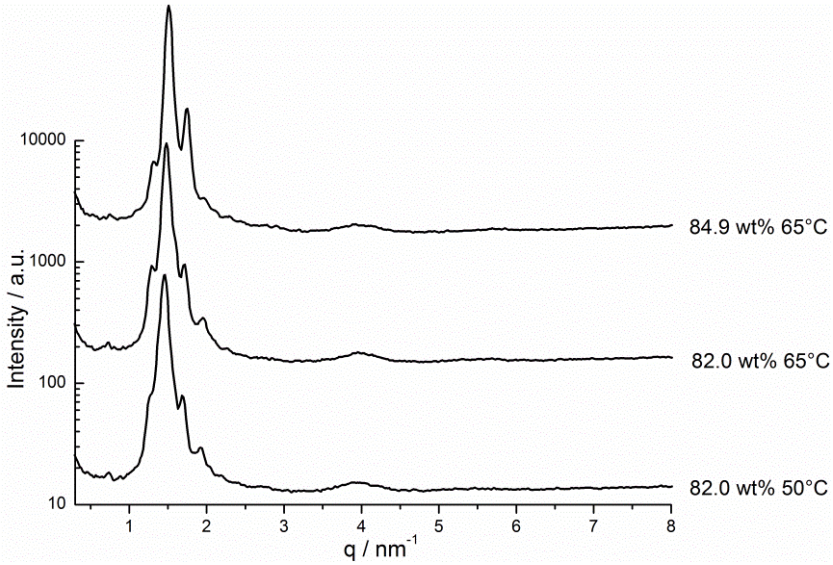

Figure D2-7. SAXS spectra of the biphasic region at different concentrations of choline hexadecylsulfate with water at 50°C and 65°C are shown. The two phases are assigned as hexagonal phase and bicontinuous cubic phase with I*a*3*d* structure.

D.2.3 Bicontinuous cubic phase with I*a*3*d* structure

D.2.3.1 SAXS data and calculated parameter

Bicontinuous cubic – I*a*3*d*											
ChS_{12}											
wt%	**T / °C**	**d_{211} / Å**	**d_{220} / Å**	**d_{321} / Å**	**d_{400} / Å**	**d_{420} / Å**	**d_{332} / Å**	**d_{422} / Å**	**a / Å**	**Φs**	**$Φ_L$**
87.1	25	36.7	31.8	24.1	22.5	20.1	19.2	18.4	90.0	0.865	0.515
89.0	25	36.5	31.6	23.9	22.4	20.0	19.1	18.3	89.4	0.885	0.527
87.1	50	35.7	30.9	23.4	22.0	19.6	-	-	87.6	0.865	0.515
89.0	50	35.5	30.8	23.2	21.7	19.4	-	-	87.0	0.885	0.527
90.9	50	35.1	31.3	23.0	21.5	19.2	18.3	17.6	86.4	0.905	0.539
91.8	50	34.9	30.2	22.9	21.4	19.2	18.3	17.5	85.6	0.915	0.545
87.0	65	35.3	30.6	23.1	21.6	19.4	-	-	86.5	0.865	0.515
87.8	65	35.1	30.4	23.0	21.5	-	-	-	86.0	0.873	0.520
89.0	65	34.9	30.2	23.1	21.4	-	-	-	85.7	0.885	0.527
79.9	90	34.7	29.6	22.8	21.3	19.0	18.2	-	84.9	0.792	0.472
84.2	90	34.5	29.4	22.6	21.2	18.9	-	-	84.3	0.835	0.498
87.1	90	34.3	29.2	22.5	21.1	18.8	18.0	-	83.9	0.865	0.515
77.4	95	33.6	29.1	22.3	20.6	18.4	-	-	82.5	0.766	0.456
79.9	95	33.1	28.6	21.6	20.3	17.9	17.3	-	80.9	0.792	0.472
ChS_{16}											
86.0	65	41.6	36.0	27.2	25.5	22.8	21.7	20.8	102.0	0.857	0.567
88.0	65	41.1	35.6	26.9	25.2	22.5	21.5		100.6	0.878	0.580
89.0	65	40.8	35.3	26.7	25.0	22.3	21.3	20.4	100.0	0.887	0.587
90.9	65	40.3	34.9	26.4	24.8	22.2	21.1	20.3	99.0	0.907	0.600
77.2	90	41.6	36.1	27.3	25.5	22.8	21.7	20.8	102.0	0.768	0.508
82.0	90	40.7	35.3	26.7	25.0	22.3	21.3	20.4	99.8	0.817	0.540

84.9	90	40.3	34.9	26.4	25.0	22.1	20.8	20.1	98.8	0.846	0.560
86.0	90	40.1	34.8	26.3	24.6	22.0	21.0	20.1	98.3	0.857	0.567
73.9	95	41.3	35.8	27.1	25.3	22.7	-	41.3	101.3	0.734	0.486
75.0	95	41.1	35.6	26.9	25.2	22.5	21.5	41.1	100.7	0.746	0.493
77.4	95	40.7	35.3	26.7	25.0	22.3	21.3	40.7	99.8	0.770	0.509
82.0	95	40.3	34.9	26.4	24.7	22.1	21.0	40.3	98.7	0.817	0.540

Table D2-3. X-ray diffraction data for the bicontinuous cubic phase with I*a*3*d* structure: The experimental d-values and the corresponding Miller indices, unit cell parameter a (Δa = 0.0 - 0.7) and volume fraction of the surfactant Φ_S and of the lipophilic part Φ_L of bicontinuous cubic phase at different concentrations of choline dodecylsulfate and choline hexadecylsulfate with water are shown.

D.2.3.2 SAXS and WAXS spectra of the bicontinuous cubic phase with I*a*3*d* structure of ChS_{12} with water

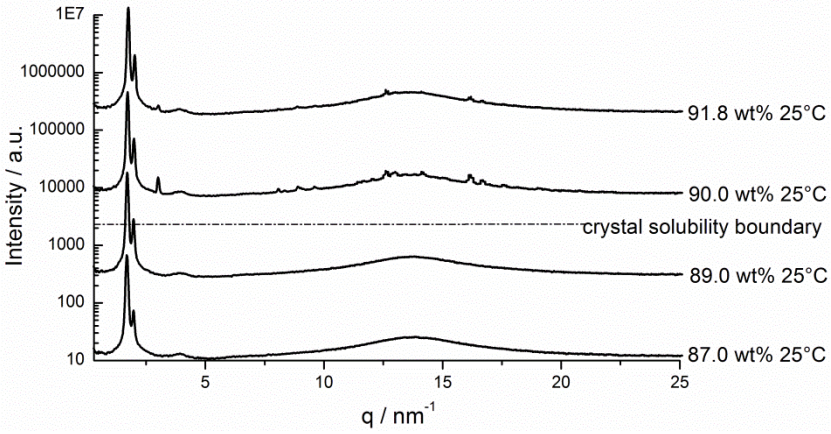

Figure D2-8. SAXS and WAXS spectra of the bicontinuous cubic phase with I*a*3*d* structure at the different concentrations of choline dodecylsulfate with water at 25°C are shown. The transition of a liquid crystalline I*a*3*d* structure to a crystalline phase is seen between 89.0 wt% and 90.0 wt% of choline dodecylsulfate with water.

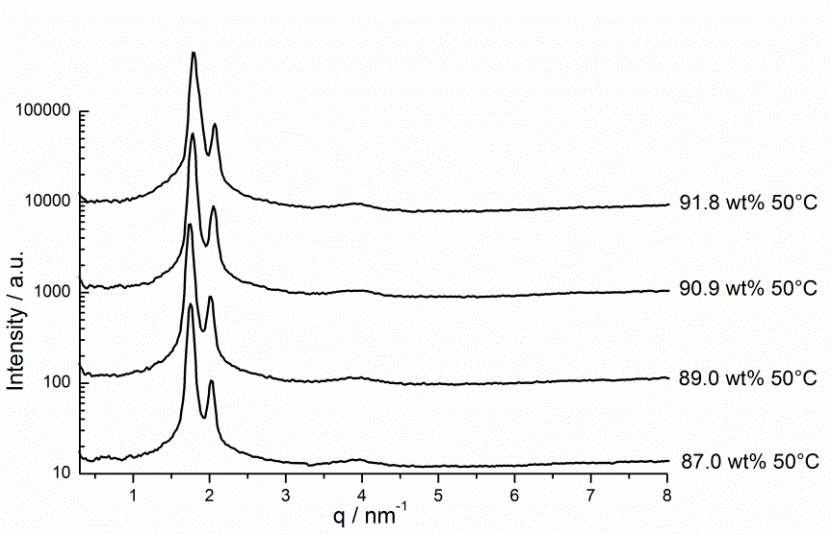

Figure D2-9. SAXS spectra of the bicontinuous cubic phase with I*a*3*d* structure at different concentrations of choline dodecylsulfate with water at 50°C are shown.

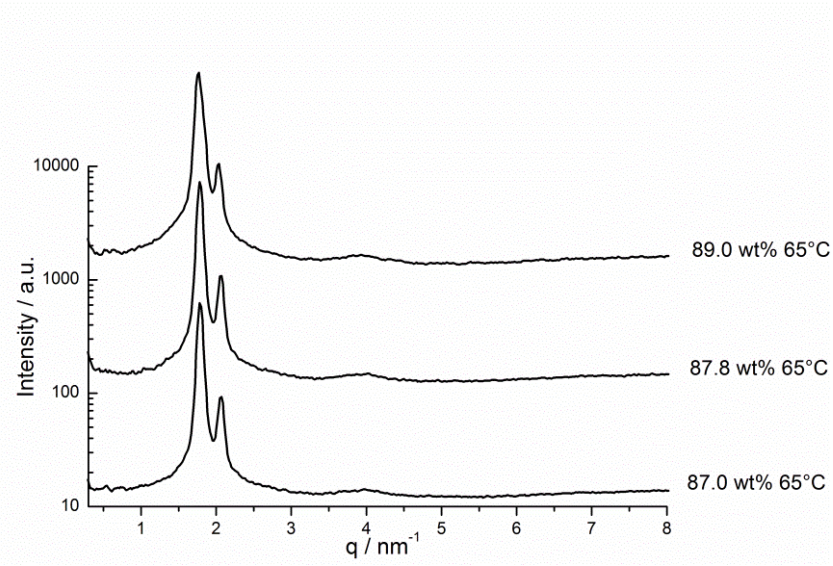

Figure D2-10. SAXS spectra of the bicontinuous cubic phase with I*a*3*d* structure at different concentrations of choline dodecylsulfate with water at 65°C are shown.

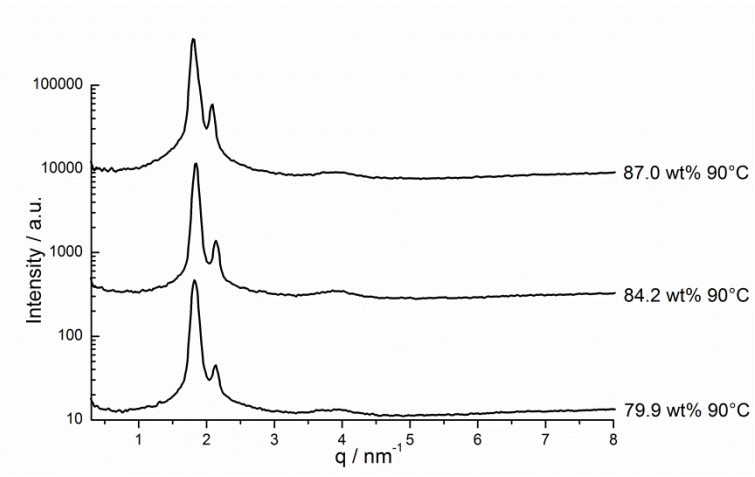

Figure D2-11. SAXS spectra of the bicontinuous cubic phase with I*a*3*d* structure at different concentrations of choline dodecylsulfate with water at 90°C are shown.

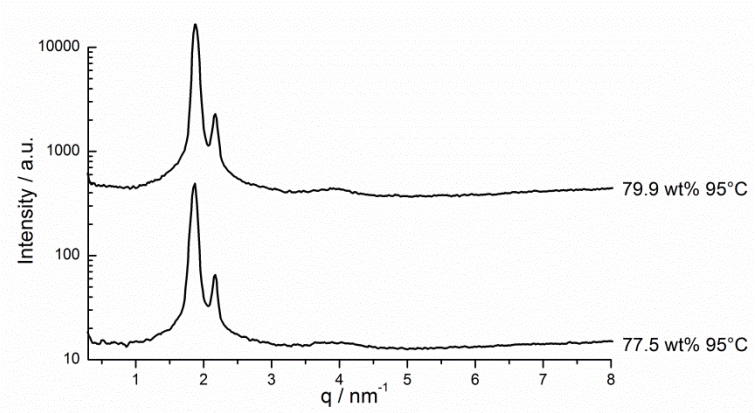

Figure D2-12. SAXS spectra of the bicontinuous cubic phase with I*a*3*d* structure at different concentrations of choline dodecylsulfate with water at 95°C are shown.

D.2.3.3 SAXS spectra of the bicontinuous cubic phase with I*a*3*d* structure of ChS_{16} with water

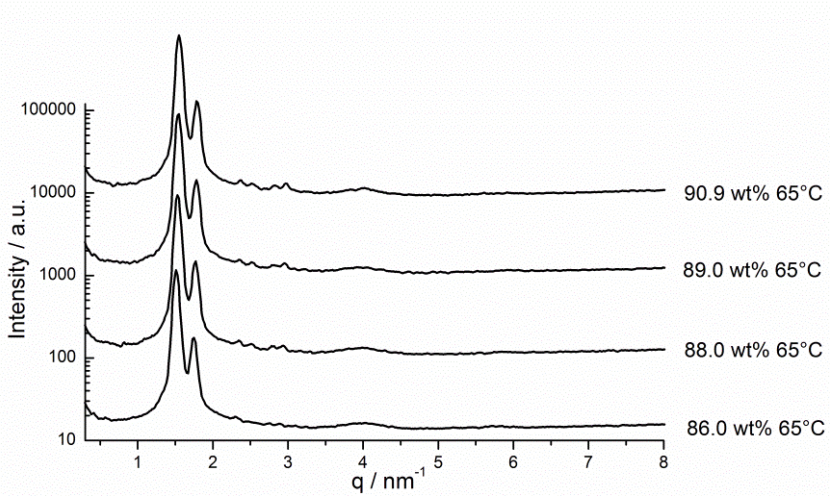

Figure D2-13. SAXS spectra of the bicontinuous cubic phase with I*a*3*d* structure at different concentrations of choline hexadecylsulfate with water at 65°C are shown.

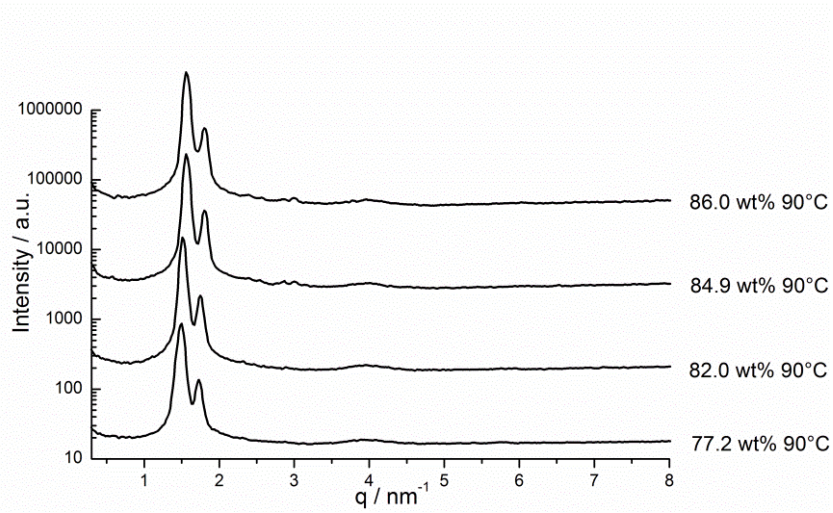

Figure D2-14. SAXS spectra of the bicontinuous cubic phase with I*a*3*d* structure at different concentrations of choline hexadecylsulfate with water at 90°C are shown.

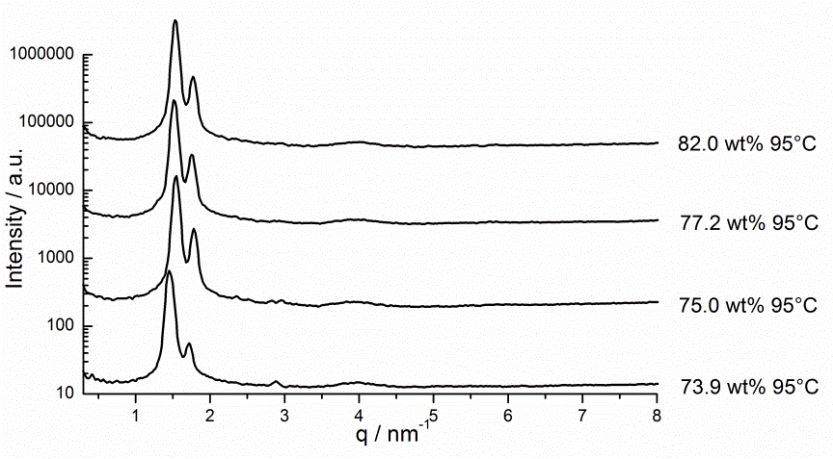

Figure D2-15. SAXS spectra of the bicontinuous cubic phase with I*a*3*d* structure at different concentrations of choline hexadecylsulfate with water at 95°C are shown.

D.2.4 Multi-phasic region: Additional bicontinuous cubic phase with I*m*3*m* structure

D.2.4.1 SAXS spectra of multi-phasic region of ChS_{12} with water

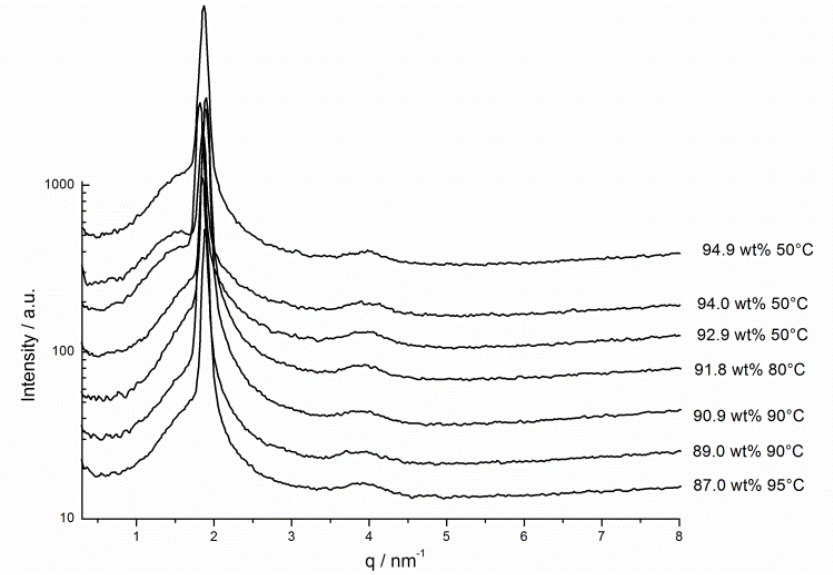

Figure D2-16. SAXS spectra of multi-phasic region at different concentrations of choline dodecylsulfate with water at 50°C, 90°C and 95 °C.

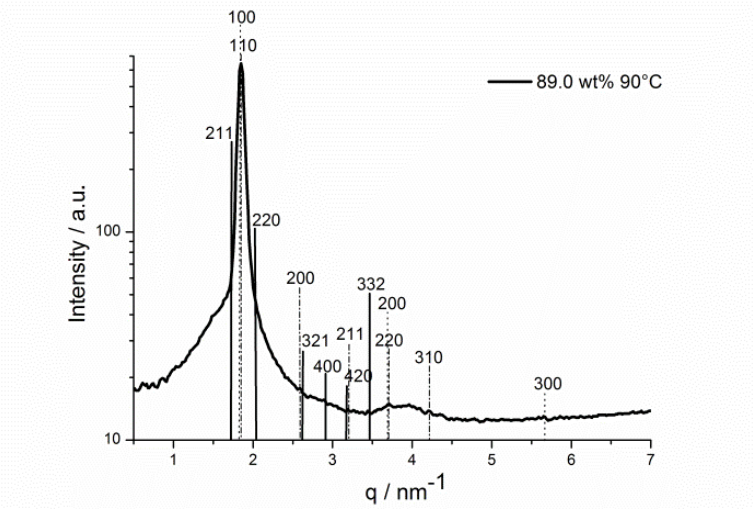

Figure D2-17. SAXS spectrum of multi-phasic region containing two bicontinuous cubic phases with I*a*3*d* and I*m*3*m* structure and a lamellar phase at 89.0 wt% choline dodecylsulfate and 90°C. The lines represent the Miller indices assigning the different structures: (_._._._) I*m*3*m*; (_____) I*a*3*d*; (…….) lamellar.

D.2.4.2 SAXS spectrum of the multi-phasic region of ChS_{16} with water

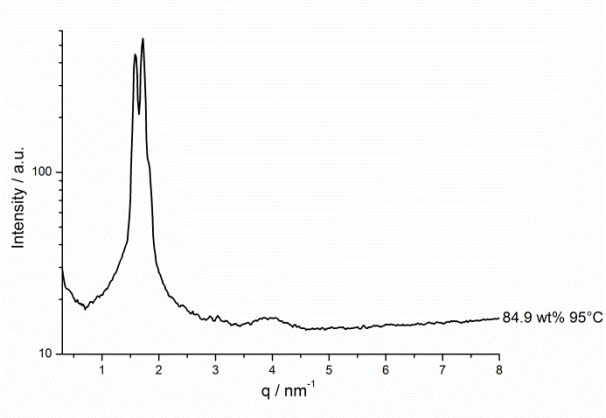

Figure D2-18. SAXS spectrum of multi-phasic region at 84.9 wt% choline hexadecylsulfate with water at 95°C.

D.2.5 Defective lamellar phase dL_α or nematic phase N

D.2.5.1 SAXS data and calculated parameter

Defective lamellar dL_α or nematic N phase							
ChS_{12}							
wt%	**T /°C**	**d_{100} / Å**	**d_{200} / Å**	**r_L / Å**	**a_S / Å^2**	**Φs**	**$Φ_L$**
95.9	50	35.7	17.8	10.2 ± 0.2	34.4 ± 0.5	0.957	0.570
92.9	90	35.7	18.4	9.8 ± 0.2	35.6 ± 0.6	0.926	0.552
95.9	90	35.1	17.6	10.0 ± 0.2	35.0 ± 0.6	0.957	0.570
97.0	90	34.9	17.5	10.1 ± 0.2	34.8 ± 0.5	0.969	0.577
89.0	95	34.5	17.2	9.1 ± 0.2	38.5 ± 0.6	0.885	0.527
ChS_{16}							
92.9	80	35.3	17.6	10.8 ± 0.2	42.3 ± 0.5	0.928	0.613
88.0	90	35.7	17.8	10.4 ± 0.2	44.2 ± 0.5	0.878	0.580
88.9	90	35.6	17.8	10.4 ± 0.2	43.9 ± 0.5	0.887	0.586
90.9	90	35.5	17.7	10.6 ± 0.2	43.0 ± 0.5	0.907	0.600
92.1	90	35.3	17.6	10.7 ± 0.2	42.7 ± 0.5	0.919	0.608
92.9	90	35.1	17.6	10.8 ± 0.2	42.5 ± 0.5	0.928	0.613

Table D2-4. X-ray diffraction data of the defective lamellar or nematic phase: The experimental d-values and the corresponding Miller indices, half length of the lipophilic bilayer r_L, area of polar-nonpolar interface a_S, volume fraction of the surfactant $Φ_S$ and of the lipophilic part $Φ_L$ of the different concentrations of choline dodecylsulfate and choline hexadecylsulfate with water are given.

D.2.5.2 SAXS spectra of the defective lamellar or nematic phase of ChS_{12} with water

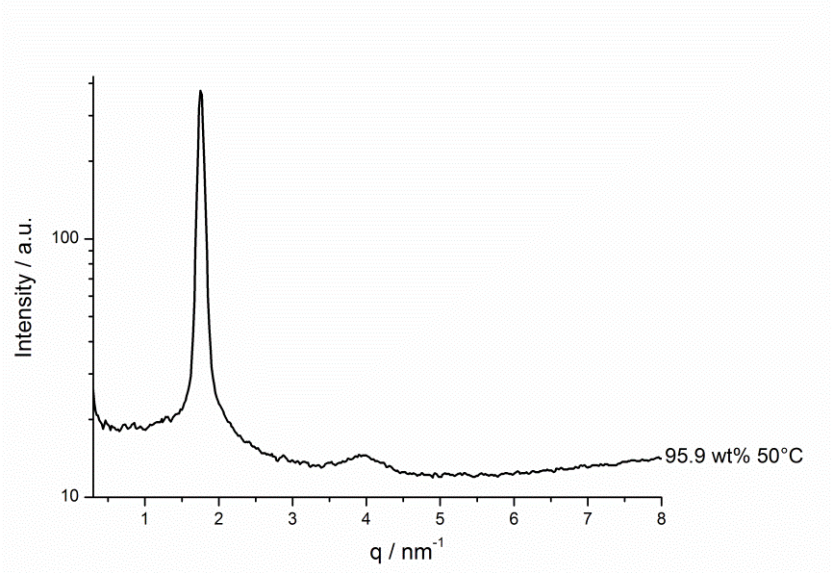

Figure D2-19. SAXS spectrum of the defective lamellar or nematic phase at 95.9 wt% choline dodecylsulfate with water at 50°C.

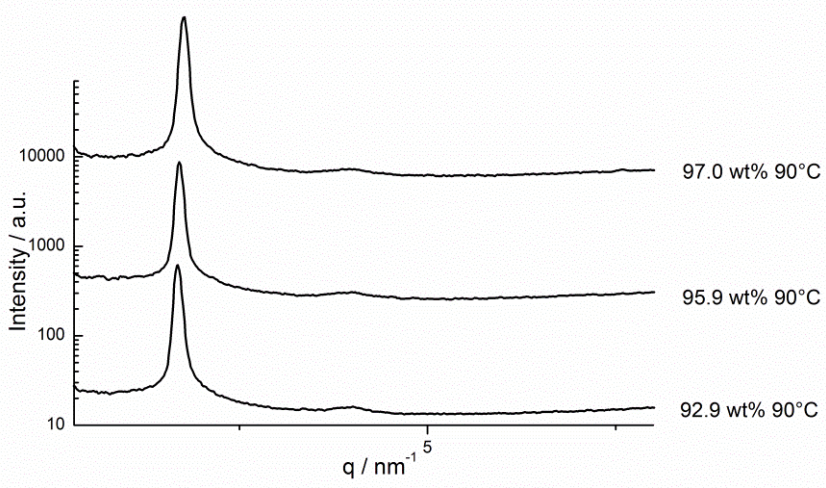

Figure D2-20. SAXS spectra of the defective lamellar or nematic phase at different concentrations of choline dodecylsulfate with water at 90°C.

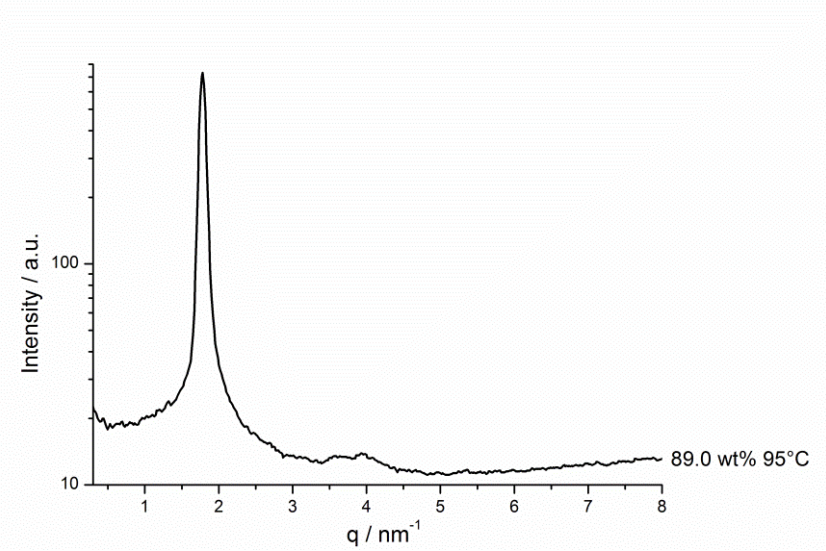

Figure D2-21. SAXS spectrum of the defective lamellar phase of 89.0 wt% of choline dodecylsulfate with water at 95°C.

D.2.5.3 SAXS spectra of the defective lamellar or nematic phase of ChS_{16} with water

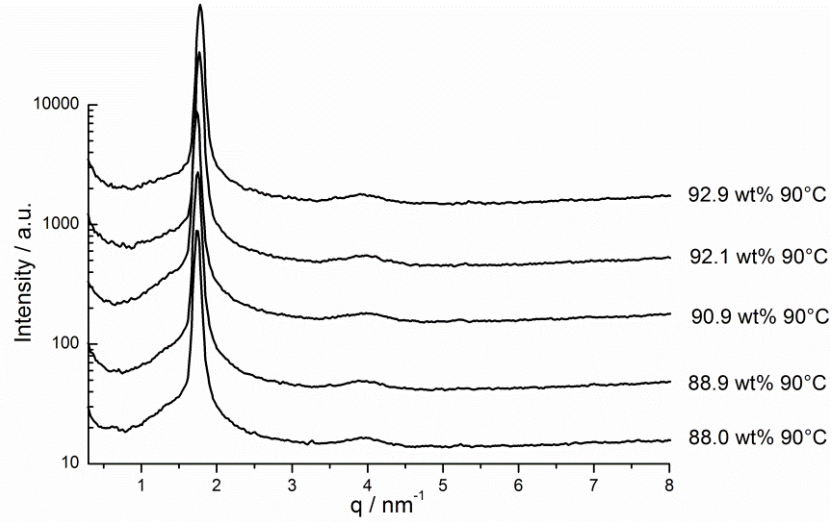

Figure D2-22. SAXS spectra of the defective lamellar or nematic phase at different concentrations of choline hexadecylsulfate with water at 90°C.

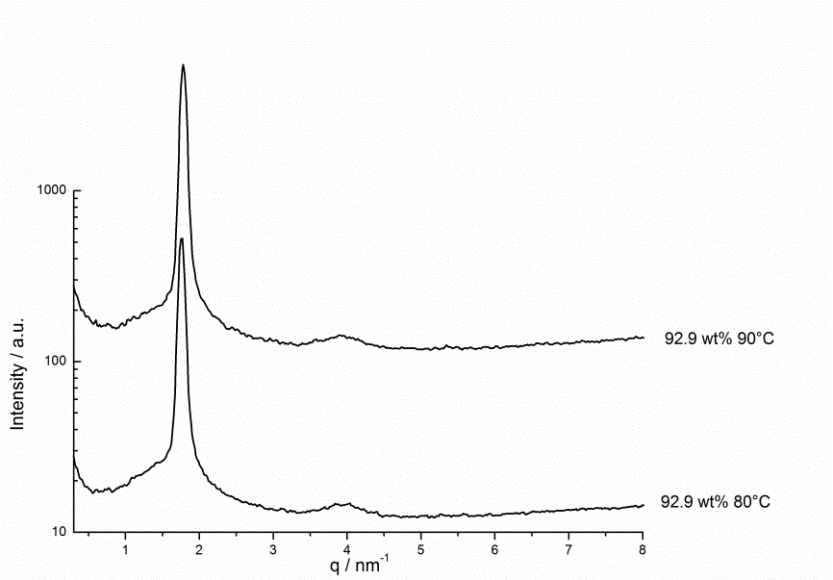

Figure D2-23. SAXS spectra of the defective lamellar or nematic phase at 92.9 wt% of choline hexadecylsulfate with water at 80°C and 90°C.

D.2.6 SAXS and WAXS spectra below the crystal solubility boundary

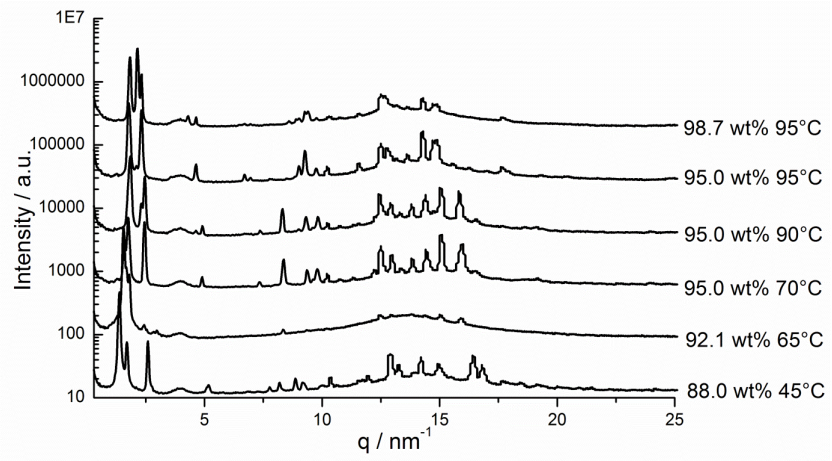

Figure D2-24. SAXS and WAXS spectra at different concentrations of choline hexadecylsulfate with water below the crystal solubility boundary.

Appendix E Thermotropic phase behavior of choline alkylsulfates ChS_m with m = 12, 16

E.1 Polarizing optical microscopy

E.1.1 Choline dodecylsulfate

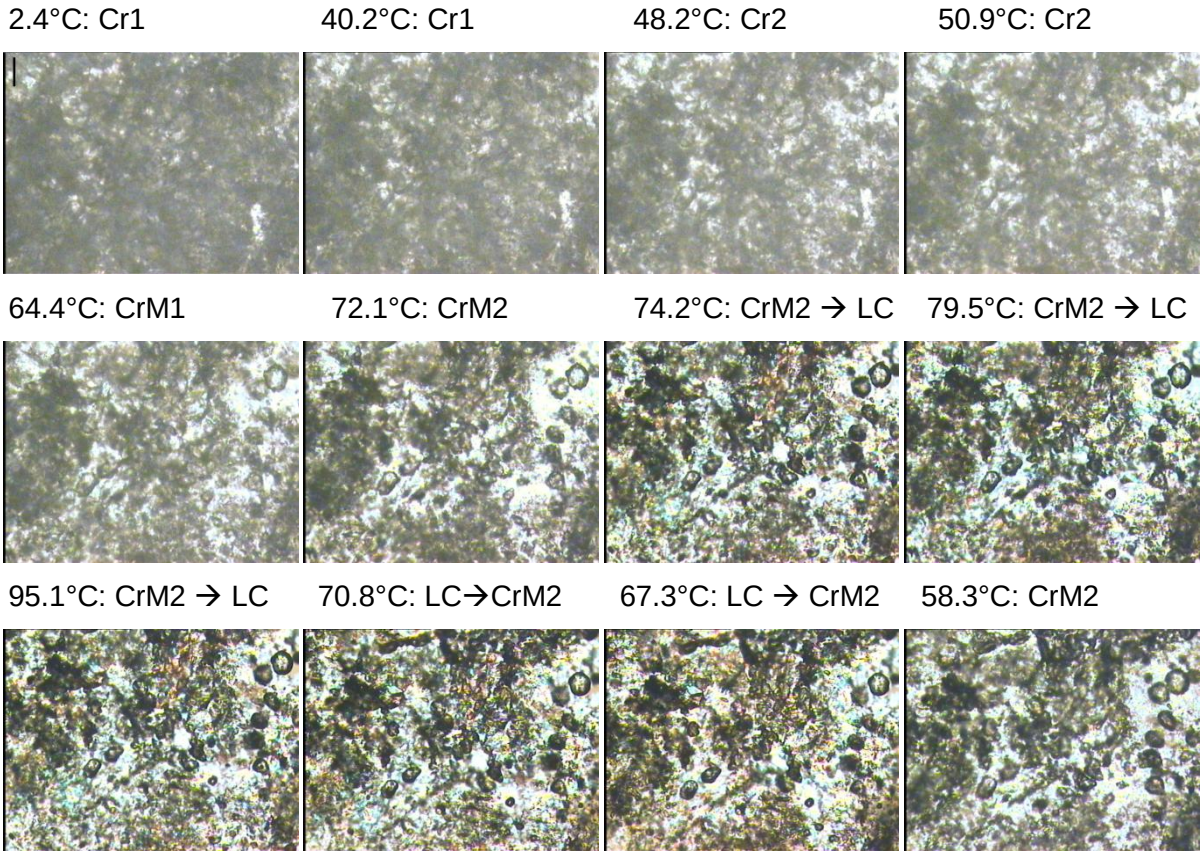

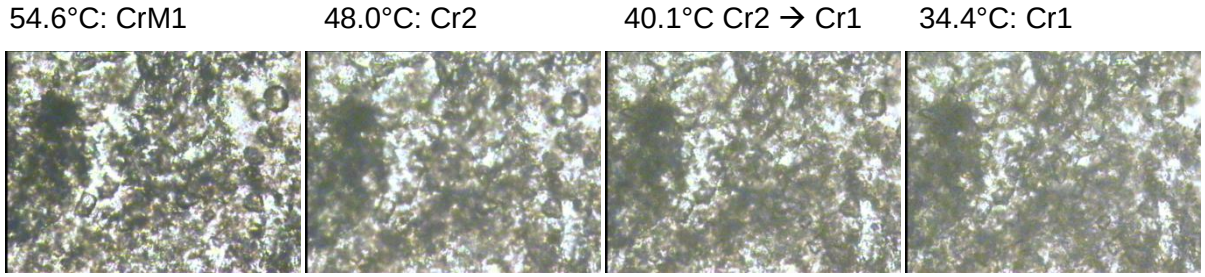

Figure E1-1. Polarizing optical light microscopy images of the second heating and cooling cycle of neat choline dodecylsulfate. The second cycle measured with a heating rate of 10 K min^{-1} is shown. With increasing temperature the following phases appear: first crystalline phase Cr1, second crystalline phase Cr2, first semi-crystalline phase CrM1, second semi-crystalline phase CrM2. The transition to the liquid crystalline phase LC is very slow. The scale bar (see image recorded at 2.4°C) is 100 µm. It is the same for the other images.

E.1.2 Choline hexadecylsulfate

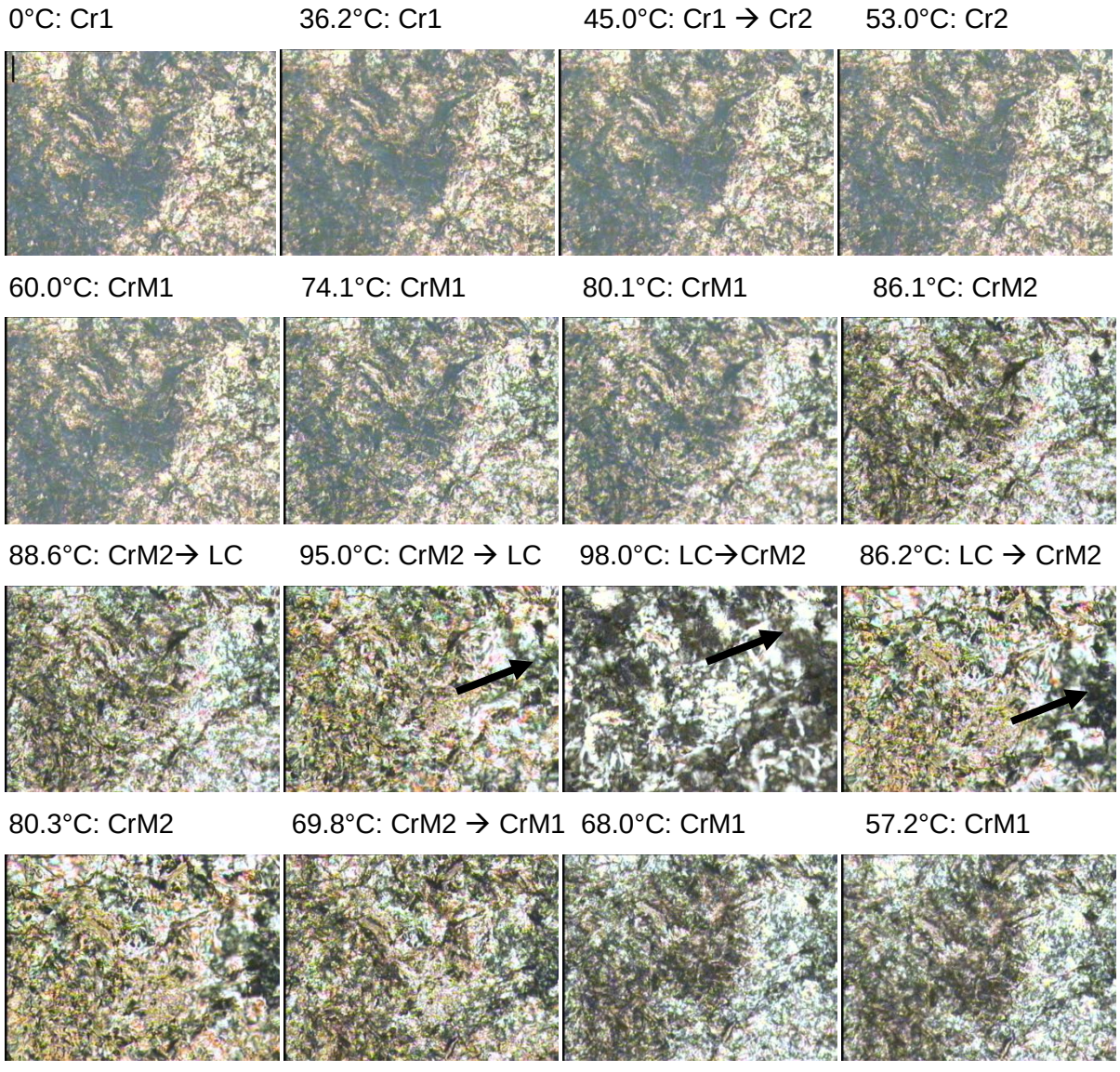

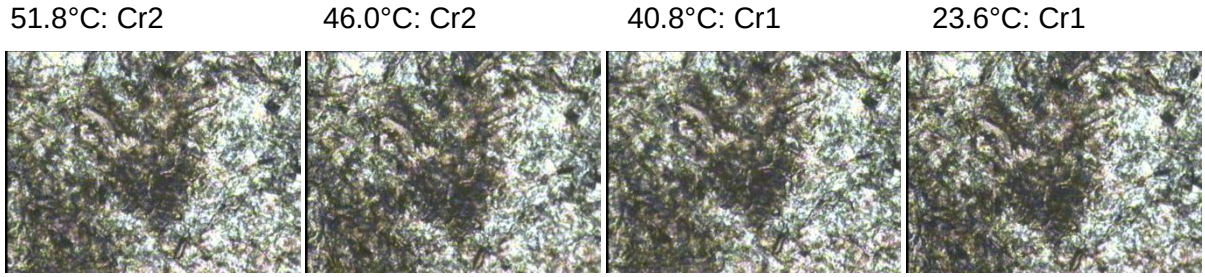

Figure E1-2. Polarized optical light microscopy images of the thermotropic phases of choline hexadecylsulfate ChS_{16} in the temperature range between 0°C and 98°C are shown. The second heating and cooling cycle is shown with a heating rate of 10 K min^{-1}. With increasing temperature the following phases appear: first crystalline phase Cr1, second crystalline phase Cr2, first semi-crystalline phase CrM1, second semi-crystalline phase CrM2. The transition to the liquid crystalline phase LC is very slow. The arrows mark the liquid crystalline phase. The scale bar (see image recorded at 0°C) is 100 µm. It is the same for the other images.

E.2 Differential scanning calorimetry (DSC)

	ChS_{12}				ChS_{16}			
	T_1 / °C	T_2 / °C	T_3 / °C	T_4 / °C	T_1 / °C	T_2 / °C	T_3 / °C	T_4 / °C
1. heating	50.0	57.3	70.8	77.4	48.1	58.8	85.0	90.9
1. cooling	39.8	50.2	56.1	67.9	45.0	56.3	70.3	81.4
2. heating	44.5	53.8	70.2	76.6	48.5	58.8	85.1	90.9
2. cooling	39.7	50.0	56.1	68.2	44.9	56.5	70.4	81.9
3. heating	44.3	53.8	70.2	76.5	48.2	59.0	85.1	91.0
3. cooling	39.4	49.8	56.2	67.8	44.6	56.5	70.7	82.1

Table E2-1. Transition temperatures of the different phase transitions of neat choline alkylsulfates ChS_m with m = 12 and 16 obtained from the DSC measurements. The value of the transition temperature was taken from the peak maximum (heating) or peak minimum (cooling). Three cycles were recorded in the temperature range of 0°C to 95°C with a heating rate of 1 K min^{-1}.

	ChS_{12}		ChS_{16}	
	$\sum\Delta H$ / kJ mol^{-1}	$\sum\Delta S$ / J $mol^{-1}K^{-1}$	$\sum\Delta H$ / kJ mol^{-1}	$\sum\Delta S$ / J $mol^{-1}K^{-1}$
1. heating	47.9	141.7	54.2	158.6
1. cooling	-37.9	-115.6	-52.7	-157.0
2. heating	38.1	113.4	53.8	156.8
2. cooling	-37.6	-114.8	-53.0	-157.9
3. heating	37.9	112.8	54.6	159.3
3. cooling	-37.5	-114.4	-53.0	-157.7

Table E2-2. Sum of all enthalpies or entropies of the phase transitions of the neat choline alkylsulfate ChS_m with m = 12 and 16 at the heating or cooling cycle in the temperature range from -50°C to 95°C. Of each sample three cycles were recorded with DSC.

E.3 NMR proton spin-spin relaxation times T_{2eff}

	ChS_{12} - first cycle		ChS_{12} - second cycle		ChS_{16} - first cycle		ChS_{16} - second cycle	
T / °C	***T_{2eff} / µs***	***percent / %***	***T_{2eff} / µs***	***percent / %***	***T_{2eff} / µs***	***percent / %***	***T_{2eff} / µs***	***percent / %***
10	6.3	11.9	5.7	12.2	-	-	-	-
25	-	-	-	-	7.0	15.1	6.6	15.9
33	6.4	14.1	7.0	12.0	-	-	-	-
45	12.6	7.4	11.7	9.6	-	-	-	-
50	-	-	-	-	8.5	20.2	6.7	19.3
54	14.3	9.9	14.9	10.0	-	-	-	-
60	17.9	13.5	17.3	11.4	-	-	-	-
70	22.2	18.4	20.4	19.4	-	-	-	-
75	-	-	-	-	16.7	22.4	19.8	23.3
79	99.0	15.4	74.3	16.5	-	-	-	-
82	-	-	-	-	21.9	26.9	21.5	19.1
84	-	-	-	-	25.2	22.6	23.2	24.5
90	114.0	17.0	114.3	17.8	61.9	11.5	61.93	21.5
92	-	-	-	-	99.4	8.4	99.1	16.2
96	-	-	-	-	106.2	12.1	107.4	13.6
86	-	-	-	-	-	-	33.0	20.4
82	-	-	-	-	23.6	18.7	-	-
75	-	-	82.6	12.4	20.4	12.0	17.9	19.4
69	22.0	16.4	20.9	16.5	19.8	7.5	17.7	19.4
59	-	-	-	-	17.1	6.6	17.3	6.9
55	18.1	9.4	15.6	11.0	-	-	-	-
49	12.4	9.9	12.7	10.7	8.3	21.5	6.2	20.0
42	11.8	11.6	11.6	11.0	-	-	-	-
37	8.5	14.7	9.9	13.0	-	-	-	-
35	-	-	-	-	7.9	15.9	-	-
25	7.7	18.6	7.5	20.4	-	-	6.6	14.0

Table E3-1. Temperature dependent spin-spin relaxation time T_{2eff} is given for the main structure of the thermotropic phases of choline dodecylsulfate and choline hexadecylsulfate. Further, the amount of the main structure of the whole phase was given in percent of the overall intensity obtained from NMR peak.

Appendix F Choline alkylsulfates as a biological alternative to common washing powder surfactants

F.1 Washing tests on cotton fiber

Tenside	ΔL*	ΔE*ab
SDS 9.5 mM	-7.035 ± 0.8288	7.239 ± 0.812
SDS 14.8 mM	-10.566 ± 1.9214	10.740 ± 1.959
SDS 0.5 wt% (17.33 mM)	-11.298 ± 0.967	11.494 ± 0.942
SDS 0.7 wt% (24.27 mM)	-12.313 ± 1.348	12.568 ± 1.401
SDS 1 wt% (34.67 mM)	-14.650 ± 1.962	14.969 ± 1.956
ChS_{12} 9.5 mM	-8.186 ± 0.787	8.281 ± 0.802
ChS_{12} 14.8 mM	-11.635 ± 0.488	11.739 ± 0.459
ChS_{12} 0.5 wt% (13.53 mM)	-12.320 ± 0.167	12.618 ± 0.142
ChS_{12} 0.7 wt% (18.94 mM)	-12.756 ± 2.739	12.884 ± 2.789
ChS_{12} 1 wt% (34.67 mM)	-14.507 ± 1.294	14.749 ± 1.309
ChS_{16} 9.5 mM	-8.212 ± 0.928	8.307 ± 0.917
ChS_{16} 14.8 mM	-10.760 ± 1.089	11.002 ± 1.108
ChS_{16} 0.5 wt% (11.74 mM)	-9.275 ± 2.208	9.493 ± 2.170
ChS_{16} 0.7 wt% (16.44 mM)	-10.87 ± 0.834	11.000 ± 0.857
ChS_{16} 1 wt% (23.495 mM)	-11.730 ± 0.806	11.816 ± 0.787
Choline oleate 9.5 mM	-4.942 ± 1.968	5.017 ± 2.608
Choline oleate 14.8 mM	-6.265 ± 1.944	6.288 ± 1.937
Choline oleate 0.5 wt% (12.97 mM)	-5.337 ± 0.821	5.439 ± 0.808
Choline oleate 0.7 wt% (18.15 mM)	-5.896 ± 1.202	5.946 ± 1.220
Choline oleate 1 wt% (25.93 mM)	-5.963 ± 1.092	6.108 ± 1.1.32
NaDB 9.5 mM	-9.050 ± 1.92	9.171 ± 1.9528
NaDB 0.5 wt% (14.8 mM)	-10.468 ± 1.136	10.630 ± 1.126
NaDB 0.7 wt% (20.08 mM)	-11.036 ± 0.976	11.212 ± 0.965
NaDB 1 wt% (28.69 mM)	-14.835 ± 1.067	15.179 ± 1.134
ChS_{16}:NaDB (1:1mol) 9.5 mM	-10.773 ± 1.610	10.876 ± 1.577
ChS_{16}:NaDB (1:1mol) 14.8 mM	-15.267 ± 0.435	15.429 ± 0.451
ChS_{16}:NaDB (1:1mol) 0.5 wt% (12.92 mM)	-14.985 ± 2.871	15.313 ± 2.968
ChS_{16}:NaDB (1:1mol) 0.7wt% (18.08 mM)	-18.463 ± 0.397	18.890 ± 0.507
ChS_{16}:NaDB (1:1mol) 1 wt% (25.84 mM)	-18.285 ± 0.488	18.712 ± 0.529
ChS_{16}:ChS_{12} (1:1mol) 9.5mM	-9.810 ± 0.781	9.870 ± 0.763
ChS_{16}:ChS_{12} (1:1mol) 14.8 mM	-15.370 ±1.262	15.667 ± 1.466
ChS_{16}:ChS_{12} (1:1mol) 0.5 wt% (12.58 mM)	-12.520 ± 0.853	12.762 ± 0.819
ChS_{16}:ChS_{12} (1:1mol) 0.7 wt% (17.6 mM)	-15.780 ± 0.834	15.982 ± 0.864
ChS_{16}:ChS_{12} (1:1mol) 1 wt% (25.15 mM)	-17.867 ± 1.176	18.158 ± 1.279

Table F1-1. Calculated values of ΔE*ab and ΔL* obtained from color difference of a dyed cotton fiber, which was washed with the different surfactant/surfactant mixture solution at these concentrations: 9.5 mM, 14.8 mM, 0.5 wt%, 0.7 wt% and 1 wt%. The washing temperature was 40°C.

List of figures

List of tables

List of publications

(1) M. Baglioni, D. Rengstl, D. Berti, M. Bonini, R. Giorgi, and P. Baglioni, Removal of acrylic coatings from works of art by means of nanofluids: understanding the mechanism at the nanoscale. *Nanoscale*, 2010, **2**, 1723-1732.

(2) W. Kunz, E. Maurer, R. Klein, D. Touraud, D. Rengstl, A. Harrar, and S. Dengler, Low Toxic Ionic Liquids, Liquid Catanionics, and Ionic Liquid Microemulsions. *Journal of Dispersion Science and Technology,* 2011*,* **32**, 1694-1699.

(3) J. Eiblmeier, M. Kellermeier, D. Rengstl, J. M. Garcia-Ruiz, and W. Kunz, Effect of bulk pH and supersaturation on the growth behavior of silica biomorphs in alkaline solutions. *CrystEngComm*, 2013, **15**, 43-53.

(4) D. Rengstl, B. Kraus, M. Van Vorst, G. D. Elliott, and W. Kunz, Effect of choline carboxylate ionic liquids on biological membranes. To be submitted to *Biotechnology and Bioengineering* (Chapter 3)

(5) D. Rengstl, O. Diat, R. Klein, and W. Kunz, Aqueous behavior of choline carboxylates: Influence of chain length and double bond. *Langmuir*, 2013, ***29***, 2506-19. (Chapter 4)

(6) D. Rengstl, G. J. T. Tiddy, I. Shenderovich, J. Eiblmeier, and W. Kunz, Influence of chain length and double bond on the thermotropic phase behavior of choline carboxylate soaps. To be submitted to *Colloids and Surfaces A: Physicochemical and Engineering Aspects* (Chapter 5)

(7) D. Rengstl, O. Diat, and W. Kunz, Aqueous behavior of choline alkylsulfates - Influence of chain length. To be submitted to *Journal of Physical Chemistry* (Chapter 6)

(8) D. Rengstl, G. J. T. Tiddy, I. Shenderovich, J. Eiblmeier, and W. Kunz, Thermotropic phase behavior of choline alkylsulfates. To be submitted to *Journal of Molecular Liquids* (Chapter 7)

(9) D. Rengstl, and W. Kunz, Deep eutectic solvents based on choline glutarate. To be submitted to *Physical Chemistry Chemical Physics* (Chapter 9)

List of oral and poster presentations

05/2012 **Bunsentagung**, Leipzig (Germany)
„Aqueous Phase Behavior of Choline Carboxylate Ionic Liquids – Influence of Chain Length and Double Bond“ (Poster)

02/2012 **Scholarship meeting of “Fonds der Chemischen Industrie”**, Erlangen (Germany)
„Choline Carboxylates and Sulfates – Biocompatible Surfactants and Ionic Liquids” (Talk)

06/2011 **4th International Congress on Ionic Liquids,** Washington DC (USA)
„Biocompatible choline carboxylate ionic liquids: Influence of chain length and double bond on the thermotropic phase behavior” (Talk)

06/2010 **Formula VI**, Stockholm (Sweden)
„Biocompatible, Green – From Ionic Liquid to Surfactant“ (Poster)

09/2010 **ECIS**, Prague (Czech Republic)
“Biocompatible Choline Carboxylates – From Ionic Liquid to Surfactant” (Poster)

Eidesstattliche Erklärung

Ich erkläre hiermit an Eides statt, dass ich die vorliegende Arbeit selbstständig ohne unzulässige Hilfe Dritter und ohne Benutzung anderer als der angegebenen Hilfmittel angefertigt habe; die aus anderen Quellen direkt übernommenen Daten und Konzepte sind unter Angabe des Literaturzitats gekennzeichnet.

Regensburg, den 28. Mai 2013

Doris Rengstl